US Army Corps of Engineers

GEOTECHNICAL LABORATORY

(6)

MISCELLANEOUS PAPER GL-88-14

A PRESSUREMETER METHOD FOR SINGLE PILES SUBJECTED TO CYCLIC LATERAL LOADS IN SAND

by

Robert L. Little, Jean-Louis Briaud

Geotechnical Division

Civil Engineering Department
Texas A&M University
College Station, Texas 77843

June 1988
Final Report

Prepared for Minerals Management Service
US Department of Interior, Reston, Virginia 22090

and

Department of Research
Federal Highway Administration, Washington, DC 20590

and

US Army Engineer Division, Lower Mississippi Valley
PO Box 80, Vicksburg, Mississippi 39180-0080

Monitored by Geotechnical Laboratory
US Army Engineer Waterways Experiment Station
PO Box 631, Vicksburg, Mississippi 39180-0631

Under Contract No. DACW39-85-M-4380

Destroy this report when no longer needed. Do not return it to the originator.

The findings in this report are not to be construed as an official Department of the Army position unless so designated by other authorized documents.

The contents of this report are not to be used for advertising, publication, or promotional purposes. Citation of trade names does not constitute an official endorsement or approval of the use of such commercial products.

Unclassified
SECURITY CLASSIFICATION OF THIS PAGE

REPORT DOCUMENTATION PAGE

Form Approved
OMB No. 0704-0188
Exp. Date: Jun 30, 1986

1a. REPORT SECURITY CLASSIFICATION Unclassified	1b. RESTRICTIVE MARKINGS
2a. SECURITY CLASSIFICATION AUTHORITY	3. DISTRIBUTION/AVAILABILITY OF REPORT Approved for public release; distribution unlimited
2b. DECLASSIFICATION/DOWNGRADING SCHEDULE	
4. PERFORMING ORGANIZATION REPORT NUMBER(S) Research Report No. 5357	5. MONITORING ORGANIZATION REPORT NUMBER(S) Miscellaneous Paper GL-88-14
6a. NAME OF PERFORMING ORGANIZATION See reverse. / 6b. OFFICE SYMBOL (If applicable)	7a. NAME OF MONITORING ORGANIZATION Geotechnical Laboratory, USAEWES
6c. ADDRESS (City, State, and ZIP Code) College Station, TX 77843	7b. ADDRESS (City, State, and ZIP Code) PO Box 631 Vicksburg, MS 39180-0631
8a. NAME OF FUNDING/SPONSORING ORGANIZATION See reverse. / 8b. OFFICE SYMBOL (If applicable)	9. PROCUREMENT INSTRUMENT IDENTIFICATION NUMBER DACW39-85-M-4380
8c. ADDRESS (City, State, and ZIP Code) See reverse.	10. SOURCE OF FUNDING NUMBERS PROGRAM ELEMENT NO. / PROJECT NO. / TASK NO. / WORK UNIT ACCESSION NO.

11. TITLE (Include Security Classification)

A Pressuremeter Method for Single Piles Subjected to Cyclic Lateral Loads in Sand

12. PERSONAL AUTHOR(S)
Little, Robert L., and Briaud, Jean-Louis

13a. TYPE OF REPORT	13b. TIME COVERED	14. DATE OF REPORT (Year, Month, Day)	15. PAGE COUNT
Final report	FROM _____ TO _____	June 1988	334

16. SUPPLEMENTARY NOTATION
Available from National Technical Information Service, 5285 Port Royal Road, Springfield, VA 22161.

17. COSATI CODES			18. SUBJECT TERMS (Continue on reverse if necessary and identify by block number)
FIELD	GROUP	SUB-GROUP	Cohesionless soils; Single piles; Cyclic lateral loading; Pressuremeter

19. ABSTRACT (Continue on reverse if necessary and identify by block number)

A method is proposed to predict the response of piles in sand subjected to cyclic horizontal loading on the basis of cyclic pressuremeter tests. This method is an extension of the pressuremeter method proposed for piles subjected to monotonic horizontal loading. The pressuremeter-derived monotonic P-y curve is reduced by a multiplier N^{-a} to obtain the cyclic PN^{-a}-y curve. The parameter a is obtained readily from cyclic pressuremeter tests.

This pressuremeter method was used to predict the response of a 10.75-in.-diam pipe pile embedded in 9.5 ft of sand and subjected to two-way cyclic horizontal loads with full reversal of loading. This pressuremeter method was also used to predict the response of 12 model pile tests in sand subjected to one-way and two-way cyclic horizontal loads. In addition, a data base of full-scale cyclic horizontal load tests was analyzed.

(Continued)

20. DISTRIBUTION/AVAILABILITY OF ABSTRACT	21. ABSTRACT SECURITY CLASSIFICATION
☒ UNCLASSIFIED/UNLIMITED ☐ SAME AS RPT. ☐ DTIC USERS	Unclassified
22a. NAME OF RESPONSIBLE INDIVIDUAL	22b. TELEPHONE (Include Area Code) / 22c. OFFICE SYMBOL

DD FORM 1473, 84 MAR 83 APR edition may be used until exhausted. All other editions are obsolete.

6a. NAME OF PERFORMING ORGANIZATION (Continued).

Geotechnical Division
Civil Engineering Department
Texas A&M University

8a. & 8c. NAME AND ADDRESS OF FUNDING/SPONSORING ORGANIZATIONS AND ADDRESSES (Continued).

Minerals Management Service
US Department of Interior
Reston, VA 22090

Department of Research
Federal Highway Administration
Washington, DC 20590

US Army Engineer Division, Lower Mississippi Valley
PO Box 80
Vicksburg, MS 39180-0080

19. ABSTRACT (Continued).

The results show that (a) two-way cyclic horizontal loading of piles in sand leads to minimal if not negligible degradation, (b) one-way cyclic horizontal loading of piles in sand leads to significant degradation, (c) the proposed method predicts with very good accuracy the degradation of piles in sand subjected to one-way cyclic horizontal loads, and (d) the proposed method cannot predict the degradation (or lack of it) of piles in sand subjected to two-way cyclic horizontal loads because the pressuremeter is a one-way cyclic test.

PREFACE

This study was performed by the Geotechnical Division, Civil Engineering Department, Texas A&M University, College Station, TX, under contract to the US Army Engineer Waterways Experiment Station (WES), Vicksburg, MS, for the Minerals Management Service, US Department of Interior; the Department of Research, Federal Highway Administration; and the US Army Engineer Division, Lower Mississippi Valley. The report was performed under Contract No. DACW39-85-M-4380.

This report was prepared by Mr. Robert L. Little and Dr. Jean-Louis Briaud, Texas A&M University, and reviewed by Mr. Gerald B. Mitchell, Chief, Engineering Group, Soil Mechanics Division (SMD), Geotechnical Laboratory (GL), WES. General supervision was provided by Mr. Clifford L. McAnear, Chief, SMD, and Dr. William F. Marcuson III, Chief, GL.

COL Dwayne G. Lee is Commander and Director of WES. Dr. Robert W. Whalin is Technical Director.

ACKNOWLEDGEMENTS

This project was sponsored by the US Army Engineer Waterways Experiment Station. Mr. Britt Mitchell who was the technical contact is thanked for his readiness to help, for his constructive advice, and for his wonderfully contagious positive attitude.

The cooperation of Professor Reese and Professor O'Neill is very much appreciated. Professor Reese was always ready to share the data that he and Mr. Morrison collected in the 10.75 inch diameter pile load test at the University of Houston. Professor O'Neill allowed this research team repeated access to his research site at the University of Houston for pressuremeter testing.

Others at Texas A&M University contributed to this project. Mr. Makarim and Mr. Tucker helped in performing the pressuremeter tests. Mr. Tucker's talent in microcomputer programming was invaluable in the reduction of the PMT data and in the preparation of the microcomputer program PYPMT.

TABLE OF CONTENTS

TABLE OF CONTENTS (continued)

TABLE OF CONTENTS (continued)

TABLE OF CONTENTS (continued)

LIST OF TABLES

LIST OF TABLES (continued)

LIST OF FIGURES

LIST OF FIGURES (Continued)

LIST OF FIGURES (Continued)

LIST OF FIGURES (Continued)

LIST OF FIGURES (Continued)

LIST OF FIGURES (Continued)

LIST OF FIGURES (Continued)

LIST OF FIGURES (Continued)

LIST OF FIGURES (Continued)

LIST OF FIGURES (Continued)

LIST OF FIGURES (Continued)

LIST OF FIGURES (Continued)

LIST OF FIGURES (Continued)

LIST OF FIGURES (Continued)

LIST OF FIGURES (Continued)

1. INTRODUCTION

1.1 Project Purpose

Pressuremeter tests offer an array of advantages over present day methods employed in the design of laterally loaded piles. The pressuremeter method allows for the design of piles based on a series of P-y curves developed from point-by-point in-situ measurements, rather than curves derived from one or two measured parameters. The pressuremeter is a versatile instrument and can be employed in virtually any soil type including those for which there are no existing recommendations for the derivation of P-y curves. The pressuremeter allows for direct modeling of the pile installation method: pre-bored pressuremeter tests for drilled shafts and driven pressuremeter tests for driven piles. The pressuremeter is also capable of simulating the expected pile loading conditions: sustained pressure increment tests, unload-reload cyclic tests, and rapid inflation tests yield site-specific soil responses to creep loading, cyclic loading, and dynamic loading respectively.

These advantages over existing methods prompted this project. The chief objective was to incorporate cyclic loading effects into the derivation of P-y curves obtained from pressuremeter tests in order to predict the response of piles in sand subjected to cyclic lateral loading.

1.2 Project Approach

The approach employed toward this end included three separate phases. Existing data on cyclic laterally loaded pile tests in sands were analyzed in the first phase. In the second phase, predictions were made of the cyclic response of the 10.75 inch pipe pile load tested by Morrison and Reese (1986) at the University of Houston Foundation Test Facility sand site. These predictions were prepared using previously performed pressuremeter test results together with a degradation model selected in phase one. The predictions were then compared to the results measured during the full-scale cyclic lateral load tests performed by Morrison and Reese (1986). The third phase of the project consisted of a series of model pile cyclic load tests conducted in the Texas A&M University laboratories and of a similar series of cone pressuremeter tests. The degradation model was again employed to predict the cyclic responses of the model piles; the results were compared to the measured responses.

2. ANALYSIS OF EXISTING DATA

2.1 Data Base for Cyclic Laterally Loaded Piles in Sand

By surveying the available literature, 16 pile load tests where piles had been subjected to cyclic horizontal loads were found. These 16 tests were performed in 5 different studies: 2 in dense sand, 2 in dense sand and gravel, and 1 in sandy clay loam. The list of load tests is presented in Table 1. The essential data from each load test may be found in Appendix A. The data base included sands with SPT blowcounts ranging from 10 to 40. The test piles varied from 1 to 4 feet in diameter with lengths varying from 16.5 to 73 feet. The number of cycles performed at any given load level ranged from 25 to 100. The data base included both one-way and two-way cyclic tests.

2.2 Degradation Model

Using the horizontal load versus horizontal displacement curves at the top of the piles, a secant stiffness, Ks(N), was defined for the N^{th} cycle at each cyclic level (Figure 1). This secant stiffness is a function of the cycle number. The following model was used to fit the evolution of the secant stiffness with increasing number of cycles:

$$\frac{Ks(N)}{Ks(1)} = N^{-a} \qquad (1)$$

This model is credited to Idriss, et al. (1978) and has been used with success by several authors including Riggins

Pile Test No.	Date	Site	Pile Type	Soil	Cyclic Data	Reference
1.1	1967	Mustang Is.	2.0' Steel Pipe	Dense Sand	20x100,2-way	Reese, Cox, and Grubbs, 1967.
1.2	1967	Mustang Is.	2.0' Steel Pipe		20x100,2-way	Reese, Cox, and Koop, 1967.
2.1	1978	U.S.S.R.	1.0' Sq. R.C.	Sandy Clay Loam	1x55,2x100, 1-way	Fayans, et al., 1978.
2.2	1978	U.S.S.R.	1.0' Sq. R.C.		5x30,1-way	
3.1	1978	L & D 26	1.0' Timber	Dense Sand and Gravel	1x30,1-way	Perez and Holloway, 1979.
3.2	1978	L & D 26	1.0' Timber Post-grouted		1x30,1-way	
3.3	1978	L & D 26	1.1' H-Pile		1x30,1-way	
3.4	1978	L & D 26	1.2' Steel Pipe		1x30,1-way	
3.5	1978	L & D 26	1.1' H-Pile Post-grouted		1x30,1-way	
3.6	1978	L & D 26	1.2' Steel Pipe Post-grouted		1x30,1-way	
3.7	1978	L & D 26	1.1' H-Pile		1x30,1-way	
3.8	1978	L & D 26	1.2' Steel Pipe		1x30,1-way	
4.1	1984	L & D 26	1.2' H-Pile	Dense Sand and Gravel	1x25,1-way	Briaud, Brasuell, and Tucker, 1984.
4.2	1984	L & D 26	1.2' H-Pile		1x25,1-way	
5.1	1984	Tampa Bay	4.0' Diam. R.C.	Dense Sand	7x40,1-way	Long and Reese, 1984.
5.2	1984	Tampa Bay	4.0' Diam. R.C.		7x40,1-way	

Table 1. Data Base for Full-scale Cyclic Lateral Load Tests.

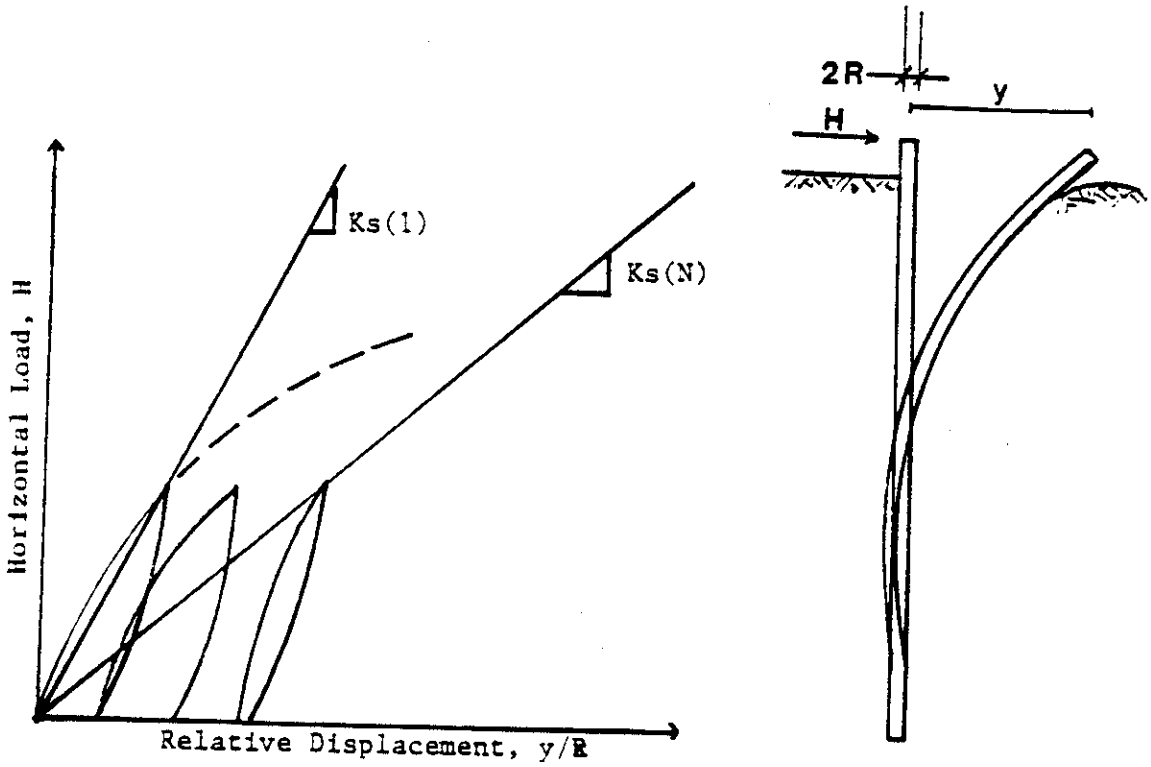

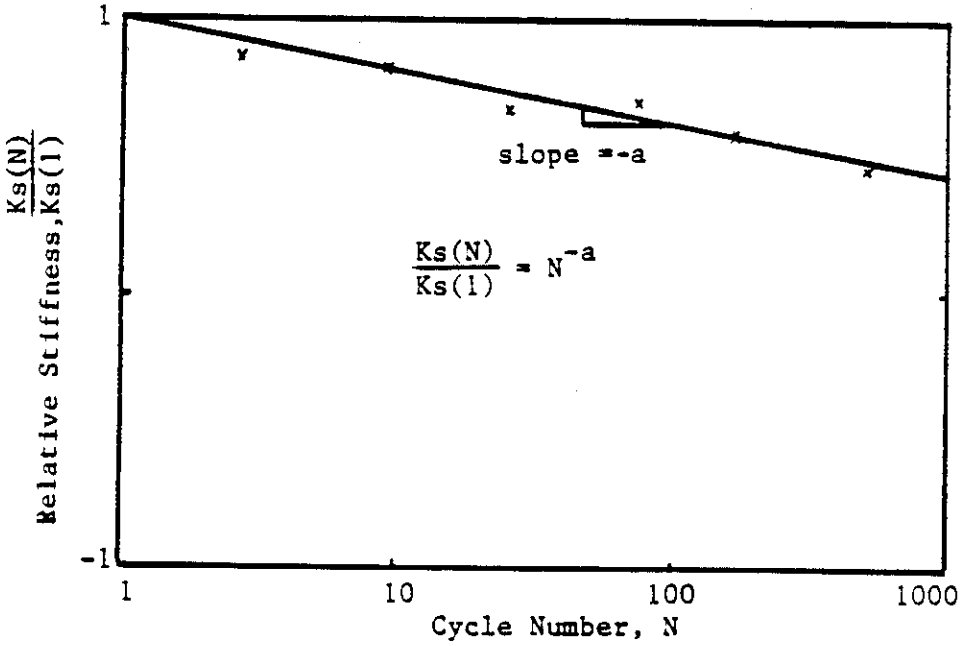

Figure 1. Cyclic Parameters Definition (After Makarim and Briaud, 1986).

(1981) for cyclic simple shear tests, Briaud and Felio (1985) for cyclic vertical loads on piles, and Makarim and Briaud (1986) for cyclic lateral loads on piles in clay. The exponent a is an indication of how rapidly the stiffness of the pile-soil assembly decreases under cyclic loading and is called the cyclic degradation parameter. An increase in the magnitude of a means an increase in the rate at which the secant stiffness Ks(N) decreases with increasing numbers of cycles. The values of a in equation (1) were back-calculated for each load level of each lateral load test in the pile data base.

2.4 Results of Data Analysis

The cyclic degradation parameters from the data base are plotted in Figure 2 against the relative displacement of the pile head corresponding to the peak pressure of each cyclic series. From the collected data, it can be observed that for sand:

(1) The degradation parameters varied from 0.01 to 0.27, had an average of 0.072 and a standard deviation of 0.056.

(2) The trend indicates less degradation at higher load levels within a given load test (a decreases with increasing y/R values).

(3) Degradation appears to be greater for piles subjected to one-way cyclic loading than for piles subjected to two-way cyclic loading.

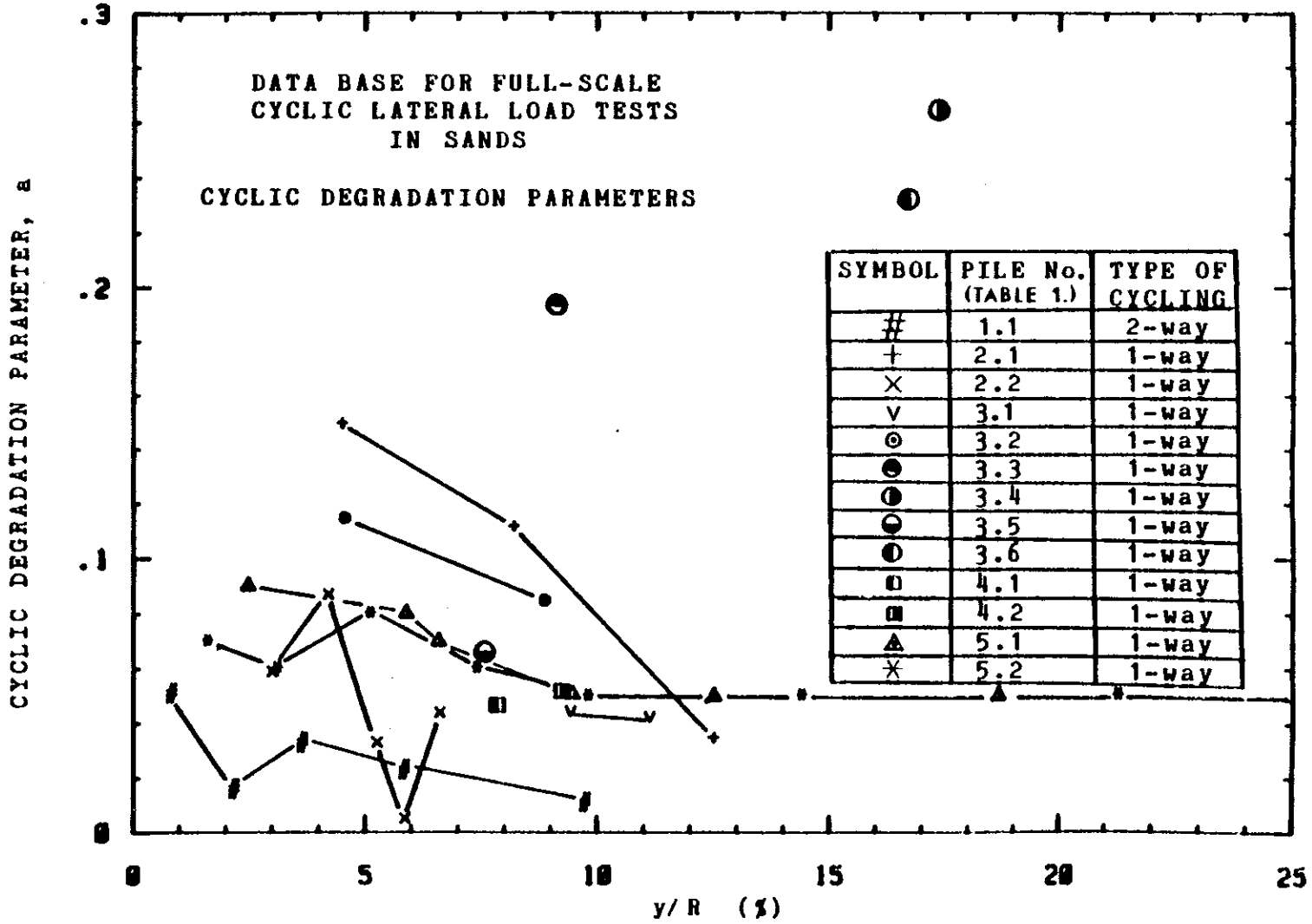

Figure 2. Cyclic Degradation Parameter a versus Relative Pile Head Displacement y/R for Piles in Sand.

The last observation is different from findings in a similar data base analysis performed for piles subjected to cyclic lateral loads in clays (Makarim and Briaud, 1986) where very little difference existed between one-way and two-way cyclic loading.

A possible explanation for this difference is as follows: In the case of two-way cyclic horizontal load tests in sand, a gap forms behind the pile upon reversal of the load. Because the sand has little cohesion, the sand falls into the gap. When the pile is loaded back in the first direction the deflection is decreased compared to the case where the gap would not have been filled. In the one-way horizontal load tests in sand, the gap does not open and therefore larger deflections upon reloading can be expected. This explains why the two-way horizontal cycling of piles in sand leads to little degradation while one-way cycling of piles in sand leads to significant degradation. In clays, for two-way cyclic horizontal loading, the gap does not collapse and therefore the two-way cycling is equivalent to two one-way cyclic tests, one on each side. This explains why there is very little difference between one-way and two-way cyclic horizontal loading of piles in clay.

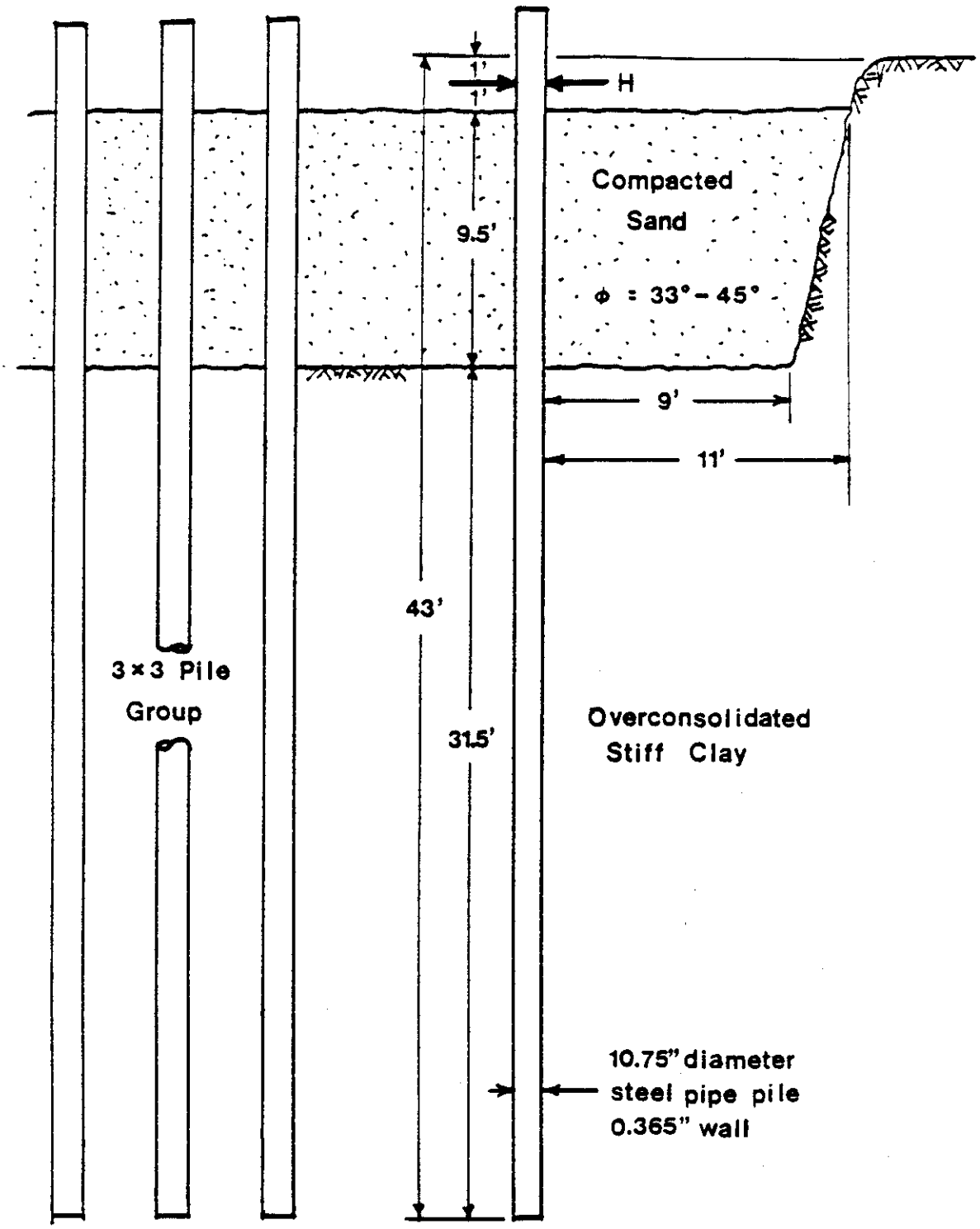

Figure 4. Profile of the 10.75 inch Diameter Test Pile and Soil Configuration at the University of Houston Foundation Test Facility Sand Site.

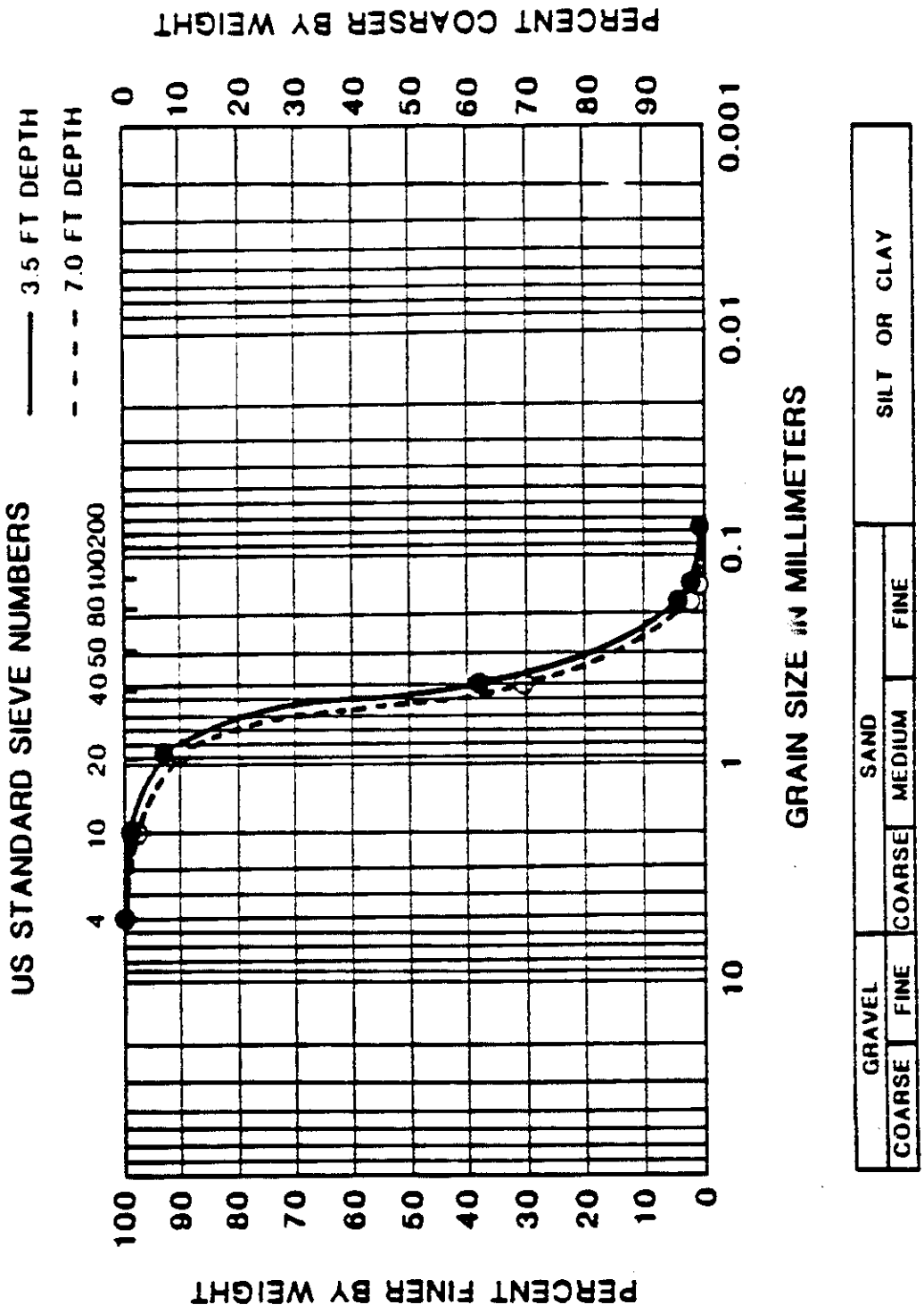

Figure 5. Grain Size Distribution of Test Site Sand (From Ochoa and O'Neill, 1986).

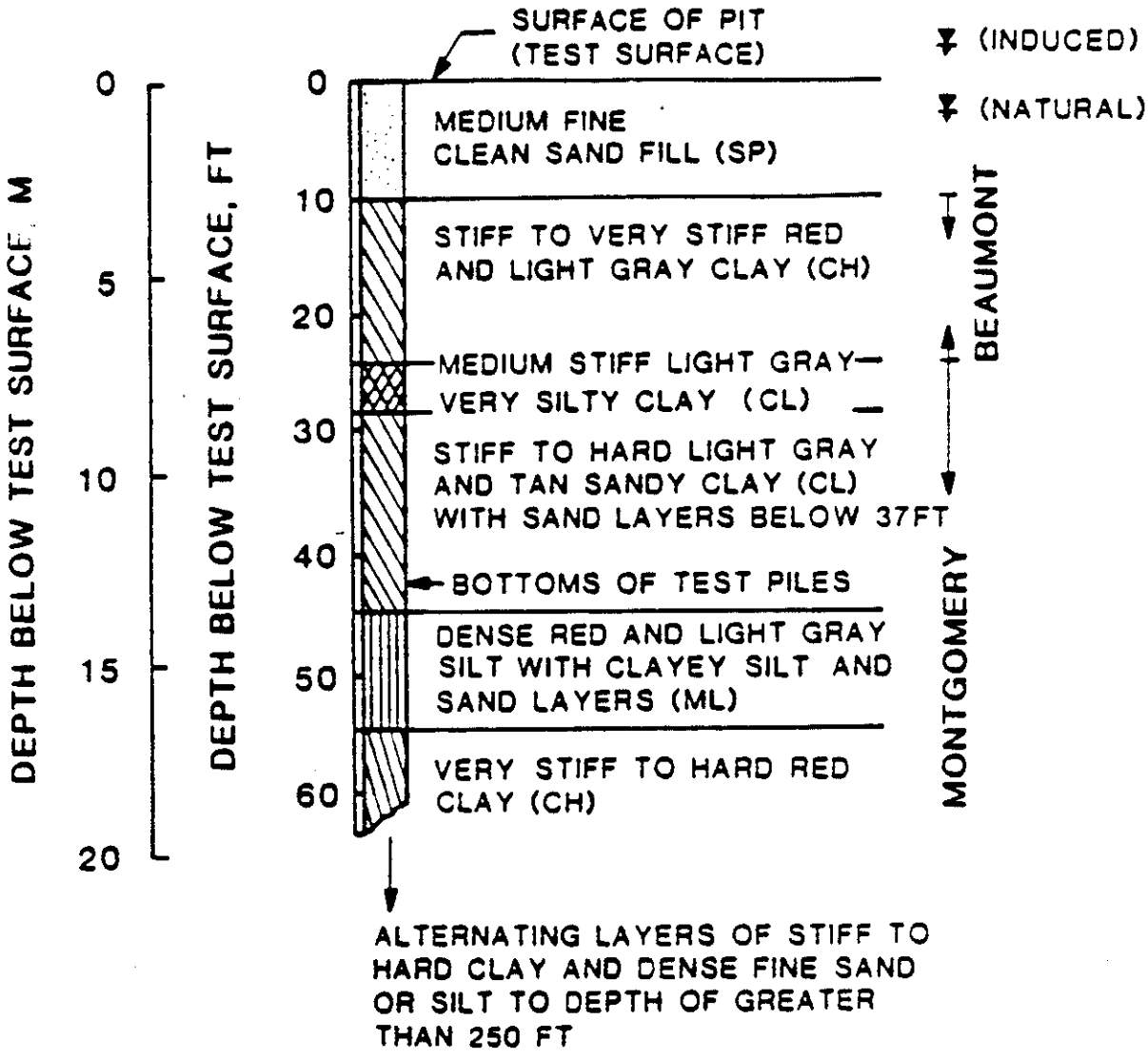

Figure 6. Test Site Stratigraphy (from Ochoa and O'Neill, 1986).

and cone penetration tests were performed at the site. The locations of these tests are shown in Figure 7. The SPT blowcounts with respect to depth in Figure 8 and the CPT results in Figure 9 are from the test locations farthest from the piles. These were presumed to be the closest to the conditions prior to the load tests.

3.3 Two-way Displacement-control Tests on the Single Pile

The 10.75 inch single pipe pile was tested under lateral cyclic loading in the fall of 1984. A 4000 lb. load was initially applied to the pile, forcing it to deflect away from the reaction pile. This was the first direction of loading. The deflection was then noted and a reverse load applied to the pile of sufficient magnitude to deflect the pile toward the reaction pile a distance equal to the deflection noted in the first direction of loading. Subsequent cycling was performed between these two deflections. A 15-second period was used for the cycles. After the desired number of cycles were completed, the pile was loaded in the first direction of loading up to the next desired load level for displacement-control cycling.

The resulting horizontal lateral load versus horizontal deflection curve is presented in Figure 10. The load-deflection history of the pile head is depicted in Figures 11 and 12. Instrumentation along the outside face of the pile allowed for the measuring of the bending moment in the pile with depth, exemplified in Figure 13. From this data, the

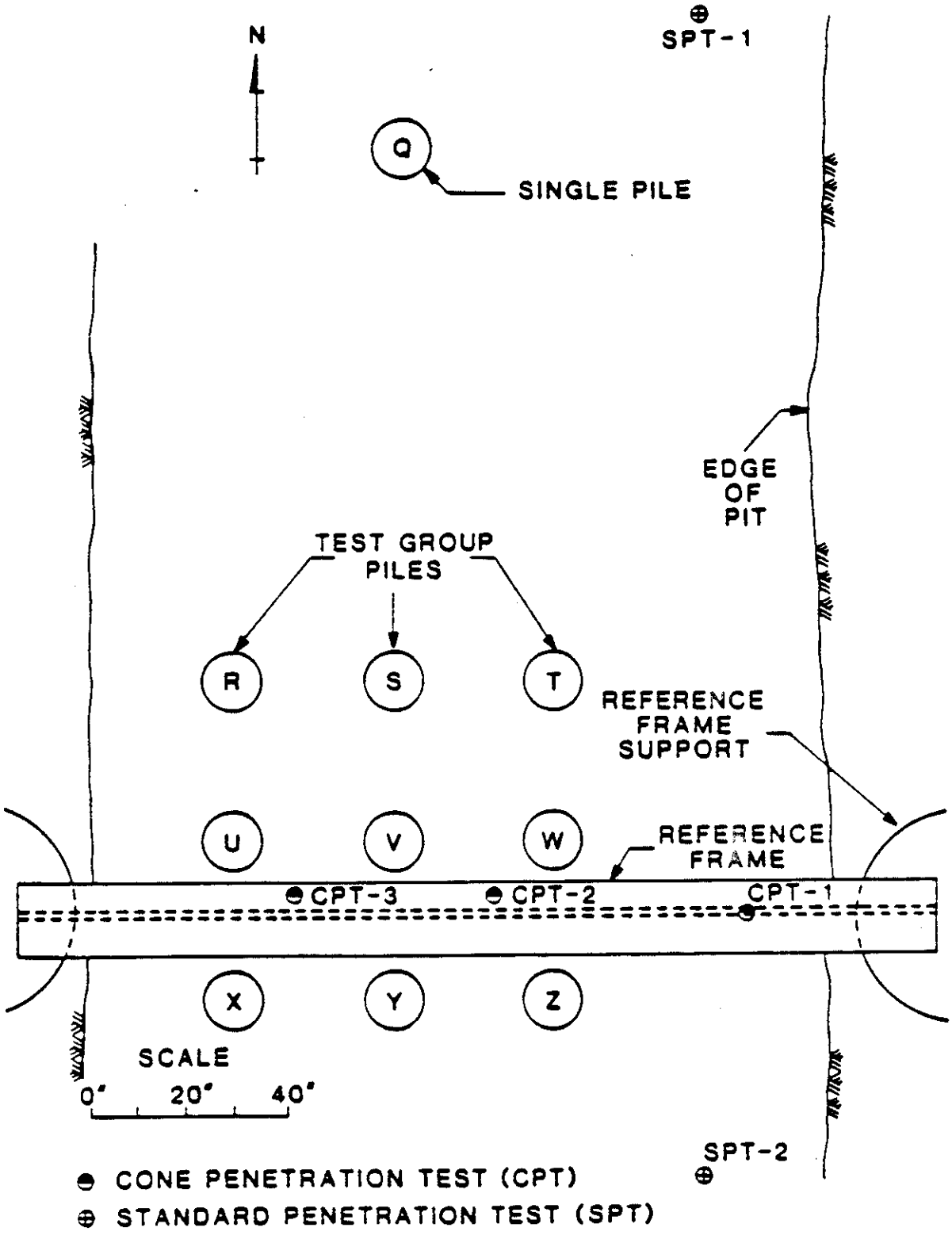

Figure 7. Locations of SPT and CPT Tests (From Ochoa and O'Neill, 1986).

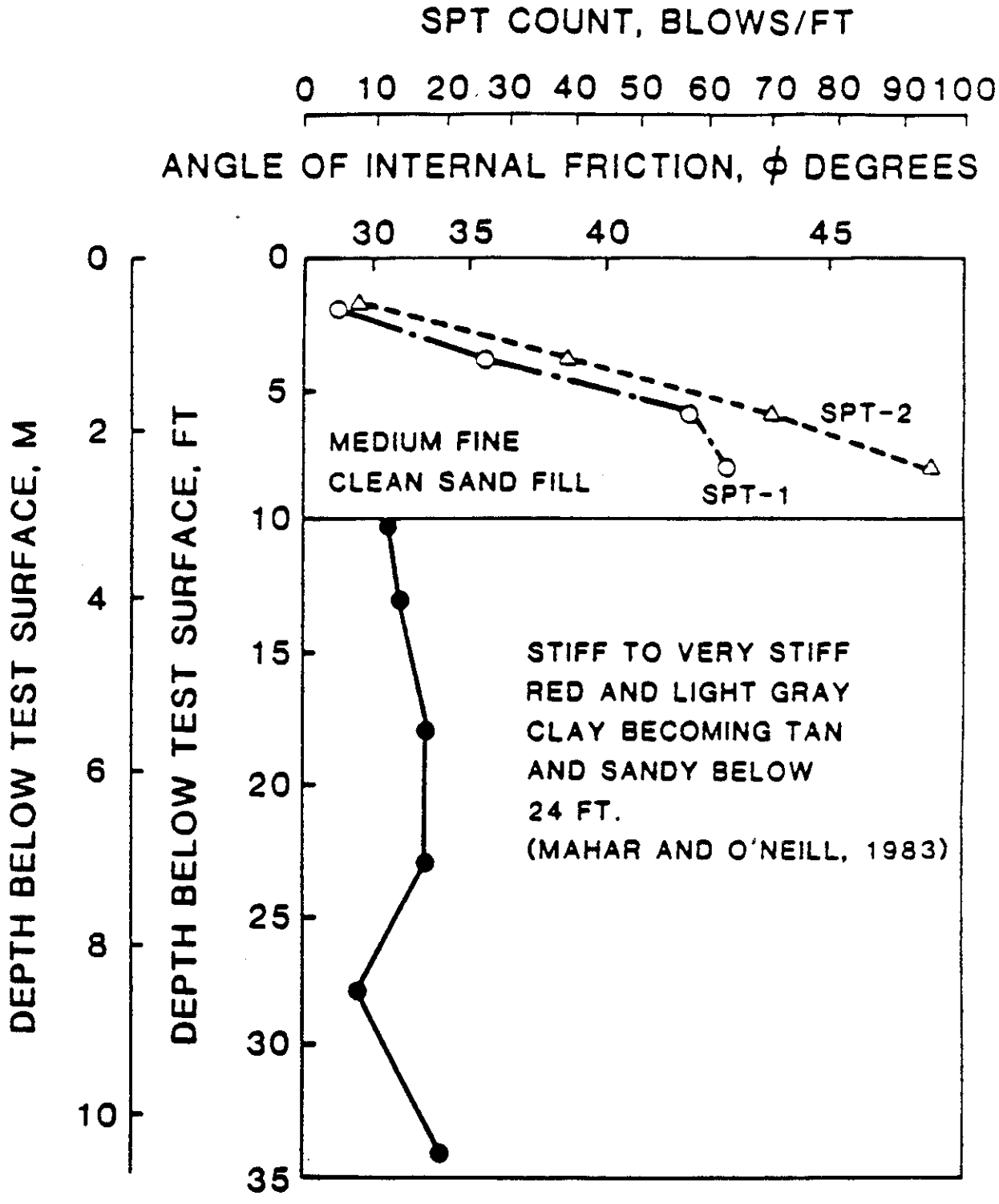

Figure 8. SPT Blowcount with Depth (From Ochoa and O'Neill, 1986).

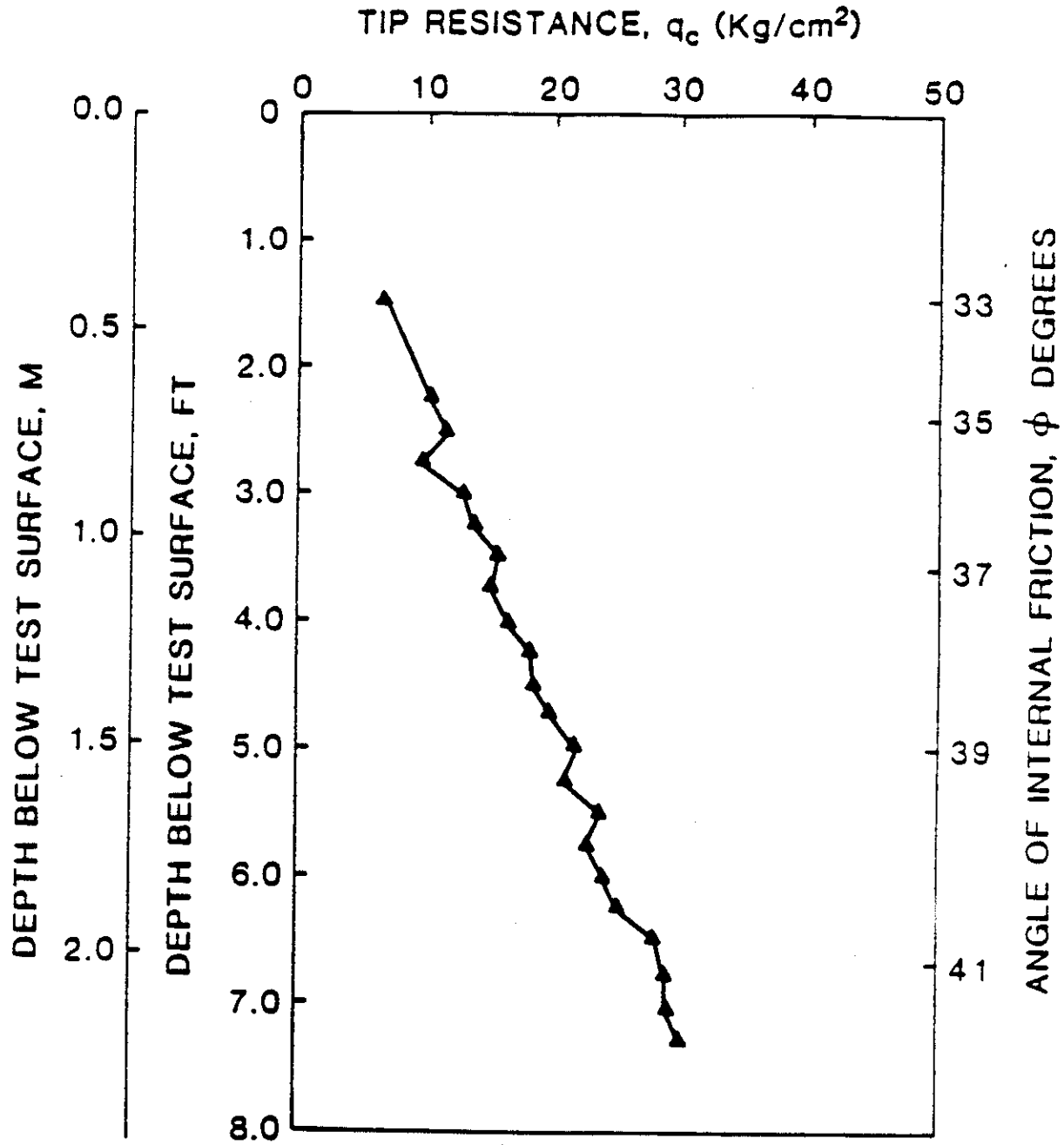

Figure 9. Angle of Internal Friction with Depth (From Ochoa and O'Neill, 1986).

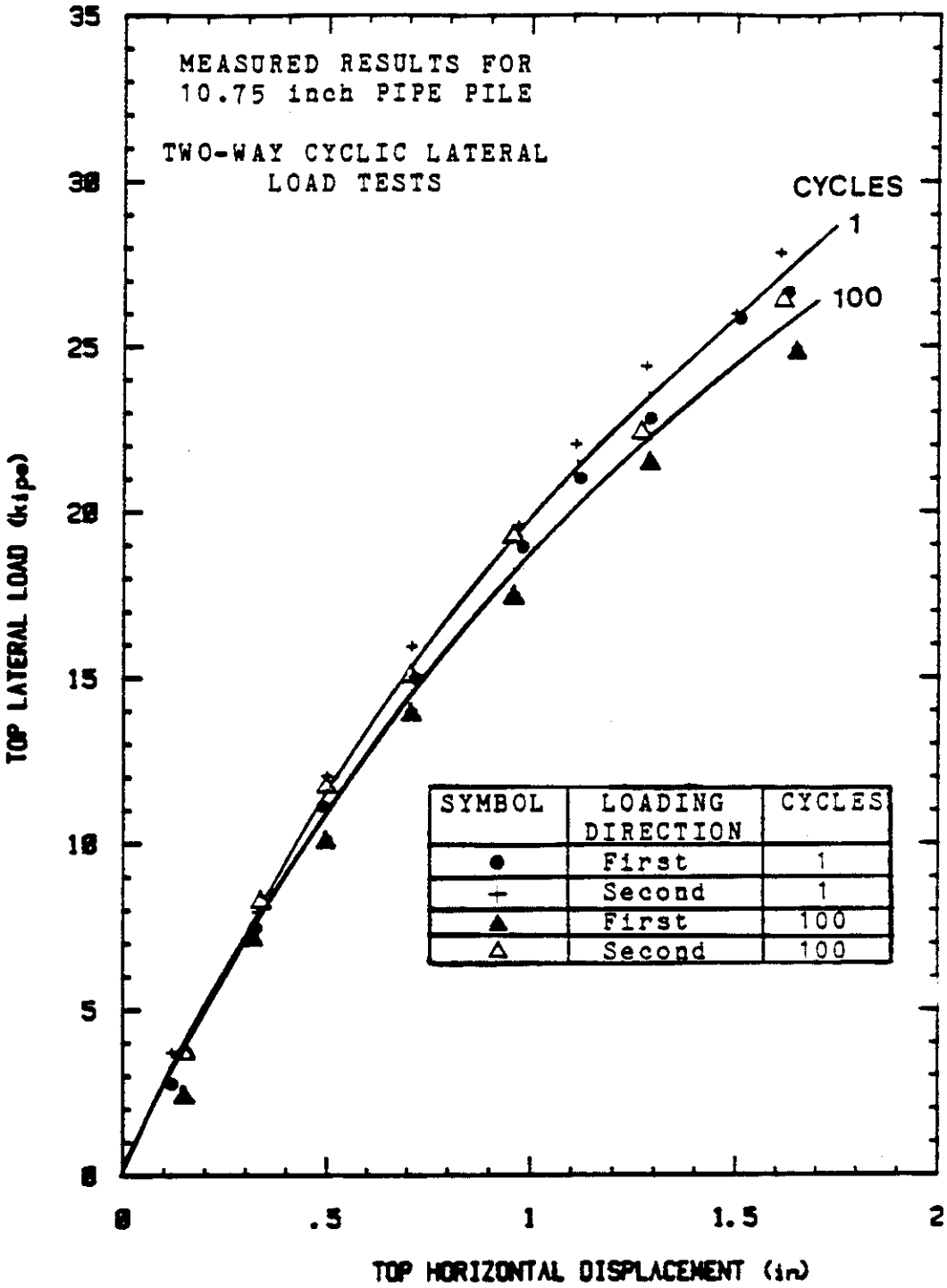

Figure 10. Single Pile Lateral Load versus Pile Head Horizontal Deflection.

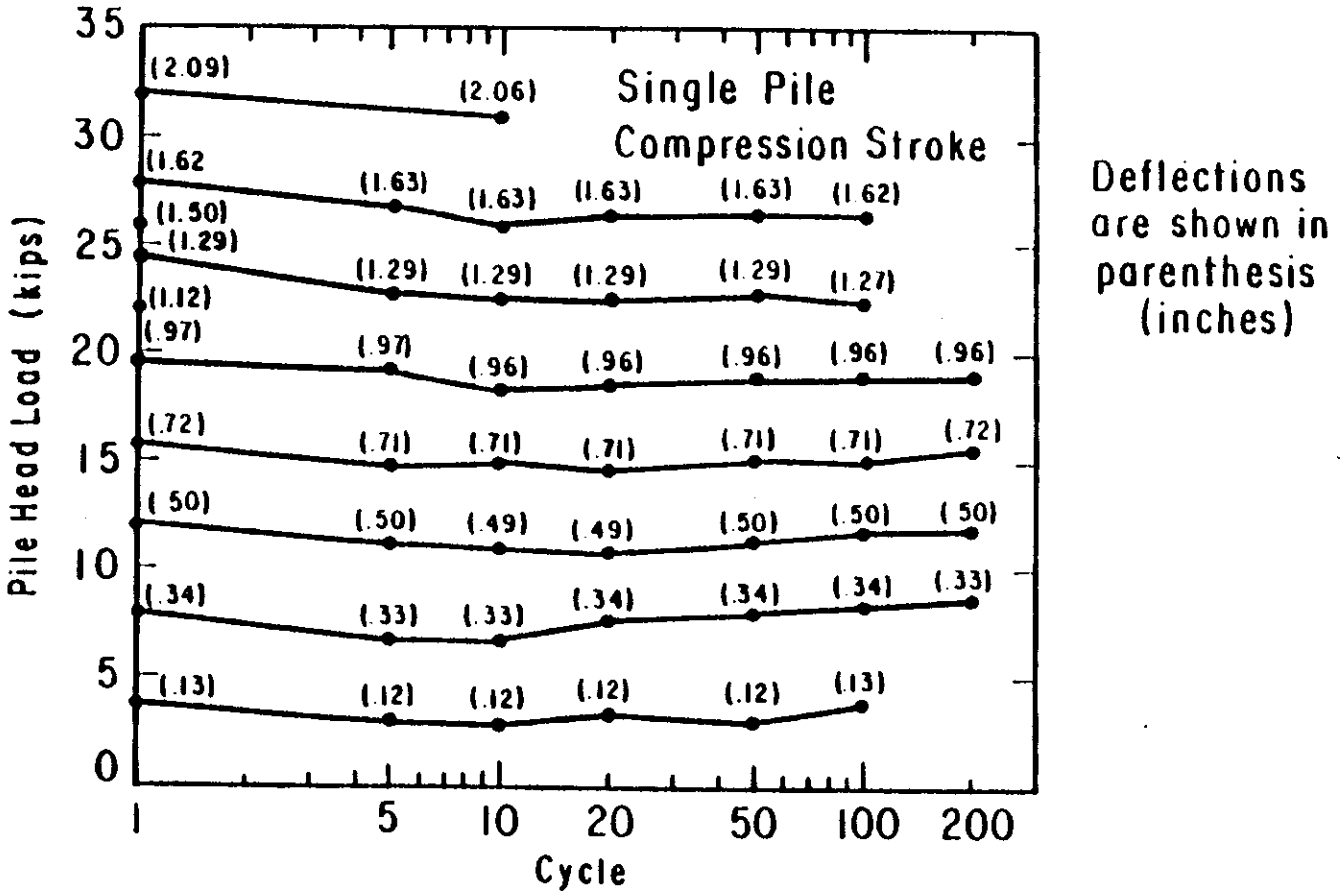

Figure 11. Dependency of Pile Head Load on the Cycle Number, First Load Direction (From Morrison and Reese, 1986).

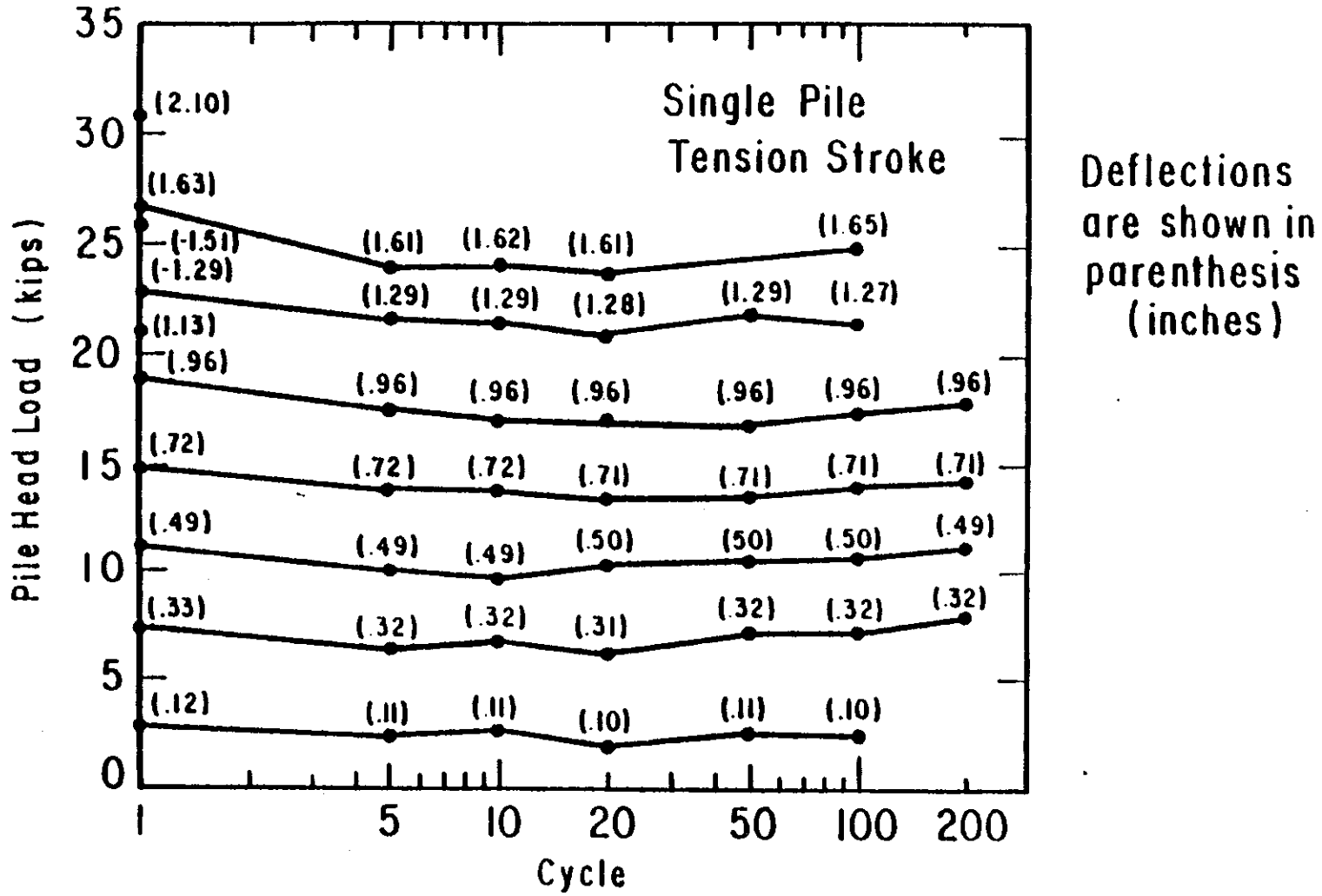

Figure 12. Dependency of Pile Head Load on the Cycle Number, Second Load Direction (From Morrison and Reese, 1986).

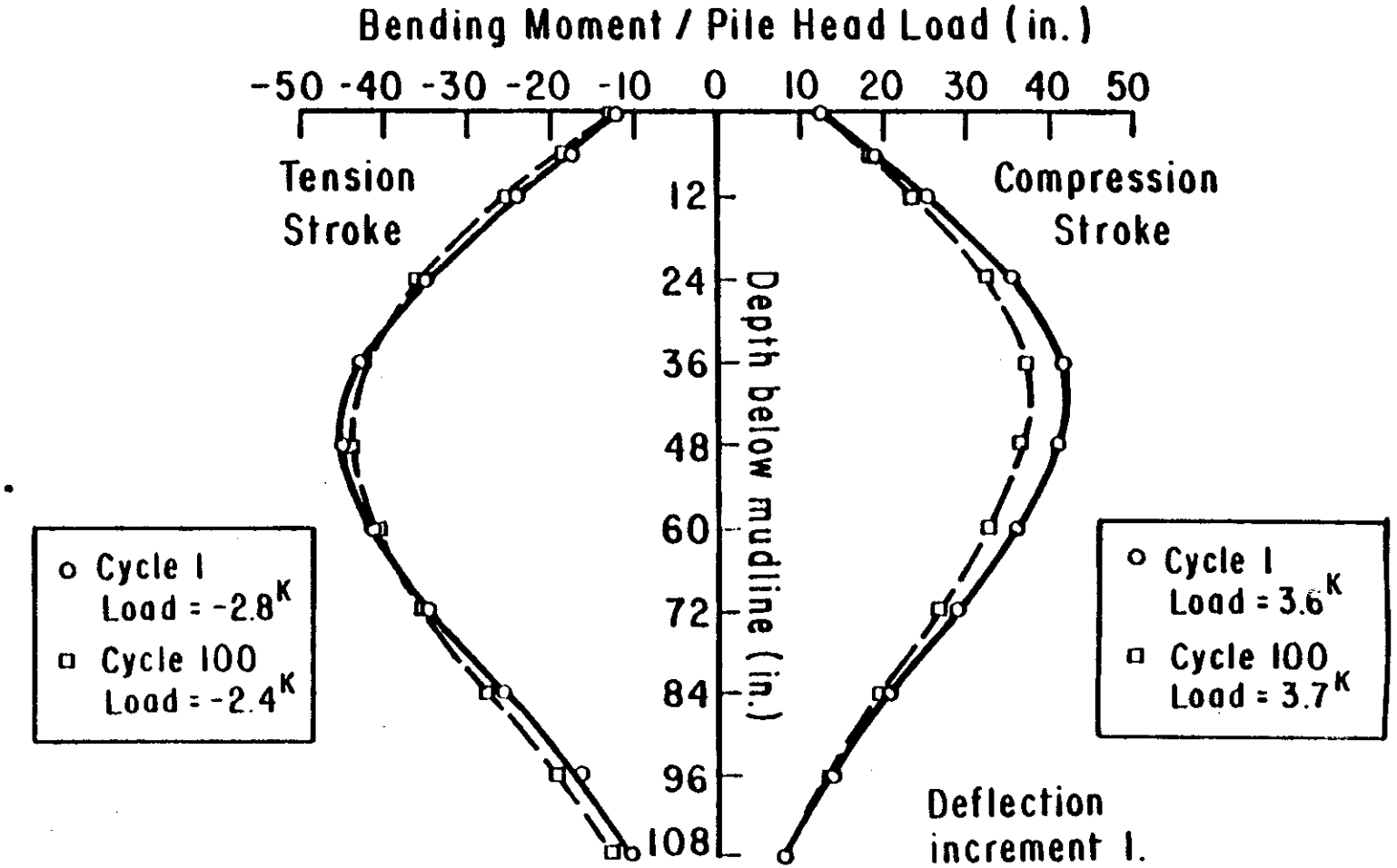

Figure 13. Normalized Moment Curves for Single Pile, First Deflection Increment (From Morrison and Reese, 1986).

soil resistance was generated through double integration of a polynomial function fitted to the measured bending moments using the least squares method (Morrison and Reese, 1986). The results are presented as P-y curves in Figures 14, 15, and 16.

Significant local densification of the sand surrounding the pile was evidenced by the formation of a funnel-shaped depression around the pile during the cyclic testing. At the conclusion of the 20 kip cycling series, the depression measured 9 inches in depth and had a radius of approximately 30 inches (Morrison and Reese, 1986).

3.4 Degradation Model Results

The resulting a versus y/R (%) values for the 10.75 inch single pile tests are plotted in Figure 17. The results agree with the observation made during the data base analysis that degradation in two-way cyclic tests in sand may be negligible. The average a in these two-way tests was 0.02. During some cycles the soil-pile response actually showed an increase in resistance to displacement with increased cycling (negative a).

The load tests did not display a marked decrease in the degradation parameter with increasing y/R (%). The degradation remained fairly constant with variations in the displacement level and with increasing cycles after the initial few cycles.

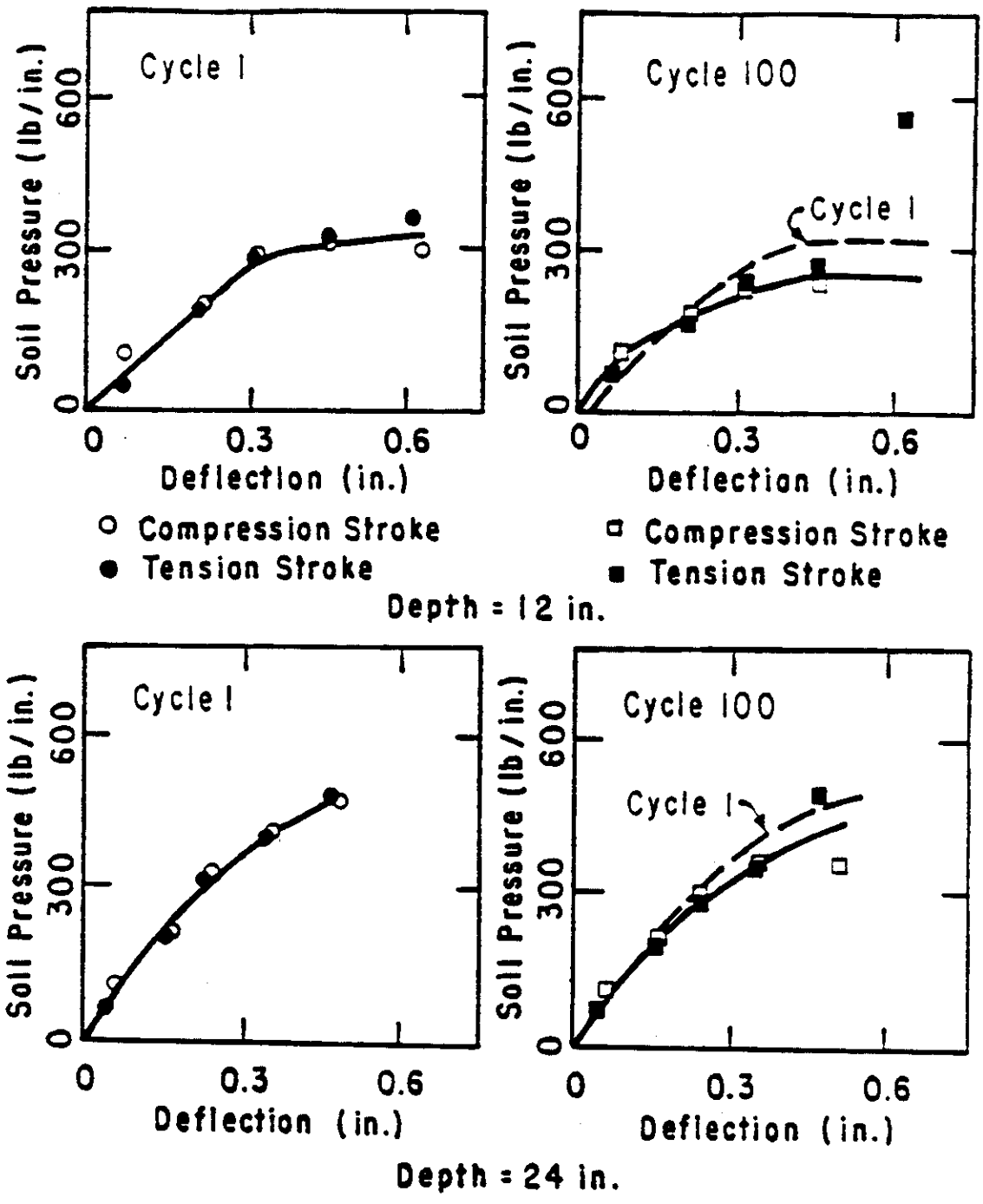

Figure 14. Experimental P-y Curves for 12 and 24 inch Depth (From Morrison and Reese, 1986).

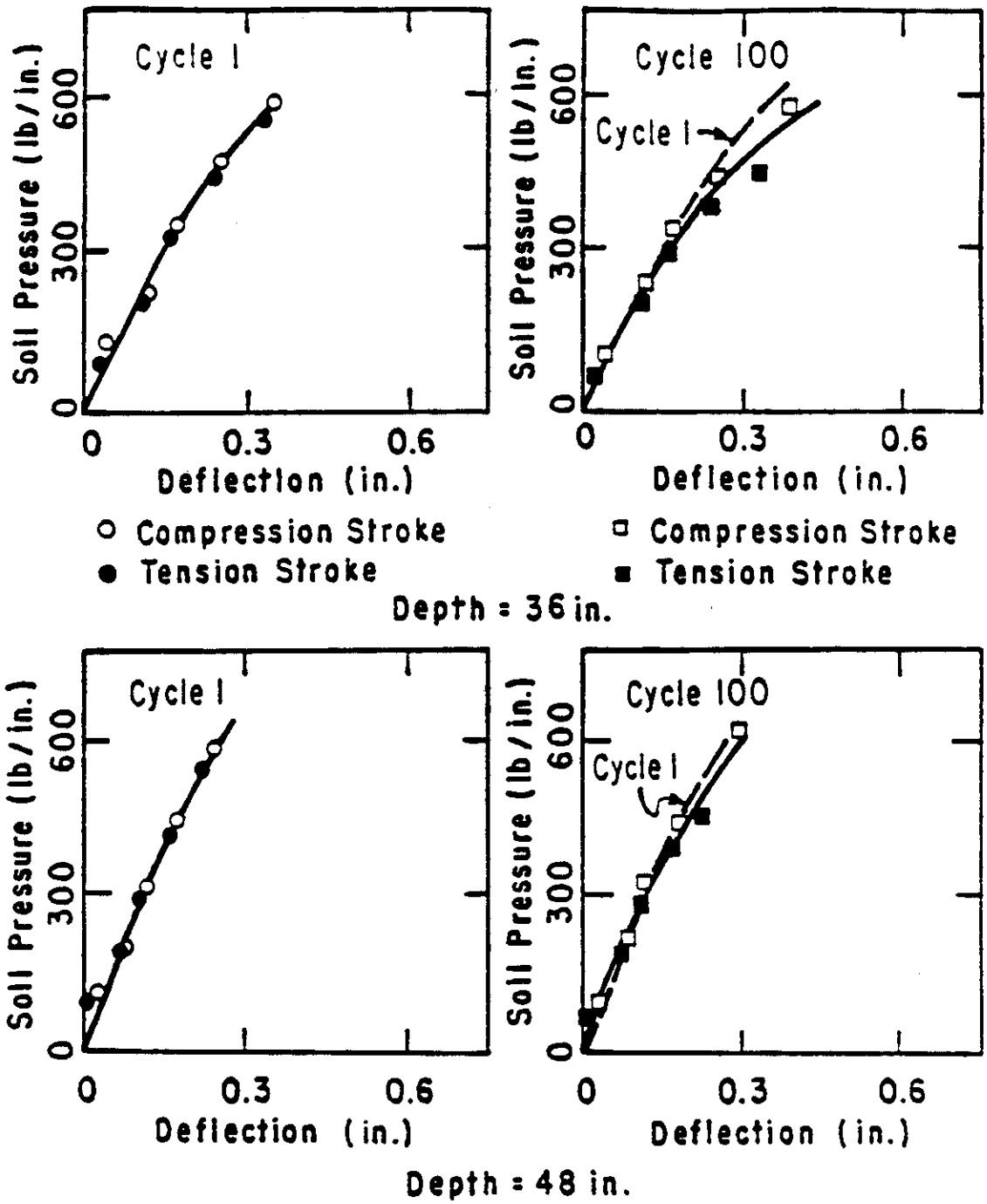

Figure 15. Experimental P-y Curves for 36 and 48 inch Depth (From Morrison and Reese, 1986).

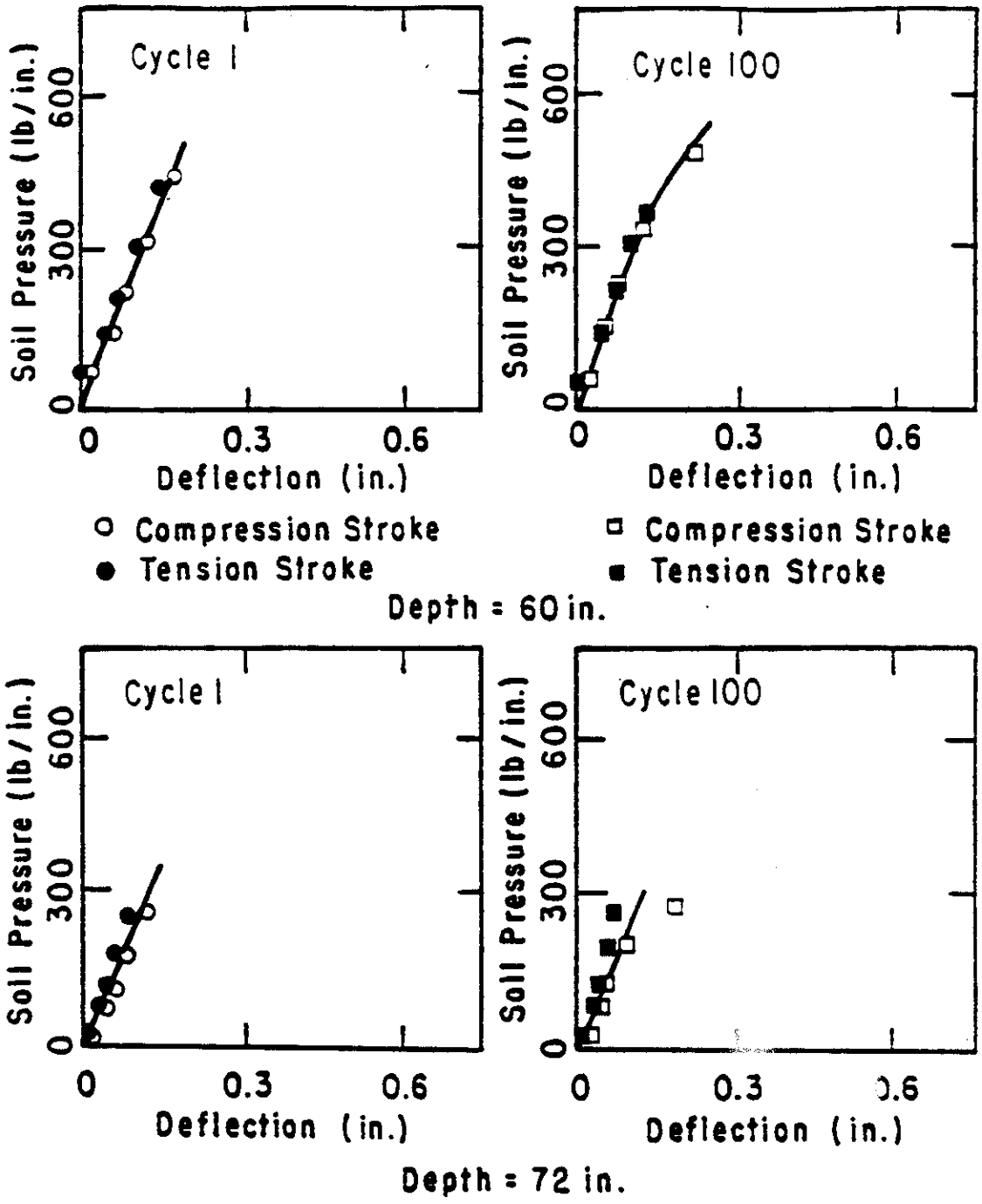

Figure 16. Experimental P-y Curves for 60 and 72 inch Depth (From Morrison and Reese, 1986).

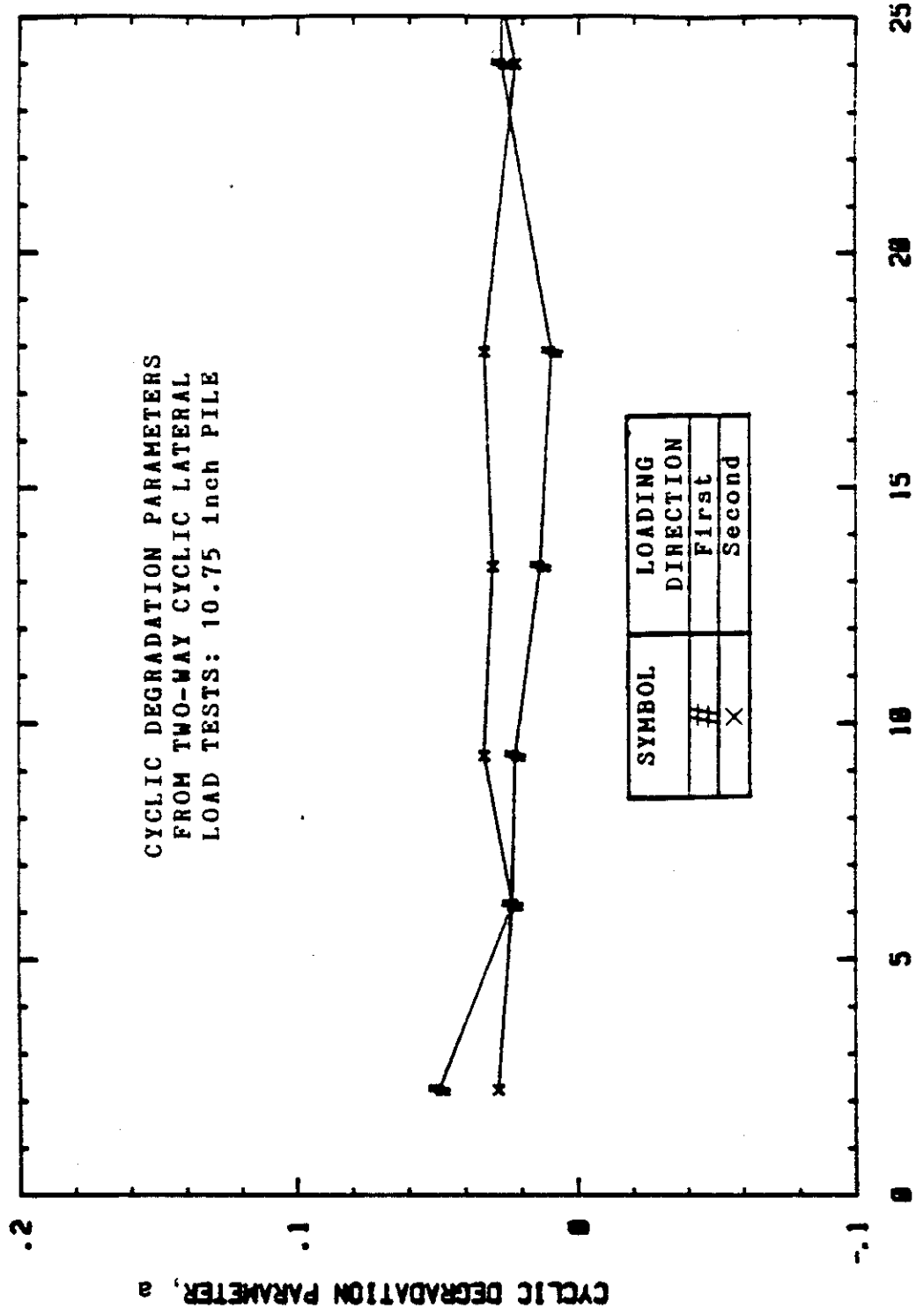

Figure 17. Cyclic Degradation Parameter versus Relative Pile Head Displacement for Single Pile in Sand.

4. MODEL PILE LOAD TESTS AT THE TEXAS A&M UNIVERSITY LABORATORIES

4.1 Model Pile Load Test Apparatus

All of the model pile cyclic lateral load tests conducted at the Texas A&M University Laboratories used the same model pile and test drum. The model pile was a solid steel rod 1.361 inches in diameter. The test drum had an inside diameter of 22.38 inches (16.44 model pile diameters). In the drum, the soil depth was approximately 33 inches (Figure 18).

The equipment for conducting the model pile load tests was initially constructed to perform only one-way load-control tests (Figures 19 and 20). This setup allowed for lateral step loading of the model pile by placing dead loads on a hanger attached to the pile by a cable-pulley system. Horizontal displacements were measured with a dial gage aligned parallel with the axis of loading and affixed on the side of the drum opposite to the cable-pulley system. A floor jack elevated the dead load weights during unload portions of the cyclic loading, relieving the cable tension and removing the lateral load on the model pile (Figure 21).

The apparatus was later modified to allow the model pile to be tested under one-way displacement-control, two-way load-control, and two-way displacement-control tests (Figure 22). The installed pile was attached through a

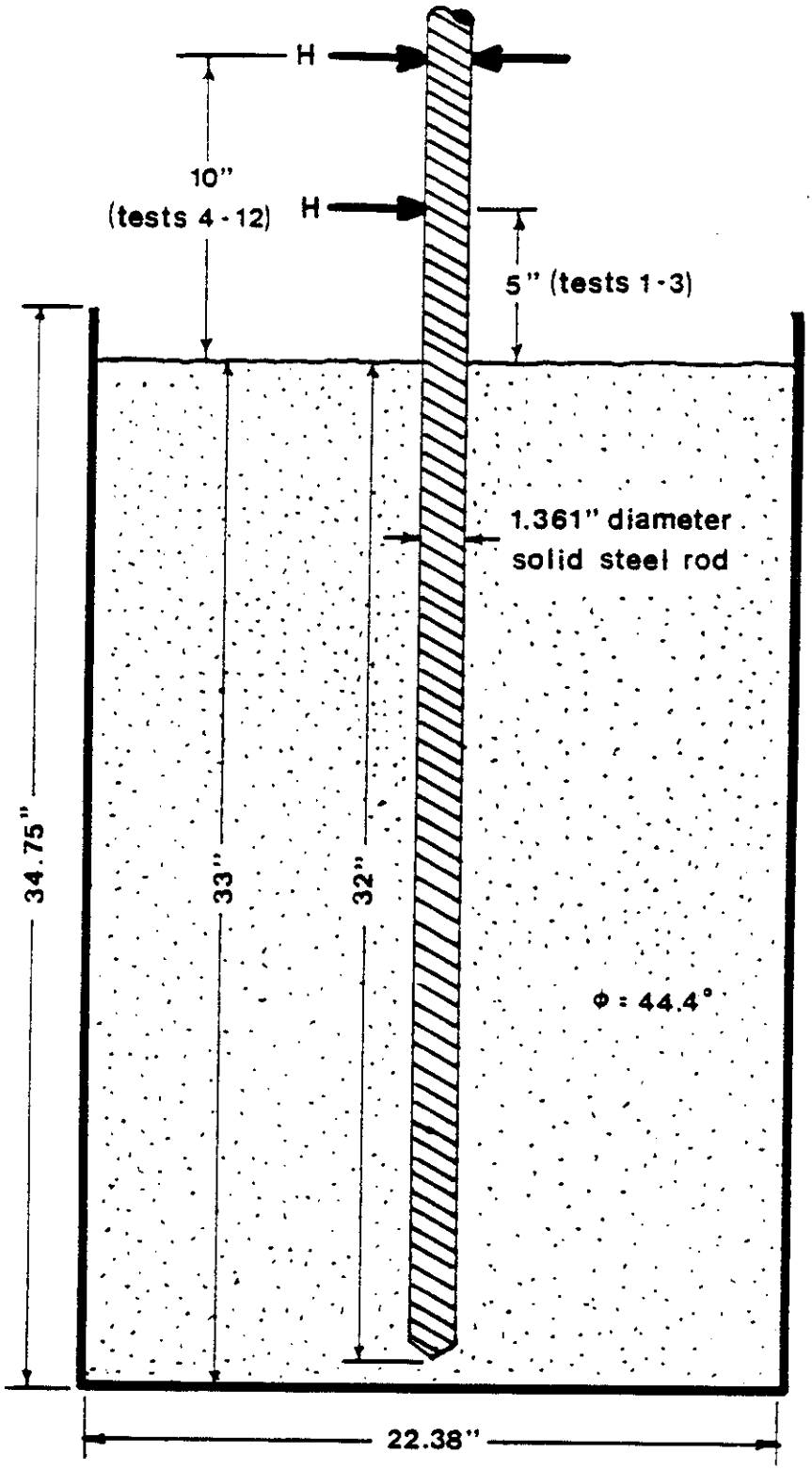

Figure 18. Profile of the 1.361 inch Diameter Model Pile and Soil Configuration at the Texas A&M University Laboratories.

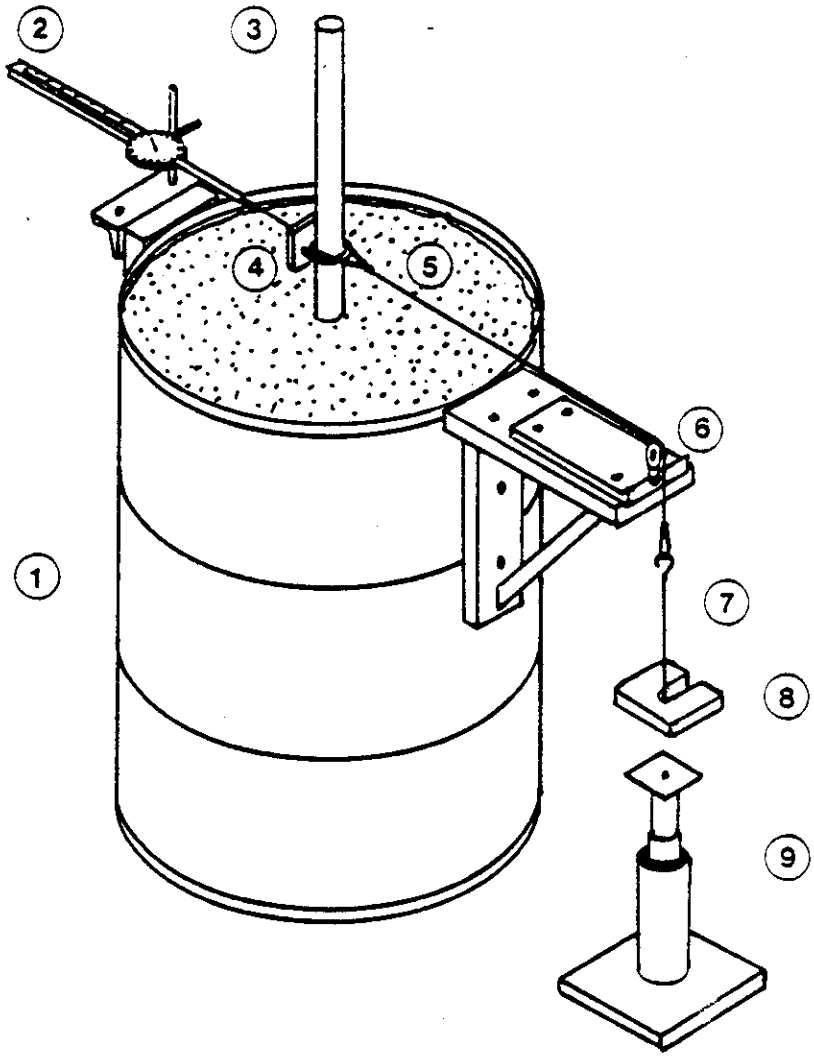

Figure 19. Schematic of Model Pile Load Test Apparatus for One-way, Load-control, Cyclic Tests: 1. Test Drum, 2. Displacement Dial Gauge, 3. Model Pile, 4. Bearing Plate for Displacement Dial Gauge, 5. Loading Cable, 6. Pulley, 7. Dead Load Hanger, 8. Dead Load Weight, 9. Floor Jack.

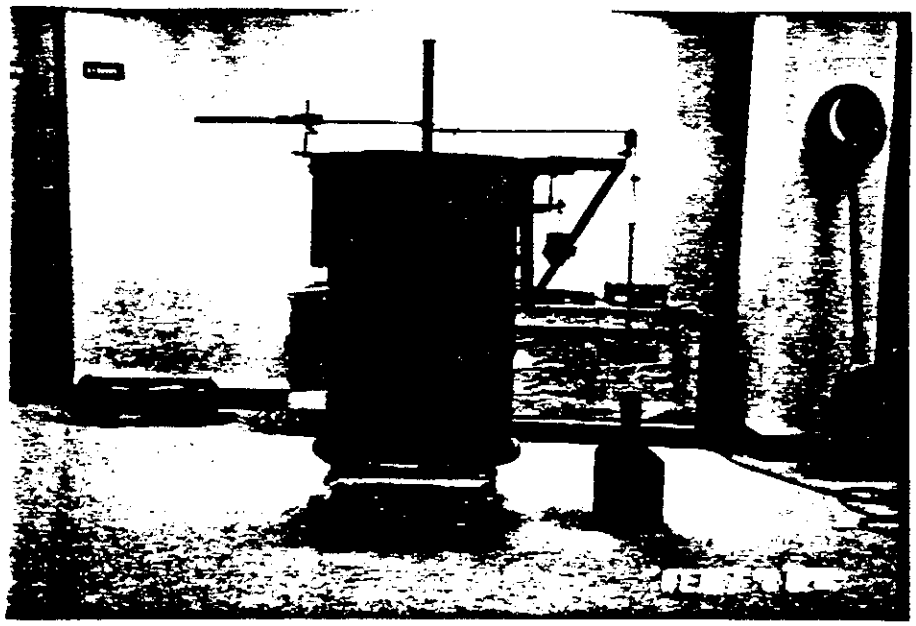

Figure 20. Model Pile Load Test Apparatus for One-way, Load-control, Cyclic Tests.

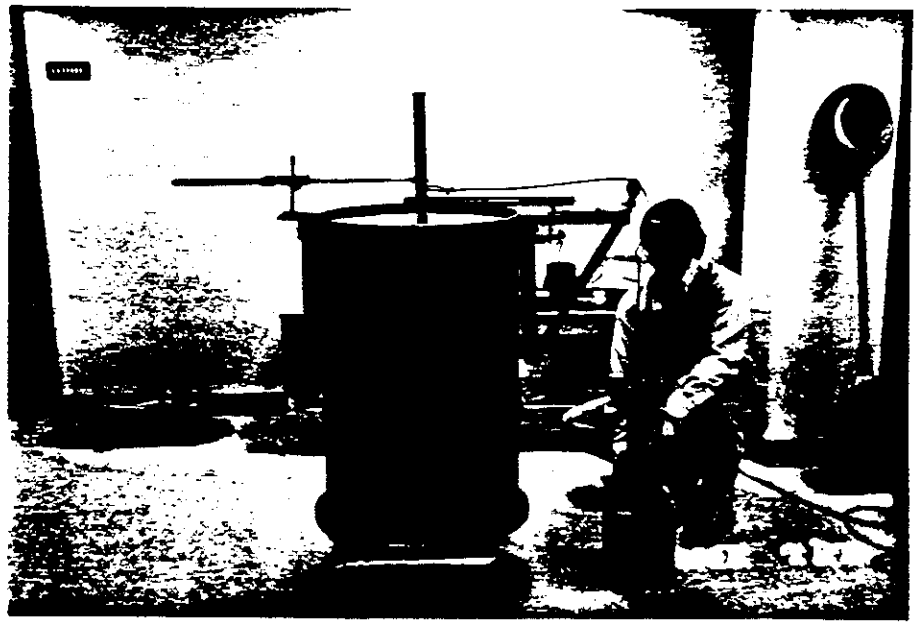

Figure 21. Unloading the Model Pile in a One-way, Load-control, Cyclic Test Series.

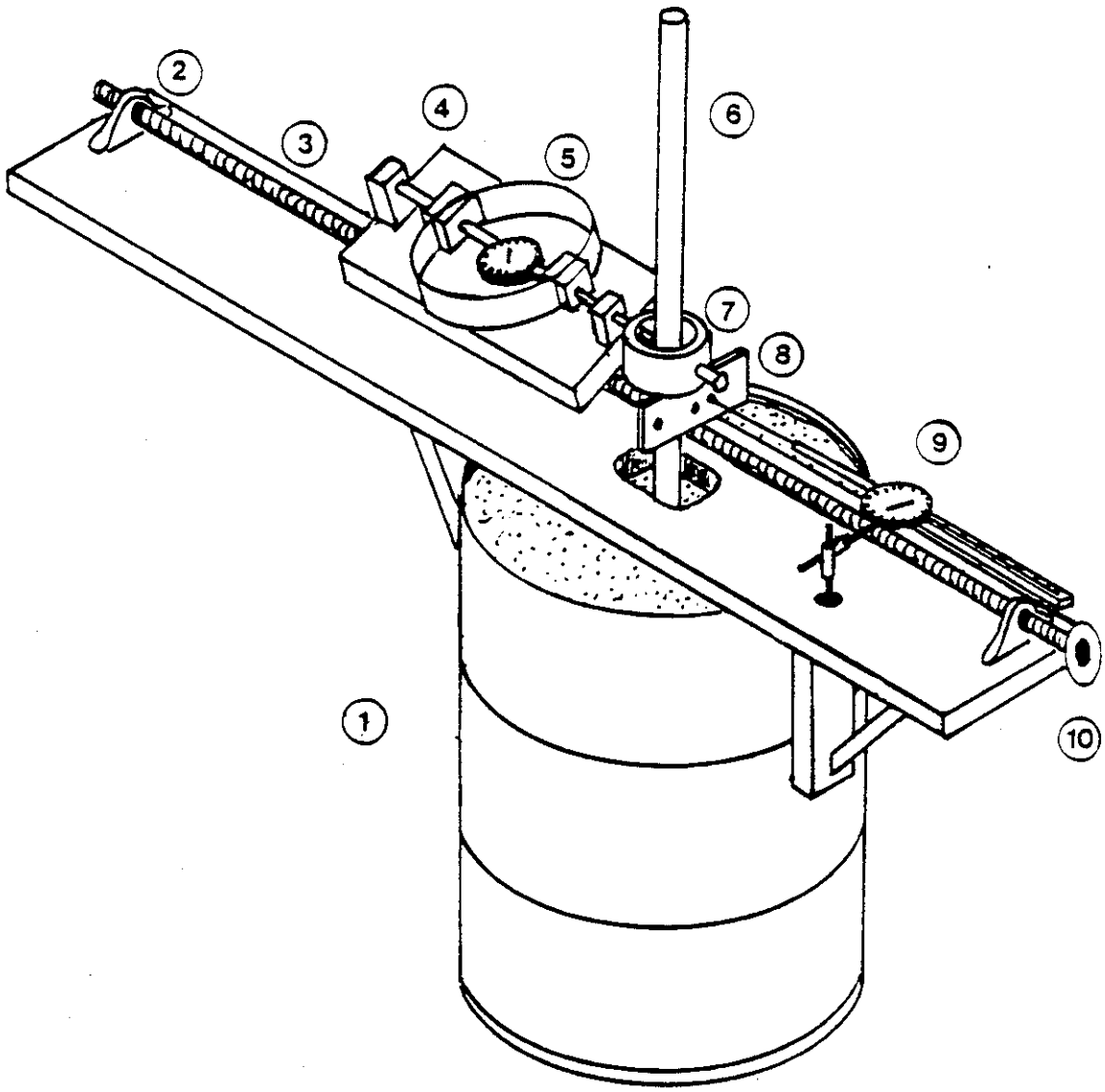

Figure 22. Schematic of Model Pile Load Test Apparatus for One-way, Displacement-control and Two-way Cyclic Tests: 1. Test Drum, 2. Lubricated Screw-Shaft Bearing, 3. Screw Shaft, 4. Proving Ring Carriage, 5. Proving Ring, 6. Model Pile, 7. Proving Ring-to-Pile Connector, 8. Bearing Plate for Displacement Dial Gauge, 9. Displacement Dial Gauge, 10. Screw-Shaft Wheel for Carriage Travel.

proving ring to a carriage riding on a screw shaft. The pile-proving ring connection was designed such that the moment in the plane of lateral loading would be negligible at small displacements (Figures 23 and 24). Loads were measured with the proving ring, which had been calibrated for both tension and compression to allow for two-way loading. Displacements were measured with a dial gage connected to the drum and aligned with the axis of loading. Loads were applied during the load-control tests by turning the screw shaft until the proving ring reading corresponded with the chosen load. Displacements were similarly applied during displacement-control tests by turning the screw shaft until the reading on the dial gage indicated the desired horizontal displacement. The screw shaft and base along which the carriage traveled were lubricated before each test to minimize friction, rendering any induced transverse loads negligible when compared to the horizontal load along the longitudinal axis of loading.

4.2 Soil Conditions and Pile Placement Procedures

To investigate variations in pile response due to installation method and soil conditions, three separate model pile placement procedures were tested:

(1) the post-compacted, single lift procedure,

(2) the pre-compacted, single lift procedure, and

(3) the post-compacted, multiple lift procedure.

The first procedure was chosen as a model of a bored pile

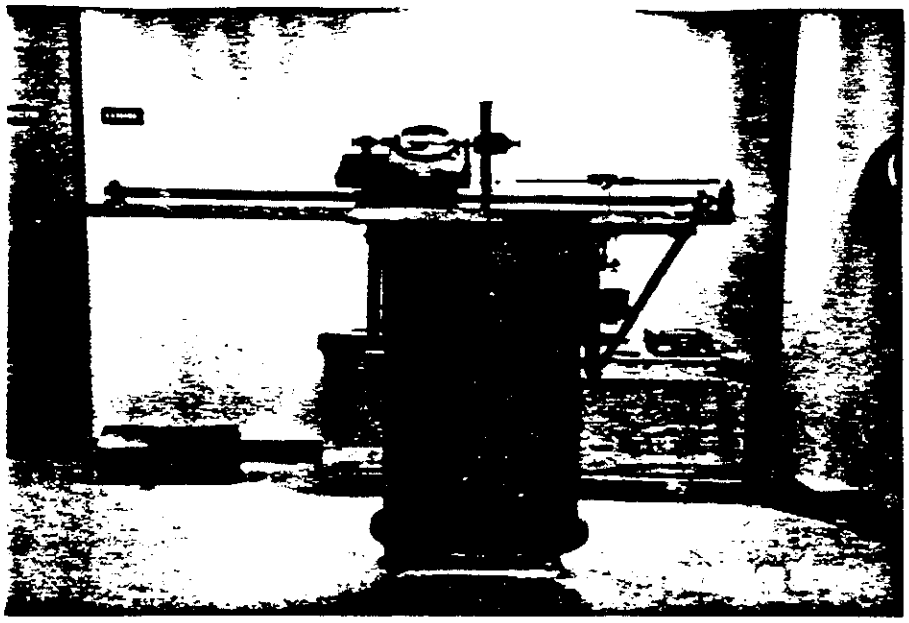

Figure 23. Model Pile Load Test Apparatus for One-way, Displacement-control and Two-way Cyclic Tests.

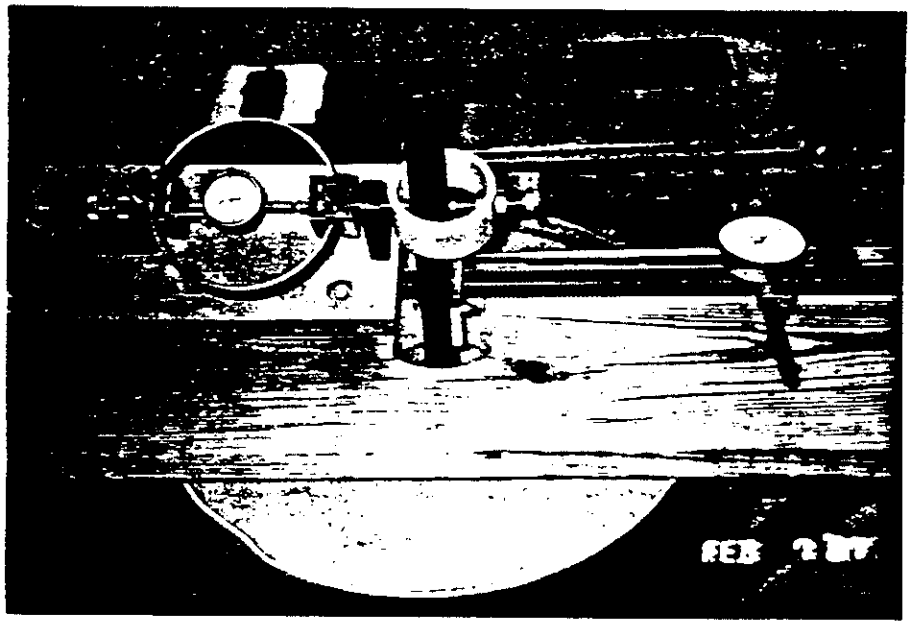

Figure 24. Pile-to-proving ring Connection and Dial Gages on Two-way Cyclic Test Apparatus.

with little soil disturbance. The drum was filled with loose sand and the pile pushed to the desired depth. The sand was then compacted in a single lift around the pile with a concrete vibrator, repeating the pattern in Figure 25a twice, penetrating fully, and the pattern in Figure 25b once, penetrating to half of the soil depth. The second procedure modeled the conditions of a driven pile. After completing a pile test from the first procedure, the pile was removed and the sand recompacted using the pattern in Figure 25b penetrating fully into the drum (Figure 26). The model pile was then driven into the sand with a rawhide mallet until the desired depth was achieved (Figure 27). The third procedure simulated the installation conditions of the 10.75 inch pile tested by Morrison and Reese (1986) at the University of Houston sand site. The model pile was first placed in the empty drum and sand was added in six lifts, each compacted around the pile independently, and each approximately six inches thick. Compaction was achieved by repetitively plunging the concrete vibrator into the lift beginning near the model pile and spiralling outward toward the drum perimeter (Figures 25c and 28).

The weight and the volume of the sand in the drum were measured for each type of pile placement procedure. The resulting unit weights, presented in Table 2, indicated a slight increase in the average density of the sand for the post-compaction, multiple lift procedure over the post-

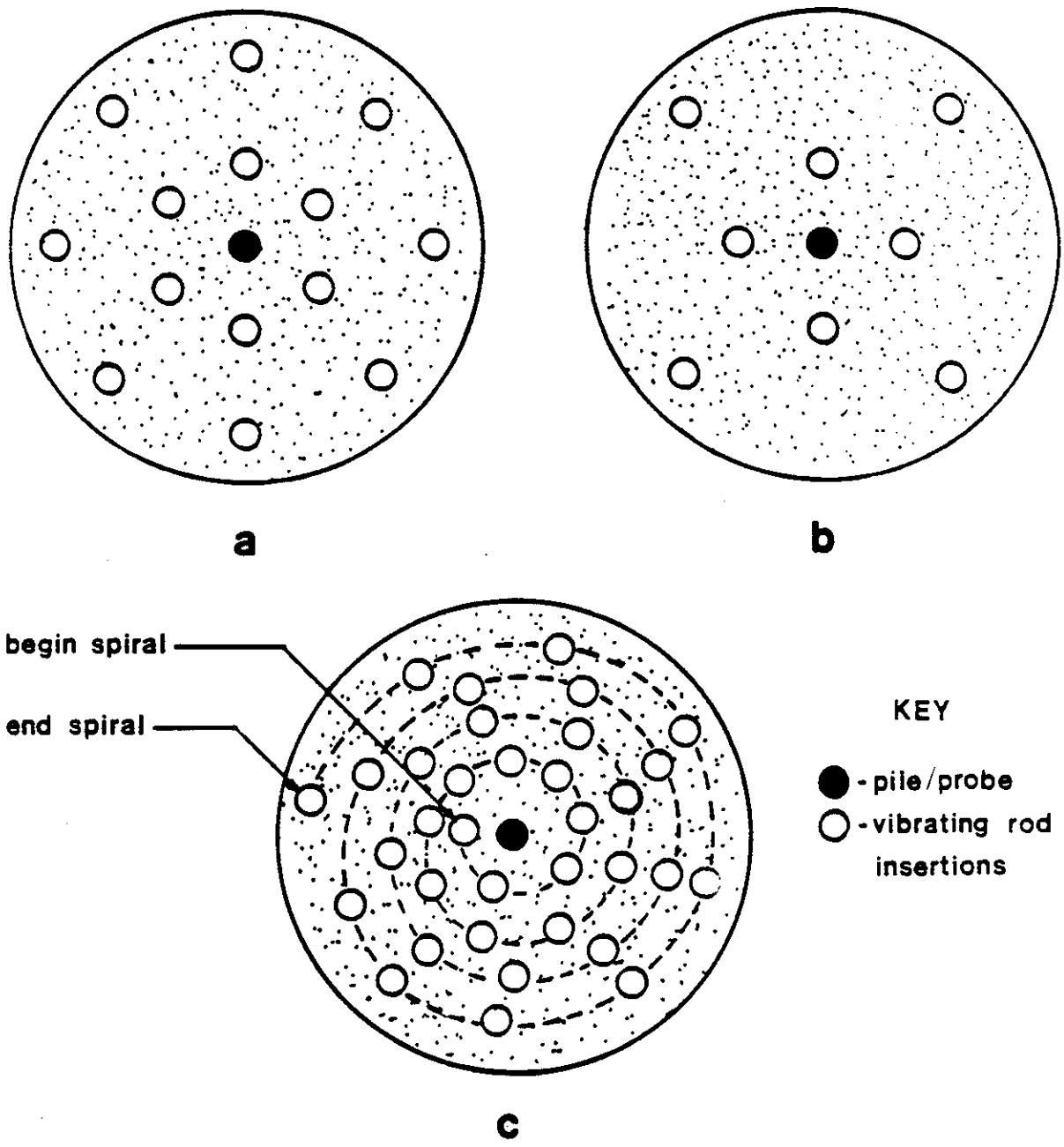

Figure 25. Compaction Patterns for Model Pile Load Test Sand.

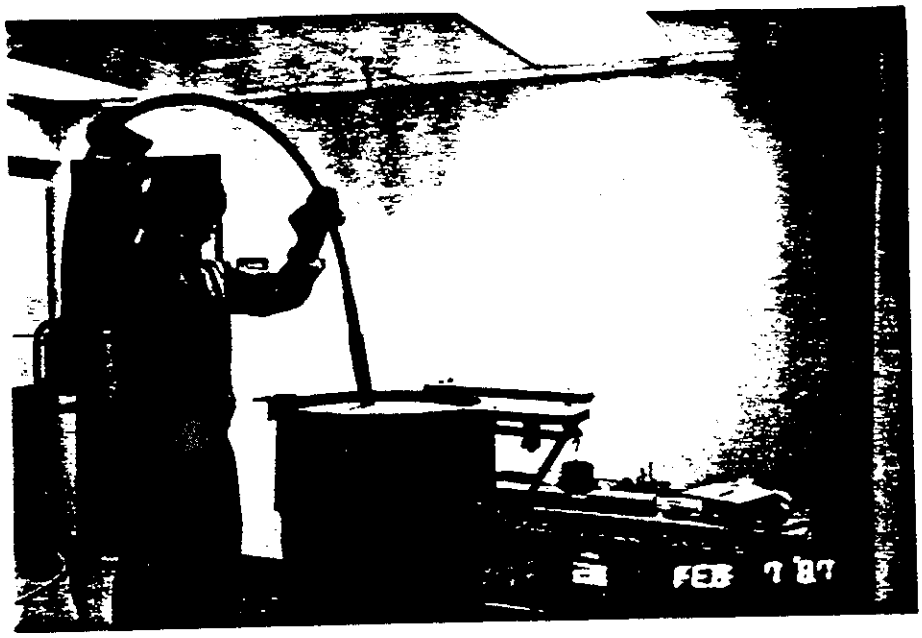

Figure 26. Pre-compacting the Sand with the Vibrating Rod.

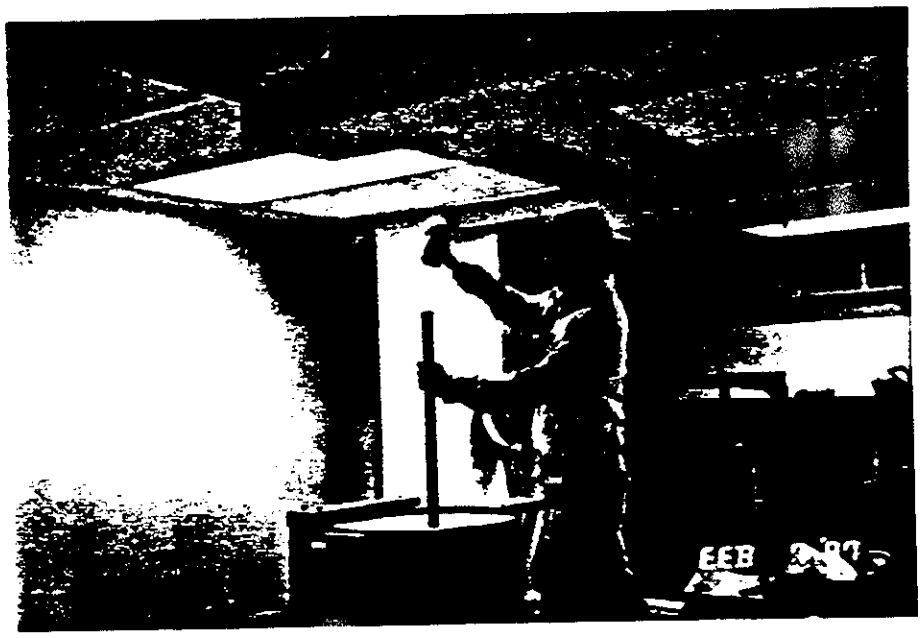

Figure 27. Driving the Model Pile to Test Depth.

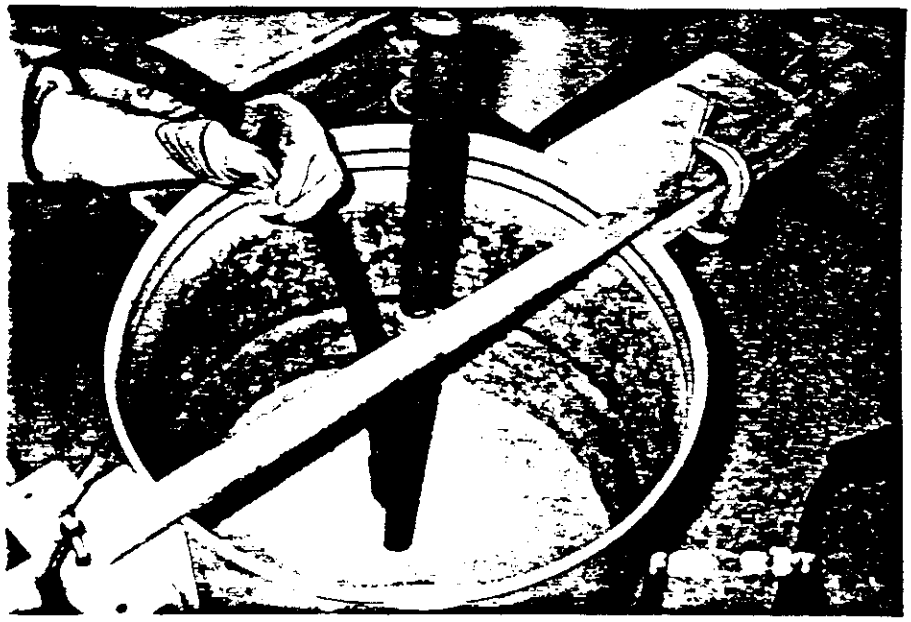

Figure 28. Post-compacting Sand in Multiple Lifts.

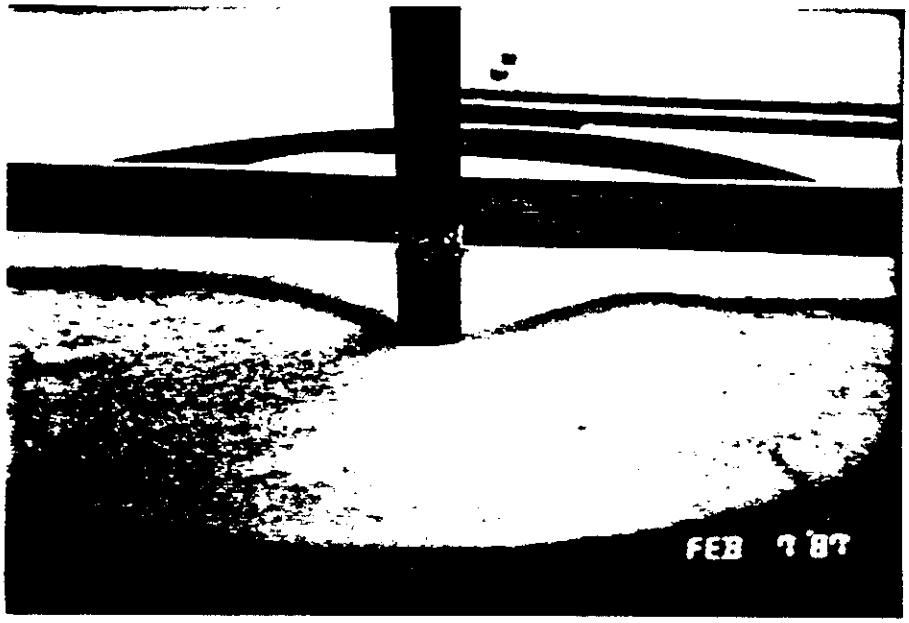

Figure 29. Cone of Depression Around Driven Model Pile.

Soil Conditions and Placement Procedure	Average Unit Weight (lbs/ft^3)
Post-compacted Single Lift	111.2
Pre-compacted Single Lift Driven Pile	114.4
Post-compacted Multiple Lifts	111.7

Table 2. Unit Weights of the Various Soil Preparations at the Texas A&M University Laboratories.

compaction, single lift procedure. With the driven pile, significant compaction occurred in the immediate vicinity of the pile during pile driving. This was evidenced not only by the higher unit weight, but also by a cone of depression that appeared around the pile during insertion (Figure 29). After driving, this depression was generally about eight inches in diameter and one and one-half inches deep.

The soil for all of the tests was a poorly graded medium sand with little or no fines (Figure 30). The average moisture content for the tests was 0.03% and was constant with depth. The angle of internal friction of the sand at a unit weight of 110 pounds per cubic foot was 44.4°.

4.3 One-way Load-control Tests

One-way load-control tests were performed for each placement procedure with the apparatus pictured in Figure 20. The pile was in a free-head condition. Loading increments of 4 kg (8.8 lbs.) were applied and pile displacement readings taken 30 seconds after each load application. Therefore, the period of cycles was one minute. Twenty cycles were conducted at three different peak load levels. The resulting lateral load versus horizontal displacement curves are presented in Figures 31, 32, and 33.

4.4 One-way Displacement-control Tests

The new apparatus employed in the one-way displacement-control tests and the two-way tests allowed for a quicker

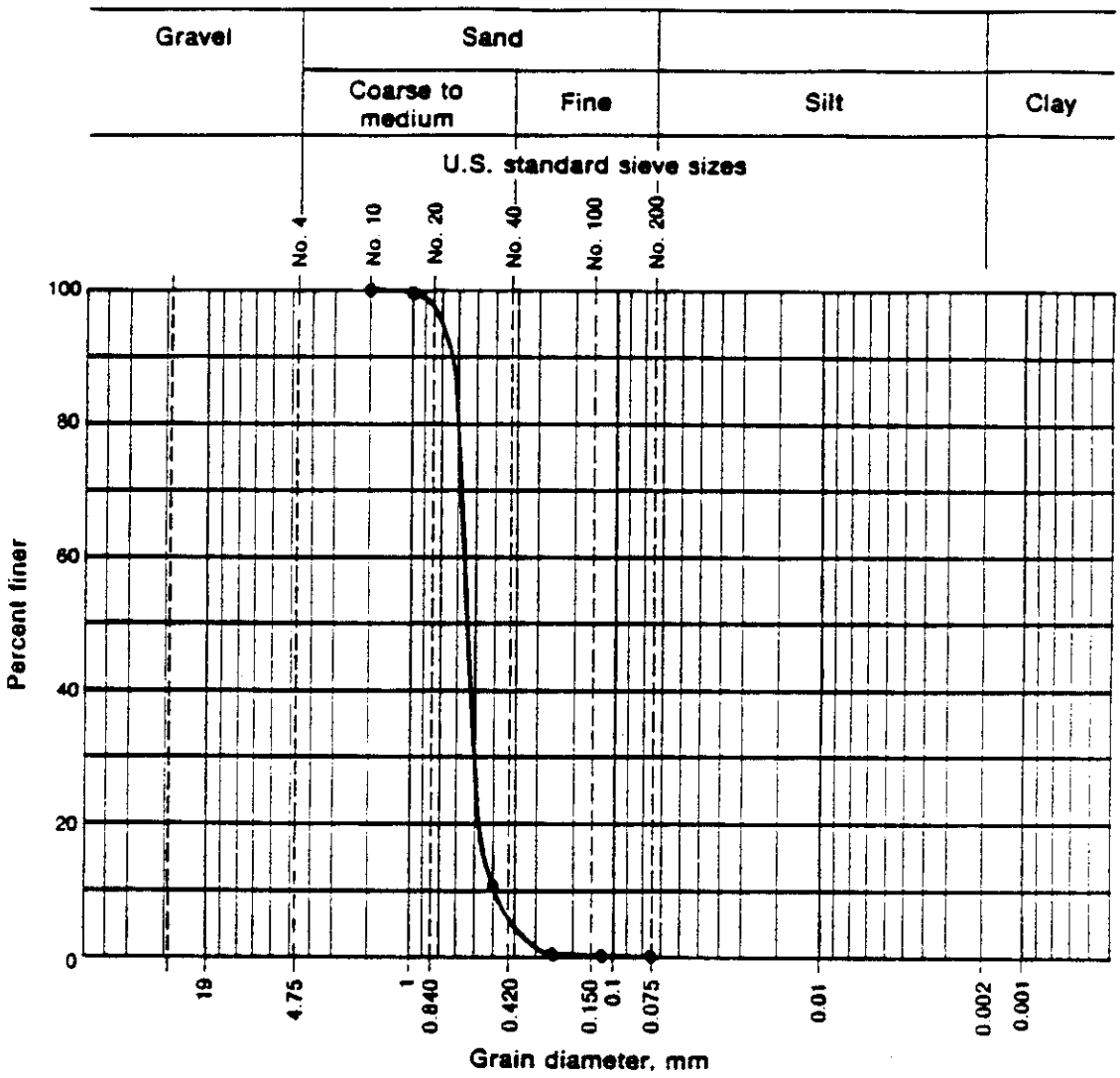

Figure 30. Grain Size Distribution of Model Pile Test Sand.

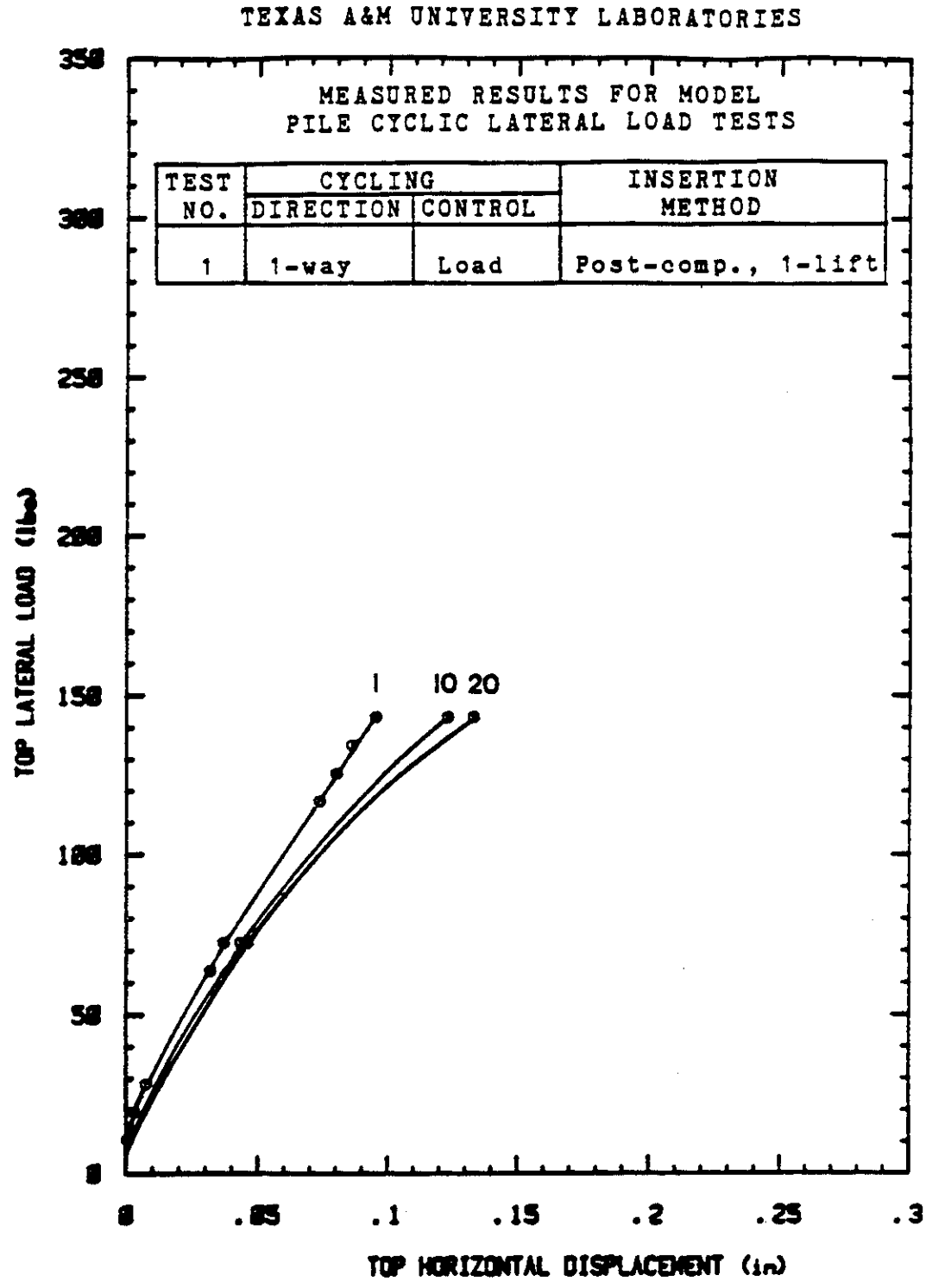

Figure 31. Lateral Load versus Horizontal Displacement of Pile Head for One-way, Load-control Test: Post-compacted, Single Lift, Pile Placement Procedure.

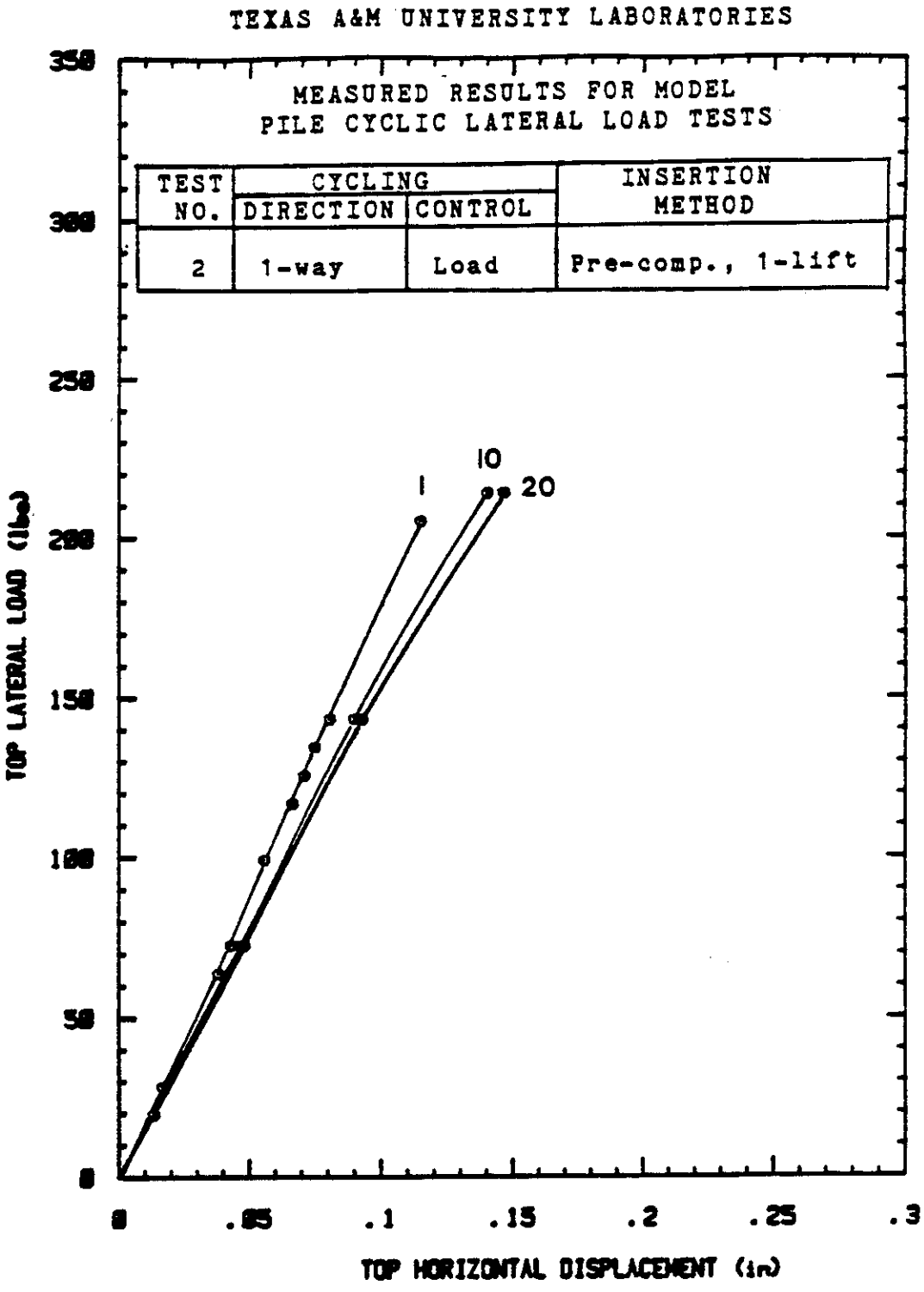

Figure 32. Lateral Load versus Horizontal Displacement of Pile Head for One-way, Load-control Test: Pre-compacted, Single Lift, Pile Placement Procedure.

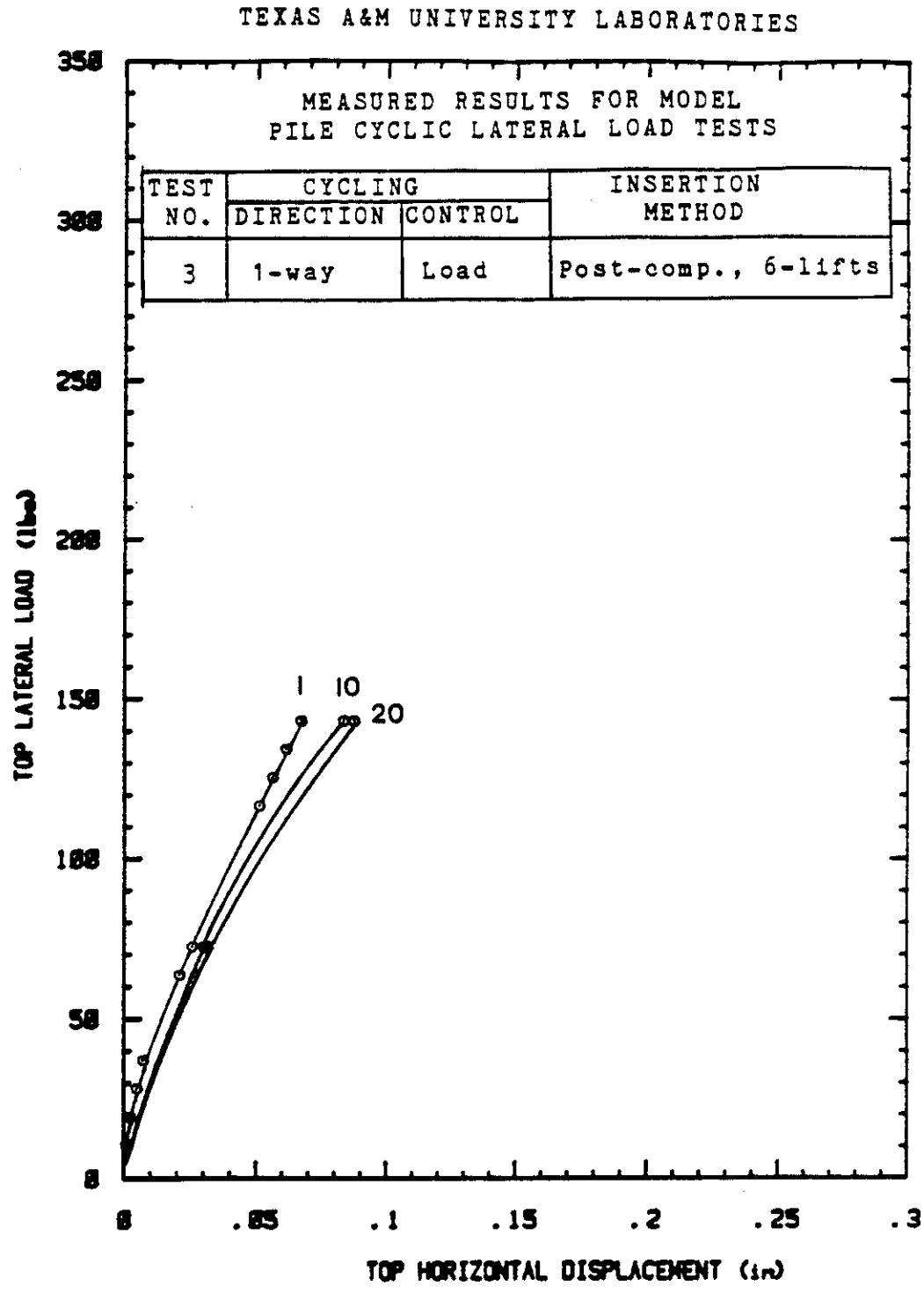

Figure 33. Lateral Load versus Horizontal Displacement of Pile Head for One-way,Load-control Test: Post-compacted, Multiple Lift, Pile Placement Procedure.

application of specified displacements or loads. The period of cycles was 40 seconds. Load readings were taken every 20 seconds following the forced displacements, which were applied in 0.005 inch increments. The pile was in a free-head condition. Twenty cycles were conducted at each of three displacements levels: 0.040 inches, 0.080 inches, and 0.125 inches, which corresponded to relative displacements (y/R) of 5.9%, 11.8%, and 18.4%. The bottom of each cycle corresponded to that displacement where the lateral load returned to zero (Figure 34). The lateral load versus horizontal displacement curves are presented in Figures 35, 36, and 37.

4.5 Two-way Load-control Tests

The two-way load-control tests were conducted by applying loads in 5 lb. increments every 20 seconds in one direction until the desired load level for cycling was reached. The same load was then applied in the opposite direction and a reading of the corresponding displacement was made. The load was then applied in the original direction, completing the cycle. The period of cycles was 40 seconds and the pile was in a free-head condition. The resulting lateral load versus horizontal displacement curves are presented in Figures 38, 39, and 40.

4.6 Two-way Displacement-control Tests

The two-way displacement-control tests were conducted by forcing incremental displacements of 0.005 inches every

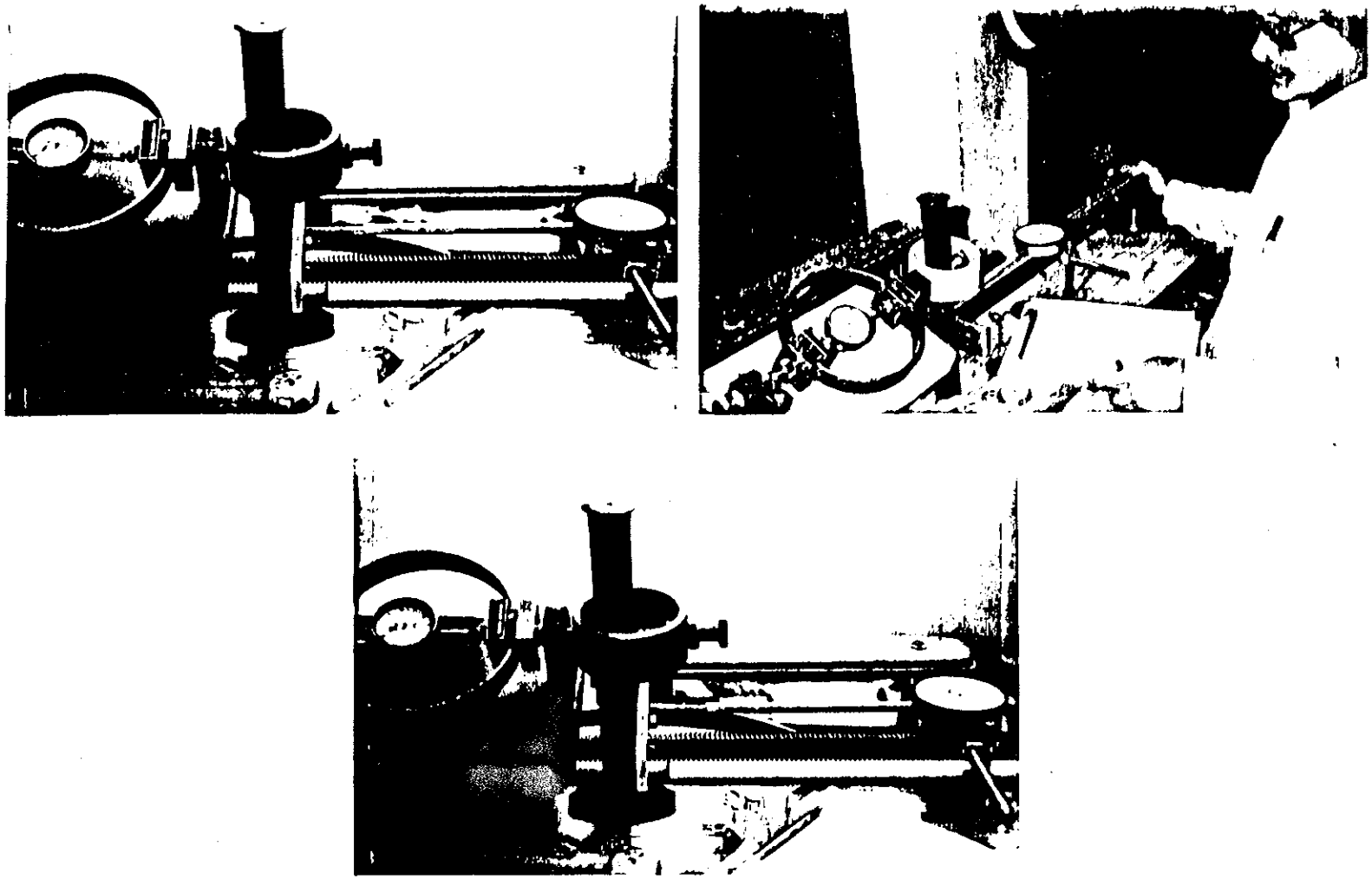

Figure 34. Performing the One-way, Displacement-control Cyclic Test.

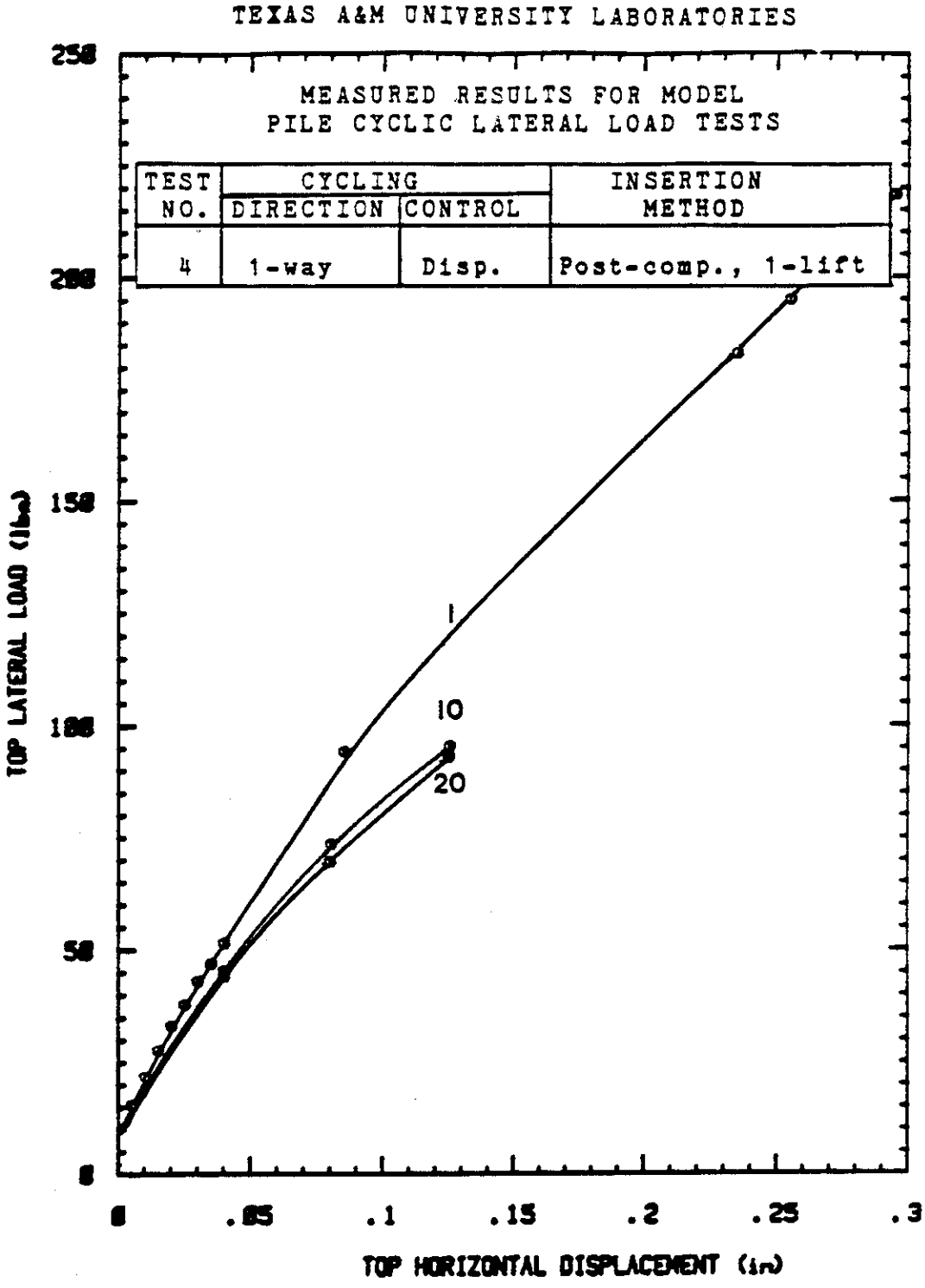

Figure 35. Lateral Load versus Horizontal Displacement of Pile Head for One-way, Displacement-control Test: Post-compacted, Single Lift, Pile Placement Procedure.

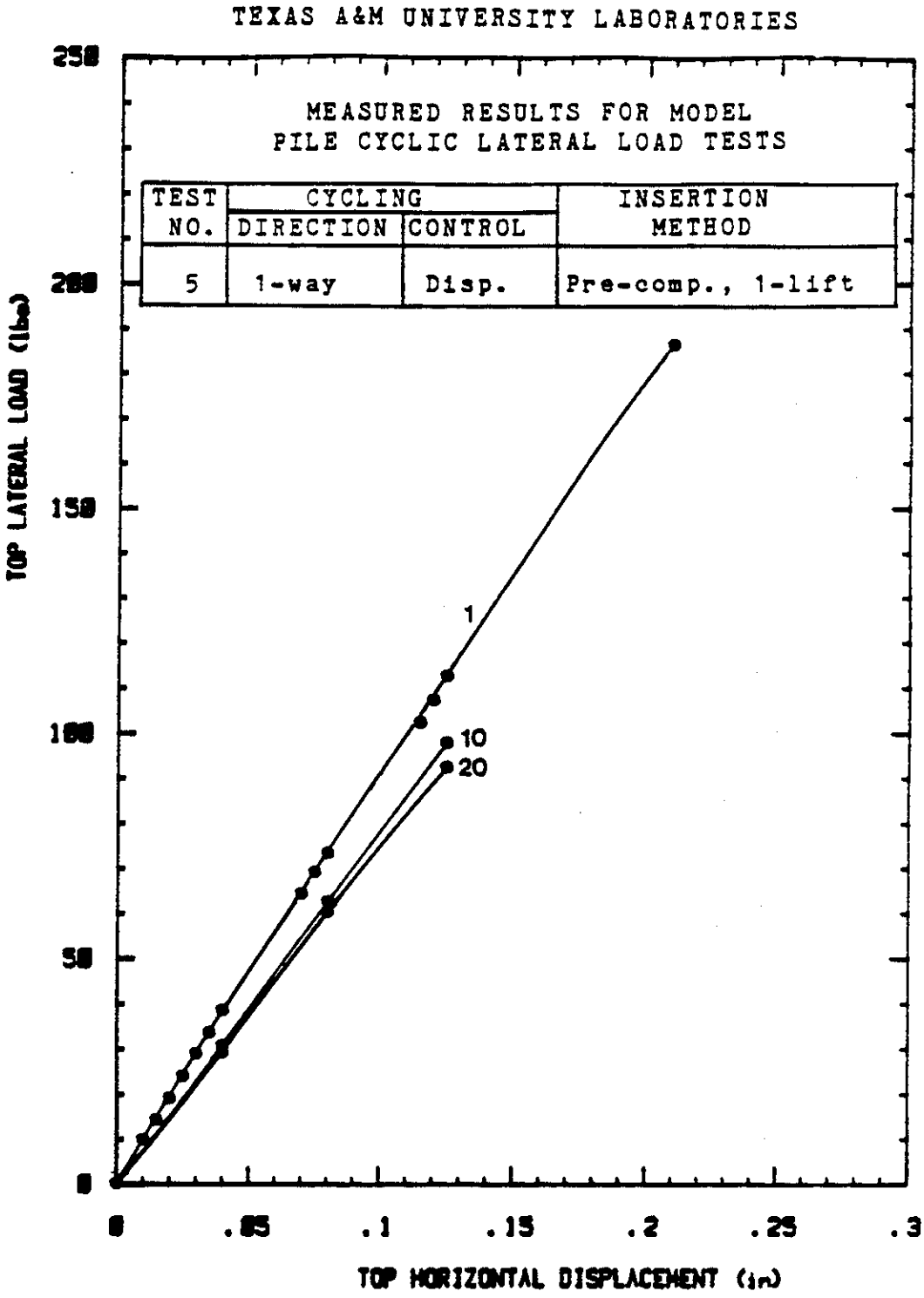

Figure 36. Lateral Load versus Horizontal Displacement of Pile Head for One-way, Displacement-control Test: Pre-compacted, Single Lift, Pile Placement Procedure.

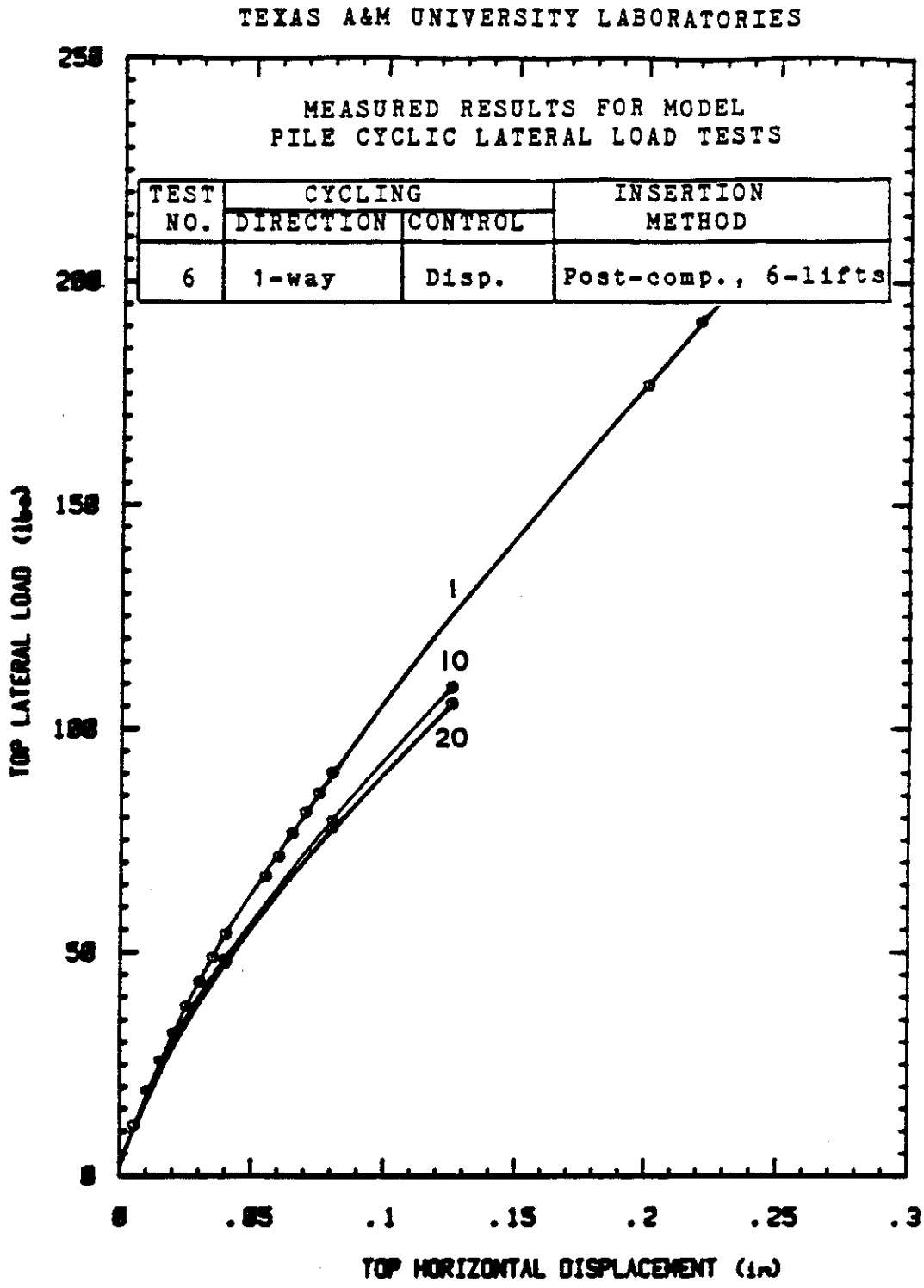

Figure 37. Lateral Load versus Horizontal Displacement of Pile Head for One-way, Displacement-control Test: Post-compacted, Multiple Lift, Pile Placement Procedure.

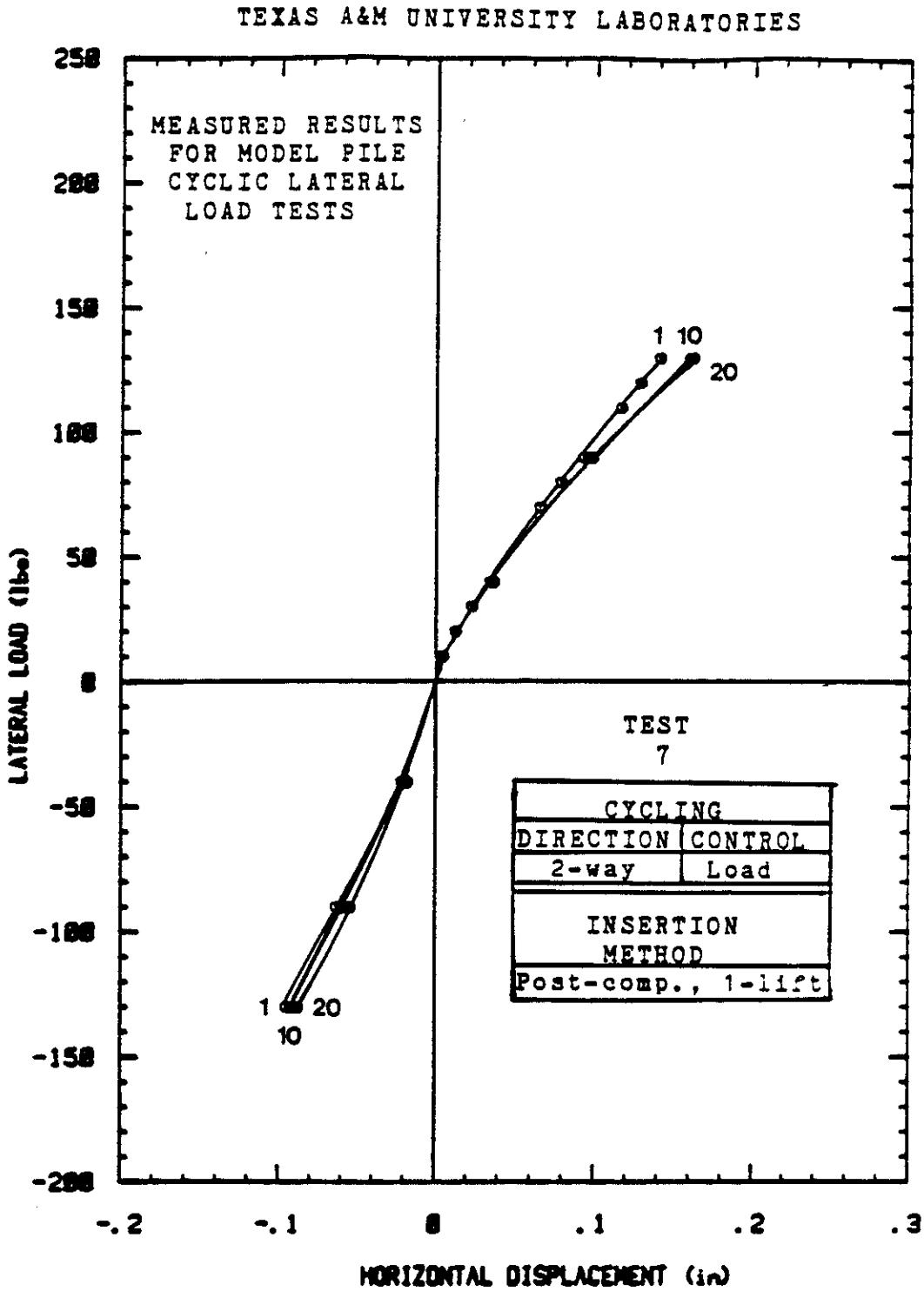

Figure 38. Lateral Load versus Horizontal Displacement of Pile Head for Two-way, Load-control Test: Post-compacted, Single Lift, Pile Placement Procedure.

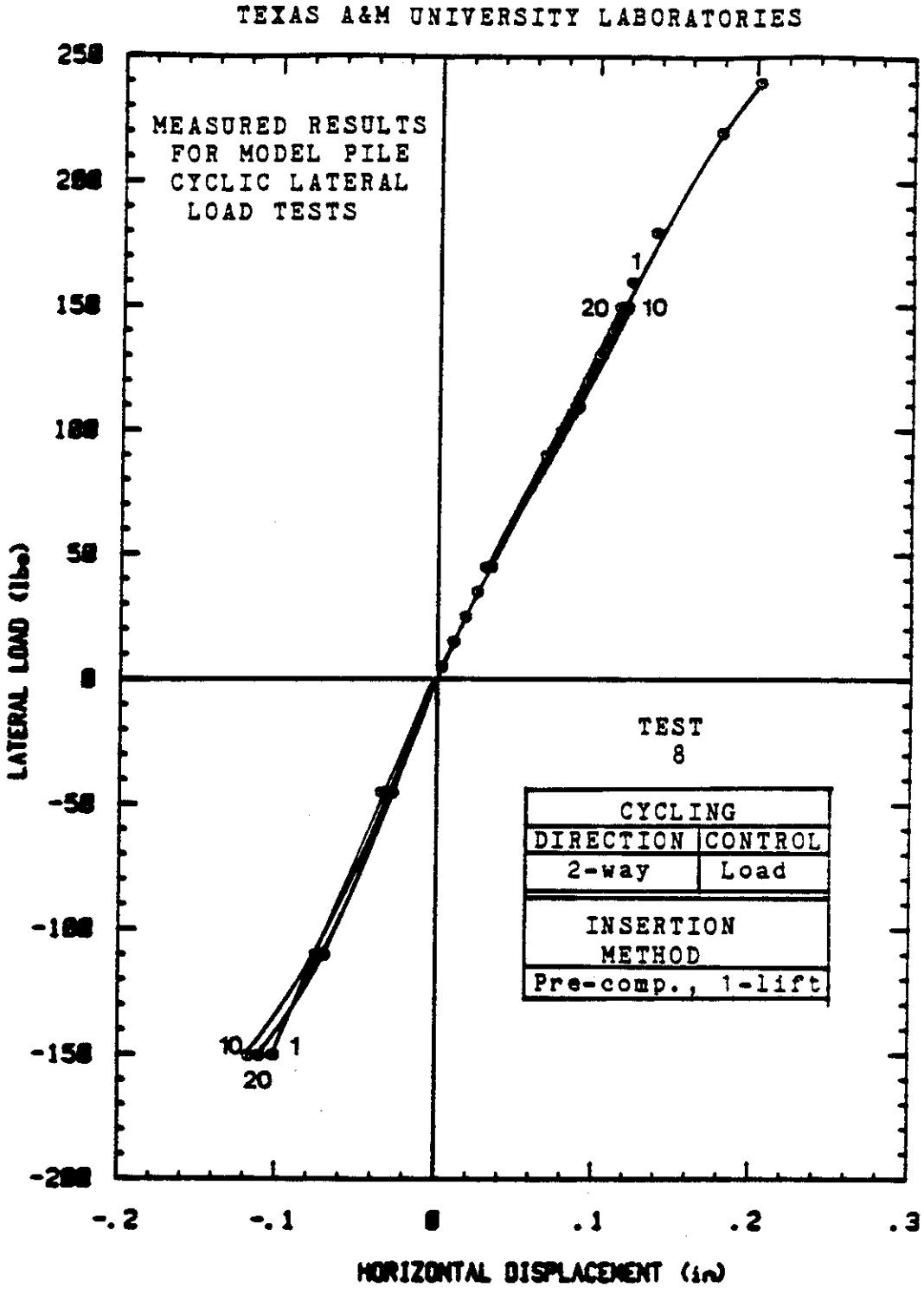

Figure 39. Lateral Load versus Horizontal Displacement of Pile Head for Two-way, Load-control Test: Pre-compacted, Single Lift, Pile Placement Procedure.

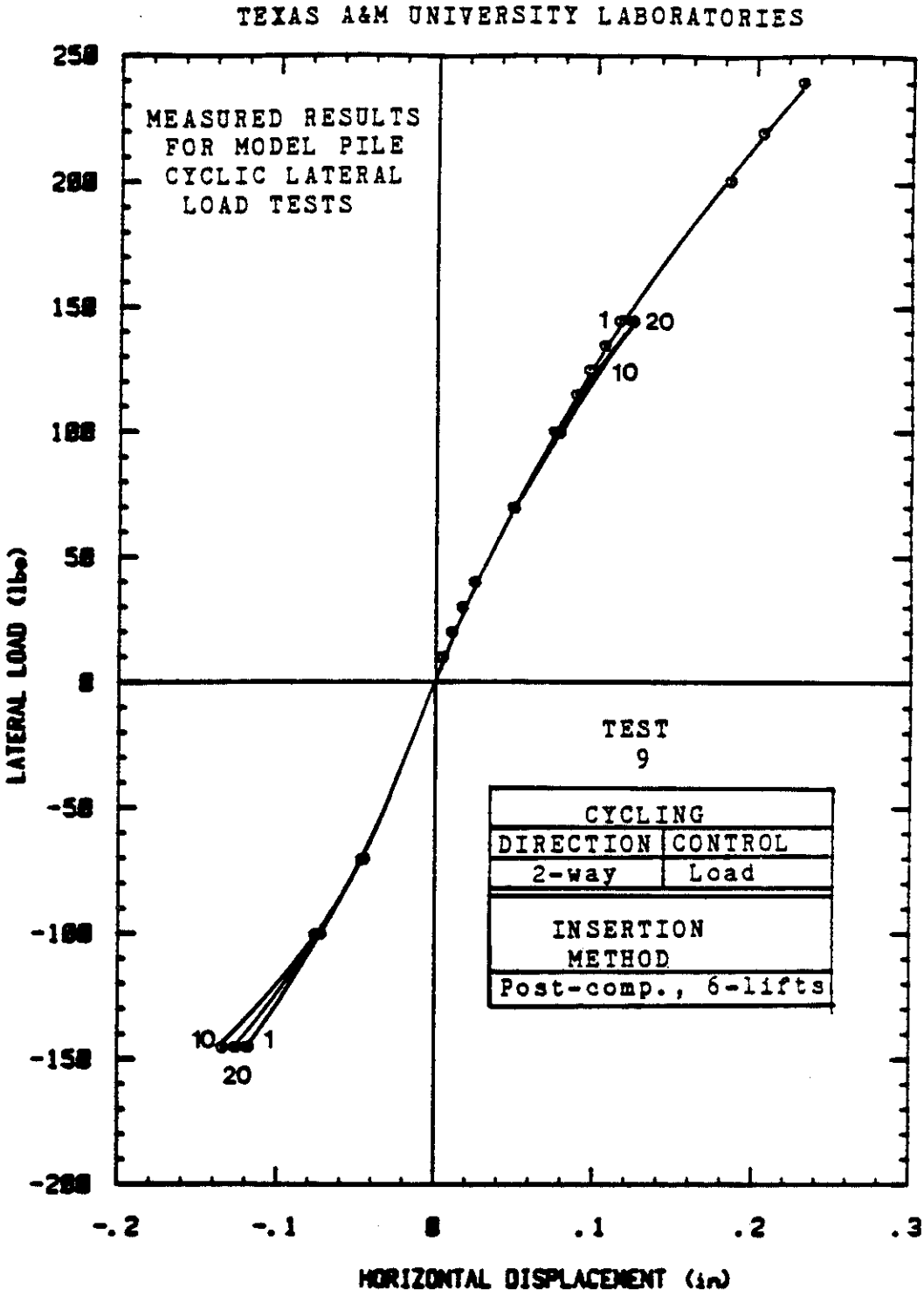

Figure 40. Lateral Load versus Horizontal Displacement of Pile Head for Two-way, Load-control Test: Post-compacted, Multiple Lift, Pile Placement Procedure.

20 seconds in one direction until the desired displacement level for cycling was achieved. An increasing load was then applied in the opposite direction until the same magnitude of displacement was reached in the opposite direction of travel. Readings of load and negative deflection were recorded after the 20-second interval, and an increasing load was then reapplied to the pile in the original direction until the displacement recorded during the first loading was matched, completing the first cycle. The period of cycles was 40 seconds and the pile was in a free-head condition. The lateral load versus horizontal displacement curves resulting from this test series are shown in Figures 41, 42, and 43.

4.7 Model Pile Monotonic Response Envelopes

A comparison of the monotonic response envelopes of the one-way model pile load tests reveals a softer response for the model piles subjected to displacement-control loading than for the model piles subjected to load-control loading (Figure 44). This variation is primarily a reflection of the difference in the elevations at which the loads were applied. The apparatus for the one-way load-control model pile test (Figure 19) applied the lateral loads at approximately 5 inches above the sand surface. The apparatus for the one-way displacement-control model pile test (Figure 22) applied the lateral loads at an elevation of approximately 10 inches. The elevation at which the deflections were

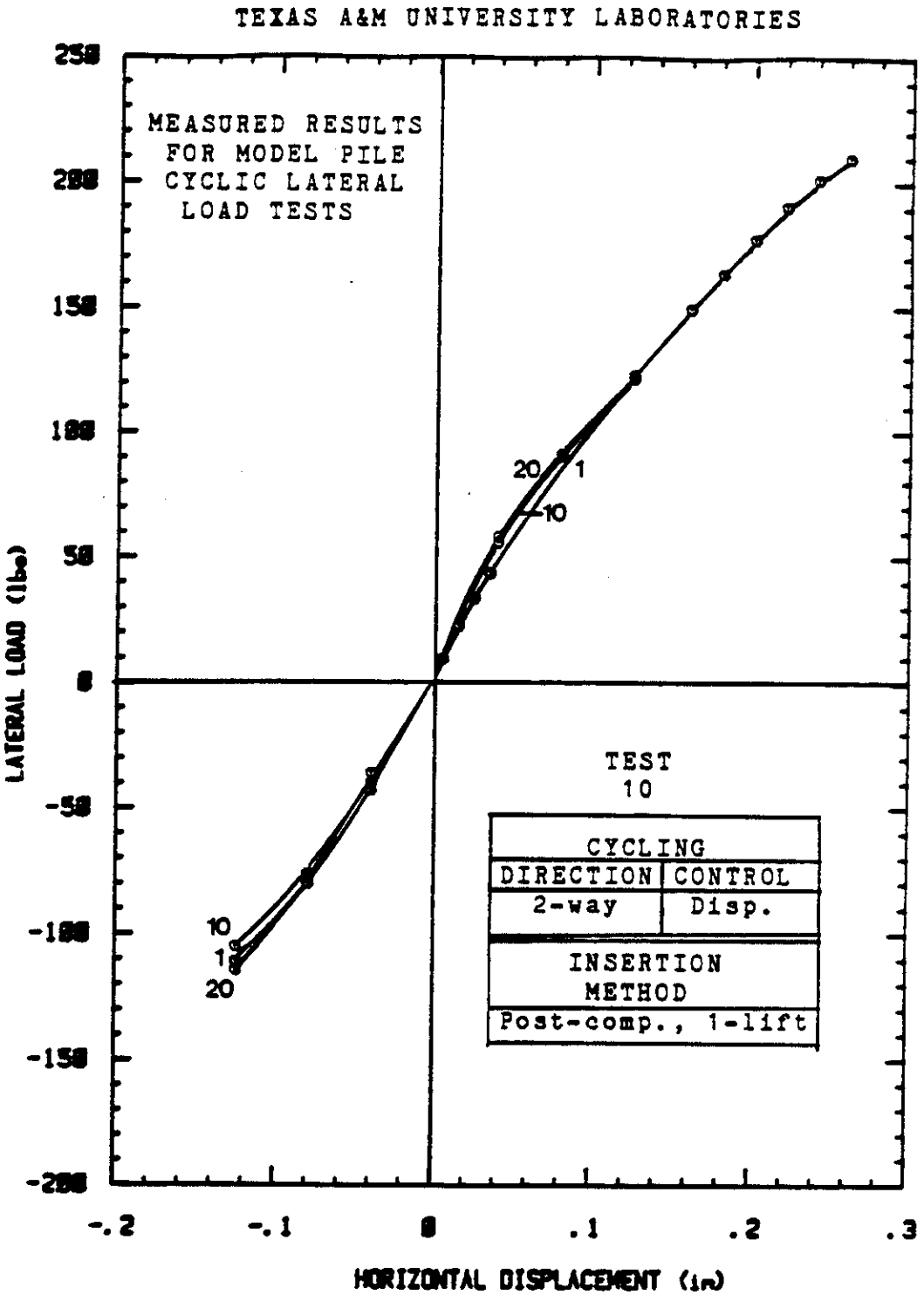

Figure 41. Lateral Load versus Horizontal Displacement of Pile Head for Two-way, Displacement-control Test: Post-compacted, Single Lift, Pile Placement Procedure.

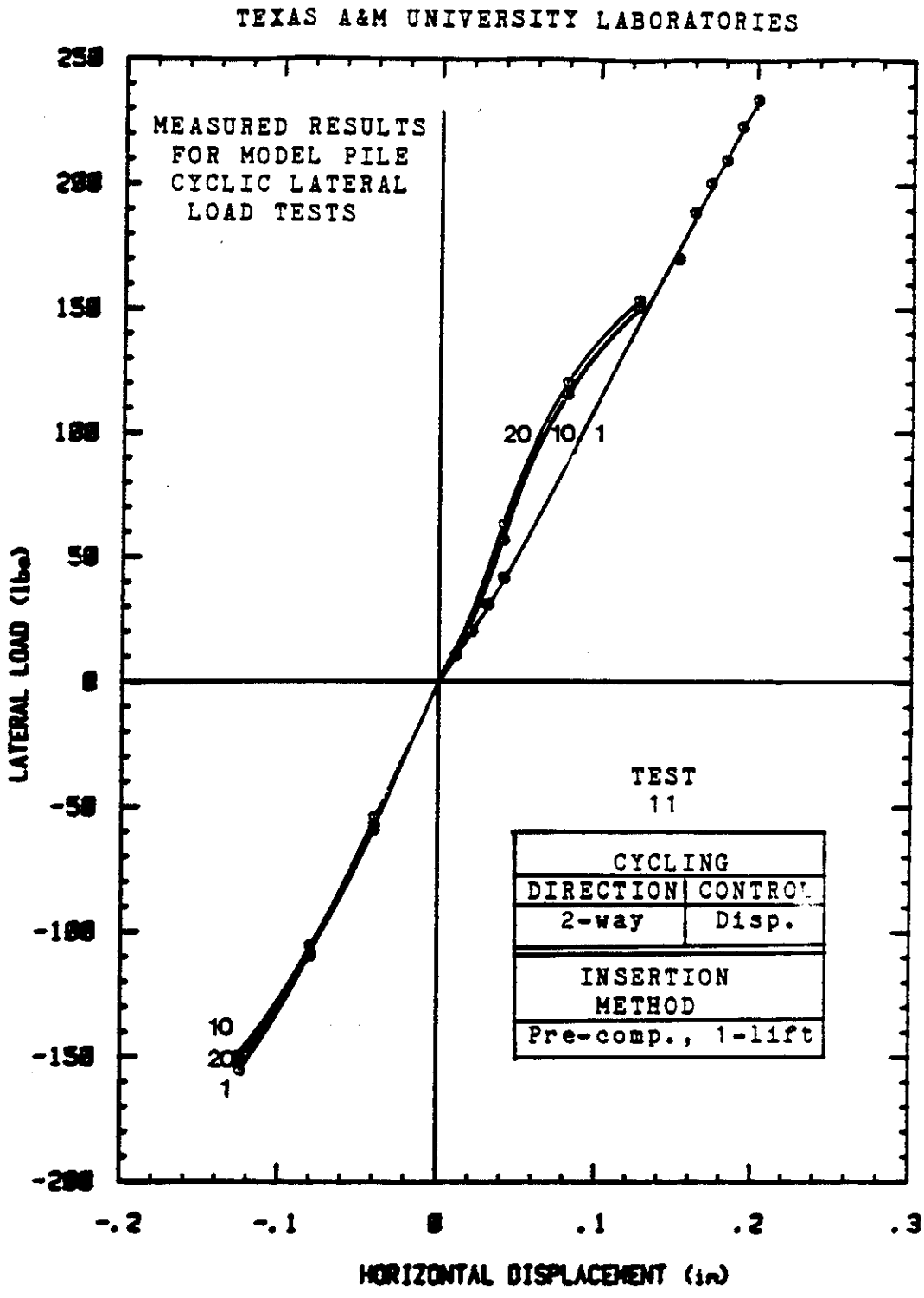

Figure 42. Lateral Load versus Horizontal Displacement of Pile Head for Two-way, Displacement-control Test: Pre-compacted, Single Lift, Pile Placement Procedure.

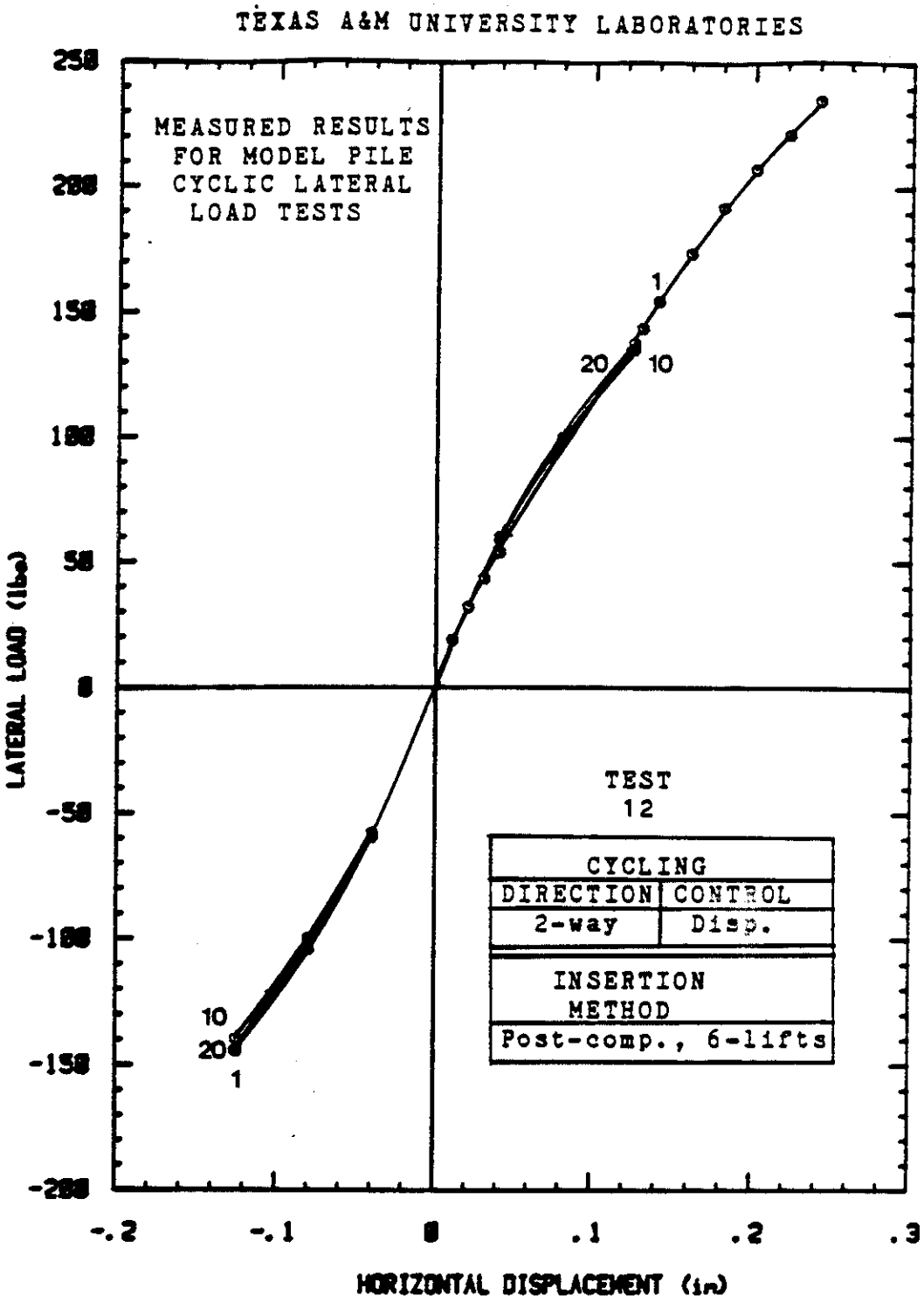

Figure 43. Lateral Load versus Horizontal Displacement of Pile Head for Two-way, Displacement-control Test: Post-compacted, Multiple Lift, Pile Placement Procedure.

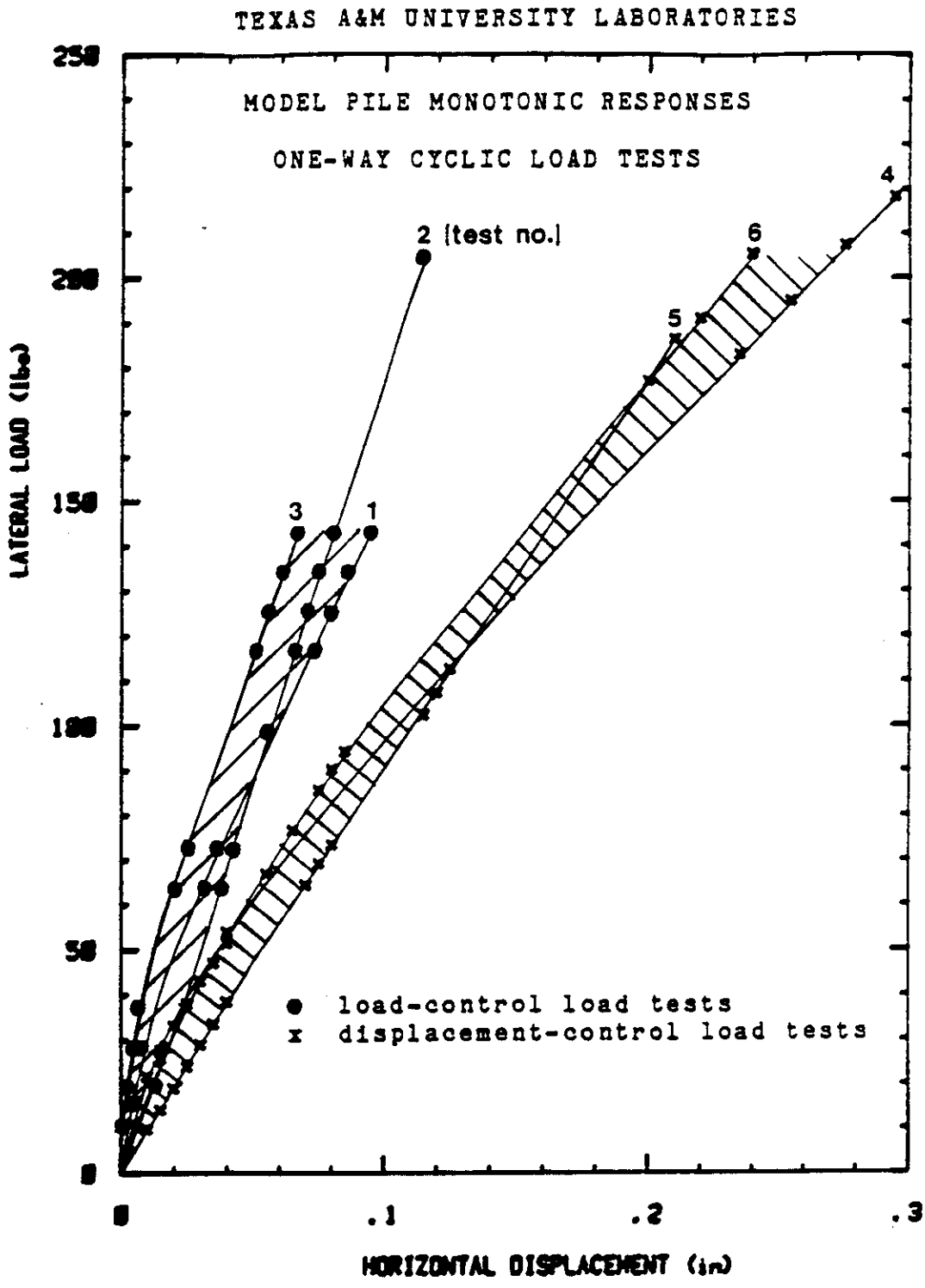

Figure 44. Range of Monotonic Responses in the Model Pile One-way Cyclic Load Tests at the Texas A&M University Laboratories.

measured was approximately 5 inches for both series of tests.

Both two-way cyclic test series were conducted using the second apparatus (Figure 22). As a result, the loads were applied at essentially the same elevation for both of the two-way cyclic loading series. The range of monotonic response envelopes of the load-control and the displacement-control two-way cyclic tests generally coincide (Figure 45).

Within each test series the model pile driven into pre-compacted sand generally had the softest monotonic response at low load levels and the stiffest response at high load levels (Figures 44 and 45). This suggests that driving the model pile densified the sand in the test drum, resulting in a higher ultimate soil/pile stiffness; however, the driving of the pile was not completely straight causing an initially weaker response. Also within each series, the post-compacted multiple-lift insertion method resulted in a stiffer response than the post-compacted single-lift insertion method (Figures 44 and 45). This may be attributed to the higher density reached when compacting the sand in multiple lifts (Table 2).

4.8 Degradation Model Results and Discussion

The percent loss of pile-soil stiffness with increasing numbers of load cycles is calculated from the cyclic pile response envelopes as depicted in Figure 46. The percent losses measured at deflections of 0.03 inches and 0.10

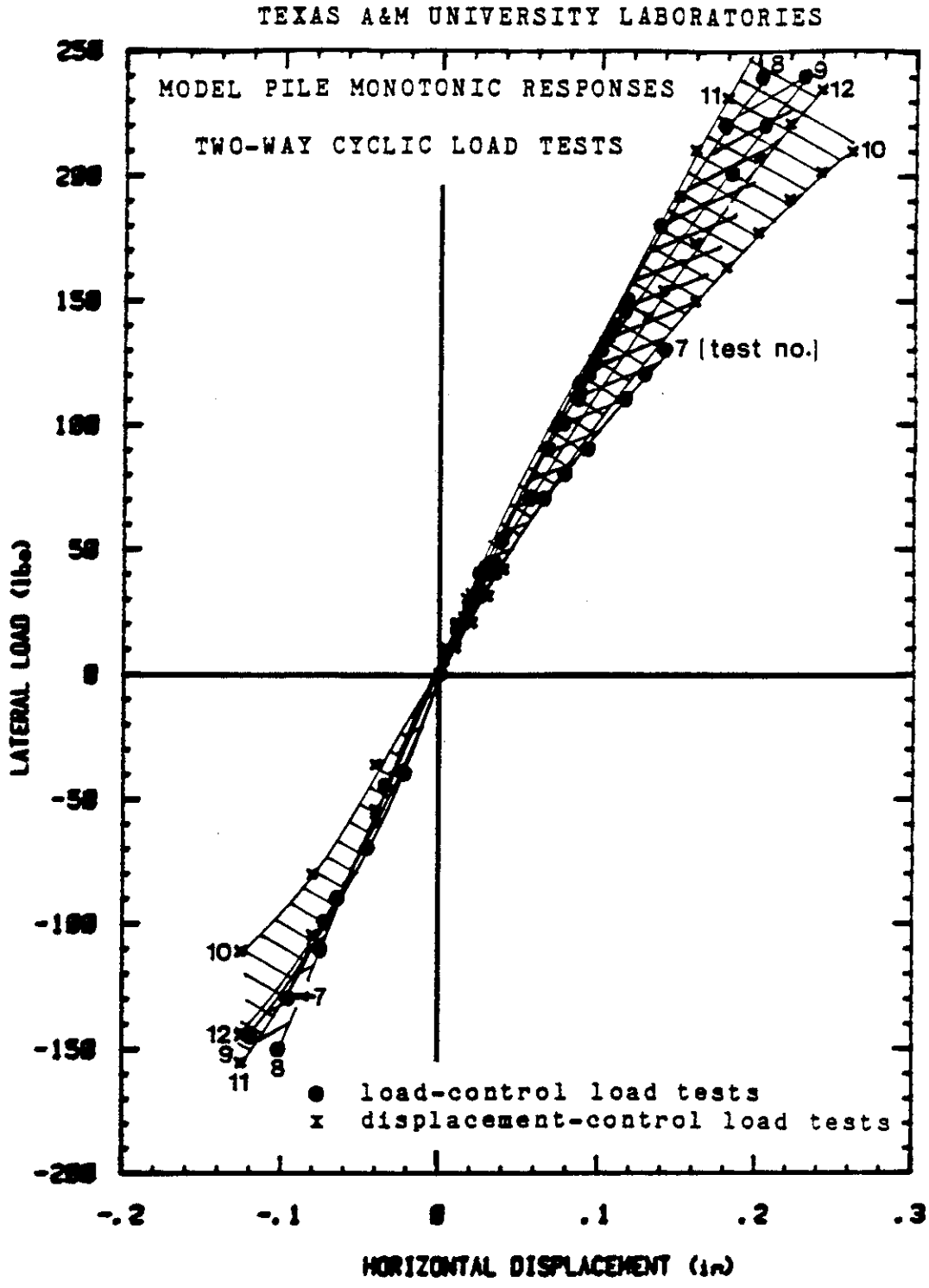

Figure 45. Range of Monotonic Responses in the Model Pile Two-way Cyclic Load Tests at the Texas A&M University Laboratories.

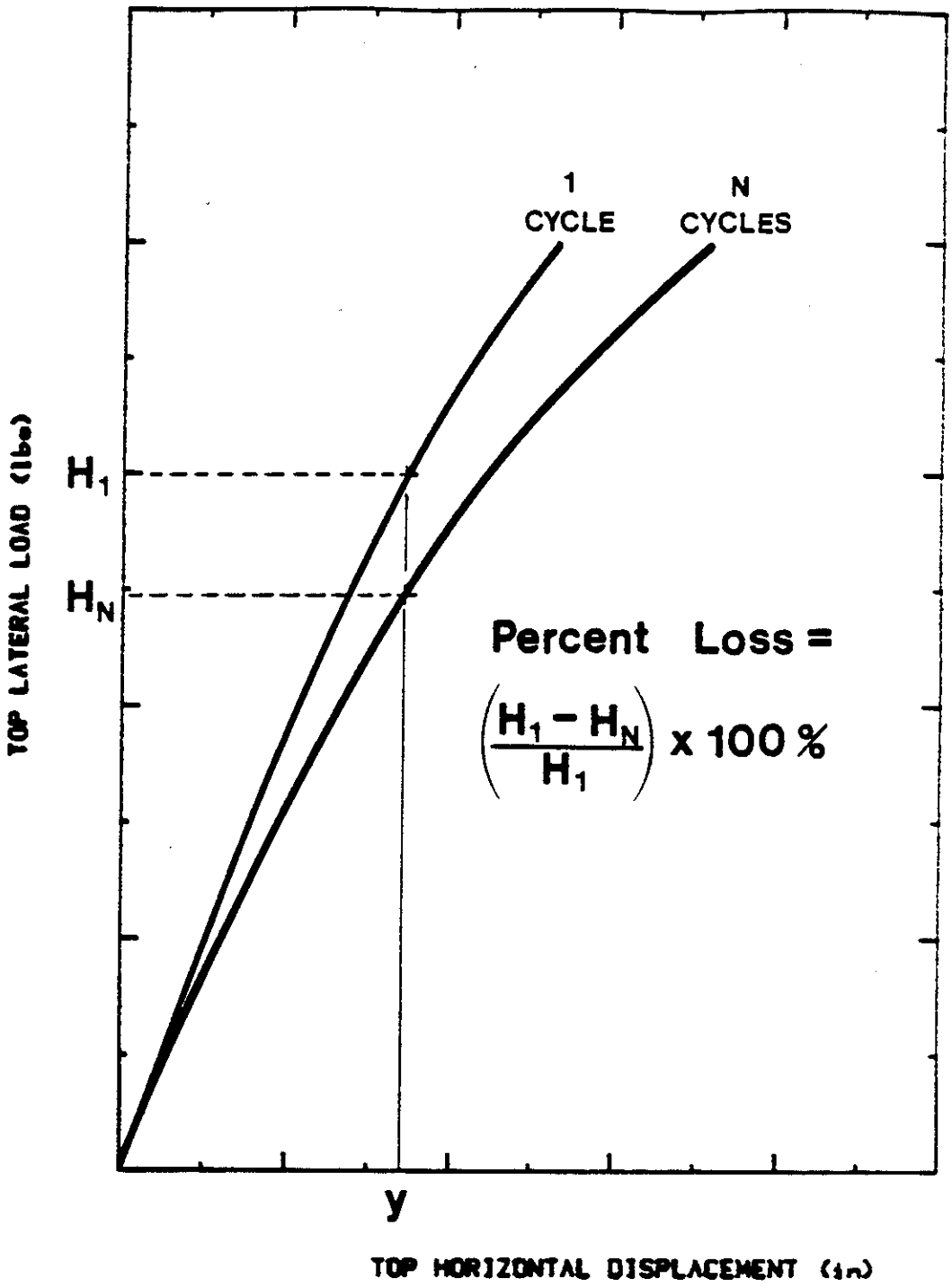

Figure 46. Determination of Percent Loss of Soil-pile Response with Increasing Cycle Number.

inches (approximately 2% and 8% of the model pile diameter) after 20 load cycles are presented in Table 3. Also, the back-calculated $\underline{a}$ values from the model pile tests are plotted in Figure 47.

The results agree with the observation made during the pile data base analysis that, in sand, one-way cycling results in greater degradation than two-way cycling. Degradation was minor and in some cases negative (strengthening of the soil) for the two-way cyclic tests (Table 3 and Figure 47). The average percent loss after 20 cycles in the first-load direction of the two-way cyclic tests was -11% (Table 3). For the one-way cyclic tests, on the other hand, significant degradation developed (Figure 47), and the average percent loss after 20 cycles was 17% (Table 3).

As with the single pile at the University of Houston sand site, after the initial few cycles, the degradation parameter $\underline{a}$ remained fairly constant with increasing cycle numbers. Also, the rate of degradation of the model pile-soil stiffness response ($\underline{a}$) tended to increase slightly with increasing displacement levels (y/R (%) in Figure 47).

The results also indicate that the stiffness degradation of piles subjected to one-way displacement-control cycling is generally greater than the stiffness degradation of piles subjected to one-way load-control loading (Table 3). The average percent loss was 19% after 20 one-way displacement-control cycles, but was only 16% after 20 one

Cycling Method	Soil/Placement Procedure	Model Pile Test No.	Percent Loss of Stiffness After 20 Load Cycles			
			First Load Direction		Second Load Direction	
			y=0.03"	y=0.10"	y=0.03"	y=0.10"
One-way Load Control	Post-comp., 1 lift	1	17	18	-	-
	Pre-comp., 1 lift	2	11	14	-	-
	Post-comp., 6 lift	3	14	20	-	-
averages for 1-way load-control tests			14	17	-	-
combined average at both y values			16			
One-way Displacement Control	Post-comp., 1 lift	4	17	23	-	-
	Pre-comp., 1 lift	5	25	18	-	-
	Post-comp., 6 lift	6	12	17	-	-
averages for 1-way disp.-control tests			18	19	-	-
combined average at both y values			19			
average of all 1-way tests			17			
Two-way Load Control	Post-comp., 1 lift	7	0	9	-12	-7
	Pre-comp., 1 lift	8	-13	-2	-19	4
	Post-comp., 6 lift	9	-	4	-	4
averages for 2-way load-control tests			-7	4	-16	0
combined average at both y values			0		-6	
Two-way Displacement Control	Post-comp., 1 lift	10	-23	-3	-12	0
	Pre-comp., 1 lift	11	-56	-20	0	3
	Post-comp., 6 lift	12	-10	-3	0	3
averages for 2-way disp.-control tests			-30	-9	-4	2
combined average at both y values			-19		-1	
average of all 2-way tests			-11		-3	

Table 3. Measured Percent Loss of Soil-Pile Stiffness after 20 Horizontal Load Cycles in the Model Pile Load Tests at Texas A&M University.

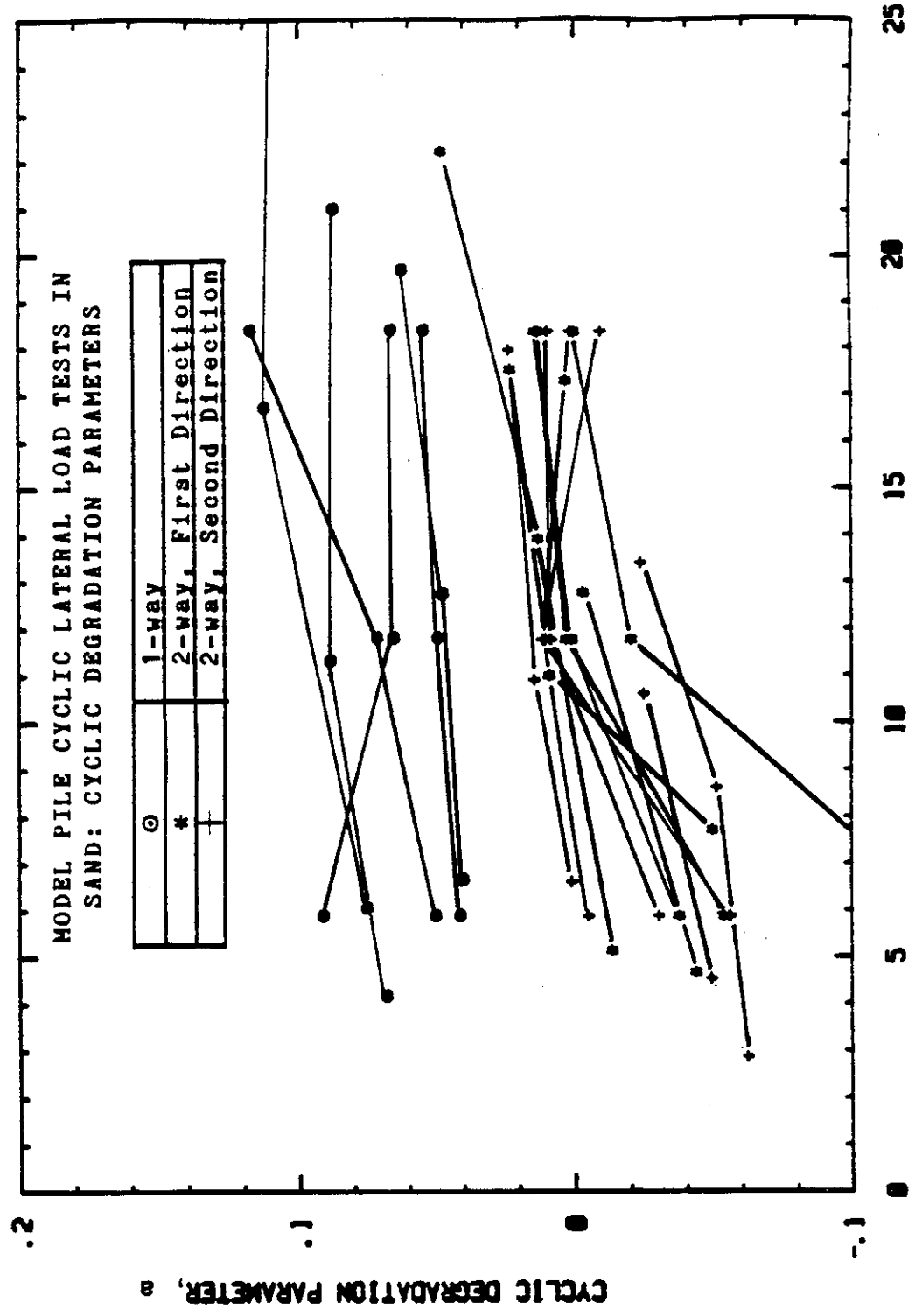

Figure 47. Cyclic Degradation Parameter a versus Relative Pile Head Deflection for Model Pile Tests.

way load-control cycles (Table 3). This variation may be partially attributed to the difference in the extent of the zone of soil influenced during these two different pile loading methods. In displacement-control cyclic tests, the zone of influence remains essentially limited after the initial few cycles since the maximum pile travel is held constant. Continued cycling, therefore, continues to weaken the same soil zone. Load-control cyclic tests, on the other hand, do not limit the pile travel. As the initially affected soil zone weakens, the pile deflects further on successive cycles, enlarging the zone of soil influenced. New soil, as yet unaffected by previous cycles (and, therefore, not yet weakened) is thus continually encountered.

This variation in the zones of influence may also help to explain why the two-way displacement-control cyclic load tests resulted in greater soil strengthening than the two-way load-control cyclic load tests. The two-way displacement-control tests averaged a percent gain in pile-soil stiffness of 19% (a negative percent loss in Table 3). The two-way load-control tests gained an average of 0%. Continued cycling during a displacement-control test may increasingly densify the same soil zone; whereas, during a load-control test, some of the energy from each cycle is expended to enlarge the zone of influence. As a result, the zone influenced during the displacement-control tests develops a higher degree of densification than the larger

zone influenced during the load-control tests.

The model pile tests were conducted in dry sand and the influence of the degree of saturation was not directly investigated. The dry sand model pile tests under two-way cyclic loading definitely showed a tendency for stiffer response with increasing cycles at low displacement levels. This phenomenon was not observed in the full-scale pile load test at the University of Houston Foundation Test Facility, where the sand was fully saturated. The cyclic degradation parameter back-calculated from the 10.75 inch pile generally remained above zero. The effect of sand saturation on cyclic lateral loading of piles needs to be more fully explored.

5. PRESSUREMETER EQUIPMENT AND TEST PROCEDURES

5.1 The TEXAM Pressuremeter Equipment

The TEXAM pressuremeter test equipment was developed at Texas A&M University between 1980 and 1983 and is now sold commercially by ROCTEST. It is composed of a portable control unit and a probe with a single inflatable cell (Figure 48). The control unit houses a fluid storage tank connected to the probe by very high strength tubing. The tubing has an 8 mm outside diameter and experiences negligible volume expansion under pressure (0.02 $cm^3/kg/cm^2$ per linear meter of tubing).

Pressure is developed in the system through the use of a piston-cylinder assembly within the control unit. A screw jack is employed to advance the piston, forcing fluid from the storage tank, through the tubing, and into the probe's inflatable cell. Any of three pressure gages mounted on the control unit may be used to monitor the system pressure, depending on the range of pressures encountered during the test. A dial gage tracks the piston travel. Since piston displacements are directly related to the volume of water injected into the tubing and probe, readings from the piston displacement dial gage will be referred to as injected volume readings in this report.

The pre-bored pressuremeter probe employed in this study is made of a single inflatable cell 40 cm in length

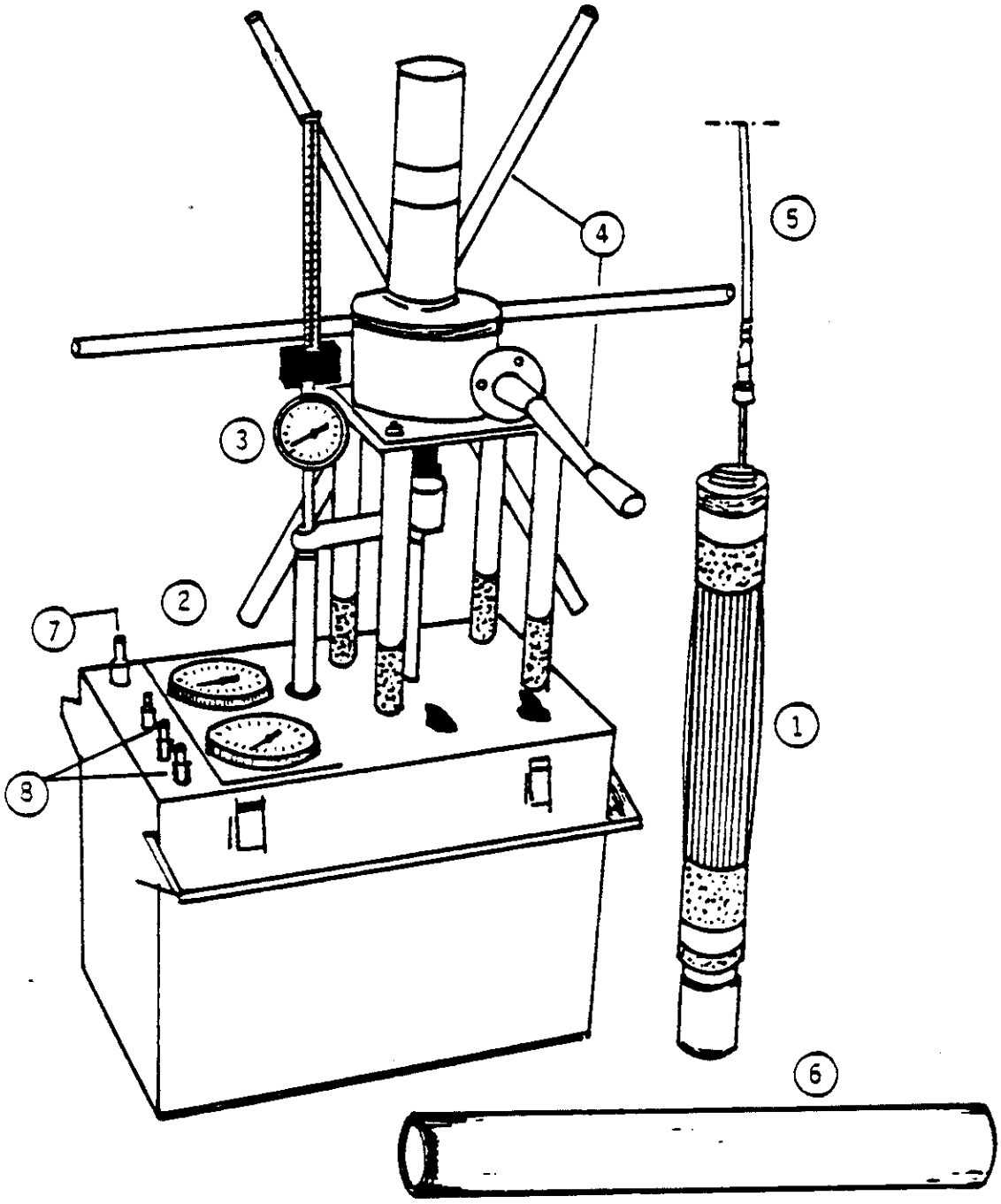

Figure 48. Schematic of Pre-boring Pressuremeter Model TEXAM. 1. Probe, 2. Pressure Gauges, 3. Volume/ Displacement Indicator, 4. Manual Actuator, 5. Tubing, 6. Calibration Tube, 7. Connection for Probe, 8. Connection to the Water Reservoir (After Makarim and Briaud, 1986).

and with a deflated diameter of 5.8 cm. The cell membrane is a rubber cylinder protected against puncture by a series of overlapping steel strips rubber-glued to the membrane. The probe itself is hollow to allow drilling fluid and subsurface water to pass freely through the probe during insertion.

5.2 The Cone Pressuremeter Equipment

The cone pressuremeter test equipment is also composed of a portable control unit and a probe with a single inflatable cell (Figure 49). It is sold commercially by ROCTEST under the name of PENCEL. The control unit and probe, however, are more compact than those of the TEXAM.

Pressure is similarly developed in the system through the use of a piston-cylinder arrangement; however, rather than reading the piston displacement with a dial gage, a counter connected to the screw jack which advances the piston indicates the volume of fluid displaced in cubic centimeters. A single pressure gage indicates fluid pressure within the system.

The inflatable cell in the probe has a length of 23 cm and a deflated diameter of 3.2 cm and is made up of a rubber membrane protected against puncture by a series of overlapping steel strips rubber-glued to the membrane. A dummy cone penetrometer point was mounted on the bottom of the probe during these tests. The probe connects with standard cone rods and may be advanced into the soil either by

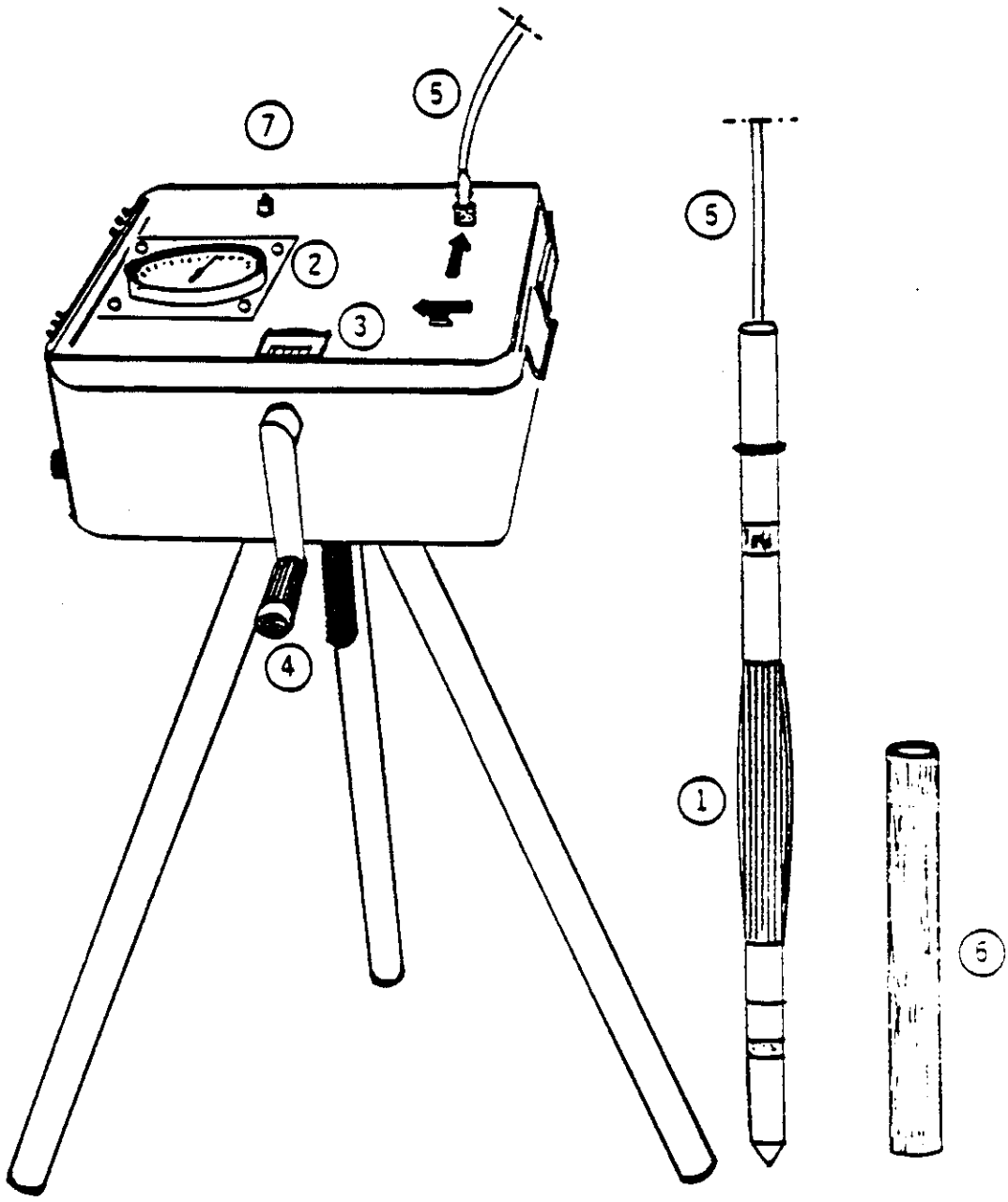

Figure 49. Schematic of Cone Pressuremeter Model PENCEL. 1. Probe, 2. Pressure Gauge, 3. Volume/ Displacement Indicator, 4. Manual Actuator, 5. Tubing, 6. Calibration Tube, 7. Connection to the Water Reservoir (After Makarim and Briaud, 1986).

pushing, as with the cone penetrometer, or by driving, to simulate the insertion of a driven pile.

5.3 TEXAM Pressuremeter Test Procedure

Before beginning a series of pressuremeter tests, the control unit storage tank was filled with water. The probe was then connected to the unit through the flexible tubing and the entire system checked for saturation and leaks.

5.3.1 Necessary Monotonic Calibrations

Once in the field, two calibrations were performed: a volume calibration and a membrane resistance calibration. Before calibration, the probe was inflated in the air a few times to exercise the system components. Then the inflatable portion of the probe was inserted into a tight-fitting steel calibration tube (74.5 mm inside diameter) and inflated to a pressure equivalent to the anticipated limit pressure of the soil to be tested. At this time the system was again checked for leakage. The pressure was then dropped until the probe could first be pulled from the steel tube, at which point the "zero" volume of the probe was considered to have been reached. The control unit tank was then either bled or filled to read zero injected volume with the probe still sheathed in the steel tube. The calibration procedure could then begin.

Since the control unit-tubing-probe system is not entirely incompressible, a volume calibration was necessary to determine the "apparent" volumetric increase in the

system associated with an increase in the internal system pressure. This apparent volumetric increase includes expansion of the tubing and compression of the inflatable cell and system fluid, and does not include inflation of the probe (Section 6.4). With the probe tightly fitting inside the steel tube, the system pressure was increased in twenty 15-second pressure increments equal to 1/20th of the anticipated maximum soil limit pressure. The injected volume and system pressure were recorded at the end of each 15-second interval (Figure 50).

The membrane resistance calibration was necessary to determine the pressure required to inflate the probe in the air to any given injected volume. This membrane pressure must be subtracted from the pressure recorded during a test since this membrane pressure is not applied to the borehole wall (Section 6.3). With the probe removed from the steel volume calibration tube and simply supported to allow for free cell expansion, the probe was inflated in forty 15-second volume increments equivalent to approximately 1/40th of the fully inflated probe volume. At the end of each increment, the pressure and injected volume were recorded (Figure 50).

5.3.2 Cyclic Degradation Calibrations

For cyclic testing it was also necessary to determine cyclic degradation parameters for the volume and membrane resistance calibrations.

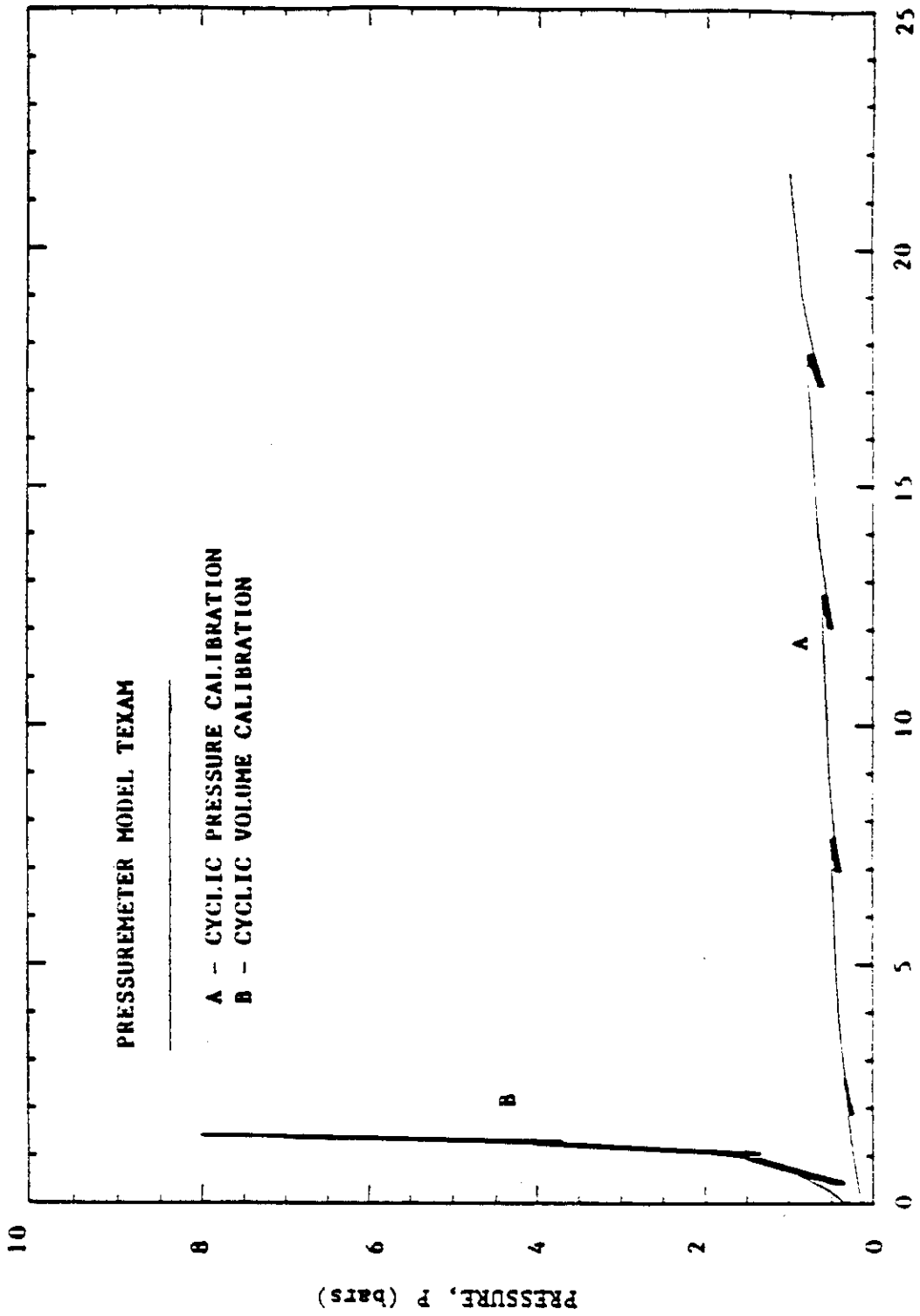

Figure 50. Cyclic Pressure and Volume Calibrations for the TEXAM Pressuremeter.

To determine the cyclic degradation parameters for the volume calibration, the probe was inserted into the steel calibration tube and the pressure increased in a series of steps as in the case of the standard volume calibration procedure. When the pressure was approximately equal to the pressure level at which cyclic testing in the soil was performed, the pressure was then decreased to approximately half of its peak value. This pressure was maintained until the end of the 15-second interval, the pressure and the injected volume values were recorded, and then the probe was reinflated until the initial pressure was reached again, completing one cycle. As many as three sets of 100 cycles each were performed on the TEXAM pressuremeter system with negligible degradation (Figure 50). As a result, additional volume losses associated with cyclic degradation were disregarded in the reduction of raw pressuremeter data.

The cyclic degradation parameter for the membrane resistance was similarly determined by cycling during a standard membrane resistance calibration at injected volumes equivalent to those anticipated during the actual soil testing (Figure 50). The difference between the cyclic membrane resistance and the monotonic membrane resistance was of sufficient magnitude to warrant the use of the cyclic membrane resistance in the reduction of the cyclic test data.

5.3.3 Soil Testing Procedures

After the calibrations were completed, the probe was ready for the actual soil testing. The borehole was drilled and the pressuremeter probe was inserted down to the test depth. The probe was then inflated in approximately thirty-five injected volume increments equivalent to 1/40th of the total fully inflated capacity of the probe. Readings of pressure and injected volume were taken at the end of each 15-second interval.

Cycling was performed either between preset values of injected volume or preset values of pressure. Cycling between preset injected volume values (volume-control tests) was chosen when modeling the response of displacement controlled cyclic pile load tests, whereas cycling between preset pressure values (pressure-control tests) was used to model load controlled cyclic pile load tests.

Generally, two or three series of 20 to 100 cycles each were performed in each test at pressure levels between 25% and 75% of the anticipated soil limit pressure.

During the volume-control tests, the probe was inflated in volume increments equal to $1/40^{th}$ of the probe's deflated volume (V_o), each lasting 15 seconds. This was done until the pressure was reached where cycling began. At the end of that 15-second interval the injected volume, V_{cp}, and the system pressure, P_{cp}, were recorded (Figure 51). Then the probe was deflated to a pressure, P_r, equivalent to

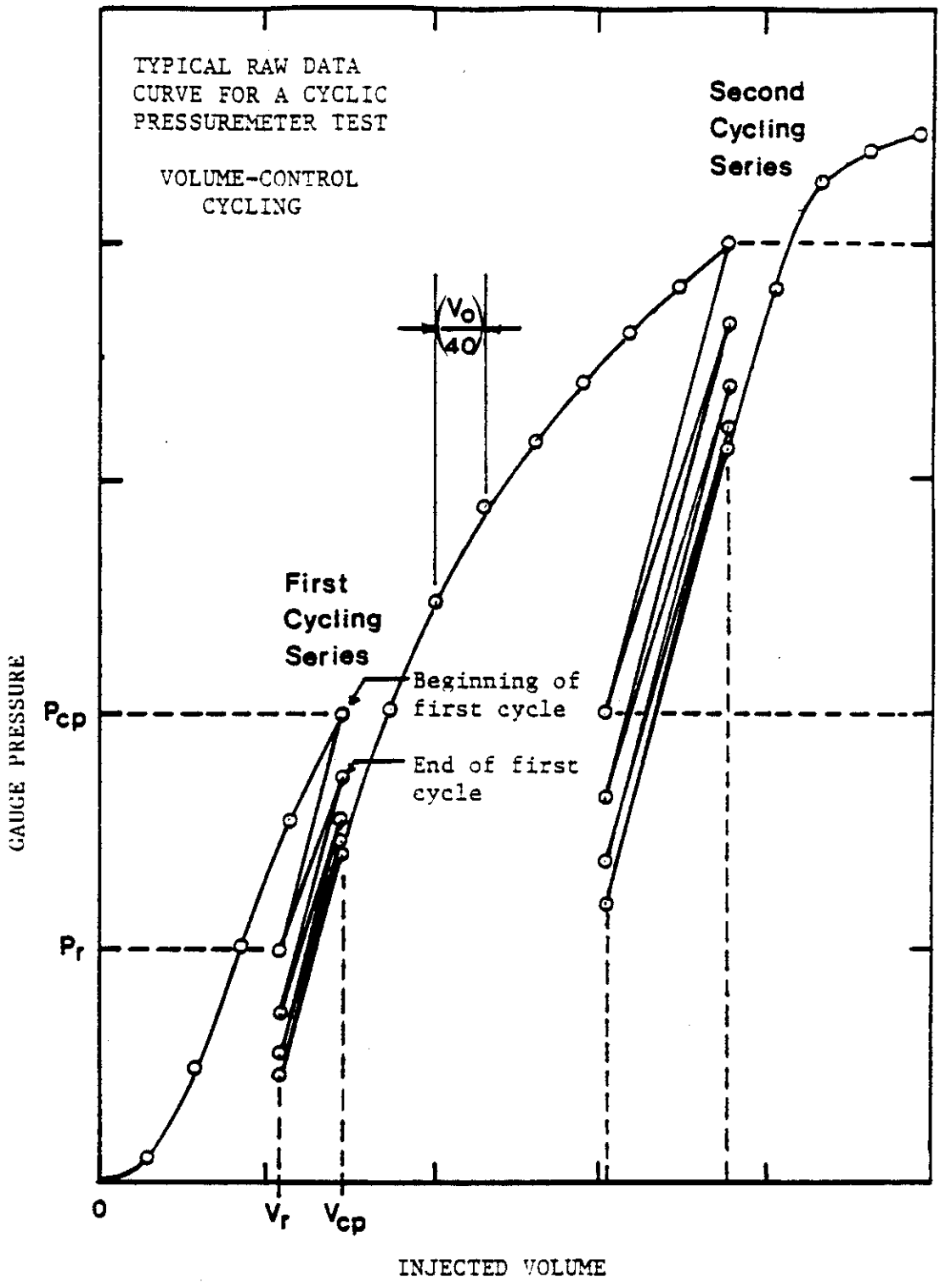

Figure 51. Steps in the Performance of a Cyclic Pressuremeter Test: Volume-control.

approximately half of the pressure P_{cp}. At the end of this 15-second interval, the pressure, P_r, and the volume, V_r, were noted (Figure 51). The probe was then reinflated to the volume V_{cp} and the new pressure was recorded after 15 seconds, concluding the first cycle. The probe was then deflated to a volume of V_r, beginning the next cycle. As many as 100 cycles were run in this manner between the volumes V_{cp} and V_r after which the probe inflation was continued in the standard manner until the next cycling level was achieved (Figure 51). The cycling process was then repeated between the new values of V_{cp} and V_r (Figure 51).

Pressure-control tests began in the same manner, incrementally advancing the injected volume until the desired pressure for the first cyclic series was achieved. As in the volume-control tests, the injected volume V_{cp} and the system pressure P_{cp} were recorded and the probe was deflated to P_r and V_r. At this point, however, the probe was reinflated until the pressure P_{cp} was regained and after maintaining the pressure P_{cp} for 15 seconds the new injected volume reading was recorded, concluding the first cycle (Figure 52). The probe was then deflated until the pressure had once again dropped to P_r (Figure 52). After the desired number of cycles had been run, the probe inflation was continued in the standard manner up to the next cycling level. The cycling process was then repeated between the new

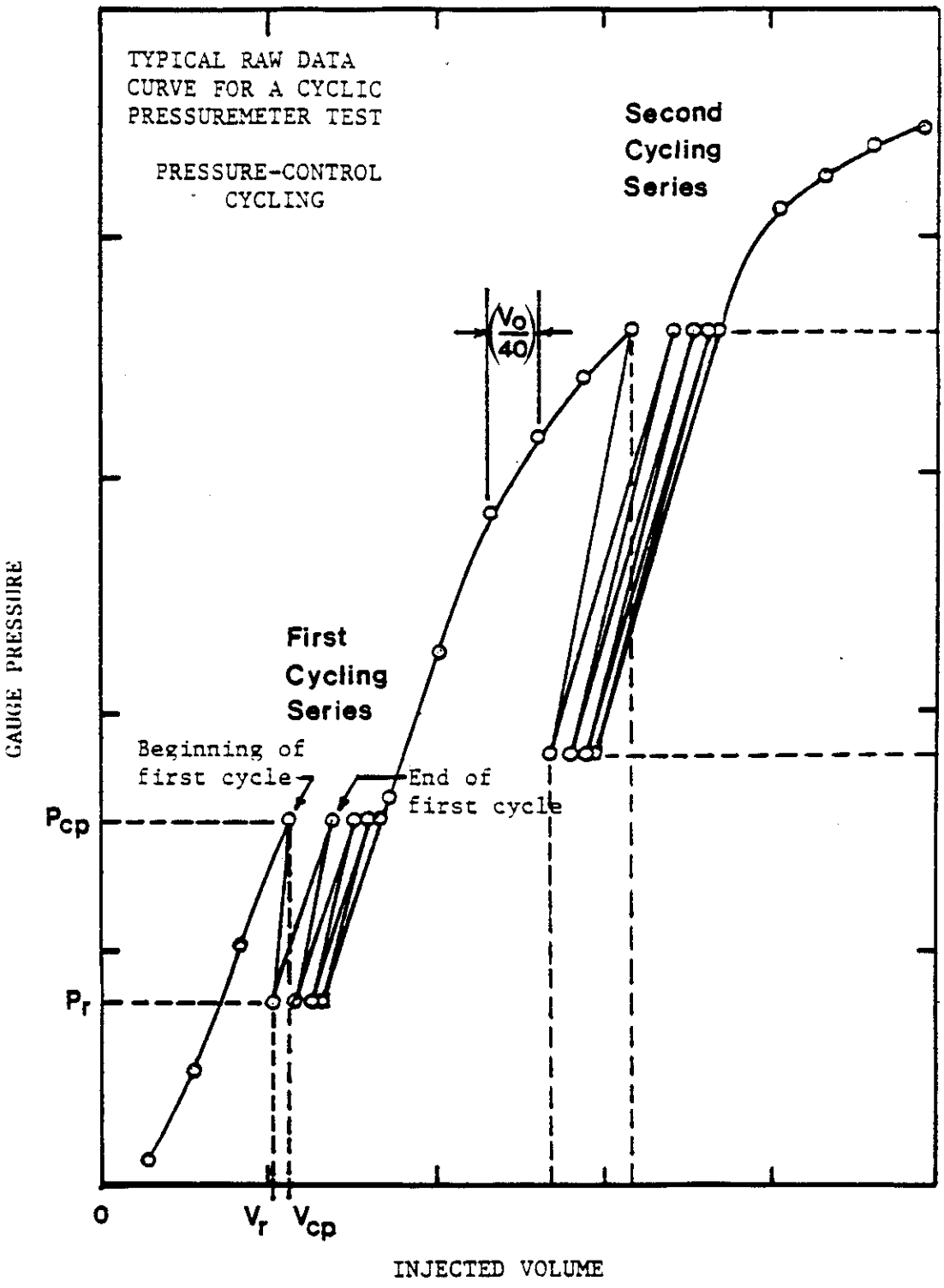

Figure 52. Steps in the Performance of a Cyclic Pressuremeter Test: Pressure-control.

values of P_{cp} and P_r (Figure 52).

After completing a test, the probe was removed from the borehole and cleaned to prevent a buildup of soil particles between the protective steel strips. The borehole was then advanced to the next test depth and the soil testing procedure repeated.

5.4 Cone Pressuremeter Test Procedure

Before beginning a series of pressuremeter tests, the control unit storage tank was filled with water. The probe was then connected to the unit through the flexible tubing and the entire system checked for saturation and leaks.

5.4.1 Necessary Monotonic Calibrations

The calibration procedures for the cone pressuremeter were identical to those for the TEXAM (Section 5.3.1). The steel calibration tube used in the cone pressuremeter calibration had an inside diameter of 33.4 mm.

5.4.2 Cyclic Degradation Calibrations

The cyclic degradation parameters for the cone pressuremeter volume and membrane resistance calibrations were found through testing procedures identical to those described for the TEXAM (Section 5.3.2). The cyclic volume calibration was negligible and so the monotonic volume calibration curve was used in the reduction of test data. The difference between the cyclic membrane resistance and the monotonic membrane resistance was significant, and so the cyclic membrane resistance was used in the reduction of

cyclic test data.

5.4.3 Soil Testing Procedures

The soil testing techniques for the cone pressuremeter were the same as those employed in the TEXAM tests except for the insertion method. In the field tests at the University of Houston Foundation Test Facility, the cone pressuremeter was either pushed into the soil at a constant rate of 0.1 ft/sec (Figure 53), or driven with a 28 lb hammer dropping approximately 4 feet, accelerated by hand, and hitting an anvil clamped to the cone rods (Figure 54). During the model pile tests in the drum at Texas A&M University, the probe was either driven to depth with a rawhide mallet or positioned at a predetermined depth in the test drum and the soil backfilled and compacted around the pile. This latter technique was chosen to simulate the conditions surrounding the 10.75 inch pile at the University of Houston. More specific details on this insertion technique will be given in Section 8.2.

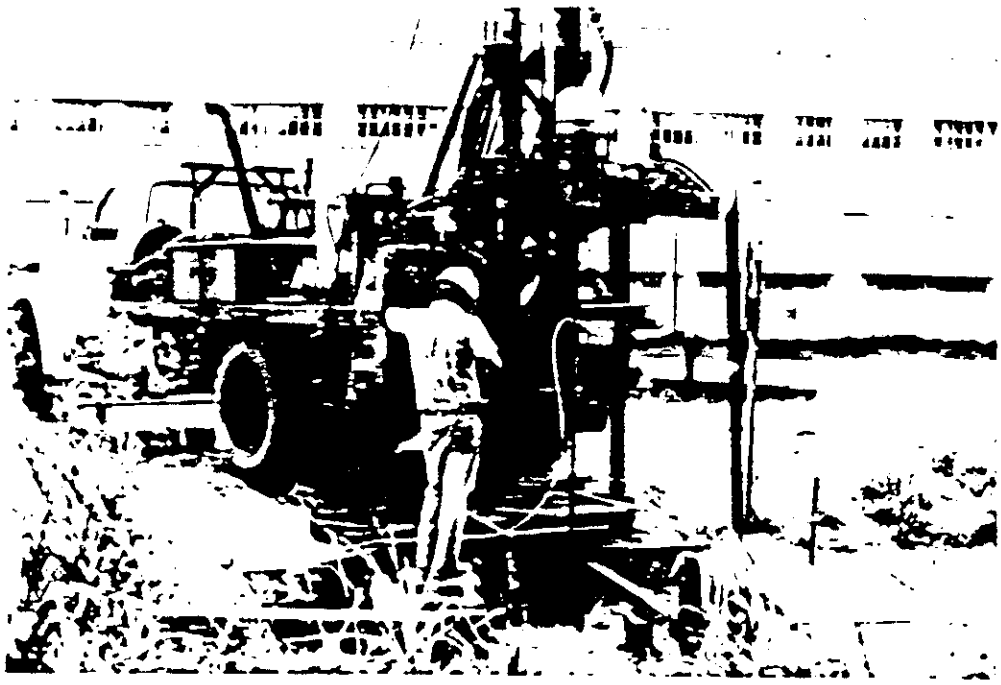

Figure 53. Pushed-in Insertion Method
for the Cone Pressuremeter.

Figure 54. Driven-in Insertion Method
for the Cone Pressuremeter.

6. PRESSUREMETER DATA REDUCTION TECHNIQUES

6.1 Initial Pressure Reading

Before each test, a pressure reading, P_i, is taken with the probe simply supported in the air at the same elevation as the pressure gages mounted on the control unit. This reading may not equal zero due to temperature variations during the testing period, gage error, or excess pressure necessary to inflate the probe cell to its "zero" calibration volume (Section 5.3.1). This initial pressure is not exerted on the soil cavity wall and thus must be subtracted from each raw pressure recorded during the test.

6.2 Hydrostatic Pressure

With the probe positioned at the test depth, a hydrostatic pressure exists within the inflatable cell. Due to this pressure, there is a difference between the pressure reading on the control unit and the pressure which exists in the probe. This pressure difference, P_h, is equal to the unit weight of the system fluid multiplied by the difference in elevation between the pressure gage and the cell. Since this pressure is not registered on the pressure gage, it must be added to each value recorded during the pressuremeter test.

6.3 Membrane Resistance

The membrane resistance calibration curve is a measure of the pressure necessary to inflate the probe in air. The

raw pressure from PMT test data at any given injected volume must be corrected by subtracting the membrane resistance pressure, P_c, corresponding to the same injected volume. The pressure P_c is necessary just to expand the probe and is not transfered to the soil cavity walls.

For cyclic tests, the membrane resistance degradation must also be considered (Figure 50). Following the degradation model presented in Section 2.2 (Idriss, et al., 1978), the formula for determining P_{cn} at a given value of injected volume and cycle number N may be presented as:

$$P_{cn} = P_c N^{-a} \qquad (2)$$

where

P_{cn} = membrane resistance pressure at N cycles

P_c = monotonic membrane resistance pressure

N = number of cycles at which the membrane resistance pressure is desired

a = membrane resistance degradation parameter.

For the TEXAM pressuremeter the a was 0.02, while for the cone pressuremeter the a was 0.03.

6.4 Compressibility

The volume calibration curve is a measure of the increase in volume of the unit-tubing-probe system when the pressure is increased but the probe is prevented from expanding by sliding it into a steel casing. Depending on the fit of the calibration casing, this curve may require adjustment to account for the probe's seating against the

casing wall. This is accomplished by translating the injected volume origin to coincide with the point of intersection between the injected volume axis and a projection from the calibation curve where contact with the casing wall is evident (Figure 55). Raw injected volume data from pressuremeter tests at any given pressure must be corrected by subtracting the adjusted volume calibration volume, V_c, corresponding to that same pressure. The volume V_c is not associated with the cell expansion. The degradation parameter for the volumetric increase was found to be negligible; therefore, no additional corrections were needed to adjust the raw pressuremeter data for the influence of cycling on the system compressibility.

6.5 Corrected Pressuremeter Curve

The complete correction process encompassing the factors described above may be mathematically expressed as follows:

$$P_{corr}(N) = P_{rn} - P_i + P_h - P_{cn} \qquad (3)$$

$$V_{corr}(N) = V_{rn} - V_{cn} \qquad (4)$$

where

$P_{corr}(N)$ = the pressure exerted on the soil cavity wall at N cycles

P_{rn} = the raw pressure read during the test at N cycles

P_i = the initial pressure reading with probe at gage height

P_h = the hydrostatic pressure correction = H x γ

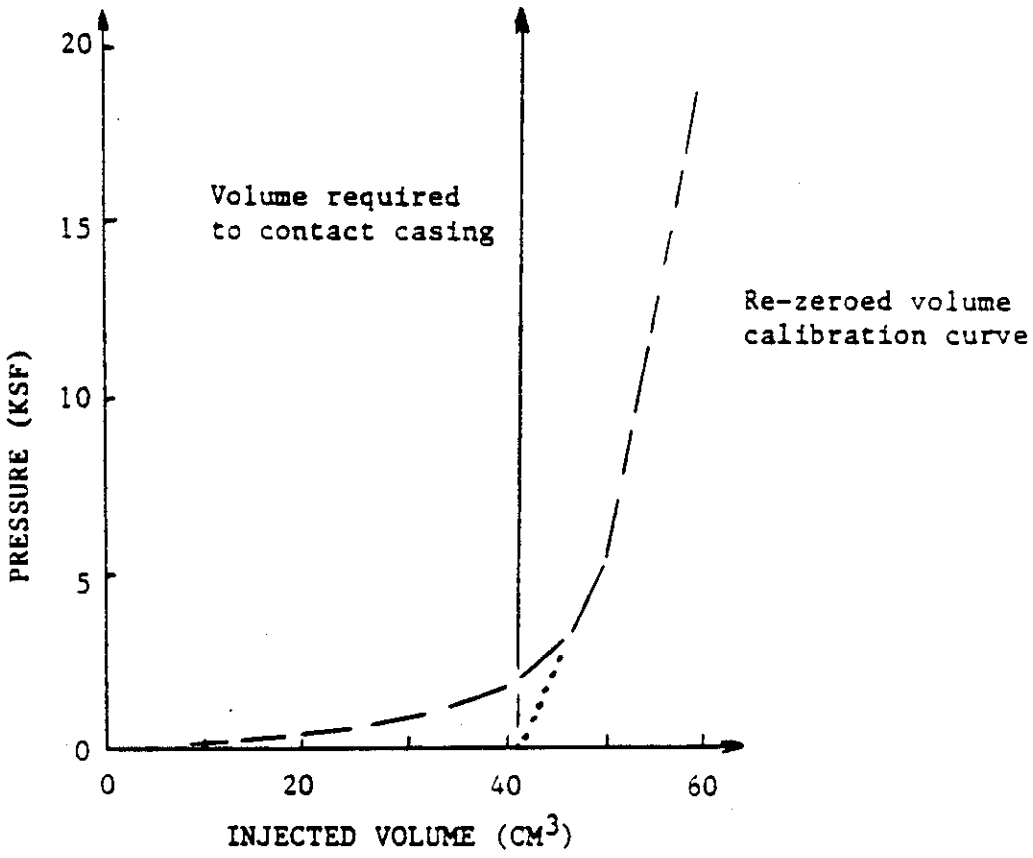

Figure 55. Adjusting the Volume Calibration Curve for Casing Size.

H = the difference between the gage elevation and the elevation at the center of the inflatable cell (test elevation)

γ = the unit weight of the system fluid

P_{cn} = membrane resistance calibration pressure at N cycles (equation 2)

N = number of cycles

a = membrane resistance cyclic degradation parameter

$V_{corr}(N)$ = the corrected injected volume at N cycles

V_{rn} = the raw injected volume read during the test at N cycles

V_{cn} = the adjusted volume calibration value associated with a pressure of $P_{corr}(N)$.

In order to normalize the final corrected pressuremeter curves, the corrected injected volume values are used to derive the relative increases in the probe cell radius. This is achieved by assuming that the cell behaves as a cylinder expanding radially, such that:

$$\left(\frac{\Delta R}{Ro}\right) = \frac{\sqrt{Vo + \Delta V} - \sqrt{Vo}}{\sqrt{Vo}} \qquad (5)$$

where

ΔR = the increase in the probe radius

Ro = the deflated probe radius

ΔV = the corrected injected volume (increase in probe volume)

Vo = the deflated probe volume.

Thus in the final form, the corrected pressuremeter curves are presented as in Figure 56, with the corrected pressure

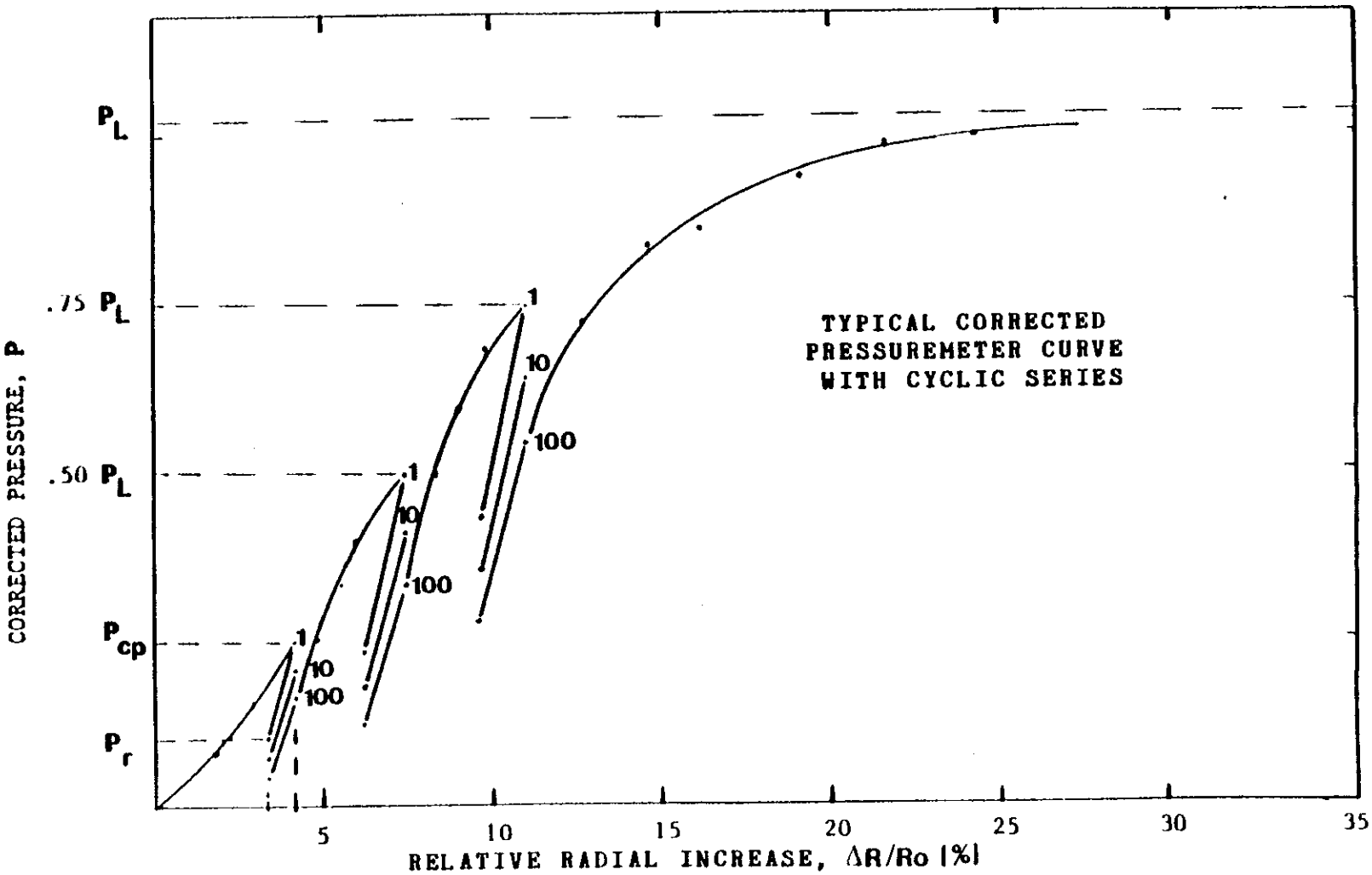

Figure 56. Typical Corrected Pressuremeter Curve with Cyclic Series.

against the borehole wall, P, along the vertical axis and the increase in probe radius divided by the deflated probe radius, $\Delta R/R_o$ (%), along the horizontal axis.

PRESRED, a microcomputer program written by L.M. Tucker (1986) to reduce monotonic pressuremeter test data, was modified to allow it to handle cyclic pressuremeter test data and used to reduce the pressuremeter data collected during this project. It should be noted that the corrected curves presented in this report do not incorporate the initial reading correction (P_i); however, this correction was performed before prediction procedures were employed.

6.6 Pressuremeter Parameters

The pressuremeter first load modulus, E_p, is calculated from Baguelin, et. al., (1978):

$$E_p = \frac{(1+\nu)\left[\left(1+\left(\frac{\Delta R}{Ro}\right)_2\right)^2+\left(1+\left(\frac{\Delta R}{Ro}\right)_1\right)^2\right](P_2-P_1)}{\left[\left(1+\left(\frac{\Delta R}{Ro}\right)_2\right)^2-\left(1+\left(\frac{\Delta R}{Ro}\right)_1\right)^2\right]} \qquad (6)$$

where ν = Poisson's ratio of the soil and is usually assumed to be 0.33. All other parameters are defined on Figure 57. The values of $(P_1,(\Delta R/Ro)_1)$ and $(P_2,(\Delta R/Ro)_2)$ are taken from the steepest initial linear portion of the corrected pressuremeter curve (Figure 57).

The pressuremeter reload modulus, E_r, is calculated using the formula:

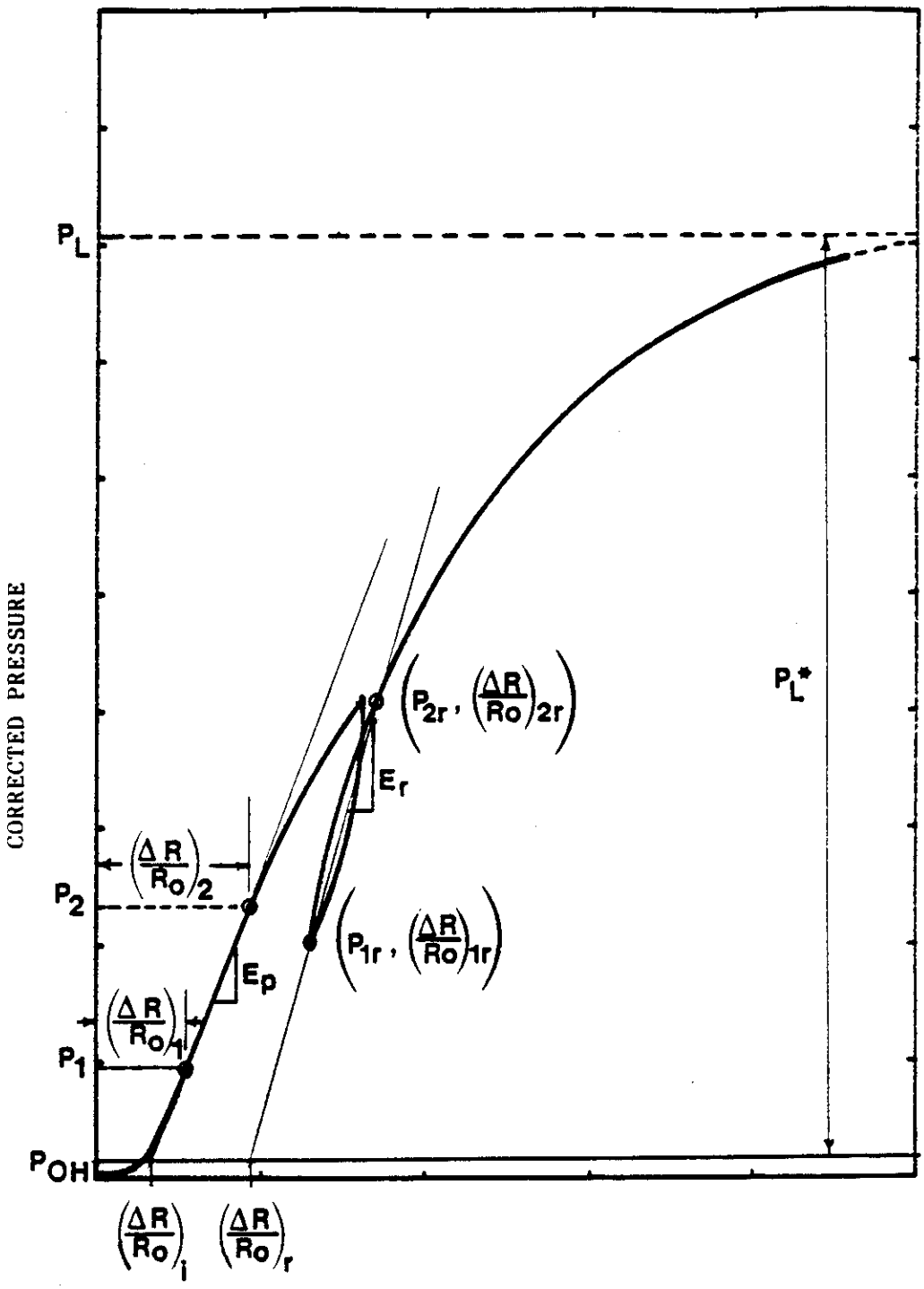

Figure 57. Pressuremeter Parameters Definition.

$$E_r = \frac{(1+\nu)\left[\left(1+\left(\frac{\Delta R}{Ro}\right)_{2r}\right)^2 + \left(1+\left(\frac{\Delta R}{Ro}\right)_{1r}\right)^2\right](P_{2r}-P_{1r})}{\left[\left(1+\left(\frac{\Delta R}{Ro}\right)_{2r}\right)^2 - \left(1+\left(\frac{\Delta R}{Ro}\right)_{1r}\right)^2\right]} \quad (7)$$

with $(P_{1r},(\Delta R/Ro)_{1r})$ and $(P_{2r},(\Delta R/Ro)_{2r})$ being the two data points on the reload portion of the pressuremeter test (Figure 57).

The horizontal earth pressure at rest, P_{OH}, is assumed to be the pressure coinciding with the point of maximum inflection on the corrected pressuremeter curve's initial portion (Figure 57).

With the pressuremeter modulus and horizontal earth pressure at rest determined, the initial borehole radius may be defined as the $(\Delta R/Ro)$ value coinciding with the intersection of the pressure P_{OH} value and a projection of the pressuremeter first load modulus line (Figure 57). The relative increase in radius necessary for the probe to seat against the borehole wall is thus denoted by $(\Delta R/Ro)_i$. For the reload curve, a similar initial reload borehole radius may be found by projecting the reload modulus to intersect P_{OH} at a relative displacement of $(\Delta R/Ro)_{ir}$.

The limit pressure, P_L, is defined as the pressure necessary to expand the volume of the soil cavity to twice its original value. This pressure corresponds to an increase in the probe radius equal to $0.41 + 1.41\ (\Delta R/Ro)_i$. Most often this requires manual extrapolation of the curve

to that level of expansion (Figure 57). The net limit pressure, P_L^*, is the difference between the limit pressure and the at rest horizontal earth pressure:

$$P_L^* = P_L - P_{OH} \tag{8}$$

From the solution of the expansion of an infinitely long cylinder in an elastic homogeneous full space, Baguelin, et al. (1978) determined that the secant shear modulus, Gs(N) for the N^{th} cycle may be calculated as follows (Figure 58):

$$Gs(N) = \left(\frac{P_{cp}}{2}\right)\left[\frac{\left(1 + \left(\frac{\Delta R_T(N)}{Ro}\right)\right)^2 + \left(1 + \left(\frac{\Delta R}{Ro}\right)_i\right)^2}{\left(1 + \left(\frac{\Delta R_T(N)}{Ro}\right)\right)^2 - \left(1 + \left(\frac{\Delta R}{Ro}\right)_i\right)^2}\right] \tag{9}$$

where

P_{cp} = peak cyclic pressure

Ro = deflated probe radius

$\left(\frac{\Delta R}{Ro}\right)_i$ = relative increase in probe radius necessary for seating against the cavity walls (Figure 57)

$\left(\frac{\Delta R_T(N)}{Ro}\right)$ = relative increase in probe radius corresponding to the peak of the Nth cycle (Figure 58)

N = number of cycles at which the secant shear modulus is desired (note that the number of cycles is counted as shown on Figure 58).

The degradation model used in this study is (Idriss, et al., 1978):

$$Gs(N) = Gs(1) \times N^{-a} \tag{10}$$

where

Gs(N) = secant shear modulus at the N^{th} cycle

Gs(1) = secant shear modulus at the first cycle

N = number of cycles

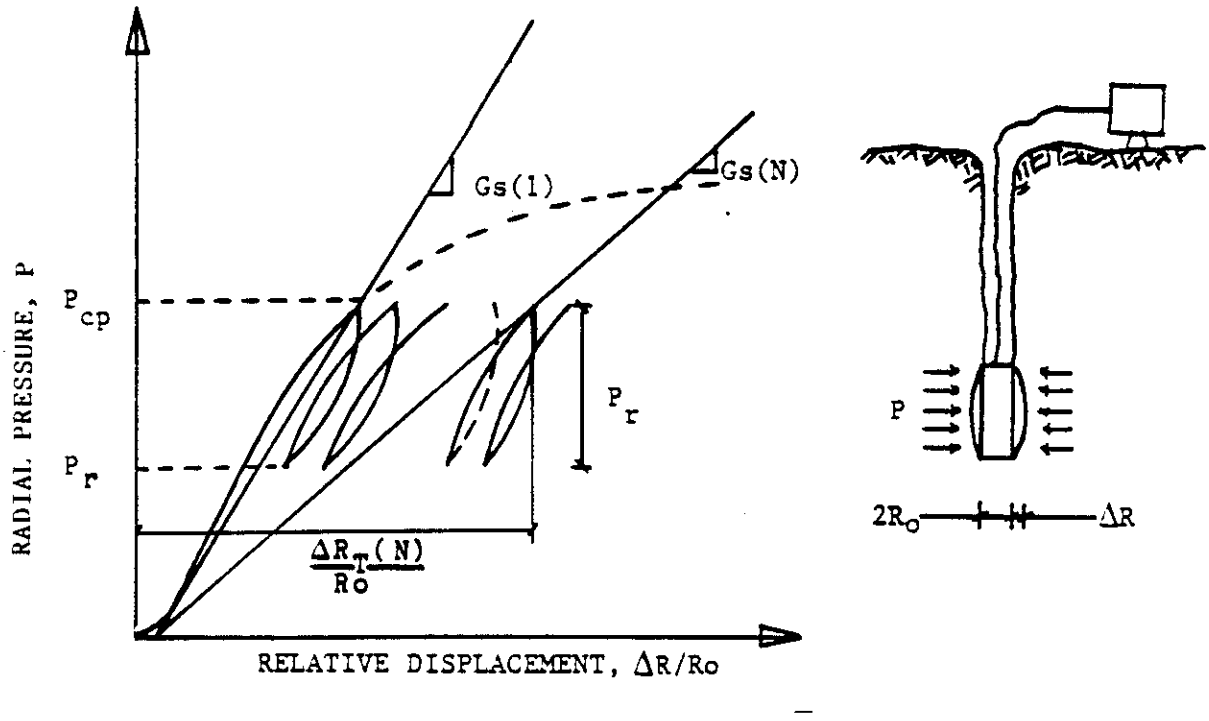

Figure 58. Definition of the Secant Shear Modulus.

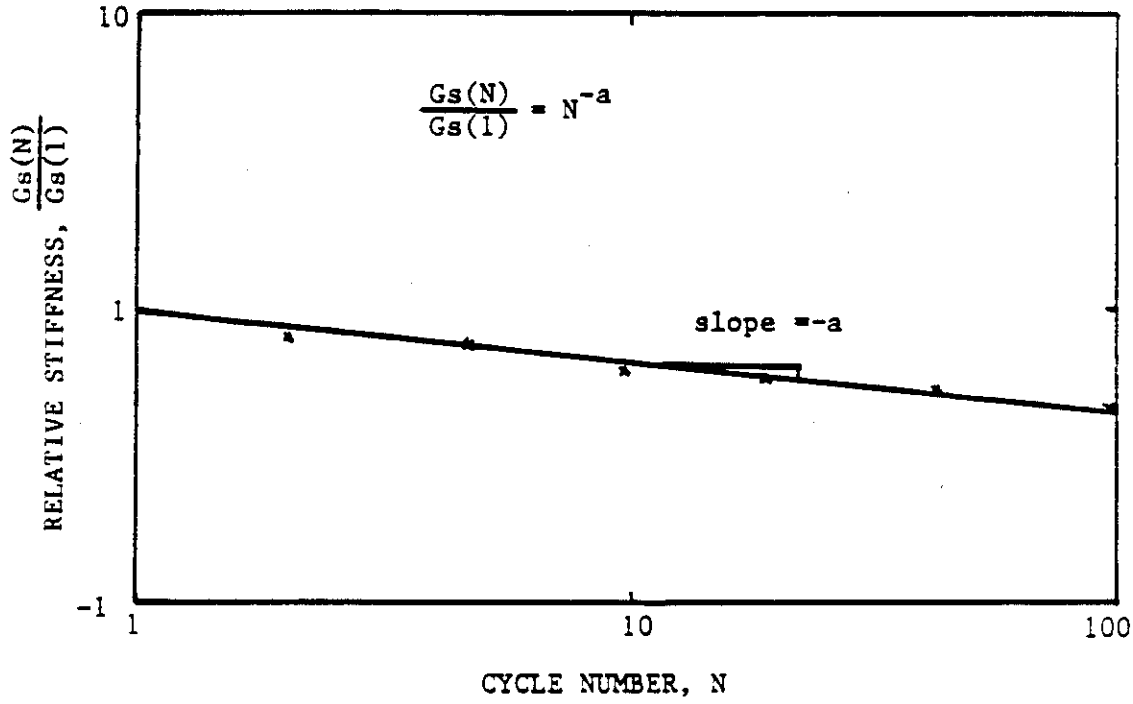

Figure 59. Definition of the Cyclic Degradation Parameter for the Secant Shear Modulus.

a = cyclic degradation parameter for the secant shear modulus.

The degradation parameter a for a particular series of cycles is equal to the negative slope of the best fit line from the plot of log (Gs(N)/Gs(1)) versus log N (Figure 59).

The cyclic shear modulus, Gc(N), for the N^{th} cycle may be calculated from pressuremeter tests as follows (Figure 60):

$$Gc(N) = \left(\frac{P_r}{2}\right)\left[\frac{\left(1+\left(\frac{\Delta R_T(N)}{Ro}\right)\right)^2 + \left(1+\left(\frac{\Delta R_B(N)}{Ro}\right)\right)^2}{\left(1+\left(\frac{\Delta R_T(N)}{Ro}\right)\right)^2 - \left(1+\left(\frac{\Delta R_B(N)}{Ro}\right)\right)^2}\right] \qquad (11)$$

where

P_r = cyclic pressure variation

Ro = deflated probe radius

$\left(\frac{\Delta R_T(N)}{Ro}\right)$ = relative increase in probe radius corresponding to the peak of the Nth cycle (Figure 60).

$\left(\frac{\Delta R_B(N)}{Ro}\right)$ = relative increase in probe radius corresponding to the bottom of the Nth cycle (Figure 60).

N = number of cycles at which the cyclic shear modulus is desired (note that the number of cycles is counted as shown on Figure 60).

Using the same degradation model (Idriss, et al., 1978) as for the secant shear modulus degradation:

$$Gc(N) = Gc(1) \times N^{-b} \qquad (12)$$

where

Gc(N) = cyclic shear modulus at the N^{th} cycle

Gc(1) = cyclic shear modulus at the first cycle

N = number of cycles

b = cyclic degradation parameter for the cyclic shear modulus.

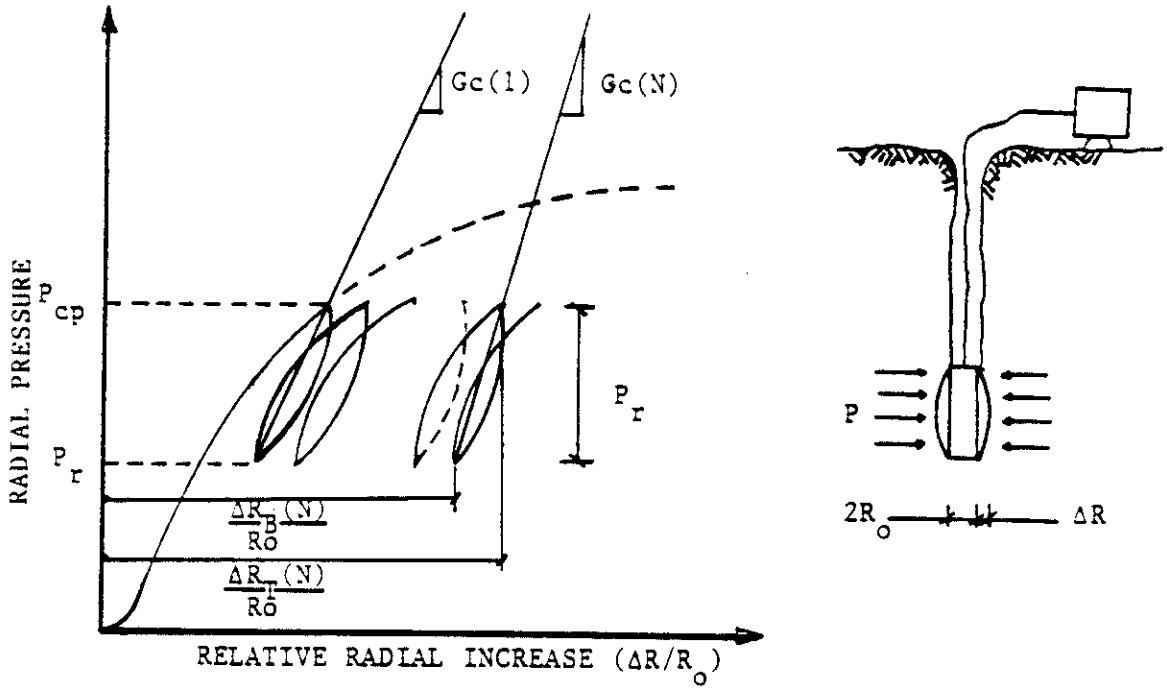

Figure 60. Definition of the Cyclic Shear Modulus.

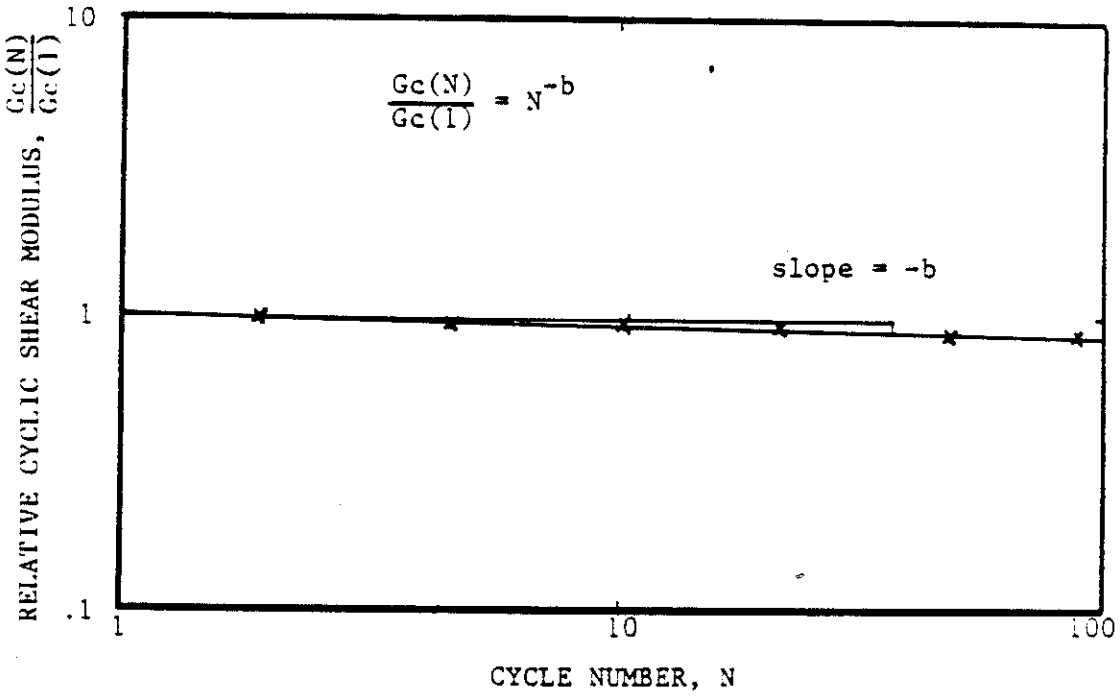

Figure 61. Definition of the Cyclic Degradation Parameter for the Cyclic Shear Modulus.

The degradation parameter $\underline{b}$ for a particular series of cycles is equal to the negative slope of the best fit line from the plot of log (Gc(N)/Gc(1)) versus log N (Figure 61).

The degradation of the cyclic shear modulus was not employed in the prediction methods used in this report. However, the plots of log (Gc(N)/Gc(1)) versus log N for the pressuremeter tests conducted during this project are presented in Appendix B.

7. PRESSUREMETER TESTS AT THE UNIVERSITY OF HOUSTON FOUNDATION TEST FACILITY SAND SITE

7.1 Test Locations, Insertion Techniques, and Pressuremeter Types

In the spring of 1985, eleven pressuremeter tests were conducted at the University of Houston Foundation Test Facility in the sand deposit surrounding the single 10.75 inch test pile. The locations, insertion techniques, and pressuremeter types are detailed in Table 4 and Figure 62.

A variety of pressuremeter insertion methods were used to study the effect of the insertion technique on the soil response. The pre-bored insertion technique was used with the TEXAM pressuremeter system. The TEXAM probe had a diameter of 5.8 cm and an inflatable length of 40 cm. The boreholes were prepared with a hand auger while pumping drilling mud vertically through the bit. The pushed pressuremeter tests were performed with the cone pressuremeter (CPMT) system. The CPMT probe had a diameter of 3.2 cm and an inflatable length of 23 cm. The probe was advanced to the test depth at a rate of 0.1 feet per second by a drilling rig (Figure 53). The driven insertion technique also employed the cone pressuremeter, driven to the test depth using a 28 lb hammer with a fall of approximately 4.0 feet, accelerated by hand, and striking an anvil clamped to the cone rods above the probe (Figure 54).

Borehole Number	Insertion Method	Pressuremeter Type	Date
T3	Pre-bored	PBPMT / TEXAM PMT	4 / 85
T4	Pre-bored	PBPMT / TEXAM PMT	4 / 85
P2	Pushed-in	PCPMT / Cone PMT	5 / 85
D1	Driven-in	DCPMT / Cone PMT	5 / 85
D3	Driven-in	DCPMT / Cone PMT	5 / 85

Table 4. Pressuremeter Tests Performed at the University of Houston Foundation Test Facility Sand Site.

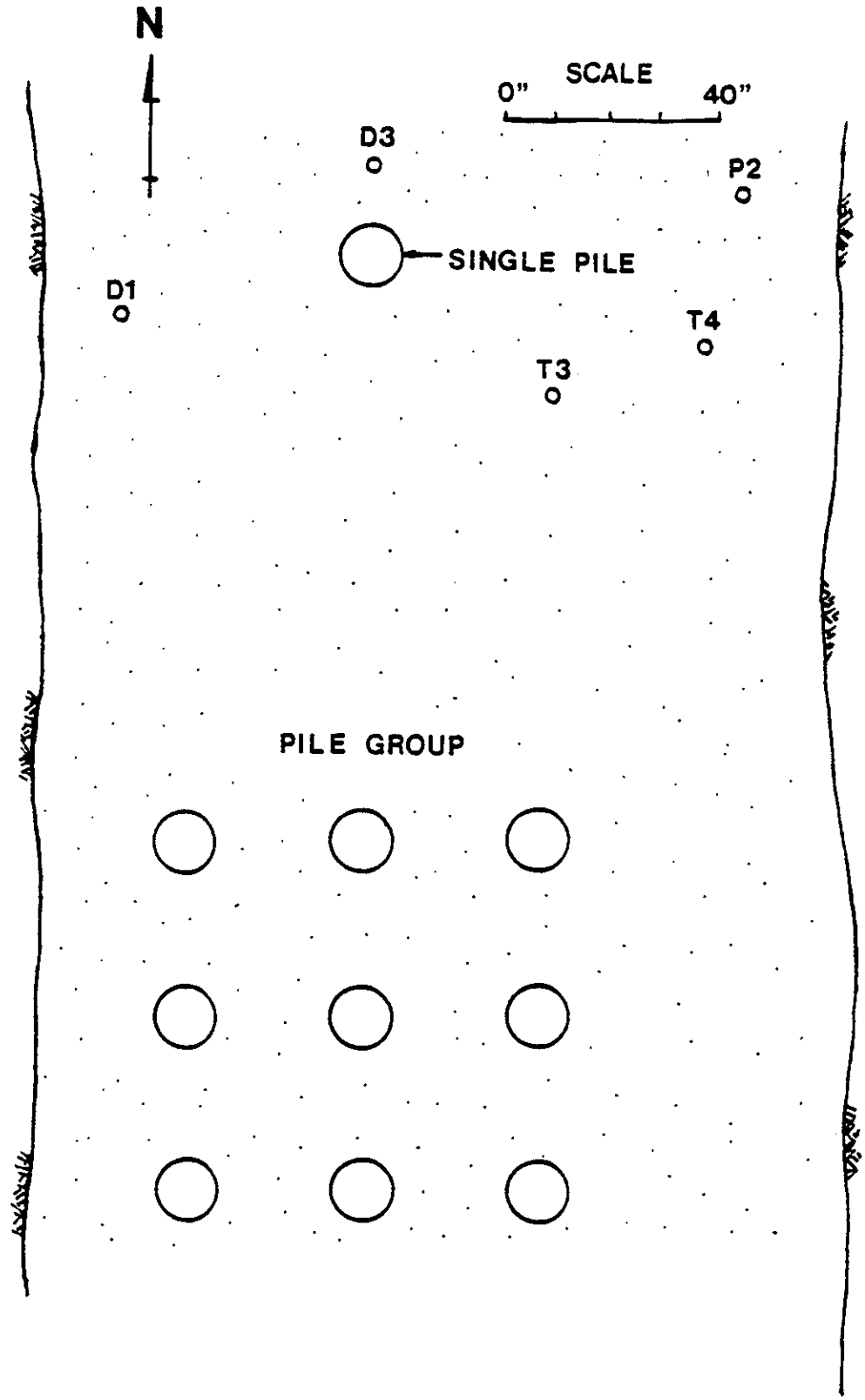

Figure 62. Pressuremeter Tests in The University of Houston Foundation Test Facility Sand Site.

7.2 Pressuremeter Moduli and Net Limit Pressure Profiles

Profiles of the pressuremeter first load modulus, pressuremeter reload modulus, and the net limit pressure are presented in Figures 63, 64, and 65. These values are also tabulated in Table 5. The stiffer response of the driven pressuremeter as well as its higher net limit pressure may be indicative of the local densification that occurred during driving. Visual evidence of the densification was provided by a cone of depression that formed around the cone rods as driving proceeded (Figure 66).

7.3 Pre-bored TEXAM Pressuremeter (PBPMT) Results

7.3.1 Corrected Pressuremeter Curves

The raw pressuremeter test data was reduced as described in Section 6. The resulting corrected pressuremeter curves, borehole pressure versus relative increase in probe radius, are presented in Figures 67 through 70. Volume-control cycling was performed to simulate the displacement-control pile load tests. In borehole T4, however, both volume-control and pressure-control cycles were performed within each cycling series.

Three sets of 100 cycles were performed at depths of 2.0 and 4.5 feet. During the test at 7.5 feet an initial series of 10 cycles was followed by a series of 100 cycles performed at a pressure level below the maximum pressures that had already been applied to the soil cavity. Additionally, a 50-minute relaxation test was performed at a y/R

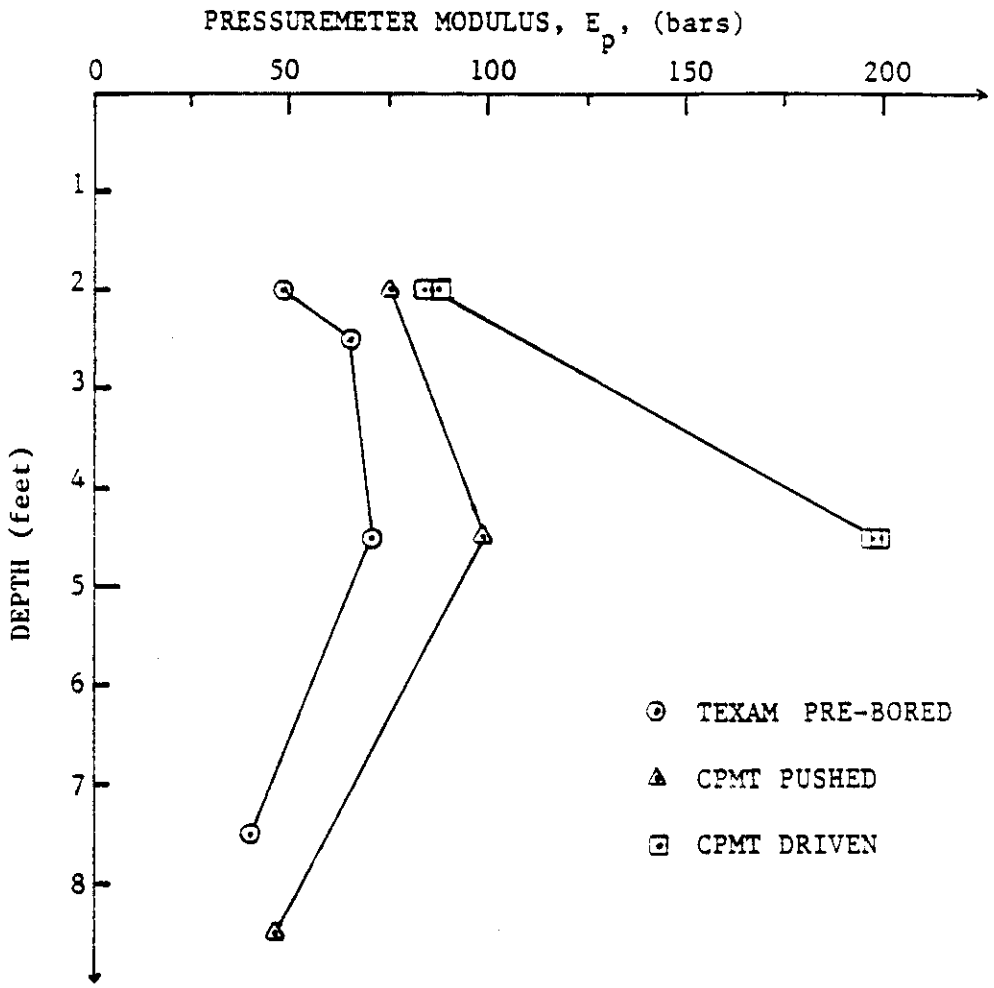

Figure 63. Pressuremeter First Load Modulus versus Depth.

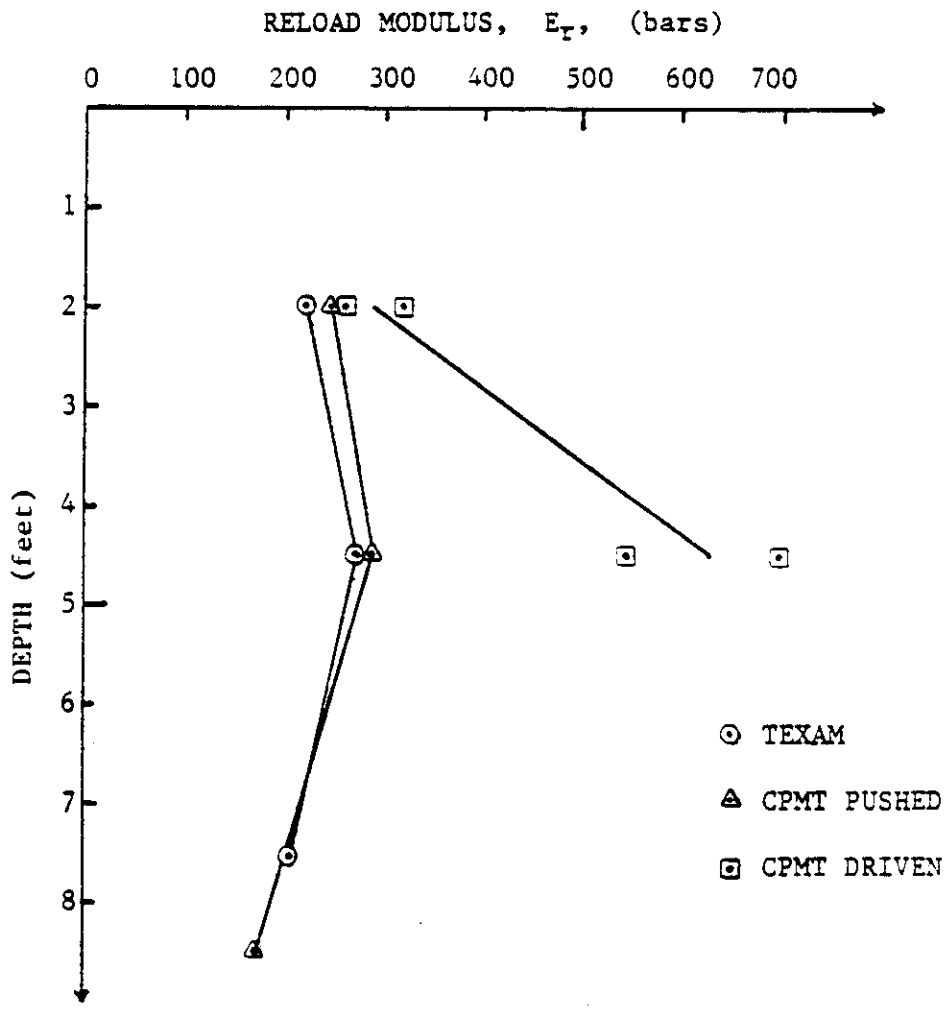

Figure 64. Pressuremeter Reload Modulus versus Depth.

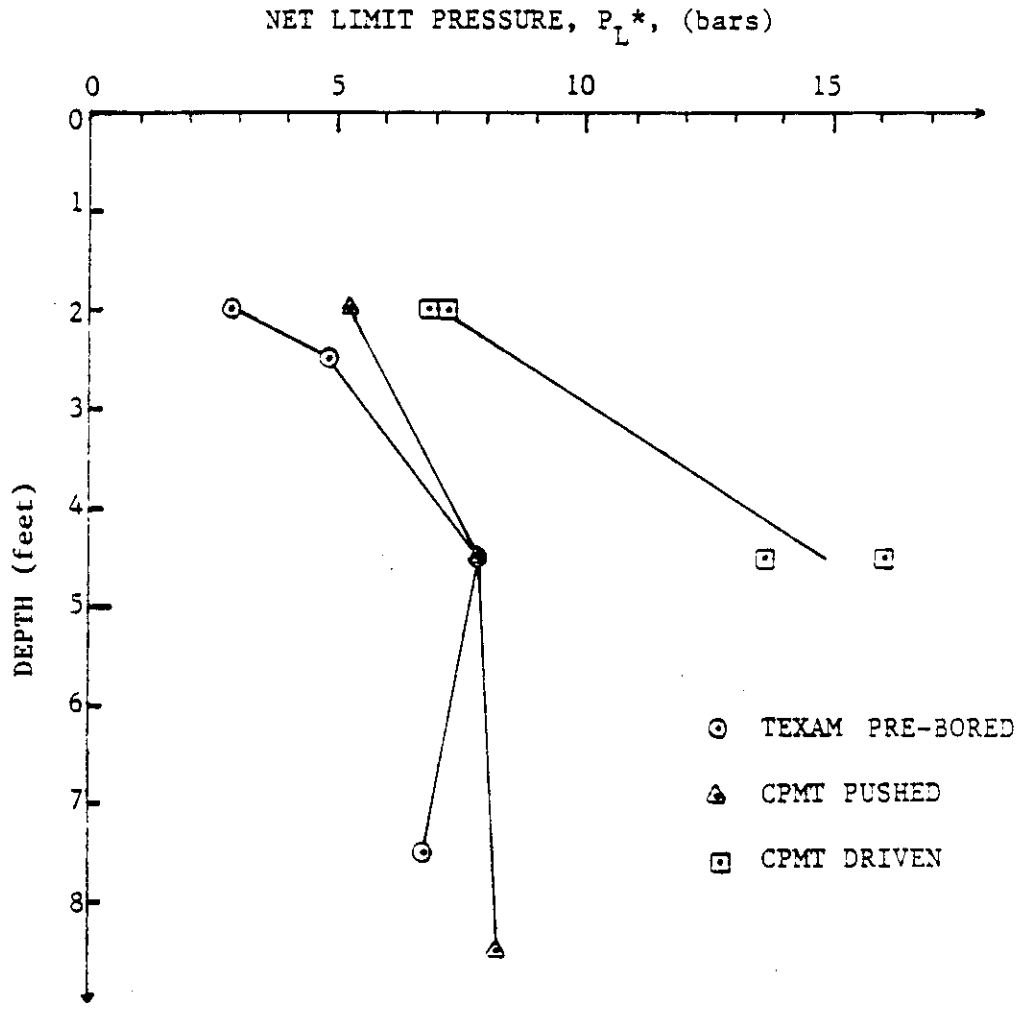

Figure 65. Pressuremeter Net Limit Pressure versus Depth.

Bore-hole	PMT Type	Depth (feet)	E_p (bars)	E_r (bars)	P_L^* (bars)
T3	PBPMT Pre-bored	2.0	49.1	219.4	2.91
		4.5	71.5	272.7	7.90
		7.5	40.3	205.7	6.84
T4	PBPMT Pre-bored	2.5	66.1	462.1	4.91
P2	PCPMT Pushed-in	2.0	75.6	249.4	5.29
		4.5	99.6	286.8	7.90
		8.5	47.2	170.2	8.31
D1	DCPMT Driven-in	2.0	84.3	318.7	7.29
		4.5	199.6	543.2	13.70
D3	DCPMT Driven-in	2.0	87.4	259.3	6.91
		4.5	198.3	696.8	16.10

Table 5. Pressuremeter Moduli and Net Limit Pressure with Depth from Tests at the University of Houston Foundation Test Facility Sand Site.

Figure 66. Cone of Depression Around Driven Cone Pressuremeter Test.

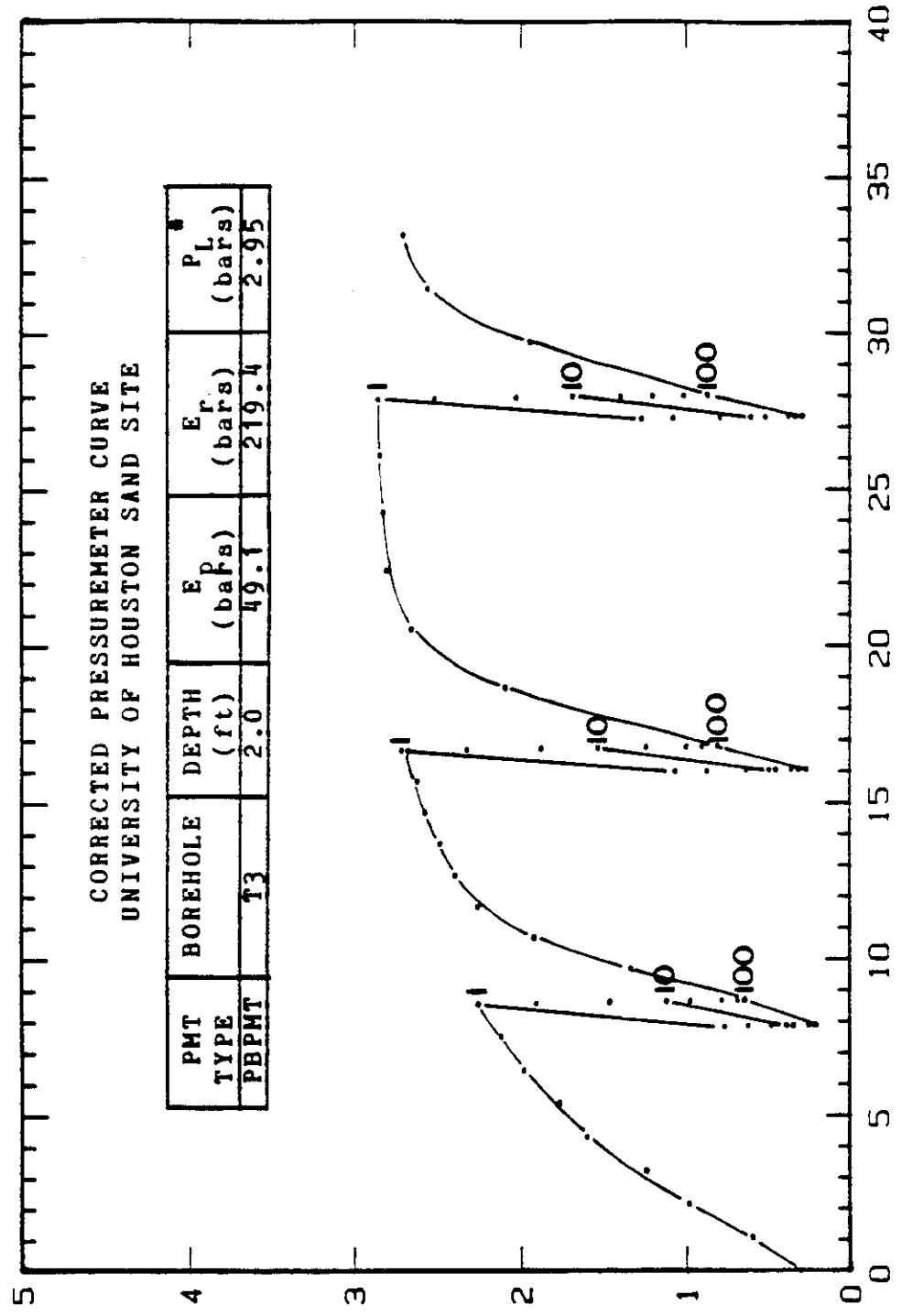

Figure 67. Pre-bored TEXAM Corrected Pressuremeter Curve, Borehole T3, 2.0 feet.

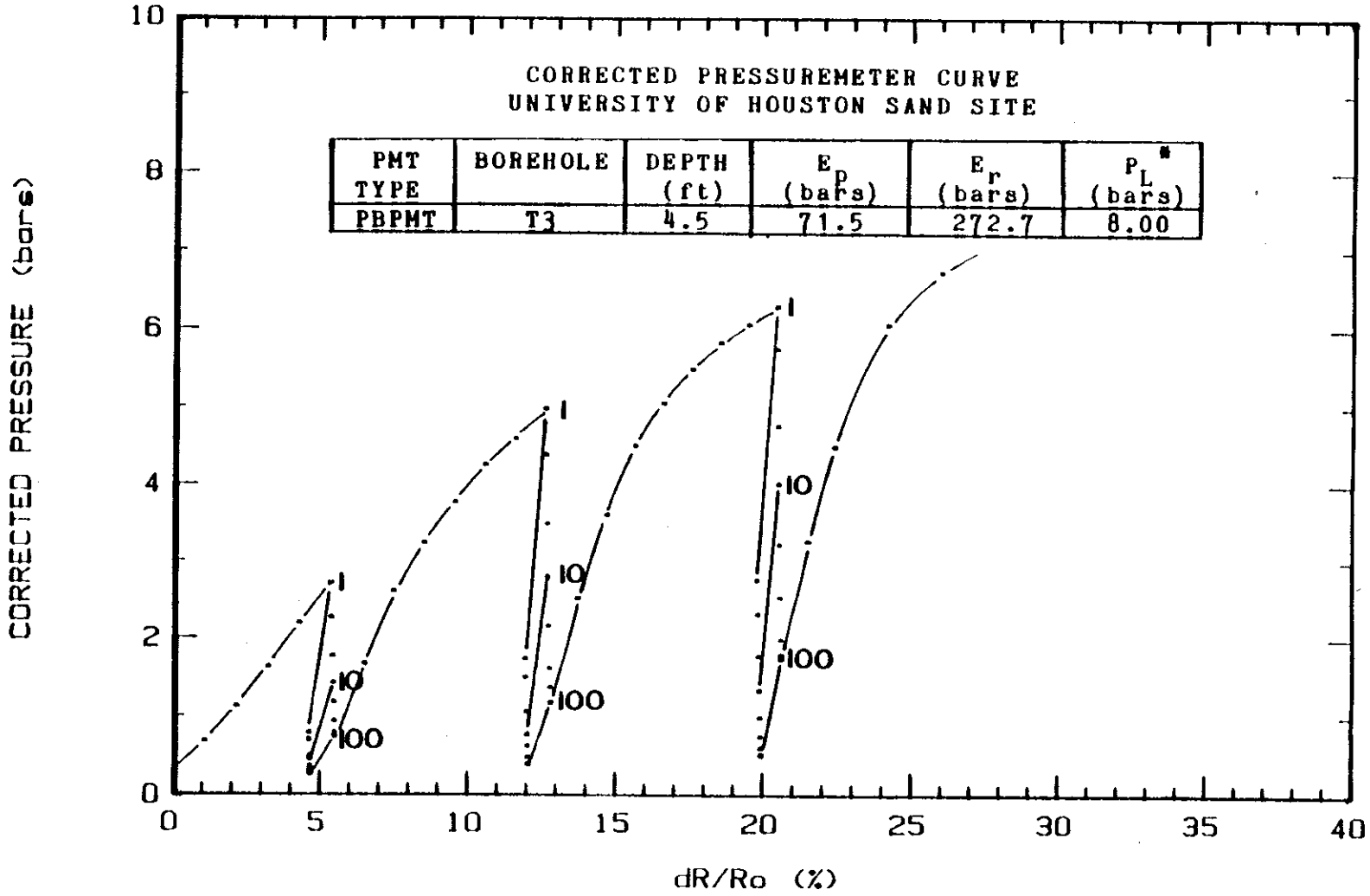

Figure 68. Pre-bored TEXAM Corrected Pressuremeter Curve, Borehole T3, 4.5 feet.

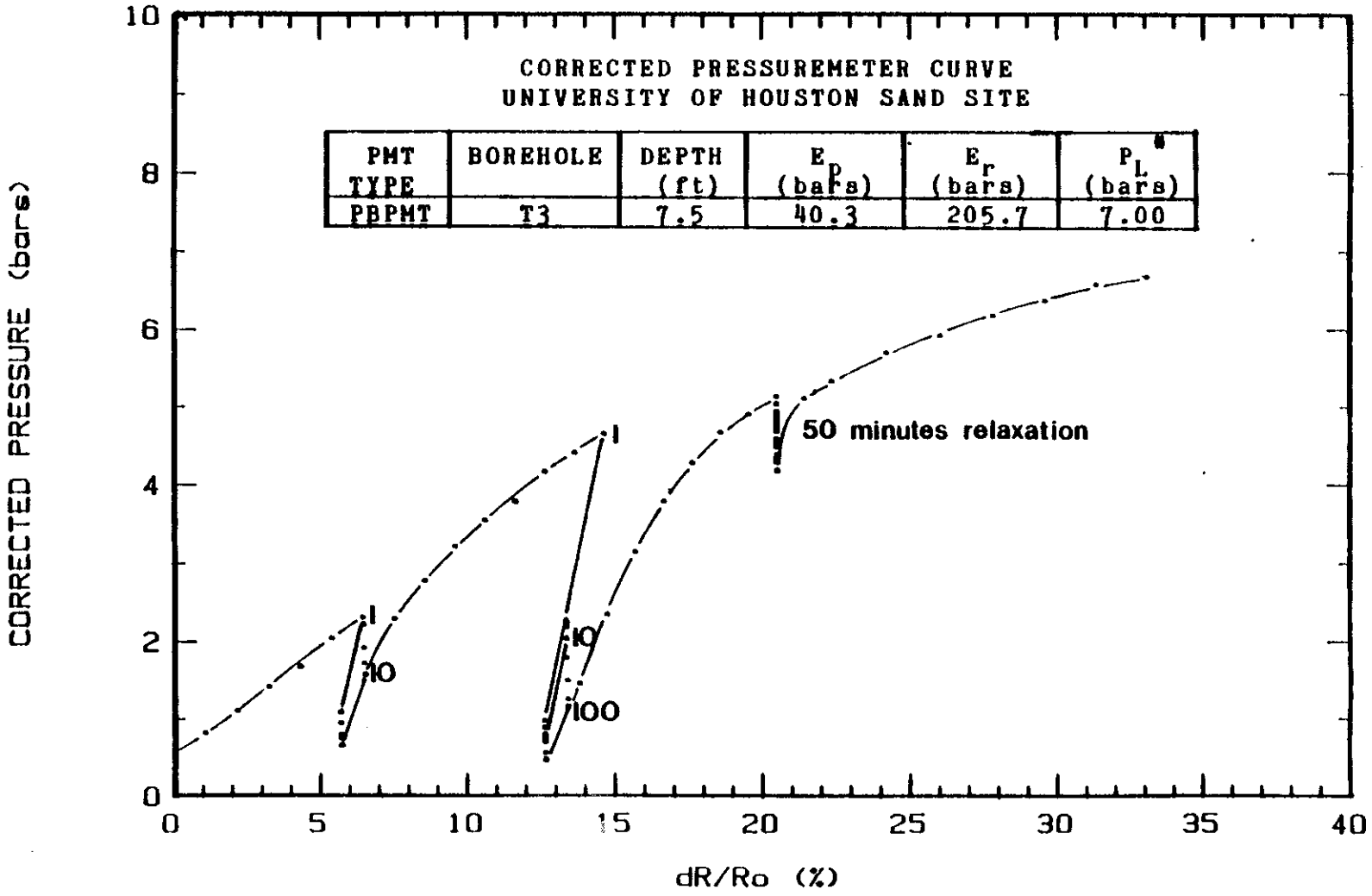

Figure 69. Pre-bored TEXAM Corrected Pressuremeter Curve, Borehole T3, 7.5 feet.

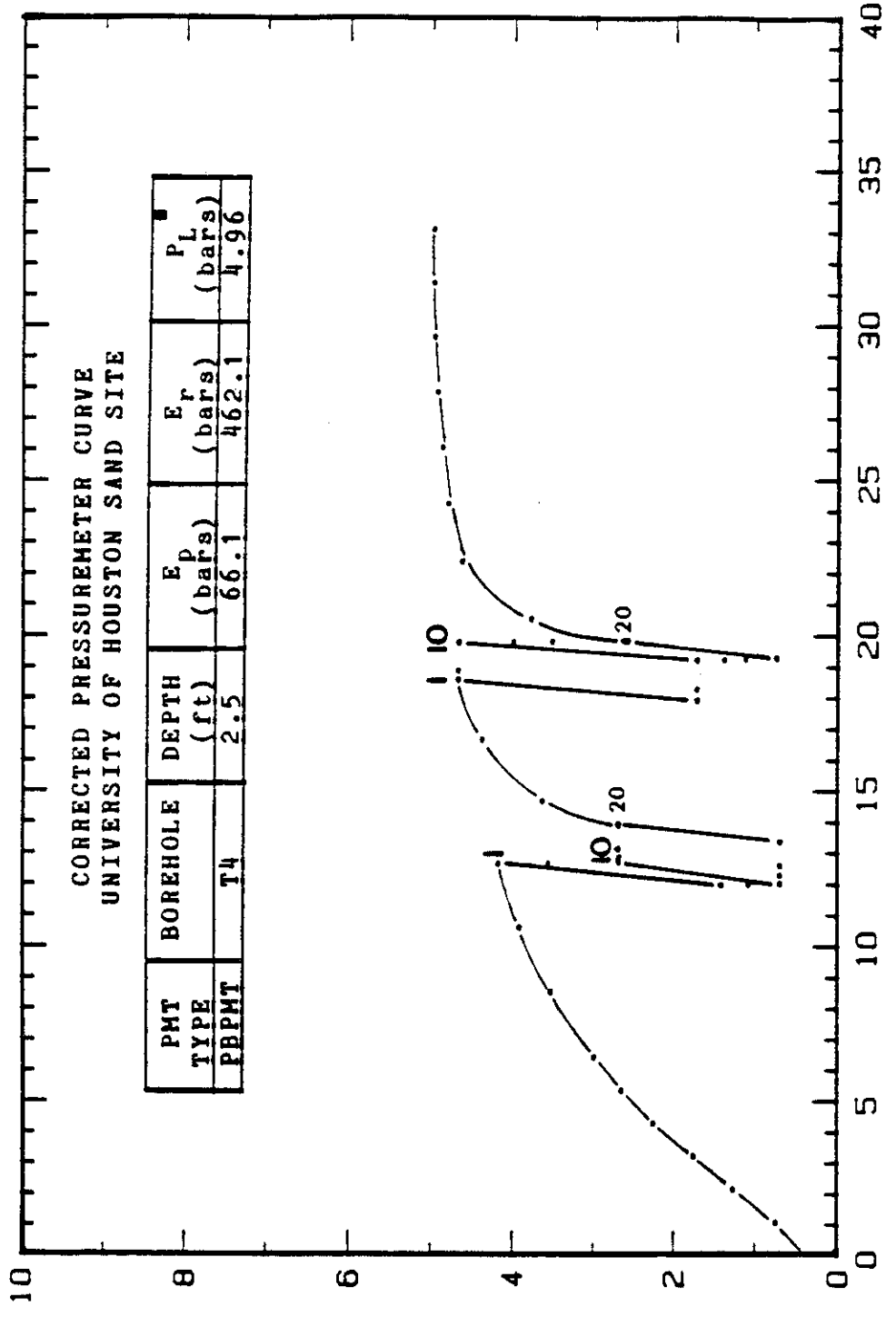

Figure 70. Pre-bored TEXAM Corrected Pressuremeter Curve, Borehole T4, 2.5 feet.

ratio of 20.5 %. Ten volume-control cycles followed by ten pressure-control cycles were conducted within one cyclic series of the pre-bored pressuremeter test at a depth of 2.5 feet. Also performed in that test was a cyclic series of ten pressure-control cycles followed by ten volume-control cycles to reveal the relative effect on the cyclic degradation parameters (Figure 70).

7.3.2 Cyclic Degradation Parameters

Figures 71 through 74 track the decrease in the secant shear modulus with increasing cycles for each pressuremeter test. The ratio of the peak cyclic pressure over the net limit pressure (P_{cp}/P_L^*) and the ratio of the increase in probe radius over the deflated probe radius (y/R) at which the cyclic test series were performed are indicated on the figures. Also shown on the figures are the values of the cyclic degradation parameter a, which is the negative slope of the regression line through each cyclic series.

Figure 73 indicates that for the second series of cycles, the preloading generated by applying a pressure higher than the pressure level at which the cycles were performed (Figure 69) lead to temporary smaller degradation. For the first ten cycles (Figure 73) the a value is very small; however, the beneficial effect of the preloading seems to disappear after 10 cycles and the a value increases. This, however, may be due in part to the fact that the bottom of the volume-control cycles became too low

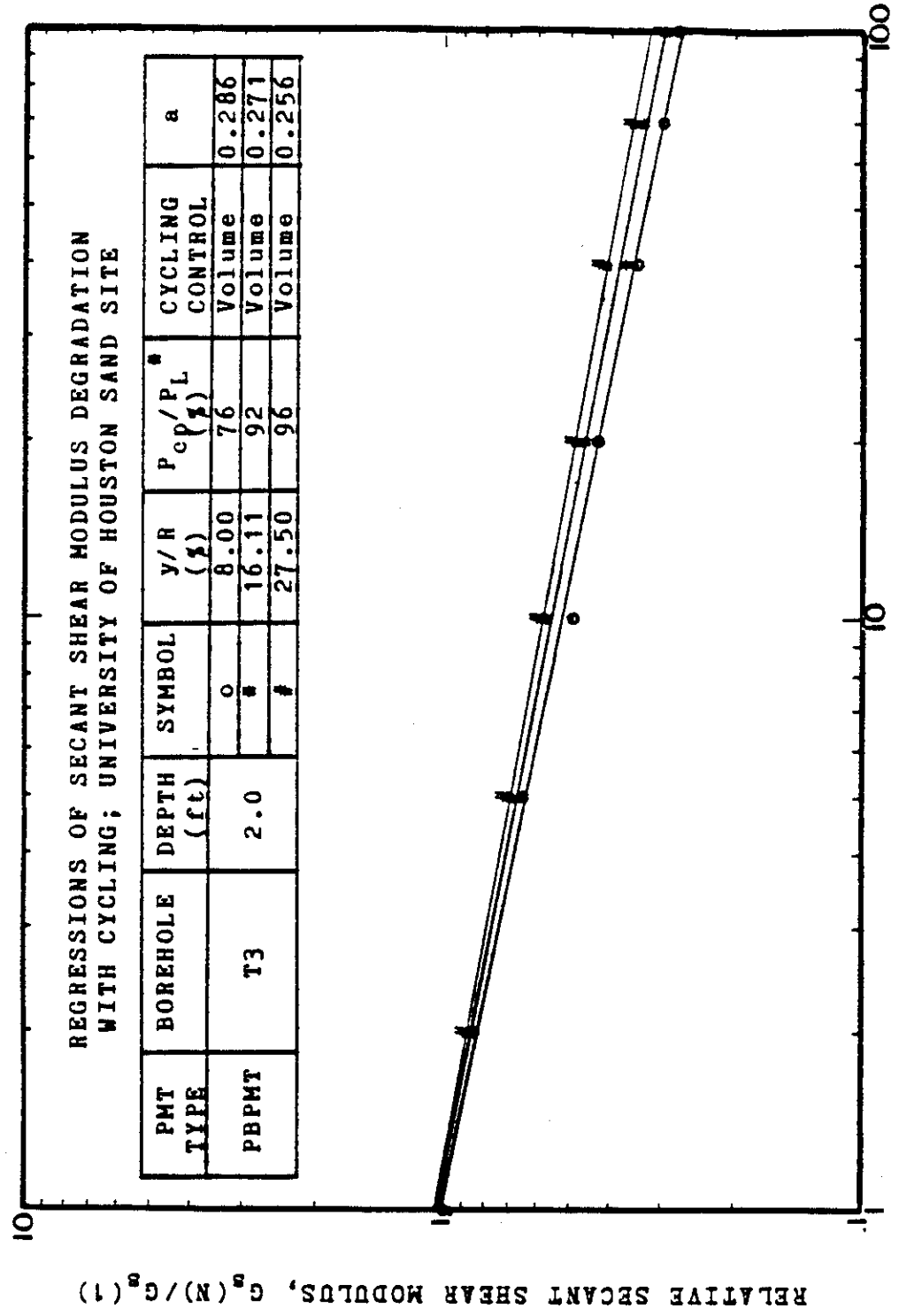

Figure 71. Secant Shear Modulus Degradation with Cycle Number, 2.0 feet, PBPMT-T3.

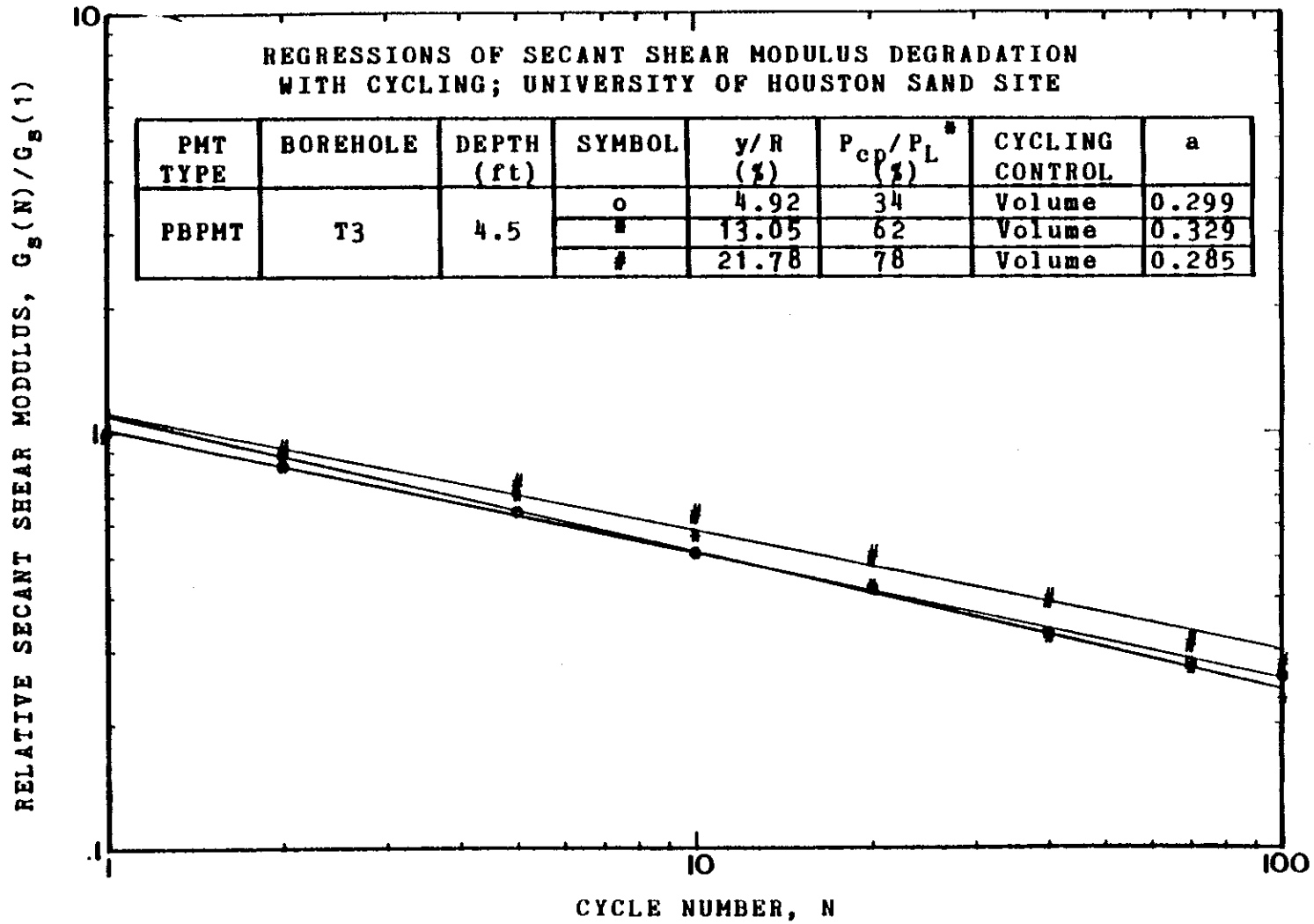

Figure 72. Secant Shear Modulus Degradation with Cycle Number, 4.5 feet, PBPMT-T3.

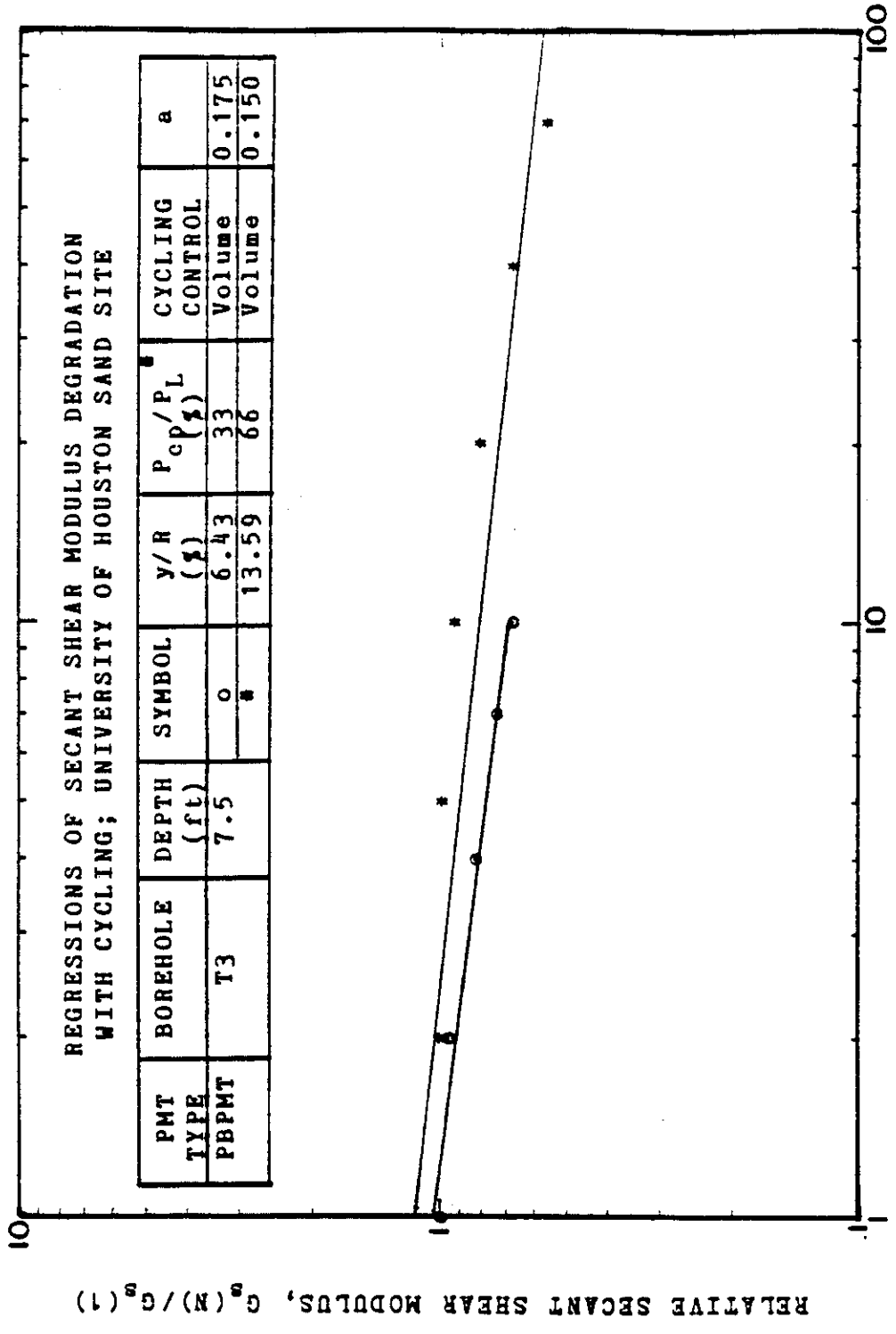

Figure 73. Secant Shear Modulus Degradation with Cycle Number, 7.5 feet, PBPMT-T3.

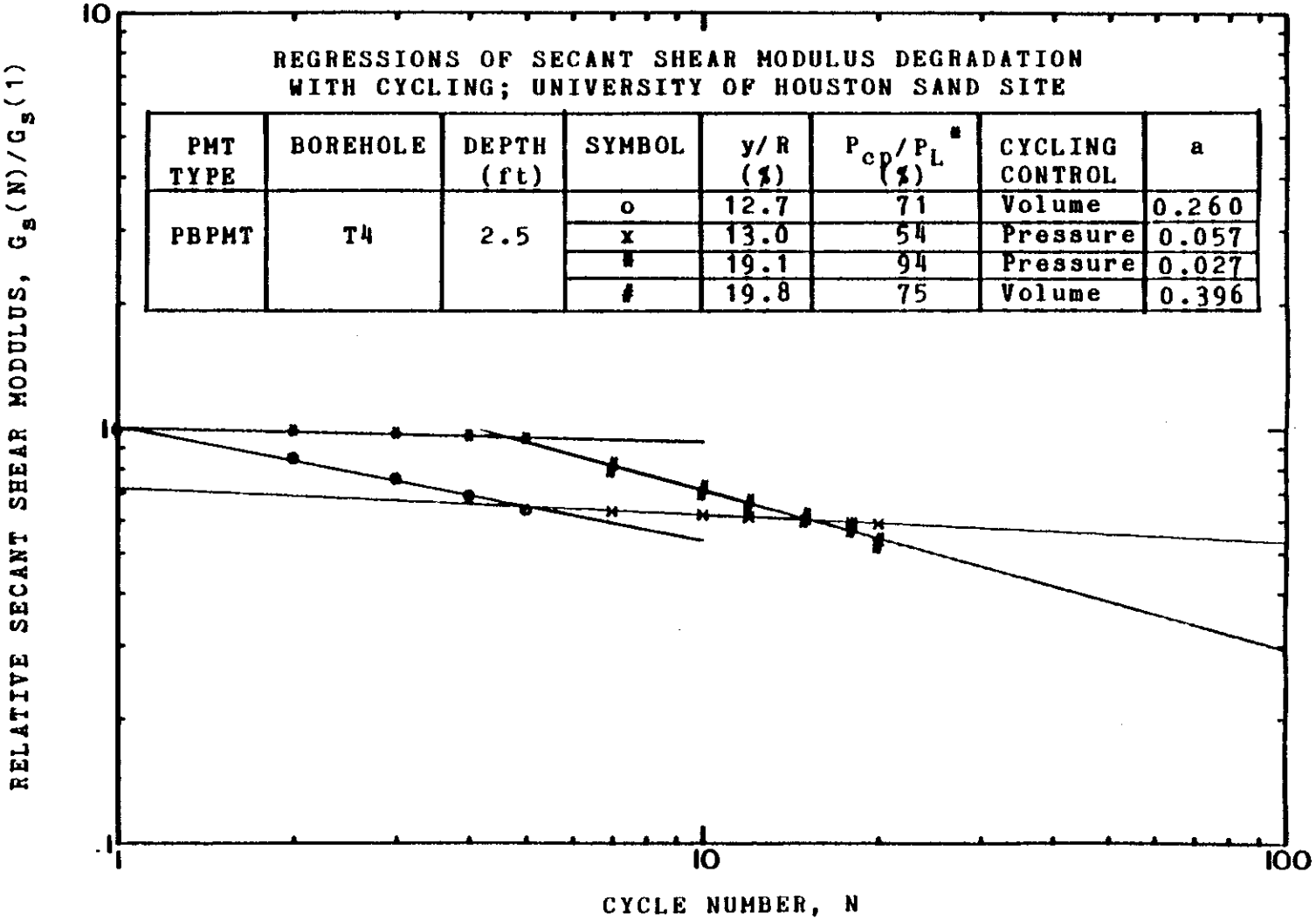

Figure 74. Comparison of Secant Shear Modulus Degradation: Pressure-control versus Volume-control Cycling.

to be reliable.

Comparing pressure-control and volume-control cyclic pressuremeter tests (Figure 74), indicates that the volume-control cycles degraded the secant shear modulus of the soil significantly more than the pressure-control cycles. This is consistent with the behavior of the one-way cyclic model pile load tests (Section 4.8).

In order to select an appropriate $\underline{a}$ value for prediction purposes, the $\underline{a}$ values found in the tests above were plotted as a function of the relative increase in probe radius (Figure 75). The volume-control versus pressure-control tests were disregarded and the average $\underline{a}$ value was calculated to be 0.26.

7.4 Pushed-in Cone Pressuremeter (PCPMT) Results

7.4.1 Corrected Pressuremeter Curves

The corrected pressuremeter curves for the pushed cone pressuremeter tests are presented in Figures 76 through 78. Volume-control cyclic tests were performed to simulate the displacment-control cyclic pile load tests. Three levels of cycling were performed in each test with the number of cycles varying between 10 and 50 at each level.

7.4.2 Cyclic Degradation Parameters

Degradation of the secant shear modulus with increasing cycle numbers with the pushed cone pressuremeter cyclic tests are shown in Figures 79 through 81. Cycling levels are referenced by giving the relative peak pressure

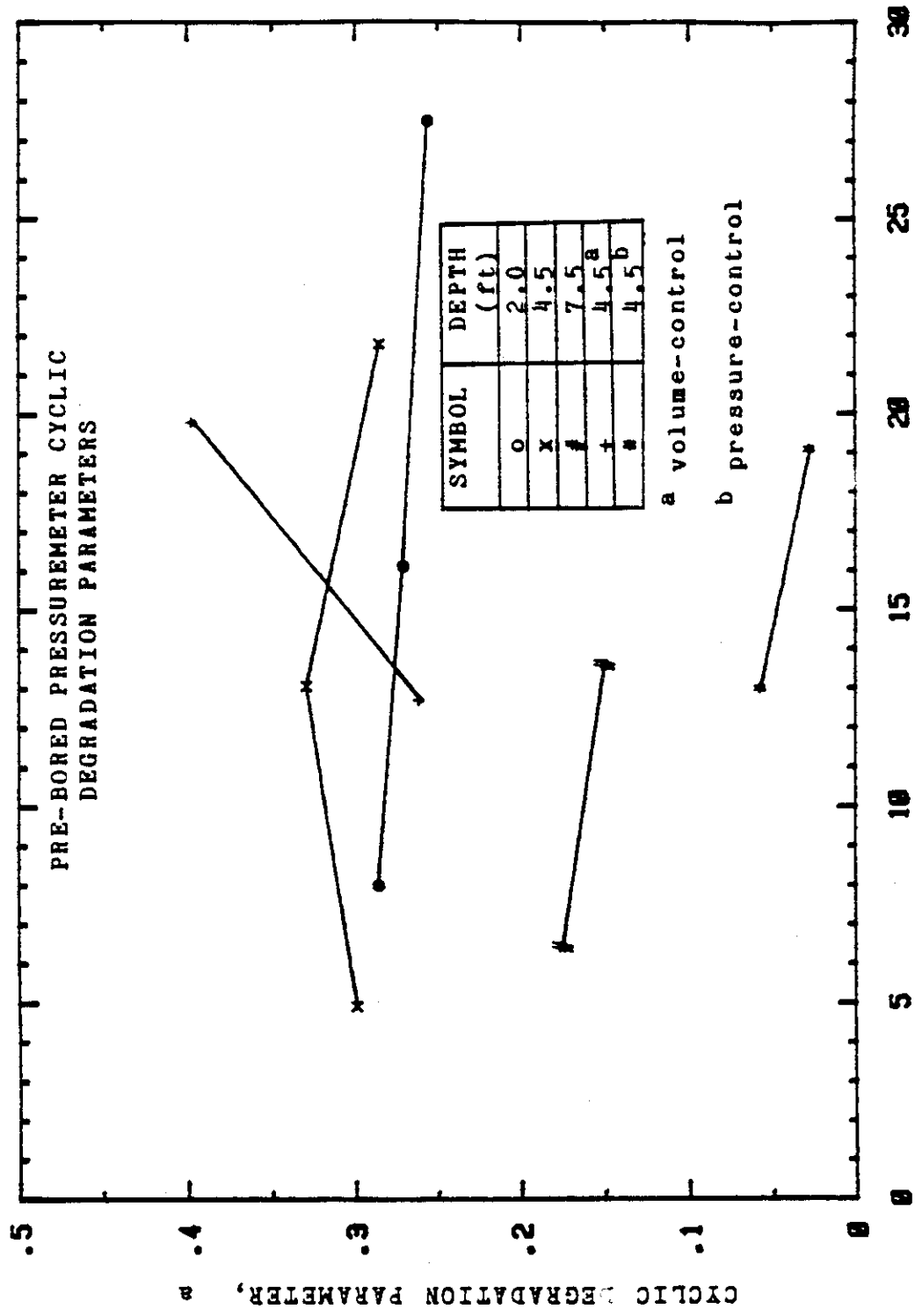

Figure 75. Cyclic Degradation Parameter versus Relative Radial Increase, PBPMT.

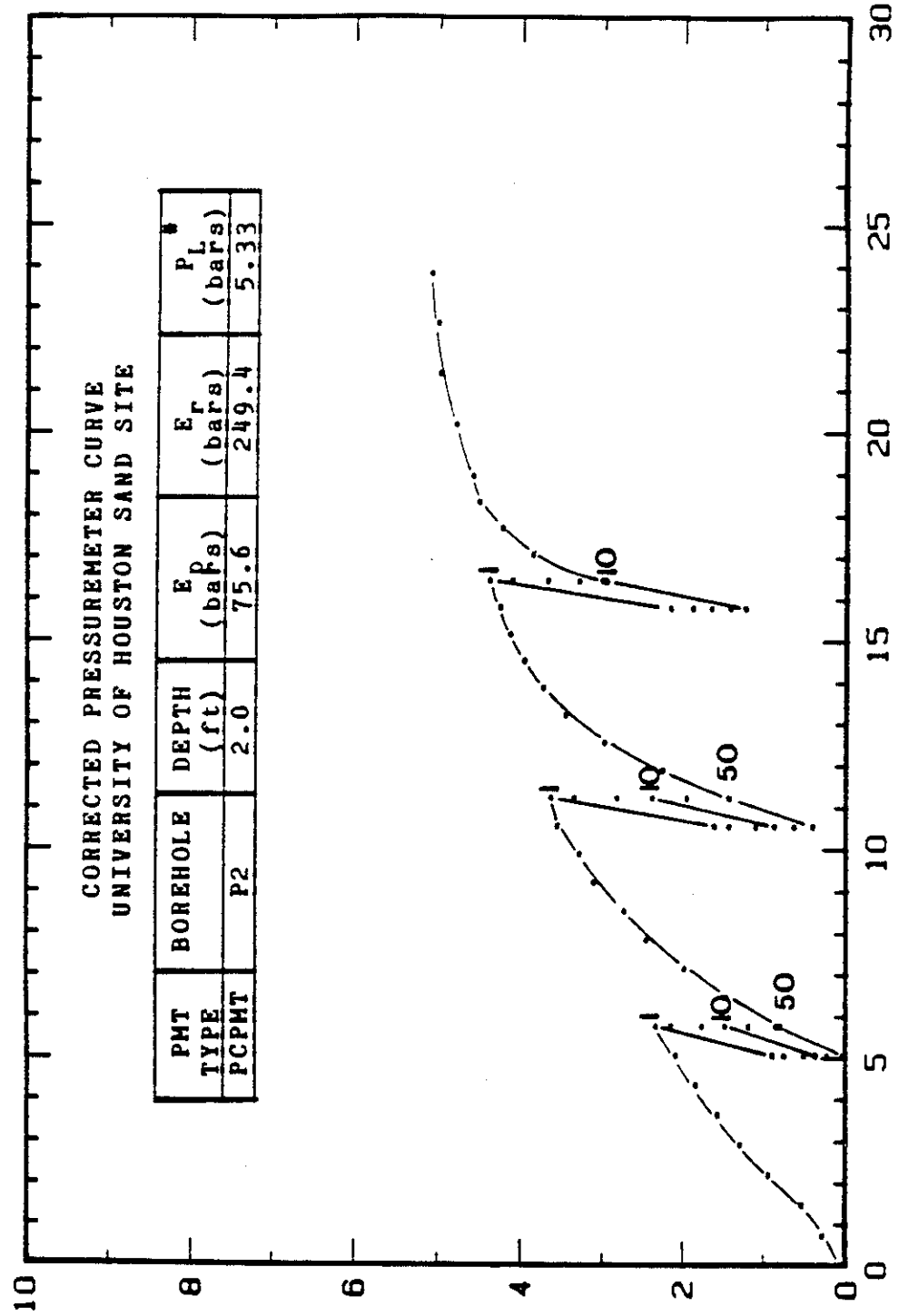

Figure 76. Pushed-in Cone Corrected Pressuremeter Curve, Borehole P2, 2.0 feet.

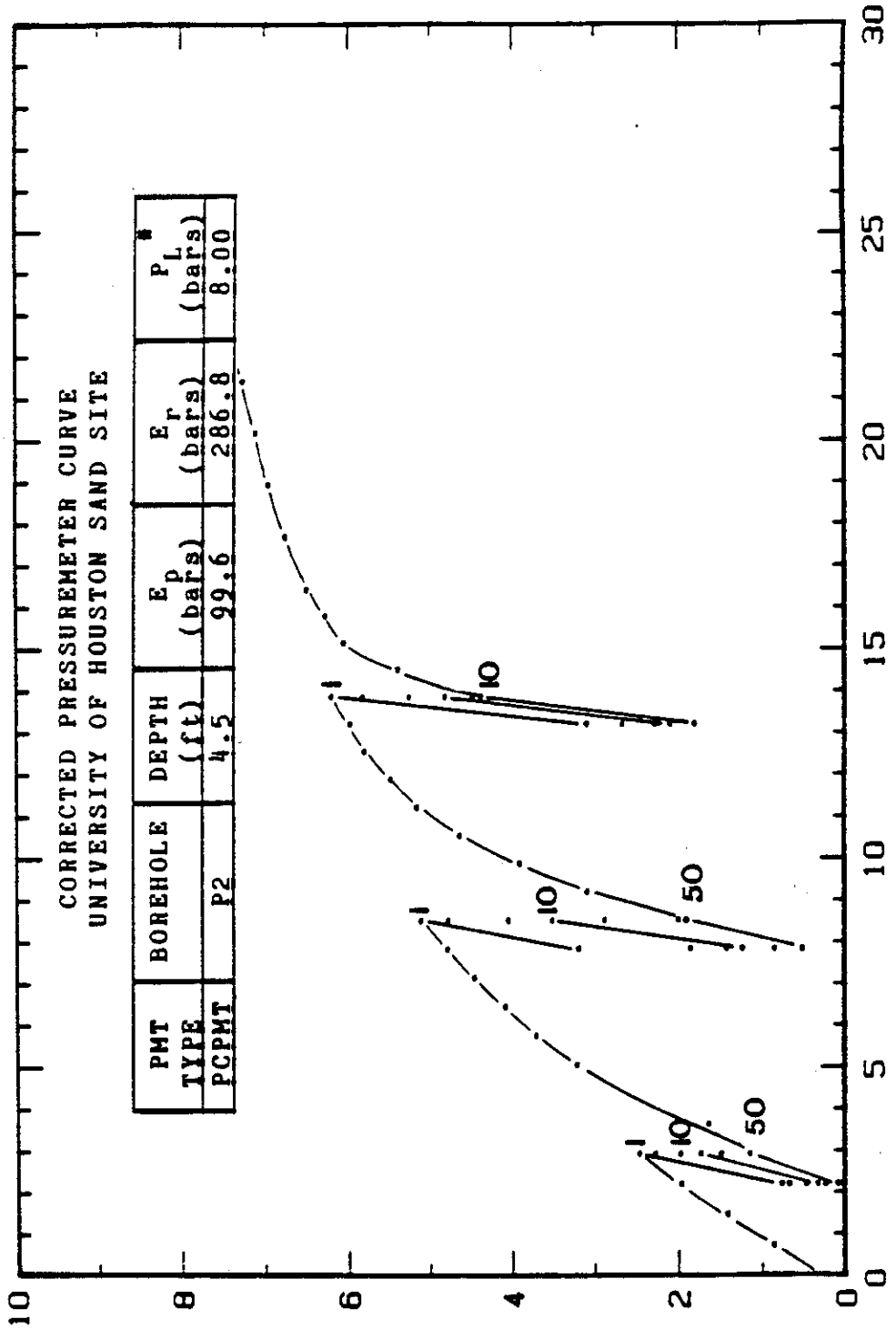

Figure 77. Pushed-in Cone Corrected Pressuremeter Curve, Borehole P2, 4.5 feet.

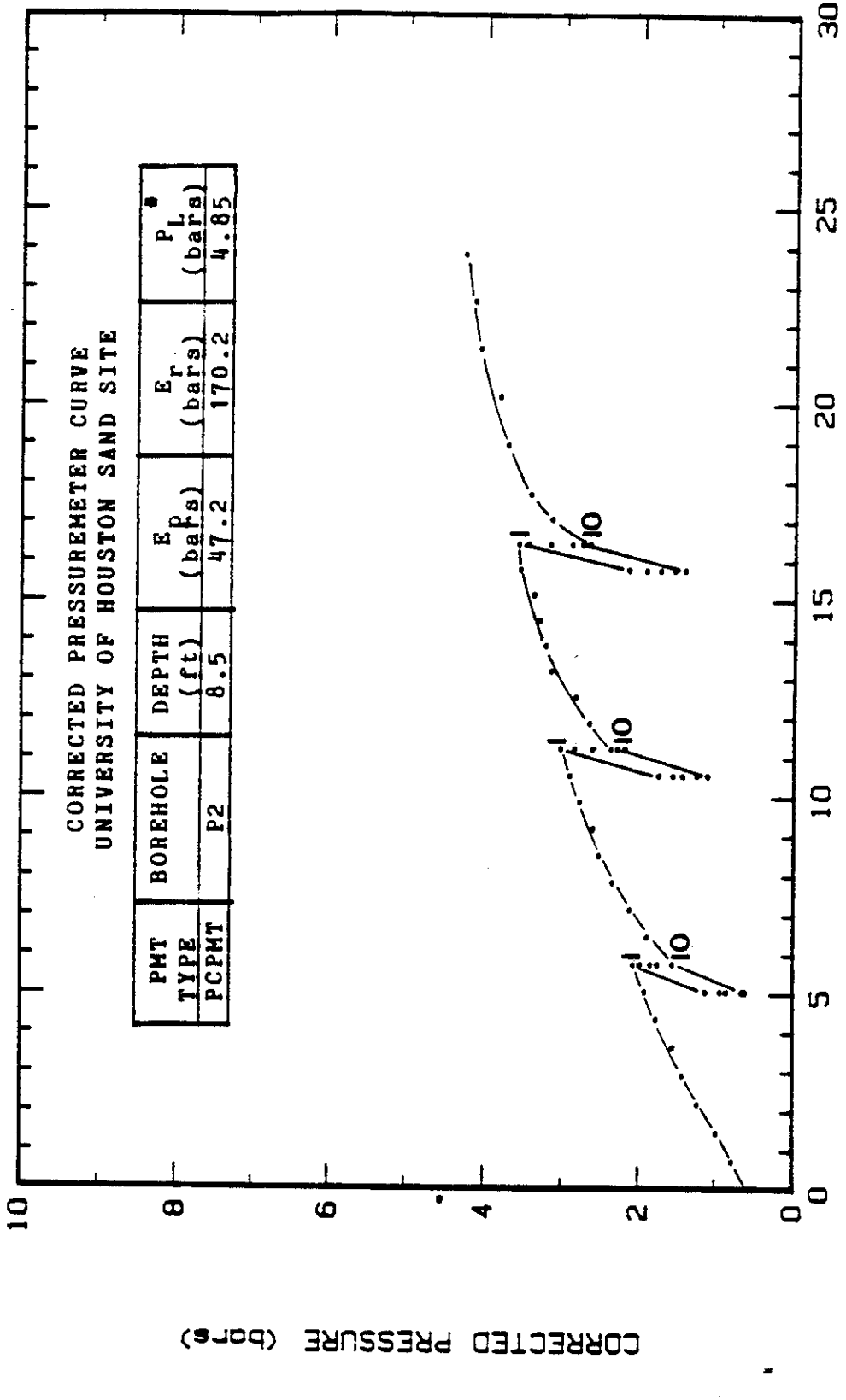

Figure 78. Pushed-in Cone Corrected Pressuremeter Curve, Borehole P2, 8.5 feet.

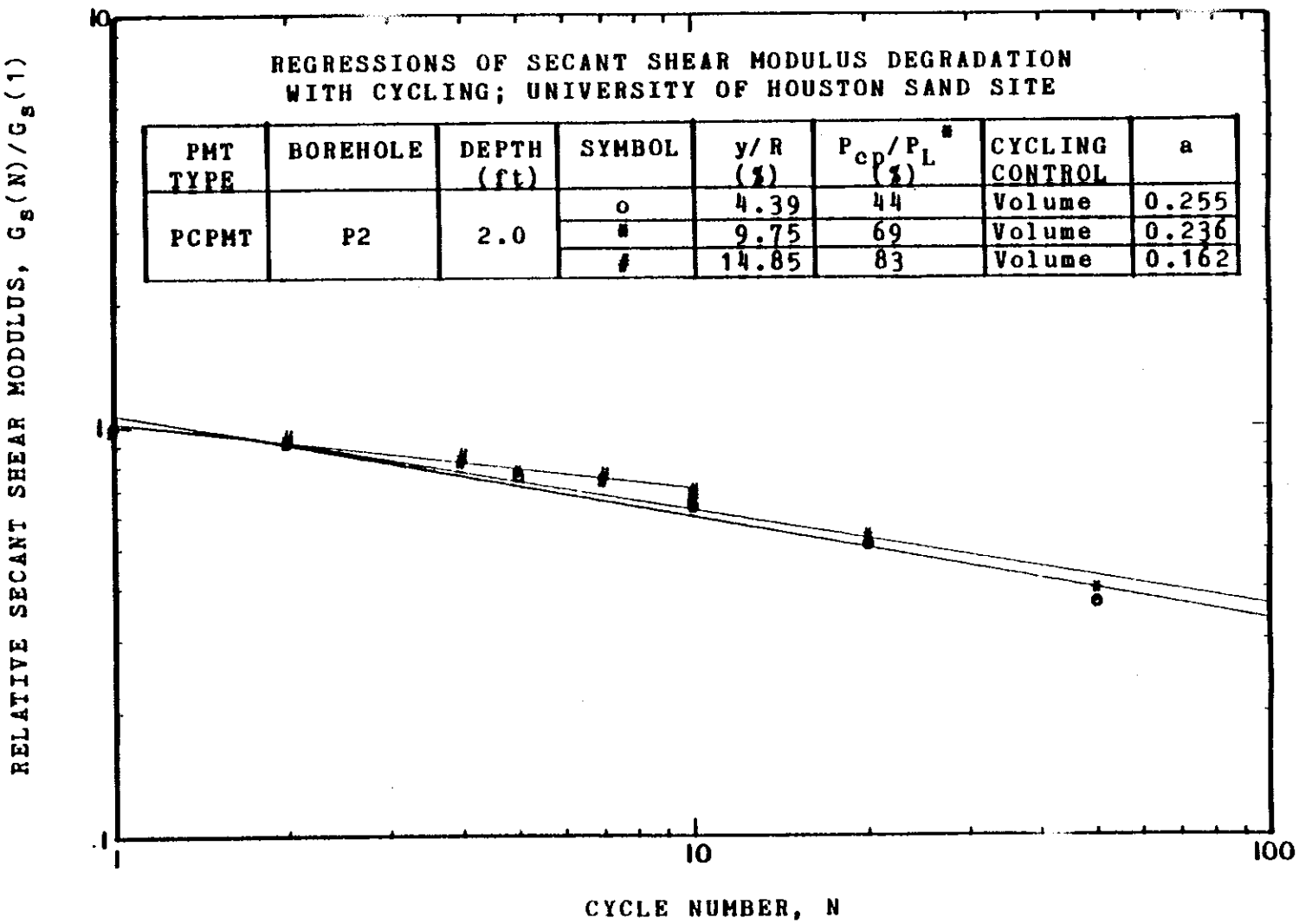

Figure 79. Secant Shear Modulus Degradation with Cycle Number, 2.0 feet, PCPMT-P2.

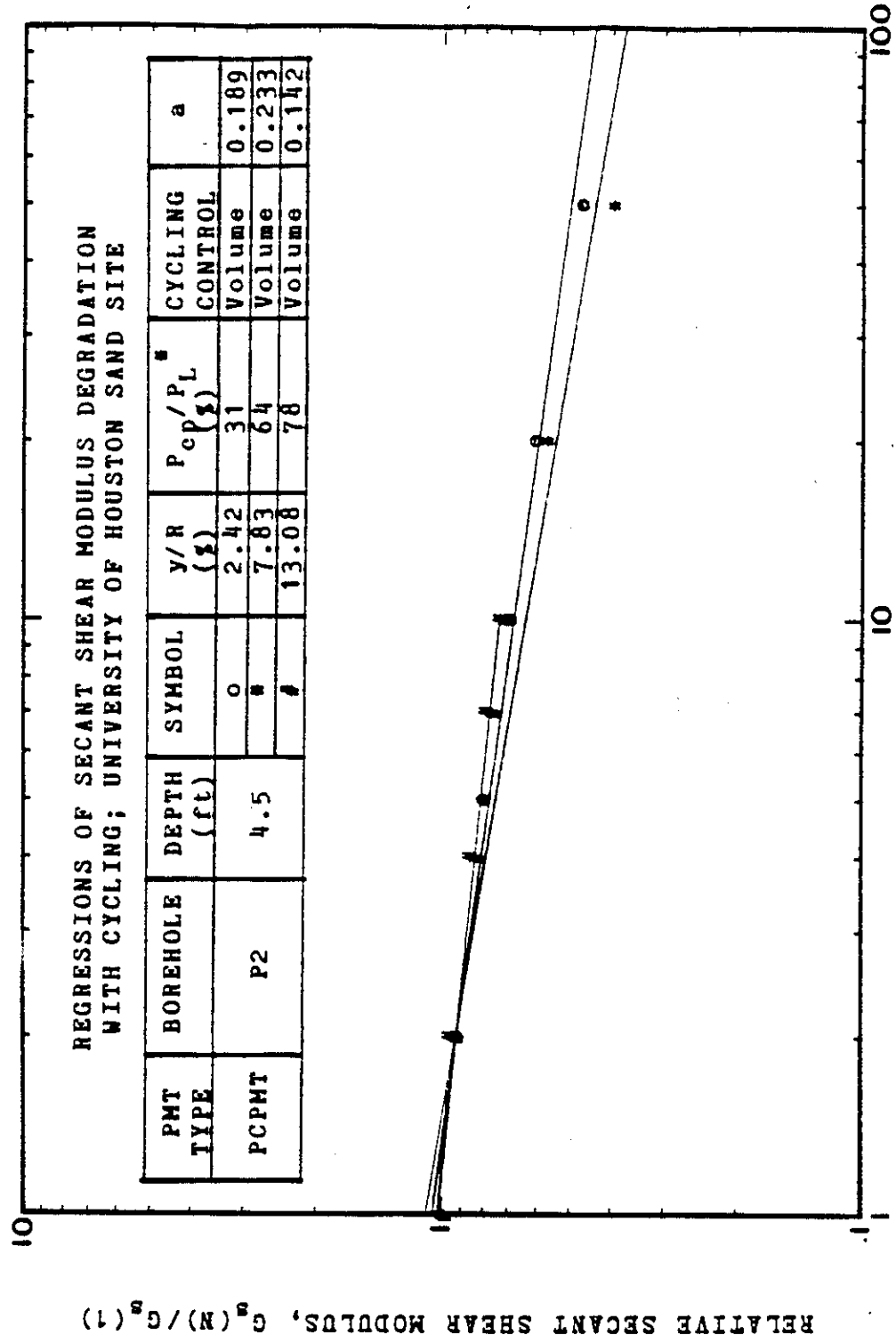

Figure 80. Secant Shear Modulus Degradation with Cycle Number, 4.5 feet, PCPMT-P2.

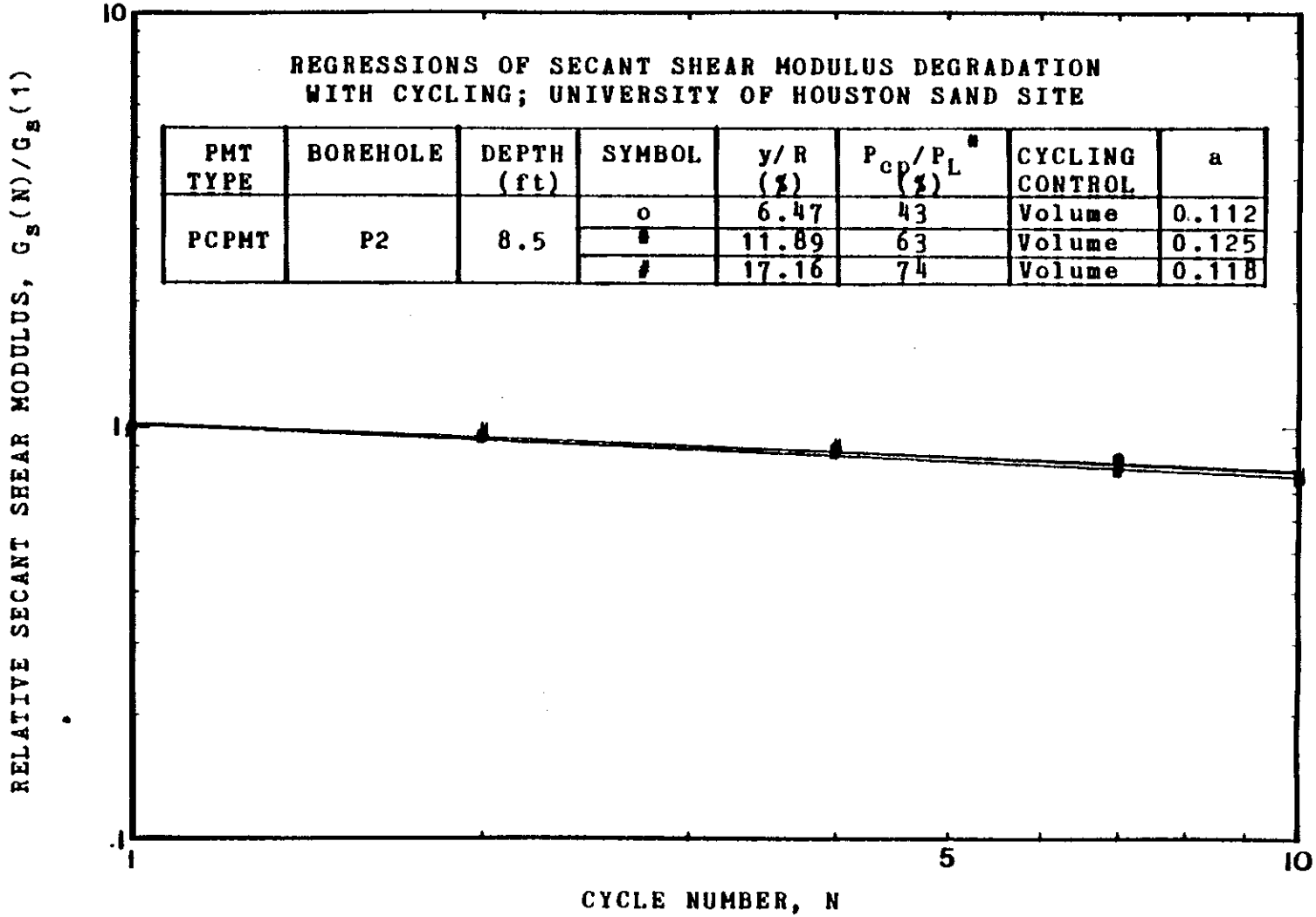

Figure 81. Secant Shear Modulus Degradation with Cycle Number, 8.5 feet, PCPMT-P2.

(P_{cp}/P_L^*) and the relative radial expansion (y/R). It should be noted on Figures 79 and 80 that the early part of the degradation curves show less degradation (smaller slope a up to approximately 10 cycles). This is possibly due to the temporary beneficial effect of the pushing of the probe. The pushing process compacts a certain zone around the probe; early cycling involves this stronger zone and leads to smaller degradation. As cycling continues, this zone weakens and the uncompacted natural soil leads to larger degradation.

The degradation parameters (a) are plotted versus the relative radial expansion in Figure 82. The average a value is 0.180 when all the data points are considered. When only the a values from the four tests with 50 cycles are averaged, the result is a degradation parameter of 0.23. This latter a value was chosen for use with the prediction method presented in this report.

7.5 Driven-in Cone Pressuremeter (DCPMT) Results

7.5.1 Corrected Pressuremeter Curves

The corrected pressuremeter curves from the driven cone pressuremeter tests are seen in Figures 83 through 86. Three series of 100 cycles each were run in the test at 4.5 feet in borehole D1; whereas three series of 10 cycles each were run during the other DCPMT tests.

7.5.2 Cyclic Degradation Parameters

The progressive decrease in the secant shear modulus

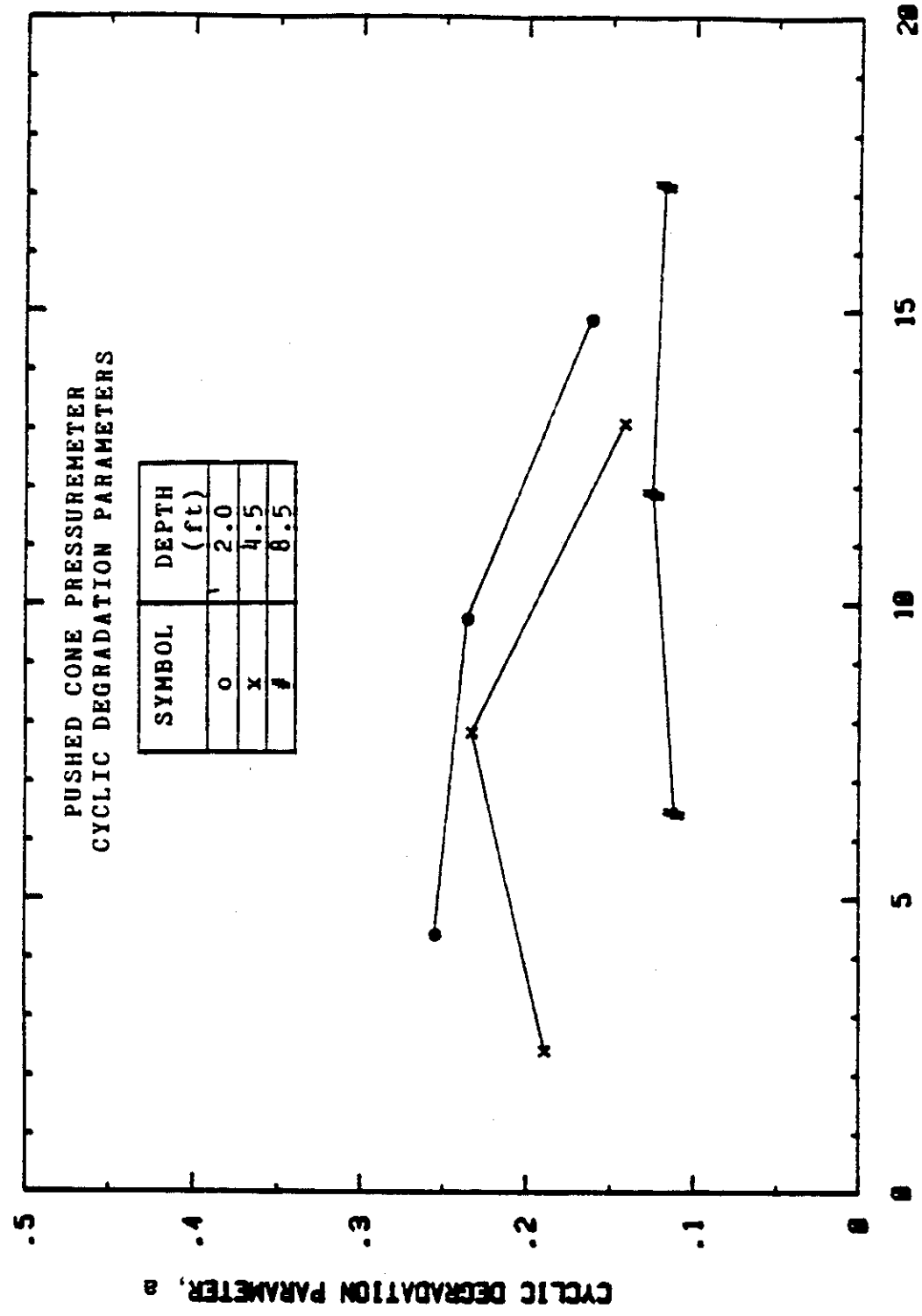

Figure 82. Cyclic Degradation Parameter versus Relative Radial Increase, PCPMT.

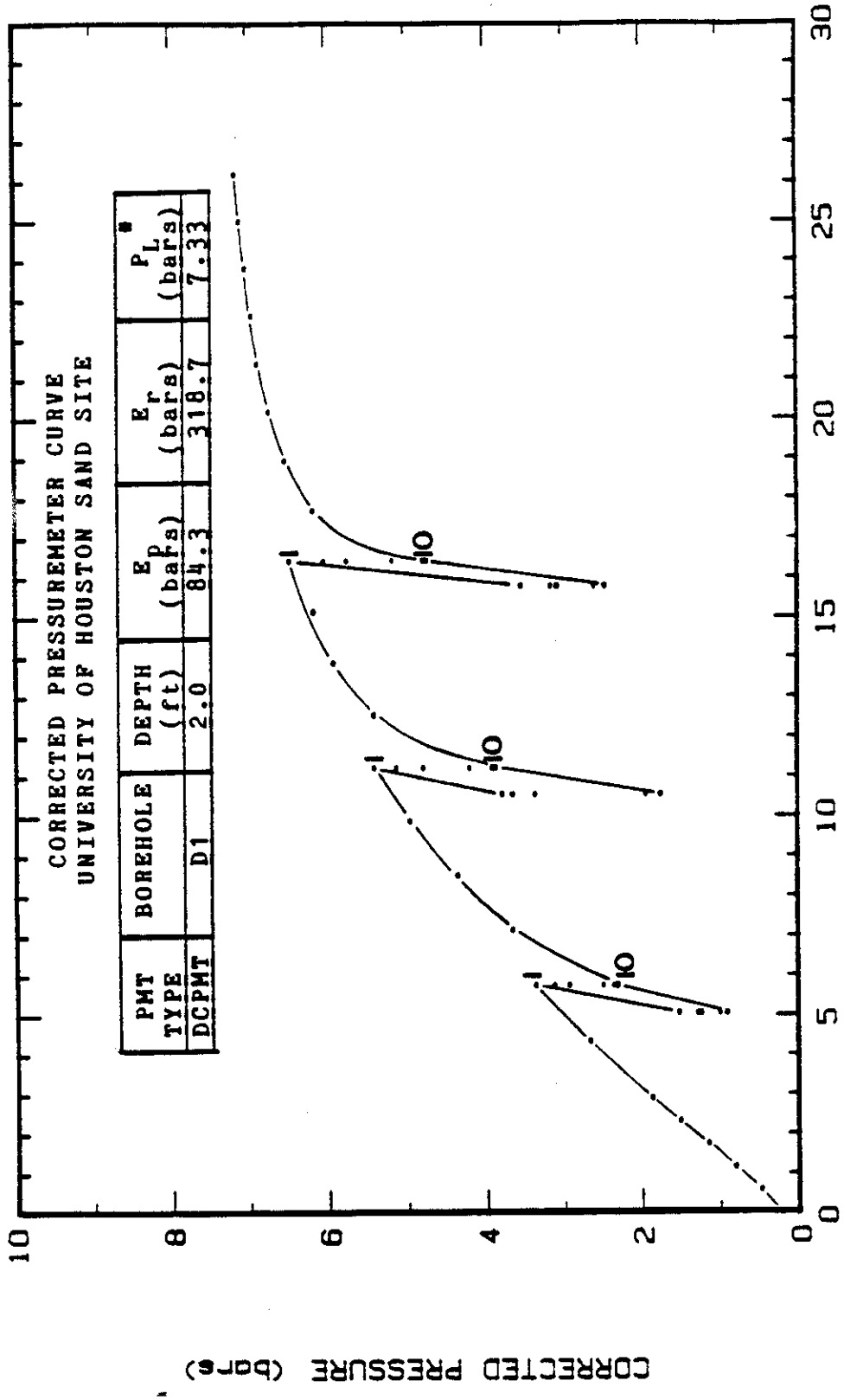

Figure 83. Driven-in Cone Corrected Pressuremeter Curve, Borehole D1, 2.0 feet.

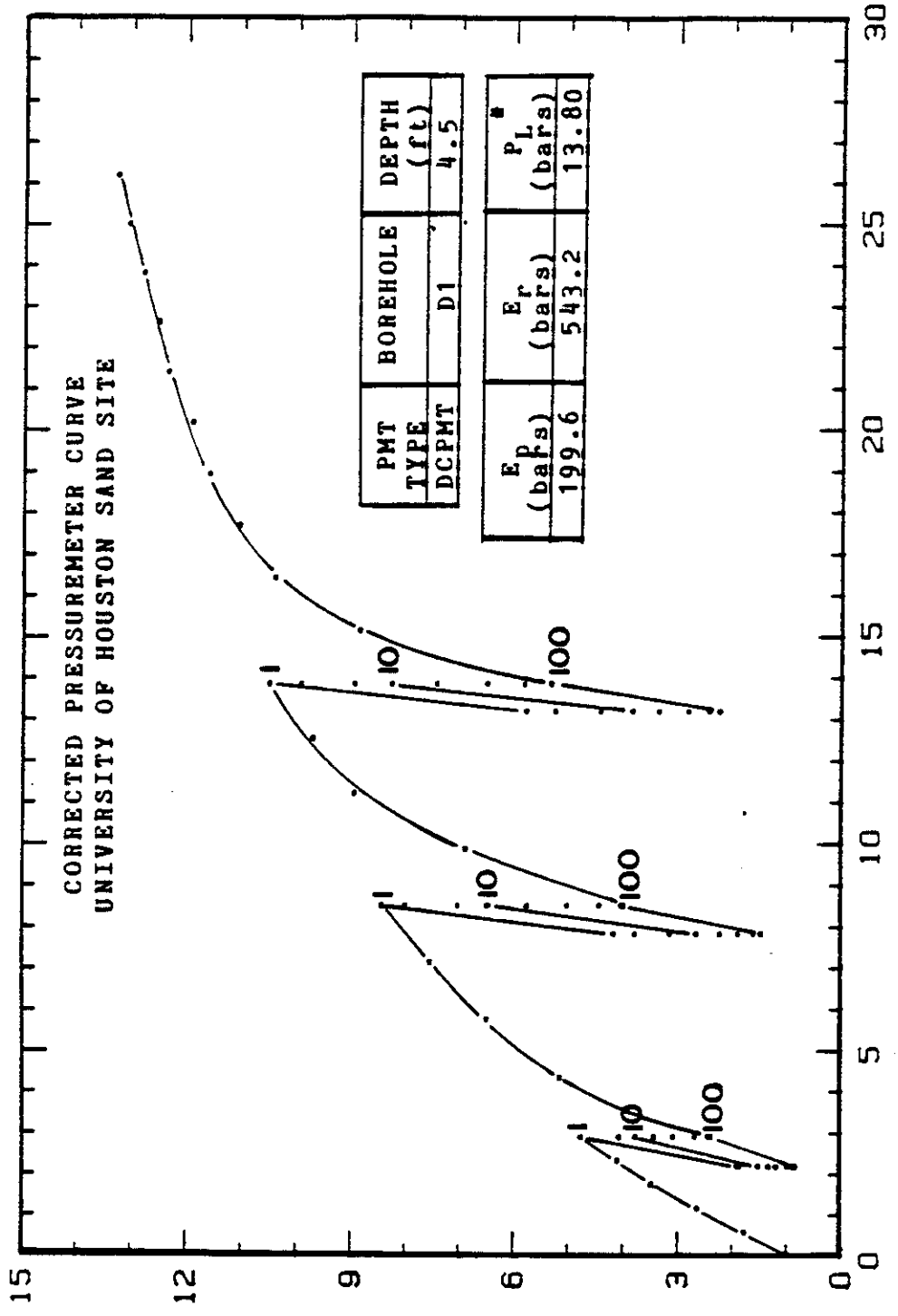

Figure 84. Driven-in Cone Corrected Pressuremeter Curve, Borehole D1, 4.5 feet.

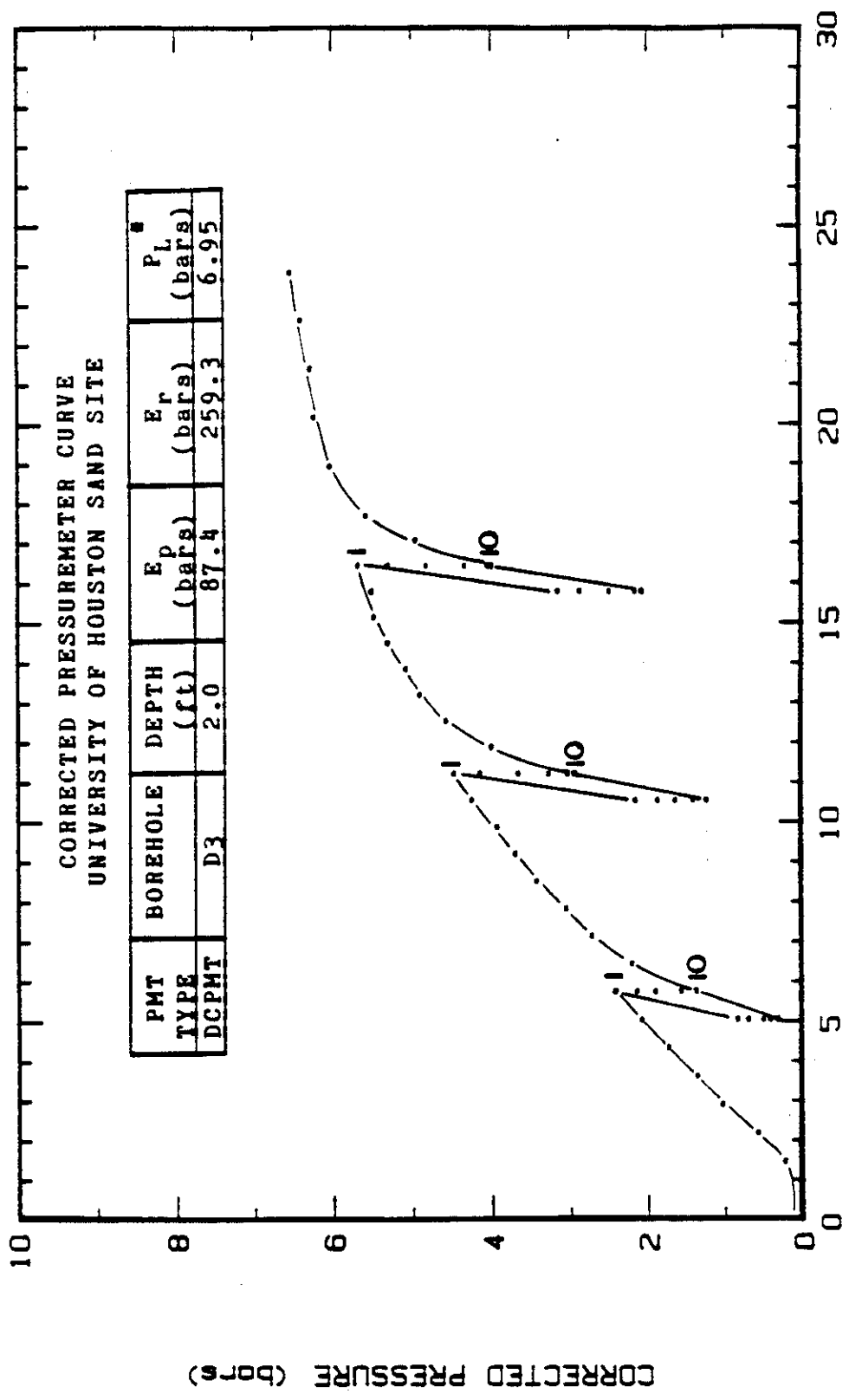

Figure 85. Driven-in Cone Corrected Pressuremeter Curve, Borehole D3, 2.0 feet.

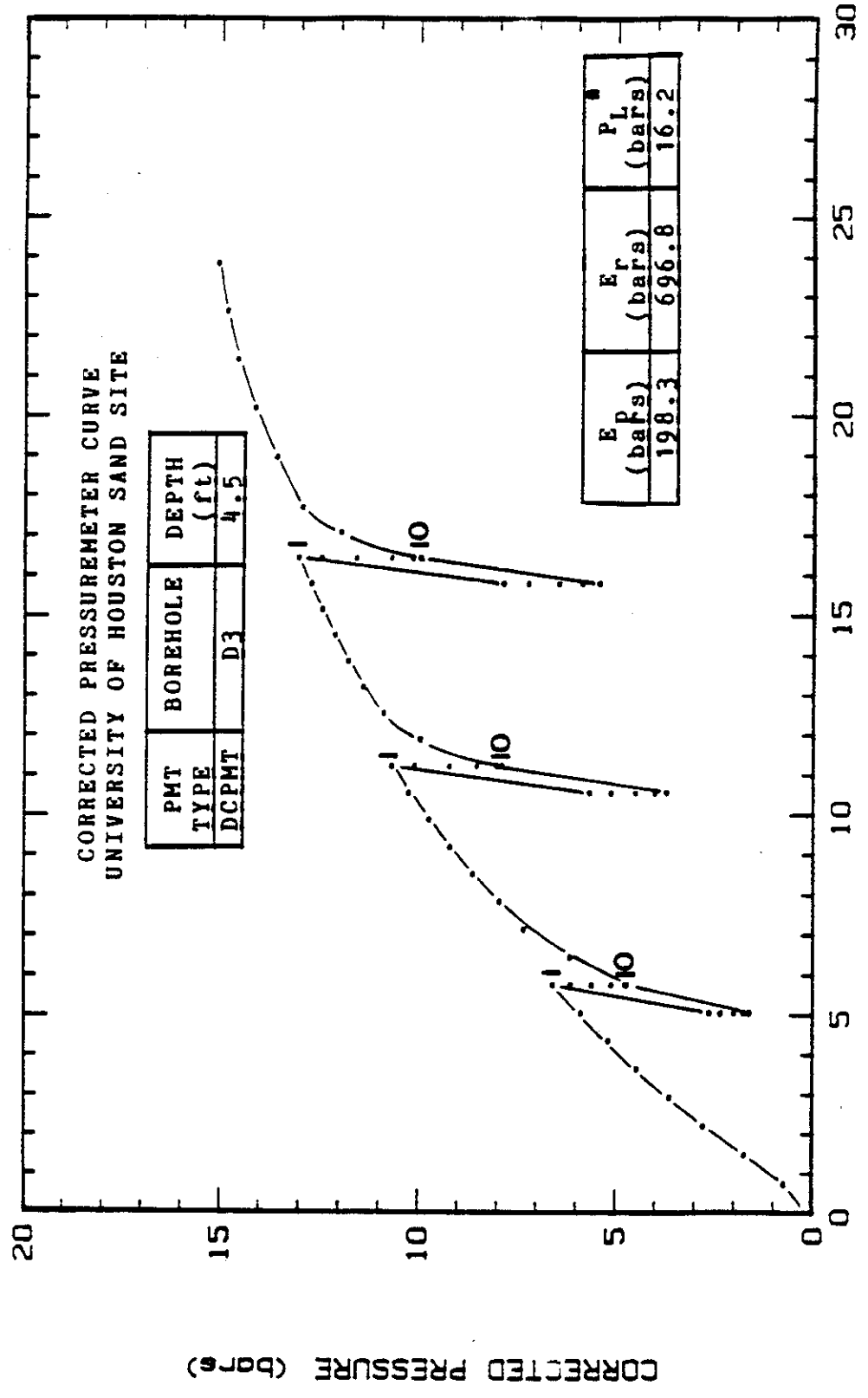

Figure 86. Driven-in Cone Corrected Pressuremeter Curve, Borehole D3, 4.5 feet.

with increasing cycle number is evident in Figures 87 through 90. In selecting the $\underline{a}$ value to use for prediction purposes, all the points except the first $\underline{a}$ value obtained in the 2.0 foot test in borehole D3 were averaged, yielding an $\underline{a}$ equal to 0.145. The data point (y/R, a) equal to (3.5, 0.248) was disregarded since its $\underline{a}$ value appeared erratic with respect to the other, more clustered, data points (Figure 91). The reasons for this erraticism may have been the result of local disturbance around the probe, the low peak pressure level, and the low number of total cycles performed in the series.

The beneficial effect described in Section 7.3.2 and 7.4.2 shows up for the driven CPMT since the average $\underline{a}$ value is 0.145 instead of 0.18 for the pushed CPMT and 0.26 for the pre-bored PMT. Judging from Figure 88, the beneficial effect does not appear to be temporary or at least seems to last longer than the beneficial effect on the pushed CPMT. This tends to indicate that the driving process densifies a zone of sand which is much larger than the zone densified by the pushing process.

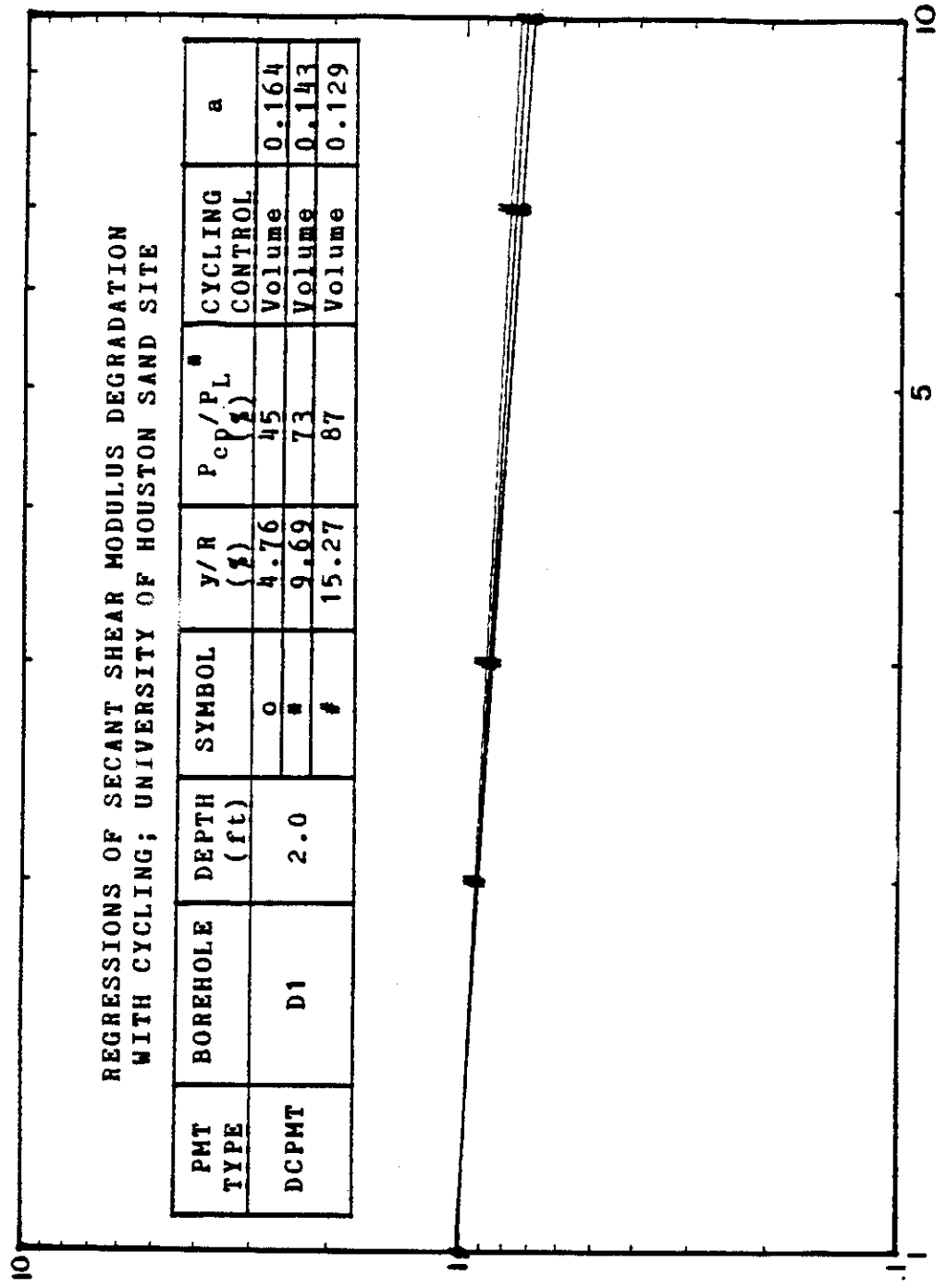

Figure 87. Secant Shear Modulus Degradation with Cycle Number, 2.0 feet, DCPMT-D1.

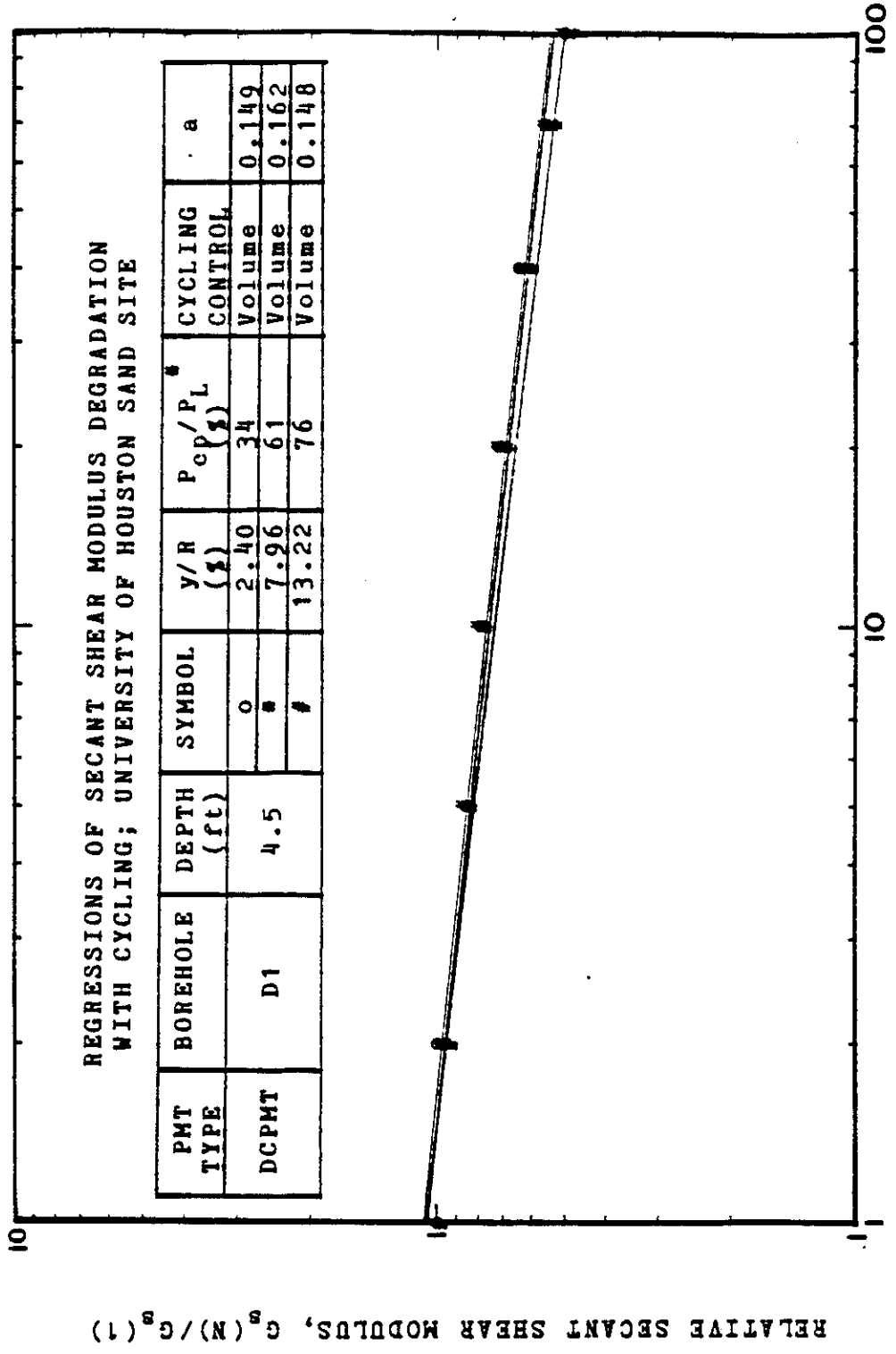

Figure 88. Secant Shear Modulus Degradation with Cycle Number, 4.5 feet, DCPMT-D1.

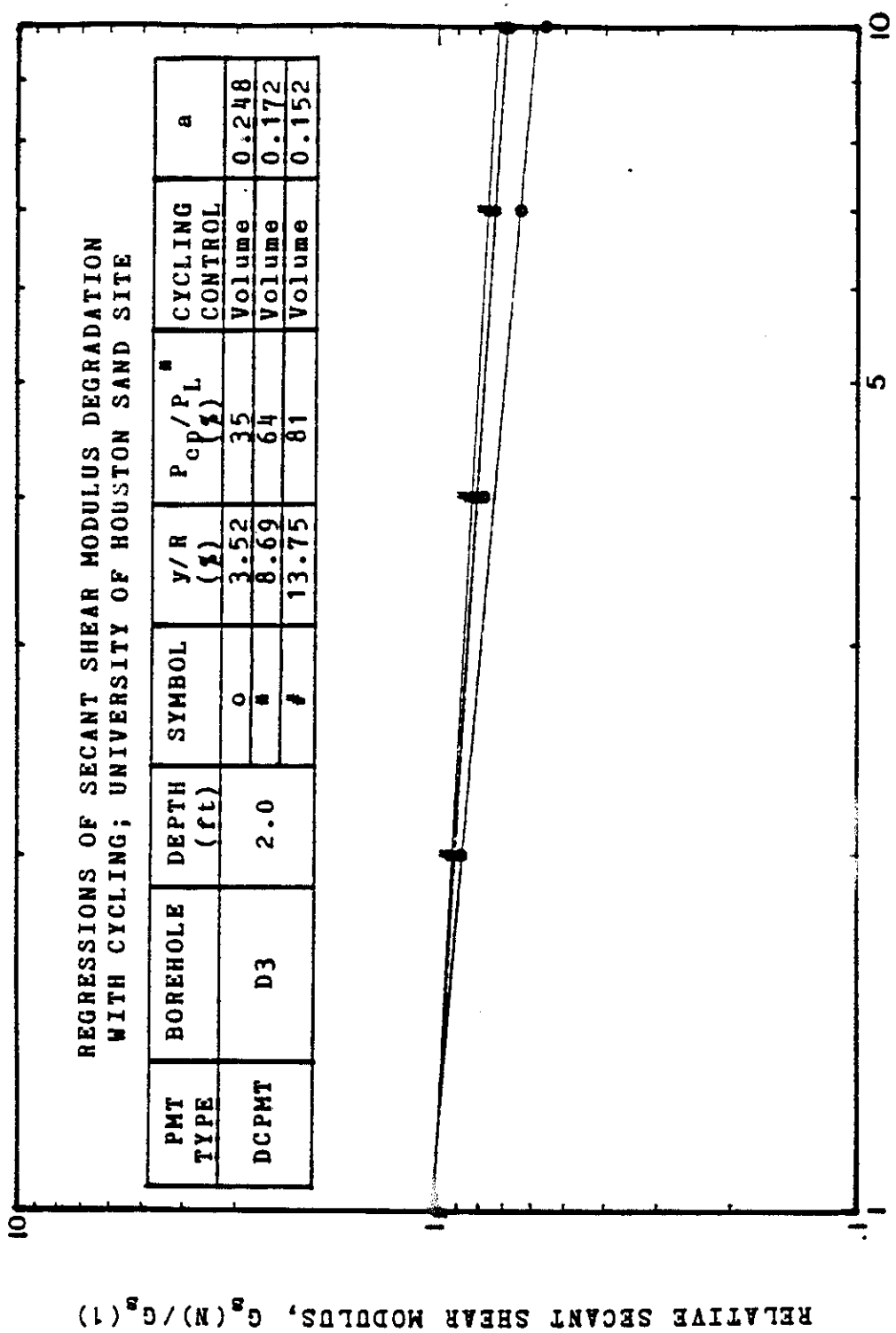

Figure 89. Secant Shear Modulus Degradation with Cycle Number, 2.0 feet, DCPMT-D3.

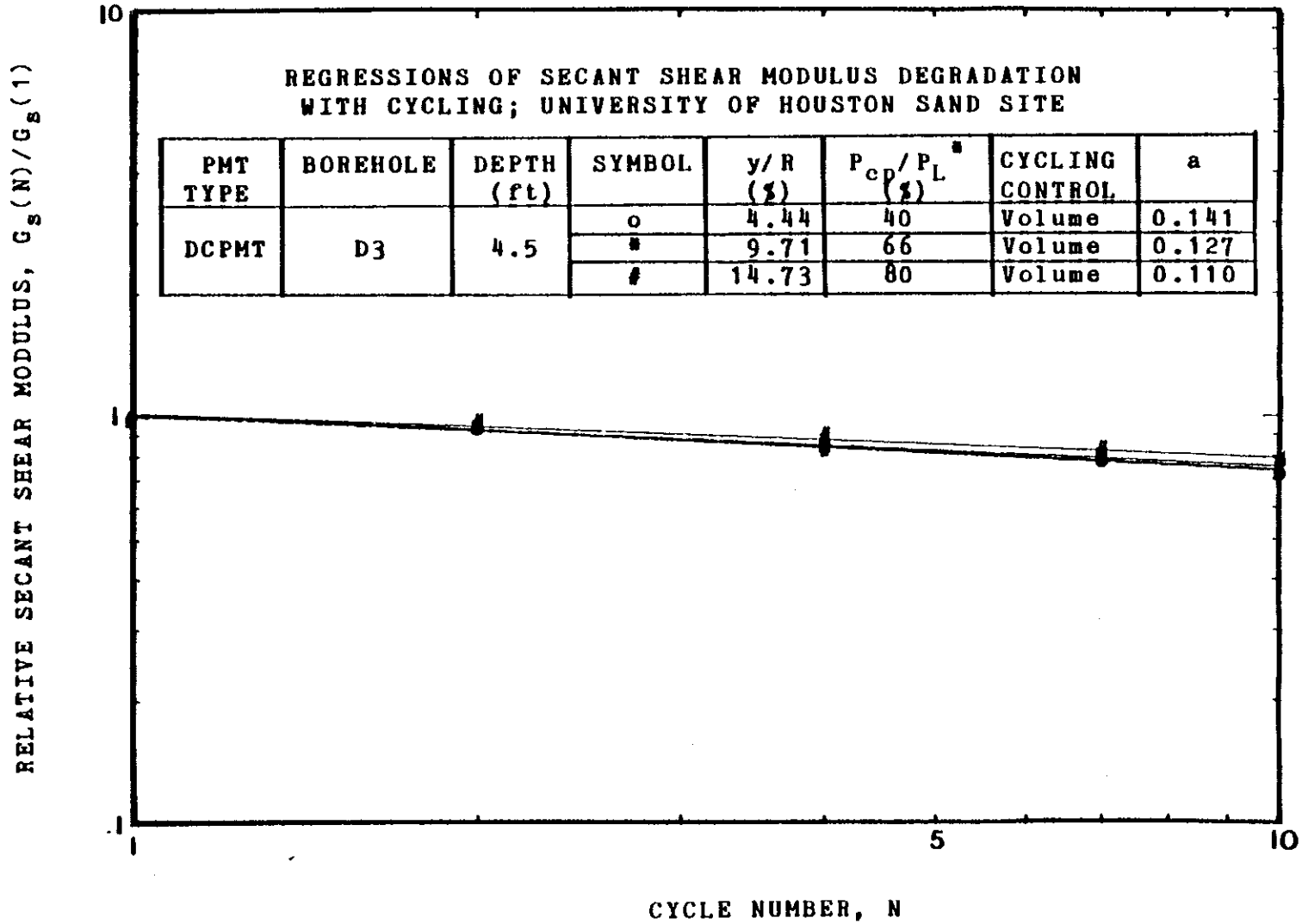

Figure 90. Secant Shear Modulus Degradation with Cycle Number, 4.5 feet, DCPMT-D3.

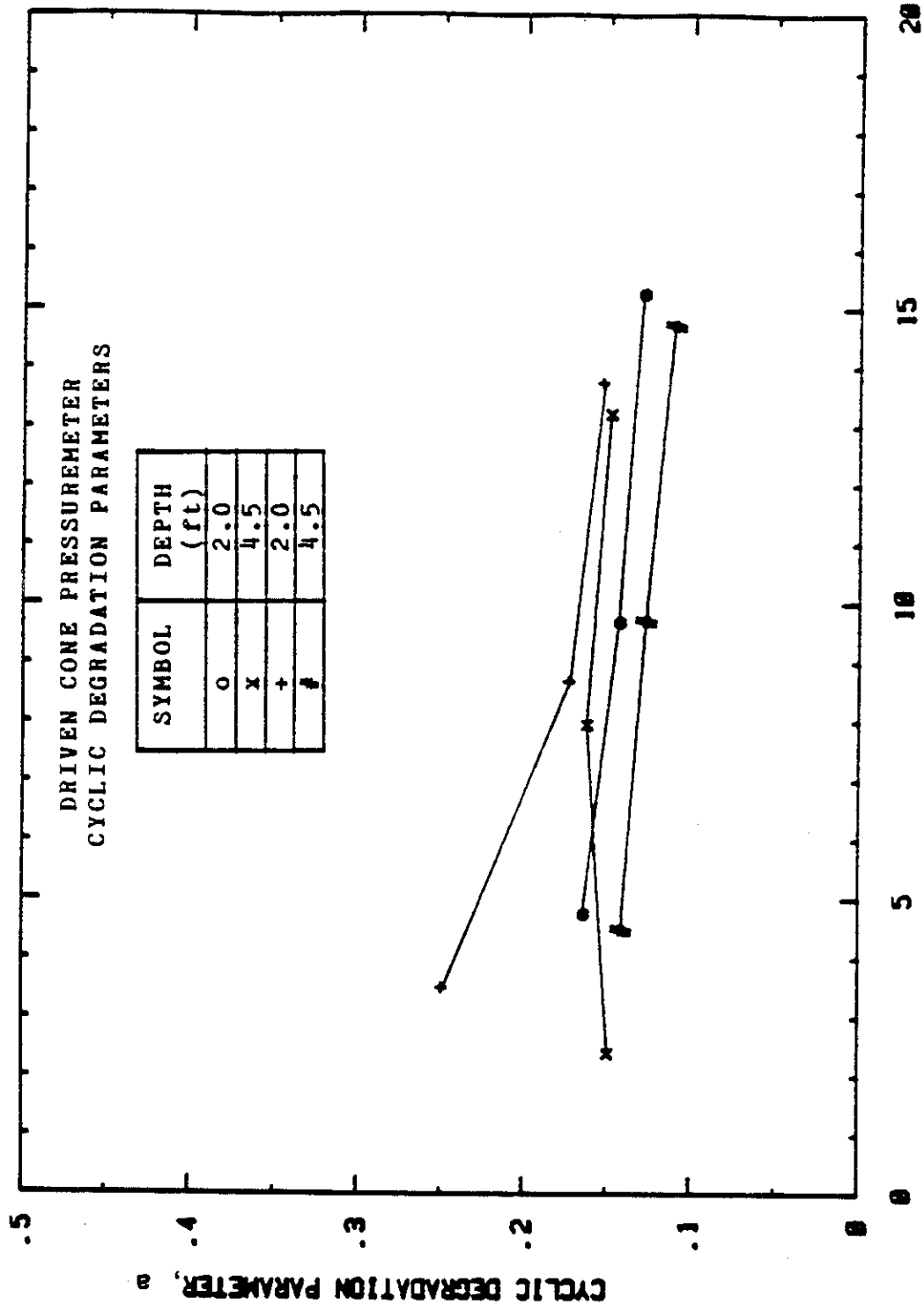

Figure 91. Cyclic Degradation Parameter versus Relative Radial Increase, DCPMT.

8. PRESSUREMETER TESTS AT TEXAS A&M UNIVERSITY LABORATORIES

8.1 Pressuremeter Type and Cycling Methods

Two pressuremeter test series were conducted in the laboratory at Texas A&M University (Table 6). The first series included pressure-control cycling to simulate the load-control model pile tests while the second series used volume-control cycling to match the displacement-control model pile tests. Each series consisted of six separate pressuremeter tests: one shallow and one deep test for each of the three different pile placement procedures employed in the model pile tests (Figure 92). The cone pressuremeter equipment and procedures (Sections 5.2 and 5.4) were employed in all of the laboratory pressuremeter tests.

8.2 Probe Placement Procedures and Soil Conditions

The probe placement procedures mirrored those of the model piles, namely:

(1) the post-compacted, single lift procedure,

(2) the pre-compacted, single lift procedure, and

(3) the post-compacted, multiple lift procedure.

In the first procedure, the drum was filled with loose sand and the probe pushed into the sand to a depth of approximately 20 inches and the soil compacted around the probe with a concrete vibrator, repeating the pattern in Figure 25a twice. The deep pressuremeter test was then

PRESSURE-CONTROL PMT TESTS						
Soil / Placement Procedure	γ (lb/ft^3)	Depth (in)	y/R (%)	a	a average	a selected
Post-compacted Single Lift	111	9.25	5.1	0.078	0.096	0.096
			18.1	0.114		
		19.25	5.6	0.062	0.056	0.056
			14.1	0.053		
			25.2	0.053		
Pre-compacted Single Lift	114	6.75	3.1	0.090	0.132	0.132
			16.9	0.174		
		19.25	3.8	0.104	0.087	0.087
			9.5	0.078		
			11.3	0.078		
Post-compacted Multiple Lift	112	6.75	11.9	0.102	0.133	0.133
			23.2	0.164		
		19.50	1.1	0.083	0.068	0.068
			2.9	0.064		
			9.2	0.058		
VOLUME-CONTROL PMT TESTS						
Soil / Placement Procedure	(lb/ft^3)	Depth (in)	y/R (%)	a	a average	a selected
Post-compacted Single Lift	111	9.75	0.9	0.262*	0.180	0.179
			7.7	0.180		
		20.75	1.4	0.095	0.151	
			7.2	0.166		
			14.6	0.191		
Pre-compacted Single Lift	114	9.25	2.1	0.112	0.136	0.138
			6.0	0.159		
		20.75	1.7	0.124	0.139	
			4.5	0.145		
			7.8	0.149		
Post-compacted Multiple Lift	112	7.25	3.4	0.121	0.128	0.140
			9.8	0.135		
		20.75	3.5	0.114	0.147	
			7.2	0.160		
			12.3	0.168		

* Disregarded when averaging a values.

Table 6. Pressuremeter Tests Performed at the Texas A&M Laboratories.

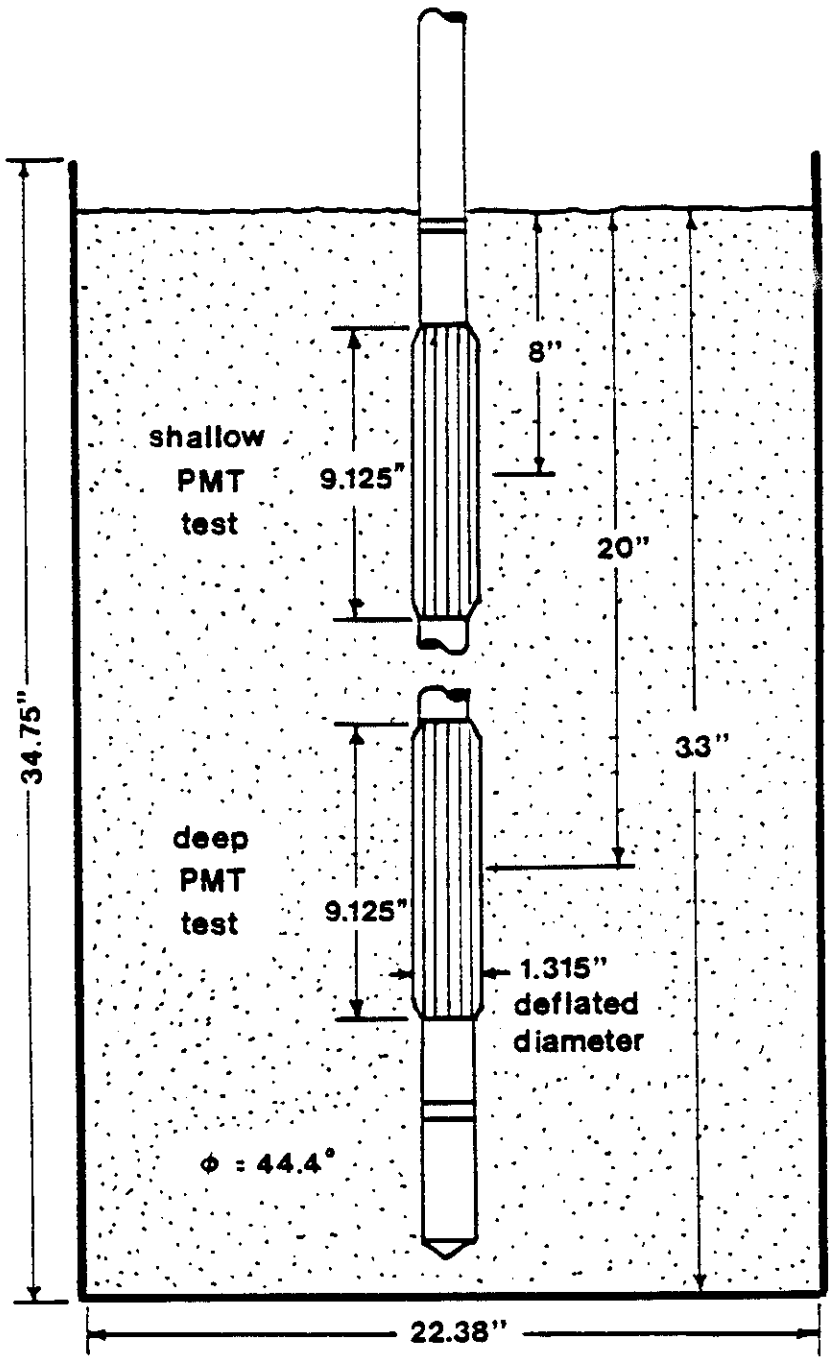

Figure 92. Profile of the Cone Pressuremeter Tests in the Model Pile Test Drum at Texas A&M University.

performed, including 3 cycling series of 20 cycles each. The probe was then carefully pulled to the shallow test position, approximately 8 inches deep, and the top half of the soil recompacted using the concrete vibrator and the pattern in Figure 25b. The shallow pressuremeter test was then performed including 2 cycling series of 20 cycles each.

The pressuremeter was then removed and the sand recompacted using the pattern in Figure 25b, with the vibrator penetrating fully into the drum. The probe was then driven into the sand with a rawhide mallet to the shallow testing depth and the pre-compacted, single lift procedure shallow pressuremeter test was performed including 2 cycling series of 20 cycles each. The probe was then driven to a testing depth of approximately 20 inches and, with no further compaction, the deep test was performed including 3 cycling series of 20 cycles each.

The drum was then emptied and the probe positioned for a deep test. Sand was then compacted around the probe in six lifts of approximately six inches each. Compaction was achieved by repetitively plunging the concrete vibrator into the lift in a spiral pattern beginning near the probe (Figure 25c). The pressuremeter test was then performed, including 3 series of 20 cycles, after which time the top 1/3 of the sand was removed. The probe was then repositioned at the shallow test depth and the sand added back to the drum in 6 inch lifts compacted as detailed above. The

shallow test was then performed with the standard 2 series of 20 cycles each.

8.3 Pressure-control Pressuremeter Test Results

8.3.1 Corrected Pressuremeter Curves

The corrected pressuremeter curves for the pressure-control test series are presented in Figures 93 through 98. On Figures 95, 97, and 98 the curve indicates that expansion of the probe was necessary to come in good contact with the soil even though the soil was compacted around the probe. This was due to the fact that sand grains became more and more entrapped between the overlapping steel strips as the testing program progressed. Indeed, it is the recompression of the grain-filled steel strips which shows up at the beginning of these pressuremeter curves. The effect of this phenomenon on the final predictions was taken into account in the preparation of the P-y curves by translating the origin of the curve to the intersection of the linear portion of the pressuremeter curve and the at rest horizontal earth pressure (Section 9.3.3).

8.3.2 Cyclic Degradation Parameters

Figures 99 through 104 display the decrease in the secant shear modulus with increasing cycle numbers for the pressure-control cyclic pressuremeter tests. The a values as found from the slope of the regression lines are plotted as a function of the relative increase in probe radius, y/R (%), in Figures 105, 106, and 107: one figure for each probe

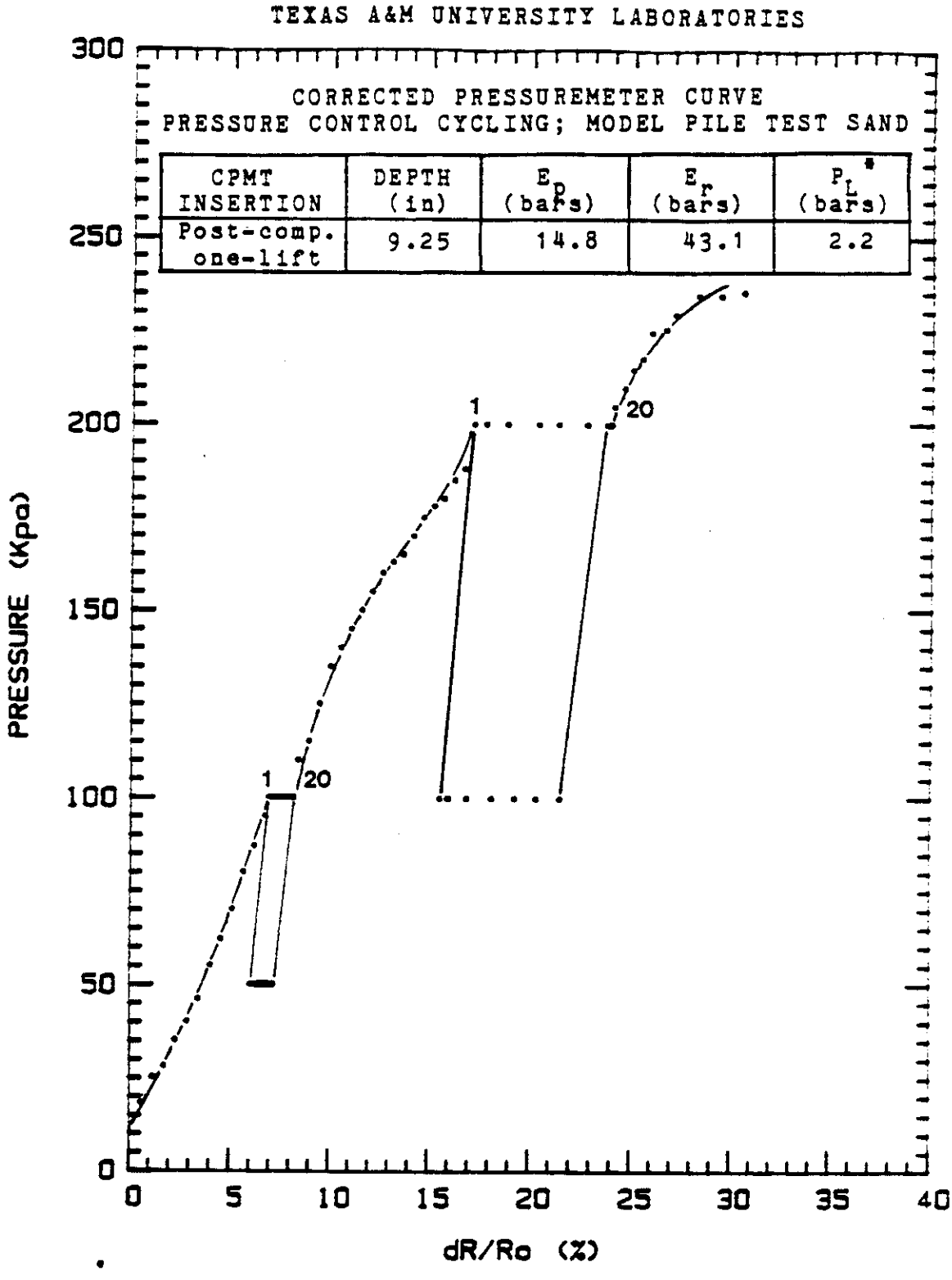

Figure 93. Shallow Corrected Pressuremeter Curve for Post-compacted, Single Lift Procedure: Pressure-control Cycles.

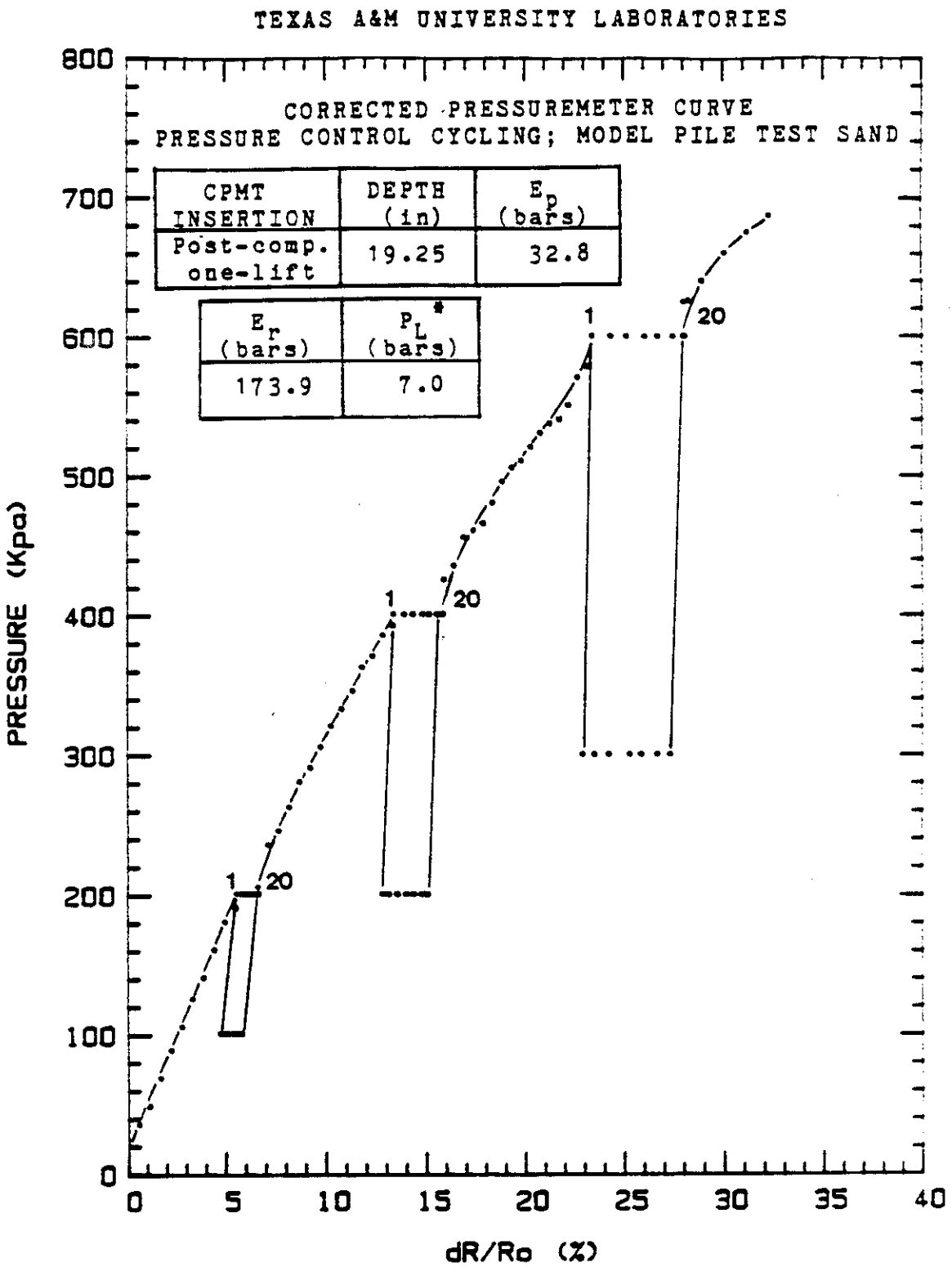

Figure 94. Deep Corrected Pressuremeter Curve for Post-compacted, Single Lift Procedure: Pressure-control Cycles.

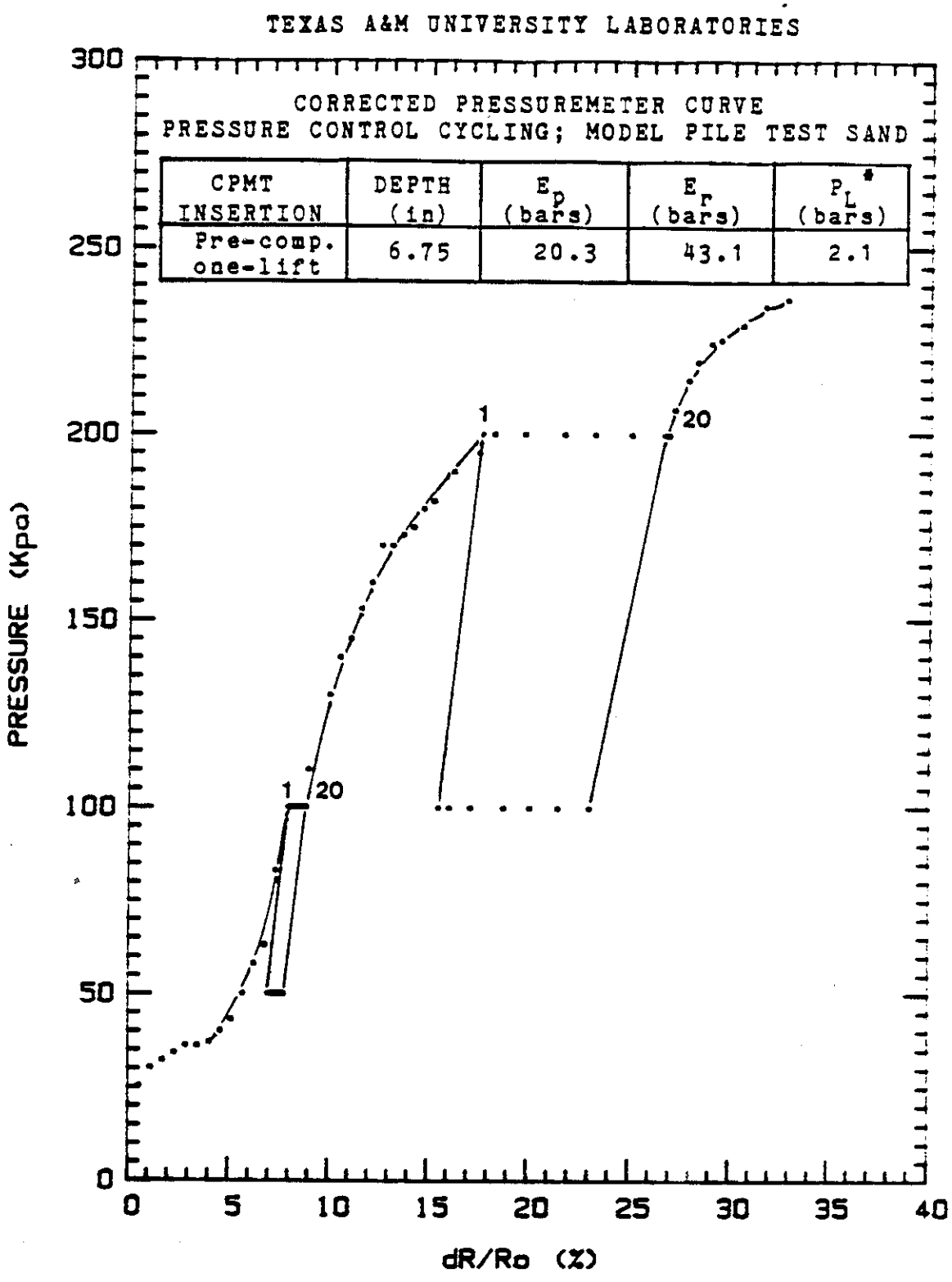

Figure 95. Shallow Corrected Pressuremeter Curve for Pre-compacted, Single Lift Procedure: Pressure-control Cycles.

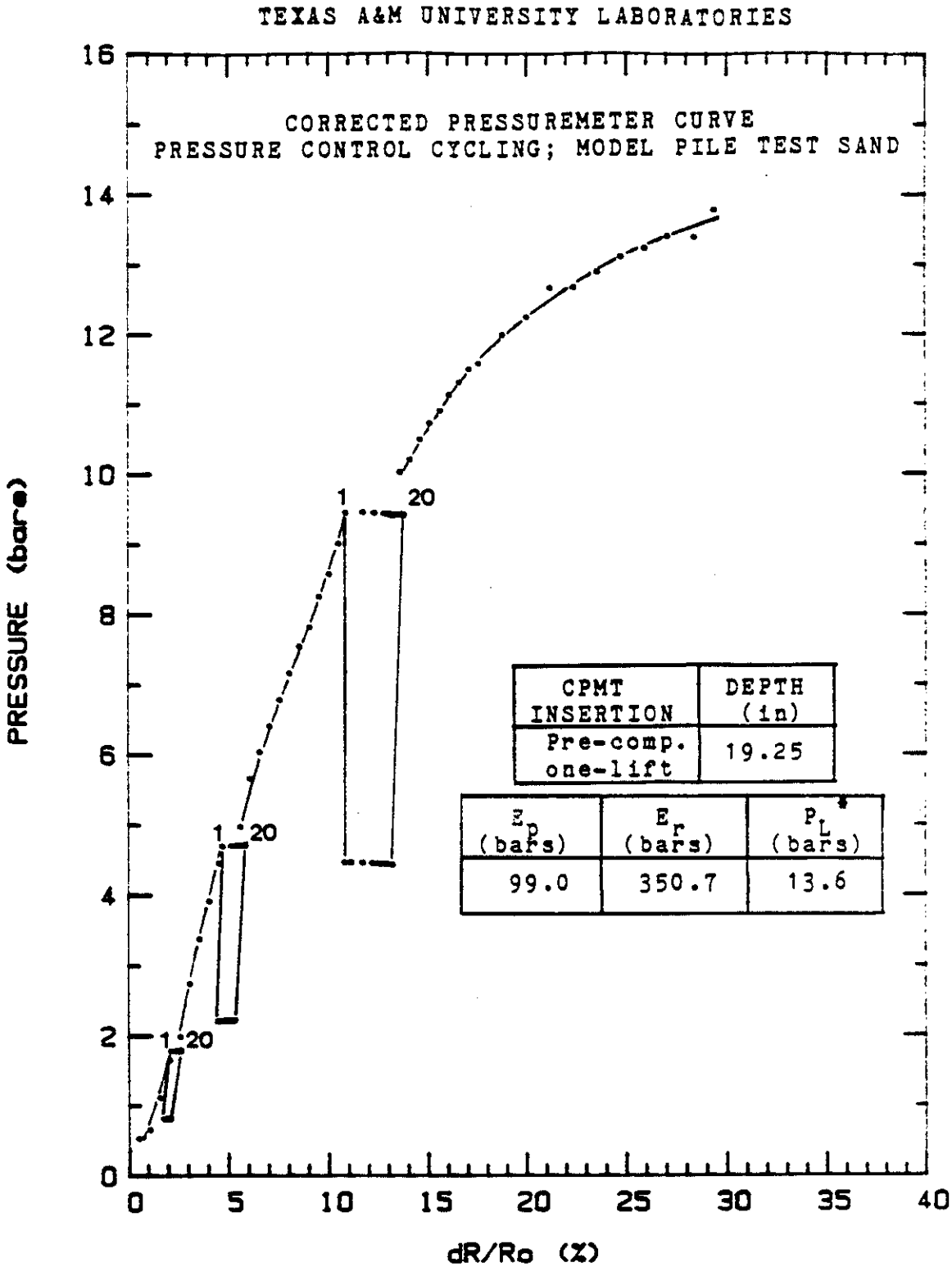

Figure 96. Deep Corrected Pressuremeter Curve for Pre-compacted, Single Lift Procedure: Pressure-control Cycles.

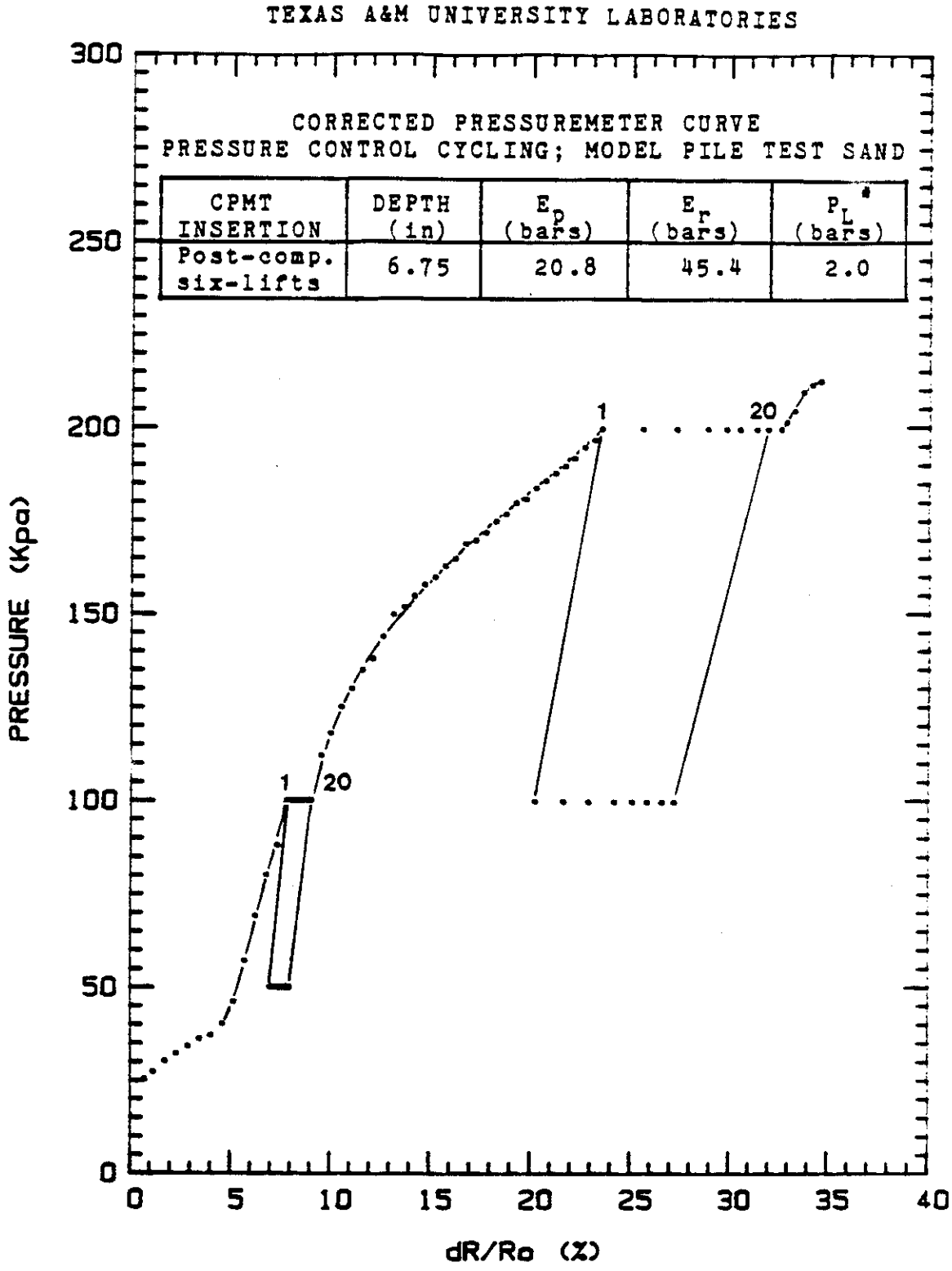

Figure 97. Shallow Corrected Pressuremeter Curve for Post-compacted, Multiple Lift Procedure: Pressure-control Cycles.

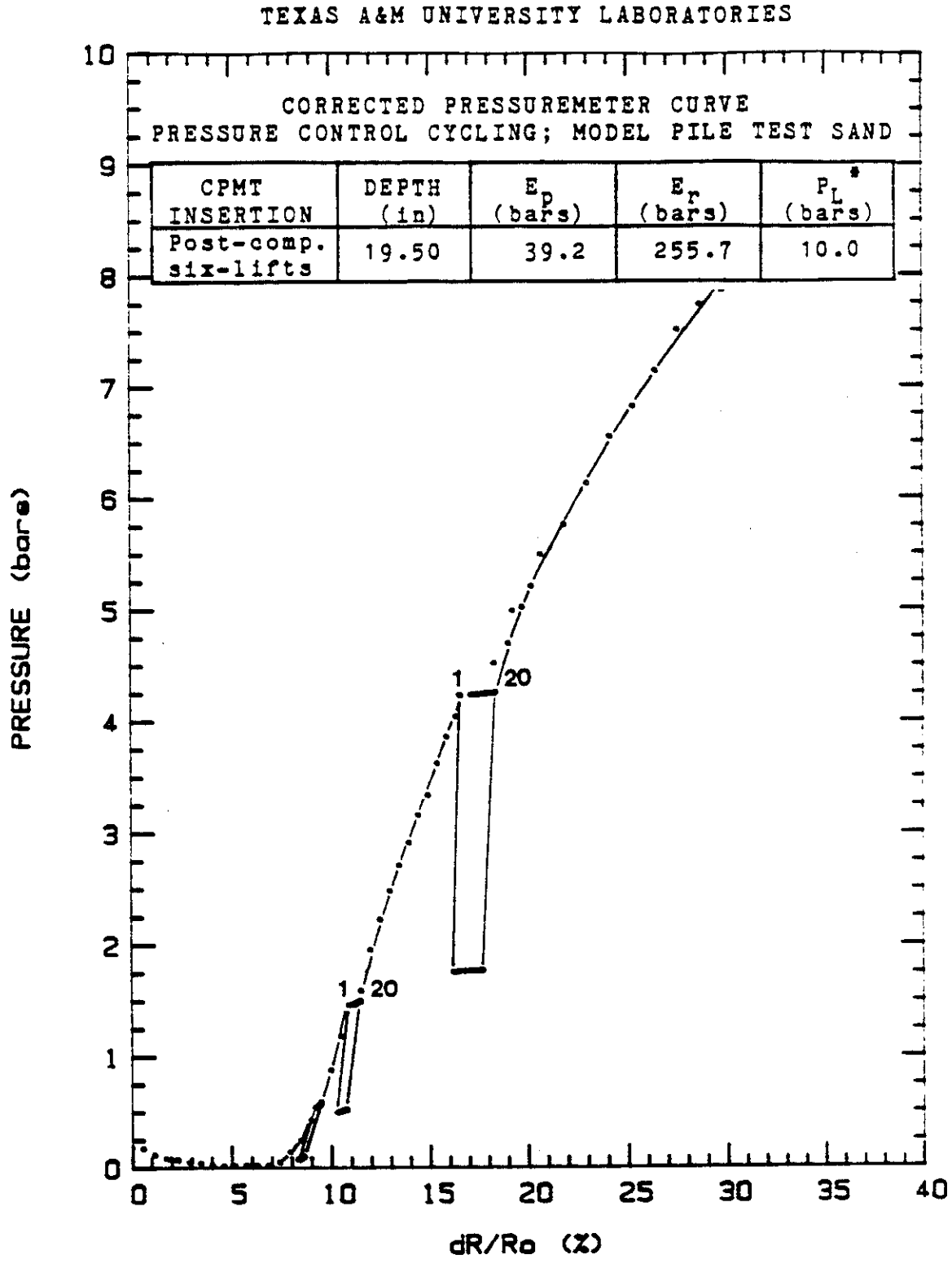

Figure 98. Deep Corrected Pressuremeter Curve for Post-compacted, Multiple Lift Procedure: Pressure-control Cycles.

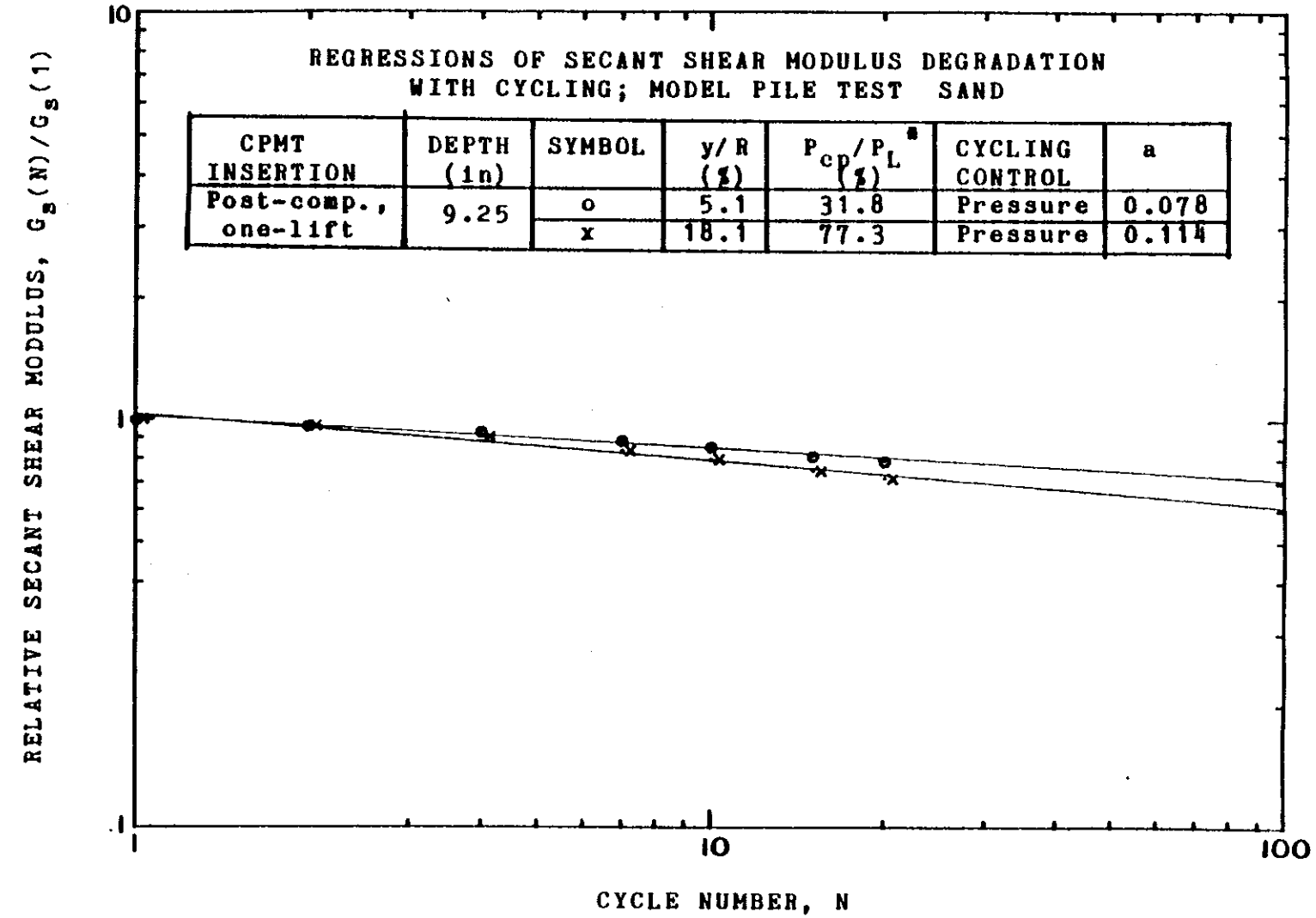

Figure 99. Secant Shear Modulus Degradation with Cycle Number, Shallow Test, Post-compacted, Single Lift Procedure: Pressure-control Cycles.

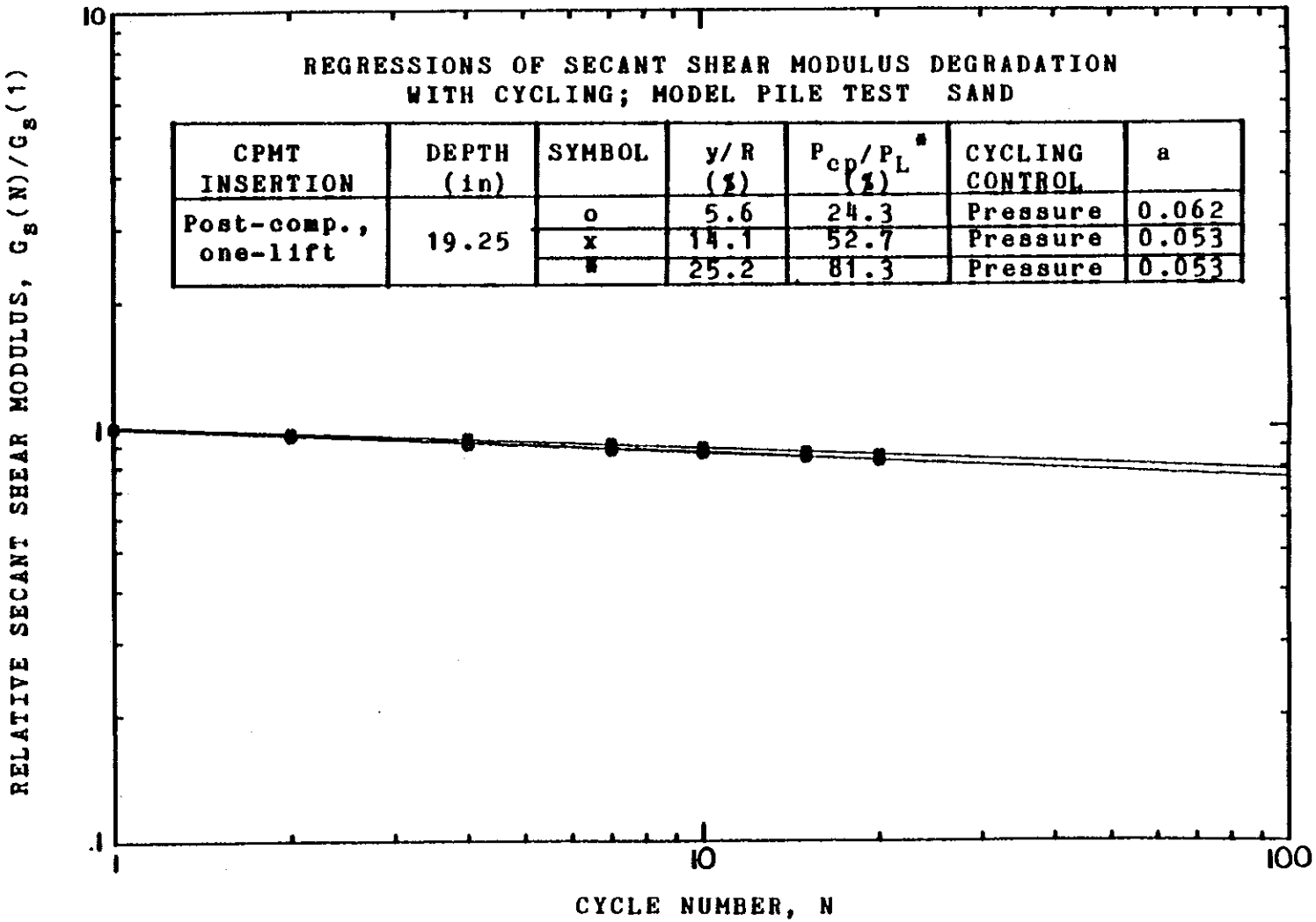

Figure 100. Secant Shear Modulus Degradation with Cycle Number, Deep Test, Post-compacted, Single Lift Procedure: Pressure-control Cycles.

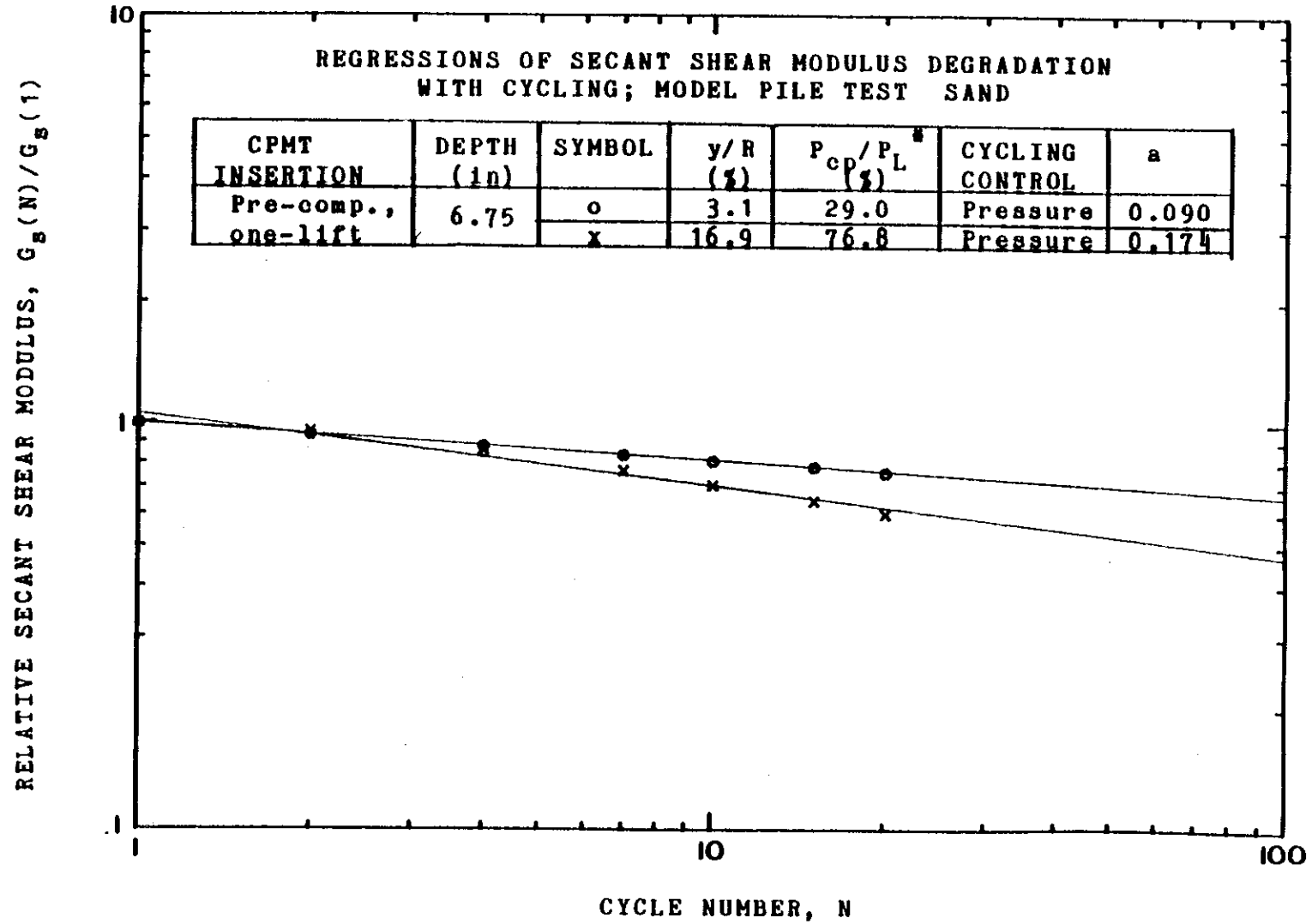

Figure 101. Secant Shear Modulus Degradation with Cycle Number, Shallow Test, Pre-compacted, Single Lift Procedure: Pressure-control Cycles.

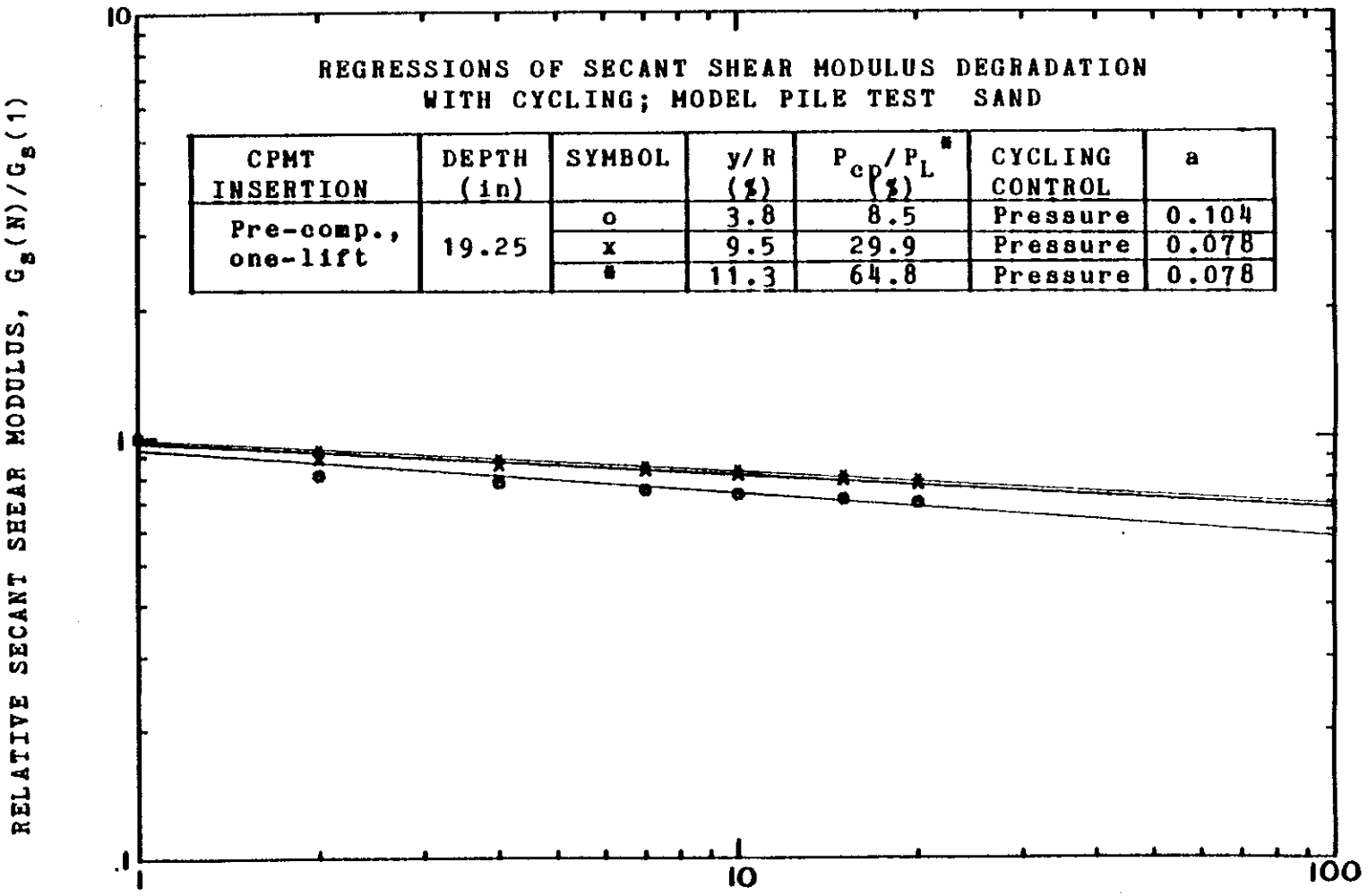

Figure 102. Secant Shear Modulus Degradation with Cycle Number, Deep Test, Pre-compacted, Single Lift Procedure: Pressure-control Cycles.

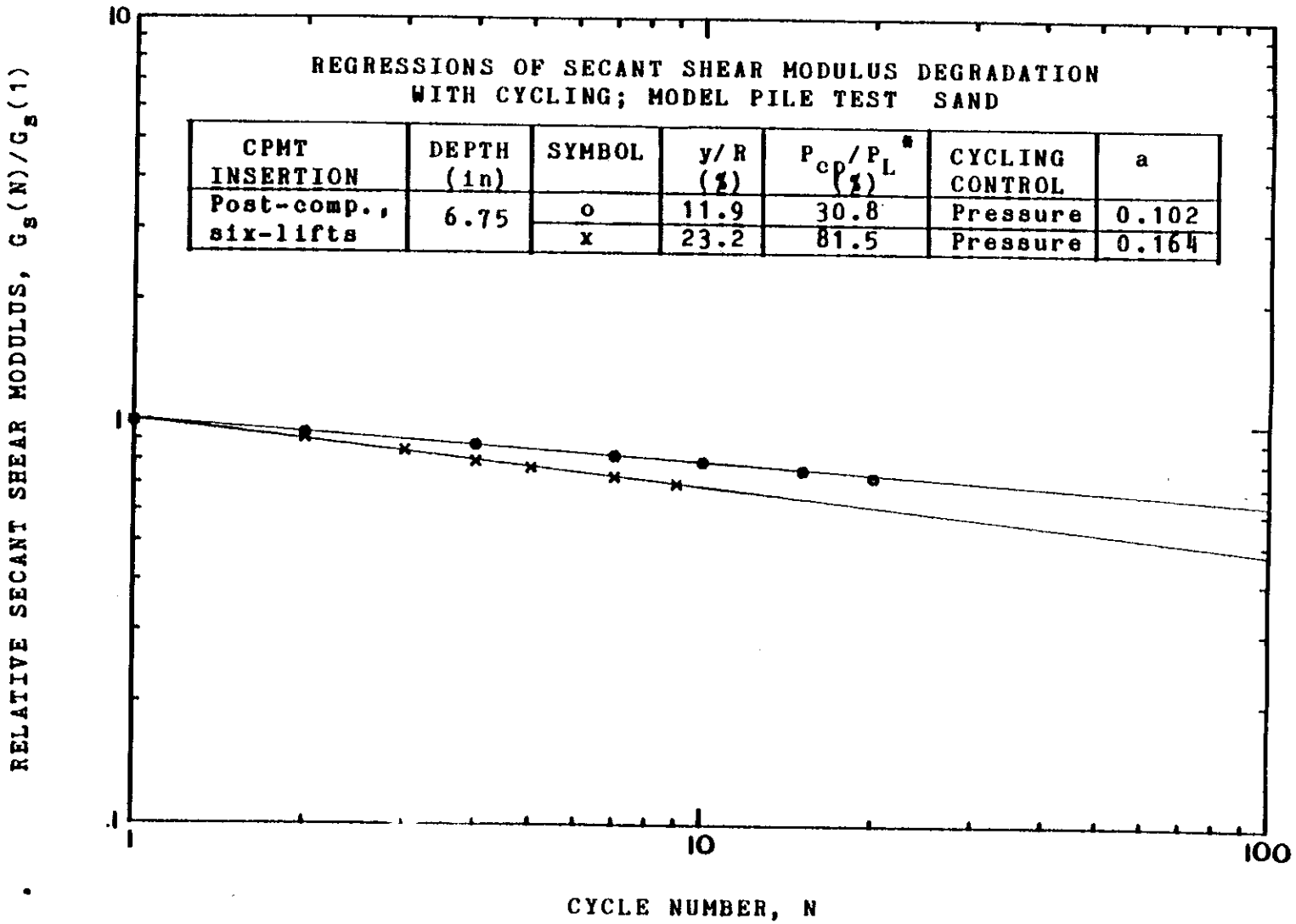

Figure 103. Secant Shear Modulus Degradation with Cycle Number, Shallow Test, Post-compacted, Multiple Lift Procedure: Pressure-control Cycles.

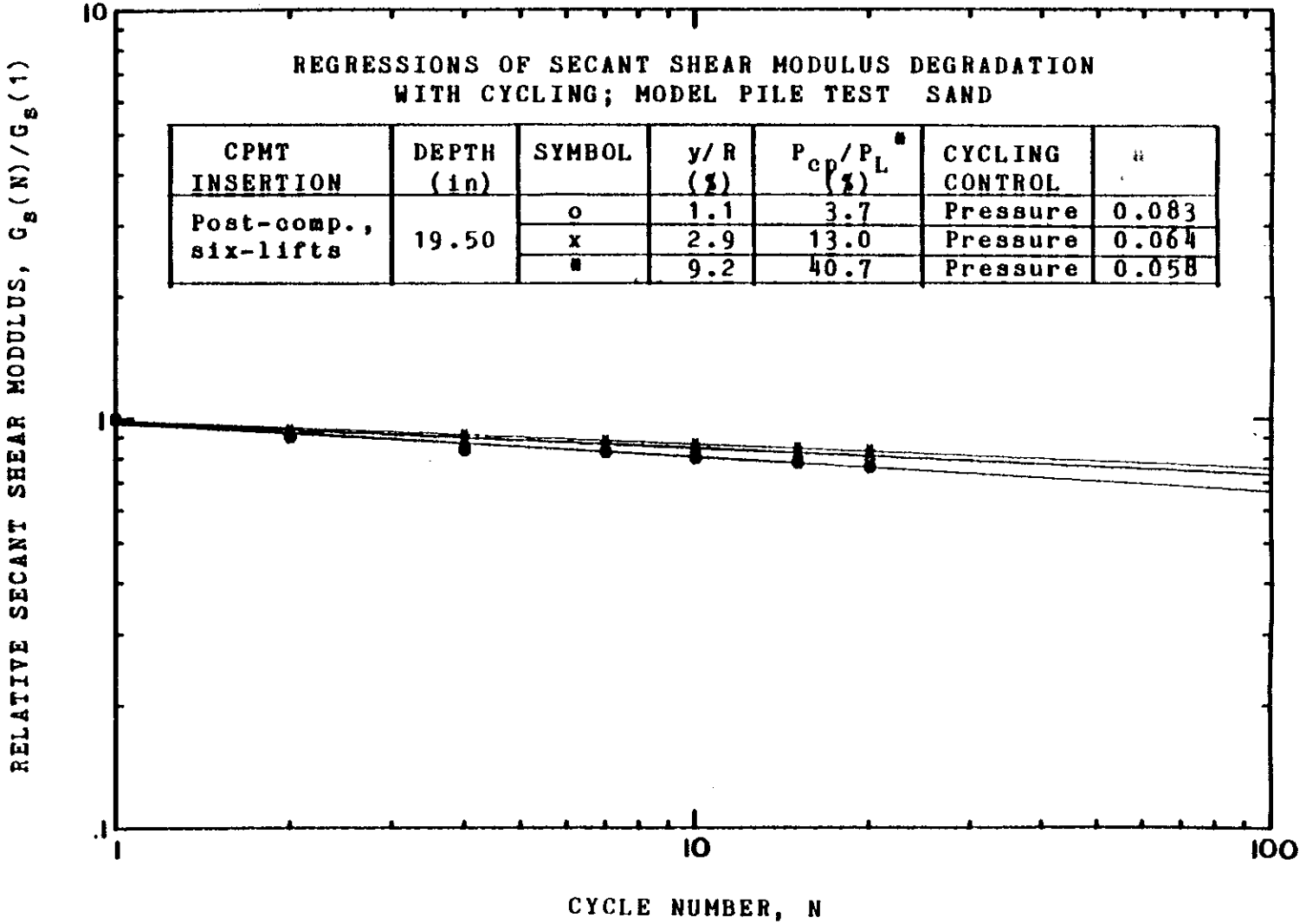

Figure 104. Secant Shear Modulus Degradation with Cycle Number, Deep Test, Post-compacted, Multiple Lift Procedure: Pressure-control Cycles.

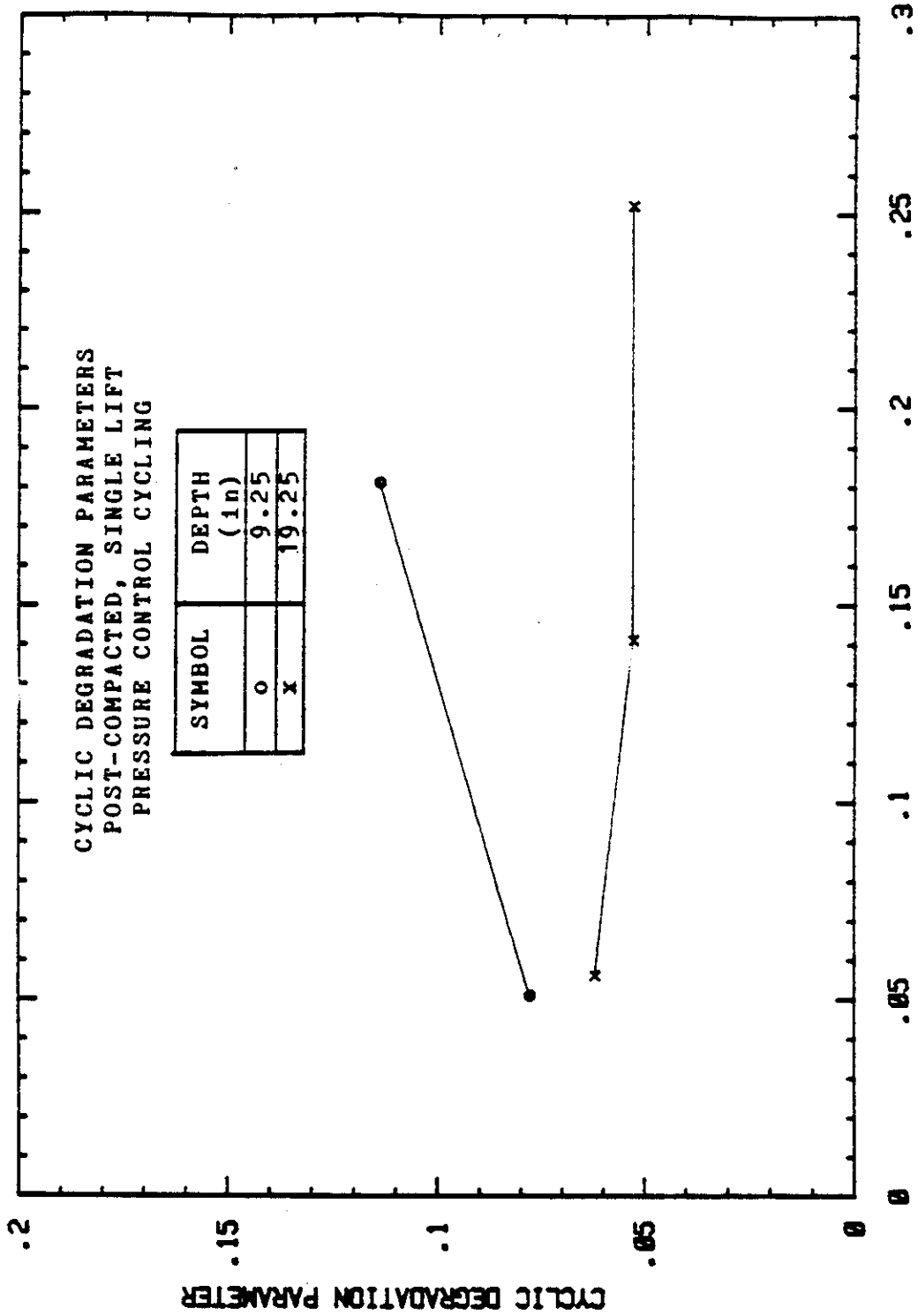

Figure 105. Cyclic Degradation Parameter versus Relative Radial Increase: Post-compacted, Single Lift Procedure, Pressure-control Cycles.

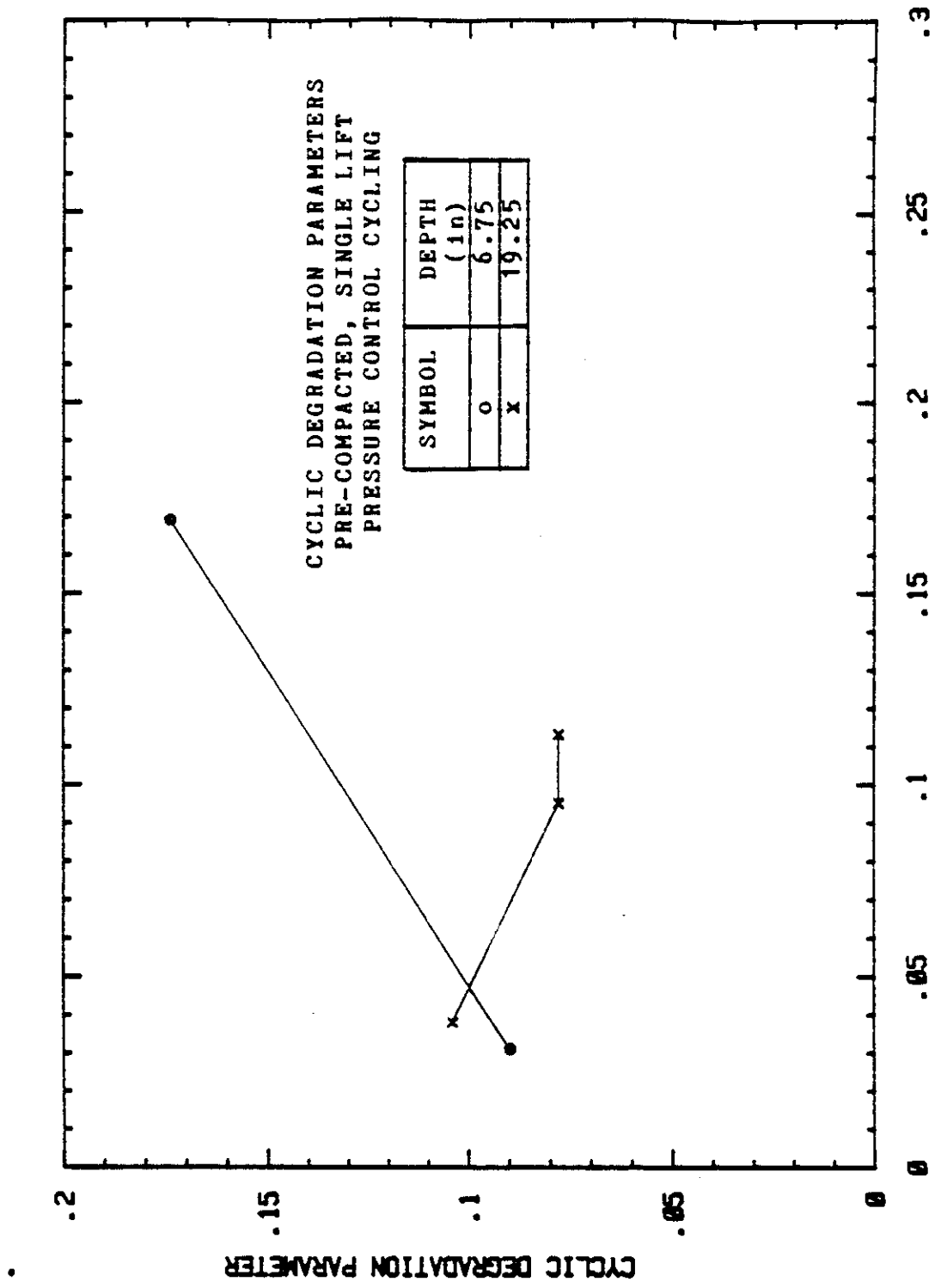

Figure 106. Cyclic Degradation Parameter versus Relative Radial Increase: Pre-compacted, Single Lift Procedure, Pressure-control Cycles.

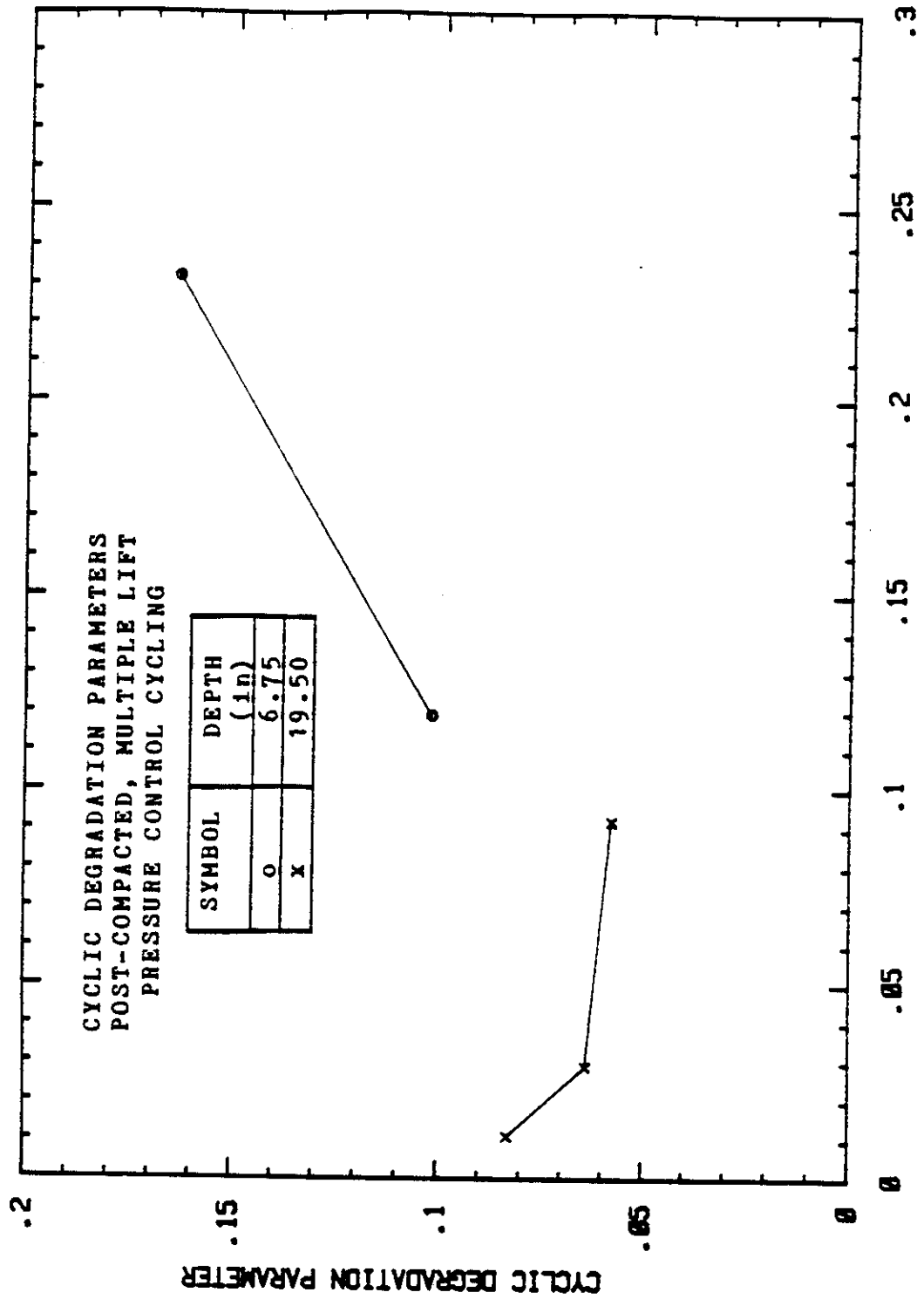

Figure 107. Cyclic Degradation Parameter versus Relative Radial Increase: Post-compacted, Multiple Lift Procedure, Pressure-control Cycles.

placement procedure. The average $\underline{a}$ values for each test series are tabulated in Table 6. Due to the dissimilar magnitudes between the shallow and deep test $\underline{a}$ values, an average value for each test depth was selected for use in the prediction process.

8.4 Volume-control Pressuremeter Test Results

8.4.1 Corrected Pressuremeter Curves

The corrected pressuremeter curves for the volume-control cyclic test series are shown in Figures 108 through 113. These curves also display the problem (described in Section 8.3.1) associated with the sand lodging between the steel strips.

8.4.2 Cyclic Degradation Parameters

The secant shear modulus degradation with increasing cycle number for the volume-control tests are seen in Figures 114 through 119. The $\underline{a}$ values are plotted versus the relative radial expansion y/R in Figures 120, 121, and 122. The variation between shallow $\underline{a}$ values and deep $\underline{a}$ values was not as pronounced as in the pressure-control tests (Table 6), and only a single average $\underline{a}$ value was chosen for each placement procedure.

The following reason is given for the above difference: Close to the surface there is a lack of vertical confinement. Due to this lack of vertical confinement a PMT test close to the surface shows a well defined limit to the horizontal pressure which can be applied (Figure 112). This

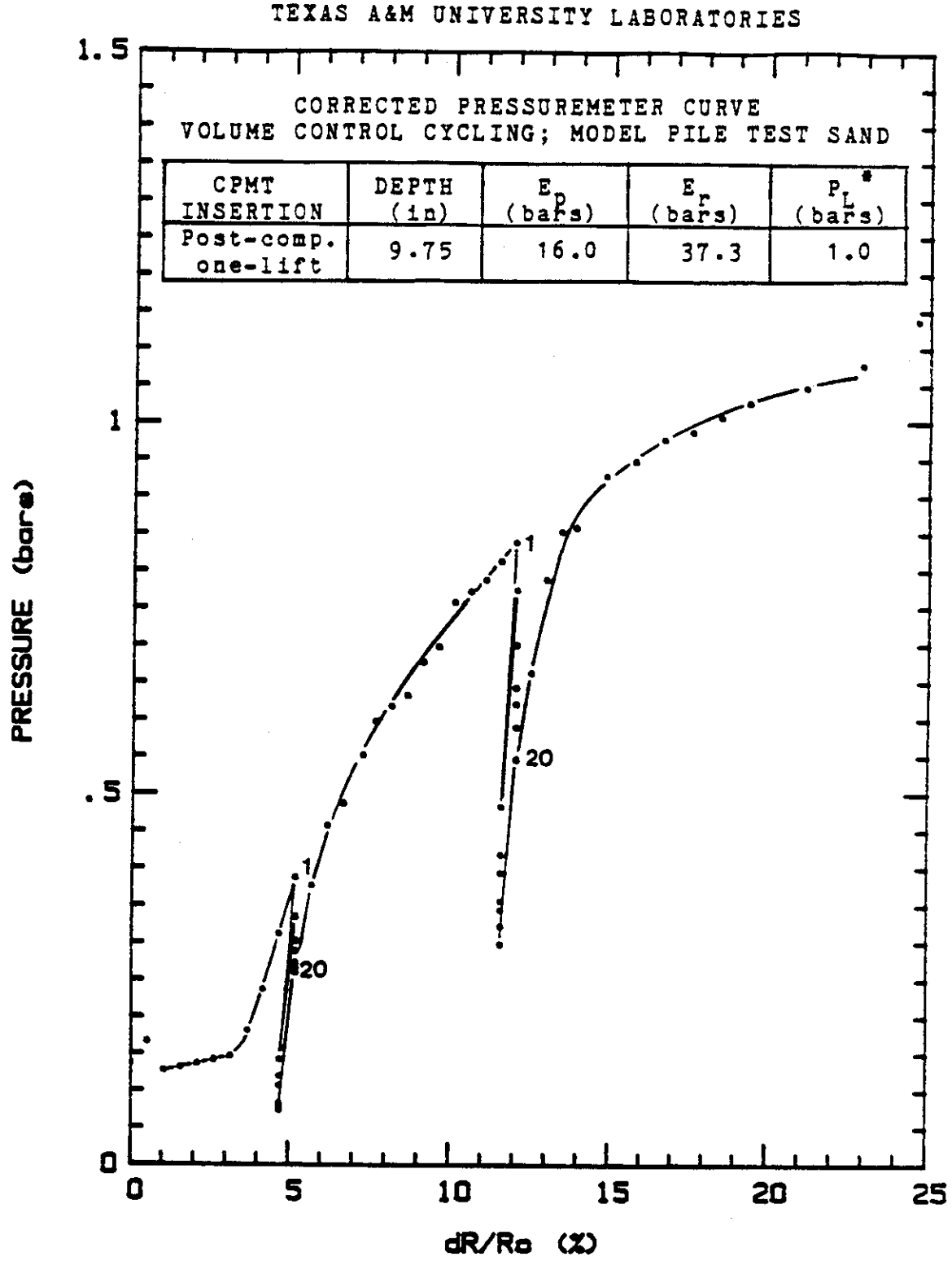

Figure 108. Shallow Corrected Pressuremeter Curve for Post-compacted, Single Lift Procedure: Volume-control Cycles.

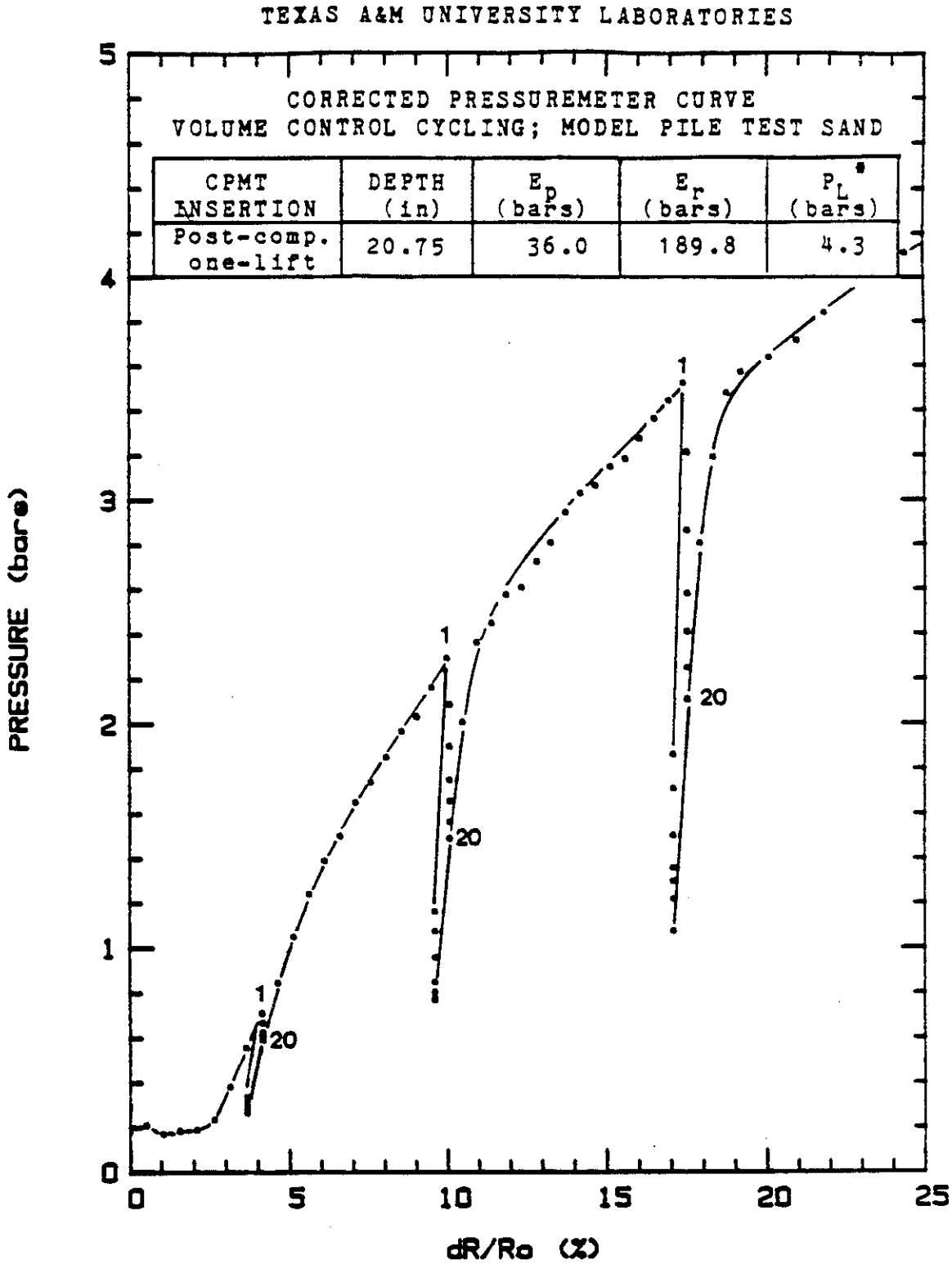

Figure 109. Deep Corrected Pressuremeter Curve for Post-compacted, Single Lift Procedure: Volume-control Cycles.

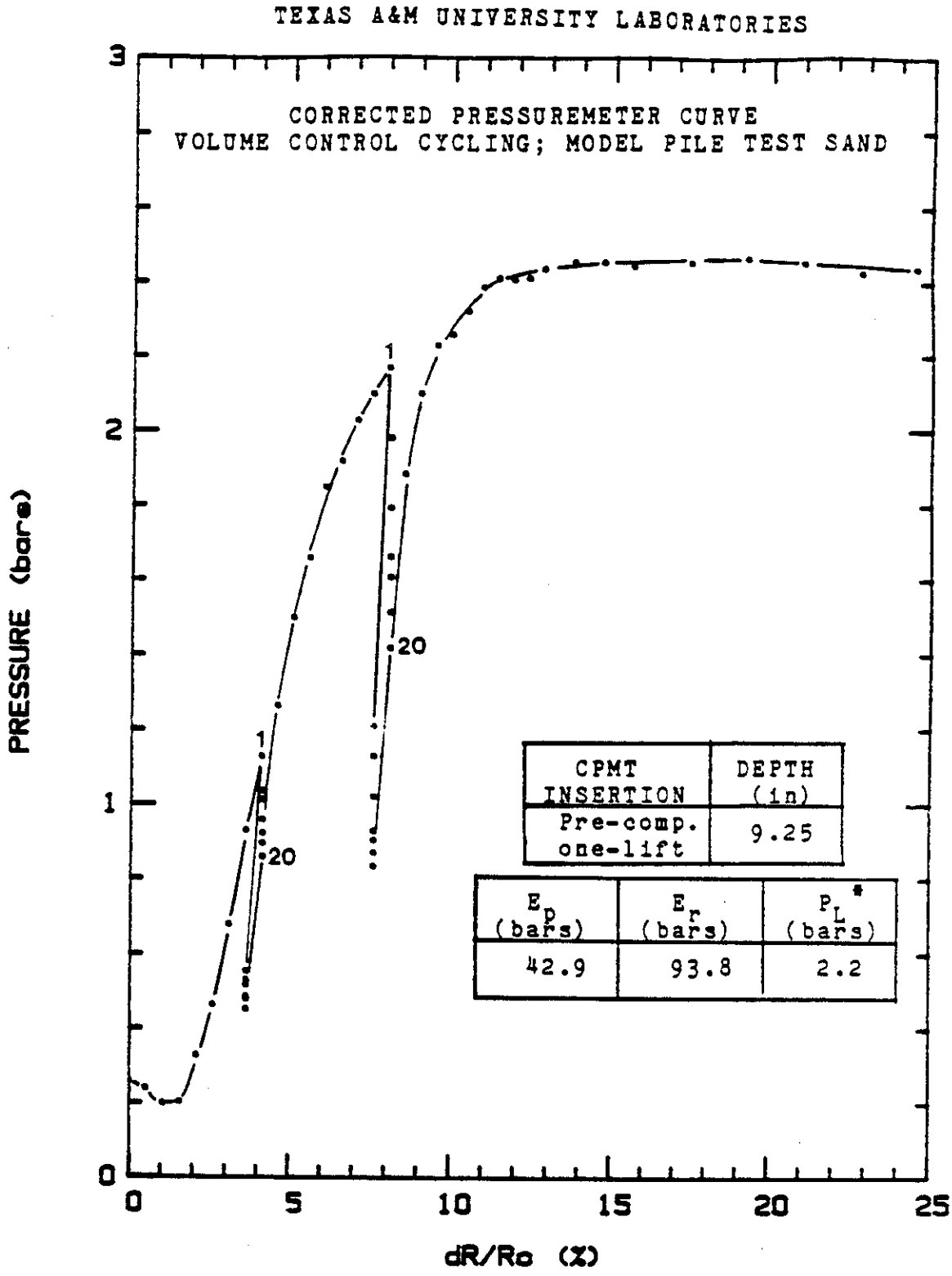

Figure 110. Shallow Corrected Pressuremeter Curve for Pre-compacted, Single Lift Procedure: Volume-control Cycles.

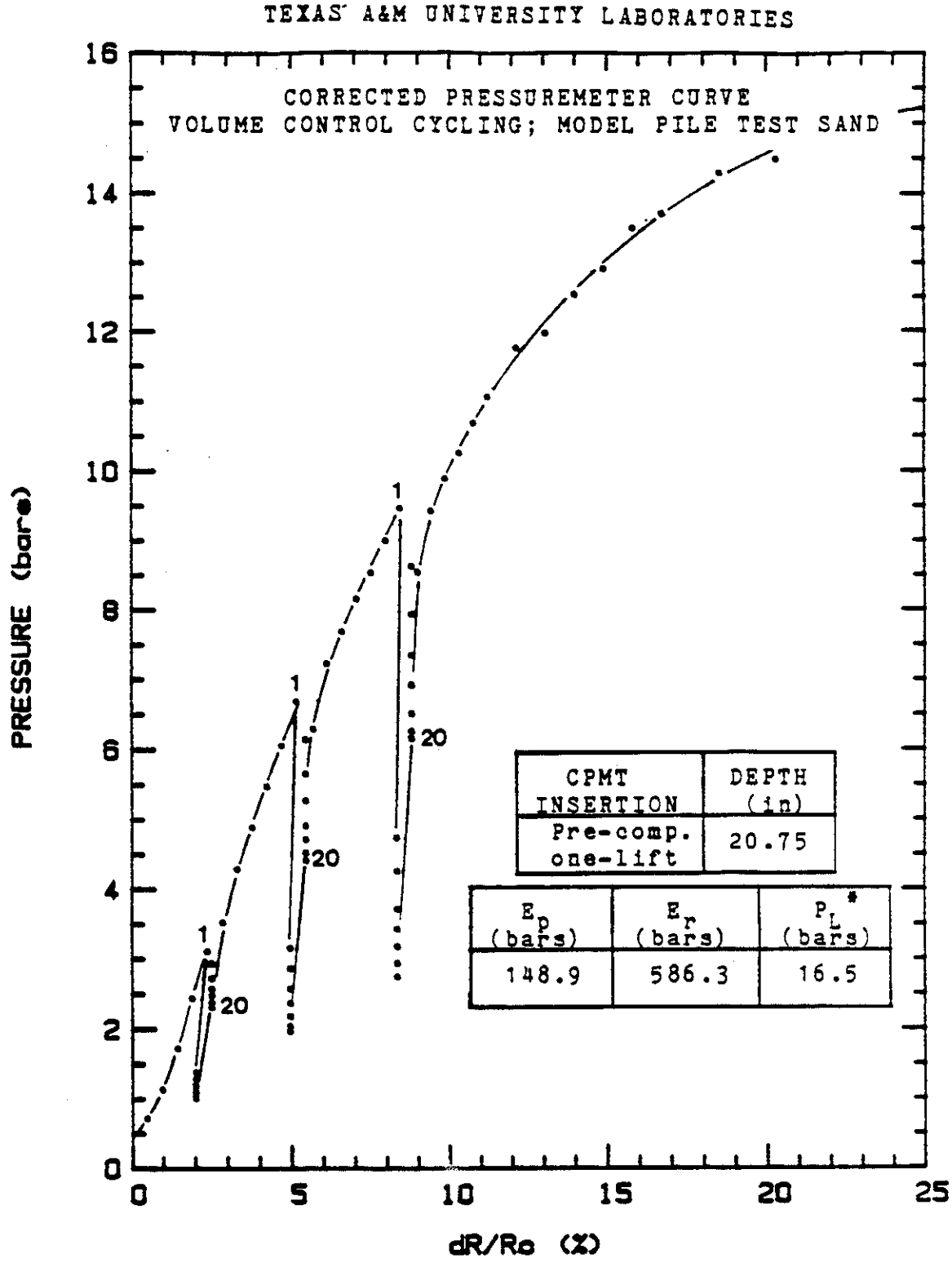

Figure 111. Deep Corrected Pressuremeter Curve for Pre-compacted, Single Lift Procedure: Volume-control Cycles.

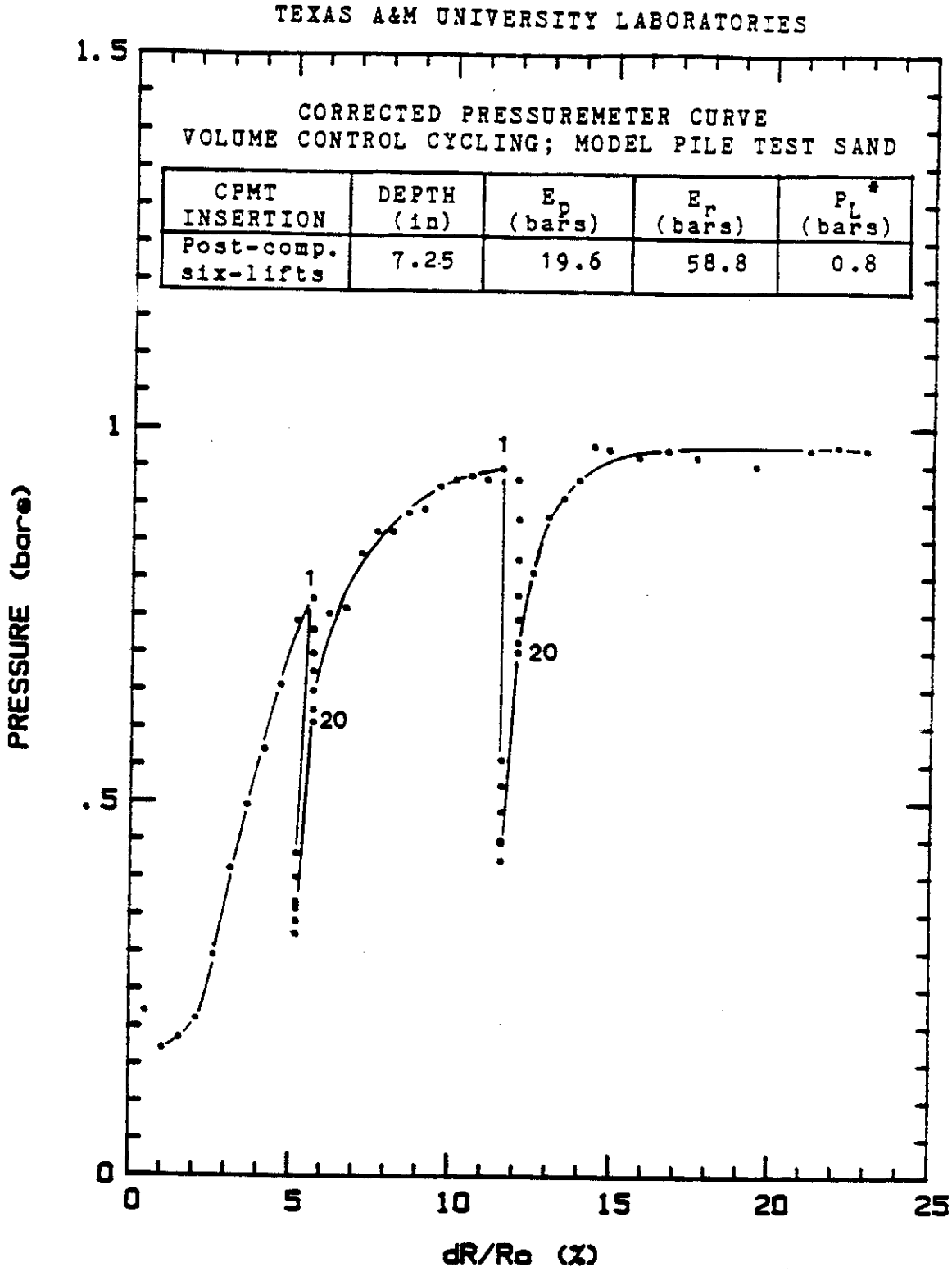

Figure 112. Shallow Corrected Pressuremeter Curve for Post-compacted, Multiple Lift Procedure: Volume-control Cycles.

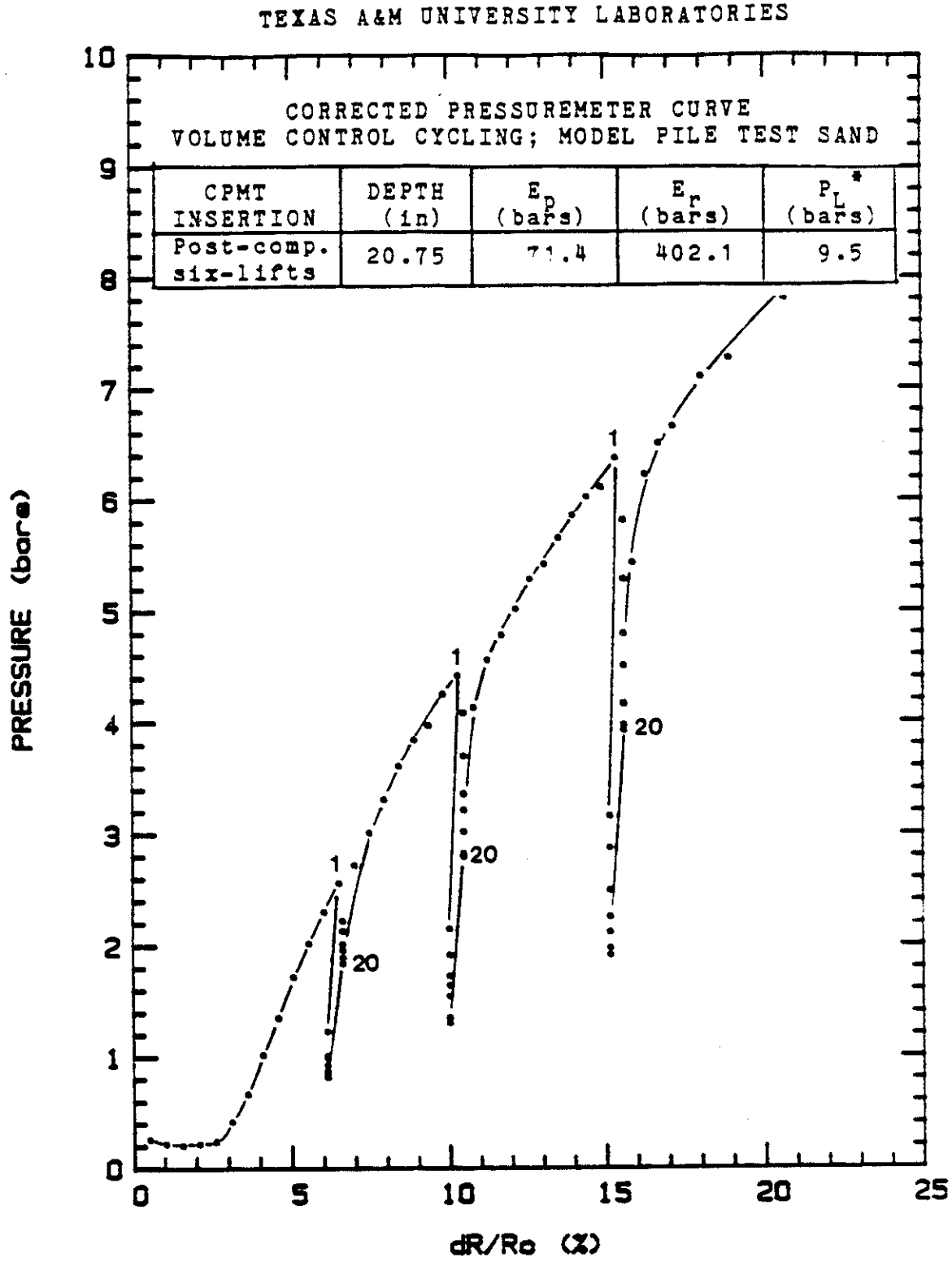

Figure 113. Deep Corrected Pressuremeter Curve for Post-compacted, Multiple Lift Procedure: Volume-control Cycles.

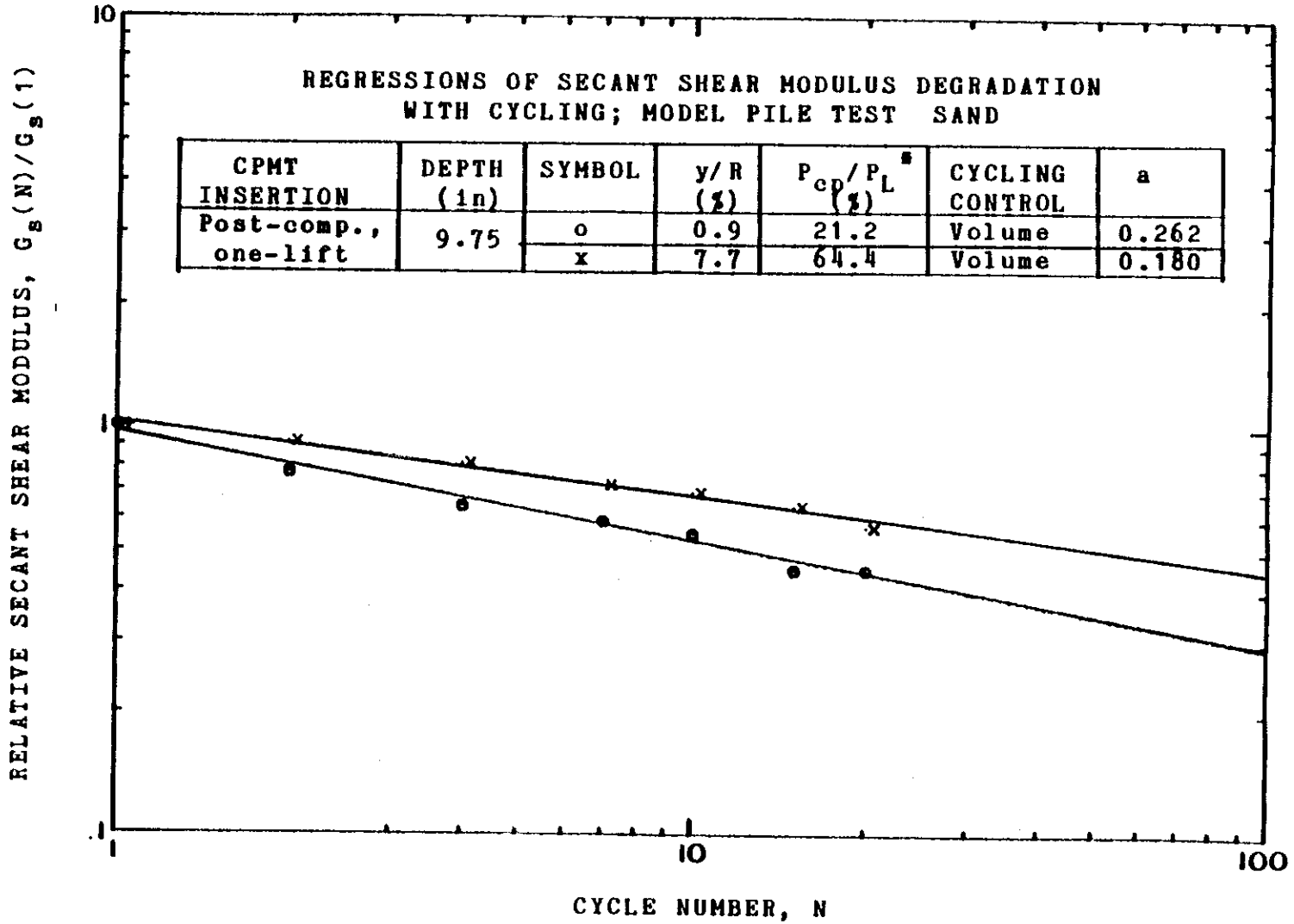

Figure 114. Secant Shear Modulus Degradation with Cycle Number, Shallow Test, Post-compacted, Single Lift Procedure: Volume-control Cycles.

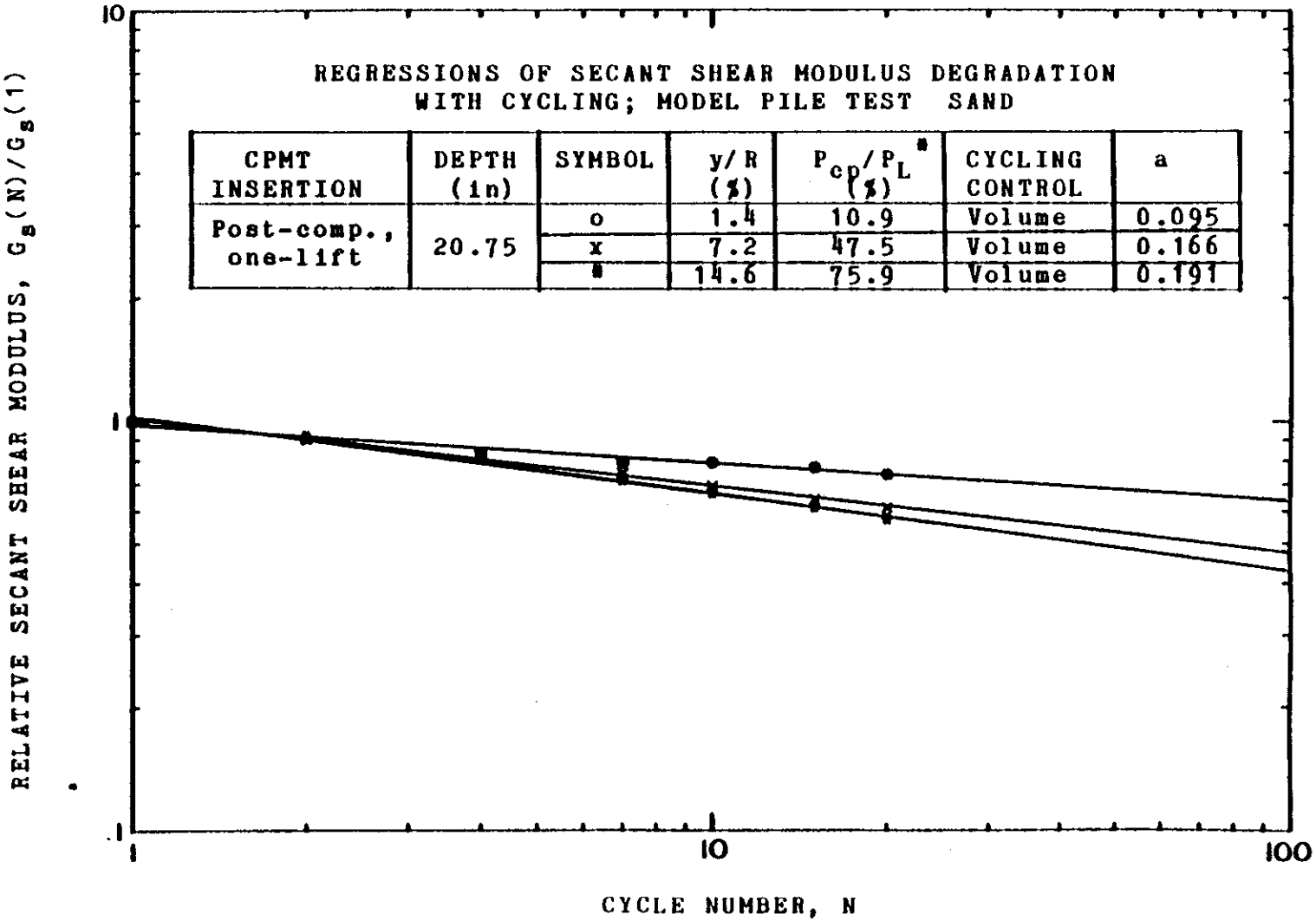

Figure 115. Secant Shear Modulus Degradation with Cycle Number, Deep Test, Post-compacted, Single Lift Procedure: Volume-control Cycles.

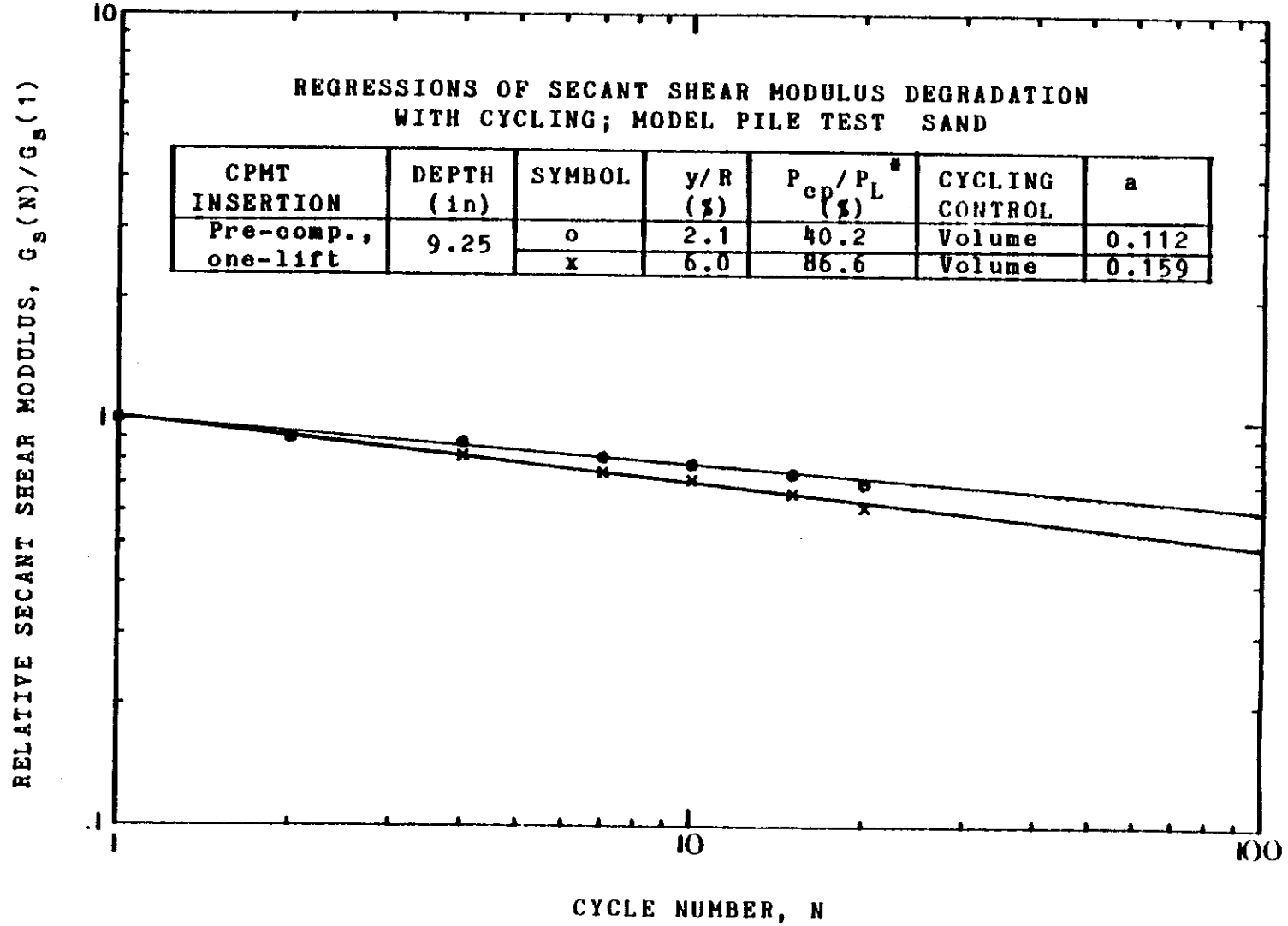

Figure 116. Secant Shear Modulus Degradation with Cycle Number, Shallow Test, Pre-compacted, Single Lift Procedure: Volume-control Cycles.

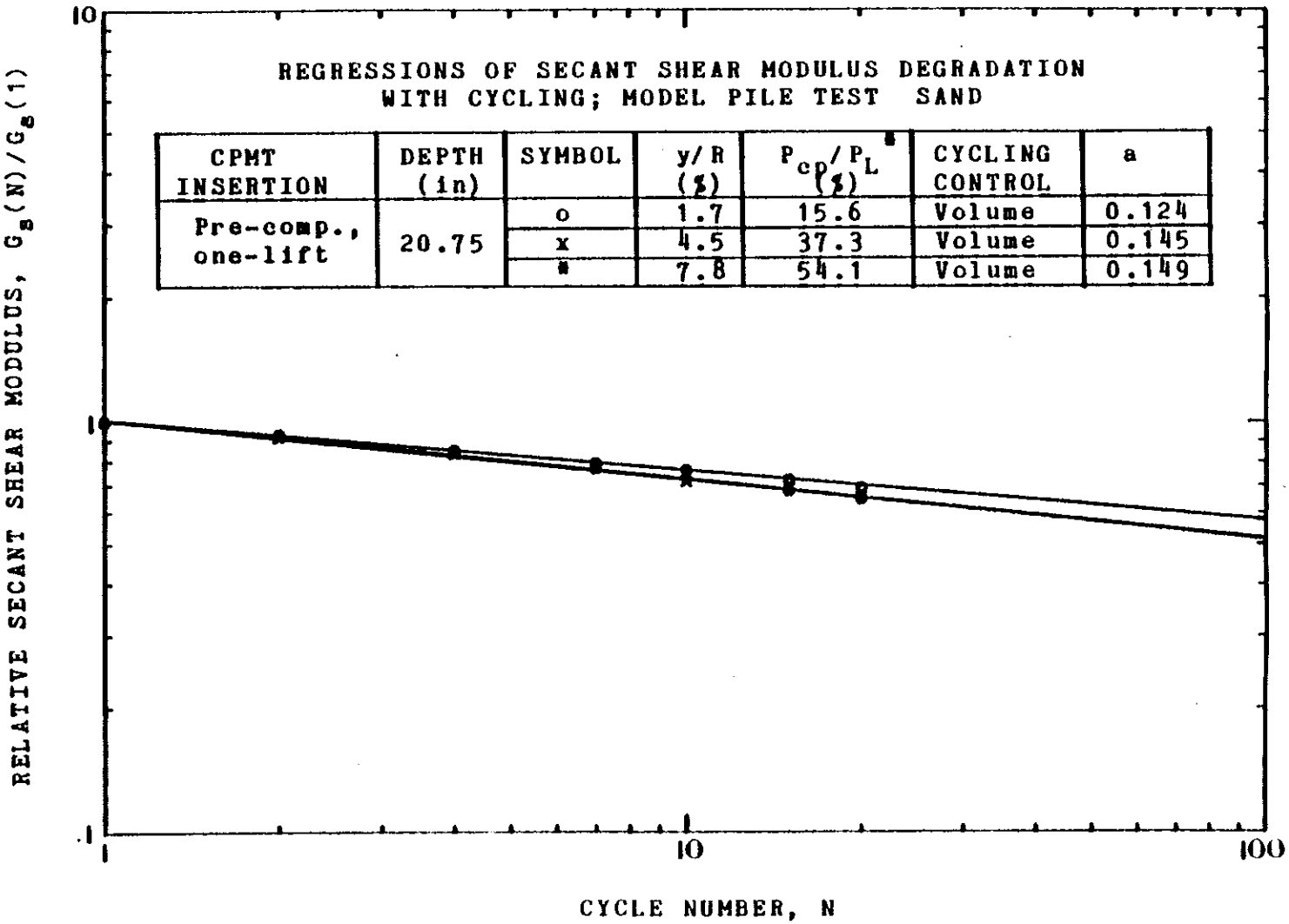

Figure 117. Secant Shear Modulus Degradation with Cycle Number, Deep Test, Pre-compacted, Single Lift Procedure: Volume-control Cycles.

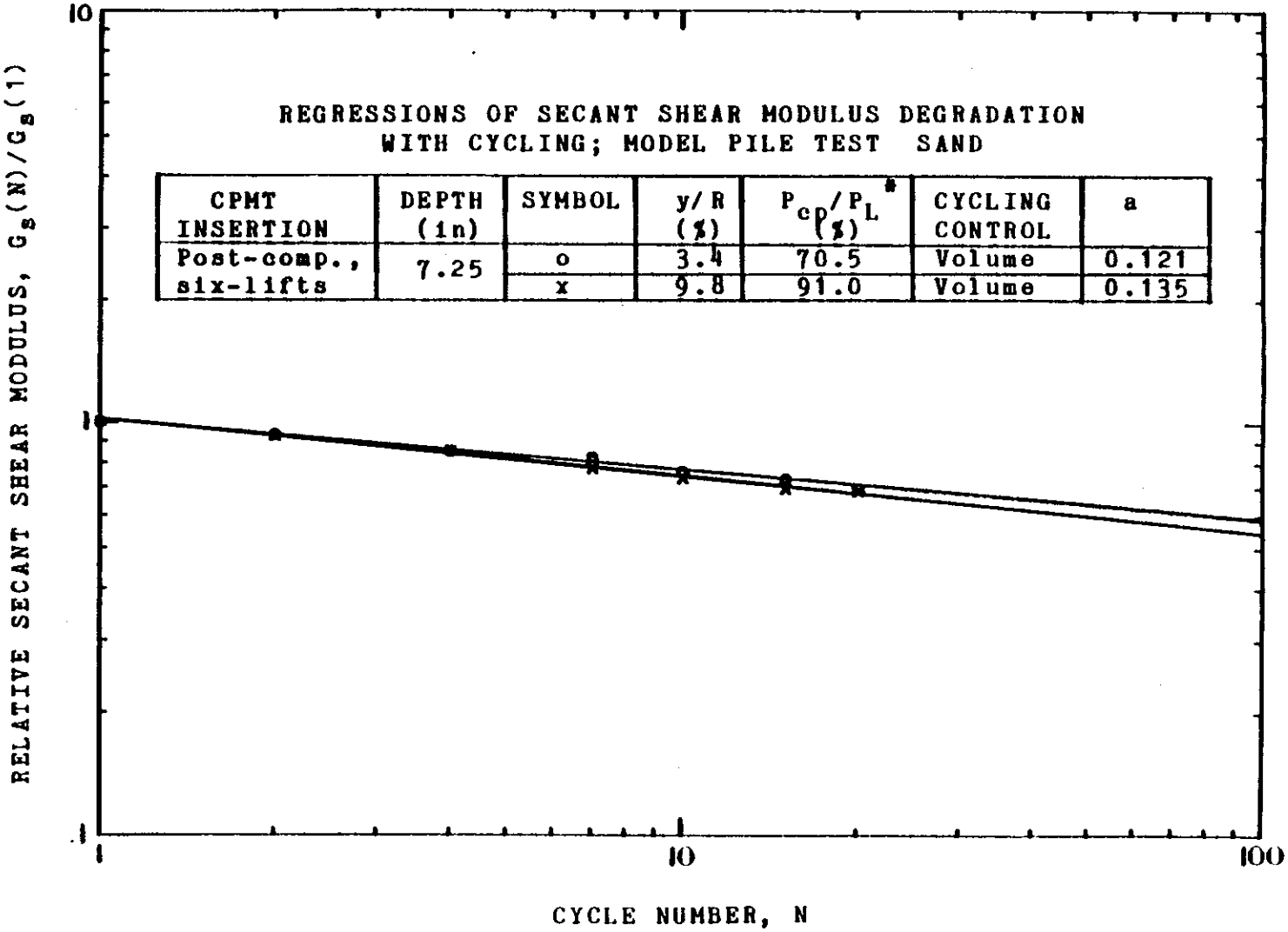

Figure 118. Secant Shear Modulus Degradation with Cycle Number, Shallow Test, Post-compacted, Multiple Lift Procedure: Volume-control Cycles.

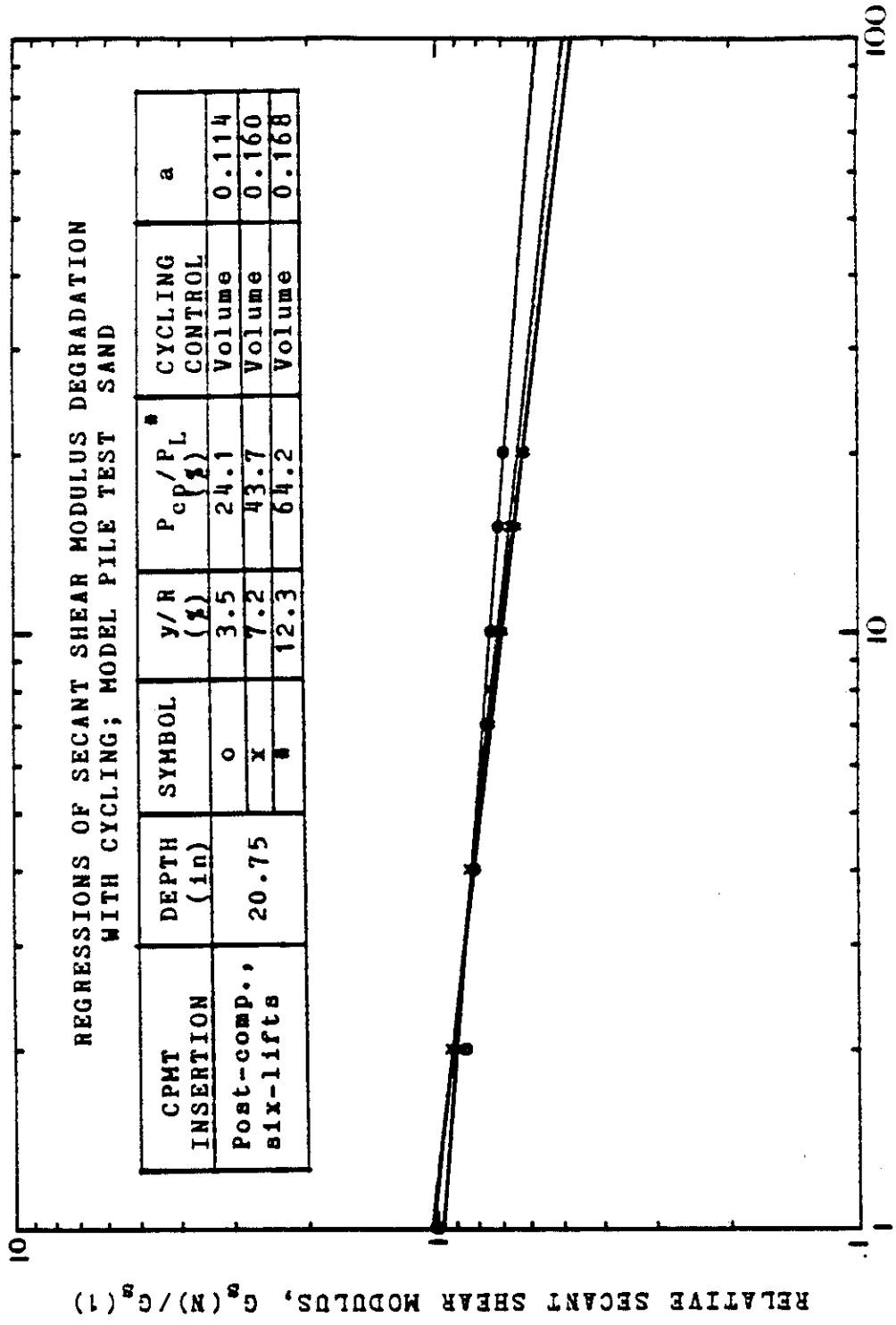

Figure 119. Secant Shear Modulus Degradation with Cycle Number, Deep Test, Post-compacted, Multiple Lift Procedure: Volume-control Cycles.

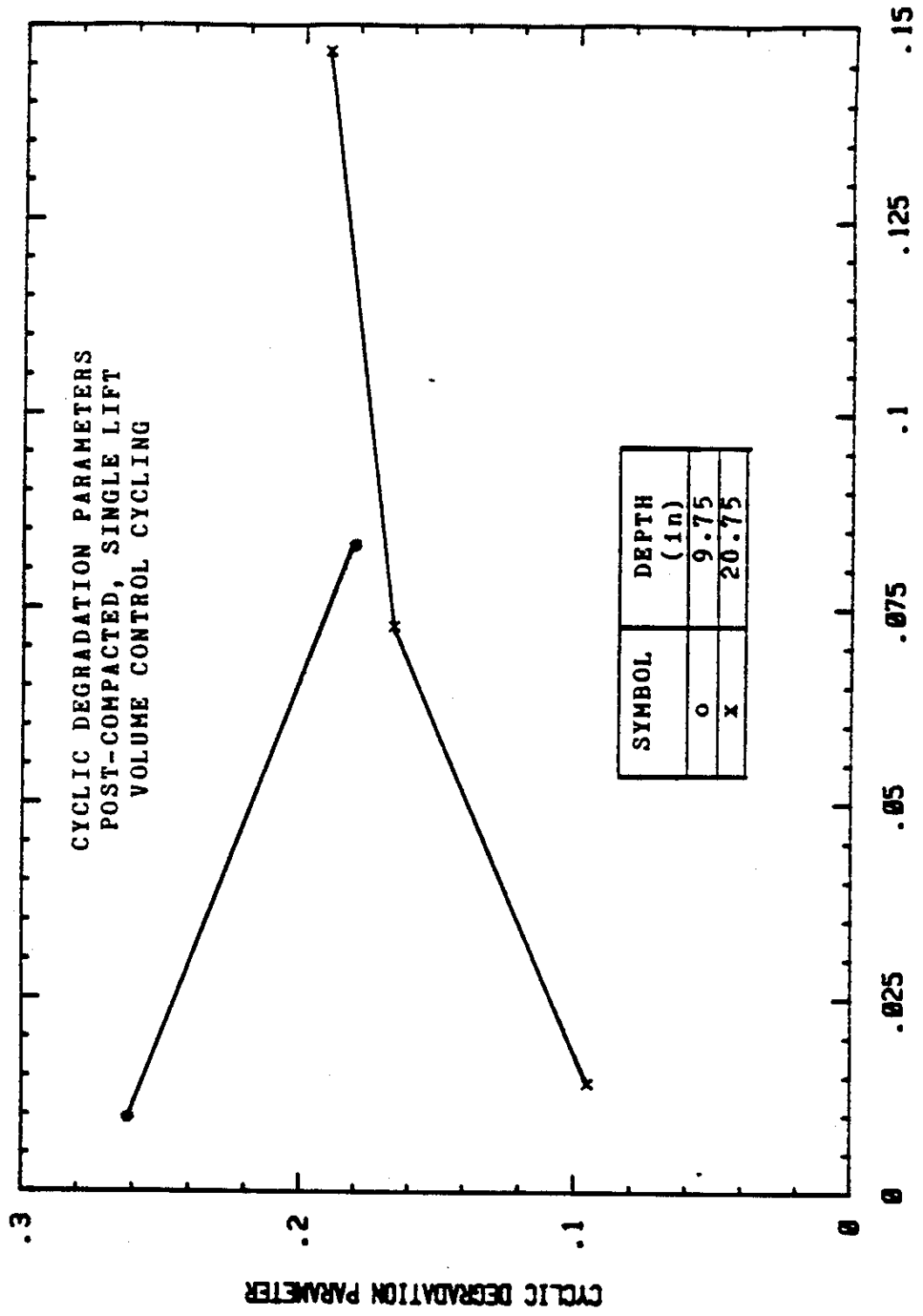

Figure 120. Cyclic Degradation Parameter versus Relative Radial Increase: Post-compacted, Single Lift Procedure, Volume-control Cycles.

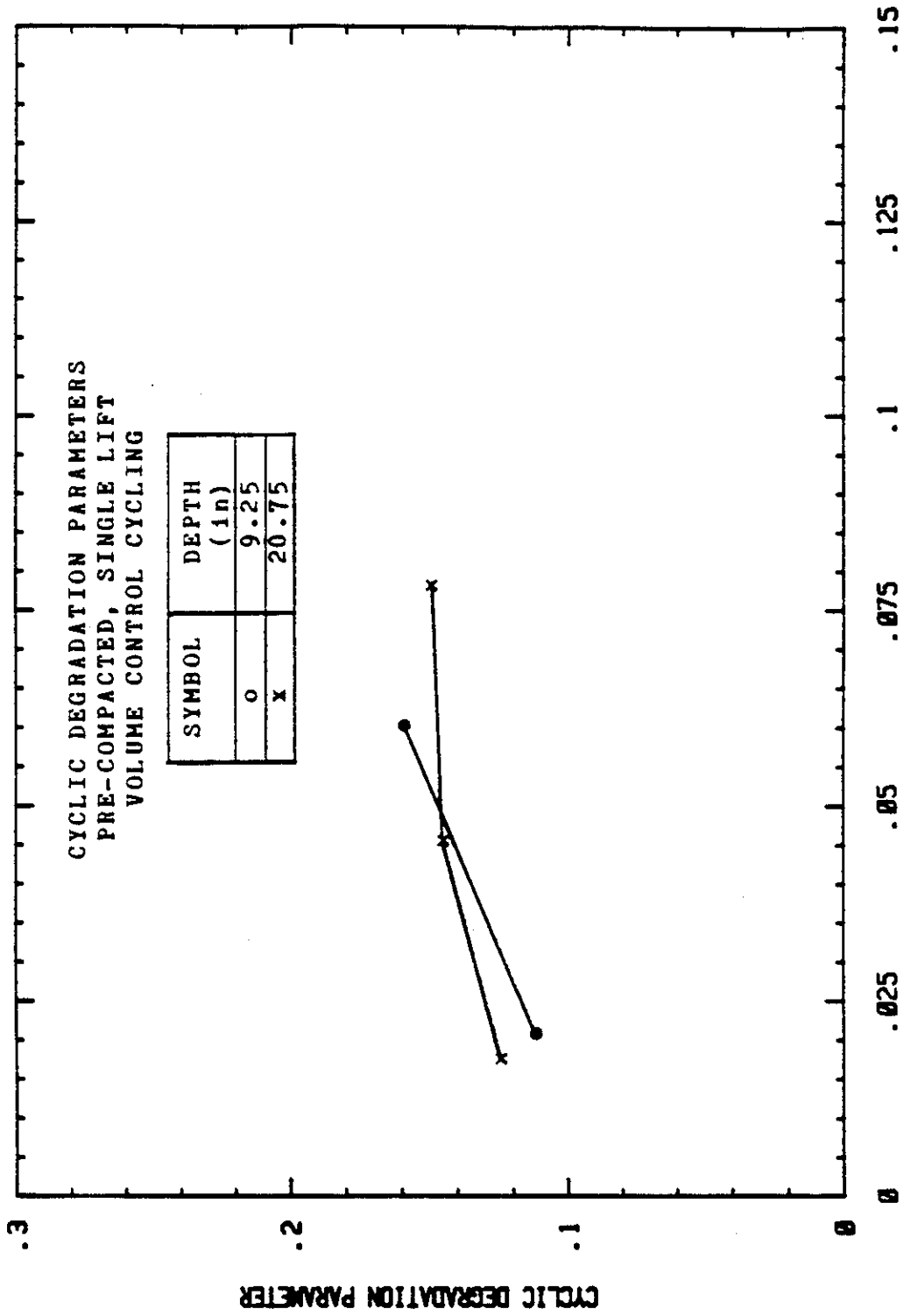

Figure 121. Cyclic Degradation Parameter versus Relative Radial Increase: Pre-compacted, Single Lift Procedure, Volume-control Cycles.

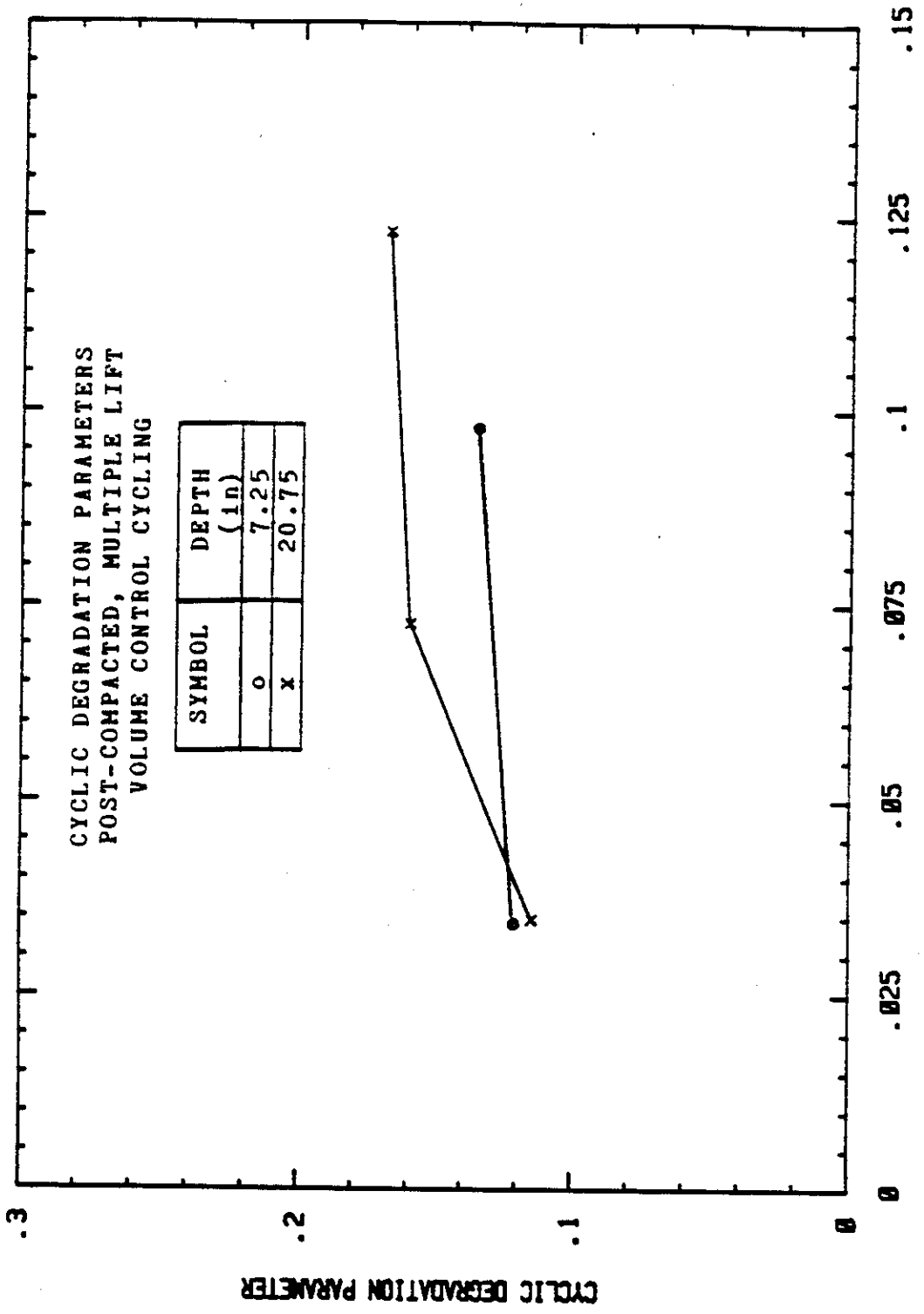

Figure 122. Cyclic Degradation Parameter versus Relative Radial Increase: Post-compacted, Multiple Lift Procedure, Volume-control Cycles.

is not the case for a deeper PMT test (Figure 113). The influence of vertical pressure confinement on the degradation in cyclic tests is that: (1) the degradation is more severe for the shallow test than for the deep test (Table 6), and (2) for shallow pressure-control tests the degradation is more severe at large y/R than at small y/R (Table 6).

8.5 Pressure-control vs. Volume-control Degradation Parameter Comparison

The degradation parameters found in all of the cyclic pressuremeter tests have been tabulated (Table 6). The results indicate higher degradation of the soils exposed to volume-control cycling than those where pressure-control cycling was executed. This result agrees with that of the pressure-control versus volume-control test performed at the University of Houston sand deposit with the TEXAM probe (Section 7.3.2).

As pointed out in section 8.4.2, degradation during pressure-control tests was more greatly influenced by overburden pressure than degradation during volume-control tests. Figures 123 and 124 present the a values from Table 6 plotted versus the test depth. The pattern for the pressure-control tests indicate decreasing a values with increasing depth. The volume-control a values do not reflect a similar trend. Also, the greater spread in data obvious in the volume-control tests may indicate that the cyclic degradation parameter a is more dependent upon the

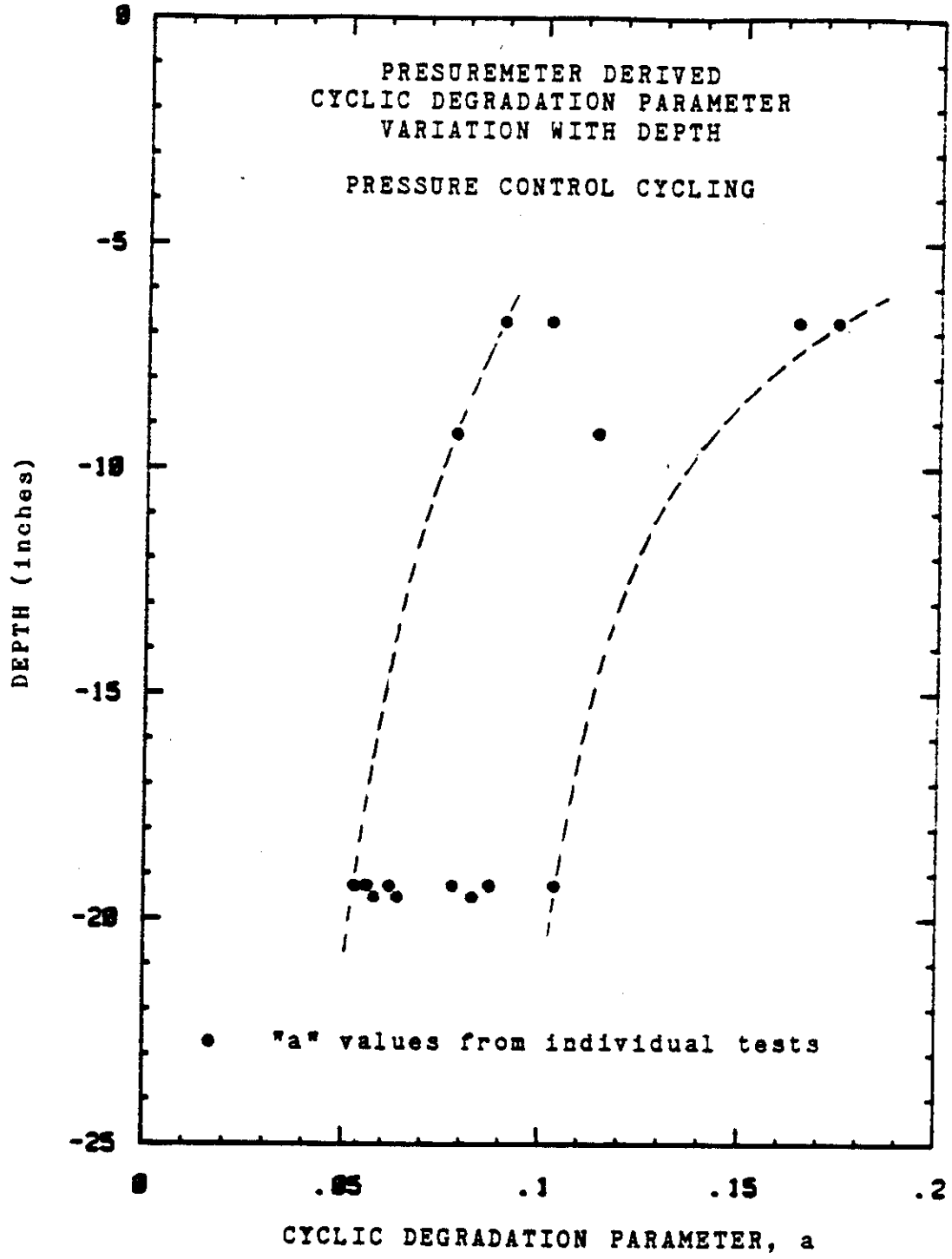

Figure 123. Cyclic Degradation Parameter as a Function of Depth: Pressure-control Cycles.

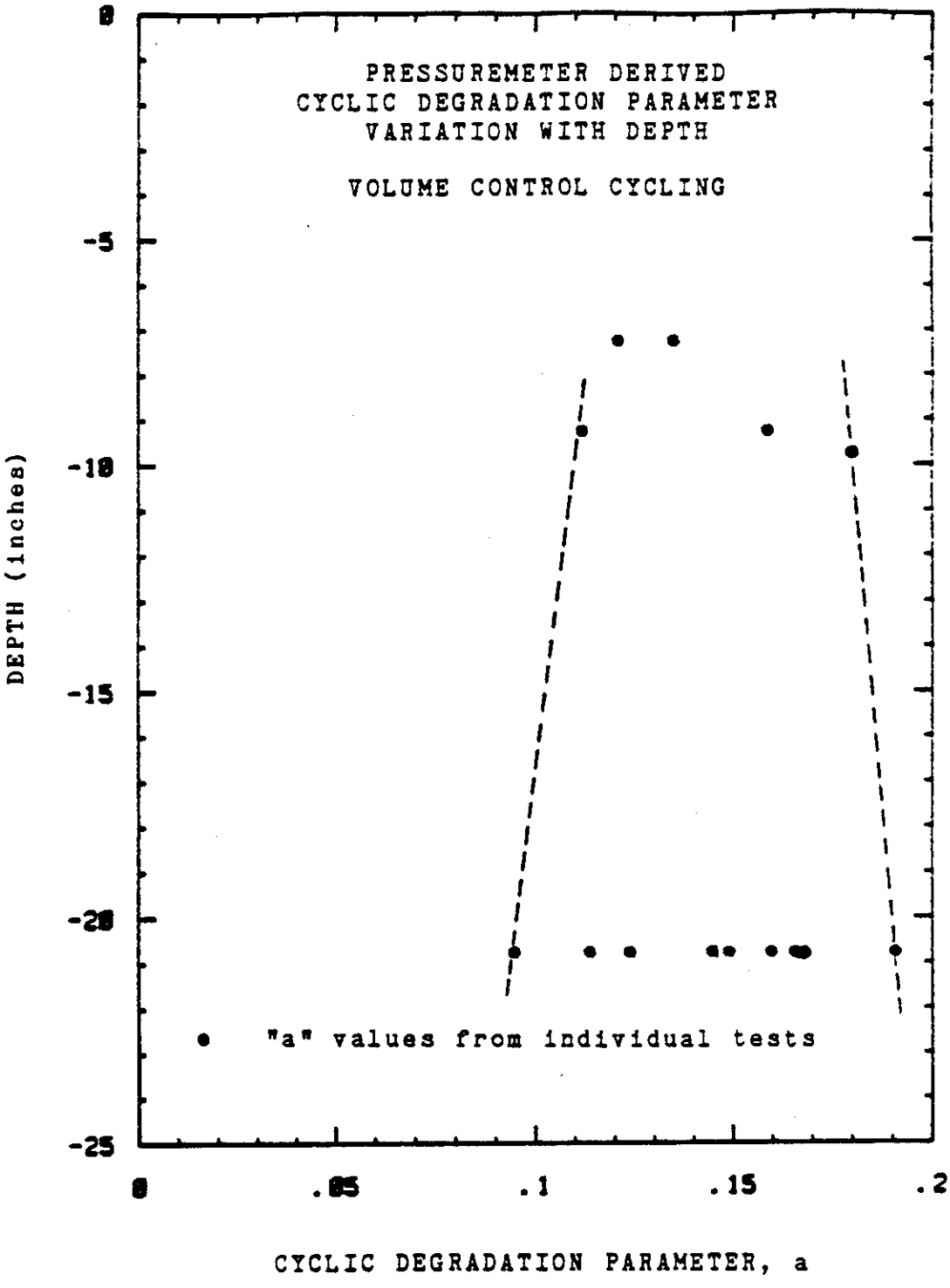

Figure 124. Cyclic Degradation Parameter as a Function of Depth: Volume-control Cycles.

relative displacement level for volume-control cycling than for pressure-control cycling. Generally, $\underline{a}$ increased with increasing load levels during volume-control cyclic tests, whereas $\underline{a}$ values did not show any particular trends as load levels were increased during pressure-control cyclic tests (Table 6). Therefore, it is advisable to pay particular care to match the load level of the pressuremeter cycles to those anticipated during the cyclic loading of the pile when modeling a displacement-control pile load test.

The sensitivity of pressure-control cycling to overburden pressure may not be as great a factor in predicting full-scale pile responses as it played in the model pile tests. It is unlikely that pressuremeter tests would be performed for full-scale pile predictions at depths as shallow as those performed for the model pile tests. As the depth of the pressure-control cyclic pressuremeter tests increased, the $\underline{a}$ values tended to stabilize (Figure 123).

9. PROPOSED PREDICTION METHOD

9.1 Prediction Approach

There is a physical analogy between the cylindrical expansion of the pressuremeter and the lateral movement of the pile. A microcomputer program, PYPMT (Little, et al., 1986), was developed during this study to generate automatically the P-y curves from the pressuremeter curves as recommended by Briaud, et al. (1985b). The P-y curves were then input into BMCOL7, a beam column program written by Hudson Matlock (Coyle, 1986), to obtain the predicted deflections of a pile subjected to a given set of loads.

9.2 Theoretical Basis

9.2.1 The P-y Curve Components

The P-y curve (Matlock, 1970, and Reese and Desai, 1977) describes the soil resistance to the lateral displacement of a horizontally-loaded pile at a particular depth. At a depth "z" along the pile, the "y" symbol represents the horizontal displacement, and the "P" symbol represents the total soil resistance in force per unit length associated with the displacement "y". Although several various stresses contribute to the total soil resistance (Figure 125), in piles with a diameter-to-length ratio greater than 3 the majority of soil resistance is the result of the front resistance, Q, and the friction resistance, F (Figure 126).

At the soil interface of a horizontally loaded pile a

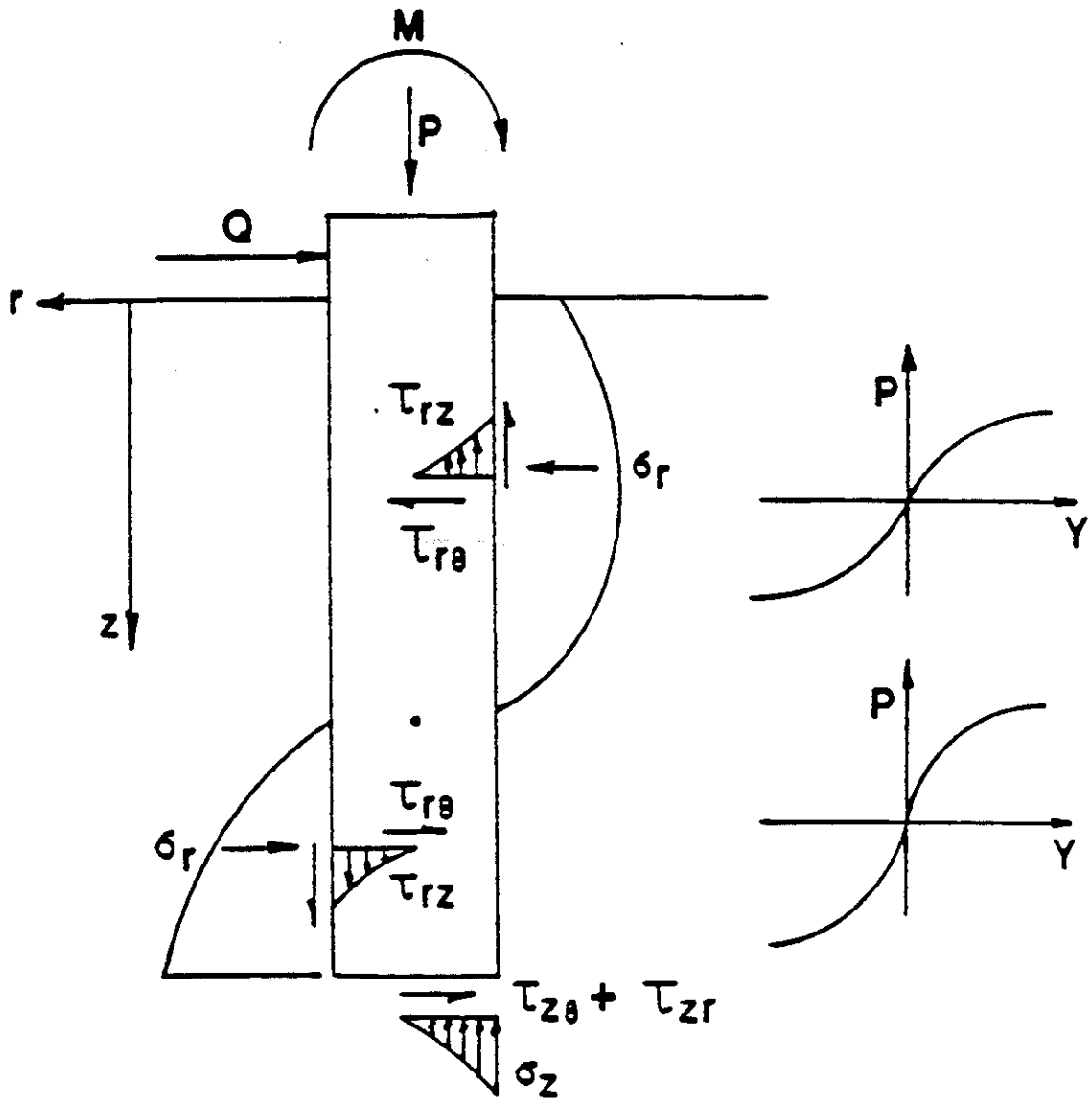

Figure 125. Stresses on a Pile that Contribute to the Soil Resistance.

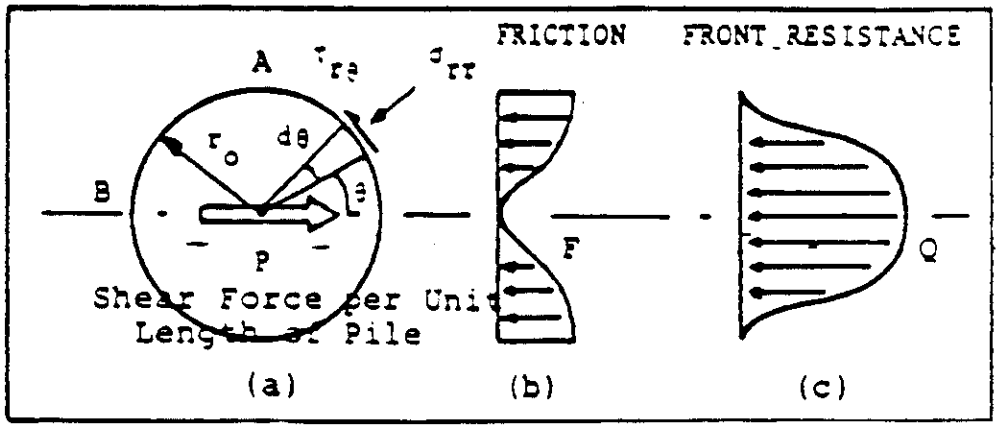

Figure 126. Normal and Shear Stresses in Opposition to the Pile's Shear Force.

normal stress, σ_{rr}, and a shear stress, $\tau_{r\theta}$, exist (Figure 126). The elementary forces per unit length of the pile may be determined by resolving the stresses into their components in the direction of loading:

$$dF = \tau_{r\theta} \; r_o \; \sin\theta \; d\theta \tag{13}$$

and

$$dQ = \sigma_{rr} \; r_o \; \cos\theta \; d\theta \tag{14}$$

where

dF = the elementary force per unit pile length due to the component of $\tau_{r\theta}$

dQ = the elementary force per unit pile length due to the component of σ_{rr}

r_o = the radius of the pile

θ = the angle between the direction of the lateral load and the direction of σ_{rr}.

If friction and front resistances on the back face of the pile (opposite to the direction of travel) are disregarded, the total friction and front resistances per unit length of the pile are obtained through integration:

$$F = \int_{-\pi/2}^{\pi/2} \tau_{r\theta} \; r_o \; \sin\theta \; d\theta \tag{15}$$

and

$$Q = \int_{-\pi/2}^{\pi/2} \sigma_{rr} \; r_o \; \cos\theta \; d\theta \tag{16}$$

where

F = the total friction resistance per unit length of pile

Q = the total front resistance per unit length of pile.

Baguelin, et al. (1977) provide expressions for the normal and shear stresses at the soil-pile interface in an elastic medium:

$$\sigma_{rr} = \sigma_{rr}(max) \cos\theta \quad (17)$$

$$\tau_{r\theta} = \tau_{r\theta}(max) \sin\theta \quad (18)$$

where

$$\sigma_{rr}(max) = P/(2\ r_o \pi/4)$$

$$\tau_{r\theta}(max) = P/(2\ r_o \pi/4)$$

P = the force per unit length in the $\theta = 0$ direction.

Solving equations (15) and (16) after substituting the expressions in (17) and (18) yield:

$$F = \tau_{r\theta}(max)\ 2r_o\ \pi/4 \quad (19)$$

and

$$Q = \sigma_{rr}(max)\ 2r_o\ \pi/4 \quad (20)$$

These two resistances, F and Q, may then be added to obtain the total soil resistance, P, per unit length of pile for a given deflection, y.

9.2.2 <u>The Q-y Curve and the Pressuremeter Curve</u>

The distribution of elementary forces per unit pile length, dQ, around the face of a pile predicted using equation (14) was found to closely match the same distribution as measured using pressure cells (A, B, and C in Figure 127) on a laterally-loaded bored pile (Briaud, et al., 1983 and

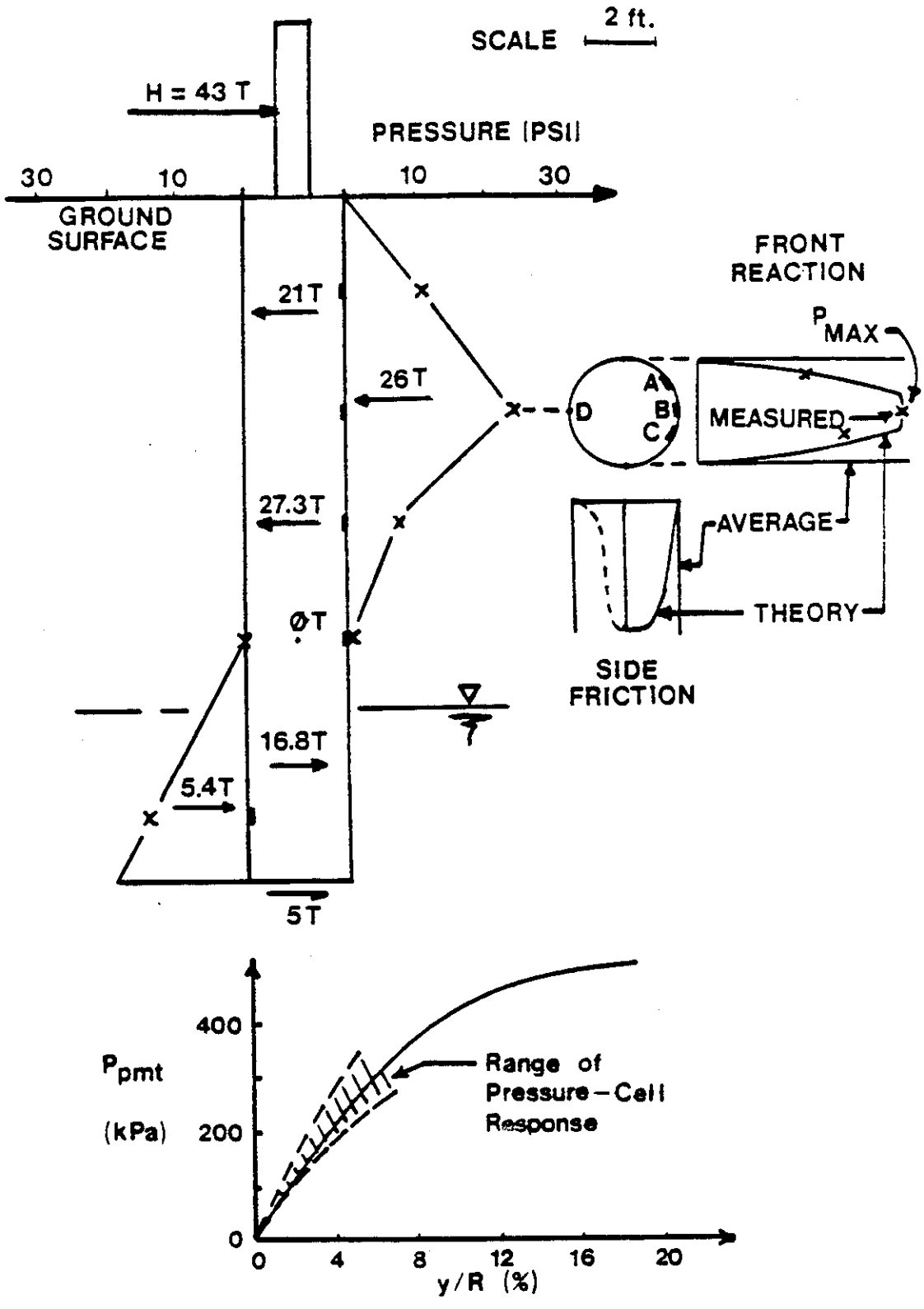

Figure 127. Example of Friction and Frontal Resistances (After Briaud, et al., 1985b).

Smith, 1983). Thus if the peak stress, $\sigma_{rr}(max)$, can be experimentally determined, the Q-y component of the P-y curve may be developed using equation (20).

Pre-bored pressuremeter tests were performed near the laterally-loaded pile (Smith, 1983). A comparison between the P versus y/R curves for the pressuremeter and the pressure cell on the pile (Figure 127) indicated very close agreement (Briaud, et al., 1983 and Smith, 1983). For the pressuremeter, P is the pressure on the borehole wall and y/R is the relative increase in cavity radius. For the pressure cell, P is the pressure against the cell located along the loading axis and y/R is the horizontal displacement of the pile over the pile radius. This supports the use of pre-bored pressuremeter tests for obtaining the predicted front resistance curve for a bored pile.

For full-displacement driven piles (either close-ended piles or open-ended piles that plug during insertion) the front resistance would most likely be different from that experienced by a bored pile in the same soil. To more closely maintain the analogy between pressuremeter and pile, it may prove most beneficial to employ driven pressuremeter results in the development of driven pile Q-y curves. An alternative approach would be to use the reload curve from pre-bored pressuremeter tests. In this approach, after placing the pressuremeter in the pre-bored hole, the probe is partially inflated once to simulate the stresses

transferred to the soil during pile driving and then the probe is reinflated to obtain a reload curve to failure. The Q-y curve is then derived from this reload curve.

9.2.3 The F-y Curve and the Pressuremeter Curve

Baguelin, et al. (1978) have shown that the soil shear stress-strain curve can be derived from the self-boring pressuremeter curve through use of the theoretical subtangent method. This same method, when applied to the results from pre-bored pressuremeter tests, consistently yielded shear moduli which were too low and peak shear strengths which were too high. However, applying the subtangent method to the reload curves of pre-bored pressuremeter tests led to shear moduli comparable to those obtained with self-boring pressuremeter tests (Baguelin, et al., 1978). Therefore, when pre-bored pressuremeter tests are used, the proposed approach is to employ the reload curve to derive the F-y component of the soil resistance curve for both driven and bored piles.

9.3 The Briaud-Smith-Meyer Method

The analogy of loading between the pressuremeter and the pile is not complete and the pressuremeter curve is not identical to the P-y curve. It has been shown that the pressuremeter curve gives the Q-y curve, and that the F-y curve can be obtained from the same curve. The P-y curve is the addition of the Q-y and F-y curves. The following is a summary of the method which is proposed to obtain the P-y

model from the pressuremeter curve (Briaud, et al., 1985b and Briaud, et al., 1985c).

9.3.1 The Pressuremeter Curve

The pressuremeter curve is a plot of the pressure on the borehole wall versus the relative increase in probe radius. Figure 128 shows a typical pressuremeter curve with one unload-reload cycle. This cycle is necessary in the application of this method. The unloading should start at the end of the linear range of the pressuremeter curve and continue until the pressure is reduced to one-half the pressure at the start of unloading (Figure 128). At this point reloading is commenced and continues until the limit pressure can be determined.

9.3.2 Total Horizontal Pressure at Rest

The total horizontal pressure at rest, P_{OH}, may be calculated as:

$$P_{OH} = \left[\left(\sigma_{ov} - U_o\right) \times K_{OH}\right] + U_o \qquad (21)$$

where,

σ_{ov} = the vertical total stress at testing depth before testing

U_o = pore water pressure at testing depth before testing

K_{OH} = estimated coefficient of horizontal earth pressure at rest.

Alternatively, P_{OH} can be taken at the point of maximum curvature on the initial part of the pressuremeter curve (Figure 57).

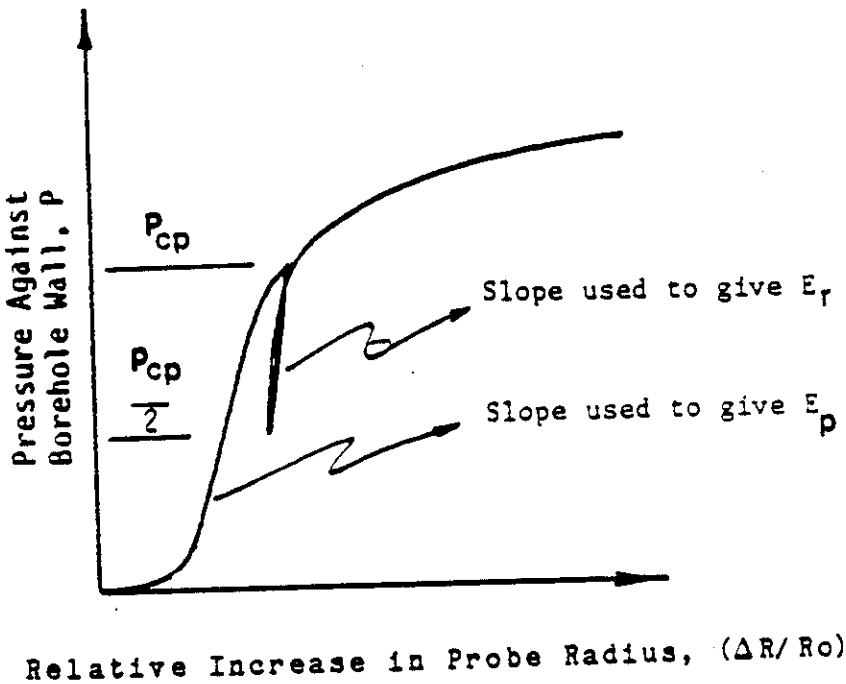

Figure 128. Typical Pressuremeter Test Curve with Unload-Reload Cycle.

9.3.3 Translation of Origin

To obtain a corrected curve, the origin must be translated to correspond with P_{OH} (Figure 129). As shown on the figure, the linear portion of the curve should be extrapolated back to P_{OH}, thus defining the new origin. If P_{OH} cannot be calculated by equation (21) it may be estimated to be equal to the pressure corresponding to the point of maximum inflection on the initial portion of the pressuremeter curve (Figure 128).

The reload cycle of a pre-bored test has been shown (Smith, 1983) to better approximate an undisturbed test and generate shear strength values in good agreement with laboratory values. The reload cycle should therefore be used to obtain the F-y curves for all piles, both driven and augered, when pre-bored pressuremeter data is used. For bored piles, or piles driven open-ended which do not plug, the front reaction, Q-y, curve is developed from the initial curve of a pre-bored test. For full-displacement piles the reload cycle is used for the front resistance. This is summarized below in Table 7:

	Pile Type	
Curve	Driven	Bored
F-y	Reload Cycle	Reload Cycle
Q-y	Reload Cycle	Initial Cycle

Table 7. When to Use the Reload and Initial Cycles in Pressuremeter-derived P-y Curve Developement.

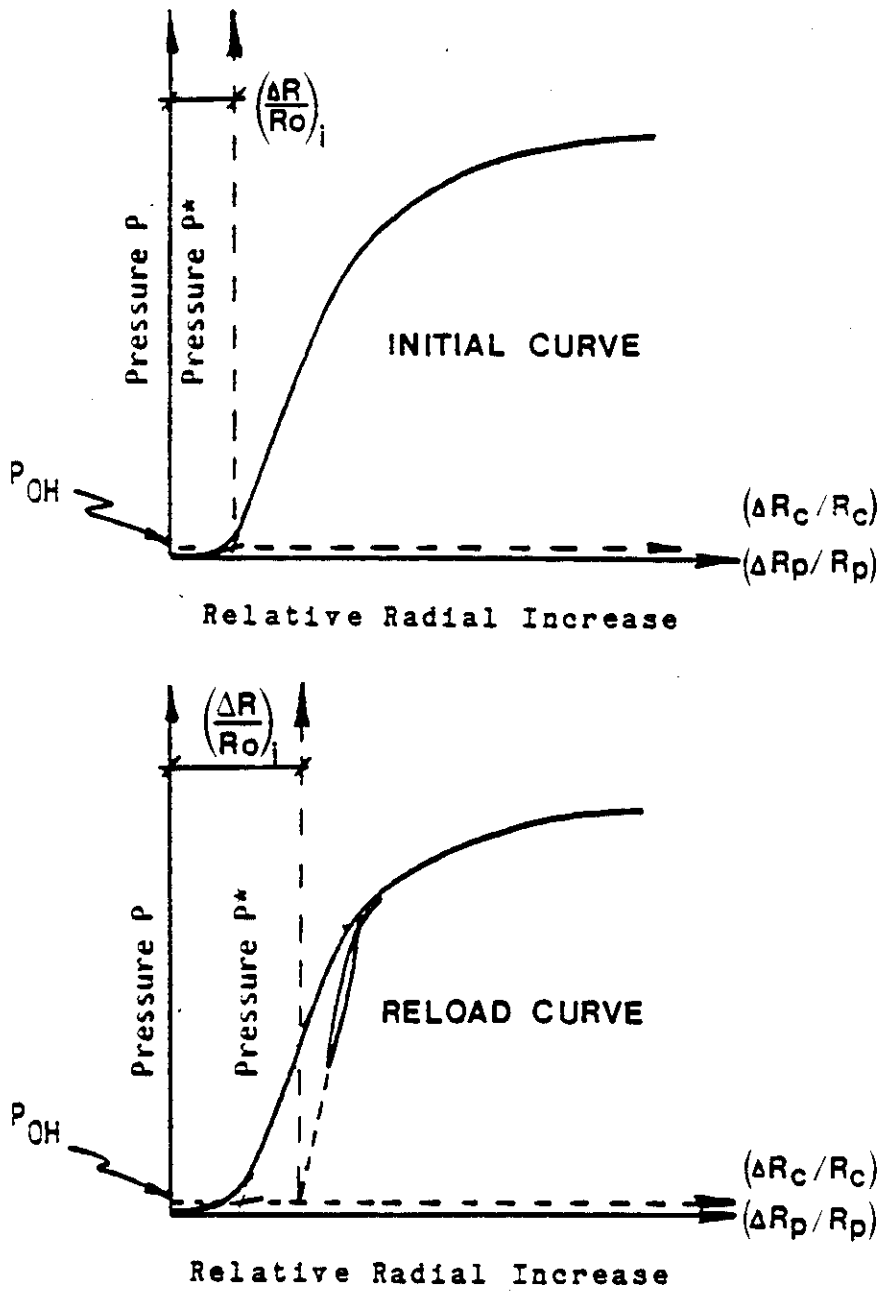

Figure 129. Translation of Pressuremeter Curve Origin.

When the reload cycle is used, the linear range is extrapolated back to P_{OH} to obtain the full curve (Figure 129).

The notation used to define these curves is as follows:

P = pressuremeter pressure

P^* = net pressuremeter pressure ($P-P_{OH}$)

P_{OH} = horizontal earth pressure at rest

Ro = initial probe radius before inflation

ΔRp = increase in probe radius

ΔR = increase in probe radius necessary to reach P_{OH}

$\left(\frac{\Delta R}{Ro}\right)_i$ = relative radial increase of probe when P_{OH} is reached

Rc = initial cavity radius = $\Delta R + Ro$

ΔRc = increase in cavity radius.

9.3.4 Critical Depth for the Pressuremeter

The pressuremeter is subject to a reduction of soil resistance at shallow depths. The reduction factor is shown in Figure 130 as a function of the ratio of the test depth, Z, to the critical depth, Z_c. The critical depth as recommended by Baguelin et al. (1978) is:

$$Z_c = 30\ R \text{ for cohesive soils}$$
$$Z_c = 60\ R \text{ for cohesionless soils} \qquad (22)$$

where R is equal to the pressuremeter radius. The pressuremeter curve is corrected into a curve which would not have the influence of shallow depth by taking:

$$P_{corr} = \frac{P^*}{\chi} \qquad (23)$$

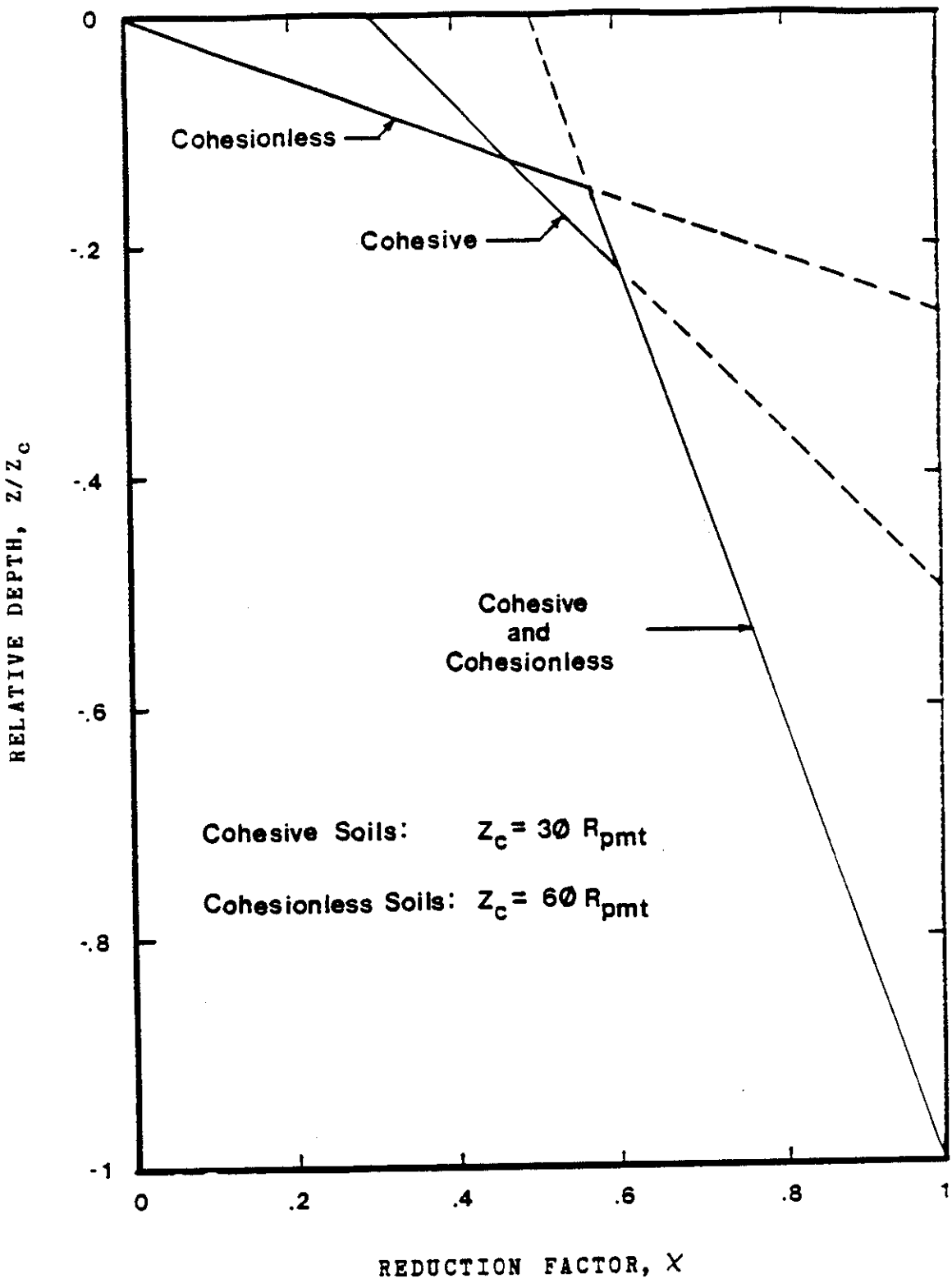

Figure 130. Proposed Reduction Factor for the Pressuremeter within the Critical Depth (From Briaud, Tucker, and Olsen, 1985).

where

P_{corr} = corrected net pressure

χ = reduction factor for pressuremeter critical depth (Figure 130).

χ is equal to unity when the pressuremeter is below its critical depth. This curve is then used to obtain the Q-y and F-y curves.

9.3.5 Front Resistance

The front Resistance of the pile, Q, is calculated by:

$$Q = \frac{P^*}{\chi} \times B \times SQ \times \psi \qquad (24)$$

where

SQ = pile shape factor: 1 for square piles loaded parallel to their sides, 0.8 for round piles and square piles not loaded parallel to their sides

B = pile diameter or width

ψ = pile front resistance reduction factor with pile critical depth (Section 9.3.6).

9.3.6 Accounting for the Pile Critical Depth

To account for the reduced soil resistance near the ground surface (within the pile's critical depth) the front reaction, Q, is multiplied by a reduction factor, ψ. The reduction factor is given in Figure 131. The average critical depth for the pile, $Z_c(av)$, is a function of the relative pile/soil stiffness and is given by the greater of:

$$Z_c(av) = (\pi/4)\ (RR-5)\ (B)$$

or (25)

$$Z_c(av) = B$$

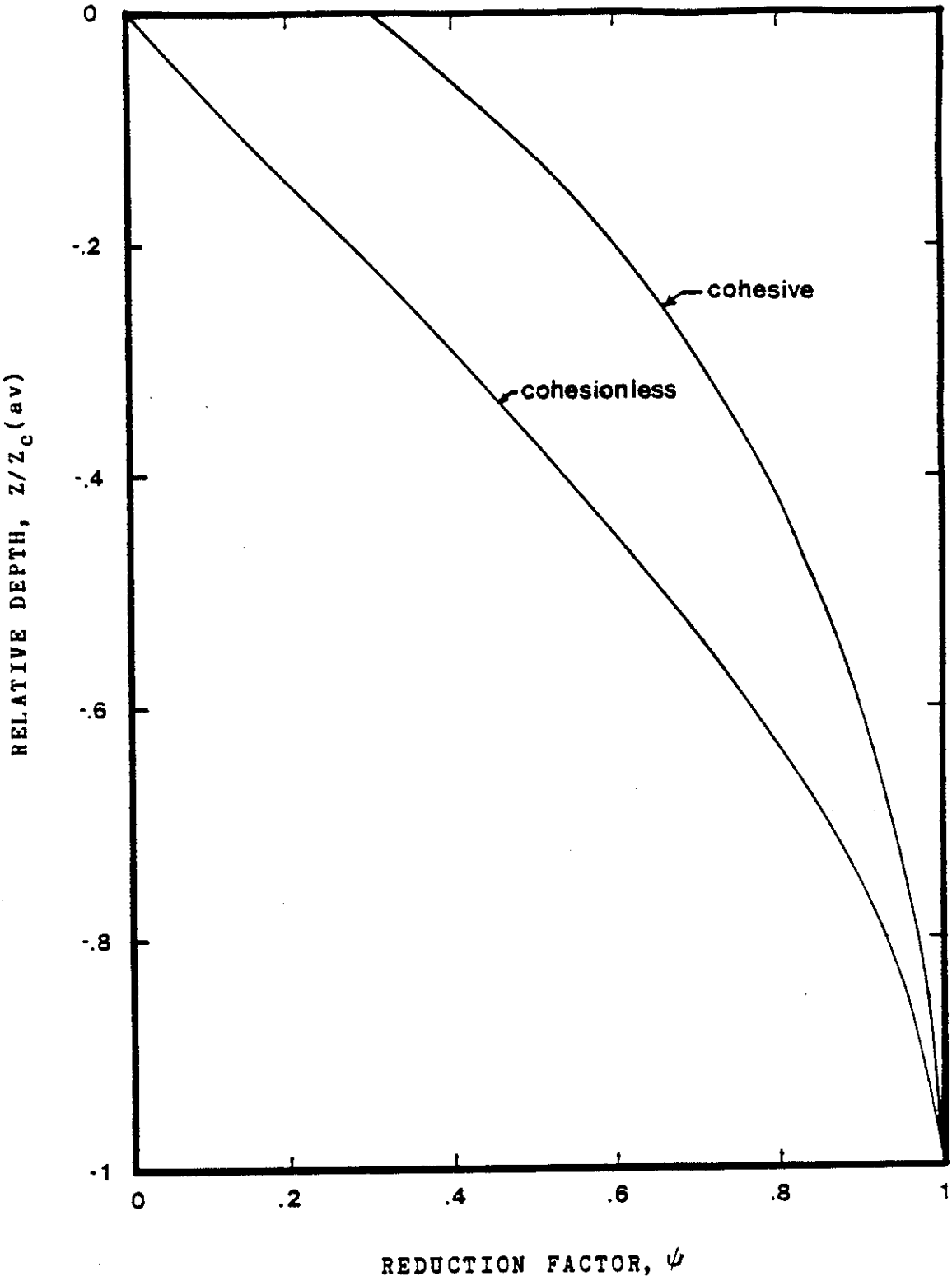

Figure 131. Proposed Reduction Factor for the Pile within the Critical Depth (From Briaud, Tucker, and Olsen, 1985).

The relative rigidity factor, RR, is given by:

$$RR = \left(\frac{1}{B}\right) \sqrt[4]{\frac{EI}{P_L^*}} \qquad (26)$$

where

EI = pile flexural stiffness

P_L^* = net pressuremeter limit pressure

The correlation between RR and $Z_c(av)/B$ is shown in Figure 132 with measured data also plotted.

9.3.7 Pile Displacement

After having translated the corrected pressuremeter curve (Figure 129 and Section 9.3.3) and rescaling the horizontal axis to the relative increase in borehole cavity radius ($\Delta Rc/Rc$), the pile displacement, y_{pile}, is then calculated by:

$$y_{pile} = \left(\frac{\Delta Rc}{Rc}\right) \times R_{pile} \qquad (27)$$

where R_{pile} is the pile radius.

9.3.8 Friction Resistance

The friction resistance is determined through the following procedure. The slope of the pressuremeter curve at a point is assumed to be the slope of the line joining the point before and the point after the point considered (Figure 133). Thus the slope of the curve may be calculated by:

$$\frac{P^*}{\chi} = \left(\frac{P_a^* - P_b^*}{\chi_a - \chi_b}\right) \frac{1}{\chi} \qquad (28)$$

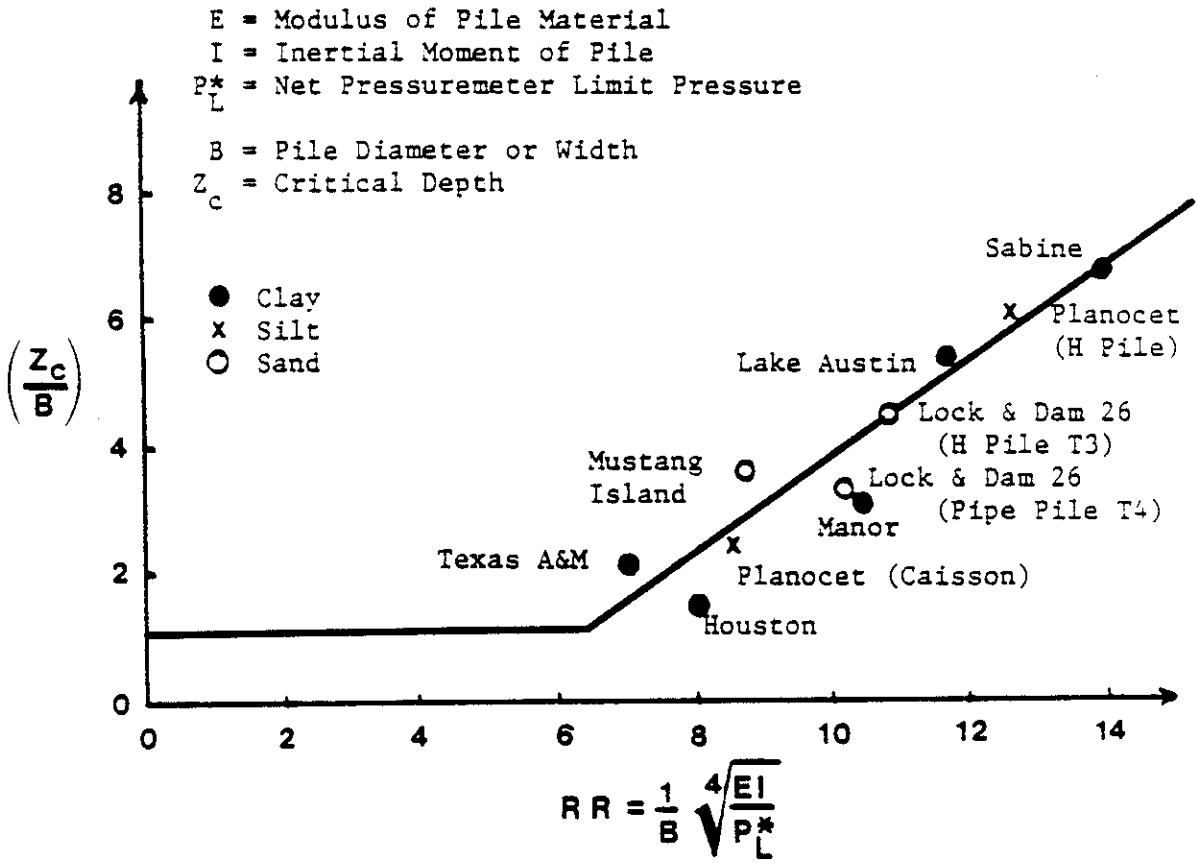

Figure 132. Critical Depth as a Function of Relative Rigidity (From Briaud, Tucker, and Olsen, 1985).

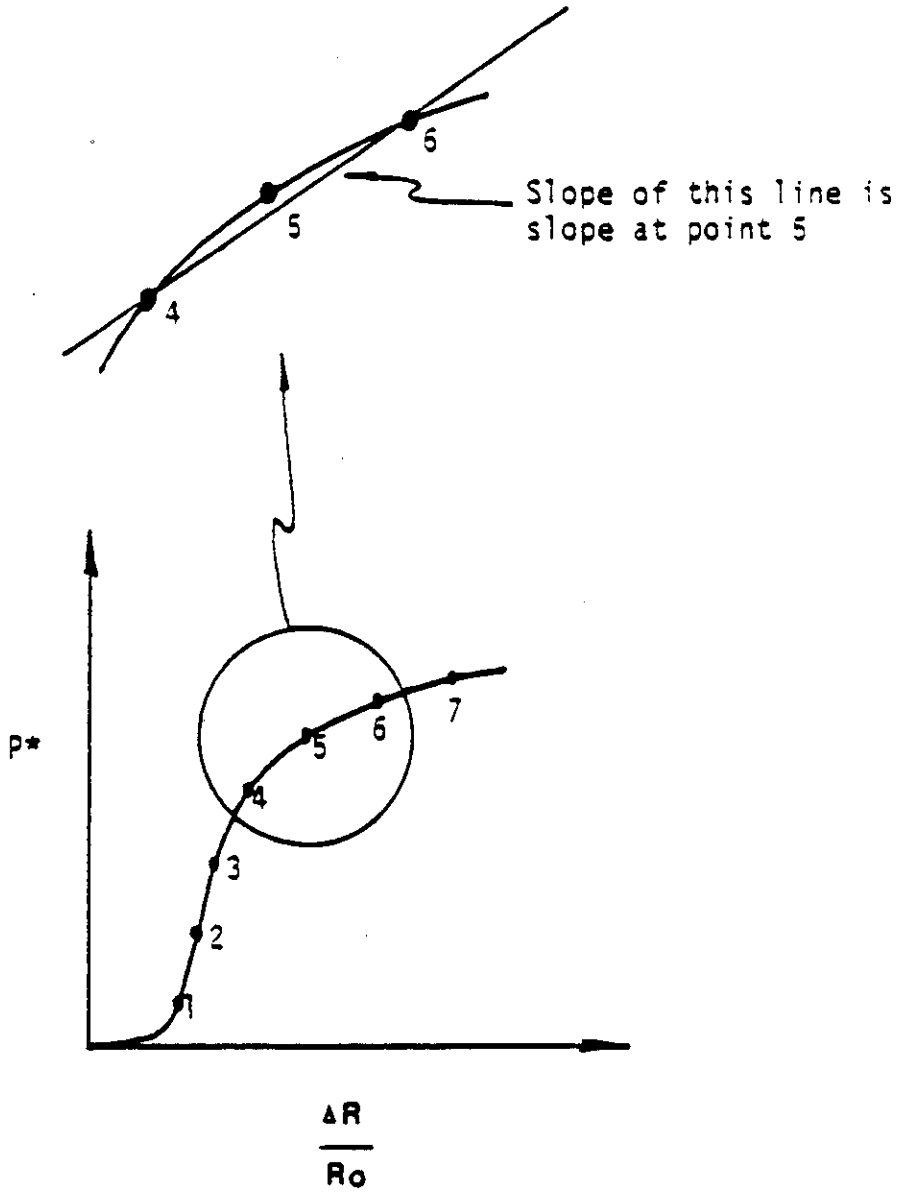

Figure 133. Determining the Slope.

where

P_a^* = net pressure for the point after the point considered

P_b^* = net pressure for the point before the point considered

X_a = relative change in radius for the point after the point considered

X_b = relative change in radius for the point before the point considered

$\left(\frac{\Delta P^*}{\Delta X}\right)$ = slope for the curve at the point considered

= reduction factor for the pressuremeter critical depth.

The shear stress, , mobilized by the pile is calculated from the slope of the curve:

$$\tau = X\ (1+X)\ \left(\frac{\Delta P^*}{\Delta X}\right)\ \left(\frac{1}{X}\right) \qquad (29)$$

where

X = the relative increase in radius for the point considered.

The friction resistance, F, mobilized on the pile is then determined as:

$$F = \tau \times B \times SF \qquad (30)$$

where

SF = shape factor for the pile: 2 for square piles loaded parallel to their sides and 1 for round piles and square piles not loaded parallel to their sides.

No pile critical depth reduction factor is applied to the friction component since overburden pressure does not appear to significantly affect frictional resistance on the pile.

9.3.9 Total Resistance

The total resistance is the sum of the front and friction resistances:

$$P = F + Q \tag{31}$$

where

P = the total soil resistance on the pile (force per unit length of pile).

9.3.10 Base Resistance on a Rigid Pile

The mobilization of shear resistance upon the base of a rigid rotating pile may be significant. The shear stress is assumed to be mobilized linearly and to reach the shear strength at a translation of 0.1 inches. If the beam column program used is not equipped with a separate base friction model, the base frictional resistance may be added to the deepest P-y curve as follows:

$$F_b = S \quad x\left(\frac{A_p}{\delta}\right) \tag{32}$$

where

F_b = base mobilized resistance

δ = finite difference increment length for the pile

A_p = area of the base

S = shear strength of soil at the depth of the base.

The units of F_b are therefore force per unit length, and consistent with those of F and Q. The base P-y curve only is then given by:

$$P = Q + F + F_b \tag{33}$$

9.4 Precision of the Briaud-Smith-Meyer Monotonic Method

Pre-bored pressuremeter tests were conducted next to 27 piles on which horizontal load tests were performed (Table 8). P-y curves were then derived from the corrected pressuremeter results using this pressuremeter method. The P-y curves coupled with a beam-column program were used to obtain predicted horizontal load versus horizontal deflection curves for the pile tops. The pressuremeter-derived predictions were compared to the measured results at two different deflection levels: at 2% of the pile diameter to represent small, working load movements, and at 10% of the pile diameter to represent the ultimate capacity. The comparisons of the predicted and measured loads are plotted in Figures 134 and 135, showing a very satisfactory prediction of measured pile behavior using this method for static loading. It is significant to note that the load tests included a wide range of pile types and sizes as well as a variety of soils. Also, only piles 1-7 were used in the development of the method and several pile predictions were made prior to the availability of the actual load test results (Briaud, 1986).

9.5 Assumptions and Limitations in the Microcomputer Program PYPMT

Assumptions and limitations inherent in the PYPMT program (Little, et al., 1986) based on this pressuremeter method are listed below.

Pile I.D. No.	Site	Pile Type	Pile Embedded Length (m)	Pile Diameter (m)	Soil
1	Sabine	Pipe	12.2	0.32	Clay
2	Mustang Is.	Pipe	21.0	0.61	Sand
3	Lake Austin	Pipe	12.2	0.32	Clay
4	Houston	Bored	13.0	0.76	Clay
5	Texas A&M (1977)	Bored	6.1	0.91	Clay
6	Texas A&M (1978)	Bored	4.6	0.76	Clay
7	Texas A&M (1979)	Bored	4.6	0.76	Clay
8*	U. of Houston	H	11.8	0.27	Clay
9*	U. of Houston	Pipe	11.4	1.22	Clay
10	L&D 26 (1983)	HP14x73	20.4	0.36	Sand
11	L&D 26 (1983)	HP14x73	20.4	0.36	Sand
12	L&D 26 (1978)	H	15.2	0.36	Sand
13	L&D 26 (1978)	Pipe	15.2	0.36	Sand
14	Virginia	Bored	3.5	1.37	Clay
15	Carolina	Bored	4.5	1.37	Sand
16	Iowa	Bored	4.6	1.37	Clay
17*	LADWP Delta	Bored	3.0	0.74	Sand
18*	LADWP Caliente	Bored	3.0	0.74	Sand
19*	LADWP Alamo	Bored	3.0	0.65	Clay
20	Baytown	Bored	11.9	0.61	Clay
21*	Lackland	Bored	10.5	0.46	Clay
22	La Baule 1	R.C.	6.0	0.61	Sand/Clay
23	La Baule 2	R.C.	6.0	0.61	Sand/Clay
24	Planocet	Caisson	4.4	0.95	Silt
25	Planocet	H	6.1	0.36	Silt
26	Cubzac	Pipe	24.7	0.91	Clay
27	Provins	Pipe	23.0	0.93	Silt/Peat

* Load test results unknown at time of predictions.

Table 8. Monotonic Lateral Load Test Data Base (After Briaud, 1986).

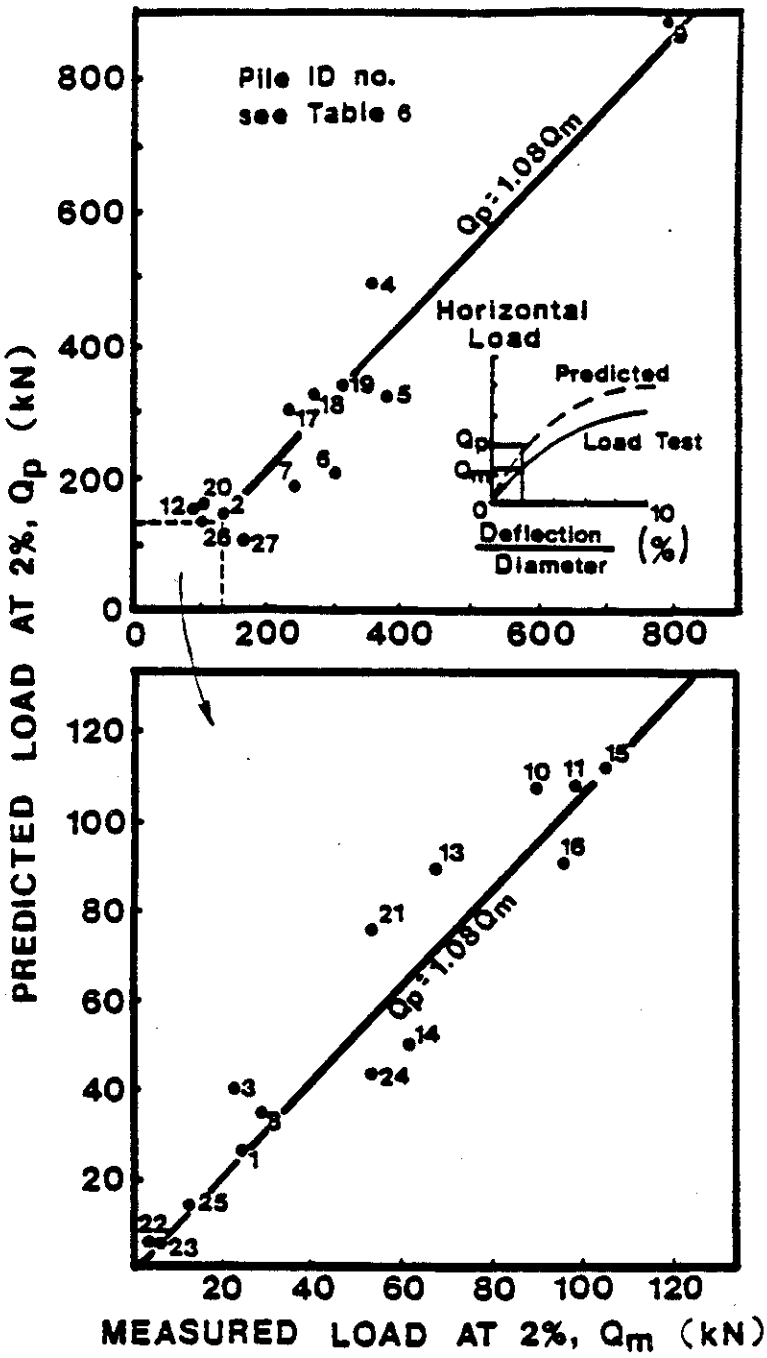

Figure 134. Predicted vs Measured Horizontal Loads for Briaud-Smith-Meyer Method at a Groundline Deflection Equal to 2% of the Pile Diameter (From Briaud, 1986).

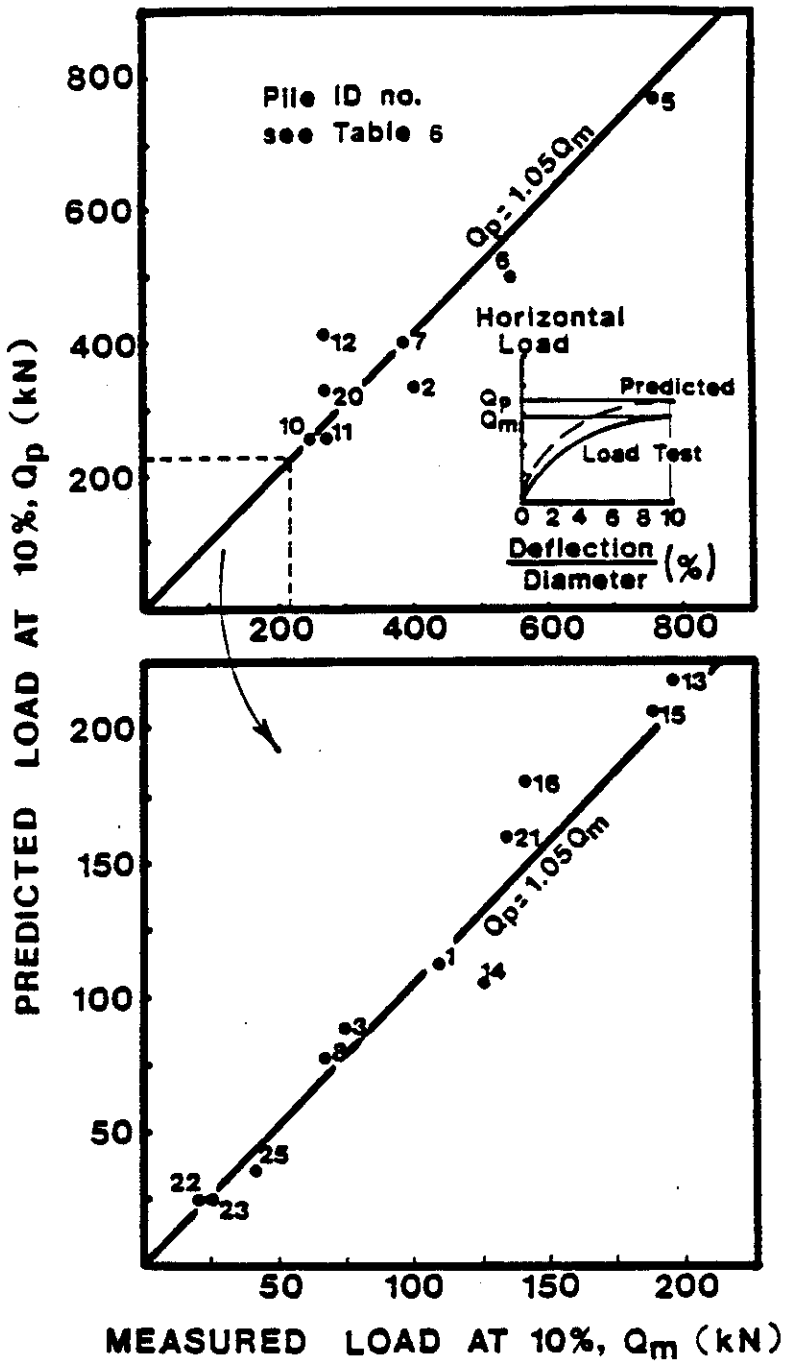

Figure 135. Predicted vs Measured Horizontal Loads for Briaud-Smith-Meyer Method at a Groundline Deflection Equal to 10% of the Pile Diameter (From Briaud, 1986).

9.5.7 Addition of the Q-y and F-y Curves

In the pre-bored pressuremeter/bored pile case the scales for the displacement values of the front and friction curves are not identical. The addition of the curves to obtain the P-y curve is achieved by linearly interpolating to determine a Q value corresponding to each y value from the F-y curve and linearly interpolating to determine an F value corresponding to each y value from the Q-y curve. When no calculated value of resistance exists beyond a y value, the last resistance value is assumed constant for any further pile displacement.

9.6 Proposed Method for Cyclic Predictions

The proposed approach for predicting the response of piles subjected to cyclic lateral loading in sands involves modifying the static P-y curves, obtained through the pressuremeter method detailed above, for cyclic degradation.

To modify a static P-y curve, the number of cycles at which the pile response is to be predicted is first determined. Each value of P from the monotonic P-y curve is then multiplied by N^{-a} to obtain P(N), the force per unit length of pile necessary to displace the soil to the corresponding y value after cycling N times. The a values were selected as detailed in Section 6.6. This is summarized in Figure 136 and in the following equations:

$$P(N) = P(1) \times N^{-a} \qquad (34)$$

$$y(N) = y(1) \qquad (35)$$

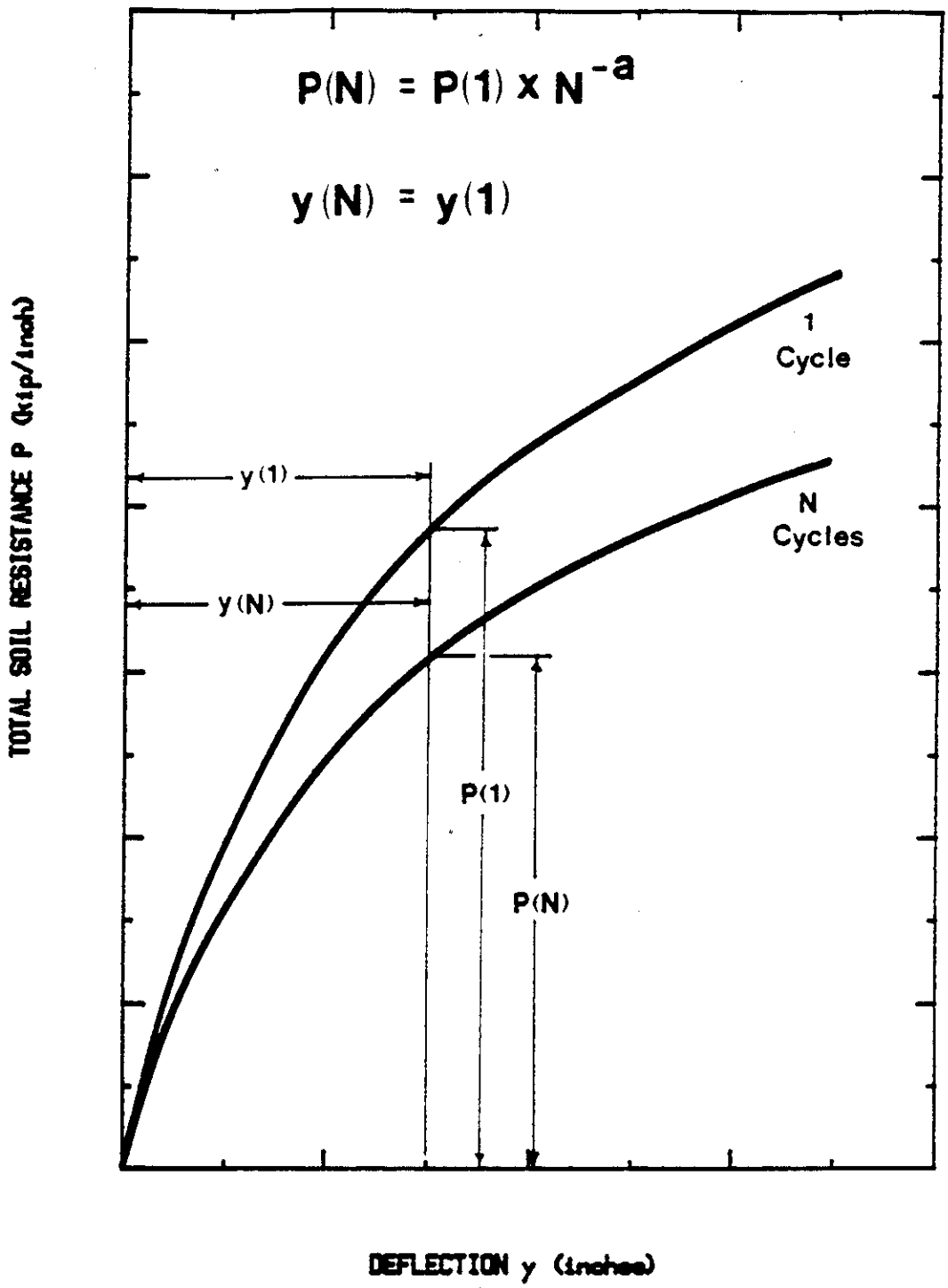

Figure 136. Generation of the Cyclic P-y Curve from a Pressuremeter-derived Monotonic P-y Curve.

where

N = cycle number for which the P-y curve is desired

P(1) = total soil resistance arrived at in static analysis

P(N) = total soil resistance arrived at after N cycles

a = cyclic degradation parameter obtained from the pressuremeter tests

y(N) = the displacement after N cycles

y(1) = the monotonic displacement.

This model has previously been employed in a study of the response of the University of Houston test piles in clay (Makarim and Briaud, 1986) with promising results.

The cyclic P-y curves were then input as resistances into a beam column program to obtain the predicted deflections of a pile subjected to a given set of cyclic lateral loads.

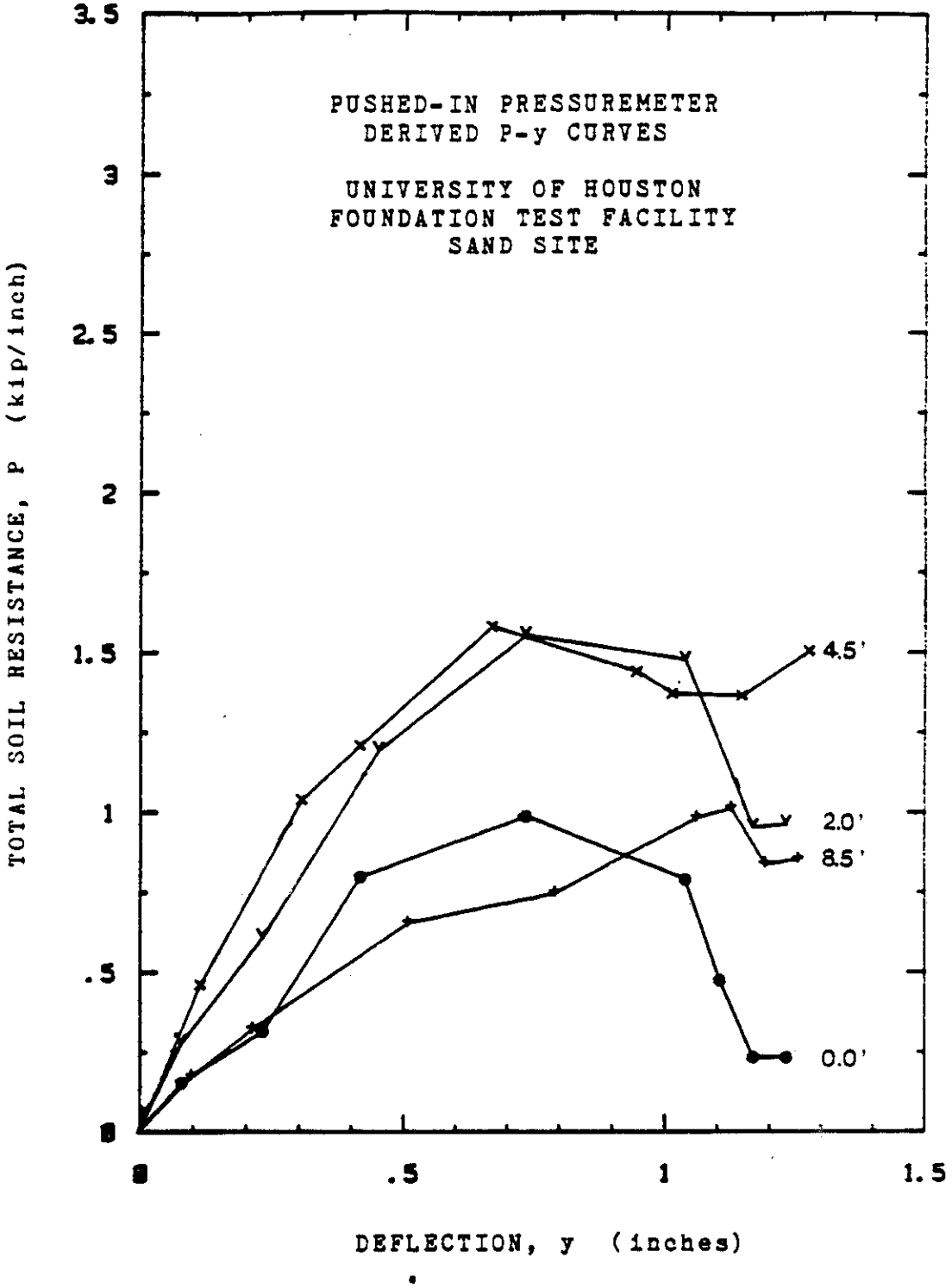

Figure 138. P-y Curves Derived from Pushed-in Cone Pressuremeter Tests at the UofH Sand Site.

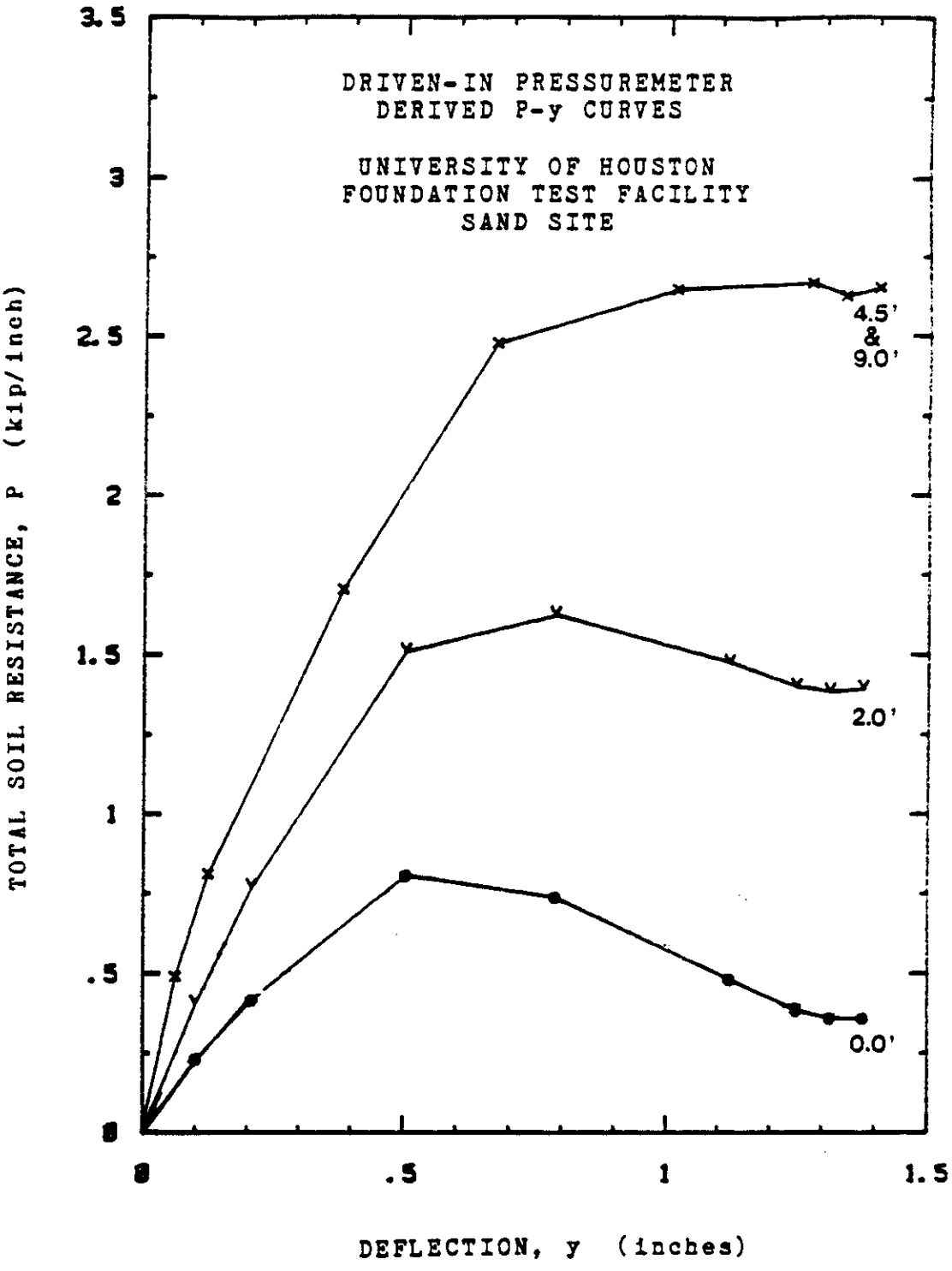

Figure 139. P-y Curves Derived from Driven-in Cone Pressuremeter Tests at the UofH Sand Site.

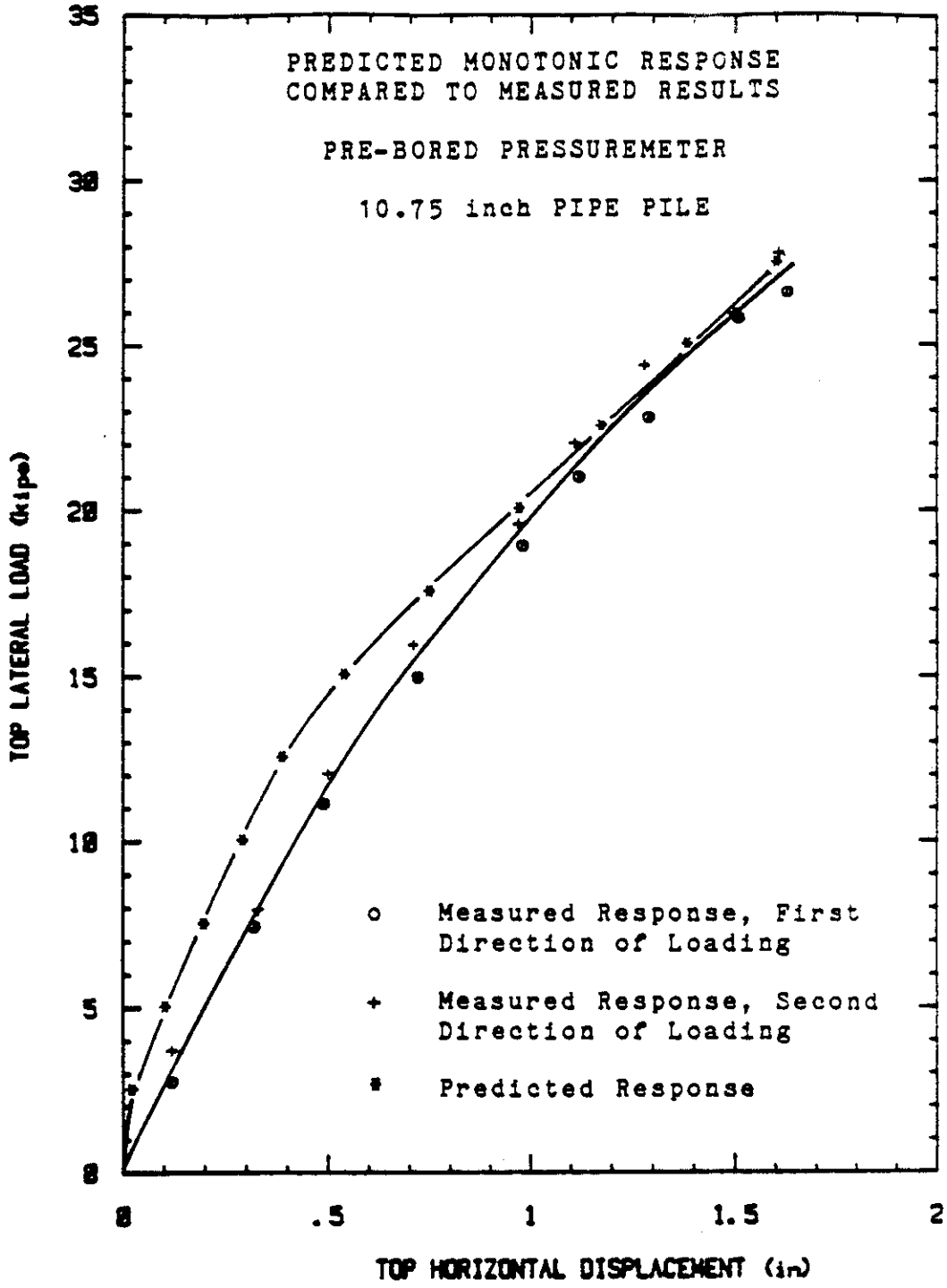

Figure 140. Predicted Monotonic Response of the Single Pile Compared to the Measured Response: Pre-bored TEXAM PMT.

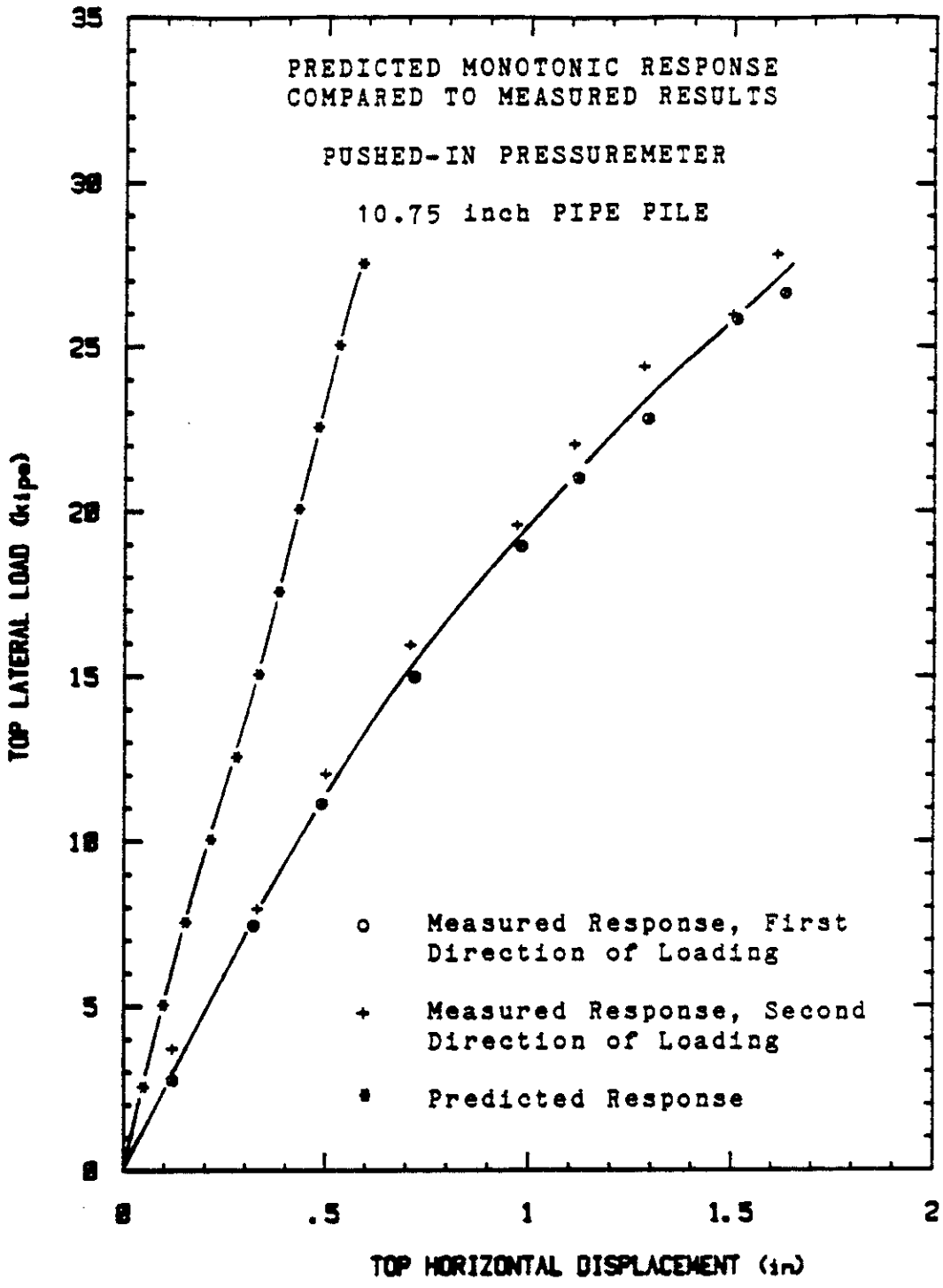

Figure 141. Predicted Monotonic Response of the Single Pile Compared to the Measured Response: Pushed-in Cone PMT.

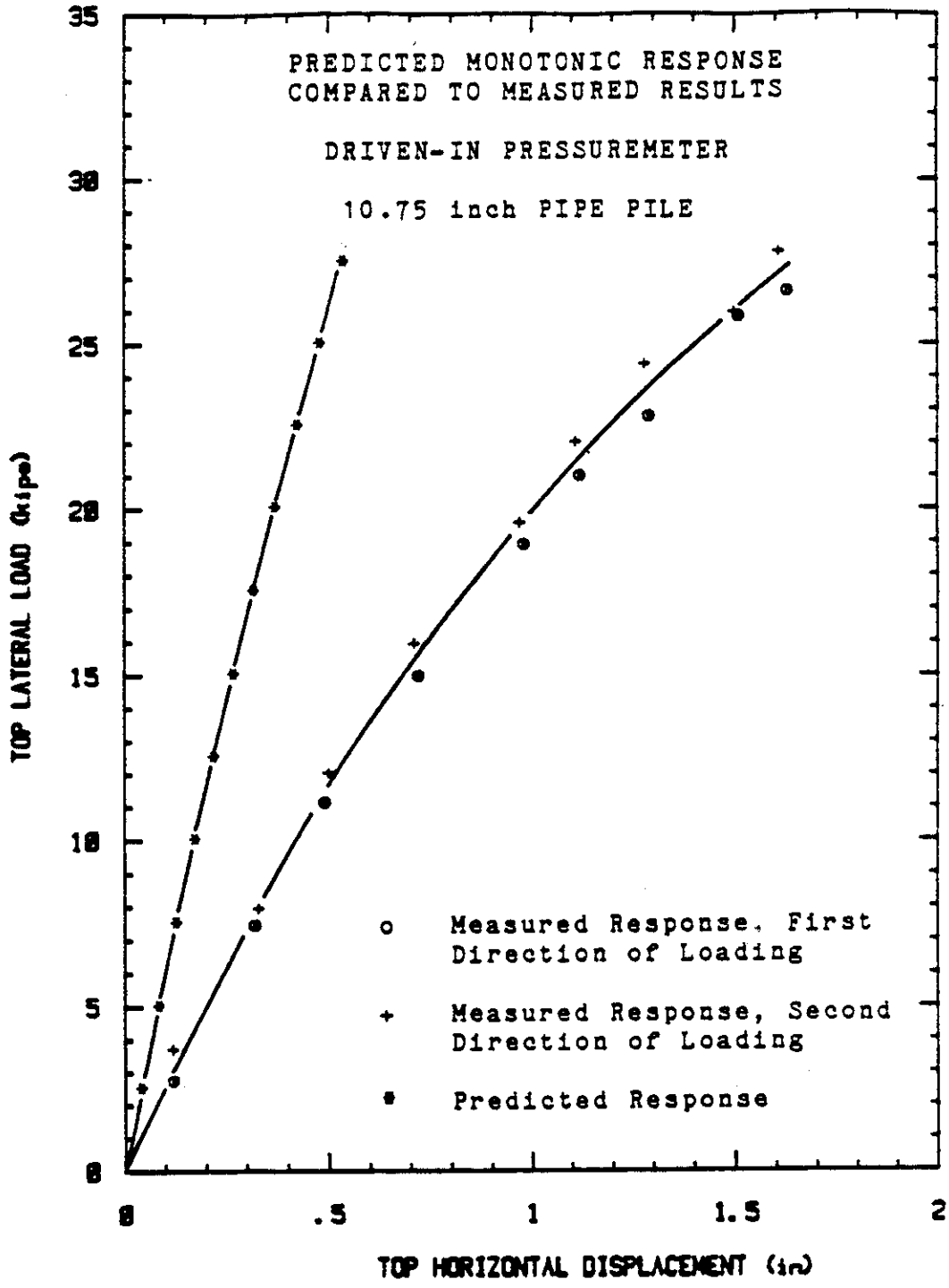

Figure 142. Predicted Monotonic Response of the Single Pile Compared to the Measured Response: Driven-in Cone PMT.

pushed pile. For the pre-bored PMT the P-y curves were obtained by assuming that the pile was a bored pile in the sand and a driven pile in the clay below. The closeness between the predicted and measured response (Figure 140) shows that the compaction of the sand around the pile simulated more closely the conditions around a bored pile.

10.2 Pressuremeter Predictions for the Model Piles at the Texas A&M University Laboratories

The predictions for the model pile tests were made using methods identical to those used in the prediction of the 10.75 inch pile behavior. For the generation of P-y curves, the model piles for which placement entailed post-compaction were treated as bored piles. The others were driven piles and treated as such.

Twelve comparisons between predicted and measured monotonic behavior are presented in Figures 143 through 154. Overall the precision of the monotonic predictions is very good both for the one-way and two-way model pile load tests as can be judged from the figures. One exception is Figure 147. In this case, the pile test is not considered as reliable. Indeed, the pile was unusally weak as compared to the similar case of Figure 153.

The monotonic measured responses are defined here as the first cycle envelopes of the cyclic tests. Also, the monotonic predictions are based on the first cycle envelopes of the PMT test curves. This may have had an effect on the

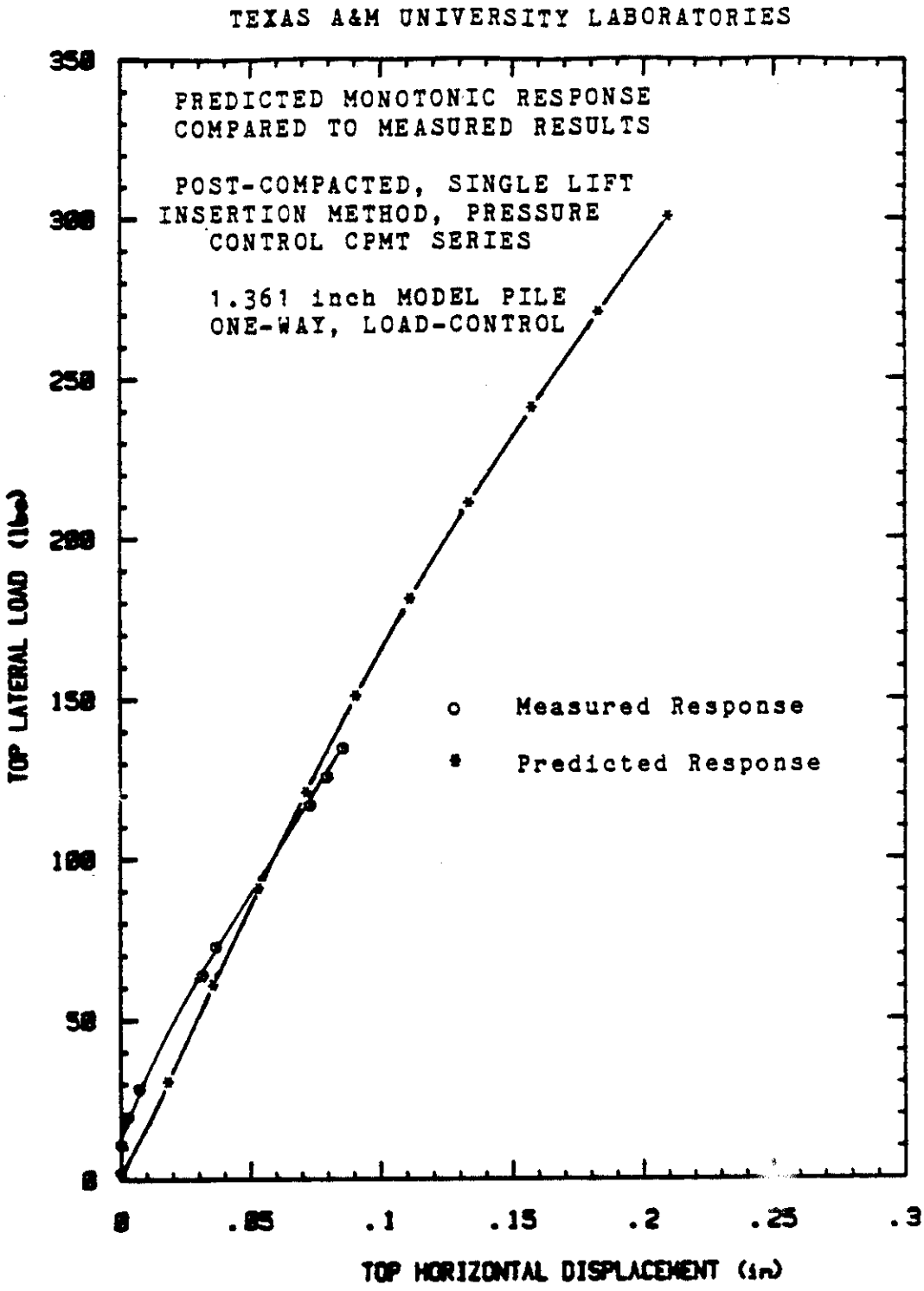

Figure 143. Predicted Monotonic Response of the Model Pile Compared to the Measured Response: Post-compacted, Single Lift, Pile Placement Procedure; One-way, Load-control Cycles.

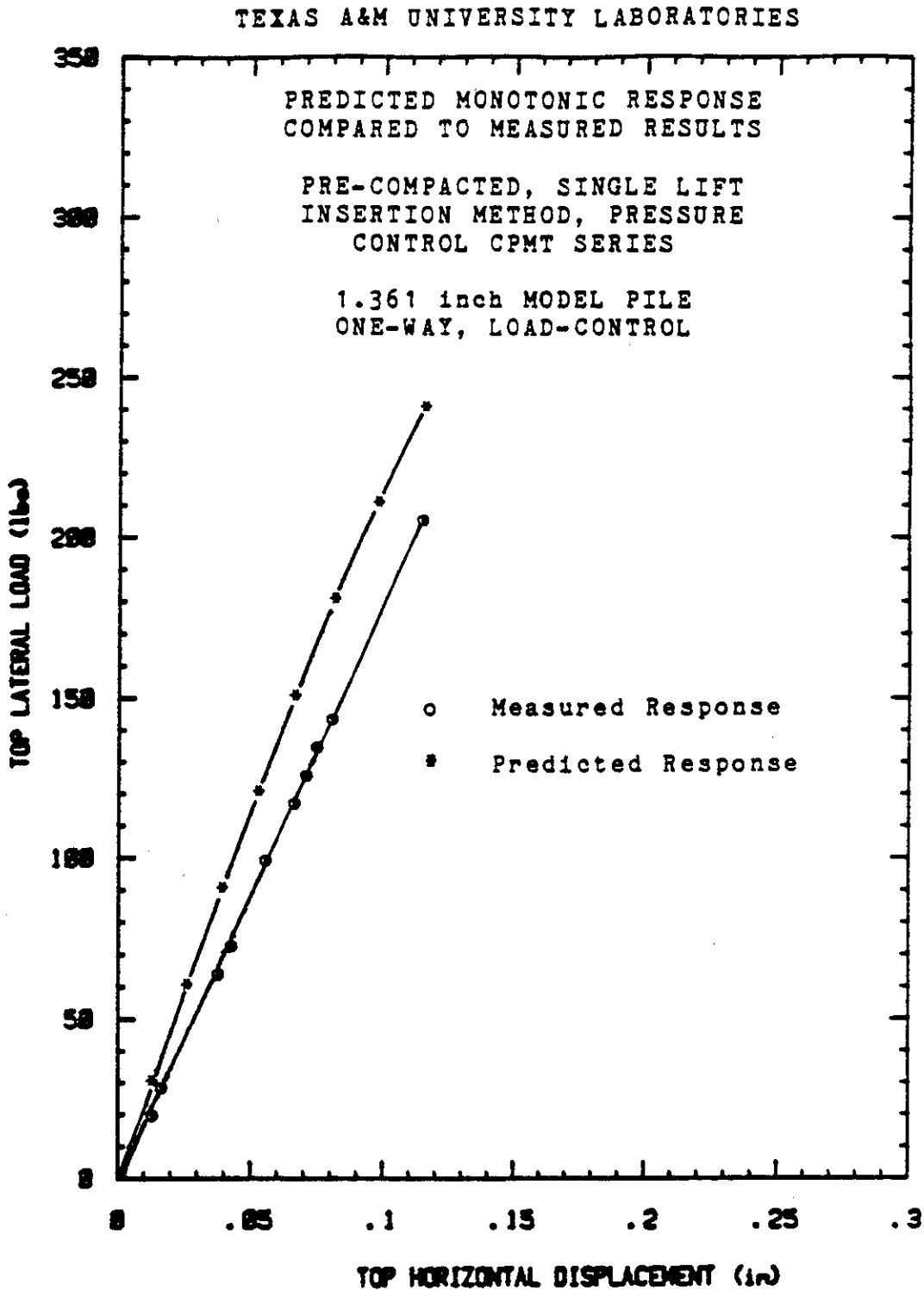

Figure 144. Predicted Monotonic Response of the Model Pile Compared to the Measured Response: Pre-compacted, Single Lift, Pile Placement Procedure; One-way, Load-control Cycles.

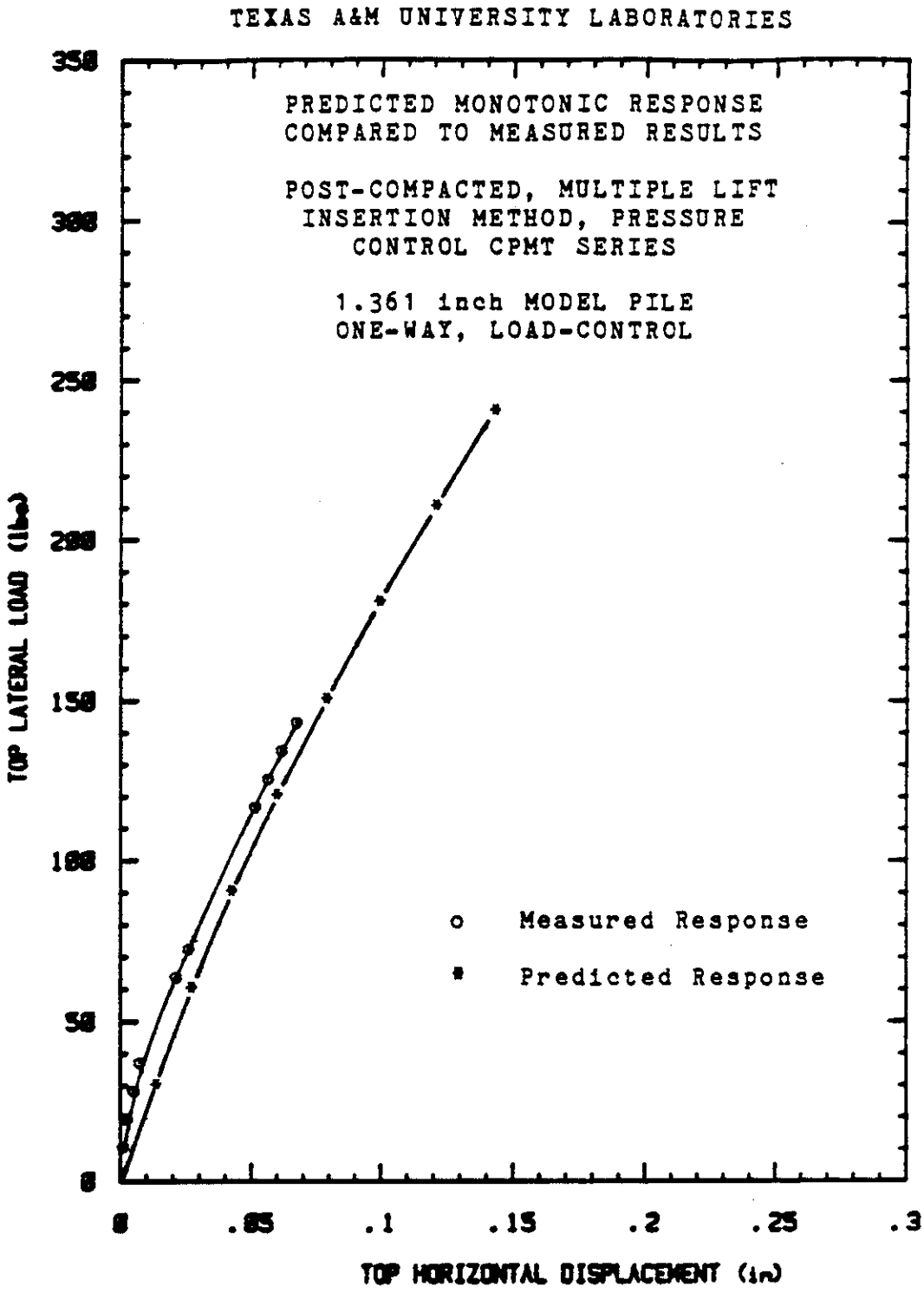

Figure 145. Predicted Monotonic Response of the Model Pile Compared to the Measured Response: Post-compacted, Multiple Lift, Pile Placement Procedure; One-way, Load-control Cycles.

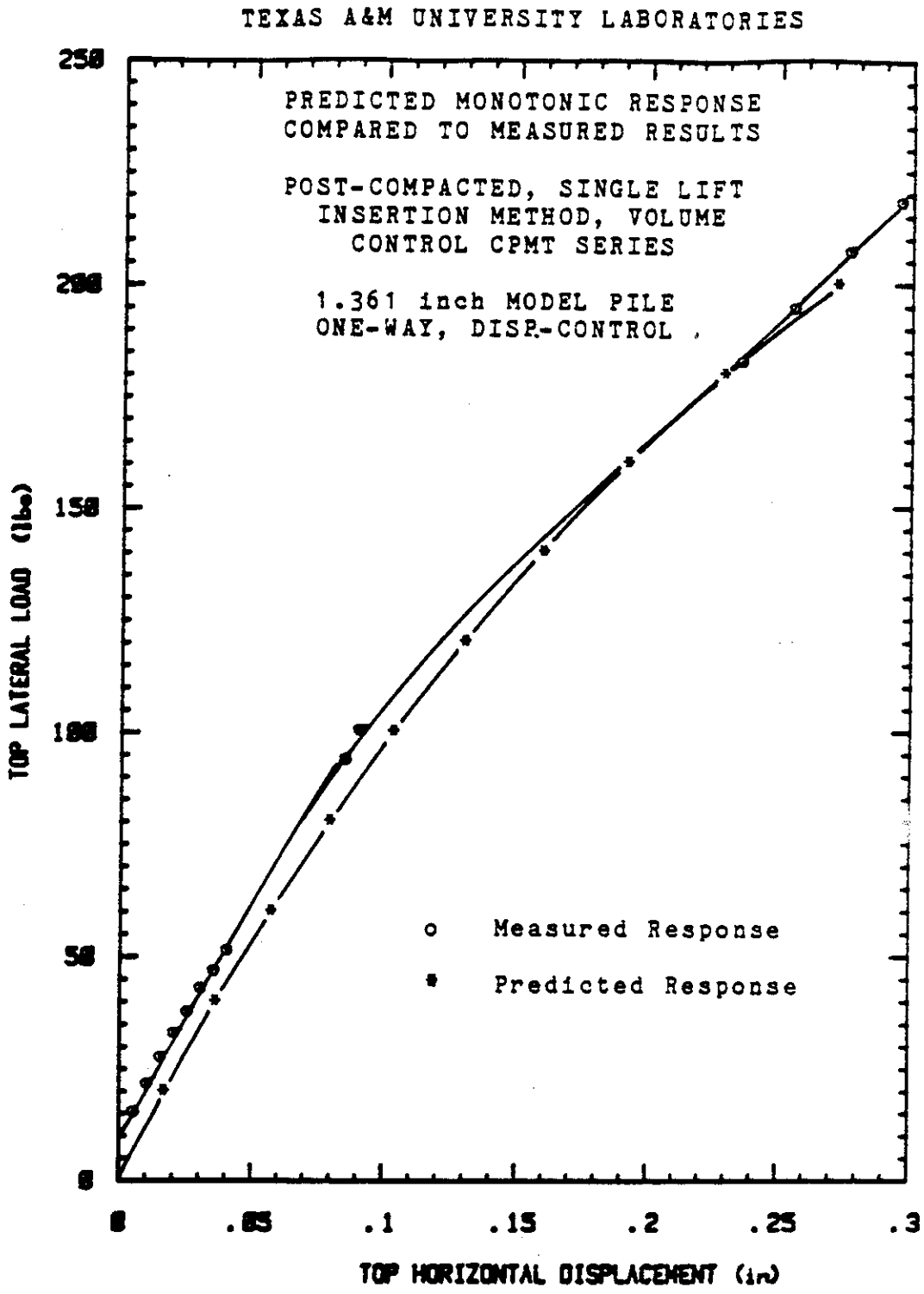

Figure 146. Predicted Monotonic Response of the Model Pile Compared to the Measured Response: Post-compacted, Single Lift, Pile Placement Procedure; One-way, Displacement-control Cycles.

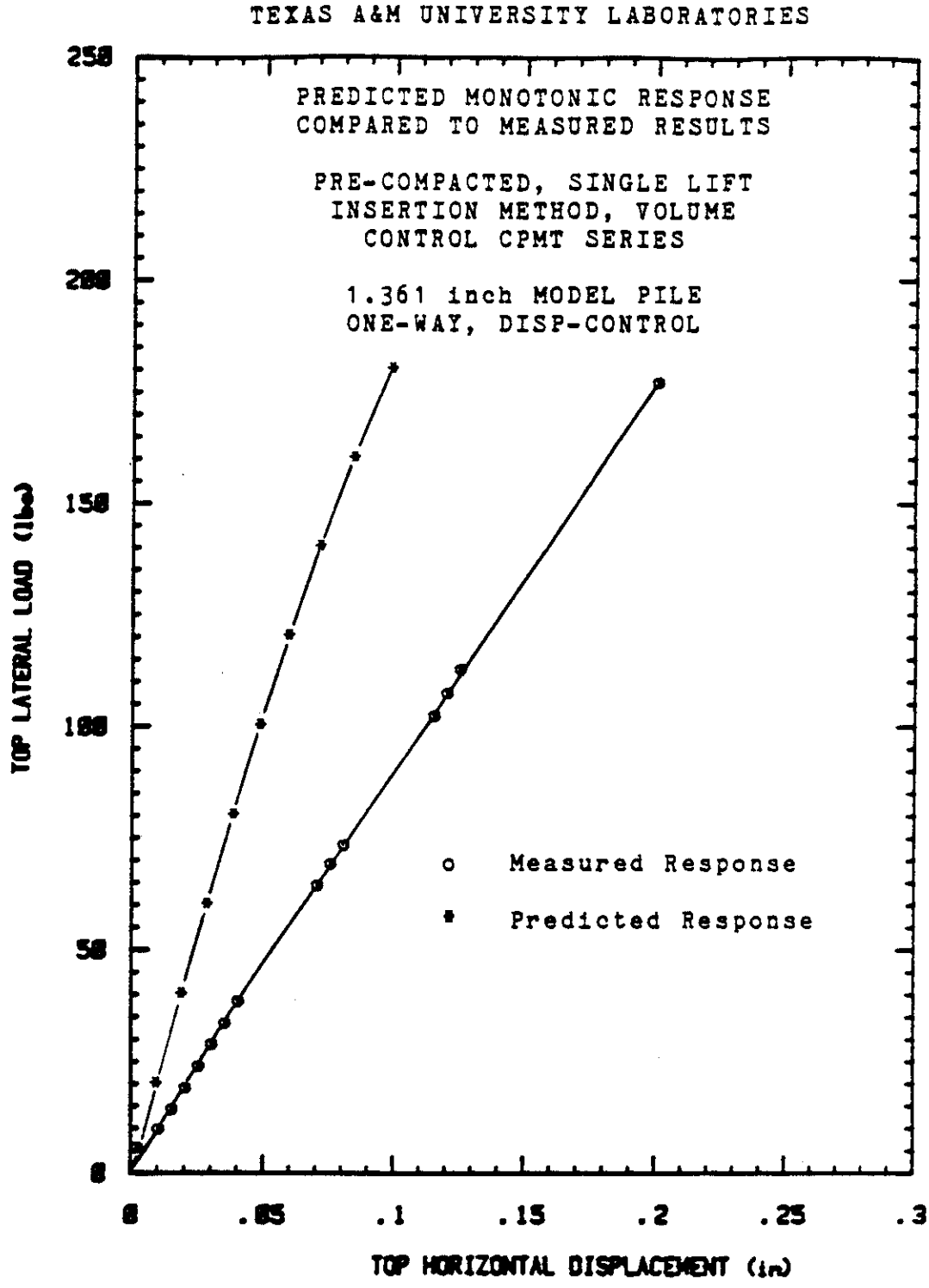

Figure 147. Predicted Monotonic Response of the Model Pile Compared to the Measured Response: Pre-compacted, Single Lift, Pile Placement Procedure; One-way, Displacement-control Cycles.

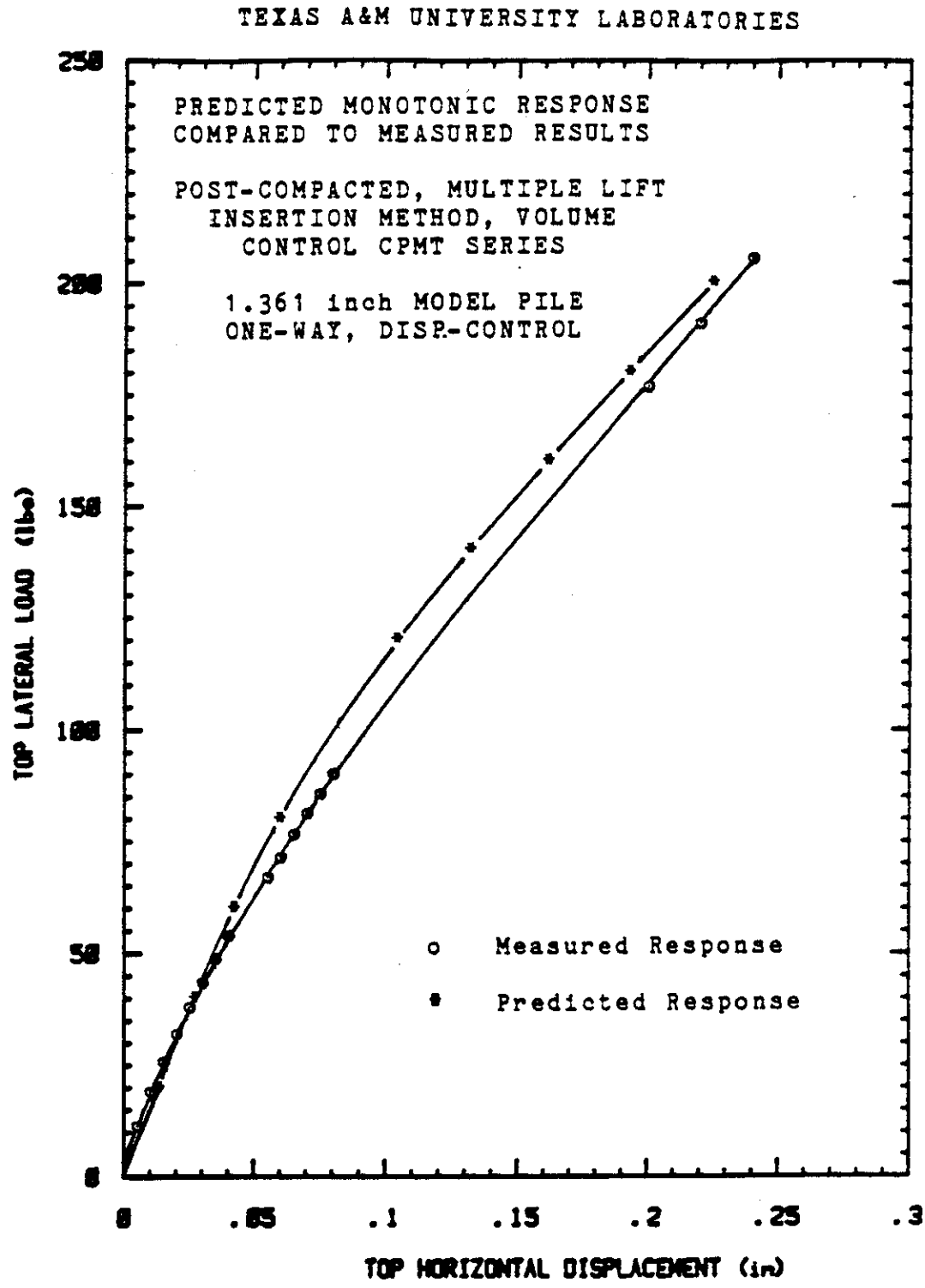

Figure 148. Predicted Monotonic Response of the Model Pile Compared to the Measured Response: Post-compacted, Multiple Lift, Pile Placement Procedure; One-way, Displacement-control Cycles.

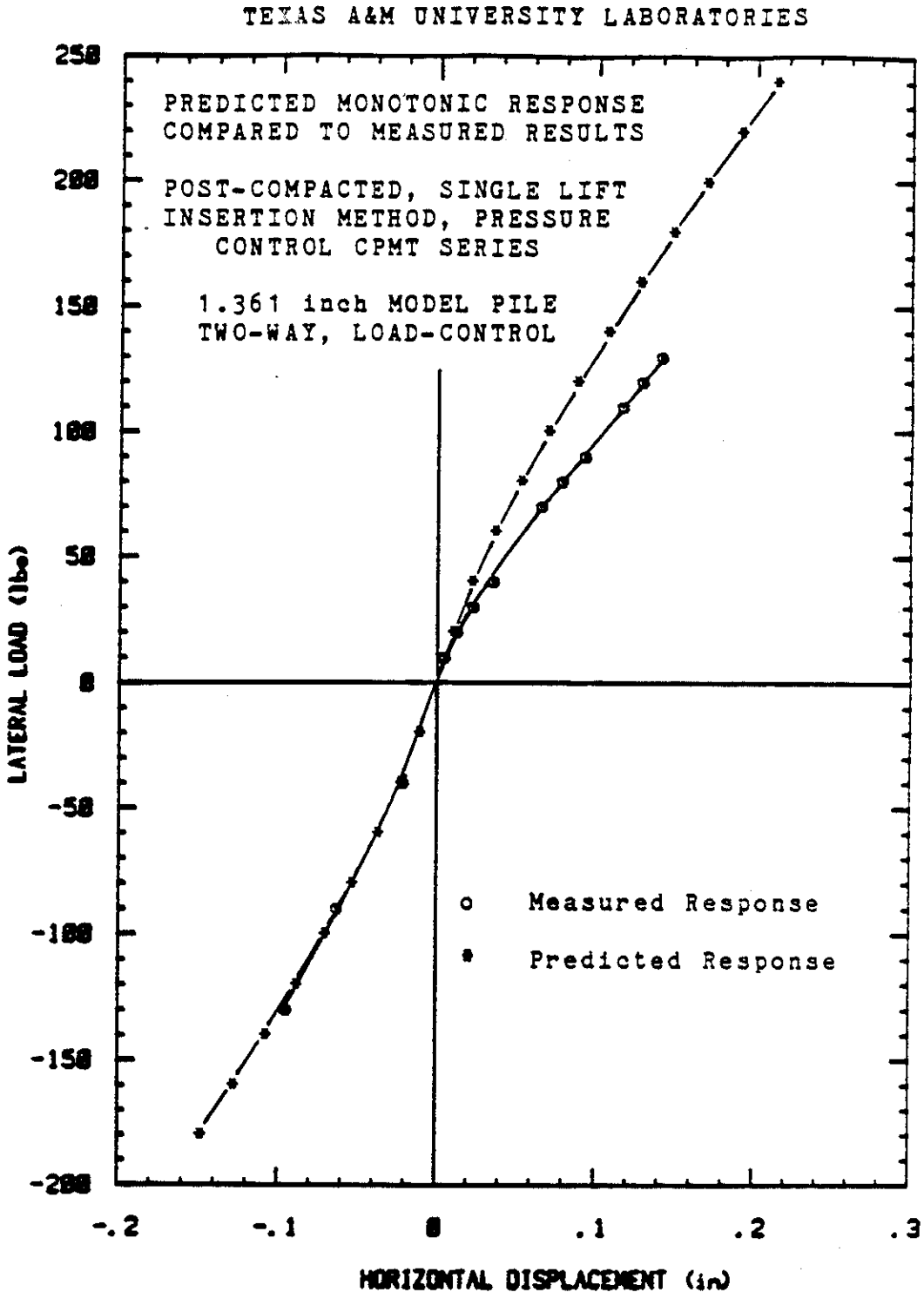

Figure 149. Predicted Monotonic Response of the Model Pile Compared to the Measured Response: Post-compacted, Single Lift, Pile Placement Procedure; Two-way, Load-control Cycles.

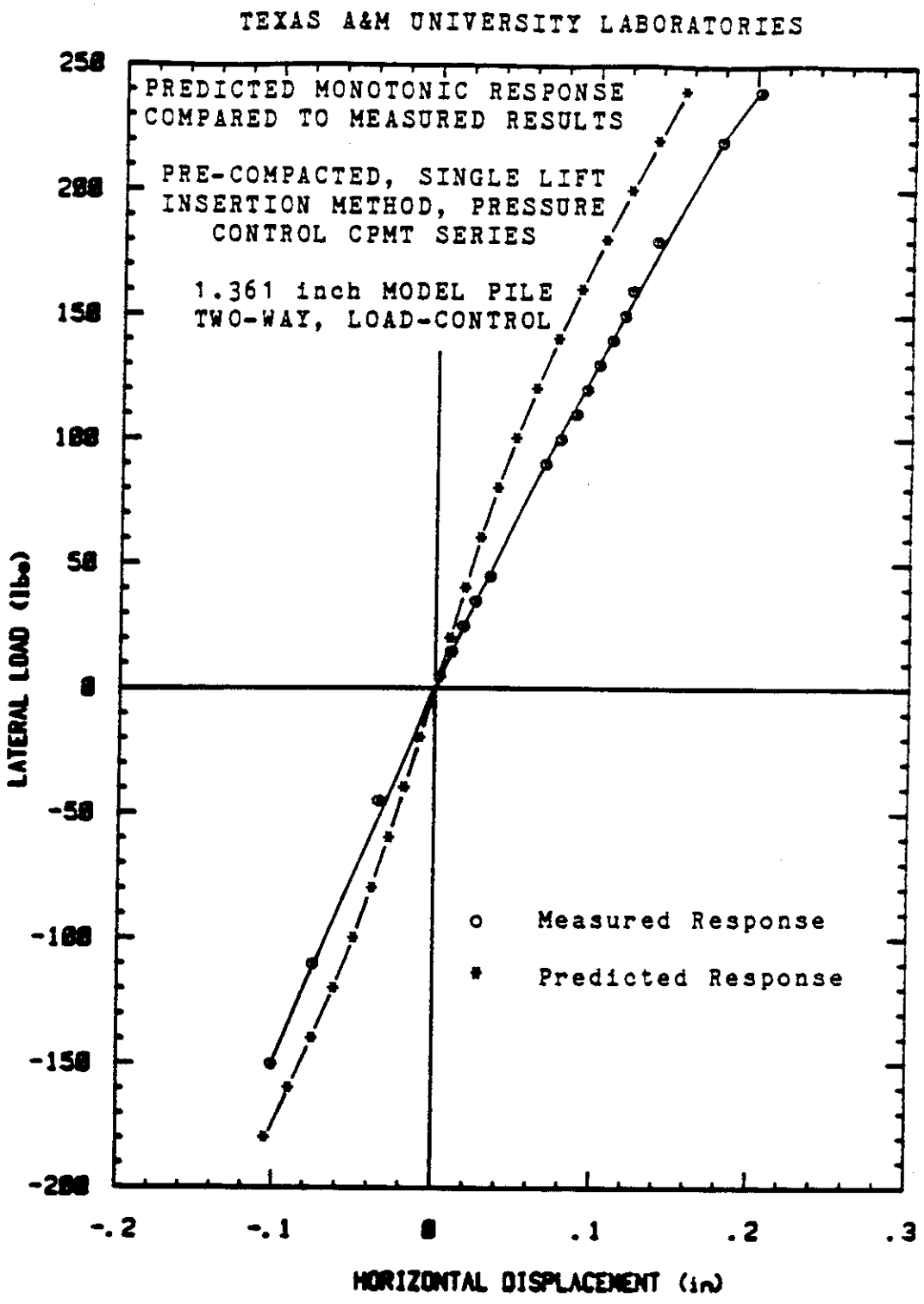

Figure 150. Predicted Monotonic Response of the Model Pile Compared to the Measured Response: Pre-compacted, Single Lift, Pile Placement Procedure; Two-way, Load-control Cycles.

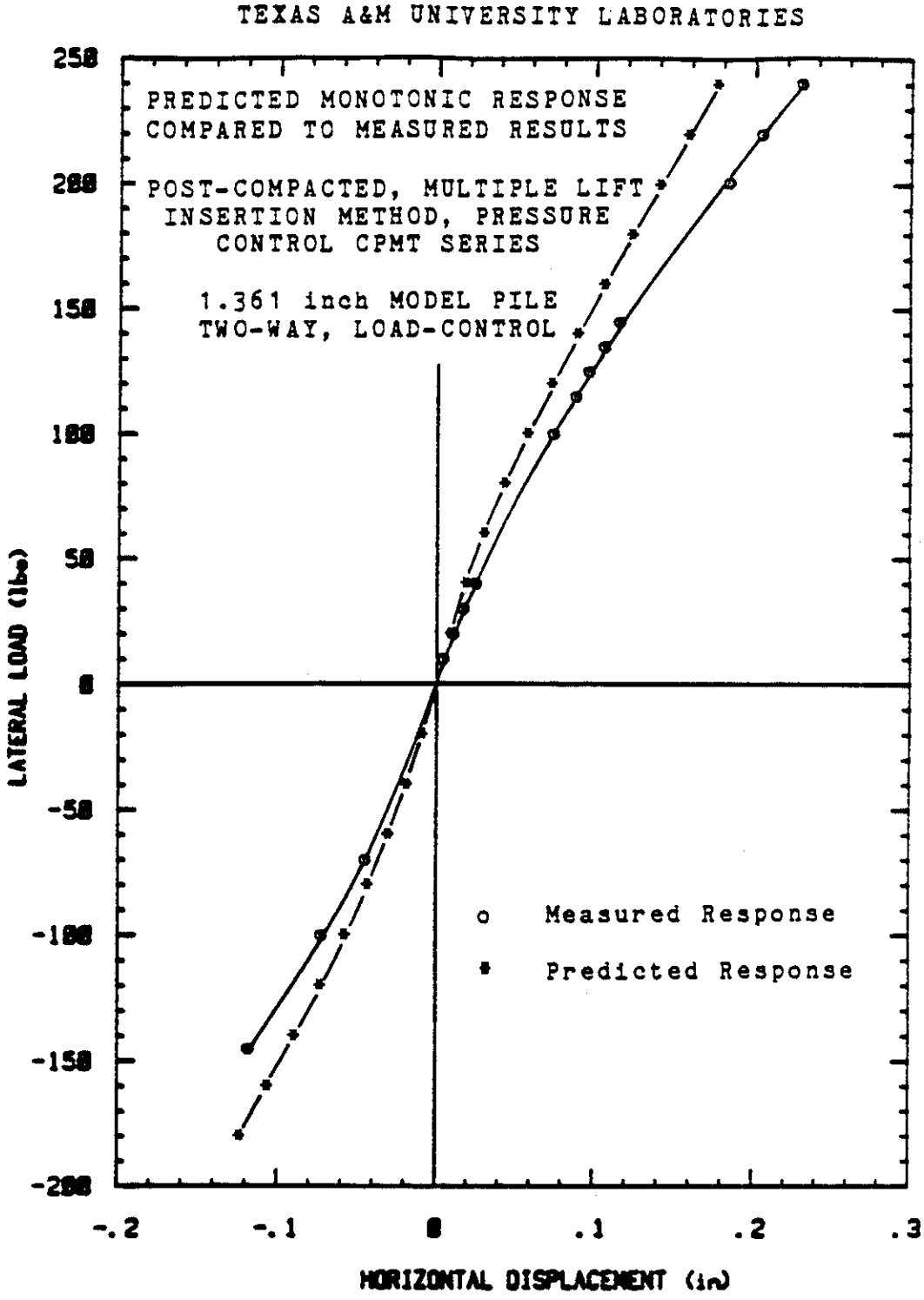

Figure 151. Predicted Monotonic Response of the Model Pile Compared to the Measured Response: Post-compacted, Multiple Lift, Pile Placement Procedure; Two-way, Load-control Cycles.

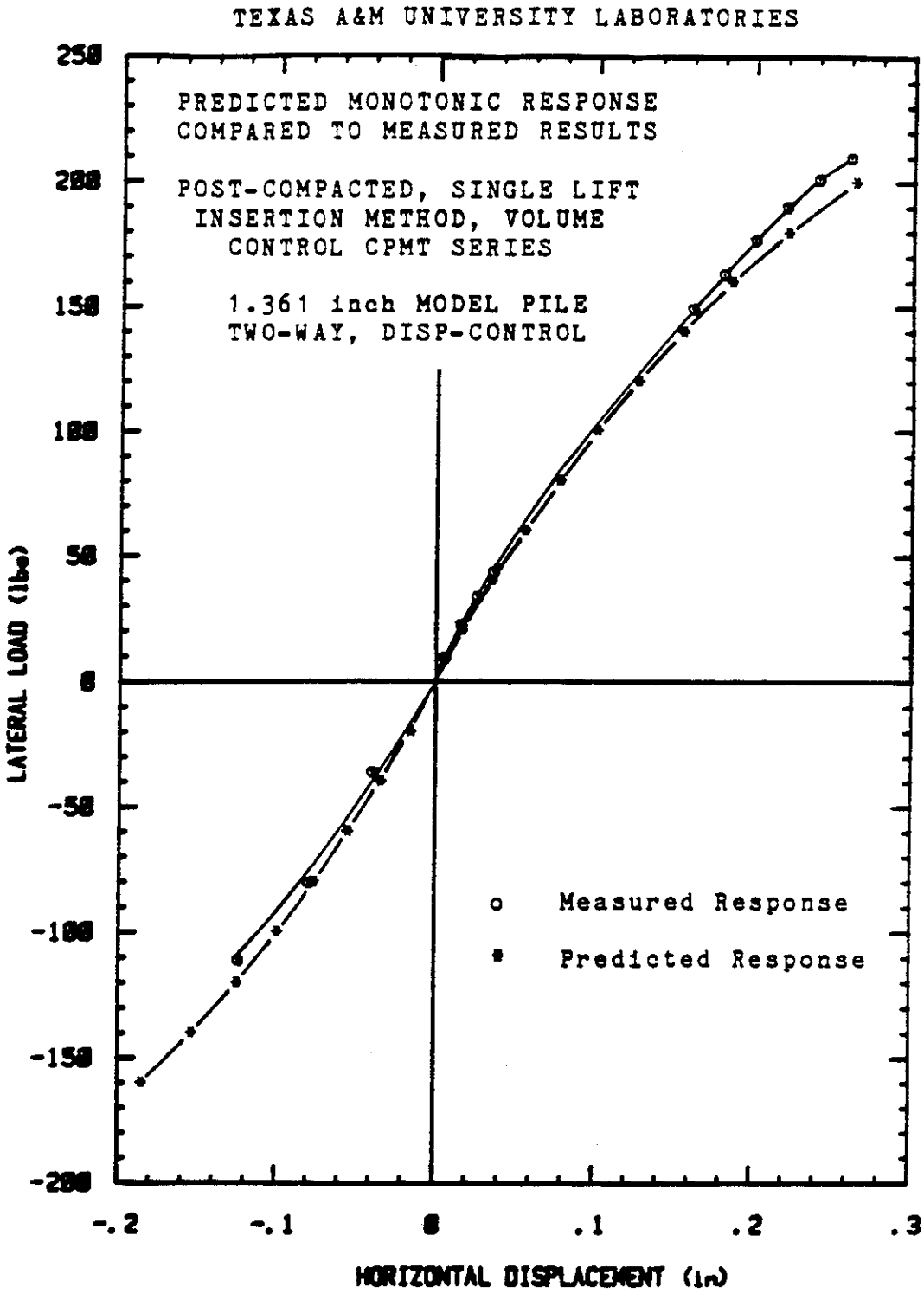

Figure 152. Predicted Monotonic Response of the Model Pile Compared to the Measured Response: Post-compacted, Single Lift, Pile Placement Procedure; Two-way, Displacement-control Cycles.

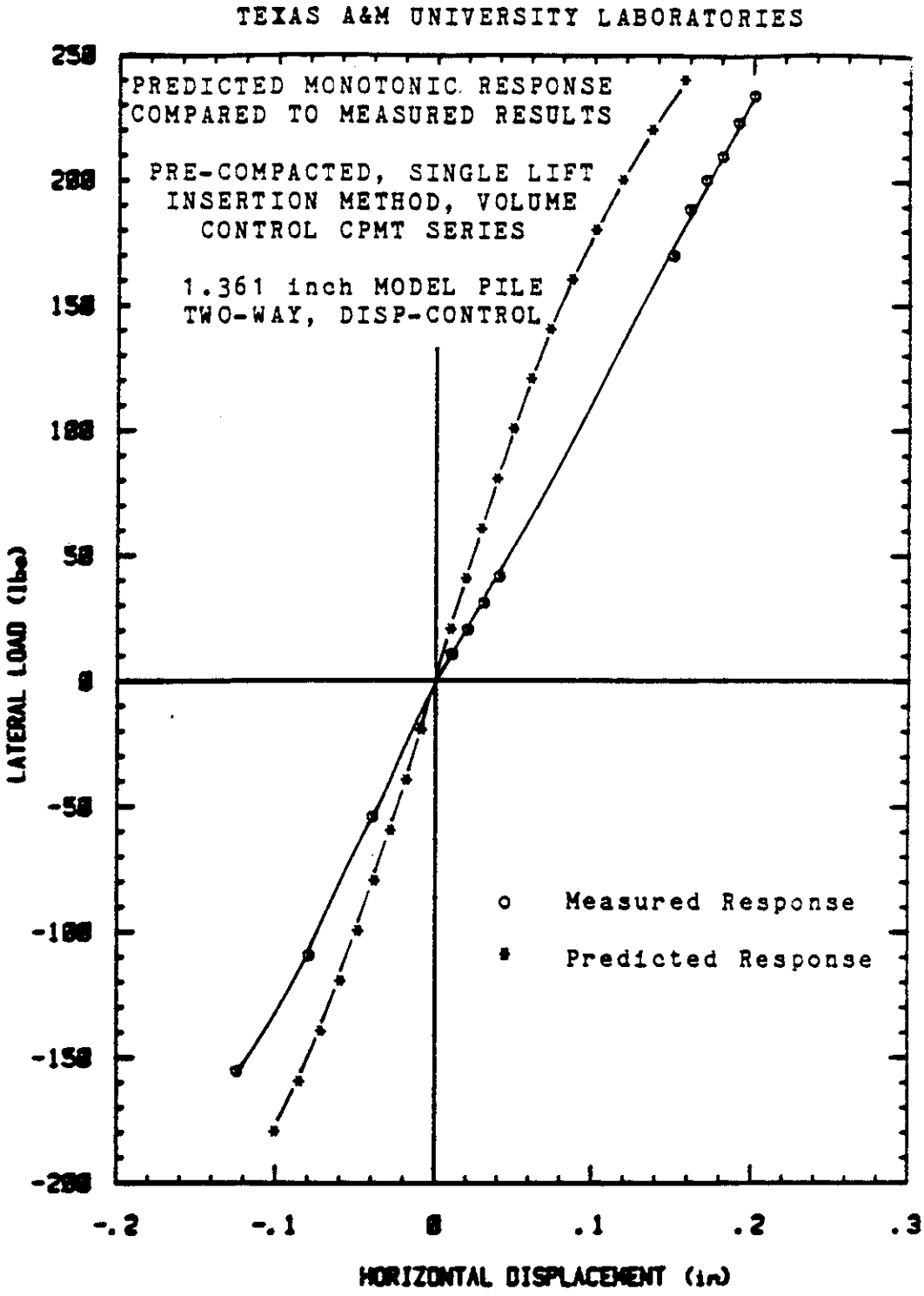

Figure 153. Predicted Monotonic Response of the Model Pile Compared to the Measured Response: Pre-compacted, Single Lift, Pile Placement Procedure; Two-way, Displacement-control Cycles.

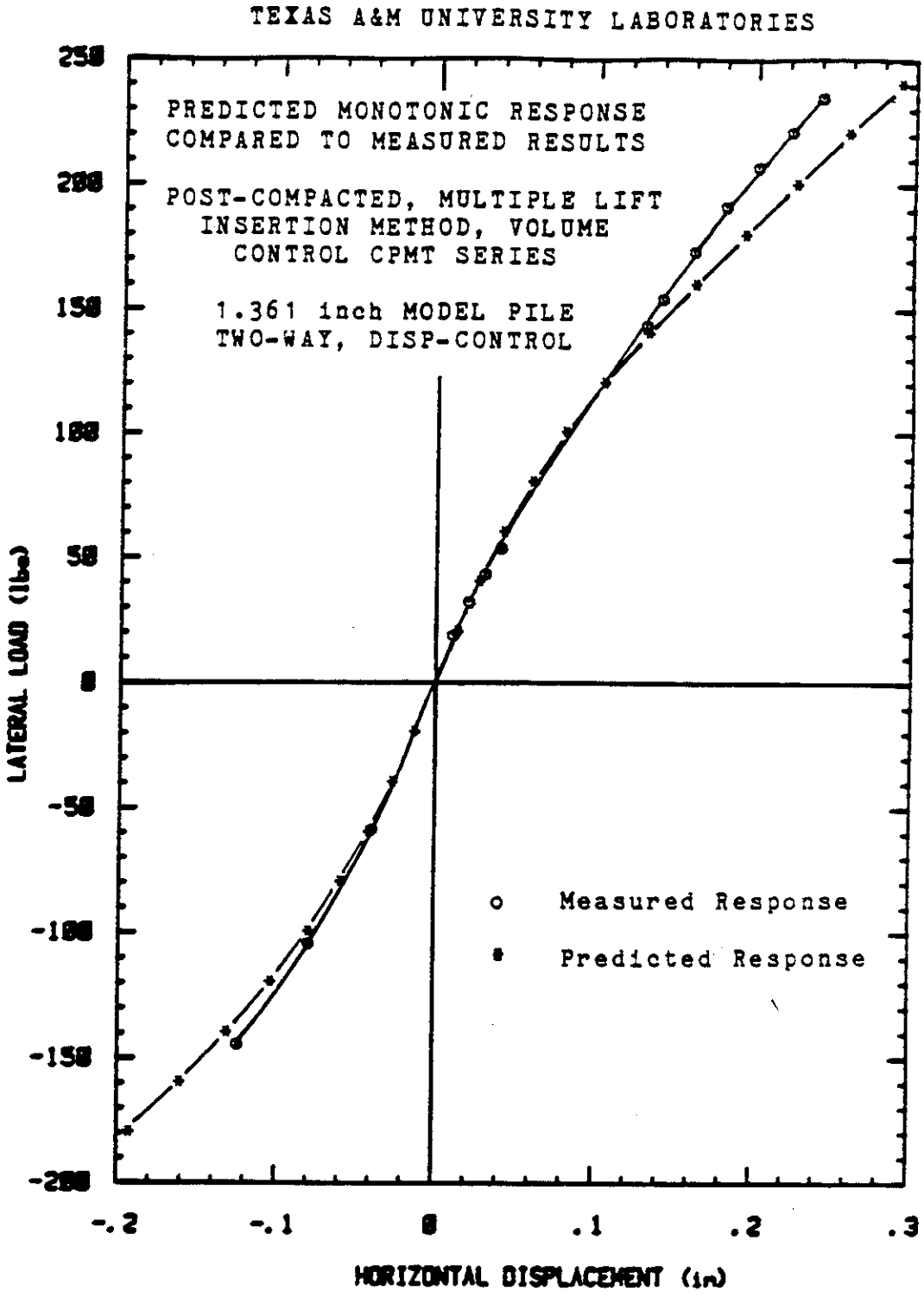

Figure 154. Predicted Monotonic Response of the Model Pile Compared to the Measured Response: Post-compacted, Multiple Lift, Pile Placement Procedure; Two-way, Displacement-control Cycles.

comparisons.

10.3 Comparison of Predicted and Measured Monotonic Responses

10.3.1 Single Pile at University of Houston

A comparison of the predicted load-displacement responses and the measured response for the 10.75 inch pipe pile (Figures 140, 141 and 142) shows that the pre-boring TEXAM probe provided the closest correlation to the actual pile response. This is due to the fact that the pre-boring pressuremeter came the closest to duplicating the pile installation technique. The stiffer initial response in the predicted curve is not surprising considering that the pressuremeter tests were conducted after the pile load tests, during which densification in the sand between the pile group and the single pile was visually evident (Section 3).

Figure 155 is a comparison of the pile's maximum bending moment as predicted by the TEXAM pre-bored tests with the measured monotonic response. The predicted moments also indicate a stiffer initial soil response than actually experienced by the pile; nonetheless, the curve does agree well with the measured results.

Pressuremeter-derived monotonic P-y curves at the measured P-y curve depths were found by linearly interpolating between the P-y curves derived from the pre-bored pressuremeter tests. The comparisons between predicted and measured monotonic P-y curves are plotted in Figures 156 through 158.

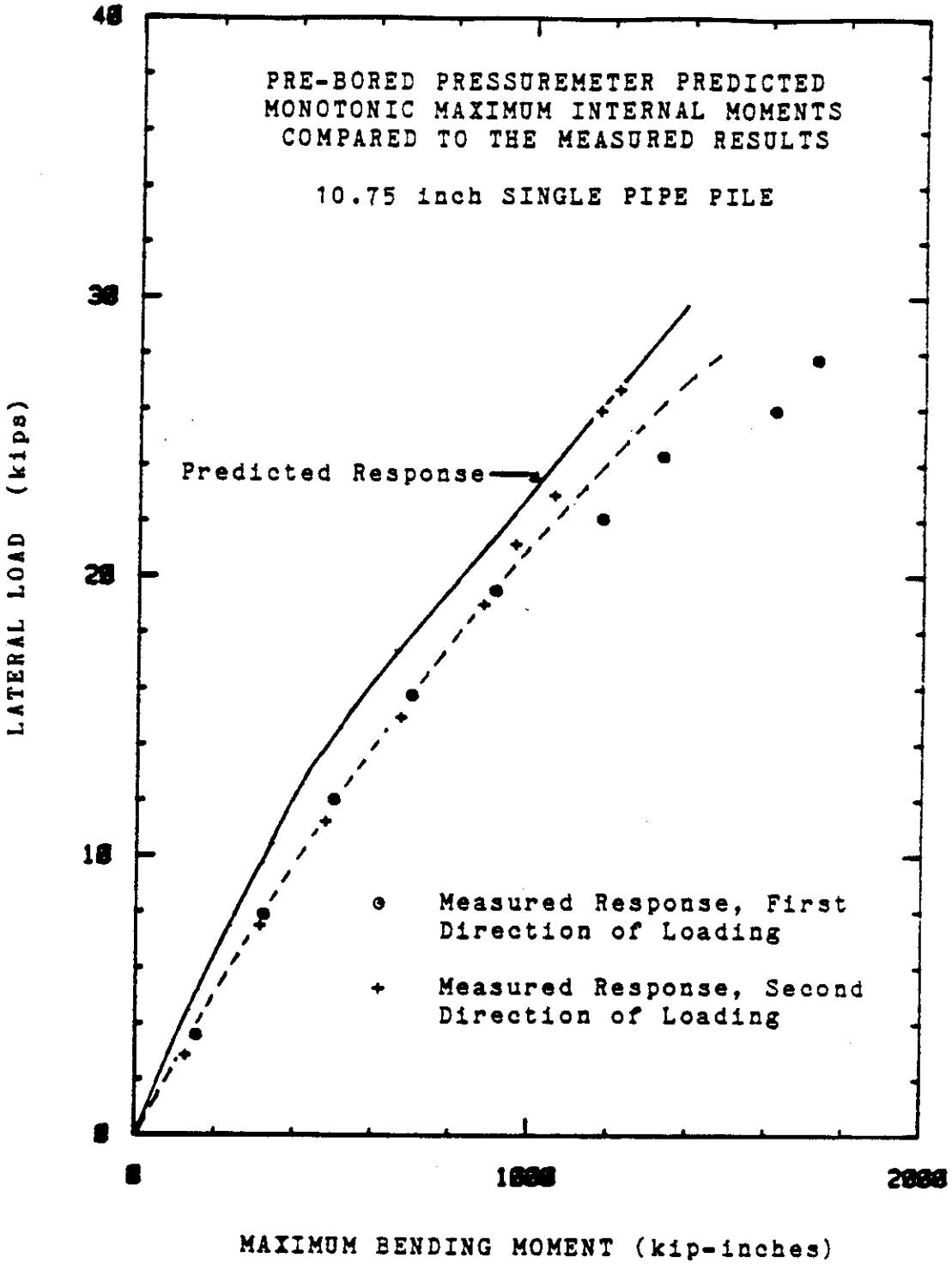

Figure 155. Predicted Maximum Internal Pile Moments Compared to the Measured Moments, Single Pile, University of Houston Sand Site.

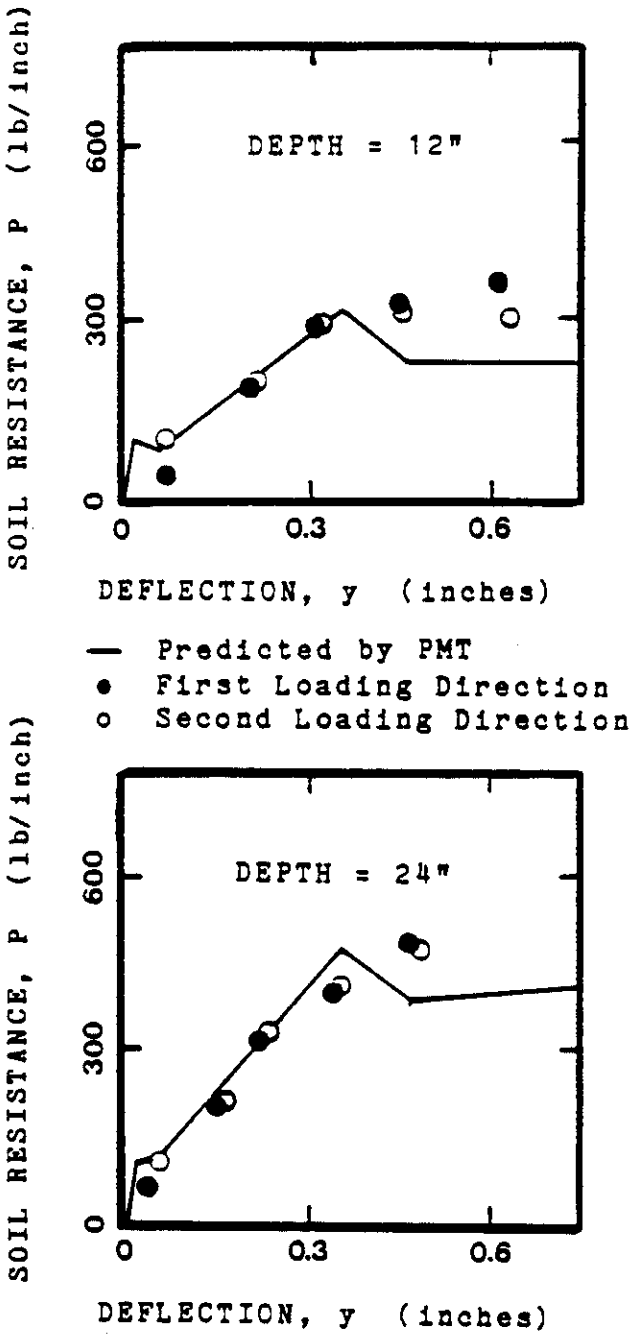

Figure 156. Pressuremeter-derived P-y Curves Compared to the Back-calculated Values for the Single Pile, 1.0 and 2.0 ft. (After Morrison and Reese, 1986).

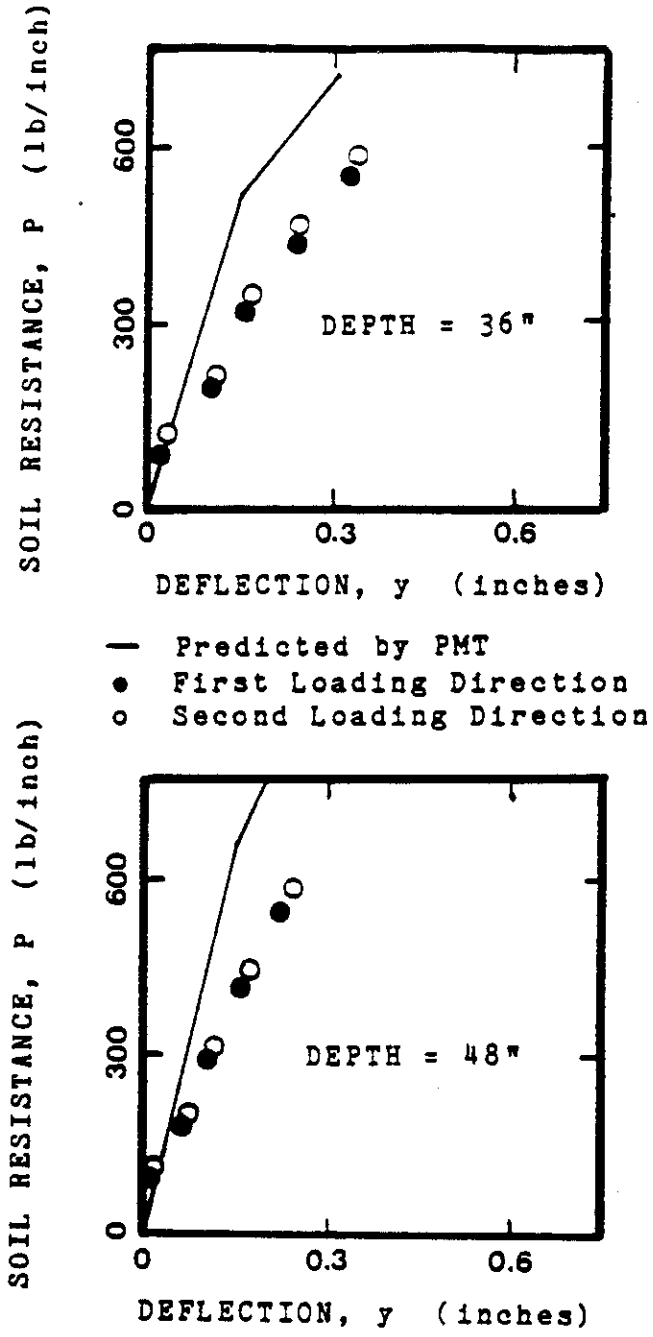

Figure 157. Pressuremeter-derived P-y Curves Compared to the Back-calculated Values for the Single Pile, 3.0 and 4.0 ft. (After Morrison and Reese, 1986).

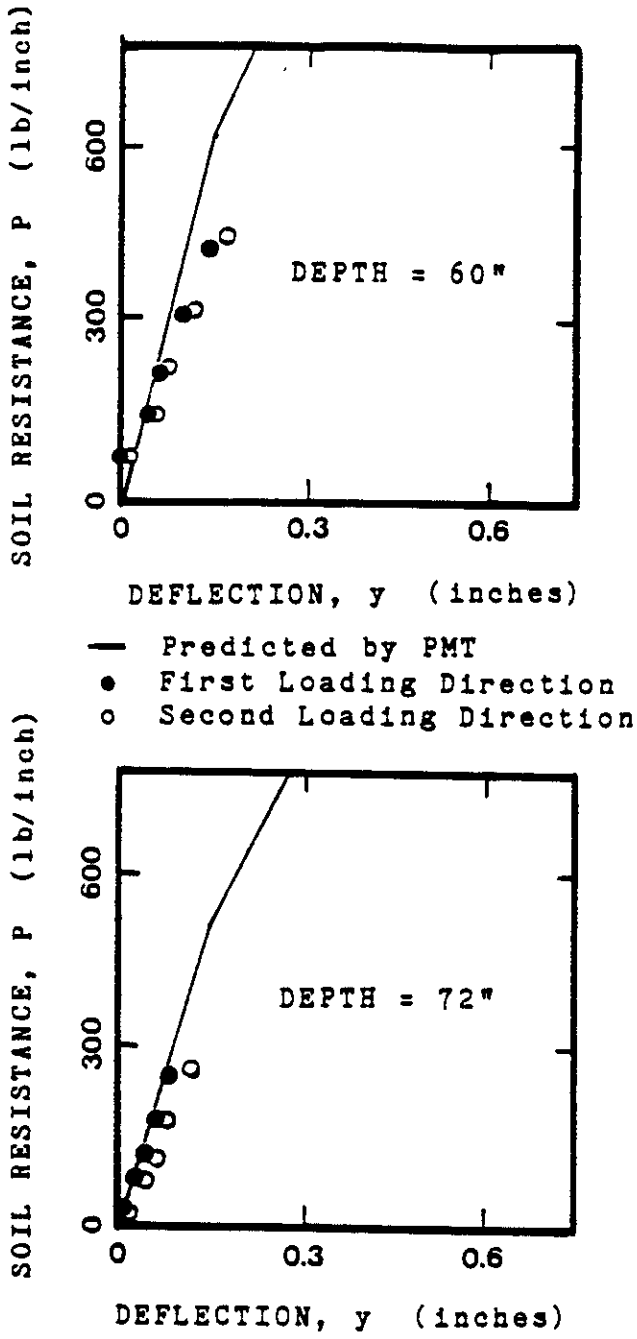

Figure 158. Pressuremeter-derived P-y Curves Compared to the Back-calculated Values for the Single Pile 5.0, and 6.0 ft. (After Morrison and Reese, 1986).

The pressuremeter P-y curves compare very favorably with the measured responses.

10.3.2 Model Piles at Texas A&M University

The static predictions for the model tests are presented with the measured results in Figures 143 through 154. The range of pressuremeter-predicted monotonic responses are compared to the range of measured responses in Figures 159 and 160. The two-way load-control and displacement-control predictions were constructed by projecting a mirror image of one-way predictions into the negative quadrants.

Overall, the predictions are very good as can be seen from the figures. Table 9 shows the ratios of predicted over measured load at deflections of 0.03 inches and 0.10 inches for all load tests. These deflections correspond approximately to 2% and 8% of the pile diameter respectively.

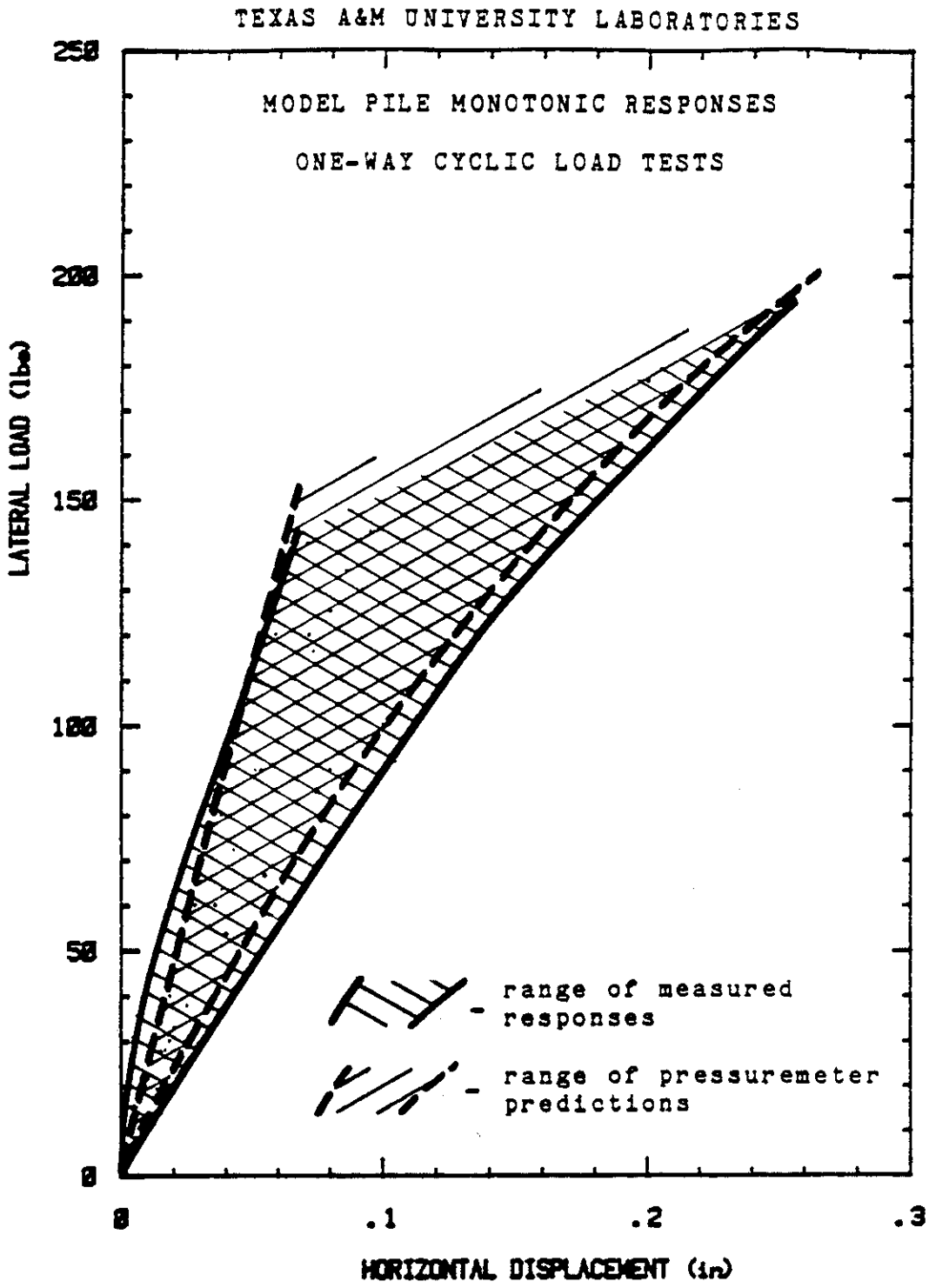

Figure 159. Range of Pressuremeter-predicted Monotonic Responses Compared to Range of Measured Monotonic Responses: One-way Cyclic Model Pile Load Tests.

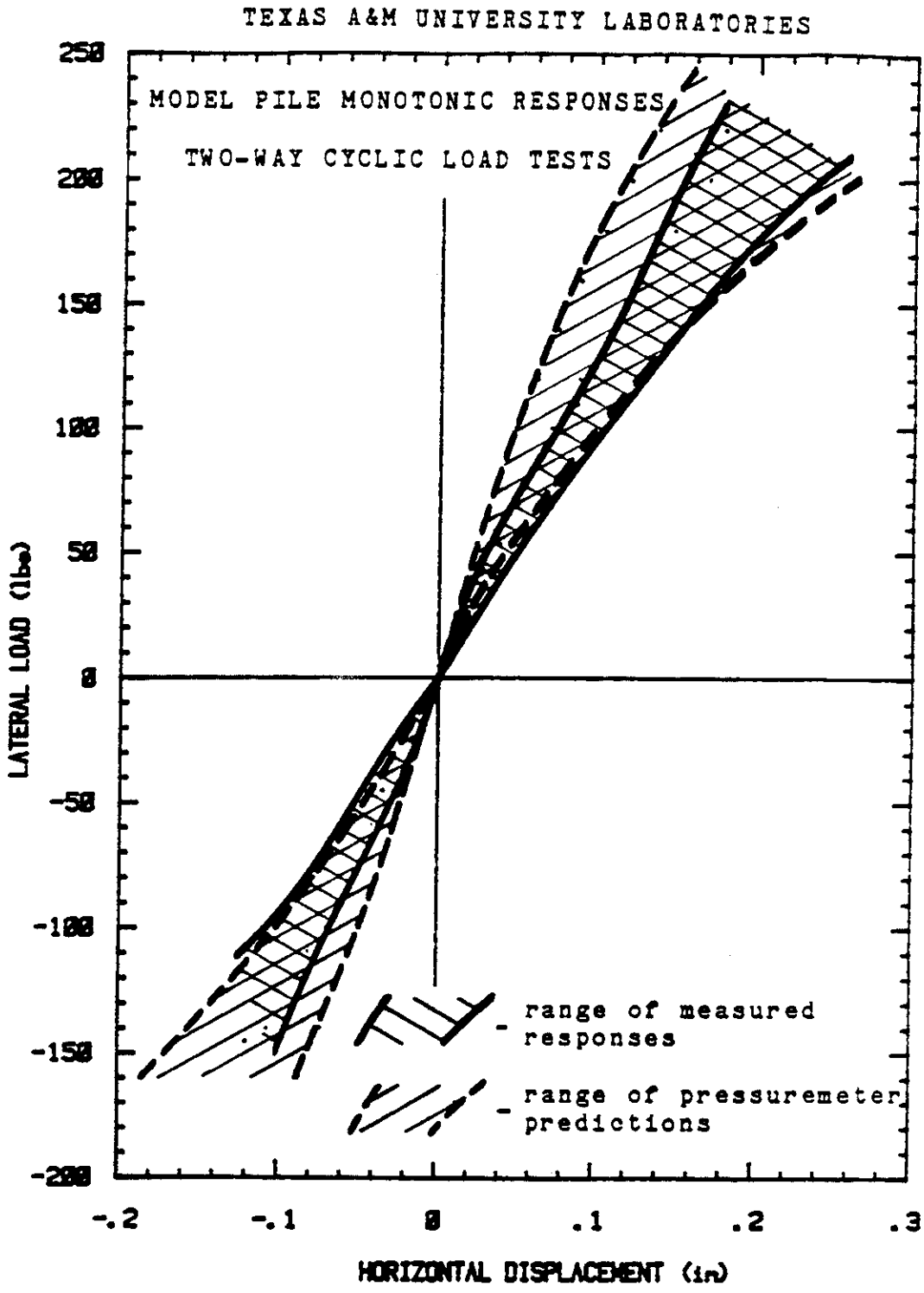

Figure 160. Range of Pressuremeter-predicted Monotonic Responses Compared to Range of Measured Monotonic Responses: Two-way Cyclic Model Pile Load Tests.

Cycling Method	Soil/Placement Procedure	Model Pile Test No.	Ratio of Predicted Monotonic Load / Measured Monotonic Load			
			First Load Direction		Second Load Direction	
			y=0.03"	y=0.10"	y=0.03"	y=0.10"
One-way Load/ Pressure Control	Post-compacted Single Lift	1	0.82	1.15	-	-
	Pre-compacted Single Lift	2	1.32	1.20	-	-
	Post-compacted Multiple Lift	3	0.83	0.97	-	-
One-way Displacement/ Volume Control	Post-compacted Single Lift	4	0.82	0.93	-	-
	Pre-compacted Single Lift	5	2.22	2.02	-	-
	Post-compacted Multiple Lift	6	1.01	1.10	-	-
averages of one-way tests			1.17	1.23		
st. dev. of one-way tests			0.55	0.40		
Two-way Load/ Pressure Control	Post-compacted Single Lift	7	1.32	1.34	1.00	0.97
	Pre-compacted Single Lift	8	1.53	1.34	1.36	1.17
	Post-compacted Multiple Lift	9	1.27	1.31	1.18	1.18
Two-way Displacement/ Volume Control	Post-compacted Single Lift	10	0.91	0.98	1.14	1.09
	Pre-compacted Single Lift	11	1.96	1.60	1.45	1.32
	Post-compacted Multiple Lift	12	1.00	1.00	0.96	0.94
averages of two-way tests			1.33	1.26	1.18	1.11
st. dev. of two-way tests			0.38	0.23	0.19	0.14

Table 9. Monotonic Predictions Compared to Measured Results for the Model Pile Load Tests at Texas A&M University.

11. CYCLIC PREDICTIONS

11.1 Predictions for the Single Pile at the University of Houston Sand Site

The cyclic degradation parameters selected from the decrease in the secant shear modulus with increasing cycles (Section 8) are presented in Table 10. These parameters were applied to the pressuremeter-derived static P-y curves to develope sets of cyclic P-y curves in the sand. In all cases, the degradation parameter for the clay was assumed to be a constant, equal to 0.06, the value found in a previous study (Makarim and Briaud, 1986). These newly derived cyclic P-y curves for the sand and the clay below were then input into BMCOL7, a bear column program written by Hudson Matlock (Coyle, 1986), to model the soil resistance. The resulting cyclic predictions are depicted in Figures 161, 162, and 163.

11.2 Predictions for the Model Piles at the Texas A&M University Laboratories

The degradation parameters selected for use in the model pile predictions (Table 6) resulted in the cyclic predictions presented in Figures 164 through 175. The method employed (Section 9) made no distinction between two-way and one-way loading.

Pressuremeter Type	Insertion Method	Cyclic Degradation Parameter Selected
TEXAM PMT	Pre-bored	0.26
Cone PMT	Pushed-in	0.23
Cone PMT	Driven-in	0.15

Table 10. Cyclic Degradation Parameters Selected for Predicting the Response of the 10.75 inch Single Pile.

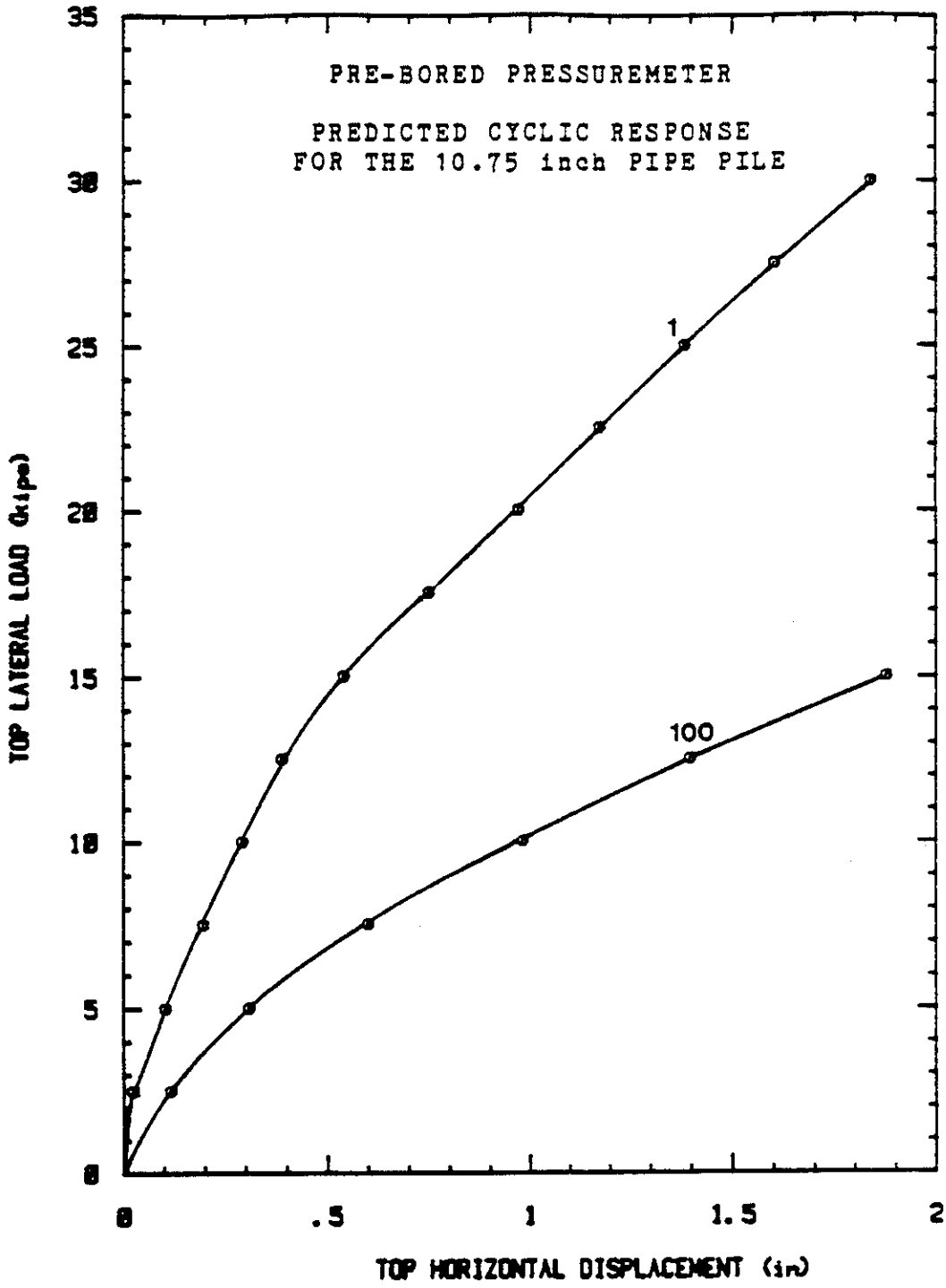

Figure 161. Predicted Cyclic Response of the Single Pile: Pre-bored TEXAM PMT.

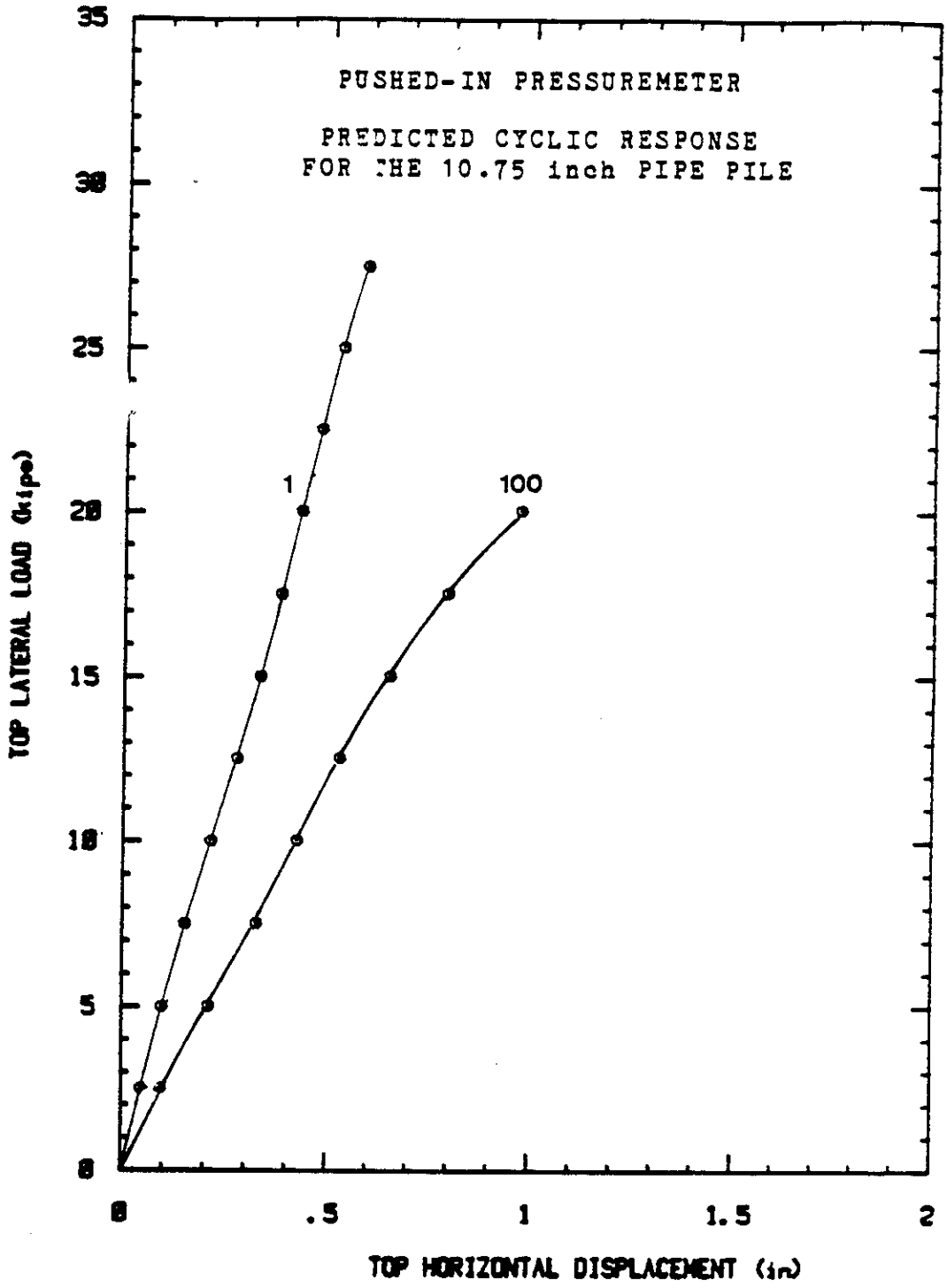

Figure 162. Predicted Cyclic Response of the Single Pile: Pushed-in Cone PMT.

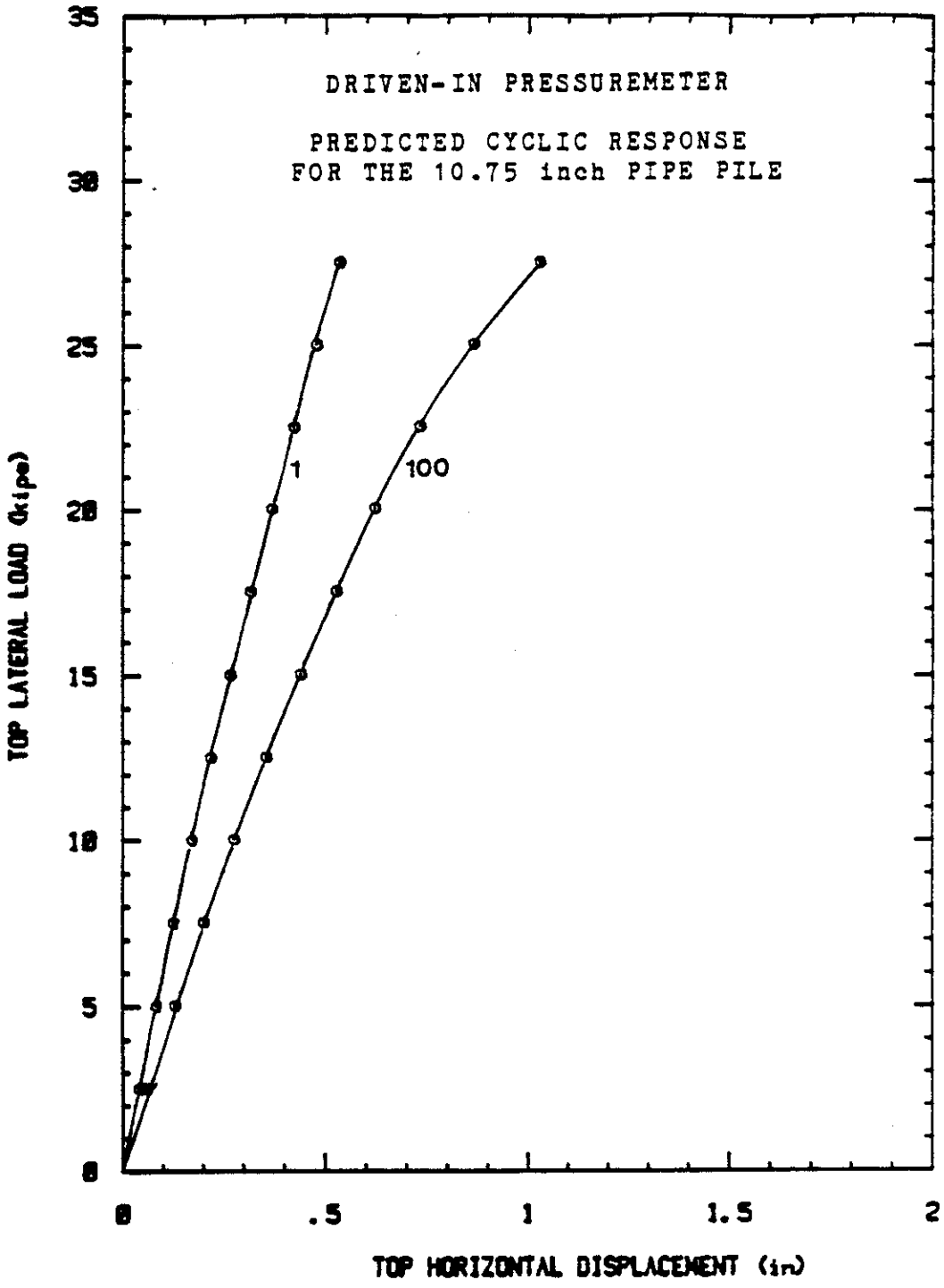

Figure 163. Predicted Cyclic Response of the Single Pile: Driven-in Cone PMT.

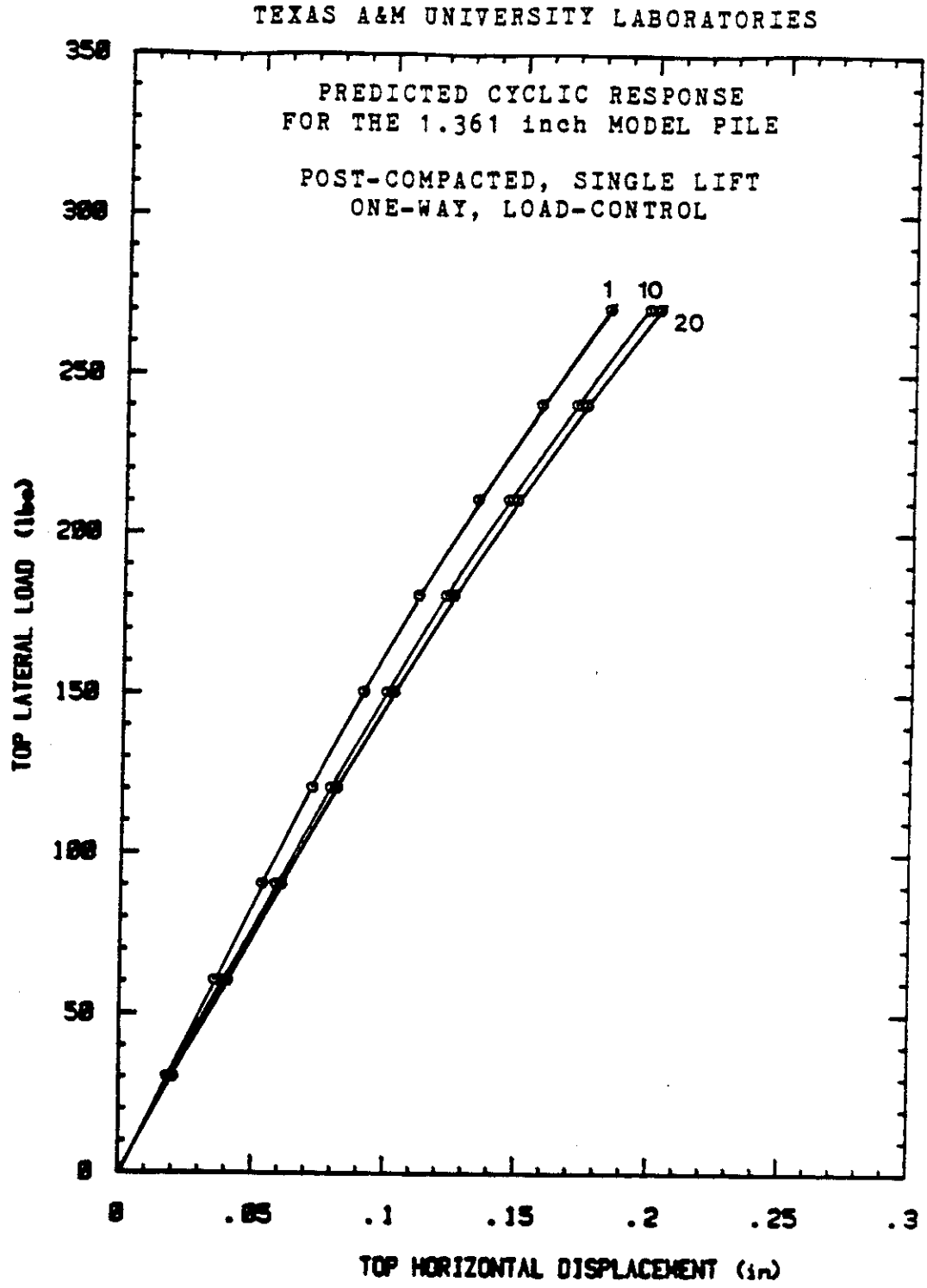

Figure 164. Predicted Cyclic Response of the Model Pile: Post-compacted, Single Lift, Pile Placement Procedure; One-way, Load-control Cycles.

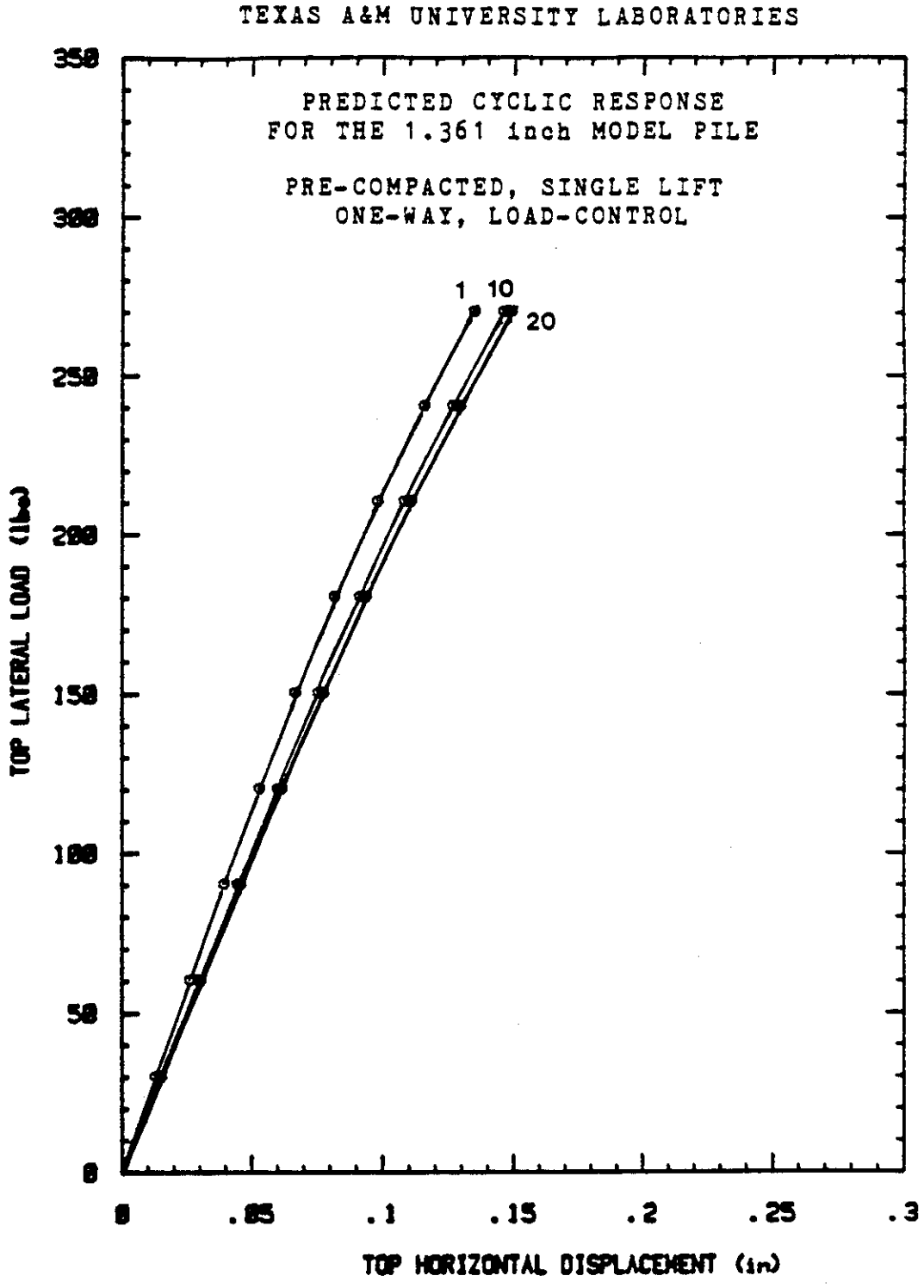

Figure 165. Predicted Cyclic Response of the Model Pile: Pre-compacted, Single Lift, Pile Placement Procedure; One-way, Load-control Cycles.

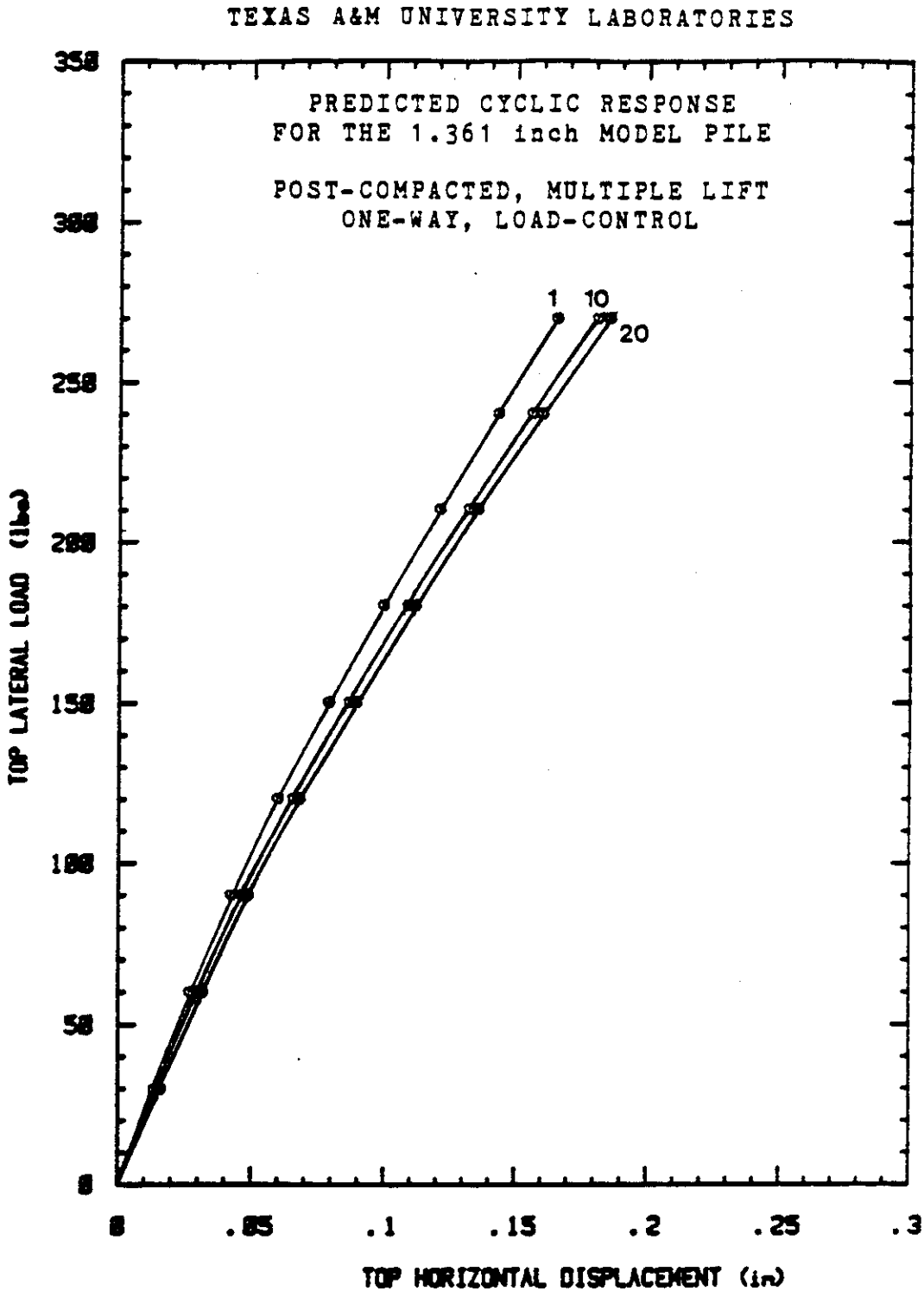

Figure 166. Predicted Cyclic Response of the Model Pile: Post-compacted, Multiple Lift, Pile Placement Procedure; One-way, Load-control Cycles.

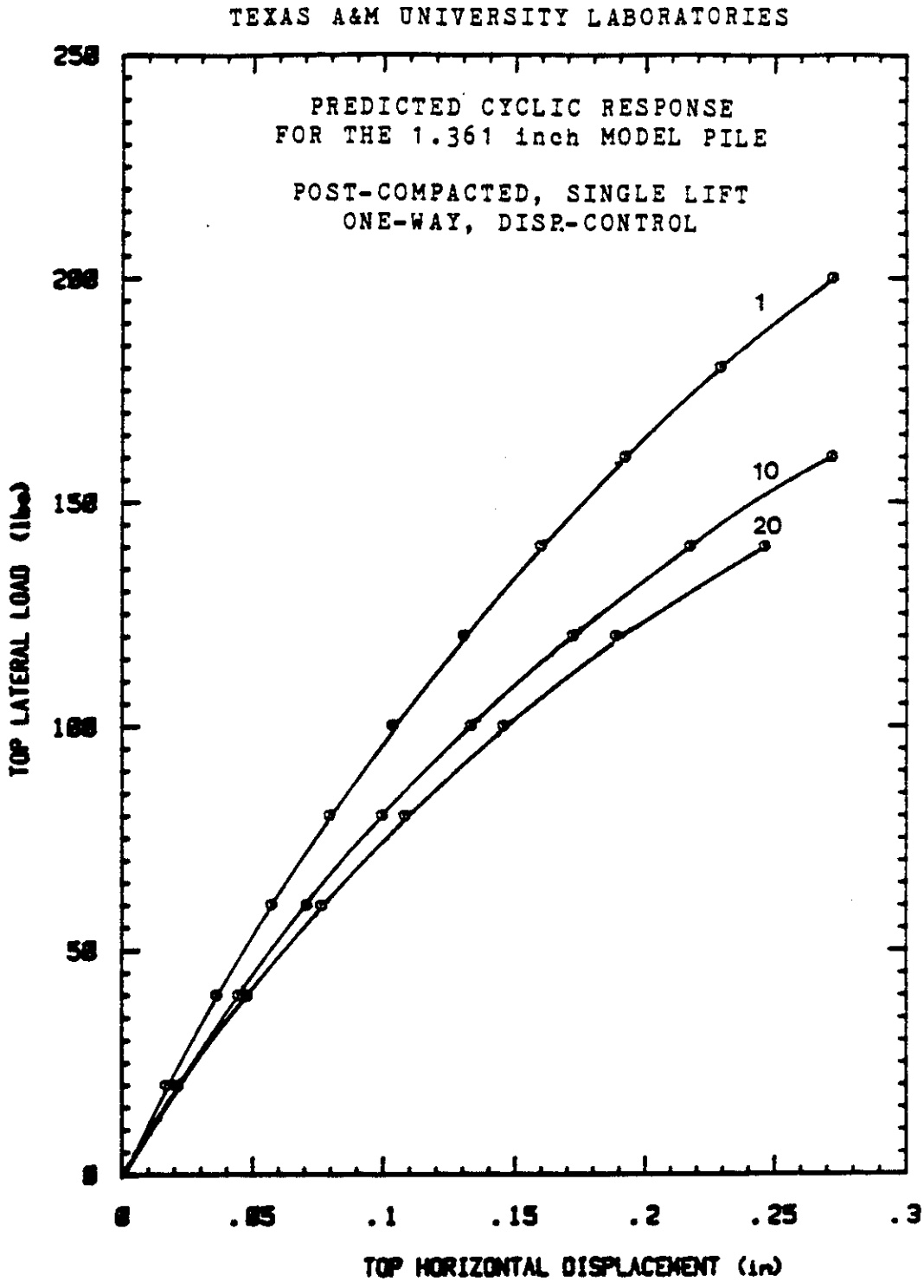

Figure 167. Predicted Cyclic Response of the Model Pile: Post-compacted, Single Lift, Pile Placement Procedure; One-way, Displacement-control Cycles.

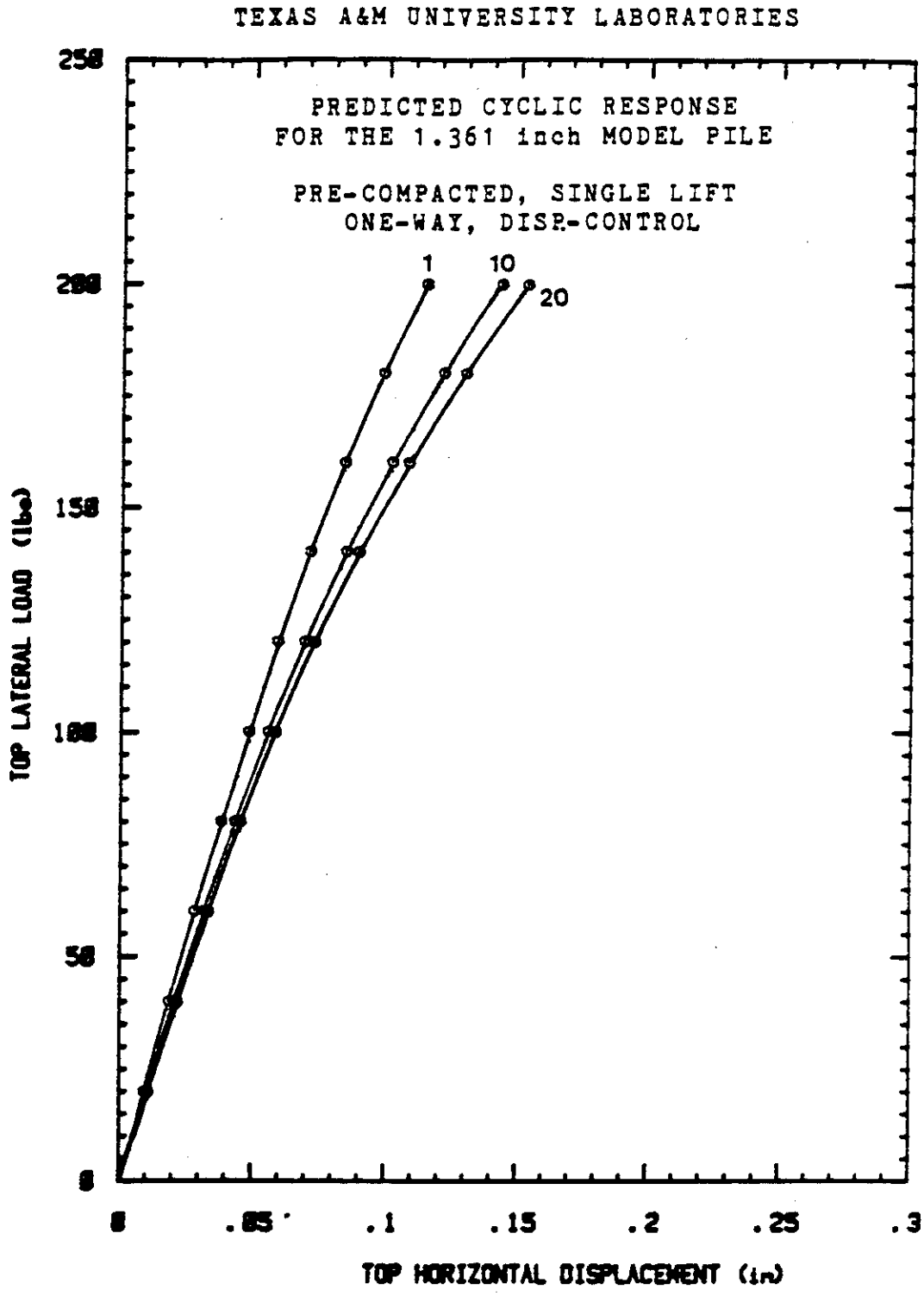

Figure 168. Predicted Cyclic Response of the Model Pile: Pre-compacted, Single Lift, Pile Placement Procedure; One-way, Displacement-control Cycles.

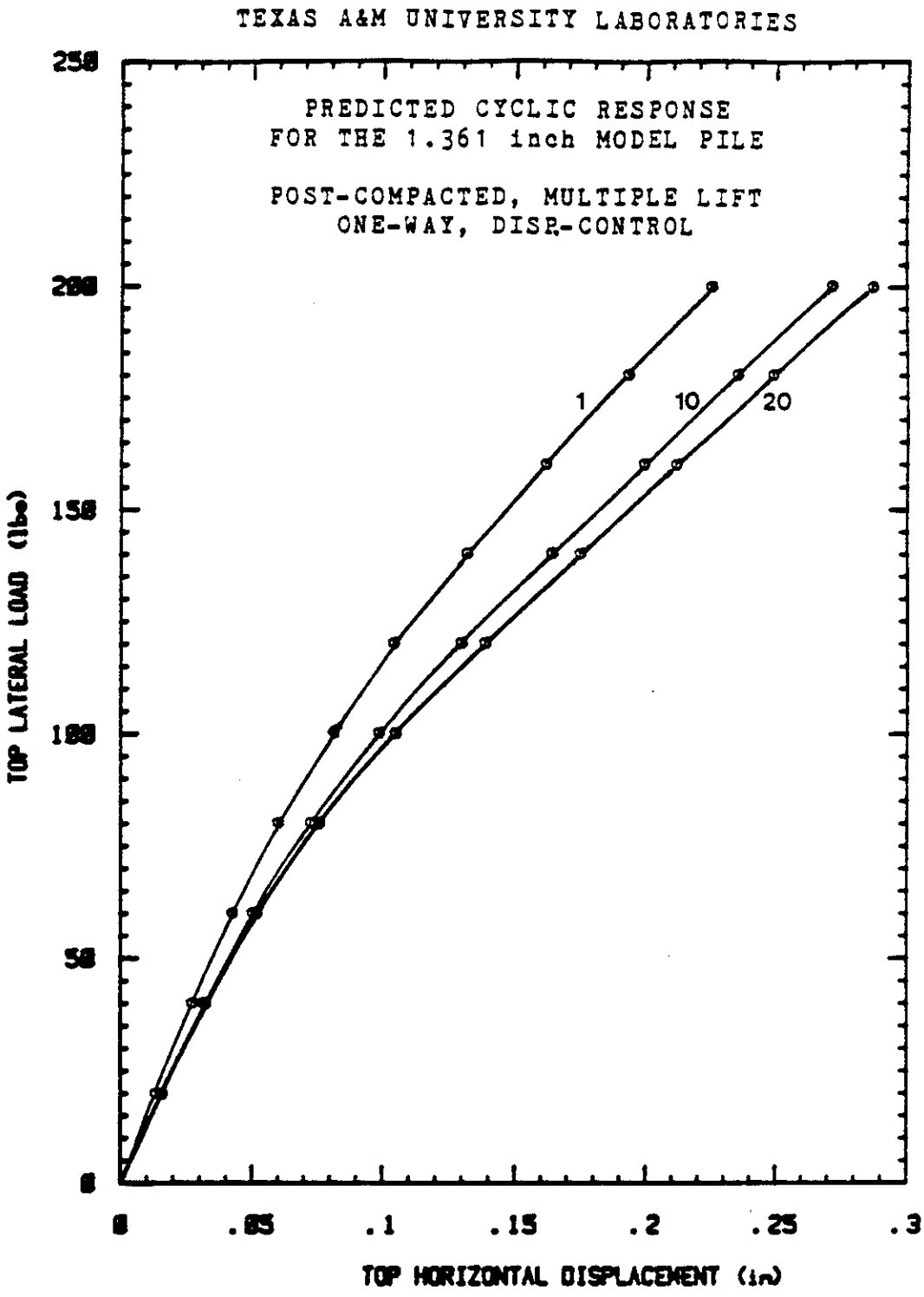

Figure 169. Predicted Cyclic Response of the Model Pile: Post-compacted, Multiple Lift, Pile Placement Procedure; One-way, Displacement-control Cycles.

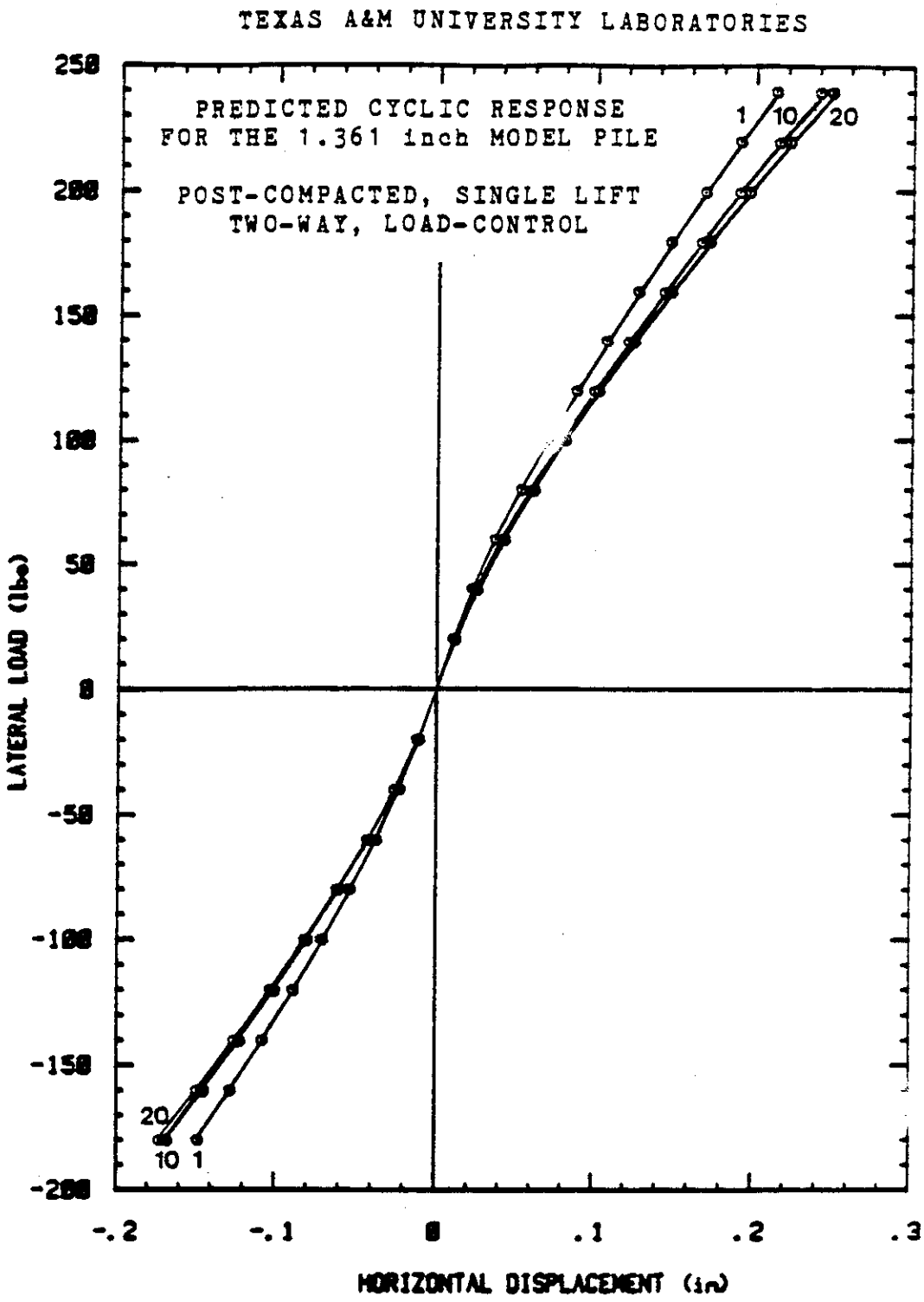

Figure 170. Predicted Cyclic Response of the Model Pile: Post-compacted, Single Lift, Pile Placement Procedure; Two-way, Load-control Cycles.

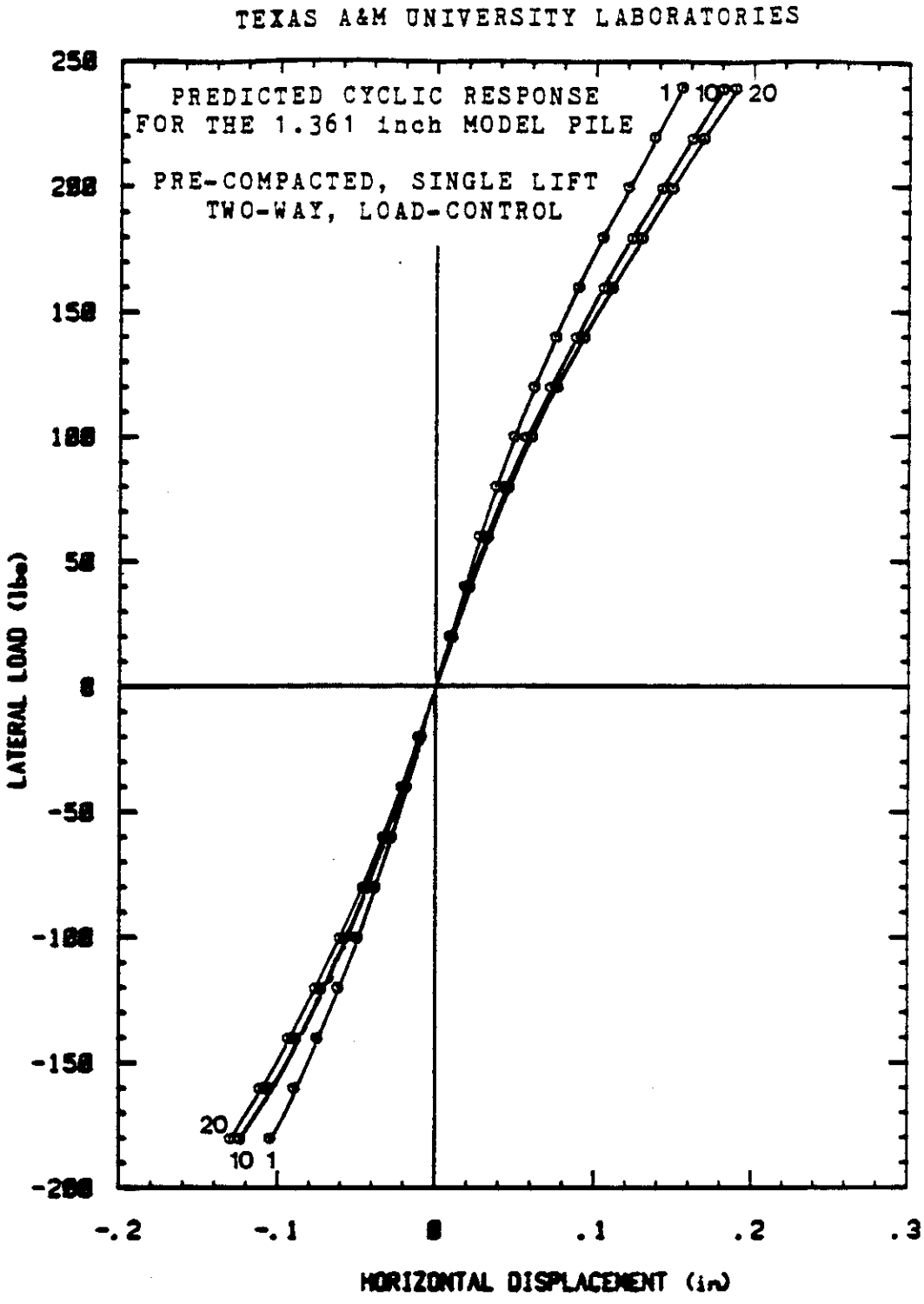

Figure 171. Predicted Cyclic Response of the Model Pile: Pre-compacted, Single Lift, Pile Placement Procedure; Two-way, Load-control Cycles.

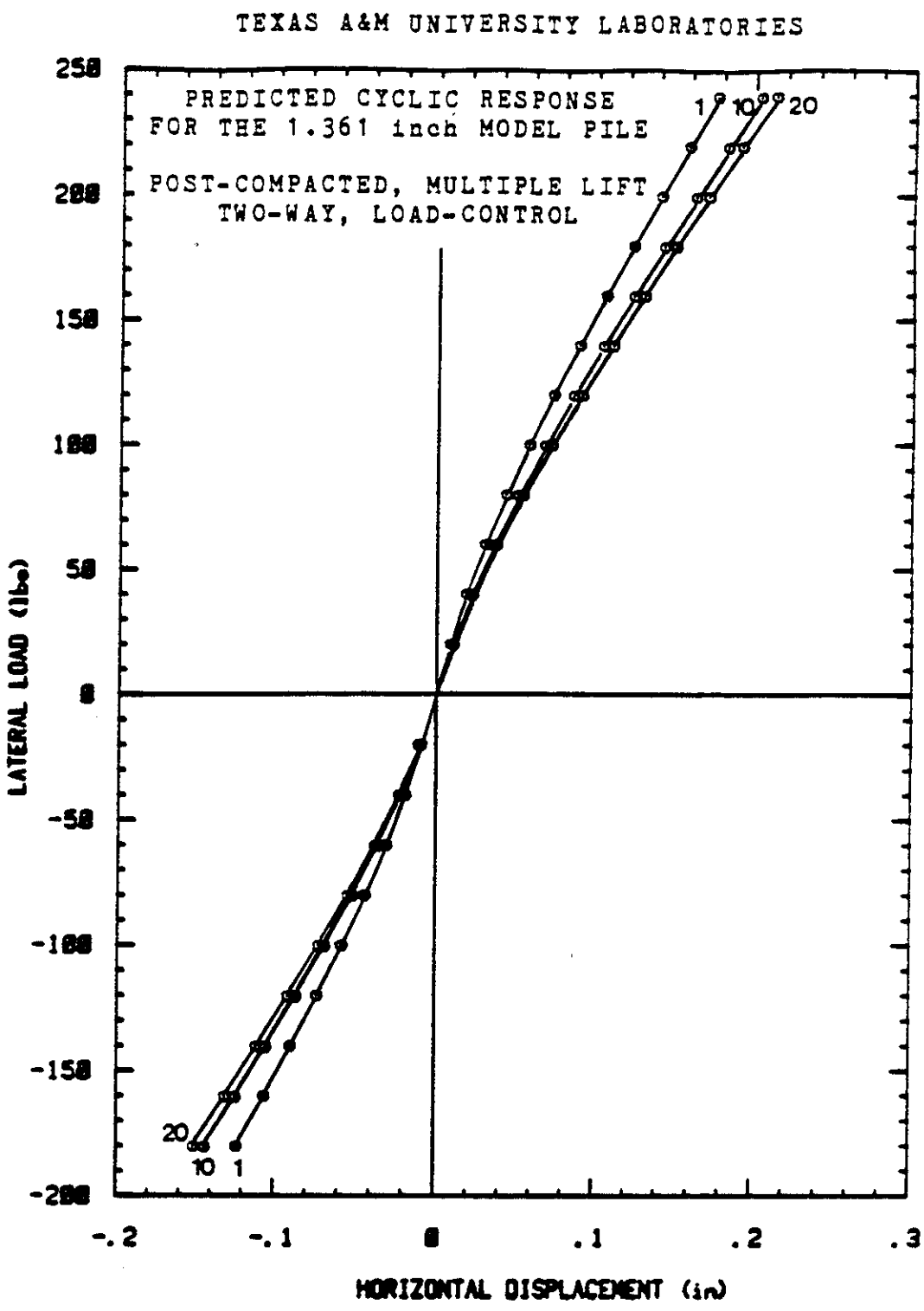

Figure 172. Predicted Cyclic Response of the Model Pile: Post-compacted, Multiple Lift, Pile Placement Procedure; Two-way, Load-control Cycles.

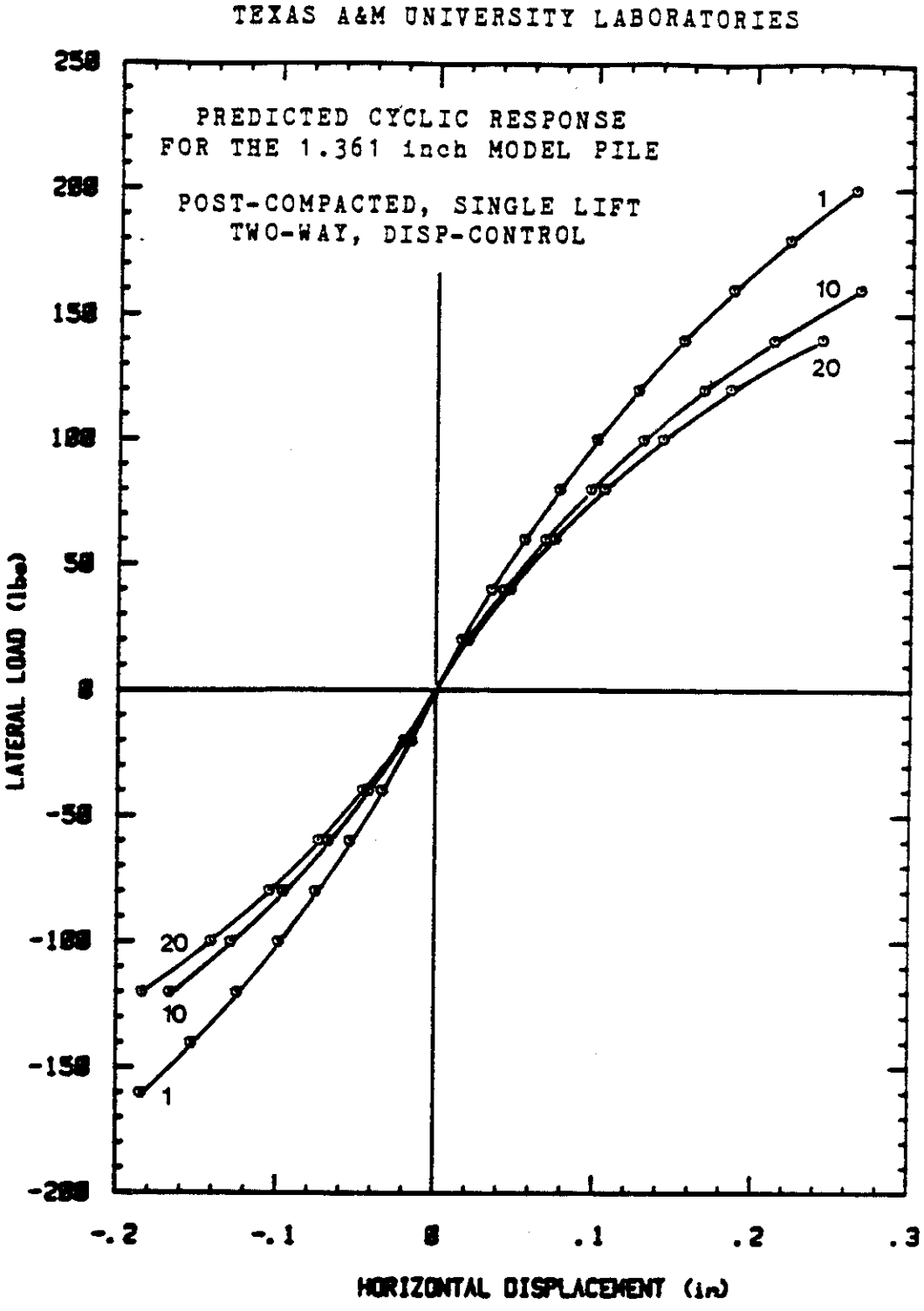

Figure 173. Predicted Cyclic Response of the Model Pile: Post-compacted, Single Lift, Pile Placement Procedure; Two-way, Displacement-control Cycles.

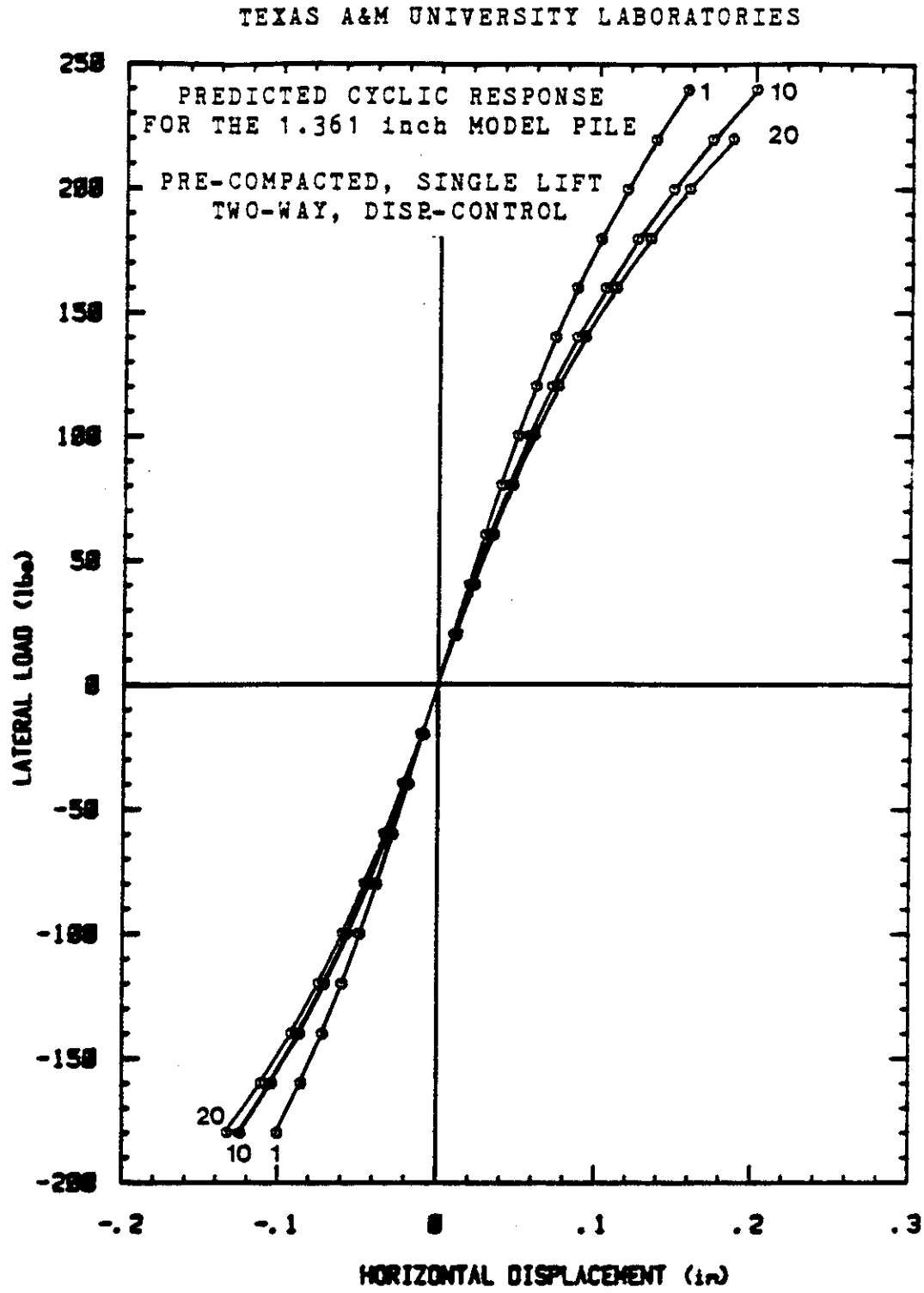

Figure 174. Predicted Cyclic Response of the Model Pile: Pre-compacted, Single Lift, Pile Placement Procedure; Two-way, Displacement Control Cycles.

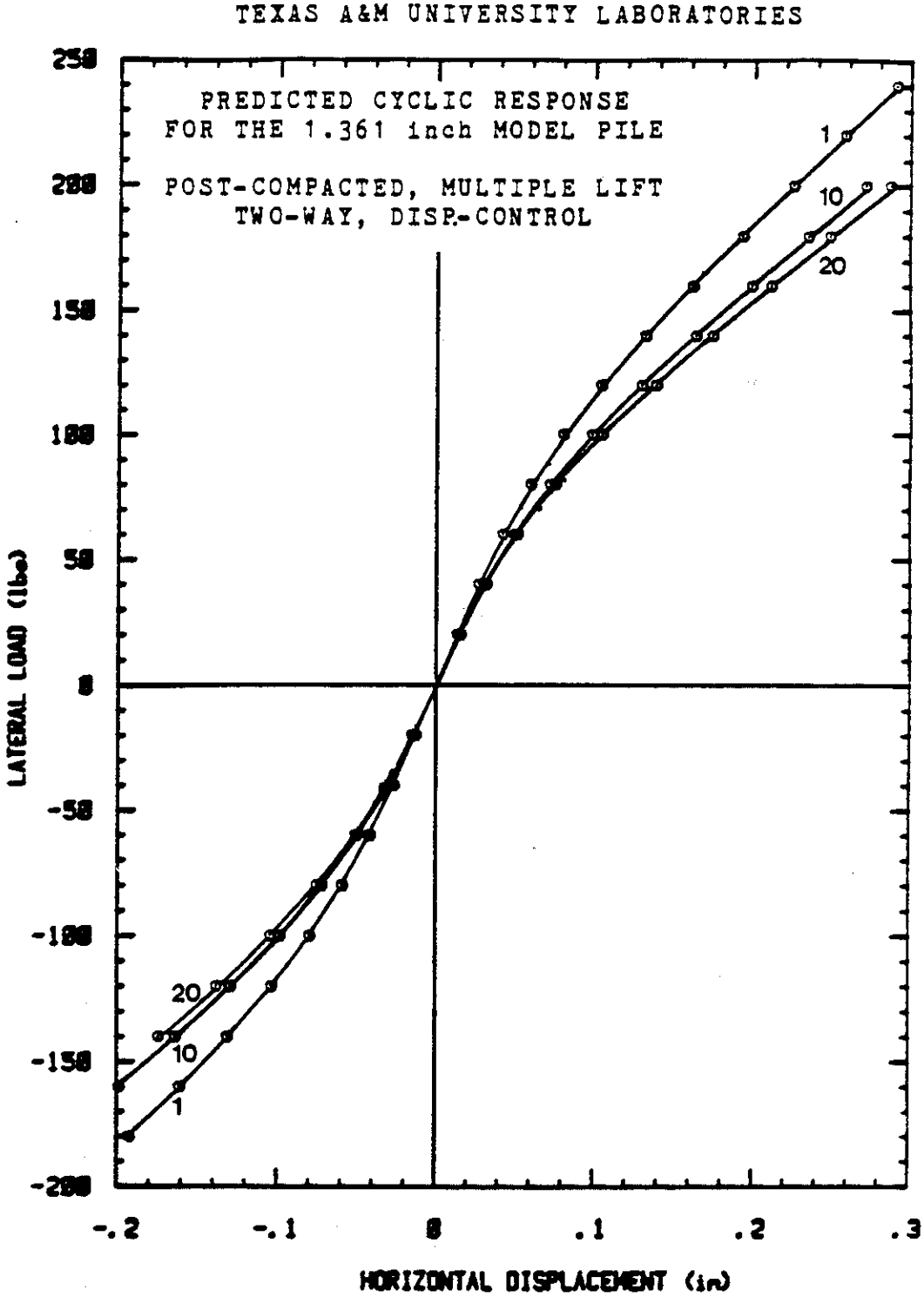

Figure 175. Predicted Cyclic Response of the Model Pile: Post-compacted, Multiple Lift, Pile Placement Procedure; Two-way, Displacement-control Cycles.

11.3 Comparison of Predicted and Measured Cyclic Responses

11.3.1 Single Pile at University of Houston

Table 11 compares the percent loss predicted at a given load and cycle number with the measured response. The percent loss is the percentage drop in the load necessary to deflect the pile to a given displacement value (Figure 46).

As can be seen in Table 11, the pressuremeter predicted a percent loss much greater than the measured percent loss. The reason for this large difference is that the pile load tests were two-way cyclic load tests while the pressuremeter is a one-way cyclic load test. As was shown in the data base study and in the model pile study, the degradation in one-way cyclic pile load tests in sand is much larger than the degradation in two-way cyclic pile load tests in sand. One can therefore speculate that had the pile load test been a one-way cyclic test the pressuremeter predictions would have been much closer. This point was confirmed by the model pile load test results.

11.3.2 Model Piles at Texas A&M University

Tables 12 through 15 compare the percent loss predicted with the measured values from the model pile tests. Overall, considering the possible variations in soil preparations, the predictions are very close to the measured behavior for the one-way cyclic pile load tests.

The two-way cyclic predictions failed to account for the stiffening of the soil-pile response encountered in the

Load (kips)	Percent Loss After 100 Cycles			
	Measured	PBPMT Predicted	PCPMT Predicted	DCPMT Predicted
10	5	52	50	36
15	6	52	48	35
20	6	50	48	35

Table 11. Predicted Loss of Stiffness Compared to the Measured Response of the 10.75 inch Single Pile: Two-way, Displacement-control Cycling.

ONE-WAY PRESSURE/LOAD-CONTROL CYCLING				
Soil/Placement Procedure	Load (lbs)	Cycle Number	% Loss Measured	% Loss Predicted
Post-compacted Single Lift	72.2	10	12	10
		20	16	13
	142.8	10	14	8
		20	18	11
	213.3	10	20	7
		20	23	9
			average 17	average 10
Pre-compacted Single Lift	72.2	10	8	15
		20	12	17
	142.8	10	10	10
		20	13	13
	209.3	10	12	8
		20	15	11
			average 12	average 12
Post-compacted Multiple Lift	72.2	10	13	7
		20	19	13
	142.8	10	12	8
		20	17	11
	170.0	10	15	7
		20	18	9
			average 16	average 9
			overall averages 15	10

Table 12. Predicted Loss of Stiffness Compared to the Measured Response of the Model Pile: One-way, Load-control Cycling.

ONE-WAY DISPLACEMENT/VOLUME-CONTROL CYCLING				
Soil/Placement Procedure	Load (lbs)	Cycle Number	% Loss Measured	% Loss Predicted
Post-compacted Single Lift	40	10	11	17
		20	15	21
	75	10	14	16
		20	18	23
	120	10	20	18
		20	22	24
			average 17	average 20
Pre-compacted Single Lift	40	10	21	10
		20	23	16
	80	10	14	11
		20	18	15
	110	10	14	12
		20	24	16
			average 19	average 13
Post-compacted Multiple Lift	40	10	7	3
		20	11	17
	80	10	11	13
		20	13	17
	120	10	13	14
		20	16	19
			average 12	average 16
			overall averages 16	16

Table 13. Predicted Loss of Stiffness Compared to the Measured Response of the Model Pile: One-way, Displacement-control Cycling.

TWO-WAY PRESSURE/LOAD-CONTROL CYCLING				
Soil/Placement Procedure	Load (lbs)	Cycle Number	% Loss Measured	% Loss Predicted
Post-compacted Single Lift	40	10	1	9
		20	-1	10
	90	10	11	8
		20	10	9
	130	10	9	8
		20	10	10
			average 7	average 9
Pre-compacted Single Lift	45	10	-5	9
		20	-10	13
	110	10	2	10
		20	-3	14
	150	10	2	11
		20	-3	15
			average -3	average 12
Post-compacted Multiple Lift	80	10	1	14
		20	0	18
	100	10	3	13
		20	-1	17
	150	10	5	11
		20	5	15
			average 2	average 15
			overall averages 2	12

Table 14. Predicted Loss of Stiffness Compared to the Measured Response of the Model Pile: Two-way, Load-control Cycling.

TWO-WAY DISPLACEMENT/VOLUME-CONTROL CYCLING				
Soil/Placement Procedure	Load (lbs)	Cycle Number	% Loss Measured	% Loss Predicted
Post-compacted Single Lift	60	10	-12	15
		20	-16	21
	120	10	0	18
		20	0	24
			average -7	average 20
Pre-compacted Single Lift	60	10	-49	6
		20	-57	11
	120	10	-15	11
		20	-18	16
			average -35	average 11
Post-compacted Multiple Lift	60	10	-9	12
		20	-10	13
	100	10	-3	13
		20	-7	15
	140	10	2	14
		20	1	17
			average -4	average 14
			overall averages -14	15

Table 15. Predicted Loss of Stiffness Compared to the Measured Response of the Model Pile: Two-way, Displacement-control Cycling.

model pile tests, and thus the predictions generally greatly overpredicted the cyclic degradation of the secant shear modulus for the two-way model pile load tests.

This points out again that the pressuremeter is a one-way cyclic tool and can predict the one-way horizontal cyclic response of piles. The degradation of soil stiffness in two-way cyclic lateral loading of piles in sand is very small compared to the degradation in one-way cyclic lateral loading and is often negligible. As a result, the pressuremeter largely overestimates the stiffness degradation of piles subjected to two-way cyclic lateral loading.

12. SUMMARY AND CONCLUSIONS

To aid in summarizing the results of this project, the cyclic degradation parameters $\underline{a}$, as defined in Figure 1, for the full-scale load test on the 10.75 inch diameter single pipe pile and for the load tests on the model pile have been plotted together with the original data base of piles subjected to cyclic lateral loading in sands (Figure 176). From this expanded data base, some general observations may be made:

(1) The $\underline{a}$ values ranged from +0.264 to -0.138 with a mean of +0.038 and a standard deviation of 0.056.

(2) The $\underline{a}$ values from the one-way load tests ranged from 0.264 to 0.005 with a mean of 0.076 and a standard deviation of 0.048.

(3) The $\underline{a}$ values from the two-way load tests ranged from 0.064 to -0.138 with a mean of 0.0015 and a standard deviation of 0.036.

(4) One-way cyclic tests in sand rarely experienced a cyclic degradation parameter less than 0.04, and in none of the observed one-way load tests did the cyclic degradation parameter drop below zero.

(5) Two-way cyclic tests in sand rarely experienced a cyclic degradation parameter greater than 0.04, and in many of the model pile tests in dry sand the cyclic degradation parameter dropped below

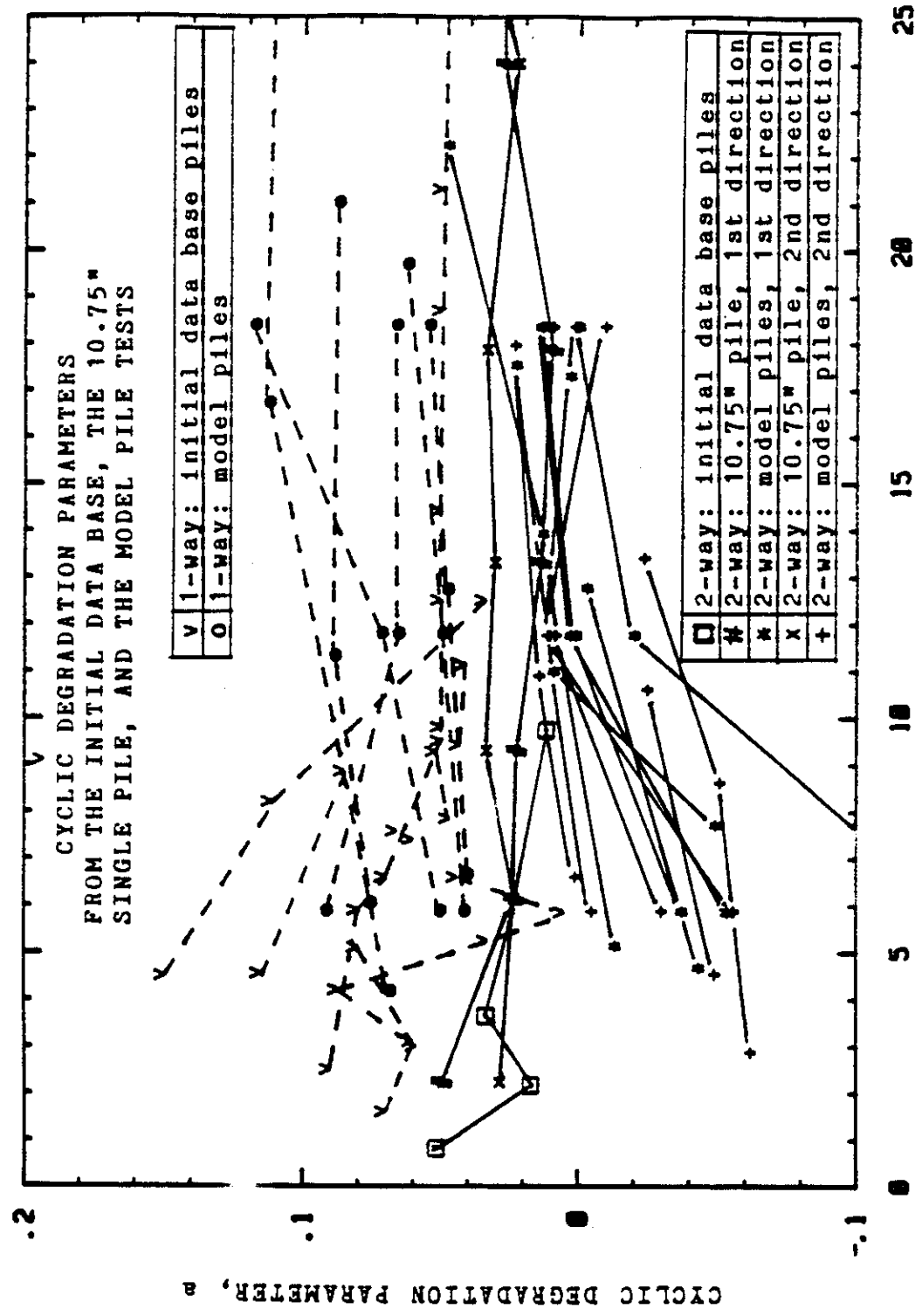

Figure 176. Cyclic Degradation Parameter a versus Relative Pile Head Displacement y/R for Initial Data Base Piles, the 10.75" Single Pile, and the Model Pile Tests.

zero, indicating a stiffening of the soil-pile response with cycling.

(6) The cyclic degradation parameter within any given test tended to become constant as y/R increased.

Therefore, one-way cyclic lateral loading of piles in sand may result in substantial degradation of the soil-pile stiffness. Two-way cyclic lateral loading of piles in sand, however, appears to be much less significant, possibly negligible, and in some cases may even result in substantial local densification of the soil and in a stiffer pile response with increasing cycles.

The pressuremeter method (Briaud, et al., 1985b) has been shown to be very accurate (Figures 134 and 135). This method was used to predict the monotonic response of the 10.75 inch diameter pipe pile tested by Morrison and Reese (1986) at the University of Houston. The predictions using the pre-boring pressuremeter results were good (Figures 140, 156, 157, and 158). The pre-boring pressuremeter usually predicts well the response of drilled shafts. The predictions using the pushed-in and driven pressuremeter results were much stiffer than the pile response (Figures 141 and 142). This shows that the way the pile was placed (sand compacted around the in-place pile) was close to simulating a drilled shaft condition.

Twelve model pile load tests were performed at Texas A&M University. The pile was 1.36 inches in diameter and

embedded 32 inches in a drum full of dry sand. Pressuremeter tests were performed in the same drum with a pressuremeter having the same diameter and placed in the sand in a manner identical to the model pile. The aforementioned pressuremeter method was used to predict the monotonic response of the model pile. Overall, the predictions were good (Figures 143 through 154).

A method was proposed to obtain the cyclic P-y curves from the monotonic P-y curves. First, the monotonic P-y is obtained from the monotonic pressuremeter test according to the method proposed by Briaud, et al. (1985b). For best accuracy, the PMT insertion technique should match the pile insertion technique (driven PMT for driven piles, pre-bored PMT for drilled shafts). Second, the pressuremeter-derived monotonic P-y curve is modified as follows to obtain the cyclic P-y curve for a number of cycles equal to N (Figure 136):

$$P(N) = P(1) \times N^{-a} \qquad (34)$$

$$y(N) = y(1) \qquad (35)$$

where the cyclic pile deflection, y(N), remains equal to the monotonic pile deflection, y(1), while the cyclic resistance, P(N), degrades with increasing cycles compared to the monotonic resistance, P(1). The parameter a is obtained directly from cyclic pressuremeter tests by applying equations (34) and (35) to the pressuremeter pressure and increase in radius of the borehole.

It is essential to match the type of cyclic loading in the pressuremeter test (pressure-control or volume-control) with the one of the pile load test (load-control or displacement-control). This was made clear by the fact that for both the pressuremeter and the piles there was a significant difference in degradation between the two types of cycling. Generally, the displacement/volume-control led to greater degradation than the load/pressure-control tests (Tables 3 and 6). Therefore, pressure-control cyclic pressuremeter tests should be chosen when modeling load-control cyclic pile load tests and volume-control cyclic pressuremeter tests should be chosen when modeling displacement-control cyclic pile load tests.

The proposed pressuremeter method to obtain the cyclic P-y curves and then predict the response of piles subjected to a given number of horizontal load cycles was used to predict the cyclic response of the 10.75 inch diameter pipe pile and the twelve model pile tests. The comparison between the predicted and measured cyclic responses of the <u>one-way</u> cyclic model pile load tests were very good (Tables 12 and 13). This seems especially important since one-way cycling proved to be the "worst case" condition in both the data base piles and in the model pile tests conducted at the Texas A&M University laboratories. The comparisons between the predicted and measured cyclic responses of the single 10.75 inch diameter pile and the two-way cyclic model pile

load tests indicated that the pressuremeter cannot predict accurately the response of piles in sand subjected to two-way horizontal cyclic loading. Indeed, the pressuremeter probe expands radially in all directions, and thus is limited to one-way cyclic loading.

A recommended modification of the proposed cyclic pressuremeter method is that if the pile is subjected to load-control cycles and, therefore, if the pressuremeter test is a pressure-control test, equations 34 and 35 may be replaced by:

$$P(N) = P(1) \tag{36}$$

$$y(N) = y(1) \times N^{+a} \tag{37}$$

where the cyclic resistance, P(N), remains equal to the monotonic resistance, P(1), and the cyclic deflection, y(N), increases with increasing cycles compared to the monotonic deflection, y(1). Equations (34) and (35) would apply only to displacement-control cyclic pile load tests and volume-control pressuremeter tests.

Further research should include a series of cyclic horizontal load tests on the model pile in wet sand and especially in saturated sand. By comparing the results with those in dry sand, inferences could then be made regarding the influence of the water table.

REFERENCES

BAGUELIN, F., FRANK, R., SAID, Y.H. 1977 Theoretical study of the lateral reaction mechanism of piles. Geotechnique, Volume 27, No. 3, Institution of Civil Engineers, London, England.

BAGUELIN, F., JEZEQUEL, J.F., and SHIELDS, D.H. 1978 The Pressuremeter and Foundation Engineering, Transtech Publications, Rockport, Mass.

BRIAUD, J.-L. 1986 Pressuremeter and foundation design. Proceedings of the ASCE Specialty Conference on Use of In Situ Tests in Geotechnical Engineering, Geotechnical Specialty Publication No. 6, Virginia Tech, Blacksburg, Virginia.

BRIAUD, J.-L., BRASUELL, T.E., and TUCKER, L.M. 1984 Case history of two laterally loaded piles at lock & dam no. 26 replacement site. Research Report No. RF 4690-3, Civil Engineering Department, Texas A&M University, College Station, Texas.

BRIAUD, J.-L., and FELIO, G.Y. 1985a Influence of cyclic loading of axially loaded piles in clay. Research Report No. 4980, Civil Engineering Department, Texas A&M University, College Station, Texas.

BRIAUD, J.-L., SMITH, T.D., and MEYER, B.J. 1983 Pressuremeter gives elementary model for laterally loaded piles. International Symposium on Soil and Rock Investigation by In Situ Testing, Volume II, International Association of Engineering Geology and International Society of Soil Mechanics and Foundation Engineering, Paris, France.

BRIAUD, J.-L., SMITH, T.D., and TUCKER, L.M. 1985b A pressuremeter method for laterally loaded piles. Proceedings of the Eleventh Annual Conference on Soil Mechanics and Foundation Engineering, Volume 3, Publications Committee of XI ICSMFE, Eds., A.A. Balkema, Rotterdam, Netherlands, 1353-1356.

BRIAUD, J.-L., TUCKER, L.M., and OLSEN, R.S. 1985c Pressuremeter, Cone Penetrometer, and Foundation Design, Volume I, Civil Engineering Department, Texas A&M University, College Station, Texas.

REFERENCES (continued)

COYLE, H.M. 1986 Unpublished Class Notes for CVEN 687, Civil Engineering Department, Texas A&M University, College Station, Texas.

FAYANS, B.L., BARVASHOV, V.A., LUCHKOVSKII, I.Ya., LEKUMOVICH, G.S., and METS, M.A. 1978 Effect of cyclic horizontal loads on the behavior of piles. Translated from Osnovaniya, Fundamety i Mekhanika Gruntov, No. 3, Scientific Research Institute of Bases and Underground Structures. Kharkov State Institute for General Construction and Sanitary Engineering Planning of Industrial Establishments, U.S.S.R.

IDRISS, I.M., DOBRY, R., and SINGH, R.D. 1978 Non-linear behavior for soft clays during cyclic loading. Journal of the Geotechnical Engineering Division, ASCE Volume 104, No. GT12, 1427-1447.

LITTLE, R.L., TUCKER, L.M., and BRIAUD, J.-L. 1986 PYRMT, Civil Engineering Department, Texas A&M University, College Station, Texas.

LONG, J.H., and REESE, L.C. 1984 Testing and analysis of two offshore drilled shafts subjected to lateral loads. Laterally Loaded Deep Foundations: Analysis and Performance, ASTM STP 835, J.A. Langer, E.T. Mosley, and C.D. Thompson, Eds., American Society for Testing and Materials, Philadelphia, Pennsylvania.

MAKARIM, C.A., and BRIAUD, J.-L. 1986 Pressuremeter method for single piles subjected to cyclic lateral loads in overconsolidated clay. Research Report No. 5112, Civil Engineering Department, Texas A&M University, College Station, Texas.

MATLOCK, H. 1970 Correlations for design of laterally loaded piles in soft clay. Proceedings, Second Annual Offshore Technology Conference, Volume 1, Paper No. OTC 1204, Houston, Texas.

MORRISON, C.S., and REESE, L.C. 1986 A lateral-load test of a full-scale pile group in sand. Geotechnical Engineering Report GR86-1, Geotechnical Engineering Center, Bureau of Engineering Research, University of Texas at Austin, Austin, Texas.

REFERENCES (continued)

OCHOA, M., and O'NEILL, M.W. 1986 Lateral pile-group interaction for free-headed pile groups in sand from full-scale experiments. Report No. UHCE 86-12, Department of Civil Engineering, University of Houston-University Park, Houston, Texas.

PEREZ, J.-Y., and HOLLOWAY, D.M. 1979 Results and interpretation of pile driving effects test program - existing locks and dam no. 26, Mississippi River, Alton, Illinois. Phase IV Report, Volume III, Prepared for the U.S. Army Corps of Engineers, St. Louis District, by Woodward-Clyde Consultants, San Francisco, California.

REESE, L.C., COX, W.R., and GRUBBS, B.R. 1967 Lateral-load tests of instrumented piles in sand at Mustang Island. A Report on Laterally Loaded Pile Program for Shell Development Company, Reese and Cox Consulting Engineers, Austin, Texas.

REESE, L.C., COX, W.R., and KOOP, F.D. 1967 Analysis of laterally loaded pile tests in sand at Mustang Island. A Report on Pile Research Program Conducted for Shell Development Company, Reese and Cox Consulting Engineers, Austin, Texas.

REESE, L.C., and DESAI, C.S. 1977 Laterally loaded piles. Numerical Methods in Geotechnical Engineering, C.S. Desai and J.T. Christian, Eds., McGraw Hill Book Co., New York, 297-325.

RIGGINS, M., 1981 The viscoelastic characterization of marine sediment in large scale simple shear. Ph.D. dissertation. Civil Engineering Department, Texas A&M University, College Station, Texas.

SMITH, T.D., 1983 Pressuremeter design method for single piles subjected to static lateral loads. Ph.D. dissertation, Civil Engineering Department, Texas A&M University, College Station, Texas.

TUCKER, L.M., and BRIAUD, J.-L. 1986 User's Guide for PRESRED, Civil Engineering Department, Texas A&M University, College Station, Texas.

APPENDIX A

Pile Load Tests from the Analysis of Existing Data

Pile	Loading	Soil
TYPE: steel pipe INSERTION: driven DIAMETER: 24" EMBEDDED LENGTH: 69 feet EI: 5.9×10^7 ksi	ELEVATION OF LATERAL LOAD: 12" above G.S. APPLIED MOMENT: 0 in-kips VERTICAL LOAD: 0 kips HEAD CONDITION: free LATERAL LOAD TEST: 2-way cyclic, major:minor load = 4 : 1 CYCLIC PERIOD: 16 - 20 sec. CYCLIC CONTROL: load	TYPE: fine silty sand INDEX PROPERTIES: W_n = 17 - 33 % D_r = 27 - 100 % STRENGTH: N = 30, 10' - 40' N = 5, 40' - 50' N > 40, > 50'

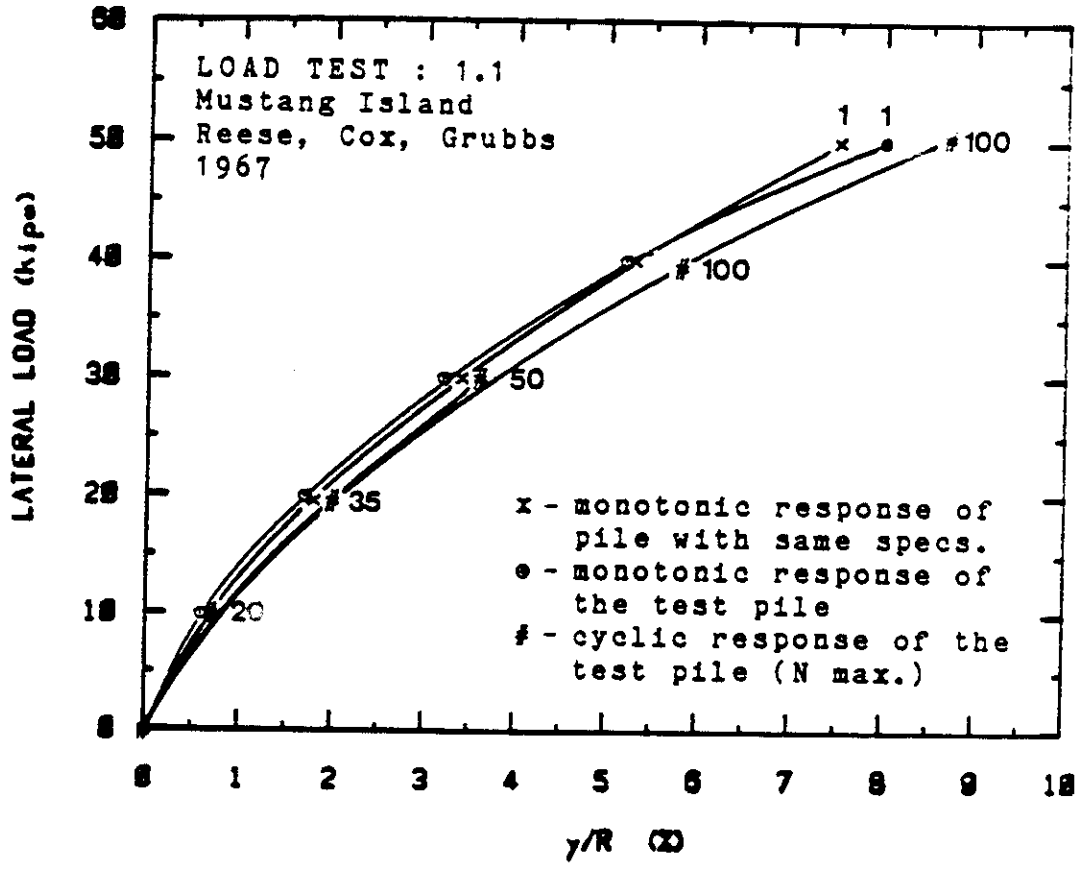

Pile	Loading	Soil
TYPE: steel pipe INSERTION: driven DIAMETER: 24" EMBEDDED LENGTH: 69 feet EI: 5.9×10^7 ksi	ELEVATION OF LATERAL LOAD: 12" above G.S. APPLIED MOMENT: 0 in-kips VERTICAL LOAD: 0 kips HEAD CONDITION: free LATERAL LOAD TEST: 2-way cyclic, major:minor load = 4 : 1 CYCLIC PERIOD: 16 - 20 sec. CYCLIC CONTROL: load	TYPE: fine silty sand INDEX PROPERTIES: W_n = 17 - 33 % D_r = 27 - 100 % STRENGTH: N = 30, 10' - 40' N = 5, 40' - 50' N > 40, > 50'

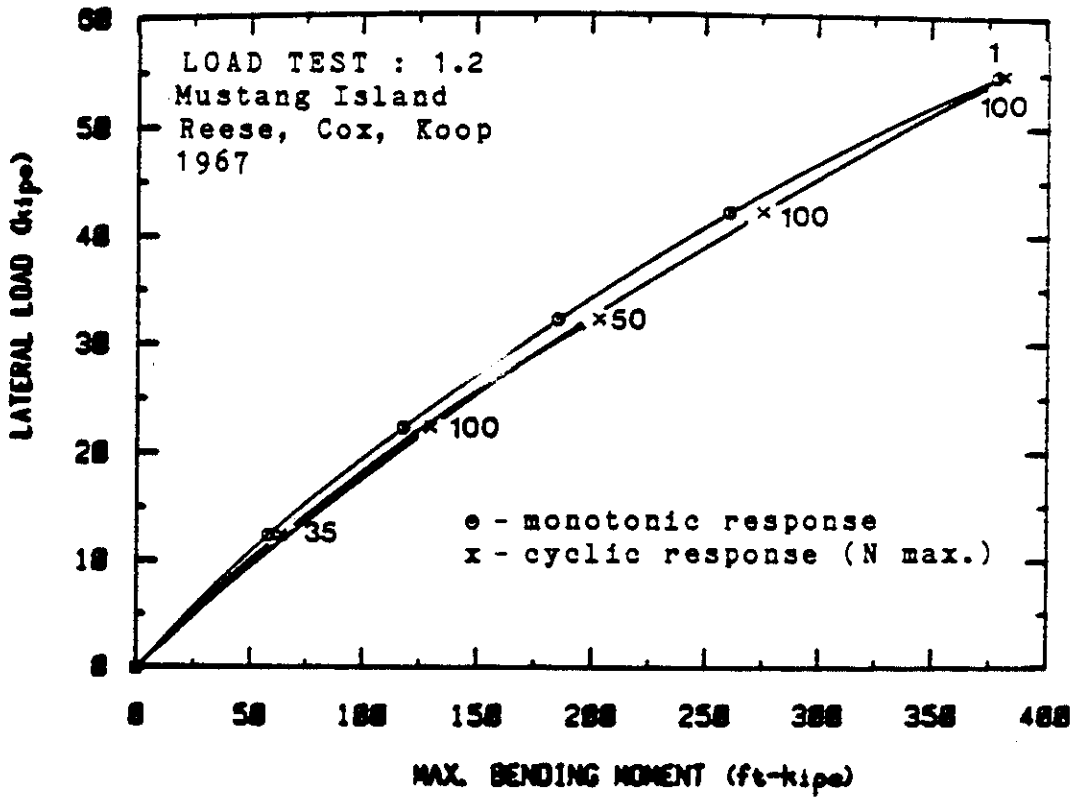

Pile	Loading	Soil
TYPE: square precast concrete INSERTION: driven SIDE DIMENSION: 11.8" EMBEDDED LENGTH: 16.4 feet EI: 4.85×10^6 ksi	ELEVATION OF LATERAL LOAD: not available APPLIED MOMENT: 0 in-kips VERTICAL LOAD: 0 kips HEAD CONDITION: free LATERAL LOAD TEST: 1-way cyclic, CYCLIC PERIOD: not available CYCLIC CONTROL: load	TYPE: sandy clay loam INDEX PROPERTIES: not available STRENGTH: not available

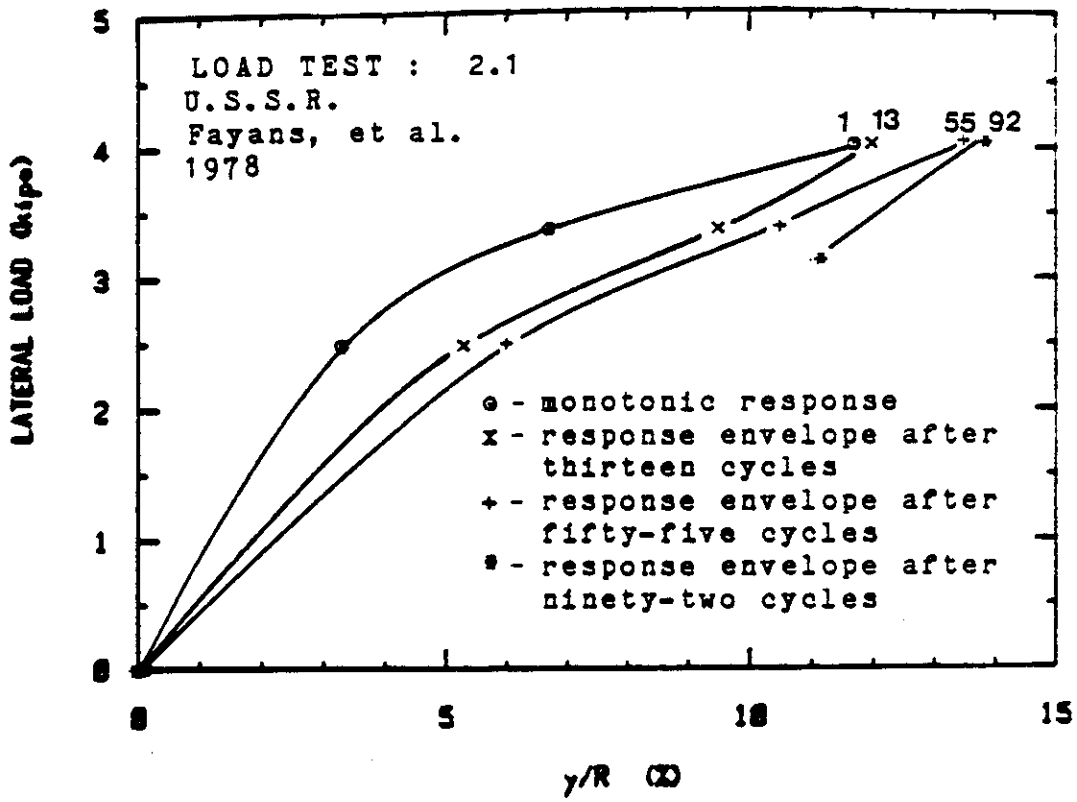

Pile	Loading	Soil
TYPE: square precast concrete INSERTION: driven SIDE DIMENSION: 11.8" EMBEDDED LENGTH: 16.4 feet EI: 4.85×10^6 ksi	ELEVATION OF LATERAL LOAD: not available APPLIED MOMENT: 0 in-kips VERTICAL LOAD: 0 kips HEAD CONDITION: free LATERAL LOAD TEST: 1-way cyclic, CYCLIC PERIOD: not available CYCLIC CONTROL: load	TYPE: sandy clay loam INDEX PROPERTIES: not available STRENGTH: not available

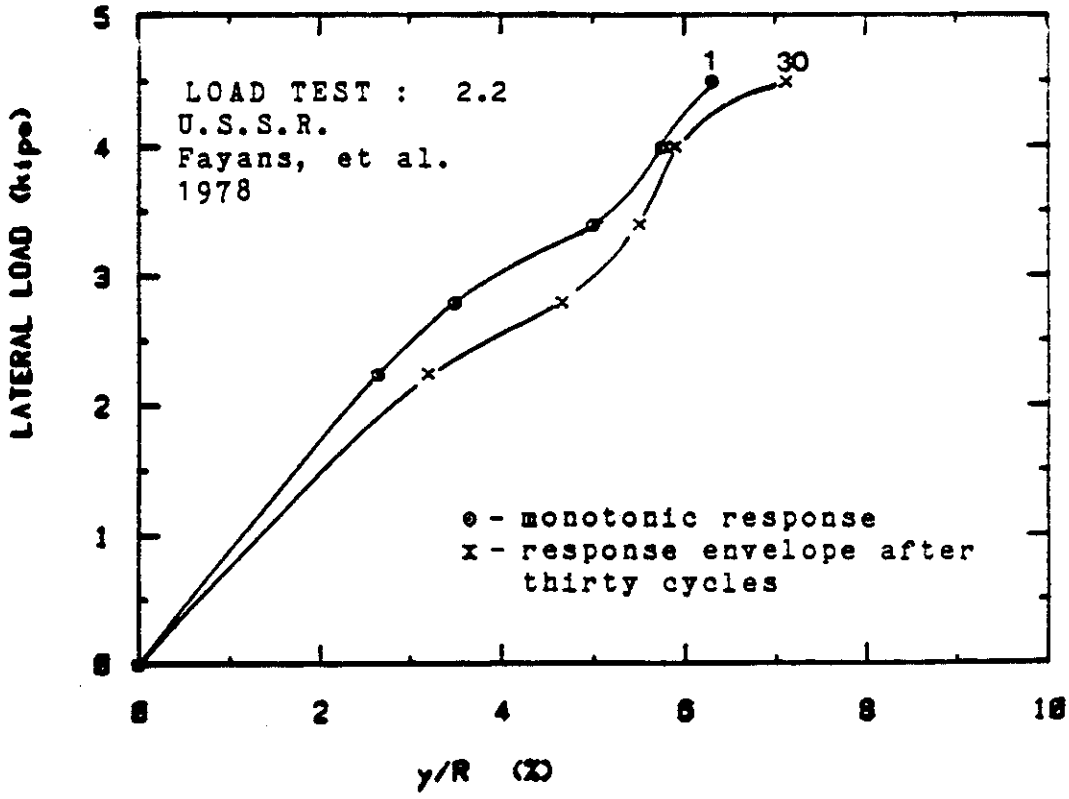

Pile	Loading	Soil
TYPE: timber INSERTION: driven DIAMETER: 14" EMBEDDED LENGTH: 35 feet EI: 3.77×10^6 ksi	ELEVATION OF LATERAL LOAD: 28" above G.S. APPLIED MOMENT: 0 in-kips VERTICAL LOAD: 60 kips HEAD CONDITION: free monolith (3x3x3 ft.) LATERAL LOAD TEST: 1-way cyclic after vertical loading to failure, and static lateral loading to 30 kips CYCLIC CONTROL: load	TYPE: sand and gravel, densed, ungrouted. INDEX PROPERTIES: D_r = 50 - 80 % STRENGTH: ϕ = 28 - 40° P_L = 20 - 90 ksf

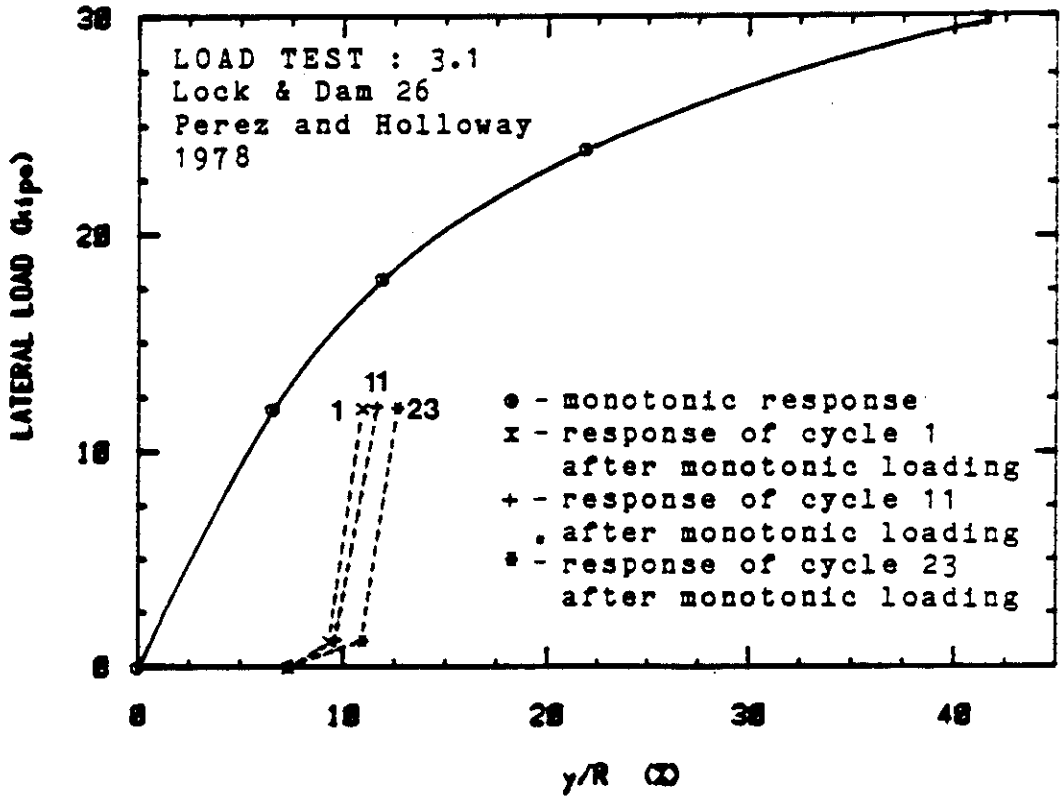

Pile	Loading	Soil
TYPE: timber INSERTION: driven DIAMETER: 14" EMBEDDED LENGTH: 35 feet EI: 3.77×10^6 ksi	ELEVATION OF LATERAL LOAD: 37.5" above G.S. APPLIED MOMENT: 0 in-kips VERTICAL LOAD: 60 kips HEAD CONDITION: free monolith (3x3x3 ft.) LATERAL LOAD TEST: 1-way cyclic after vertical loading to failure, and static lateral loading to 40 kips CYCLIC CONTROL: load	TYPE: sand and gravel, densed, grouted. INDEX PROPERTIES: D_r = 50 - 80 % STRENGTH: ϕ = 28 - 40° P_L = 20 - 90 ksf

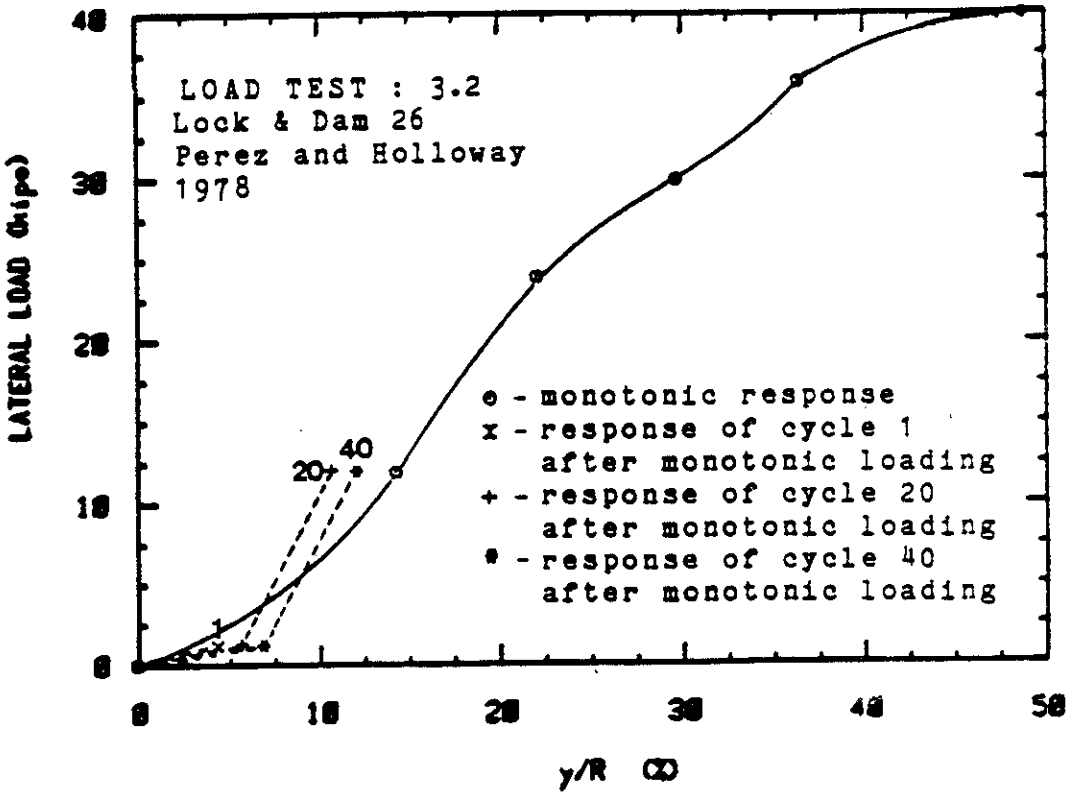

Pile	Loading	Soil
TYPE: H-pile (HP 14 x 73) INSERTION: driven SIDE DIMENSION 13.61" EMBEDDED LENGTH: 55 feet EI: 2.11×10^7 ksi	ELEVATION OF LATERAL LOAD: 0.0" above G.S. APPLIED MOMENT: 0 in-kips VERTICAL LOAD: 0 kips HEAD CONDITION: free LATERAL LOAD TEST: 1-way cyclic after monotonic lateral loading to 66 kips CYCLIC CONTROL: load	TYPE: sand and gravel, densed, ungrouted. INDEX PROPERTIES: D_r = 50 - 80 % STRENGTH: ϕ = 28 - 40° c = 0

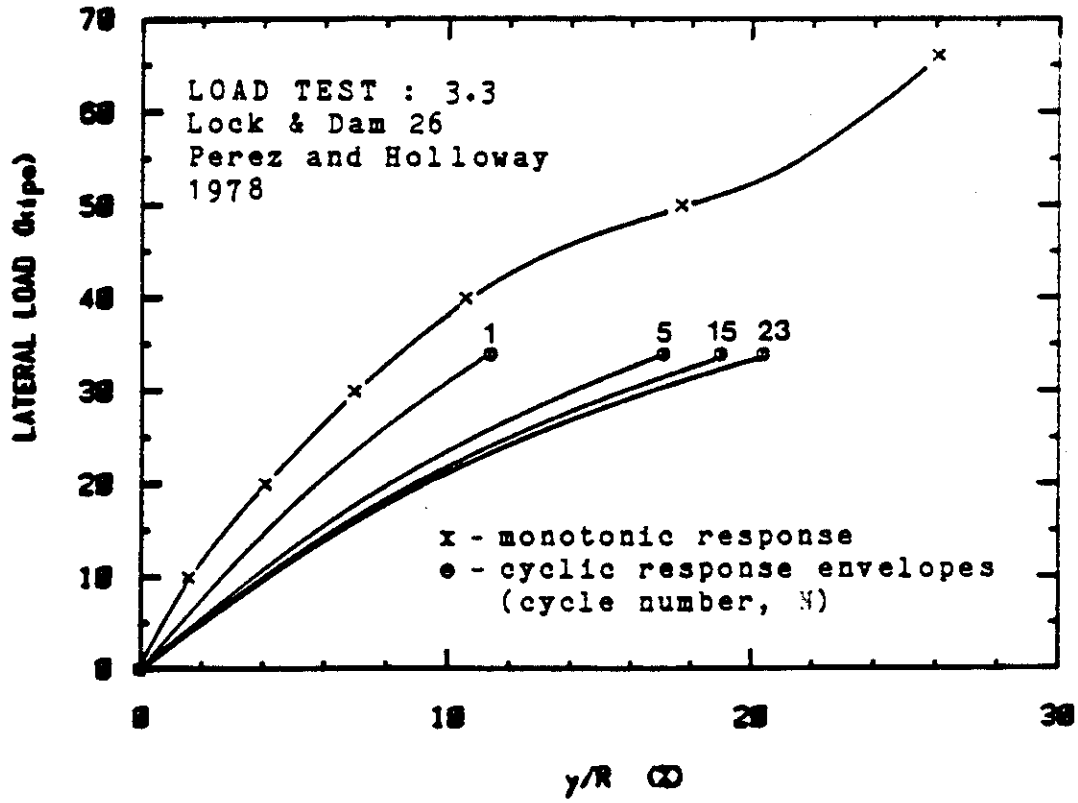

Pile	Loading	Soil
TYPE: steel pipe (PP 14 x 0.375) INSERTION: driven SIDE DIMENSION 14" EMBEDDED LENGTH: 55 feet EI: 1.08×10^7 ksi	ELEVATION OF LATERAL LOAD: 0.0" above G.S. APPLIED MOMENT: 0 in-kips VERTICAL LOAD: 0 kips HEAD CONDITION: free LATERAL LOAD TEST: 1-way cyclic after monotonic lateral loading to 66 kips CYCLIC CONTROL: load	TYPE: sand and gravel, densed, ungrouted. INDEX PROPERTIES: D^r = 50 - 80 % STRENGTH: ϕ = 28 - 40° c = 0

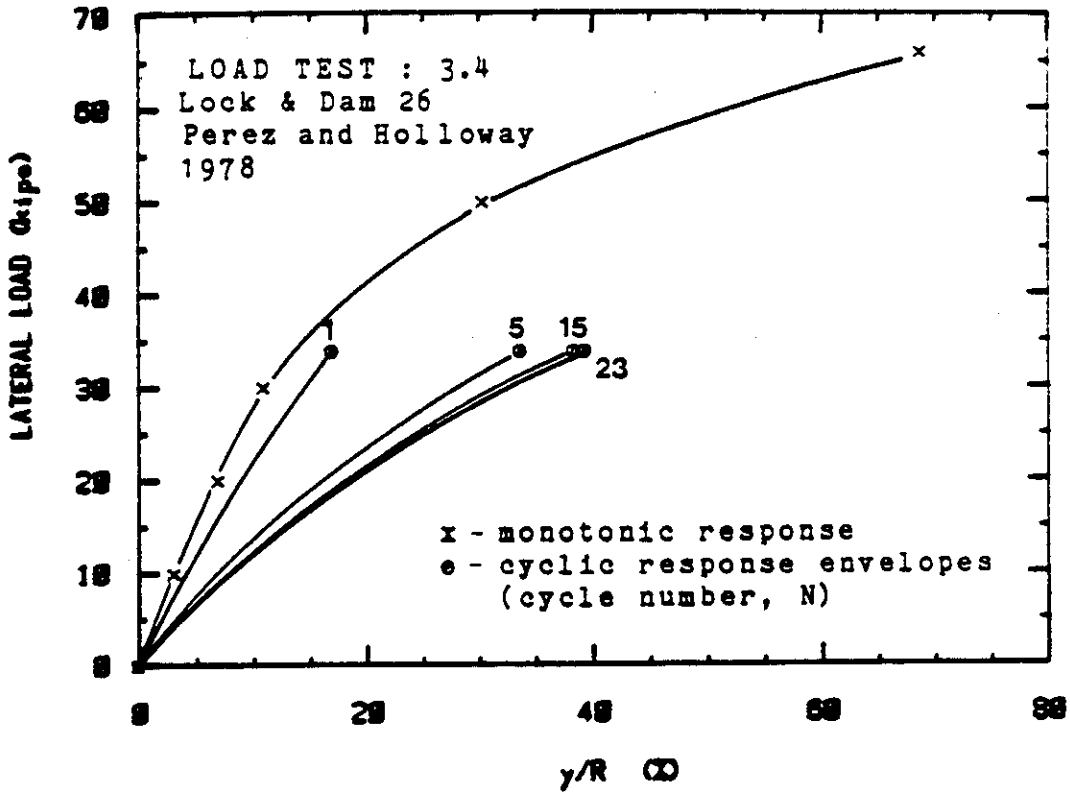

Pile	Loading	Soil
TYPE: H-pile (HP 14 x 73) INSERTION: driven SIDE DIMENSION 13.61" EMBEDDED LENGTH: 55 feet EI: 2.11×10^7 ksi	ELEVATION OF LATERAL LOAD: 0.0" above G.S. APPLIED MOMENT: 0 in-kips VERTICAL LOAD: 0 kips HEAD CONDITION: free LATERAL LOAD TEST: 1-way cyclic after monotonic lateral loading to 70 kips CYCLIC CONTROL: load	TYPE: sand and gravel, densed, post-grouted. INDEX PROPERTIES: STRENGTH: $\phi = 35^\circ$ $c = 0.7$ ksf

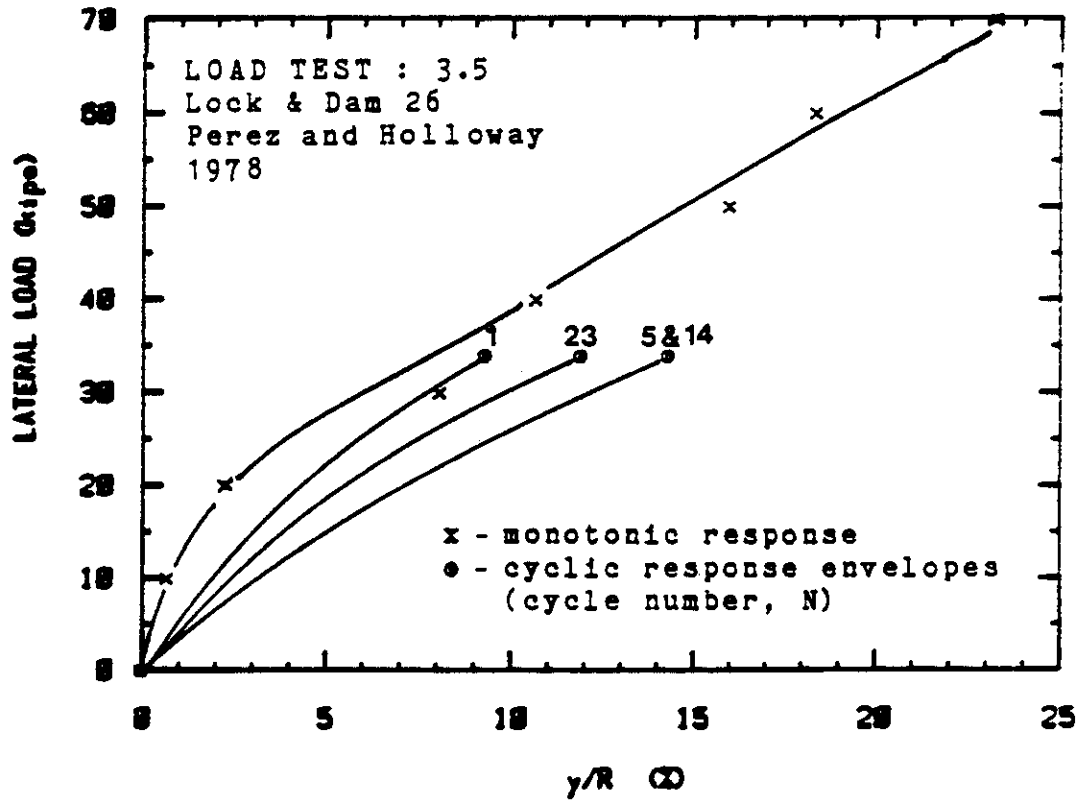

Pile	Loading	Soil
TYPE: steel pipe (PP 14 x 0.375) INSERTION: driven SIDE DIMENSION 14" EMBEDDED LENGTH: 55 feet EI: 1.08×10^7 ksi	ELEVATION OF LATERAL LOAD: 0.0" above G.S. APPLIED MOMENT: 0 in-kips VERTICAL LOAD: 0 kips HEAD CONDITION: free LATERAL LOAD TEST: 1-way cyclic after monotonic lateral loading to 70 kips CYCLIC CONTROL: load	TYPE: sand and gravel, densed, post-grouted. INDEX PROPERTIES: STRENGTH: $\phi = 35^\circ$ $c = 0.7$ ksf

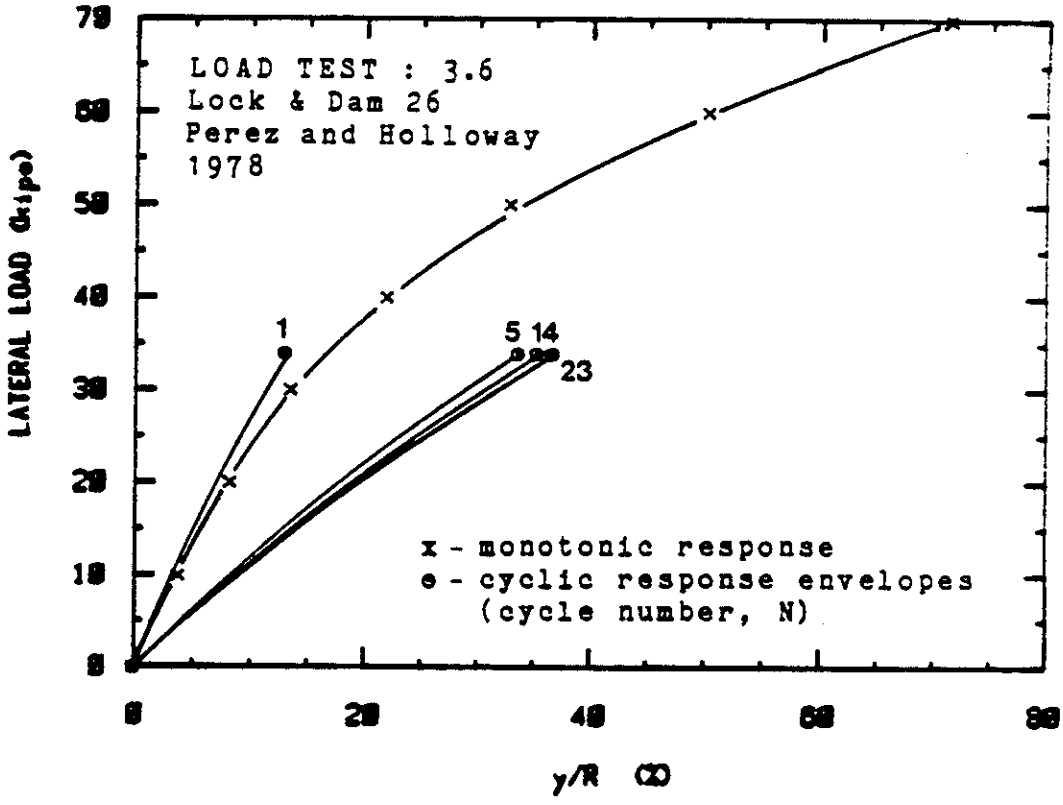

Pile	Loading	Soil
TYPE: H-pile (HP 14 x 73) INSERTION: driven SIDE DIMENSION 13.61" EMBEDDED LENGTH: 55 feet EI: 2.11×10^7 ksi	ELEVATION OF LATERAL LOAD: 0.0" above G.S. APPLIED MOMENT: 0 in-kips VERTICAL LOAD: 0 kips HEAD CONDITION: free LATERAL LOAD TEST: 1-way cyclic CYCLIC CONTROL: load	TYPE: sand and gravel, densed, post-grouted. INDEX PROPERTIES: STRENGTH: $\phi = 35^\circ$ $c = 0.7$ ksf

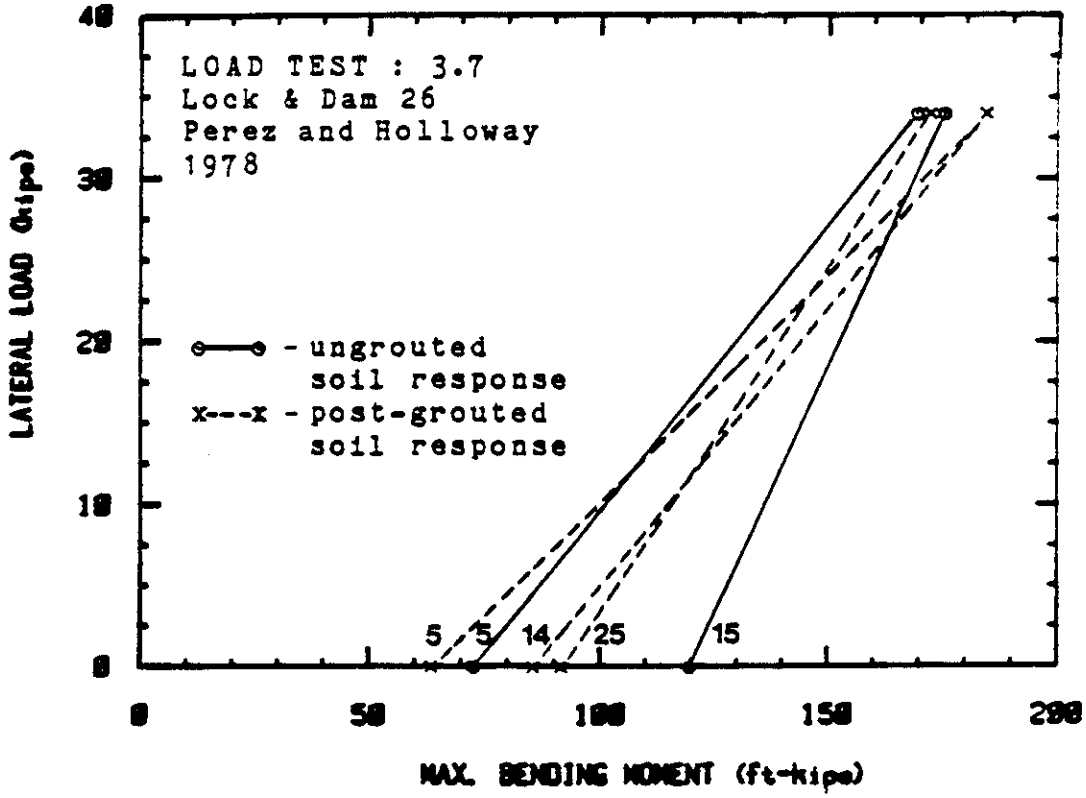

Pile	Loading	Soil
TYPE: steel pipe (PP 14 x 0.375) INSERTION: driven SIDE DIMENSION 14" EMBEDDED LENGTH: 55 feet EI: 1.08×10^7 ksi	ELEVATION OF LATERAL LOAD: 0.0" above G.S. APPLIED MOMENT: 0 in-kips VERTICAL LOAD: 0 kips HEAD CONDITION: free LATERAL LOAD TEST: 1-way cyclic CYCLIC CONTROL: load	TYPE: sand and gravel, densed, post-grouted. INDEX PROPERTIES: STRENGTH: $\phi = 35^{\circ}$ $c = 0.7$ ksf

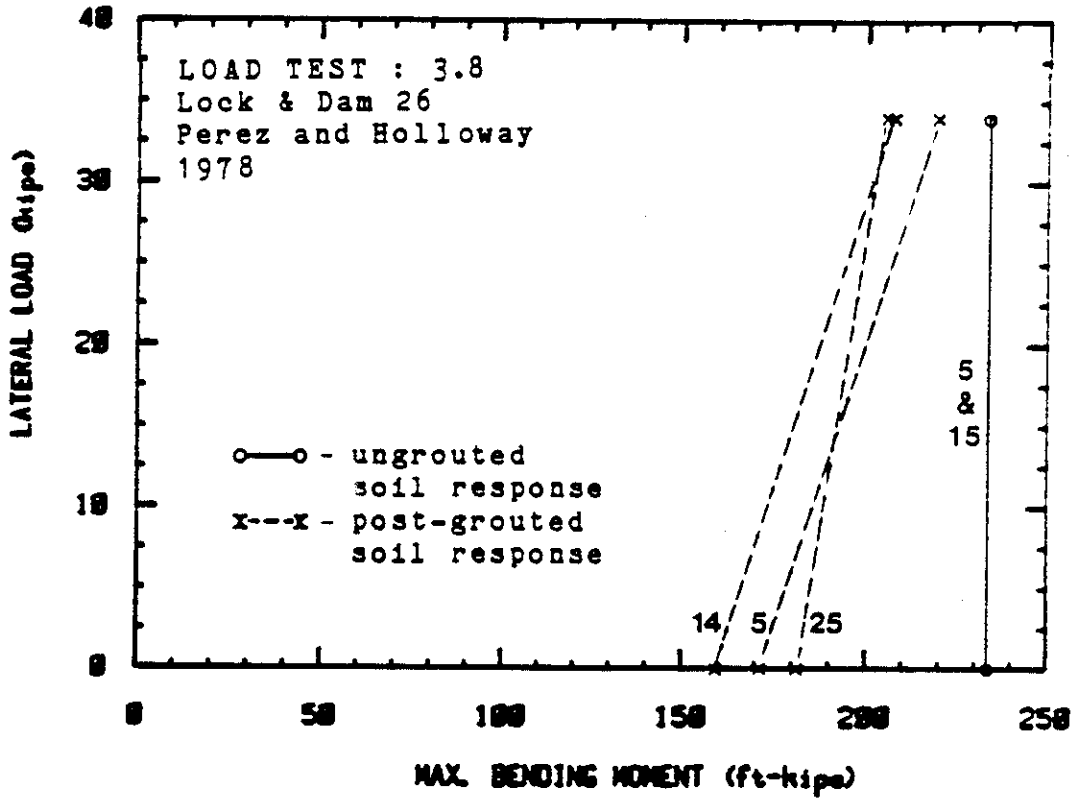

Pile	Loading	Soil
TYPE: H-pile (HP 14 x 73) INSERTION: driven SIDE DIMENSION 13.61" EMBEDDED LENGTH: 67 feet EI: 2.11×10^7 ksi	ELEVATION OF LATERAL LOAD: 6.5" above G.S. APPLIED MOMENT: 0 in-kips VERTICAL LOAD: 0 kips HEAD CONDITION: free LATERAL LOAD TEST: 1-way cyclic CYCLIC CONTROL: load	TYPE: sand and gravel, densed, ungrouted. INDEX PROPERTIES: D_r = 50 - 80 % STRENGTH: N = 15' 0' - 25' N > 40, > 25'

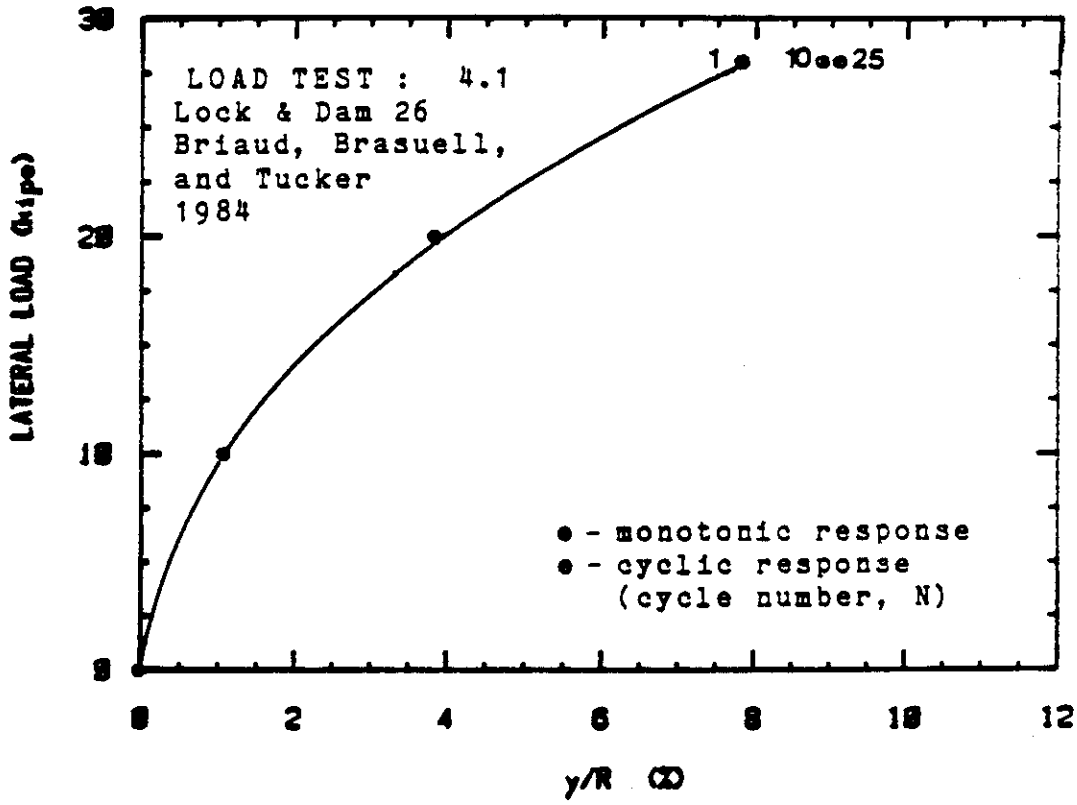

Pile	Loading	Soil
TYPE: H-pile (HP 14 x 73) INSERTION: driven SIDE DIMENSION 13.61" EMBEDDED LENGTH: 67 feet EI: 2.11×10^7 ksi	ELEVATION OF LATERAL LOAD: 6.5" above G.S. APPLIED MOMENT: 0 in-kips VERTICAL LOAD: 0 kips HEAD CONDITION: free LATERAL LOAD TEST: 1-way cyclic CYCLIC CONTROL: load	TYPE: sand and gravel, densed, ungrouted. INDEX PROPERTIES: D_r = 50 - 80 % STRENGTH: N = 15' 0' - 25' N > 40, > 25'

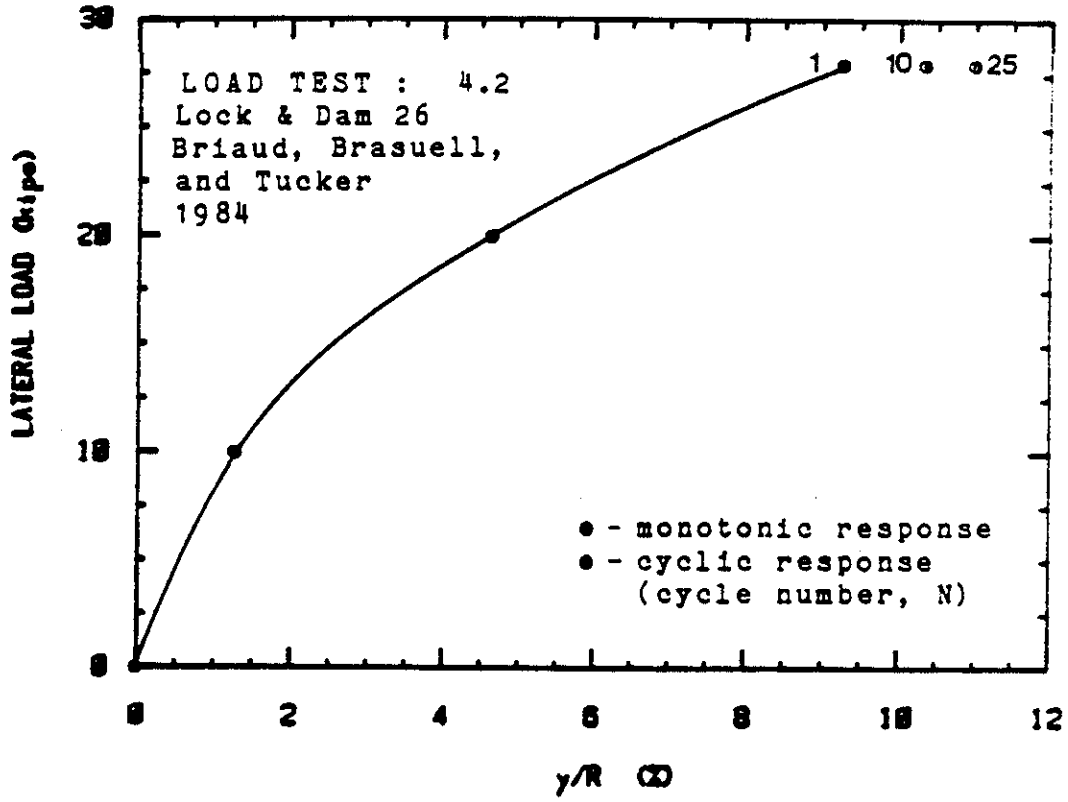

Pile	Loading	Soil
TYPE: reinforced concrete INSERTION: casing vibrated into soil 37', augured to 51', cast-in-place DIAMETER 48" EMBEDDED LENGTH: 51 feet EI: 1.00×10^9 ksi	ELEVATION OF LATERAL LOAD: 18 feet above mudline APPLIED MOMENT: 0 in-kips VERTICAL LOAD: 0 kips HEAD CONDITION: free LATERAL LOAD TEST: 1-way cyclic CYCLIC PERIOD: 2 minutes CYCLIC CONTROL: load	TYPE: dense fine sand, overlying silty, clayey sand underlain by stiff clay INDEX PROPERTIES: γ_T = 108 pcf STRENGTH: c = 0.0 ϕ = 37-38°, 0-28' = 34-38°, 28-43'

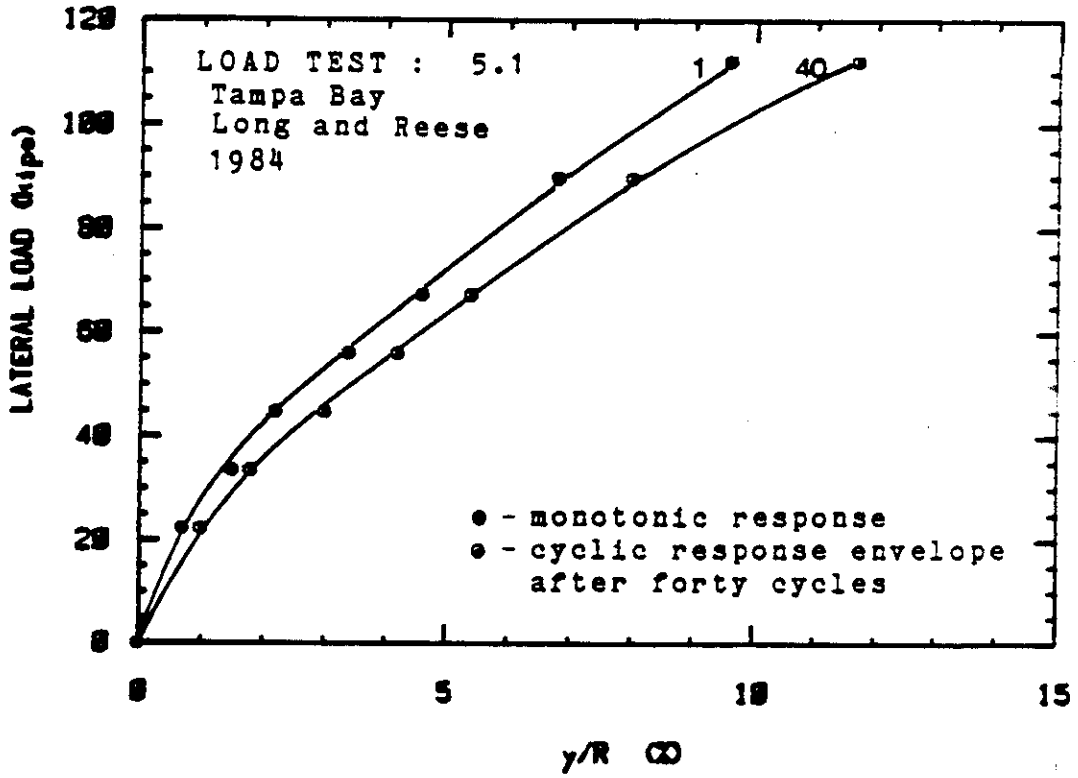

Pile	Loading	Soil
TYPE: reinforced concrete INSERTION: casing vibrated into soil 37', augured to 51', cast-in-place DIAMETER 48" EMBEDDED LENGTH: 51 feet EI: 1.00×10^9 ksi	ELEVATION OF LATERAL LOAD: 18 feet above mudline APPLIED MOMENT: 0 in-kips VERTICAL LOAD: 0 kips HEAD CONDITION: free LATERAL LOAD TEST: 1-way cyclic CYCLIC PERIOD: 2 minutes CYCLIC CONTROL: load	TYPE: dense fine sand, overlying silty, clayey sand underlain by stiff clay INDEX PROPERTIES: γ_T = 108 pcf STRENGTH: c = 0.0 ϕ = 37-38°, 0-28' = 34-38°, 28-43'

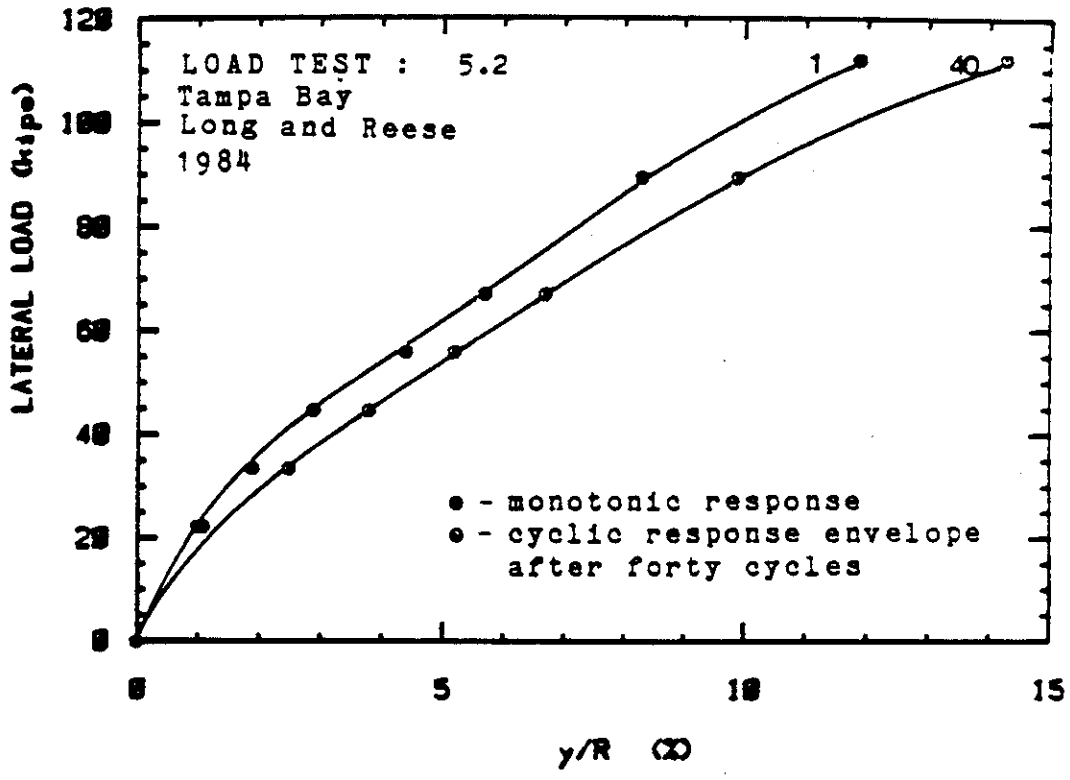

APPENDIX B

Cyclic Degradation of the Pressuremeter

Cyclic Shear Modulus

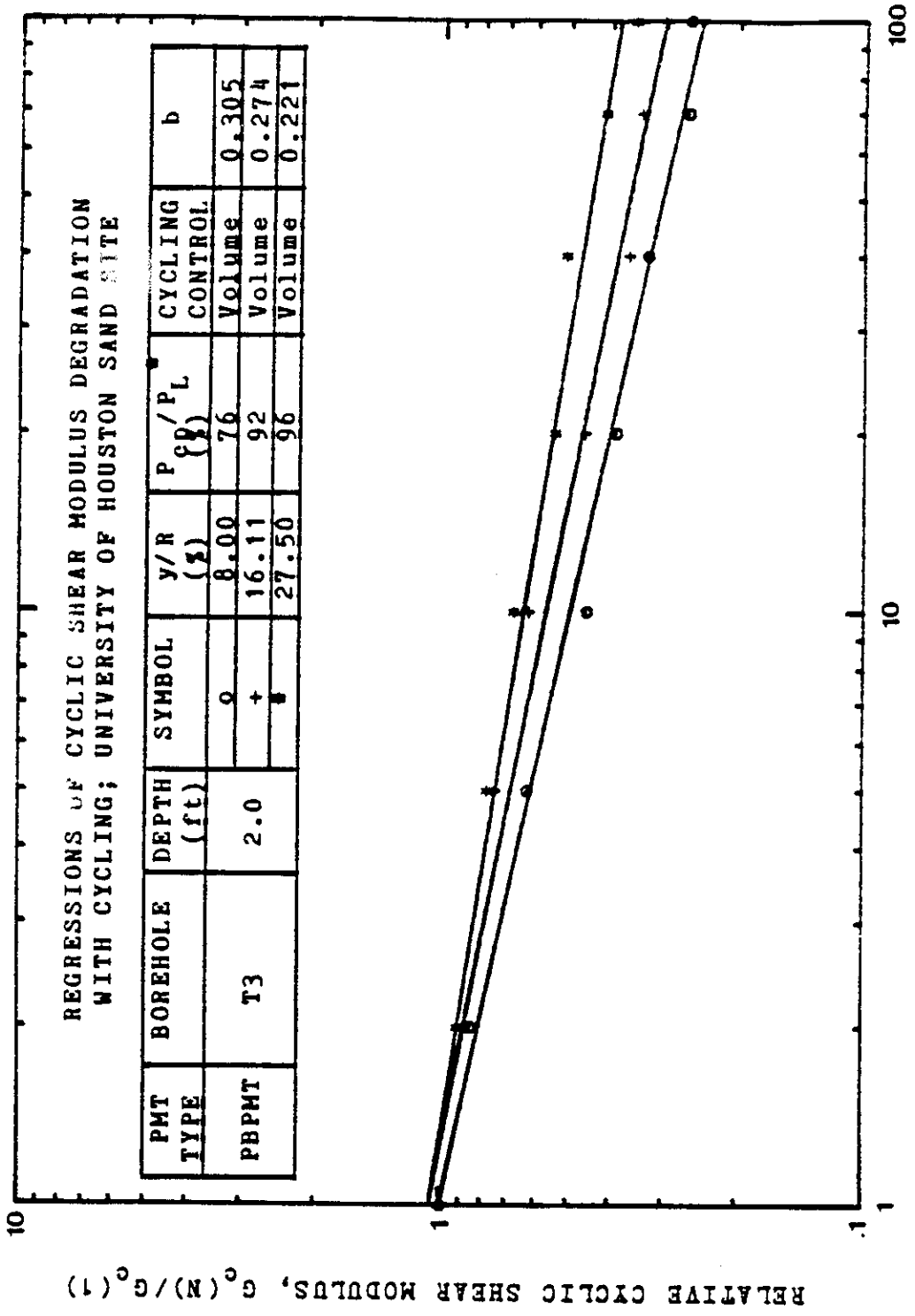
REGRESSIONS OF CYCLIC SHEAR MODULUS DEGRADATION
WITH CYCLING; UNIVERSITY OF HOUSTON SAND SITE
PMT TYPE
BOREHOLE
DEPTH (ft)
SYMBOL
y/R (%)
P_o/P_L (%)
CYCLING CONTROL
b
PBPMT
T3
2.0
o
8.00
76
Volume
0.305
+
16.11
92
Volume
0.274
*
27.50
96
Volume
0.221
10
1
.1
1
10
100
CYCLE NUMBER, N
RELATIVE CYCLIC SHEAR MODULUS, $G_c(N)/G_c(1)$

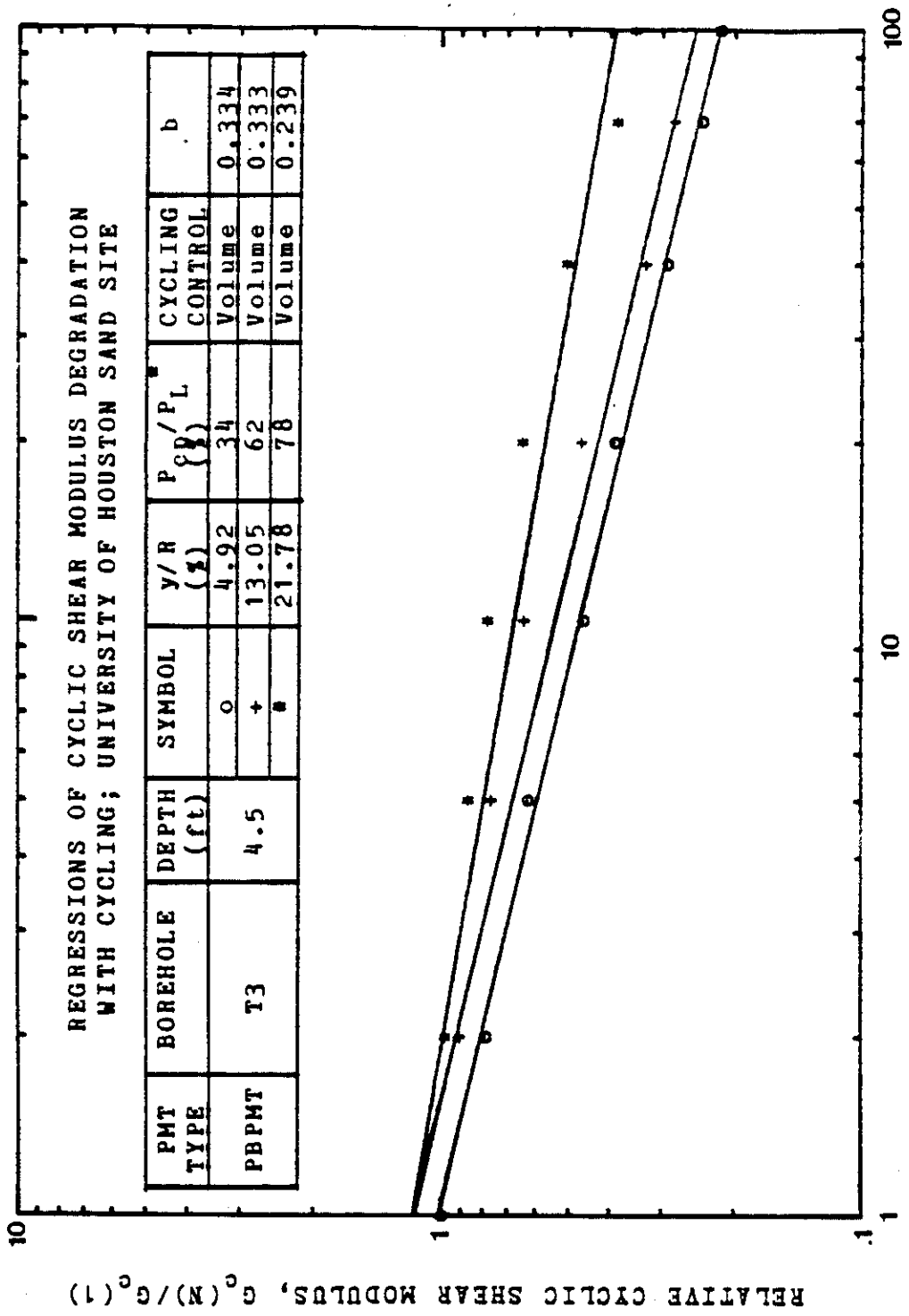
REGRESSIONS OF CYCLIC SHEAR MODULUS DEGRADATION
WITH CYCLING; UNIVERSITY OF HOUSTON SAND SITE
PMT TYPE
BOREHOLE
DEPTH (ft)
SYMBOL
y/R (%)
$P_{\ell p}/P_L$ (%)
CYCLING CONTROL
b
PBPMT
T3
4.5
o
4.92
34
Volume
0.334
+
13.05
62
Volume
0.333
*
21.78
78
Volume
0.239
10
1
.1
1
10
100
CYCLE NUMBER, N
RELATIVE CYCLIC SHEAR MODULUS, $G_c(N)/G_c(1)$

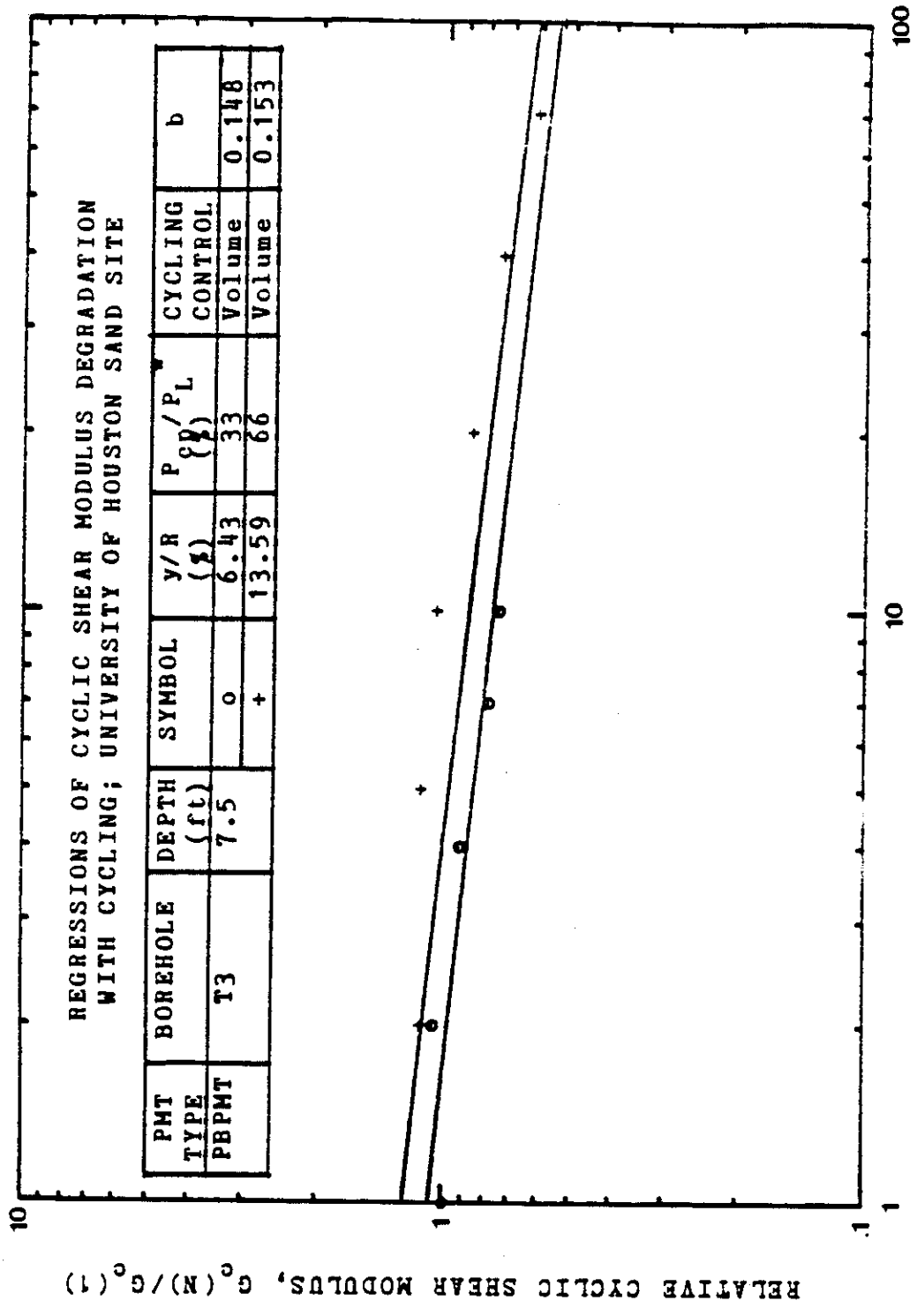
REGRESSIONS OF CYCLIC SHEAR MODULUS DEGRADATION
WITH CYCLING; UNIVERSITY OF HOUSTON SAND SITE
PMT TYPE
BOREHOLE
DEPTH (ft)
SYMBOL
y/R (%)
$P_{(D)}/P_L$ (%)
CYCLING CONTROL
b
PBPMT
T3
7.5
o
6.43
33
Volume
0.148
+
13.59
66
Volume
0.153
RELATIVE CYCLIC SHEAR MODULUS, $G_c(N)/G_c(1)$
CYCLE NUMBER, N
10
1
.1
1
10
100

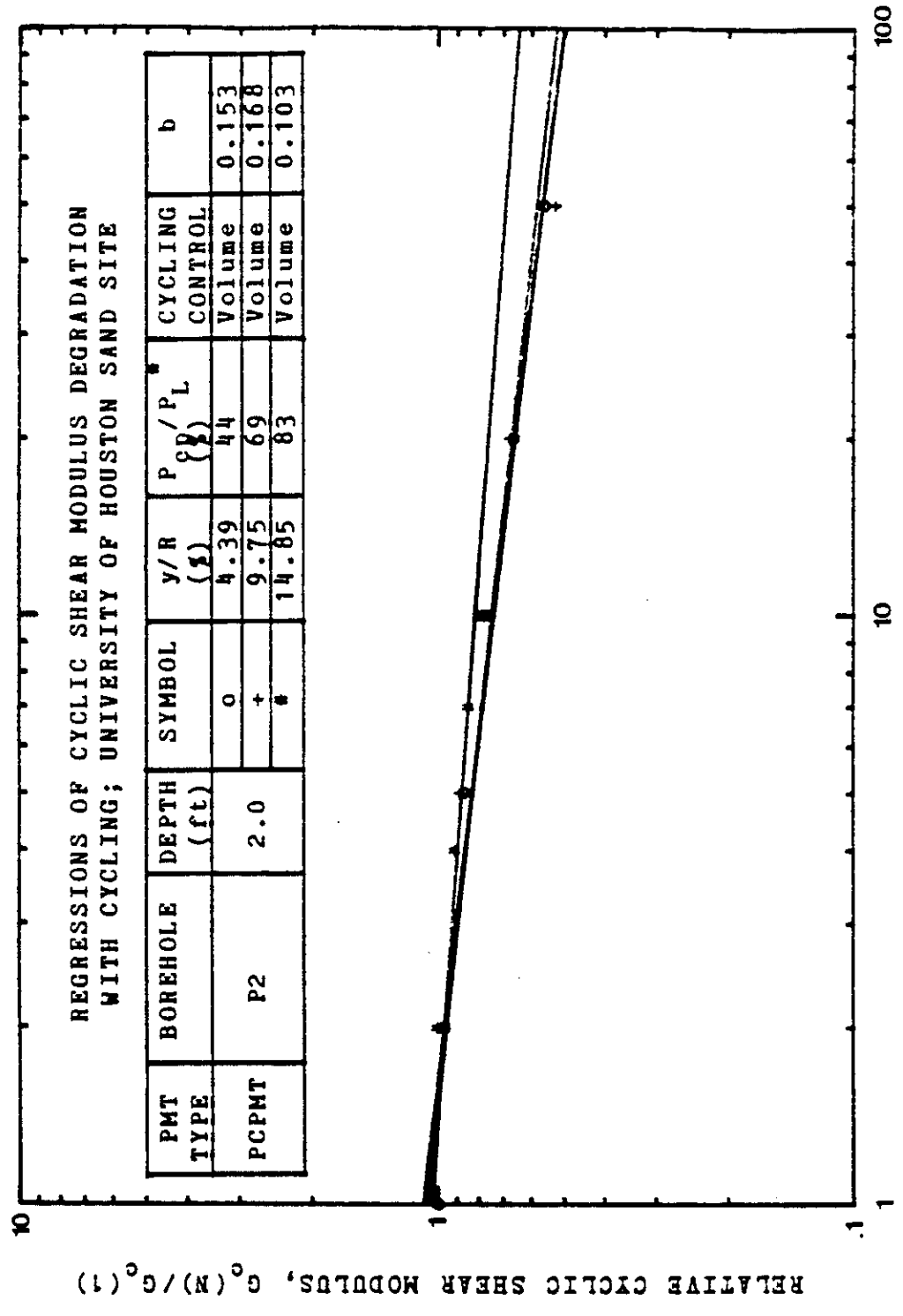
REGRESSIONS OF CYCLIC SHEAR MODULUS DEGRADATION
WITH CYCLING; UNIVERSITY OF HOUSTON SAND SITE
PMT TYPE
BOREHOLE
DEPTH (ft)
SYMBOL
y/R (%)
P_{cp}/P_L^* (%)
CYCLING CONTROL
b
PCPMT
P2
2.0
o
4.39
44
Volume
0.153
+
9.75
69
Volume
0.168
*
14.85
83
Volume
0.103
10
1
.1
1
10
100
CYCLE NUMBER, N
RELATIVE CYCLIC SHEAR MODULUS, $G_c(N)/G_c(1)$

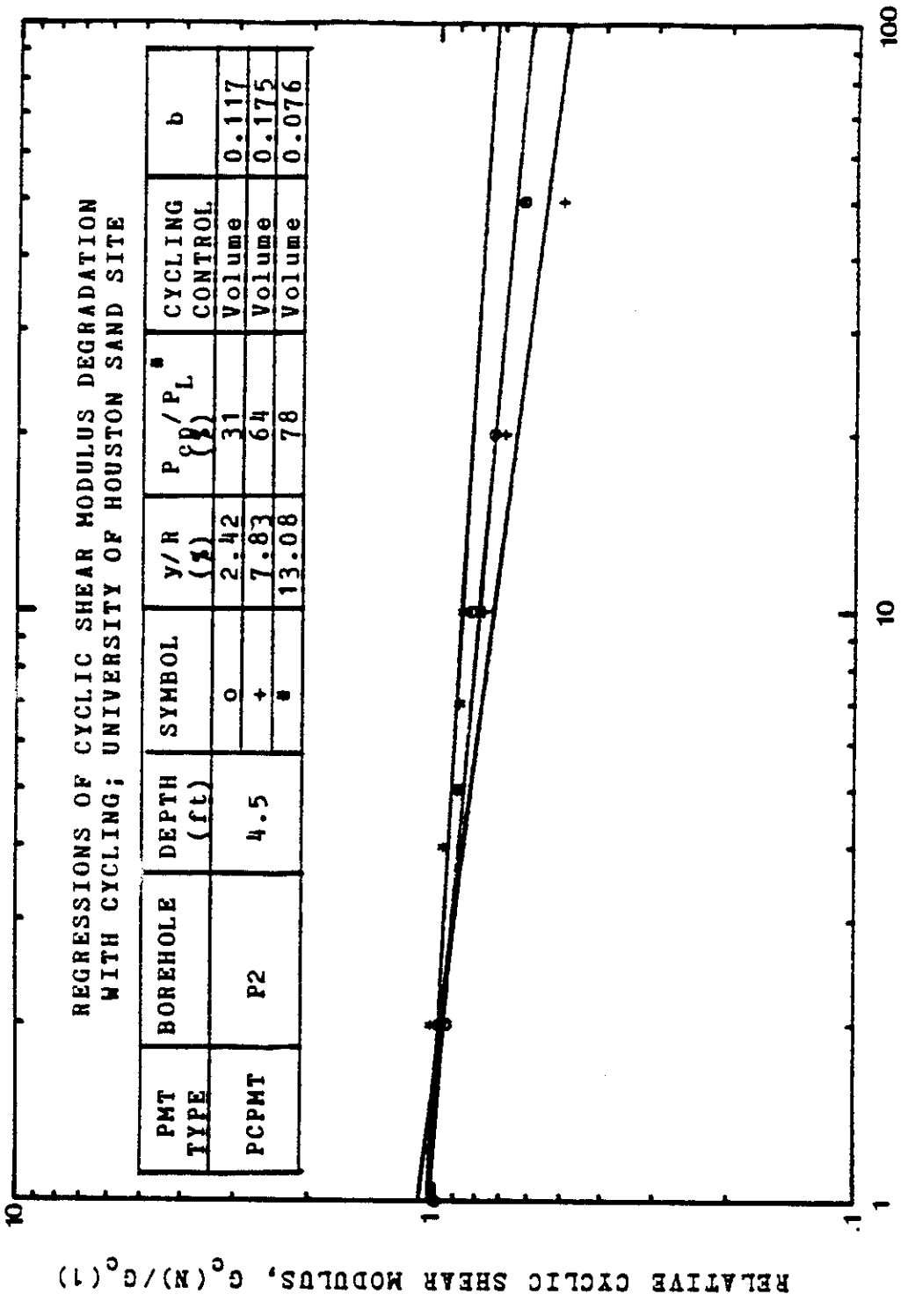
REGRESSIONS OF CYCLIC SHEAR MODULUS DEGRADATION
WITH CYCLING; UNIVERSITY OF HOUSTON SAND SITE
PMT TYPE
BOREHOLE
DEPTH (ft)
SYMBOL
y/R (%)
P_{cp}/P_L^* (%)
CYCLING CONTROL
b
PCPMT
P2
4.5
o
2.42
31
Volume
0.117
+
7.83
64
Volume
0.175
■
13.08
78
Volume
0.076
10
1
.1
1
10
100
CYCLE NUMBER, N
RELATIVE CYCLIC SHEAR MODULUS, $G_c(N)/G_c(1)$

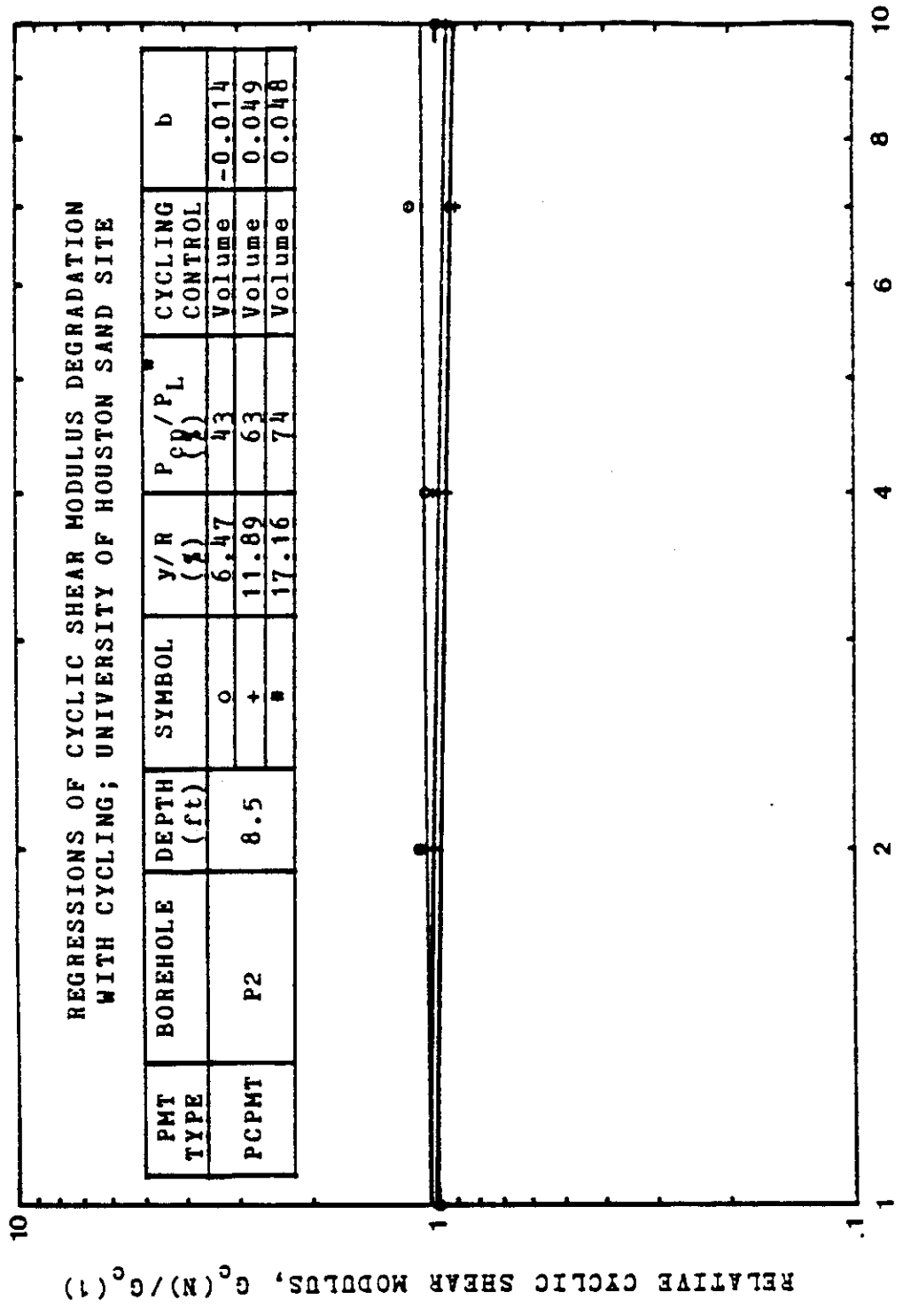
REGRESSIONS OF CYCLIC SHEAR MODULUS DEGRADATION
WITH CYCLING; UNIVERSITY OF HOUSTON SAND SITE
PMT TYPE
BOREHOLE
DEPTH (ft)
SYMBOL
γ/R (%)
P_{cp}/P_L (%)
CYCLING CONTROL
b
PCPMT
P2
8.5
o
6.47
43
Volume
-0.014
+
11.89
63
Volume
0.049
■
17.16
74
Volume
0.048
10
1
.1
1
2
4
6
8
10
CYCLE NUMBER, N
RELATIVE CYCLIC SHEAR MODULUS, $G_c(N)/G_c(1)$

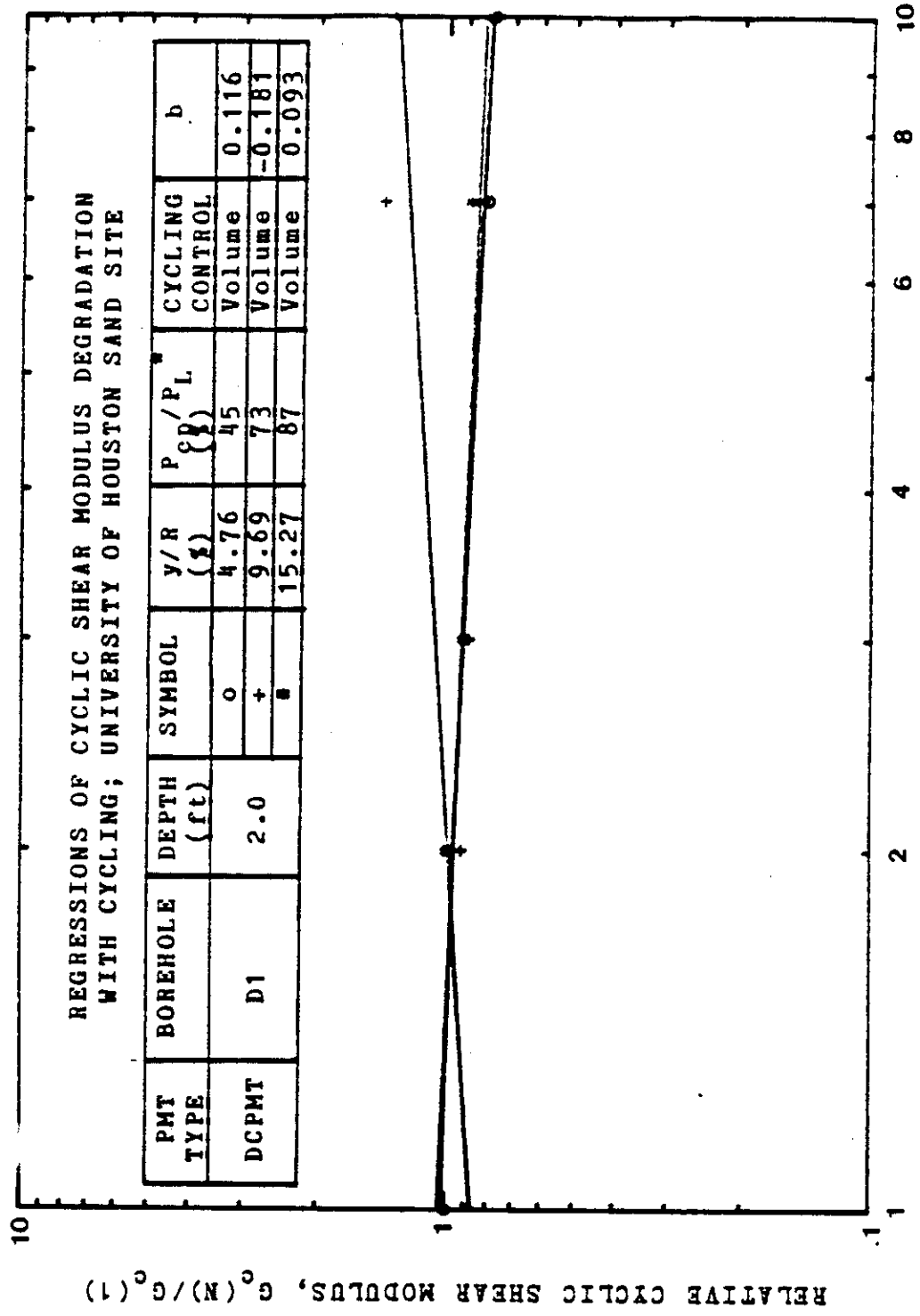
REGRESSIONS OF CYCLIC SHEAR MODULUS DEGRADATION
WITH CYCLING; UNIVERSITY OF HOUSTON SAND SITE
PMT TYPE
BOREHOLE
DEPTH (ft)
SYMBOL
y/R (%)
P_{cp}/P_L (%)
CYCLING CONTROL
b
DCPMT
D1
2.0
o
4.76
45
Volume
0.116
+
9.69
73
Volume
-0.181
■
15.27
87
Volume
0.093
RELATIVE CYCLIC SHEAR MODULUS, $G_c(N)/G_c(1)$
CYCLE NUMBER, N
10
1
.1
1
2
4
6
8
10

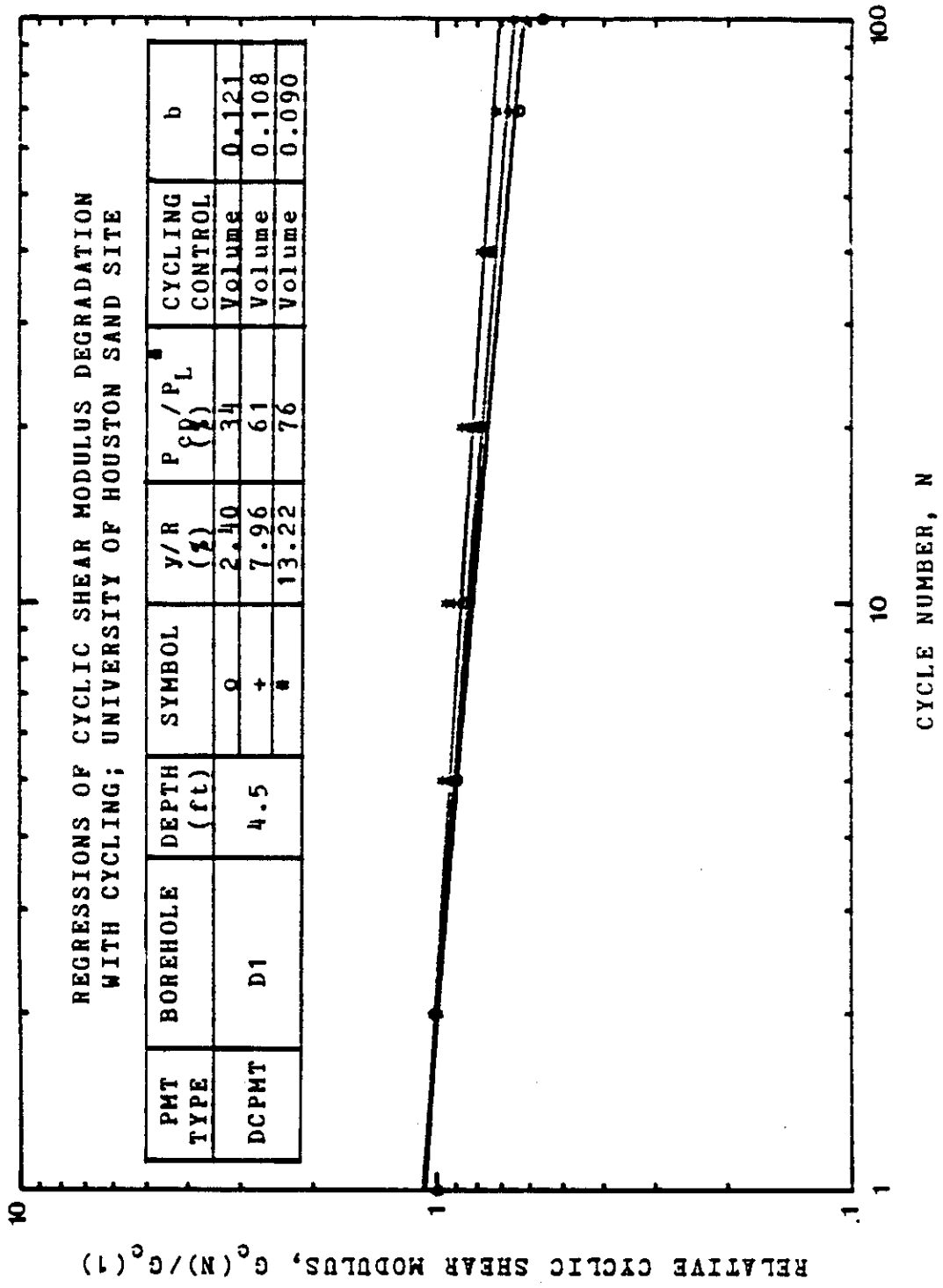
REGRESSIONS OF CYCLIC SHEAR MODULUS DEGRADATION
WITH CYCLING; UNIVERSITY OF HOUSTON SAND SITE
PMT TYPE
BOREHOLE
DEPTH (ft)
SYMBOL
γ/R (%)
P_CD/P_L (%)
CYCLING CONTROL
b
DCPMT
D1
4.5
o
2.40
34
Volume
0.121
+
7.96
61
Volume
0.108
#
13.22
76
Volume
0.090
RELATIVE CYCLIC SHEAR MODULUS, G_c(N)/G_c(1)
CYCLE NUMBER, N
10
1
.1
1
10
100

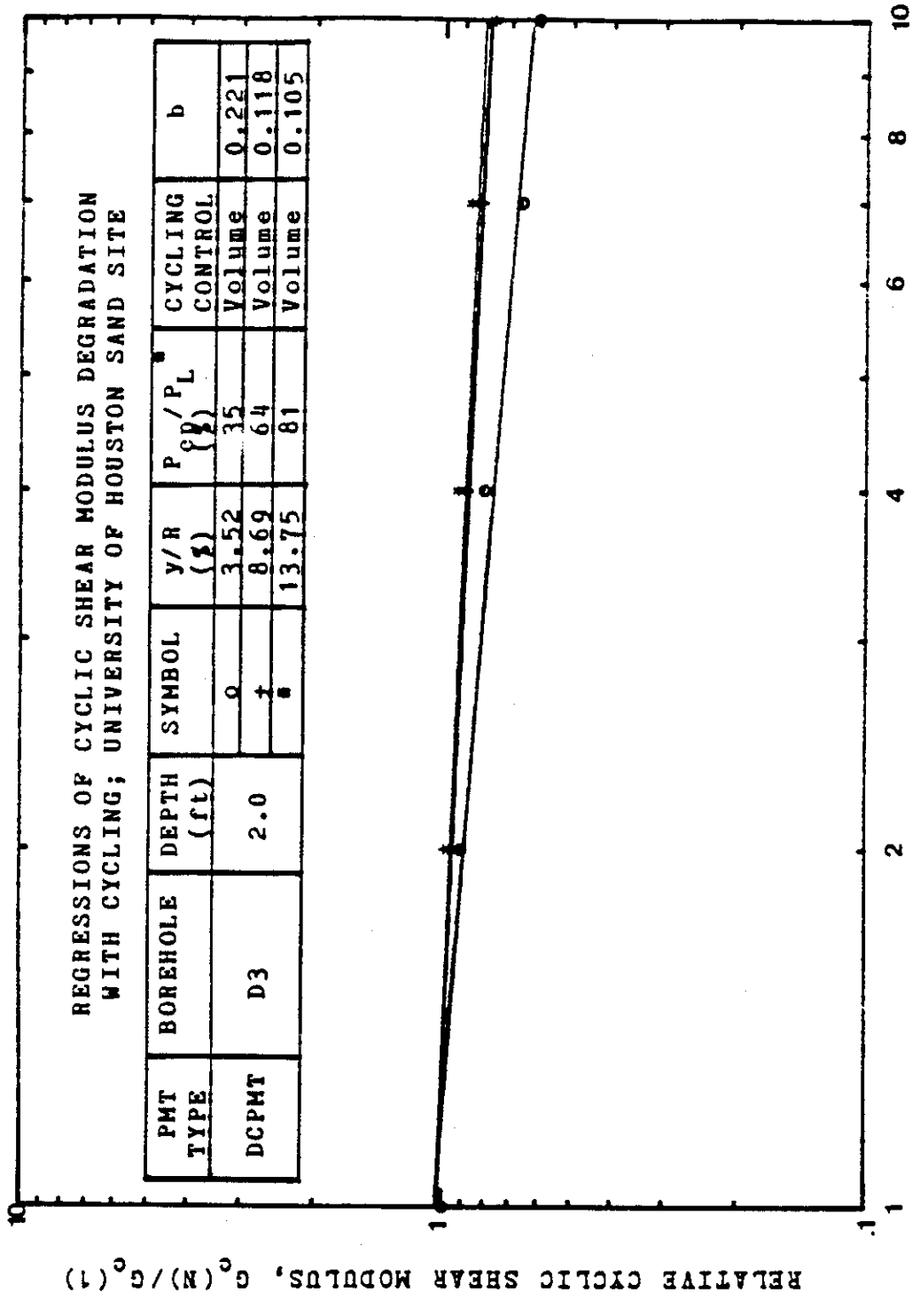
REGRESSIONS OF CYCLIC SHEAR MODULUS DEGRADATION
WITH CYCLING; UNIVERSITY OF HOUSTON SAND SITE
PMT TYPE
BOREHOLE
DEPTH (ft)
SYMBOL
γ/R (%)
P_{c0}/P_L (%)
CYCLING CONTROL
b
DCPMT
D3
2.0
○
3.52
35
Volume
0.221
+
8.69
64
Volume
0.118
■
13.75
81
Volume
0.105
RELATIVE CYCLIC SHEAR MODULUS, $G_c(N)/G_c(1)$
CYCLE NUMBER, N
10
1
.1
1
2
4
6
8
10

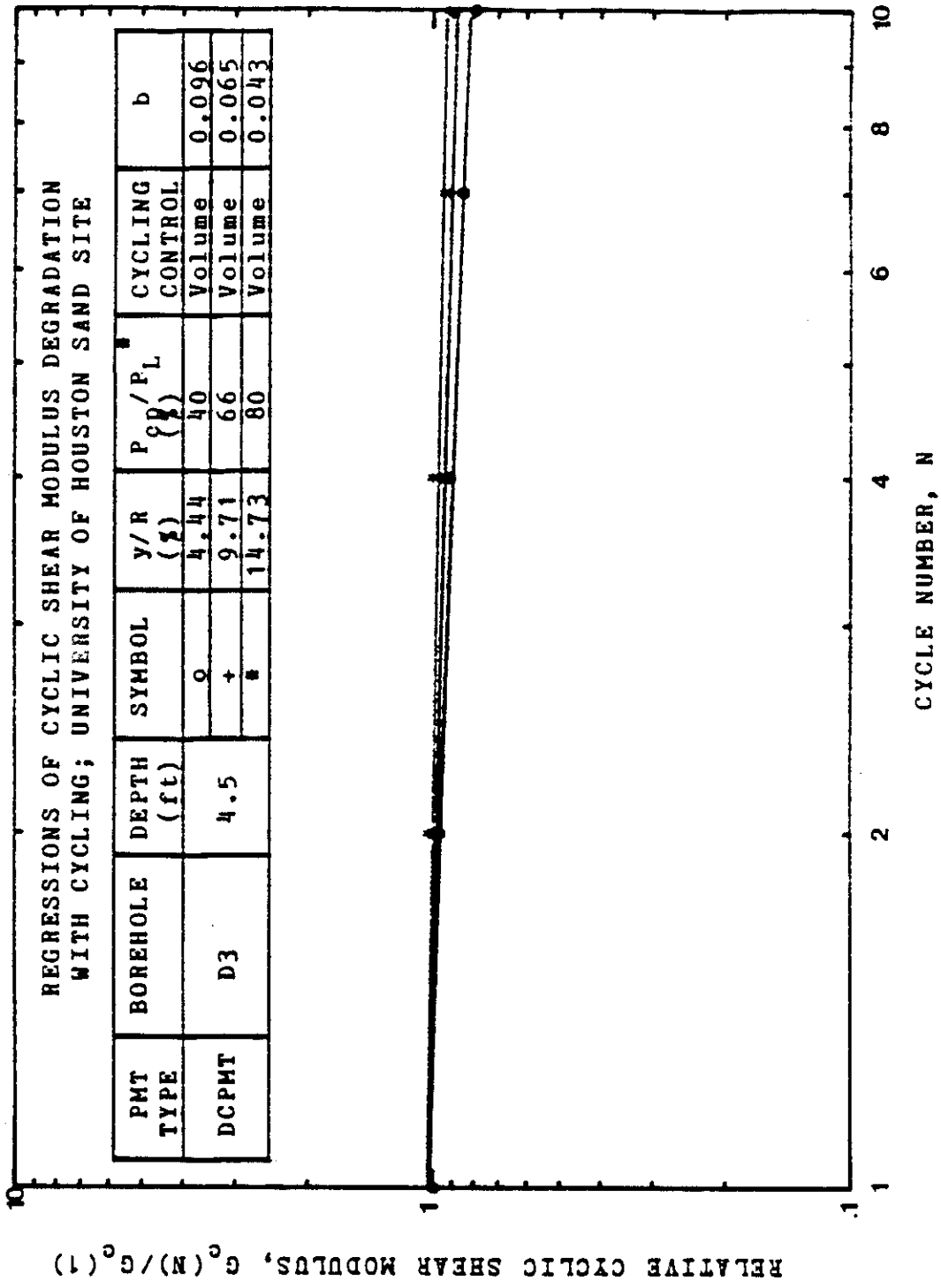
REGRESSIONS OF CYCLIC SHEAR MODULUS DEGRADATION
WITH CYCLING; UNIVERSITY OF HOUSTON SAND SITE
PMT TYPE
BOREHOLE
DEPTH (ft)
SYMBOL
γ/R (%)
P_{80}/P_L (%)
CYCLING CONTROL
b
DCPMT
D3
4.5
○
4.44
40
Volume
0.096
+
9.71
66
Volume
0.065
■
14.73
80
Volume
0.043
RELATIVE CYCLIC SHEAR MODULUS, $G_c(N)/G_c(1)$
CYCLE NUMBER, N
10
1
.1
1
2
4
6
8
10

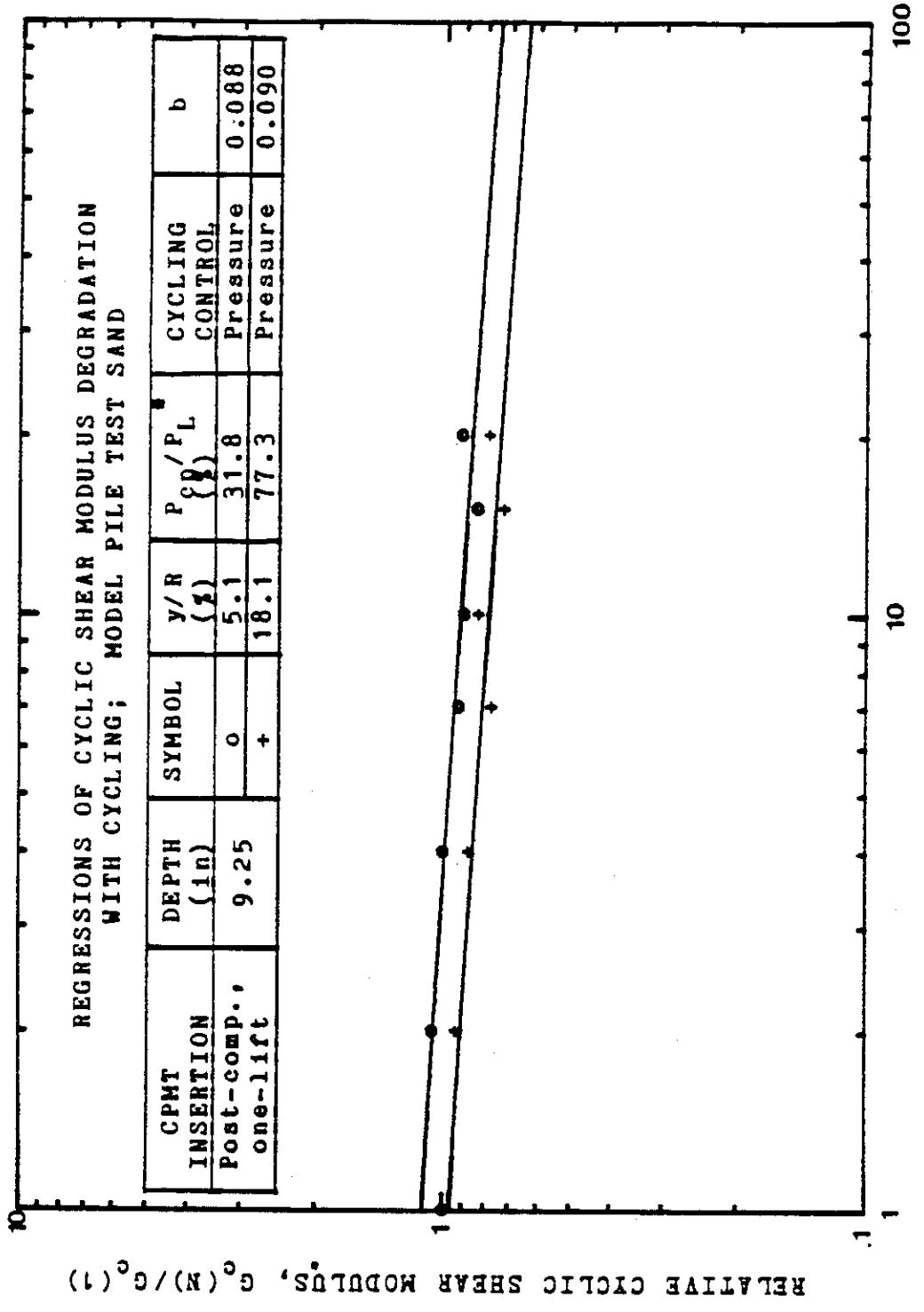
REGRESSIONS OF CYCLIC SHEAR MODULUS DEGRADATION
WITH CYCLING; MODEL PILE TEST SAND
CPMT INSERTION
DEPTH (in)
SYMBOL
y/R (%)
$P_{(0)}/P_L$ (%)
CYCLING CONTROL
b
Post-comp., one-lift
9.25
o
5.1
31.8
Pressure
0.088
+
18.1
77.3
Pressure
0.090
RELATIVE CYCLIC SHEAR MODULUS, $G_c(N)/G_c(1)$
CYCLE NUMBER, N
10
1
.1
1
10
100

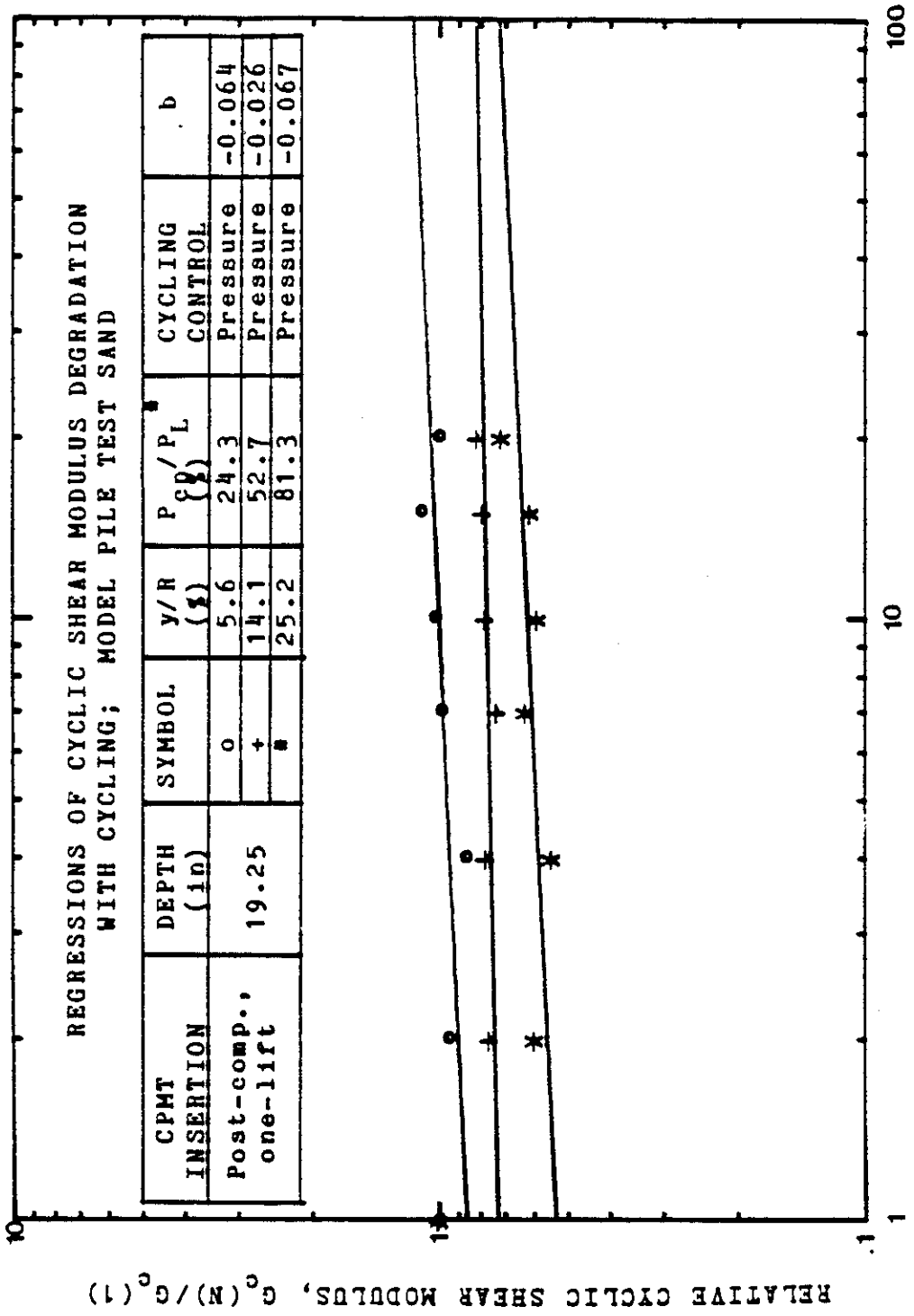
REGRESSIONS OF CYCLIC SHEAR MODULUS DEGRADATION
WITH CYCLING; MODEL PILE TEST SAND
CPMT INSERTION
DEPTH (in)
SYMBOL
y/R (%)
P_{CD}/P_L (%)
CYCLING CONTROL
b
Post-comp., one-lift
19.25
o
5.6
24.3
Pressure
-0.064
+
14.1
52.7
Pressure
-0.026
*
25.2
81.3
Pressure
-0.067
RELATIVE CYCLIC SHEAR MODULUS, $G_c(N)/G_c(1)$
CYCLE NUMBER, N
1
10
100
.1
1

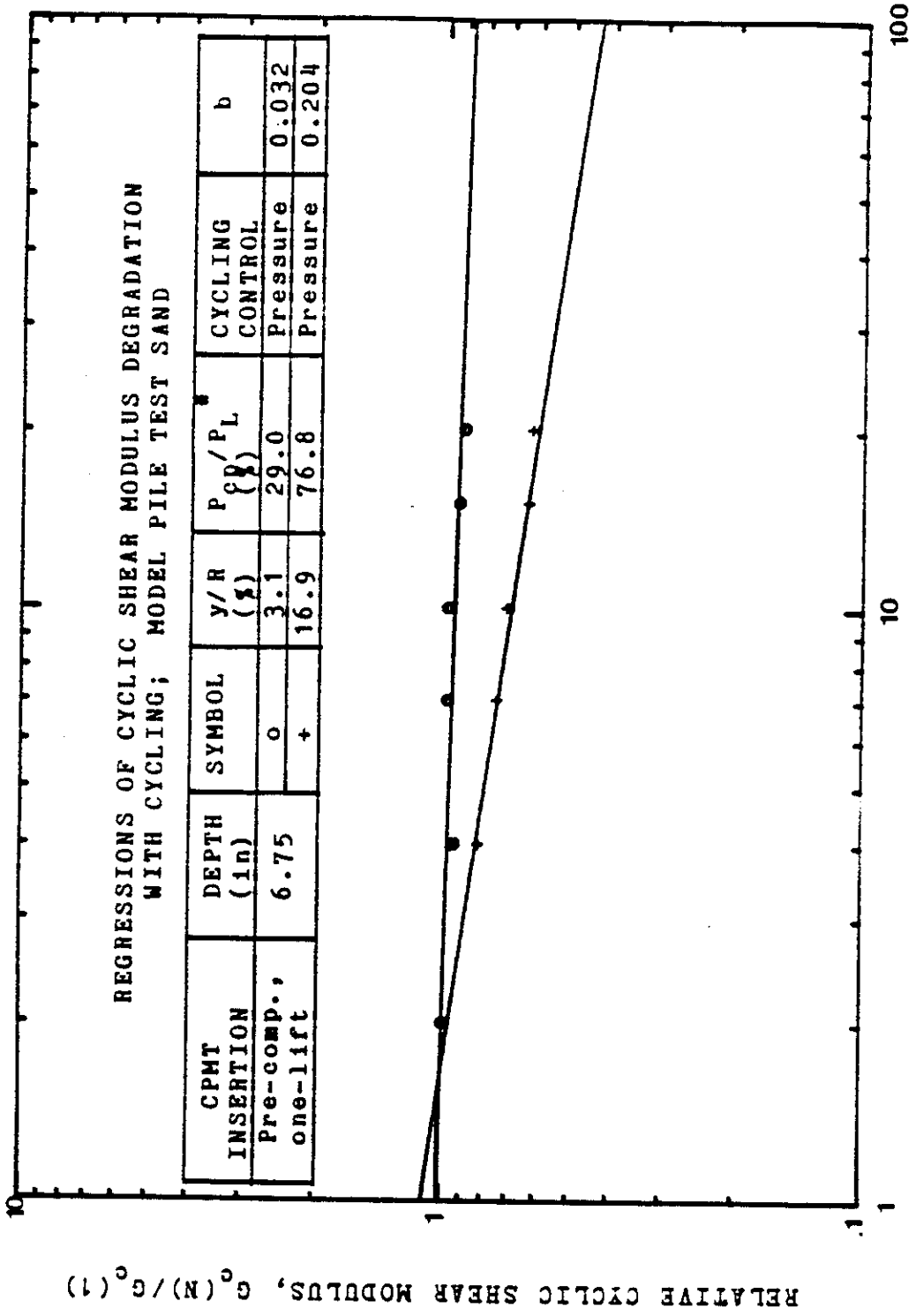
REGRESSIONS OF CYCLIC SHEAR MODULUS DEGRADATION
WITH CYCLING; MODEL PILE TEST SAND
CPMT INSERTION
DEPTH (in)
SYMBOL
y/R (%)
P_{cp}/P_L (%)
CYCLING CONTROL
b
Pre-comp., one-lift
6.75
o
3.1
29.0
Pressure
0.032
+
16.9
76.8
Pressure
0.204
RELATIVE CYCLIC SHEAR MODULUS, $G_c(N)/G_c(1)$
CYCLE NUMBER, N
100
10
1
.1
1
10

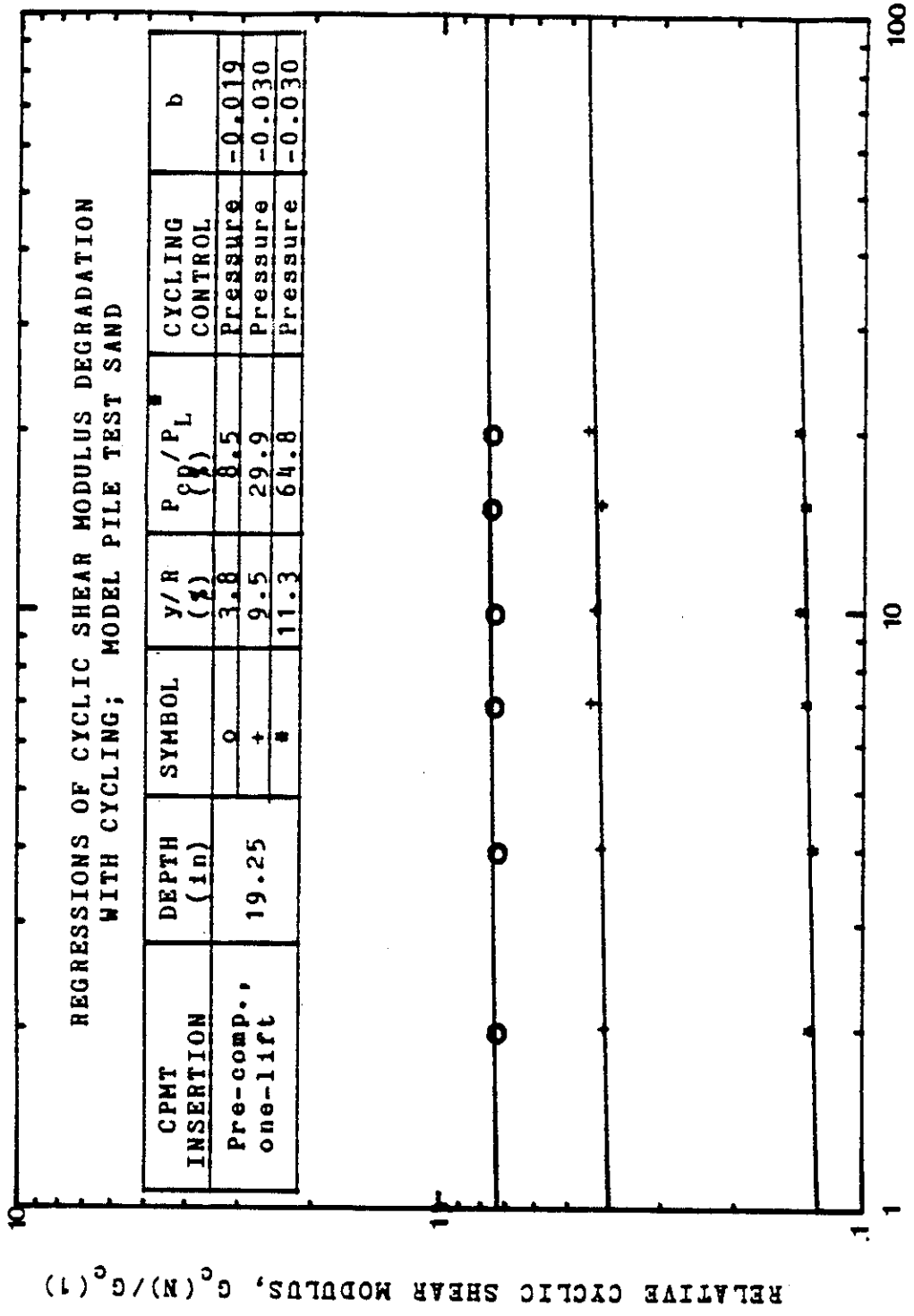
REGRESSIONS OF CYCLIC SHEAR MODULUS DEGRADATION
WITH CYCLING; MODEL PILE TEST SAND
CPMT INSERTION
DEPTH (in)
SYMBOL
y/R (%)
P_{cp}/P_L (%)
CYCLING CONTROL
b
Pre-comp., one-lift
19.25
o
3.8
8.5
Pressure
-0.019
+
9.5
29.9
Pressure
-0.030
*
11.3
64.8
Pressure
-0.030
RELATIVE CYCLIC SHEAR MODULUS, $G_c(N)/G_c(1)$
CYCLE NUMBER, N
10
1
.1
1
10
100

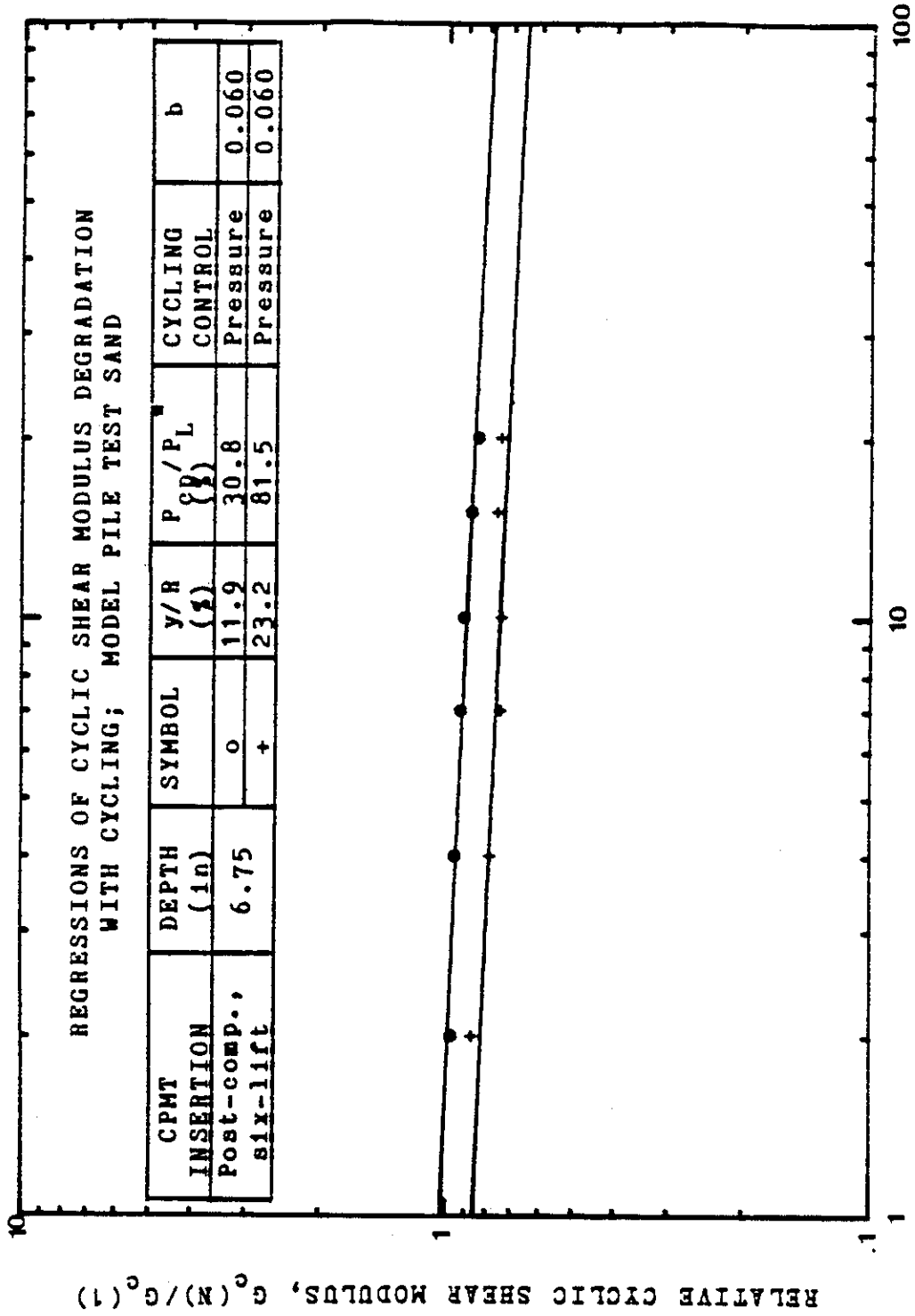
REGRESSIONS OF CYCLIC SHEAR MODULUS DEGRADATION
WITH CYCLING; MODEL PILE TEST SAND
CPMT INSERTION
DEPTH (in)
SYMBOL
y/R (%)
P_{CD}/P_L (%)
CYCLING CONTROL
b
Post-comp., six-lift
6.75
o
11.9
30.8
Pressure
0.060
+
23.2
81.5
Pressure
0.060
RELATIVE CYCLIC SHEAR MODULUS, $G_c(N)/G_c(1)$
CYCLE NUMBER, N
10
1
.1
1
10
100

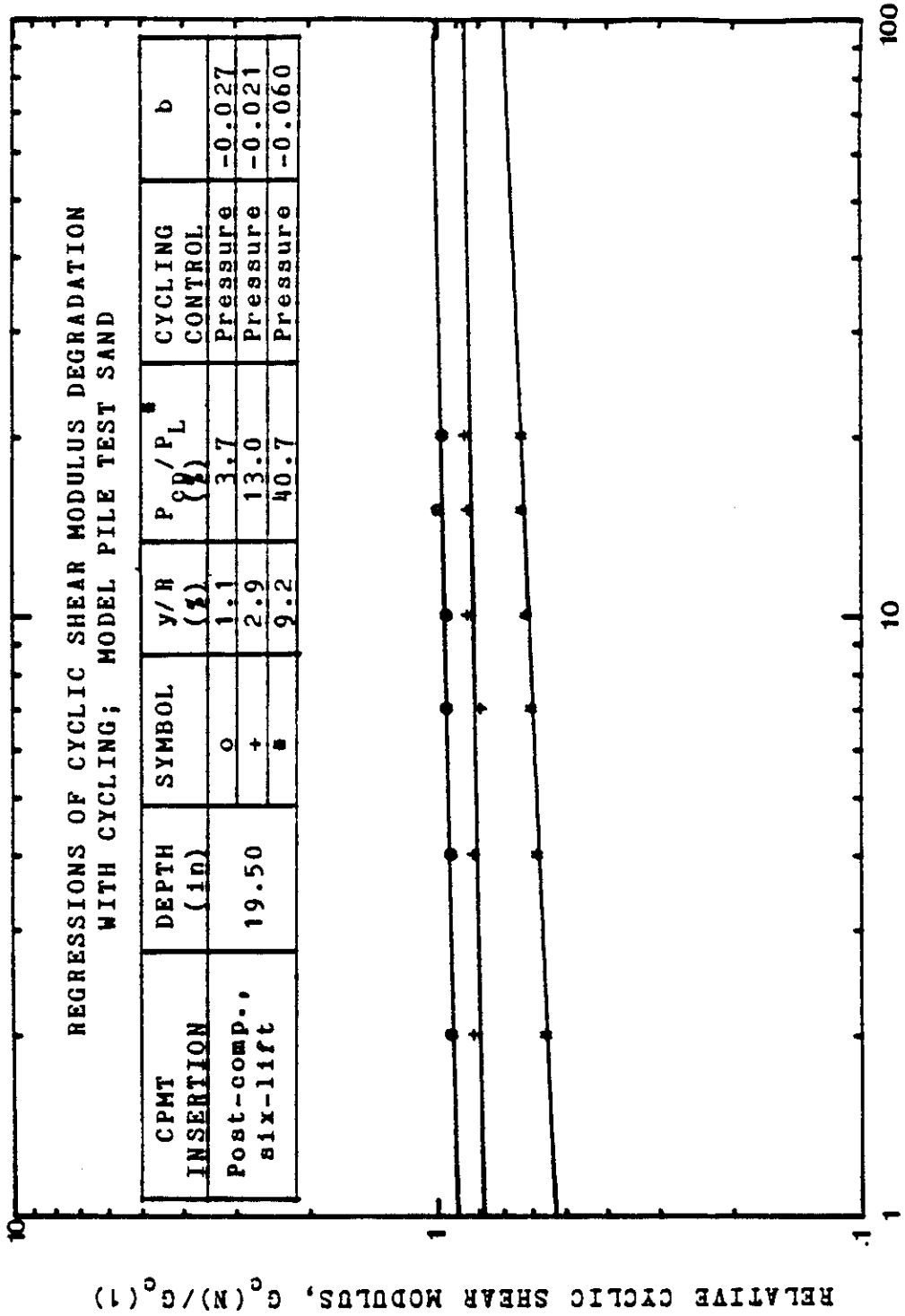
REGRESSIONS OF CYCLIC SHEAR MODULUS DEGRADATION
WITH CYCLING; MODEL PILE TEST SAND
CPMT INSERTION
DEPTH (in)
SYMBOL
y/R (%)
$P_{\ell p}/P_L$ (%)
CYCLING CONTROL
b
Post-comp., six-lift
19.50
o
1.1
3.7
Pressure
-0.027
+
2.9
13.0
Pressure
-0.021
▪
9.2
40.7
Pressure
-0.060
RELATIVE CYCLIC SHEAR MODULUS, $G_c(N)/G_c(1)$
CYCLE NUMBER, N
10
1
.1
1
10
100

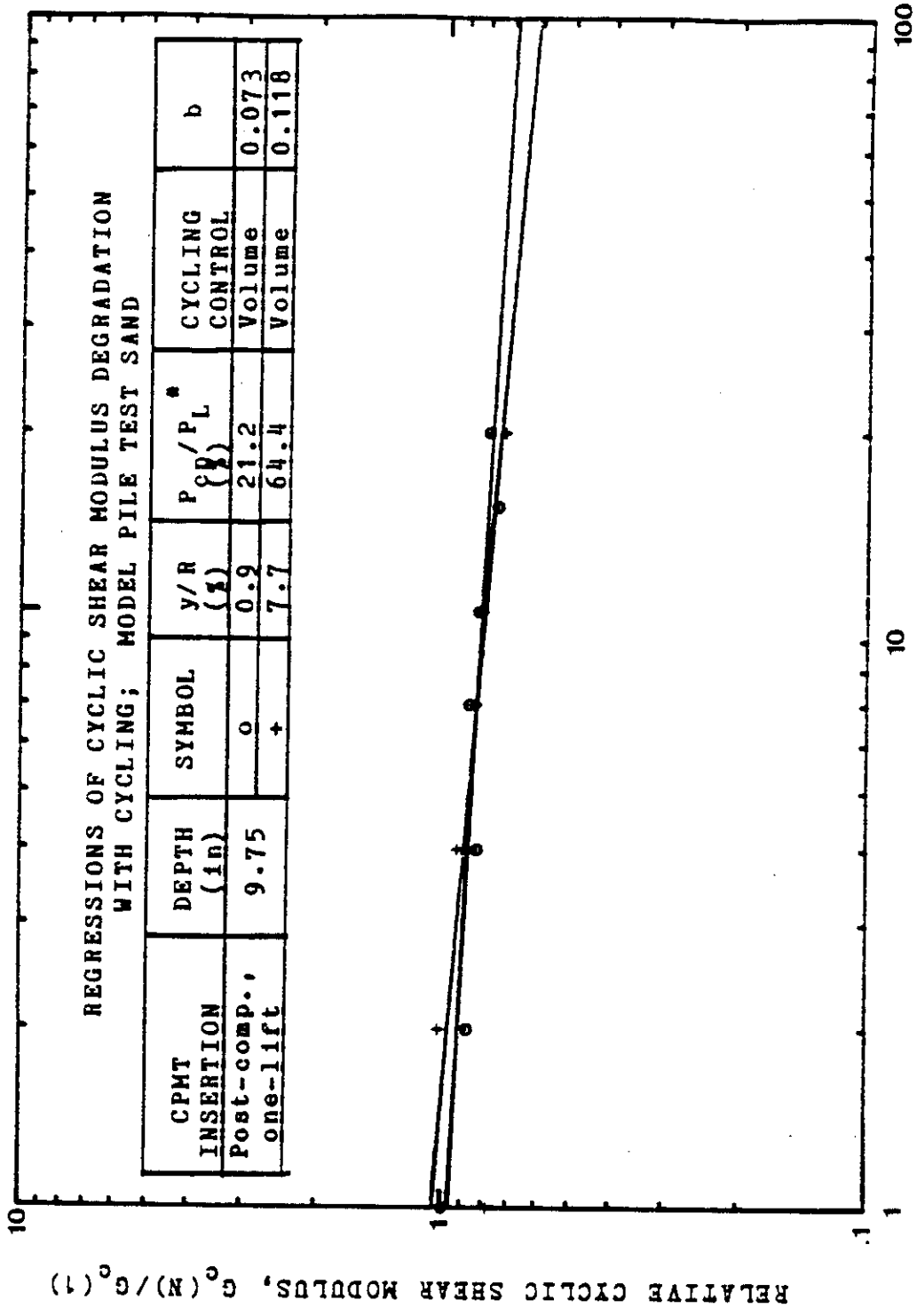
REGRESSIONS OF CYCLIC SHEAR MODULUS DEGRADATION
WITH CYCLING; MODEL PILE TEST SAND
CPMT INSERTION
DEPTH (in)
SYMBOL
y/R (%)
P_{cp}/P_L^* (%)
CYCLING CONTROL
b
Post-comp., one-11ft
9.75
o
0.9
21.2
Volume
0.073
+
7.7
64.4
Volume
0.118
RELATIVE CYCLIC SHEAR MODULUS, $G_c(N)/G_c(1)$
CYCLE NUMBER, N
10
1
.1
1
10
100

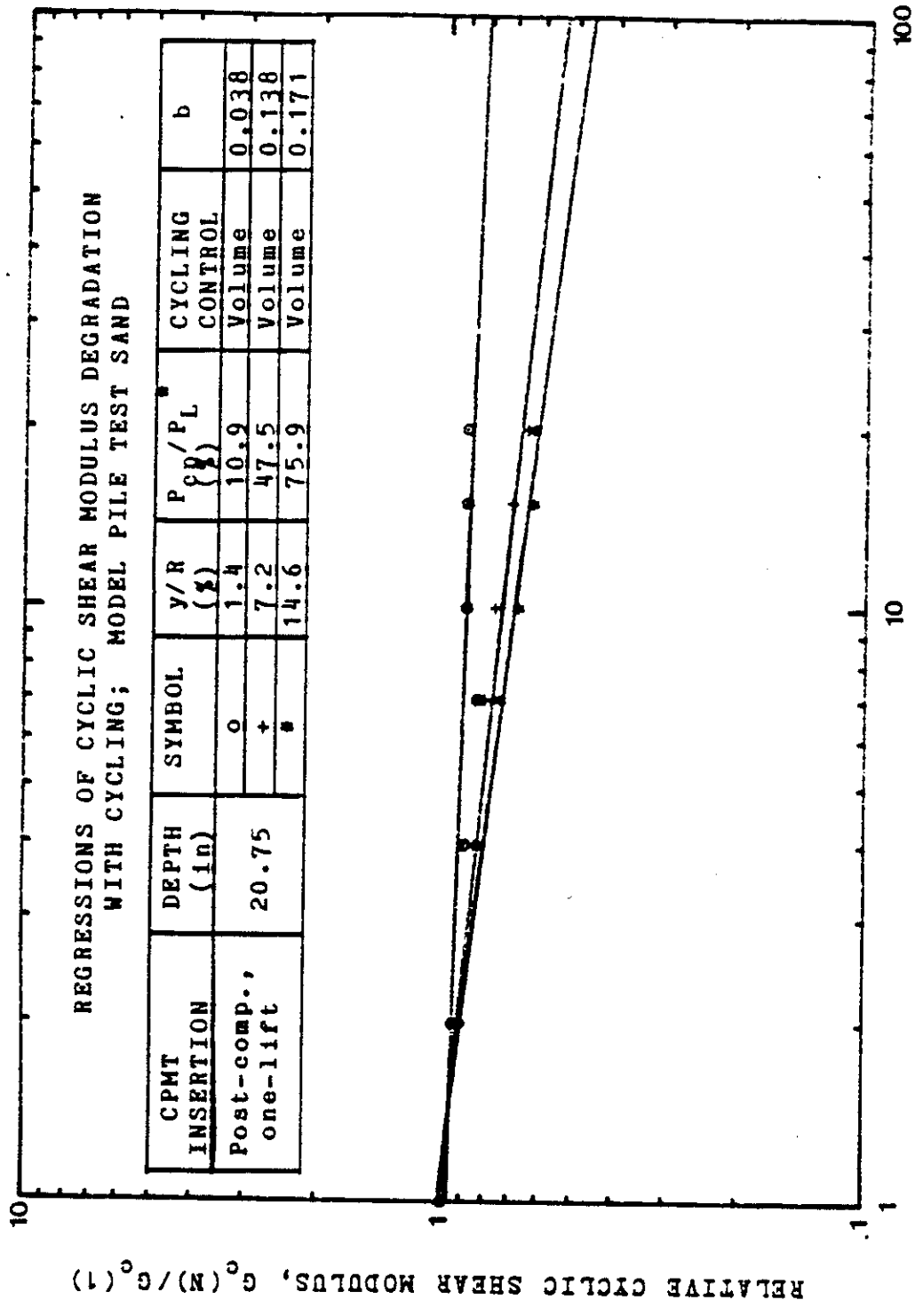
REGRESSIONS OF CYCLIC SHEAR MODULUS DEGRADATION WITH CYCLING; MODEL PILE TEST SAND
CPMT INSERTION
DEPTH (in)
SYMBOL
y/R (%)
$P_{(0)}/P_L^*$
CYCLING CONTROL
b
Post-comp., one-lift
20.75
o
1.4
10.9
Volume
0.038
+
7.2
47.5
Volume
0.138
#
14.6
75.9
Volume
0.171
RELATIVE CYCLIC SHEAR MODULUS, $G_c(N)/G_c(1)$
CYCLE NUMBER, N
10
1
.1
1
10
100

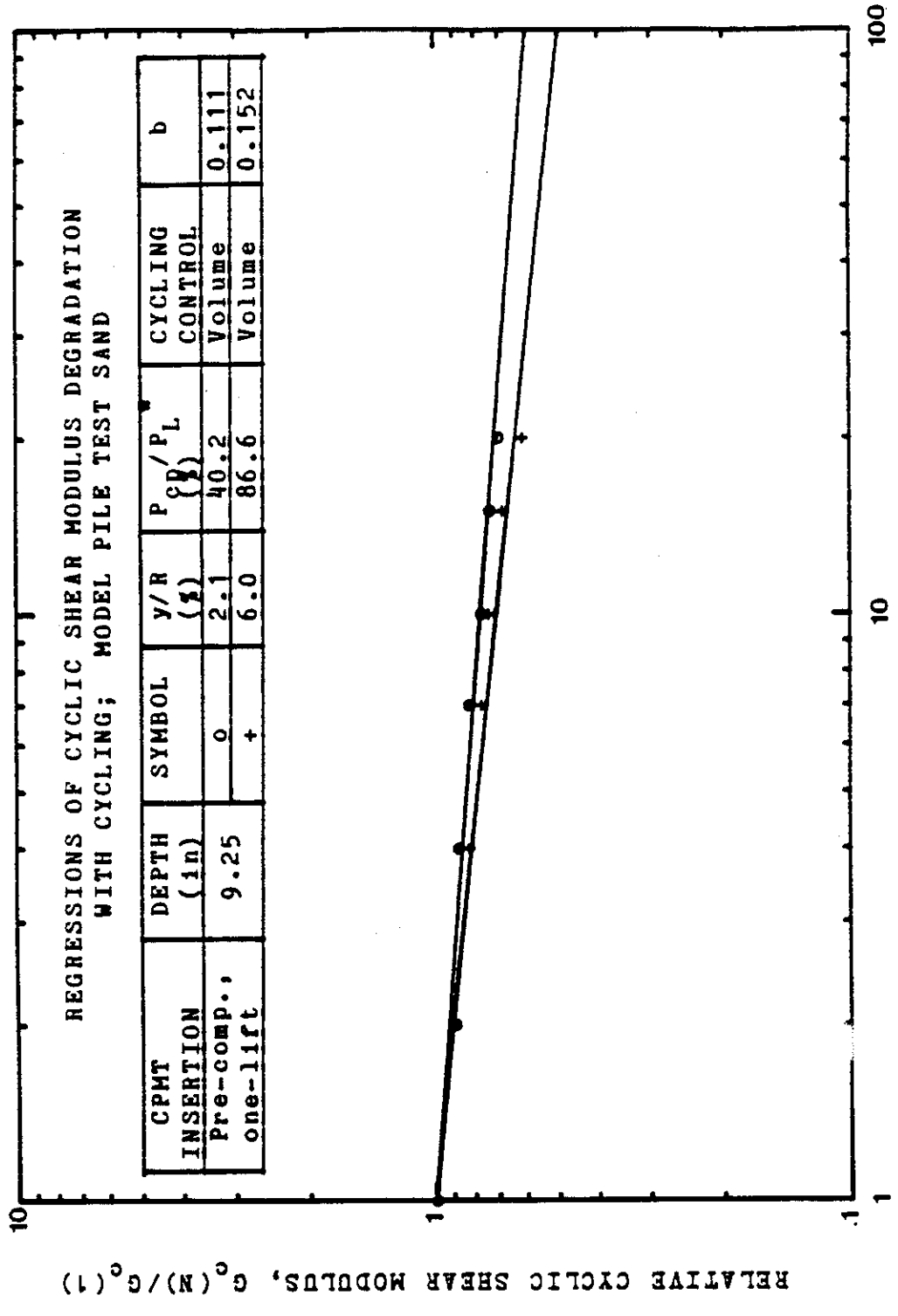
REGRESSIONS OF CYCLIC SHEAR MODULUS DEGRADATION
WITH CYCLING; MODEL PILE TEST SAND
CPMT INSERTION | DEPTH (in) | SYMBOL | γ/R (%) | P_CD/P_L (%) | CYCLING CONTROL | b
Pre-comp., one-lift | 9.25 | o | 2.1 | 40.2 | Volume | 0.111
 | | + | 6.0 | 86.6 | Volume | 0.152
RELATIVE CYCLIC SHEAR MODULUS, G_c(N)/G_c(1)
CYCLE NUMBER, N
10
1
.1
1
10
100

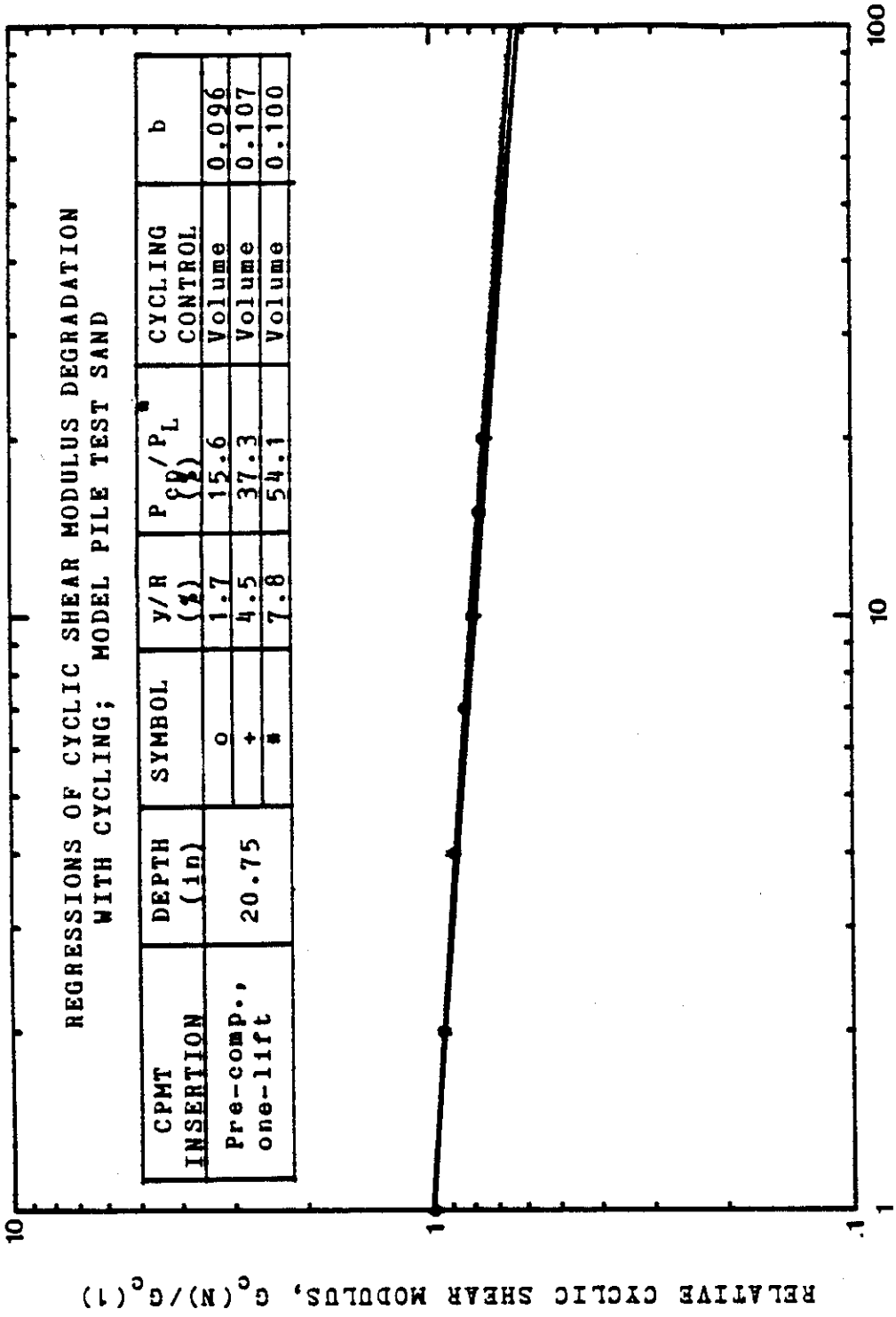
REGRESSIONS OF CYCLIC SHEAR MODULUS DEGRADATION
WITH CYCLING; MODEL PILE TEST SAND
CPMT INSERTION
DEPTH (in)
SYMBOL
γ/R (%)
P_D/P_L (%)
CYCLING CONTROL
b
Pre-comp., one-lift
20.75
o
1.7
15.6
Volume
0.096
+
4.5
37.3
Volume
0.107
*
7.8
54.1
Volume
0.100
RELATIVE CYCLIC SHEAR MODULUS, G_c(N)/G_c(1)
CYCLE NUMBER, N
10
1
.1
1
10
100

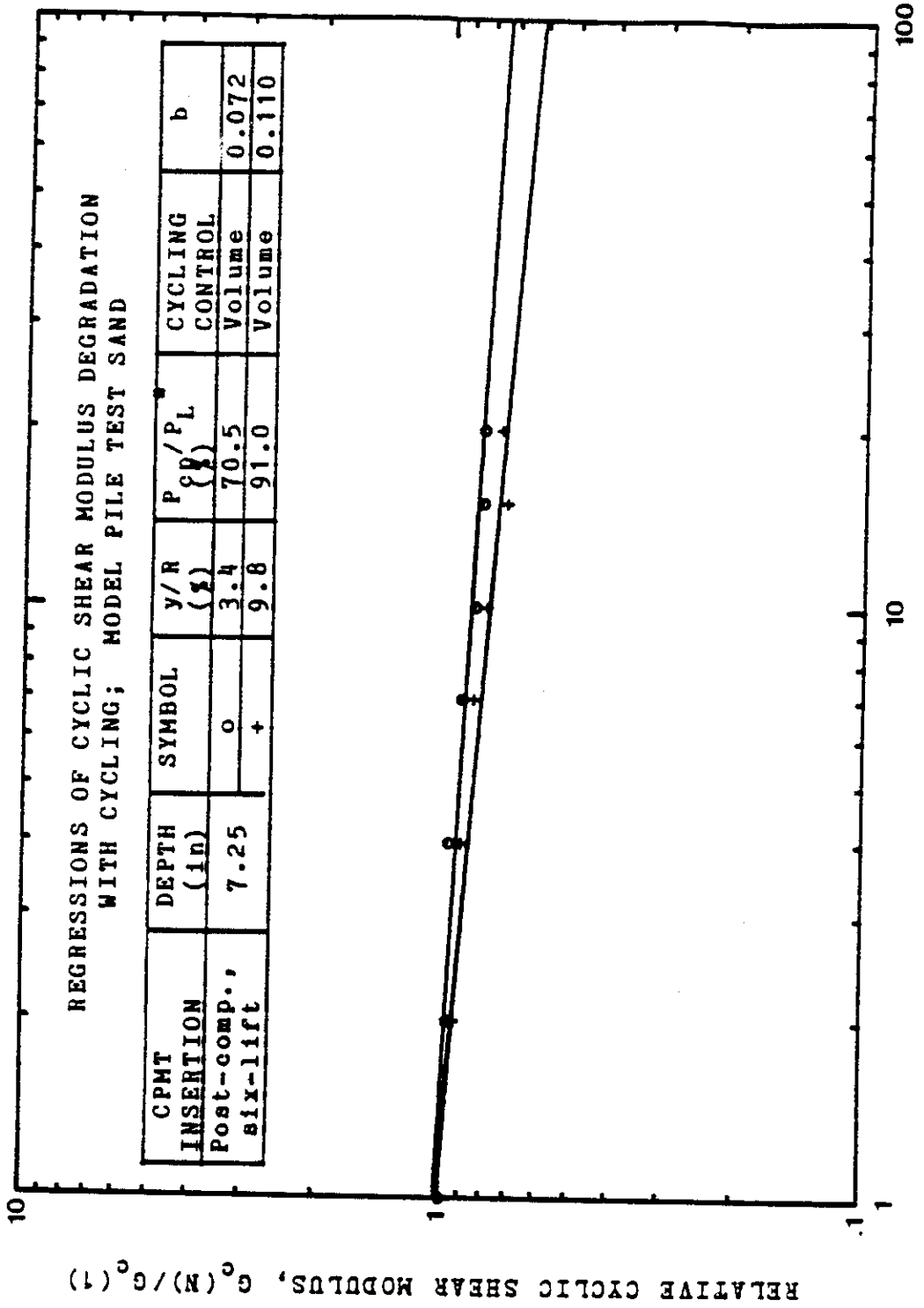
REGRESSIONS OF CYCLIC SHEAR MODULUS DEGRADATION
WITH CYCLING; MODEL PILE TEST SAND
CPMT INSERTION
DEPTH (in)
SYMBOL
y/R (%)
P_{CR}/P_L (%)
CYCLING CONTROL
b
Post-comp., six-lift
7.25
o
3.4
70.5
Volume
0.072
+
9.8
91.0
Volume
0.110
RELATIVE CYCLIC SHEAR MODULUS, $G_c(N)/G_c(1)$
CYCLE NUMBER, N
10
1
.1
1
10
100

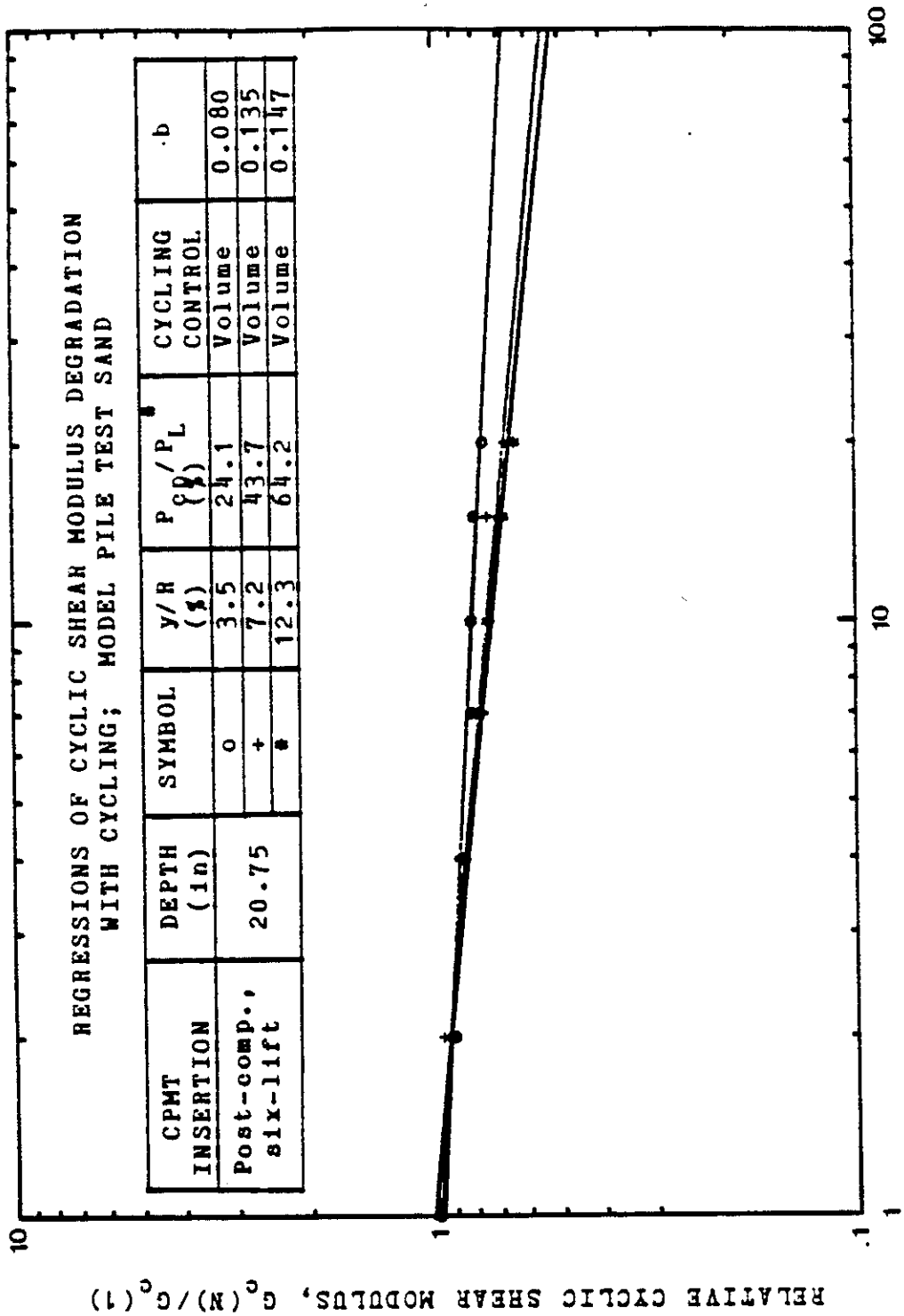
REGRESSIONS OF CYCLIC SHEAR MODULUS DEGRADATION
WITH CYCLING; MODEL PILE TEST SAND
CPMT INSERTION
DEPTH (in)
SYMBOL
y/R (%)
P_{cp}/P_L (%)
CYCLING CONTROL
b
Post-comp., six-lift
20.75
o
3.5
24.1
Volume
0.080
+
7.2
43.7
Volume
0.135
*
12.3
64.2
Volume
0.147
RELATIVE CYCLIC SHEAR MODULUS, $G_c(N)/G_c(1)$
CYCLE NUMBER, N
10
1
.1
1
10
100